Mechanistic Characterization and Development of Tailored Small Molecule Modulators of the κ-Opioid Receptor

Inaugural-Dissertation
to obtain the academic degree
Doctor rerum naturalium (Dr. rer. nat.)

submitted to the Department of Biology, Chemistry, Pharmacy
of Freie Universität Berlin

by

Kristina Sophie Puls

2024

The presented thesis was prepared from 2021 until 2024 under the supervision of Prof. Dr. Gerhard Wolber at the Institute of Pharmacy of the Freie Universität Berlin.

1st reviewer: Prof. Dr. Gerhard Wolber
2nd reviewer: Prof. Dr. Marcel Bermúdez
Date of defense: 13.06.2024

Acknowledgement

I would like to express my gratitude to Prof. Gerhard Wolber for giving me the chance to study with his research group. I always appreciated the open-minded environment and the research discussions.

I would like to thank my colleagues for their encouragement, problem-solving discussions, and friendly chats. My daily life would have been more challenging without you.

Although Marcel Bermudez has left to become a professor, I greatly benefited from his guidance at the beginning of my research. Thank you for your help.

I would also like to thank Dr. Mariana Spetea and her research group for their collaboration, which included several in vitro experiments.

Finally, I want to thank my family, especially my partner Henning Dominke, for their unwavering support. You have shared moments of great despair as well as moments of absolute happiness with me.

Independence Declaration

Herewith I certify that I have prepared and written my thesis independently and that I have not used any sources and aids other than those indicated by me. Grammarly and DeepL were used to perform a basic grammar check.

I also declare that I have not submitted the dissertation in this or any other form to any other institution as a dissertation.

Berlin, Germany

11 March 2024

Kristina Sophie Puls

Contents

Summary

Opioid receptor ligands (opioids) represent the gold standard for severe pain treatment. However, approved opioids possess many serious side effects even if they are used according to medical instructions. As a result, opioid use leads to thousands of hospitalizations and deaths each year. Four different opioid receptor subtypes exist but approved opioids mainly activate the μ-opioid receptor (MOR). Activation of the κ-opioid receptor (KOR) emerged as a promising strategy to sufficiently alleviate pain while improving the side effect profile of opioids. However, KOR-related side effects and the high structural similarity of the opioid receptor subtypes renders rational drug design challenging.

The opioid receptor system is not only involved in pain modulation, but also in the maintenance of mood homeostasis. Antagonism of the KOR recently emerged as a promising strategy for the development of novel antidepressants with fast-onset antidepressant effects that are also effective against suicidal intent. However, the chemical space of KOR selective antagonists is limited. No short-acting and selective KOR antagonists have been approved so far.

This dissertation encompasses retrospective and prospective studies that focus on *in silico* techniques to address current questions in opioid research. The first three articles, conducted retrospective *in silico* analyses of HS-731, an opioid agonist, Compound A, a KOR/MOR dual antagonist, and Salvinorin A (SalA), a non-basic, KOR-selective agonist. These analyses aimed to improve our limited understanding of the factors that determine opioid receptor activity and selectivity. The investigated compounds are of high pharmacological interest. HS-731 represents an analgesic with a potentially improved safety profile due to its exclusion from the central nervous system (CNS). Compound A has a unique scaffold that may overcome the unfavorable kinetic profile of current antidepressant opioids. SalA represents a non-basic agonist with exceptional KOR selectivity that potentially binds dissimilar to basic opioids at the KOR. Protein-ligand binding modes of the compounds at the opioid receptor subtypes were predicted and selectivity determinants rationalized. Important protein-ligand interactions responsible for the opioid receptor activity of these ligands were highlighted. A new binding site for SalA above the typical morphinan binding site that is highly non-conserved was discovered. The SalA binding mode is consistent with structure-activity relationship (SAR) data and rationalizes the exceptional receptor subtype selectivity of SalA at the KOR. In addition, a partial agonism-inducing mechanism for the KOR was hypothesized involving an interaction between the extracellular oriented parts of the transmembrane helices 5 and 6.

Typical opioids possess a basic amine moiety interacting with a conserved aspartate residue inside the binding site. Since the discover of non-basic and highly KOR-selective SalA, the design of non-basic opioids became a new and promising strategy for the selective activation of the KOR, circumventing MOR-associated severe side effects. However, the number of

1

known non-basic opioids is strongly limited and rational drug design of new non-basic opioids is the hindered by the lack of understanding about the binding mode of SalA. In the fourth article included in this dissertation, a prospective 3D pharmacophore-based virtual screening campaign was conducted. The campaign was based on the SalA binding mode postulated in the third article. The aim was to determine new non-basic and selective KOR ligands. Pharmacological *in vitro* experiments confirmed two of the suggested compounds to activate the KOR with nanomolar potency and good subtype selectivity. One hit compound possesses a full agonistic and one compound shows a partial agonistic profile at the KOR. Both hit compounds share a novel spiro-moiety-containing scaffold.

Overall, the findings of this dissertation provide new mechanistic insights into opioid receptor activation in the context of current progress in structural biology, and lay the basis for improved, rational drug design of safer analgesics and novel antidepressants with KOR activity.

Zusammenfassung

Opioide stellen die Standardmedikation für die Behandlung starker Schmerzen dar. Zugelassene Opioide besitzen jedoch viele schwerwiegende Nebenwirkungen, selbst wenn sie entsprechend der pharmazeutischen Zulassung eingenommen werden. Infolgedessen werden jährlich Tausende von Krankenhauseinweisungen und Todesfällen durch Nutzung von Opioiden verursacht. Es sind vier verschiedene Opioidrezeptor-Subtypen bekannt, doch die zugelassenen Opioide aktivieren hauptsächlich den µ-Opioidrezeptor (MOR). Agonismus am κ-Opioidrezeptor (KOR) stellt eine vielversprechende Strategie dar, um Schmerzen ausreichend lindern und gleichzeitig das Nebenwirkungsprofil von Opioiden verbessern zu können, jedoch wird ein rationales Wirkstoffdesign durch die KOR-bedingten Nebenwirkungen und die starke strukturelle Ähnlichkeit der Opioidrezeptor-Subtypen behindert.

Die Opioidrezeptoren sind nicht nur an der Schmerzmodulation, sondern auch an der Aufrechterhaltung der Stimmungshomöostase beteiligt. Vor kurzem hat sich der KOR-Antagonismus als vielversprechende Strategie für die Entwicklung neuer Antidepressiva mit schnell einsetzender antidepressiver Wirkung erwiesen, welche auch gegen Suizidabsichten wirken. Die chemische Vielfalt der selektiven KOR-Antagonisten ist jedoch stark begrenzt. Bislang sind noch keine kurz wirksamen und selektiven KOR-Antagonisten zugelassen worden.

Diese Dissertation umfasst auf retrospektive und prospektive *in silico* Studien, die aktuelle Fragen in der Opioidforschung adressieren. In den ersten drei Veröffentlichungen dieser Dissertation wurden retrospektive In-silico-Analysen von HS-731, einem Opioid-Agonisten, von Compound A, einem dualen KOR/MOR-Antagonisten, und von Salvinorin A (SalA), einem nicht-basischen, KOR-selektiven Agonisten, durchgeführt. Ziel dieser Arbeiten war es unser begrenztes Verständnis über die Faktoren zu verbessern, die die Aktivität und Selektivität an Opioidrezeptoren bestimmen. Die untersuchten Opioide selbst sind von großer pharmakologischer Relevanz. HS-731 ist ein Analgetikum mit einem potenziell verbesserten Nebenwirkungsprofil, da es nicht in das zentrale Nervensystem gelangen kann. Compound A verfügt über eine neue chemische Struktur, die das ungünstige kinetische Profil der derzeitigen antidepressiven Opioide überwinden könnte. SalA ist ein nichtbasischer Agonist mit außergewöhnlicher KOR-Selektivität und möglicherweise andersartigem KOR-Bindemodus als für basische Opioide üblich. Bindungsmodi der Opioide an den Opioidrezeptor-Subtypen sowie Selektivität determinierende Faktoren wurden bestimmt. Wichtige Protein-Ligand-Interaktionen wurden aufgezeigt, die für die Aktivität dieser Opioide an den Opioidrezeptoren verantwortlich sind. Es wurde eine neue, Bindetasche für SalA oberhalb der typischen Morphinan-Bindungsstelle entdeckt, in einem weniger konservierten Teil des Rezeptors. Der SalA-Bindungsmodus deckt sich mit den Daten zur Struktur-Aktivitäts-

Beziehung von SalA und erklärt die außergewöhnliche Rezeptorsubtypen-Selektivität von SalA am KOR. Darüber hinaus wurde eine Hypothese zur Induzierung von Partialagonismus am KOR aufgestellt, welche auf einer Interaktion zwischen den extrazellulär orientierten Abschnitten der Transmembranhelices 5 und 6 beruht.

Opioide besitzen normalerweise eine basische Amin-Gruppe, die mit einem konservierten Aspartat in der Bindetasche interagiert. Seit der Entdeckung des potenten und selektiven KOR-Agonisten SalA stellt die Entwicklung von nichtbasischen Opioiden eine neue und vielversprechende Strategie für die selektive KOR-Aktivierung dar, welche die mit dem MOR assoziierten schweren Nebenwirkungen umgehen kann. Allerdings ist die Zahl der bekannten nichtbasischen Opioide stark begrenzt. In der vierten Publikation dieser Dissertation wurde ein prospektives 3D-Pharmakophor-basiertes virtuelles Screening durchgeführt. Das Screening basierte auf dem SalA-Bindungsmodus, der in der dritten Publikation postuliert wurde. Ziel des Screenings war es, neue nicht-basische und selektive KOR-Liganden zu finden. Pharmakologische In-vitro-Experimente bestätigten zwei der von uns vorgeschlagenen Verbindungen als KOR Agonisten mit nanomolarer Potenz und guter Subtypen-Selektivität. Eine Verbindung stellt einen KOR-Vollagonisten, die andere einen KOR-Partialagonisten dar. Beide Verbindungen teilen ein neuartiges Spiro-Molekülgerüst.

Insgesamt bieten die Ergebnisse dieser Dissertation neue mechanistische Einblicke in die Opioidrezeptoraktivierung im Kontext aktueller Fortschritte in der Strukturbiologie und bilden die Grundlage für ein verbessertes, rationales Wirkstoffdesign von sichereren Analgetika und neuartigen Antidepressiva mit KOR-Aktivität.

1. Introduction

1.1. G Protein-Coupled Receptors

G protein-coupled receptors (GPCRs) are the largest family of membrane receptors in the human body [1]. They consist of a seven-transmembrane (7TM) structure embedded in the cell membrane [2]. Although the term GPCR is well established, it would be more precise to name them 7TM-receptors, as receptor family members without detectable G protein coupling are known [3,4]. GPCRs are omnipresent in the human body and play a pivotal role in a plethora of physiological and pathophysiological processes. For instance, GPCRs are linked to metabolic disorders, neurodegeneration, immune responses, and cancer [5]. Thus, GPCRs represent drug targets of high interest [5,6]. This dissertation deals with opioid receptors that belong to the GPCR family with special attention to the κ-opioid receptor (KOR).

To provide a comprehensive overview of GPCRs, the GPCR classification (section 1.1.1.), structure (section 1.1.2.), activation and signaling (section 1.1.3.), and pharmacological potential (section 1.1.4.) are described in this chapter. In the following chapter (section 1.2.) special characteristics of the opioid receptor family as the GPCRs of interest in this dissertation are highlighted.

1.1.1. Classification System of G Protein-Coupled Receptors

With over 800 distinct members in the human genome, GPCRs represent the largest family of membrane receptors [1,3]. The GPCR family comprises a large structural diversity, which makes it necessary to categorize its members into different classes to define the structural similarities shared between more similar receptors. The current classification system was developed by Fredriksson and coworkers [3] and is referred to as GRAFS classification. GRAFS is the abbreviation for the five defined classes, i.e. glutamate, rhodopsin, adhesion, frizzled/taste2, and secretin. Fredriksson and colleagues conducted a phylogenetic analysis of 802 GPCRs based on their sequences to identify the main clusters, resulting in the GRAFS classes mentioned earlier. Most of the GPCRs belong to the rhodopsin class (87.4%), followed by adhesion and frizzled/taste2 (3.0%, respectively). Fewer GPCRs were grouped into the glutamate and secretin class (1.9%, respectively). A small number of GPCRs could not be assigned to any of the five classes (2.9%). Due to the large number of receptors within the rhodopsin class the class was further divided into four main groups (α, β, γ, δ) and 13 subgroups. The only feature shared within all GRAFS classes of GPCRs is the seven-transmembrane motif.

The GRAFS classification only focuses on the human genome instead of the entirety of known GPCRs as in the competing A-F classification system [7]. There is an overlap between the GRAFS classification and the A-F-classification system with rhodopsin corresponding to class

A, secretin and adhesion to class B, glutamate to class C, frizzled to class F, and taste2 to class T [1]. Class T first belonged to class F but was later redefined as a separate class [1]. The opioid receptors discussed in this dissertation belong to the rhodopsin class according to the GRAFS classification and class A according to the A-F classification system.

1.1.2. Structural Determination and Characteristics of G Protein-Coupled Receptors

For a long time, the structural determination of GPCRs was hindered by the hydrophobic manner of GPCRs with localization within the cell membrane and their low expression levels [8]. Recent progress in X-ray crystallography facilitated the structural elucidation of GPCRs. In 2000, the first GPCR structure was published representing the inactive state bovine rhodopsin receptor covalently bound to 11-cis-retinal [9] confirming the already assumed seven-transmembrane structure of GPCRs. Nonetheless, the successful crystallization was strongly enabled by the covalent bound ligand that efficiently stabilized the inactive state receptor conformation as well as the high receptor expression, both rather untypical for other GPCRs [2]. The biologically dynamic behavior of GPCRs, i.e. the permanent fluctuation between the active and inactive conformation, regardless of the presence of ligand, usually hinders receptor crystallization leading to experimental failure or low-resolution structures [10]. Thus, experimental methods stabilizing the protein conformation of interest needed to be developed.

In 2007, Rasmussen and coworkers [11], and Cherezov and coworkers [12] successfully published crystal structures of the β_2-adrenergic receptor (β_2AR). Rasmussen's group facilitated crystallization by using an antibody against the intracellular loop 3 (ICL3) of β2AR bound to the inverse agonist Carazol. Cherezov and coworkers replaced the flexible ICL3 of β2AR with a less flexible T4 lysozyme fusion protein in the presence of Carazol. T4 lysozyme improves crystallization attempts by the reduction of flexibility in the system as well as by increasing the polar surface [2]. These crystal structures provided new insights into the structural determinants of GPCRs and the recognition of their ligands, for which Robert J. Lefkowitz and Brian K. Kobilka were awarded the Nobel Prize in 2012 [8]. The introduction of different fusion proteins at the N-terminus, C-terminus, or ICL3, as well as high-affinity antibodies and nanobodies stabilizing the receptor in a particular conformation, promoted the crystallization of several GPCRs in the following years [1]. For instance, Che and coworkers [13] used the nanobody Nb39 to stabilize the active state conformation of the KOR bound to the small molecule agonist MP1104. Further methods for improving crystallization represent the introduction of thermostabilizing mutations into the receptor to reduce conformational flexibility and the truncation of flexible regions [2].

Despite recent improvements in GPCR crystallography, several challenges remain. In particular, the structures of flexible termini and loop regions often remain unresolved due to attached fusion proteins or their flexibility in the natural state. Crystallization is a complex and time-consuming process [10], and some receptors do not crystallize. Therefore, further advancements in structural elucidation techniques are necessary.

Besides X-ray crystallography, cryogenic electron microscopy (cryo-EM), and nuclear magnetic resonance (NMR) spectroscopy are suitable methods for the structural determination of proteins [2], yet NMR spectroscopy is of secondary importance due to complex experimental validation and the need for preliminary experiments [14,15]. Cryo-EM methods for GPCR structure determination have only emerged in recent years as advances in electron detectors and data analysis facilitated the determination of protein complexes of lower molecular weight in acceptable resolution [16]. Liang and coworkers [16] published the first GPCR structure elucidated with single-particle cryo-EM in 2017. From then, the number of GPCR structures solved by cryo-EM explosively increased. Cryo-EM offers advantages over crystallography due to its lower time and resource requirements, as well as its ability to work with less stable receptors. Crystals need up to weeks to form and grow, whereby receptor conformation needs to be maintained, while cryo-EM can be performed within minutes after protein preparation [10]. Receptor crystallization often requires an iterative process of engineering to improve crystal structure resolution whereas cryo-EM tolerates flexible proteins, native wild-type receptor structures, and small amounts of sample [10]. Unlike crystallography, cryo-EM allows the determination of different conformational states within the sample that could be part of the activation mechanism [17]. In summary, cryo-EM is a valuable method for exploring the conformational space of GPCRs and may aid in revealing the structure of GPCRs that cannot be obtained through receptor crystallization. However, whether cryo-EM is applicable as a method depends on the size of the protein system. The current minimal target size for cryo-EM is about 50-60 kDa and therefore it is not yet possible to determine the structure of a single GPCR [18] as most GPCRs have a molecular weight below 40 kDA [19] Instead structures of GPCRs in complex with intracellular transducers (such as G proteins and arrestins) or antibodies are determined providing new insights into GPCR activation.

The experimentally solved GPCR structures reveal structural characteristics for the different classes of GPCRs. This study focuses on rhodopsin class GPCRs (class A) and therefore structural similarities and differences between the determined GPCR classes are only briefly described. The only structural motif conserved within the GPCR family is the seven-transmembrane motif embedded in the cell membrane [3]. The seven counterclockwise oriented α-helices are connected by three ICLs and three extracellular loops (ECLs). The N-

terminus of the receptors is extracellularly oriented, while the C-terminal end is intracellularly located (Figure 1). The N-terminal domain varies significantly among different classes: The rhodopsin class, which includes opioid receptors, has a short N-terminus, while all other classes have a long N-terminus [2,3,6]. The secretin class is characterized by an enlarged extracellular domain while the adhesion class additionally exhibits various adhesion regions attached to the N-terminus. Glutamate class GPCRs exhibit venus flytrap domains (VFTD) and cysteine-rich domains (CRD) at the large N-terminus and participate in homo- or heterodimers. Frizzled receptors are characterized by CRDs too. The GPCR orthosteric binding site is defined as the site where the endogenous ligand binds [20]. It is located within the helical bundle for rhodopsin and secretin class GPCRs [1,20] which includes the opioid receptors. In the other classes, the orthosteric binding site is placed within the extracellular domain while the helical bundle provides allosteric binding sites [1].

Extracellular side
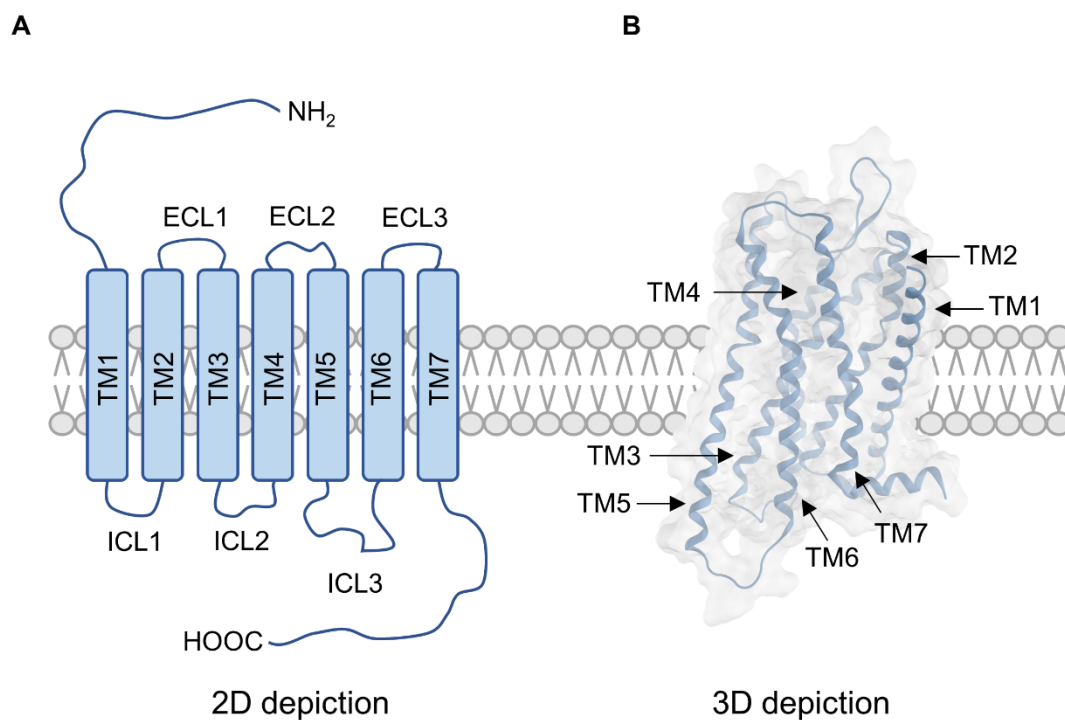
Intracellular side

Figure 1. Structural characteristics of GPCRs. A) 2D schematic of a class A GPCR (rhodopsin-like) embedded in a membrane (grey). B) 3D representation of KOR as an example GPCR (Protein data bank-ID or PDB-ID: 4DJH [21]). The 7TM domain resembles a cylindrical conformation.

Differences in sequence and structure of individual GPCRs render the comparison of receptor parts between GPCRs challenging. To facilitate the structural comparison of different GPCRs,

Ballesteros and Weinstein introduced a residue numbering scheme [22]. Each receptor amino acid is assigned an identifier that refers to the position of the amino acid within the GPCR. The identifier consists of two indices, the first refers to the closest transmembrane helix, and the second refers to the position of the amino acid with respect to a reference amino acid. The most conserved residue within each transmembrane domain serves as the reference amino acid and is assigned an arbitrary second index of 50. The most conserved residue within the sixth transmembrane helix is therefore characterized by the identifier 6.50. The amino acid five positions before in the sequence is characterized by 6.45, while the amino acid five positions later in the sequence is characterized by the identifier 6.55. In combination with the amino acid type and sequence number, a comparison between related receptors is feasible. For example, the conserved residue D138$^{3.32}$ of the KOR refers to an aspartic acid at position 138 of the KOR sequence, placed in the third transmembrane helix, eighteen positions before the most conserved residue within the third helix. This residue is conserved across the classical opioid receptors as the μ-opioid receptor (MOR) and δ-opioid receptor (DOR) exhibit the same amino acid type at the same position (D149$^{3.32}$, D128$^{3.32}$, respectively).

1.1.3. Receptor Activation and Signaling

Constitutive activity, also called basal activity, defines the activity level of a receptor in absence of a receptor-activating ligand [23]. GPCRs show constitutive activity, which varies from receptor to receptor [20]. While the human bradykinin 2 receptor (B2R) shows rather low constitutive activity, the human DOR and the viral GPCR US28 possess high constitutive activity [24,25]. The presence of constitutive activity reflects the dynamic behavior of the GPCR receptor family, which allows for transit between the inactive and active state by chance.

The activity profile of GPCRs can be modified by ligands that bind to the receptor. One can distinguish between agonists, which promote receptor activation, antagonists, which occupy the receptor binding site without altering the basal activity, and inverse agonists, which decrease receptor activation below the basal level (Figure 2) [2,8]. Partial agonists, which increase receptor activation above basal level but without a full receptor response, further expand the number of possible receptor modifications [20].

GPCR ligands are diverse and include endogenous lipids, peptides, glycosaminoglycans, biogenic amines, hormones, proteins, and glycoproteins, as well as exogenous ligands like drugs, flavoring substances, odorants, and even photons [5,8]. Adhesion class GPCRs can even interact with microbial ligands [8].
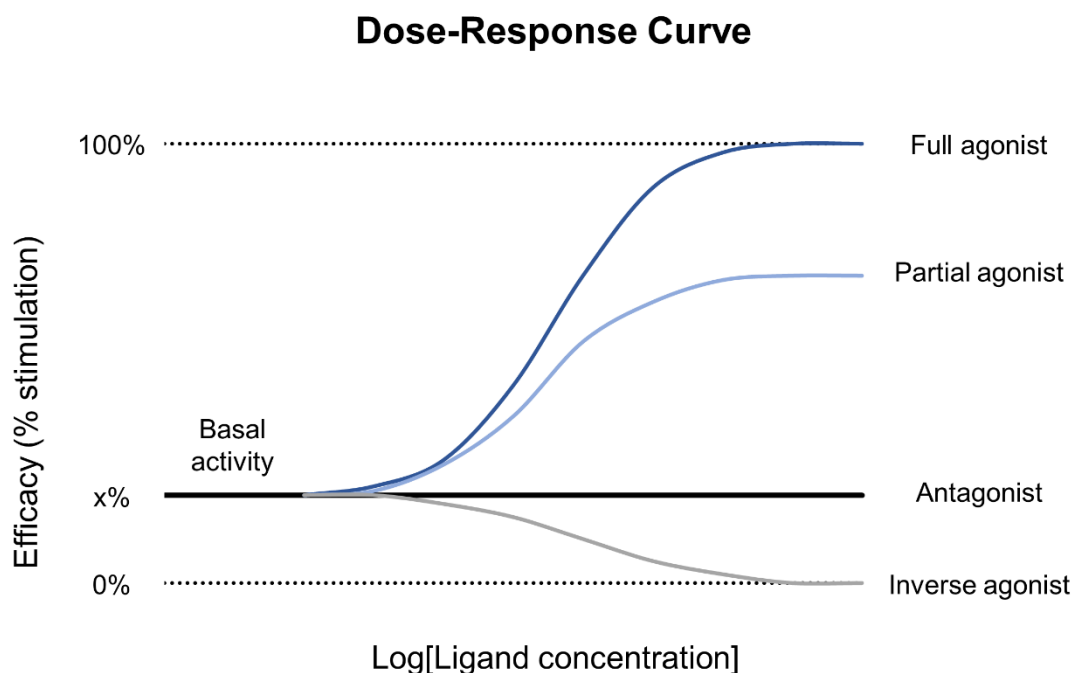
Dose-Response Curve

Figure 2. Representation of the ligand's influence on the receptor signal profile.

GPCR signaling is a highly complex process with multiple ways to fine-tune the intracellular response. Receptor signaling can be regulated by ligand binding to orthosteric and allosteric binding sites, GPCR phosphorylation by GPCR kinases (GRKs), and the dimerization or oligomerization state, all of which alter the receptor selectivity towards intracellular transducers [5]. Once the receptor adopts an active conformation, it can interact with several different intracellular transducers.

Guanosine triphosphate binding proteins, also called GTP binding proteins or G proteins, are the canonical intracellular transducers of GPCRs. There are four different families of G proteins, named G_s, $G_{i/o}$, $G_{q/11}$, and $G_{12/13}$ [26]. The heterotrimeric G protein consists of three subunits (α-, β-, γ-subunit) whose exact composition can vary by the different subtypes of the three subunits [27]. To date 16 Gα-, 4Gβ-, and 12 Gγ-subunits are known [27]. The exact composition of the G protein determines the coupling efficacy towards the activated receptor as well as the resulting pharmacological effects. Upon receptor activation, the G protein exchanges its bound GDP by GTP, followed by a dissociation into the α- and βγ-subunits which in turn modulate downstream effector proteins [28]. GKRs phosphorylate GPCRs at the intracellular domain (C-terminus and ICLs) which allows for the subsequent interaction with arrestins [29]. Four different arrestins are known, of which two (arrestin 1, 4) are exclusively for the visual system leaving two arrestins (arrestin 2, 3, also called β-arrestin 1, 2) for the remaining GPCRs [30]. Arrestins modulate GPCRs through three mechanisms [29,30]. First,

they bind phosphorylated GPCRs with high affinity thereby preventing G proteins from binding to the receptor. Second, they cause receptor desensitization by receptor internalization. Third, arrestins function as independent signal transducers leading to distinct pharmacological effects. Independent of the main signal transducers, i.e. G proteins and arrestins, GPCRs interact with PDZ-scaffold proteins [5], receptor-activating modifying proteins (RAMPs) [5], Janus kinase 2 (JAK2) [8], and Na^+-H^+ exchange regulatory factor 1 (NHERF1) [8]. The signaling process is further complicated by the modulation of GPCRs by other GPCRs, which is known as GPCR 'cross-talk'. [31].

The conformational space adopted by each GPCR defines the set of downstream mediators involved in receptor signaling and, therefore, the receptor's signaling profile. This implies the existence of a set of active conformations for one receptor rather than one defined active conformation [32]. Ligands that induce distinct receptor conformational changes lead to different signaling events, a phenomenon referred to as ligand bias [32]. Biased signaling (also referred to as functional selectivity) holds the promise of activating therapeutically desired signaling pathways while omitting those correlated with side effects [32,33].

Despite the structural diversity of GPCRs and the complex signaling pathways, class A GPCRs (rhodopsin-like GPCRs) share a similar activation mechanism [2]. Ligand binding to the receptor from the extracellular side leads to subtle conformational changes in the binding site that propagate via rearrangements of various conserved motifs within the GPCRs and eventually cause an intracellular receptor opening necessary for signal transducer recruitment [34]. The whole process is referred to as 'allosteric coupling' [26] which is described as follows for rhodopsin class GPCRs: Ligand binding to the orthosteric binding site positioned in the helical bundle [2] causes conformational rearrangements and a contraction of the binding site [26] initiating the receptor activation process (Figure 3). The small ligand-induced delocalization causes (i) the collapse of the sodium pocket releasing the sodium ion accommodated in the inactive receptor state (Figure 3F), (ii) toggle switches of $W^{6.48}$ in the CWxP motif (Figure 3E) and $Y^{7.53}$ in the NPxxY motif (Figure 3D), (iii) a rotation of $F^{6.44}$ within the PIF motif (Figure 3C), and (iv) the disruption of the 'ionic lock', a salt bridge between $D^{3.49}$ and $R^{3.50}$, within the D/ERY motif (Figure 3B) [34]. As a result, several transmembrane helices translocate, of which the outward movement of transmembrane helix 5 (TM5) and TM6 as well as the inward movement of TM7 are the most pronounced [2] (Figure 4). The helix rearrangements open the intracellular receptor interface functioning as a binding site to several transducers [34]. The aforementioned motifs participating in the receptor activation process are highly conserved within rhodopsin-like GPCRs and positioned in the lower half of the receptor. Additionally, the conformational rearrangements of these motifs during the activation process are propagated by a conserved water network within the receptor [34].
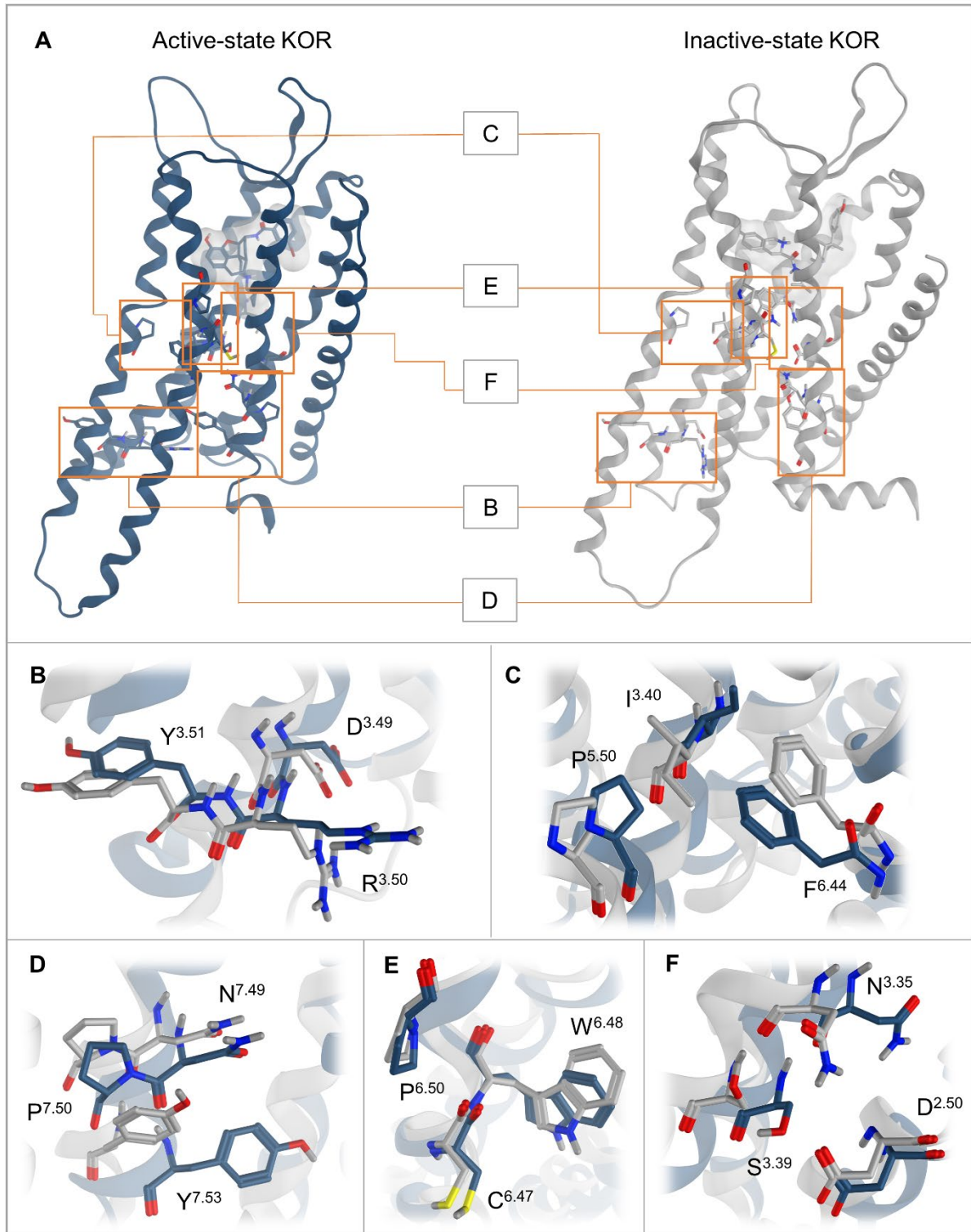
Figure 3. Comparison of active and inactive KOR with the corresponding conserved motifs. A) Active state KOR (PDB-ID: 6B73, blue) on the left and inactive state KOR (PDB-ID: 4DJH, grey) on the right. Panels B-F show enlargements of conserved motifs. B) DRY motif. C) PIF motif D) NPxxY motif. E) CWxP motif. F) Sodium binding pocket.
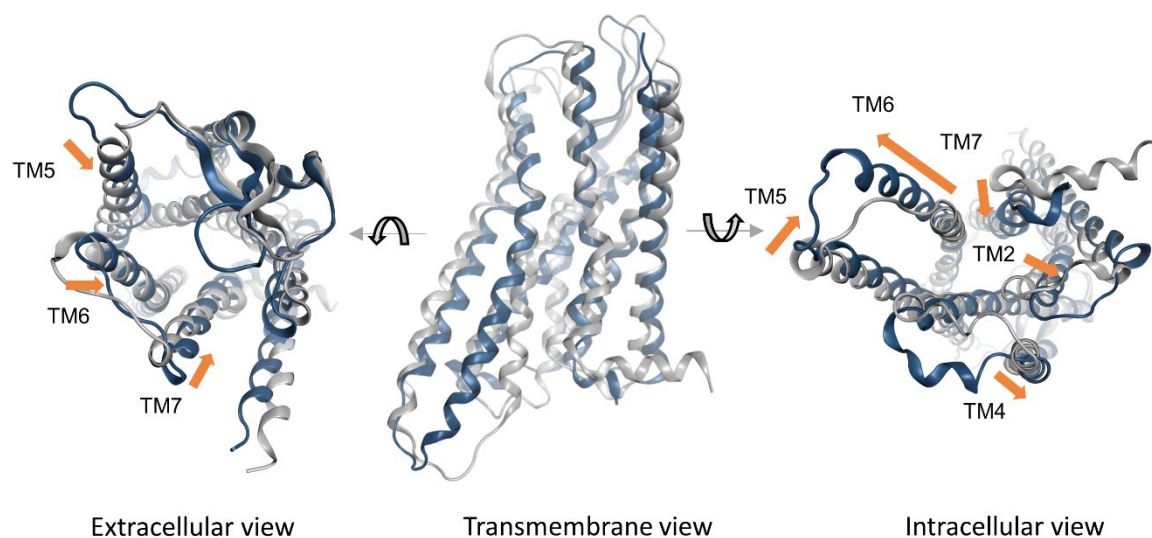
Figure 4. Schematic representation of general movements of transmembrane helices during receptor activation. The model system shown is the KOR (PDB IDs: 6B73 for active state in blue, 4DJH for inactive state in grey).

1.1.4. G Protein-Coupled Receptors as Drug Targets

Nearly half of the 802 GPCRs encoded in the human body regulate sensory perception while the remaining receptors are involved in physiological and pathophysiological processes [1,5]. GPCRs are relevant for cardiovascular, metabolic, endocrine, and neural disorders, pain modulation, immune system response, and even cancer [5,32] reflecting their high pharmacological potential.

The location of GPCRs on the cell surface makes them readily accessible to drugs in the blood system. The combination of their accessibility to drugs and their pharmacological relevance makes GPCRs promising drug targets. More than 30% of approved drugs target GPCRs [32,35] rendering GPCRs the main target for approved drugs [1]. There are more than 500 drugs that modulate rhodopsin-like (class A) GPCRs [35], with aminergic or peptidic rhodopsin-like receptors most commonly targeted [6]. Indications include nausea, insomnia, pain, hypertension, cardiovascular diseases, pulmonary disorders, cancer, multiple sclerosis, and Parkinson's disease among others [6]. A small number of drugs targeting the remaining GPCR classes are known, but these are of secondary pharmacological importance [6].

Although GPCRs are the most important drug targets, only a small fraction of individual receptors is currently targeted by drugs. Of the 802 human GPCRs, approximately 40% are considered druggable, and of these, only about half are targeted by drugs [6]. Therefore, most GPCRs escape clinical treatment [1]. Targeting neglected receptors can improve treatment in

various pathophysiological processes. However, many of these receptors are 'orphan receptors' with unknown endogenous ligands hindering rational drug design [36].

Due to structural similarities within GPCR classes, many drugs target a set of GPCRs rather than a single defined receptor [6]. In the case of bivalent ligands, which are explicitly designed to target multiple receptors simultaneously, this is a desired phenomenon [20]. However, in most cases, these additional targets ("off-targets") result in side effects rather than therapeutically desired effects [20,37].

The challenge of insufficient receptor selectivity is frequently caused by high structural similarity of the orthosteric binding site, especially between receptor subtypes or closely related receptors [2,37], such as the opioid receptor subtypes. Ligands targeting both orthosteric and allosteric binding sites can improve receptor selectivity [2,20].

1.2. Opioid Receptors

Following the general outline of GPCR classification, structure, signaling, and pharmacological potential in the previous sections, this chapter focuses on the opioid receptors as the GPCR model system studied in this dissertation. Opioid receptors consist of four receptor subtypes: KOR, MOR, DOR, and the nociceptin/orphanin FQ peptide (NOP) receptor [38]. They belong to the γ branch of rhodopsin-like (class A) GPCRs [3]. Opioid receptors participate in several physiological processes with pain modulation and mood regulation, being of special pharmacological interest [33,39]. Opioid receptors are long-studied GPCRs, many opioid receptor ligands (opioids) are known [33,40,41] and several structures experimentally solved [13,42-47]. However, the clinical value of known opioids as analgesics is limited by their severe side effects [48]. Patients might experience respiratory depression, addiction, constipation, and sedation among others [48,49]. Increased opioid prescriptions resulted in the so-called 'opioid crisis' in the United States with thousands of hospitalization events and deaths per year [50]. Besides pain perception, opioid receptors are also involved in mood regulation and have recently been suggested as new antidepressant agents [39]. Given the ongoing 'opioid crisis' in the United States [50] and the urgent need for new antidepressants [51] opioid receptor modulation, especially of the KOR, is emerging as a promising strategy to address both problems [48,51,52]. Therefore, this section describes the role of opioid receptors in pain and depression, followed by an overview of current small molecule treatment strategies for both indications, including current therapeutic issues. Subsequently, the applicability of *in silico* techniques to find solutions and optimize opioids is demonstrated by the presence of numerous opioid ligands and experimental structures. Finally, we briefly describe how new, potentially optimized opioids are evaluated *in vitro*. This dissertation focuses on the KOR, but

this receptor subtype must be viewed in the context of the remaining opioid receptors. Thus, this section will cover all opioid receptor subtypes with special attention to the KOR.

1.2.1. Physiological and Pathophysiological Role of Opioid Receptors

KOR, MOR, DOR, and NOP are expressed in the central nervous system (CNS), peripheral nervous system (PNS), neuroendocrine cells, immune cells, and ectodermal cells [40]. The opioid receptors couple to seven G protein subtypes (G_{i1}, G_{i2}, G_{i3}, G_{oA}, G_{oB}, G_z, and Gustducin) as well as ß-arrestin 1 and ß-arrestin 2 [53]. The classical opioid receptors (KOR, MOR, DOR) share 50-70% sequence identity [54] while the NOP sequence differs to a greater extent, but still shows around 50% homology [55]. Opioid receptors substantially modulate several (patho-)physiological processes such as pain perception, mood, anxiety, respiratory control, addiction, convulsions, water balance control, feeding, hormone release, and gastrointestinal transit [38,40,51,55,56]. The role of opioid receptors in pain sensation and depression is of particular interest for pharmacological treatment and is described in the following.

Pain is defined by the International Association for the Study of Pain (IASP) as 'an unpleasant sensory and emotional experience associated with, or resembling that associated with, actual or potential tissue damage' [57]. Essential physiological pain, also called nociceptive pain, can be distinguished from pathological pain [54]. The former protects the body from physiological damage by triggering reflexes in the event of acute injury [58]. Pathological pain is caused by inflammation, vascular factors, mechanical factors, nerve damage, and cancer and is part of many pain syndromes that need to be treated [59,60]. Pain syndromes include postoperative pain, wounds, neuropathic pain, cancer, and arthritis among many others [54], and often represent chronic conditions. Pathological pain may persist even if the initial trigger for the pain has been successfully treated [59]. Pain represents one of the main reasons for medical treatment [59] rendering the sufficient treatment of high pharmacological interest.

Pain perception is physiologically reduced by endogenous opioid peptides that activate opioid receptors. Of note, all individual OR subtypes facilitate analgesic effects, but their side effect profiles differ [40,61] (Table 1). Upon agonist binding, opioid receptors recruit G proteins that subsequently dissociate from their heterotrimeric state into G_α and $G_{\beta\gamma}$ subunits [62]. The subunits, in turn, modulate ion channels [51,63] (Figure 5). The G_α subunit inhibits adenylyl cyclases and subsequent cyclic adenosine monophosphate (cAMP) production [40]. The $G_{\beta\gamma}$ subunit directly interacts with ion channels, resulting in decreased Ca^{2+} influx at pre- and postsynaptic Ca^{2+} channels and activation of rectifying K^+ channels (GIRKs, G protein-coupled inwardly-rectifying potassium channels) [54]. As a result, the increased K^+ efflux and decreased Ca^{2+} influx cause cell hyperpolarization with a reduction in neuronal excitability and therefore decreased pain signaling [54]. In addition to the ion channels mentioned above,

modulation of Na$^+$ channels, hyperpolarization-activated cyclic nucleotide-gated cation channels (HCN channels or I$_h$ channels), transient receptor potential vanilloid-1 (TRPV1) channels, and acid-sensing ion channels (ASICs) contribute to inhibitory effects of opioid receptor activation in pain perception [40,54,64].

Table 1. Selected effects of opioid receptor activation with clinical relevance.

| KOR	MOR	DOR	NOP
Analgesia [40,65]	Analgesia [40,65]	Analgesia [40]	Analgesia (spinal) [55]
Dysphoria [40,65,66]	Respiratory depression [40,48,65]	Seizure [40,66]	Hyperalgesia (brain) [55]
Sedation [40,65]	Euphoria [40]	Reward [40]	Constipation [55]
Aversion [48]	Reward [40]	Respiratory depression [40]	Vasodilatation [55]
Anhedonia [66]	Sedation [40]	Anxiety [40]	Antitussive effect [55]
Itch-relief [67]	Constipation [40,48,65]	Antidepressant effects [65]	Anxiolytic effects [55]
Anxiety [66]	Dependence [48]		Reward antagonism [55]
Diuresis [40]	Nausea [40,65]		Sedation [55]
	Vomiting [40,65]		
	Tolerance [48,65]		
	Itch [48]		
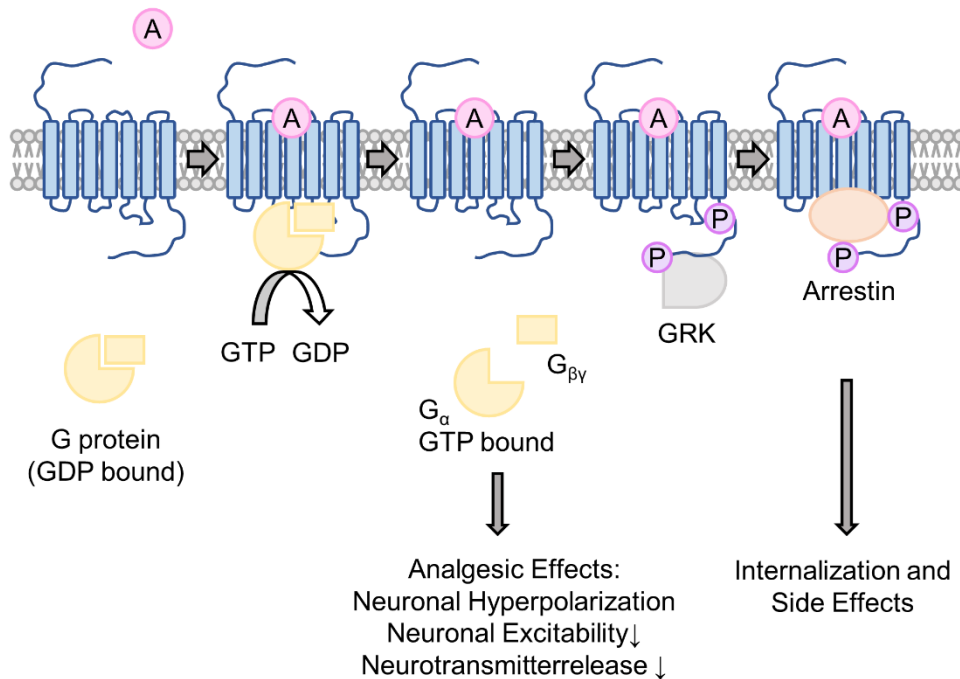
Figure 5. Opioid receptor signaling scheme. Abbreviations used: A = Agonist, GTP = Guanosine triphosphate, GDP = Guanosine diphosphate, Pi = inorganic phosphate, GRK = G protein-coupled receptor kinase.

After the receptor is phosphorylated by GRKs, β-arrestin binds to the receptor, preventing G proteins from binding and causing the receptor to be internalized with subsequent partial degradation [54,63] This mechanism reduces G protein signaling. Furthermore, GPCR-bound β-arrestin induces G protein-independent signaling cascades [68] including for example mitogen-activated protein kinases (MAPK) [69], or Src family tyrosine kinases [70]. Typically, β-arrestin and G protein signaling result in different desired or undesired pharmacological effects [69]. It has been proposed that opioid receptor-induced G protein signaling leads to analgesia, while β-arrestin signaling leads to side effects [48,66]. However, this hypothesis was recently questioned [71,72].

In addition, changes in opioid receptor signaling may occur as a result of adjustments in receptor expression levels, receptor trafficking to the cell membrane, and signaling capabilities based on the duration of pain-evoking signals [54].

Besides pain, opioid receptors modulate depression symptoms [39,56,73]. Major depressive disorder (MDD) is a severe form of depression characterized by depressed mood, cognitive impairment, loss of energy, and suicidal ideation [74]. MDD has a high prevalence [75] and is a leading cause of work disability. [76]. Its high prevalence and liability for comorbidities render MDD a serious public health issue [76]. MDD is caused by the disruption of the complex

interplay of neuronal transmitter release and signaling that regulates mood homeostasis [51]. As a result, current antidepressants mainly target monoamine neurotransmission, particularly the dopamine, serotonin (5-HT), and noradrenalin systems [74]. However, these medications only elicit efficacy after weeks or months of treatment, providing a high potential for non-response, are ineffective against suicidal intent, and are insufficient for cognitive impairment [51]. Some standard antidepressants can initially cause anxiety in patients, which may affect their adherence [39]. Thus, there is an urgent need for the development of new antidepressant agents [51].

The opioid receptor system is substantially involved in mood homeostasis and represents a major pharmacological target for the treatment of MDD. All four opioid receptors (KOR, MOR, DOR, NOP) are involved in the modulation of the mood homeostasis (Table 1). DOR and MOR agonism but KOR and NOP antagonism appear to be beneficial in the treatment of MDD whereas KOR agonism induces dysphoria [55,56,76]. However, as described in the next section KOR antagonism is most promising for the treatment of depression. The influence of opioid receptors on mood homeostasis involves modulation of the dopamine, 5-HT, and noradrenaline systems, gene transcription, neurogenesis, and stress adaptation [51,56,77]. However, their influence on mood is only partially understood and opioid receptors may act differently in different parts of the brain.

The dopamine system is strongly connected to aversion and reward [78]. KOR is expressed at dopaminergic neurons in the nucleus accumbens (NAc), inhibiting the release of dopamine [78]. Depressive symptoms worsen by provoking increased KOR activation [56], suggesting that decreased dopamine levels increase MDD symptoms. KOR additionally controls dopamine reuptake [63]. However, the release of dopamine is also regulated by the activation of DOR and MOR [56]. This makes it difficult to draw conclusions about the significance of individual receptors for dopamine balance. The interplay between the opioid and the dopamine systems is complex, but dopamine 2 receptor (D2R) inactivation seems to potentiate beneficial DOR agonistic effects [79]. The D2R is coupled to an inhibitory G_i protein [80]. Short-term MOR agonism leads to increased dopamine levels [56]. NOP is expressed in dopaminergic neurons in the ventral tegmental area (VTA) and NAc with NOP activation reducing dopamine release in the NAc [55].

5-HT signaling influences depressive symptoms and the KOR system modulates the 5-HT system in several ways. KOR activation increases 5-HT release and decreases 5-HT transporter (SERT) expression, thereby increasing the concentration of available 5-HT in the synaptic cleft [63]. Inhibitory GABAergic neurons, which control 5-HT release, express KOR, resulting in increased 5-HT activity when KOR is activated in specific parts of the brain [63]. KOR-mediated effects of the 5-HT system in turn modulate dopaminergic neurons in the NAc which is assumed to produce dysphoria [56]. The MOR strongly controls the activity of 5-HT

neurons, with short-term MOR activation leading to increased 5-HT levels, which is beneficial for depressed patients, and sustained agonism leading to decreased 5-HT release, which promotes depression [56]. NOP activation decreases 5-HT release in the dorsal raphe nucleus (DRN), the major source of 5-HT in the brain [55]. However, modulation of the 5-HT system via NOP appears to be more complex [55].

The role of noradrenaline signaling in the pathogenesis of MDD is complex and still under investigation [81]. However, noradrenaline signaling is likely reduced in patients with MDD [56] as noradrenaline reuptake inhibitors are effective antidepressants [81]. Noradrenaline signaling is known to adapt to stress [81]. NOP activation decreases noradrenaline release in the locus coeruleus (LC) which represents the main source of noradrenaline in the brain [55]. Persistent MOR activation induces noradrenaline system hyperactivity, correlated with aversion [56].

In addition to modulating mood homeostasis through monoamine signaling, opioid receptors have mood-altering effects through several other mechanisms. Phosphorylated and internalized opioid receptors can activate MAPK pathways associated with gene transcription and cell differentiation, such as extracellular signal-regulated kinase (ERK), c-Jun N-terminal kinase (JNK), and p38 [63]. These pathways correlate with the development of dysphoria [82]. For example, KOR activation-mediated p38 signaling produces aversion [83,84]. DOR and MOR antagonism impairs neuronal stem cell proliferation and differentiation reducing neural plasticity [56]. However, sustained MOR agonism decreases neuronal proliferation [85]. Both KOR antagonism and DOR agonism increase brain-derived neurotrophic factor (BDNF) activity, which relieves the symptoms of MDD [86,87]. Stress situations cause an adaption of the KOR system and its endogenous ligand dynorphin, thereby modulating mood. Chronic stress increases KOR expression and decreases dynorphin levels, while acute stress elevated dynorphin levels [63]. In addition, epigenetic modulation of the KOR gene results from stress and may influence mood control [63].

The control mechanisms by which the opioid system influences mood homeostasis are extremely complex and not fully understood. Different parts of the brain do not respond identically to opioid receptor activation. In addition, other parameters such as environmental factors, gender, and stress also modulate the response [77]. Studies evaluating stressors that have a strong impact on the KOR/dynorphin system are difficult to evaluate because different types of stress, such as acute stress, prolonged stress, social isolation, and threat, result in different signaling events and experimental outcomes [77].

The strong link between the opioid system and pain perception or mood homeostasis renders opioid receptor modulation a promising strategy for the treatment of both severe pain and depression. The following section describes how opioid receptors can be modulated by endogenous and exogenous ligands to treat these indications.

1.2.2. Opioid Receptor Modulation

Opioid receptors are modulated by endogenous and exogenous ligands [40]. The endogenous peptides are derived from four main precursors, specifically pro-opiomelanocortin, proenkephalin, prodynorphin, and pronociceptin [38]. Post-translational modifications of these precursors generate more than 20 different opioid peptides [88]. The opioid peptides share the YGGF motif at their N-termini except for opioid peptides belonging to the nociception family exhibiting the FGGF at the N-terminus instead [38]. The first four amino acids at the N-terminus represent the 'message' motif responsible for receptor activation by binding deep into the opioid receptor binding site [43]. In the past, opioid peptides of the endorphin family were thought to signal exclusively through MOR, the enkephalin family exclusively through DOR, and the dynorphin family exclusively through KOR [88]. A recent study by Gomes and coworkers showed that many of the opioid peptides signal through all three classical opioid receptors, albeit with different selectivity profiles [88]. Several opioid peptides additionally exhibit functional selectivity at opioid receptors further complicating the modulation of the opioid system by endogenous ligands [88]. The atypical chemokine receptor 3 (ACKR3) binds and scavenges opioid peptides [89] suggesting a regulatory mechanism of ACKR3 for opioid receptor modulation by controlling opioid peptide concentrations.

The long tradition of opioid receptor modulation by exogenous ligands began over 3,000 years ago with the use of opioid alkaloids from the opium poppy (*Papaver somniferum*) for pain management and recreational purposes [52]. Exogenous ligands can be divided into natural, semi-natural, and synthetic ligands according to their origin [90]. Salvinorin A (Article C) is an example of a naturally occurring opioid receptor ligand while the peripherally acting HS-731 (Article A) represents a semisynthetic ligand. Compound A (Article B) is an example of a synthetic ligand [40].

The most pharmacologically relevant indication for modulation of the opioid system is the treatment of severe pain, such as post-operative pain, chronic pain and cancer-related pain. Nevertheless, as discussed in the previous section, the opioid system is involved in the regulation of numerous physiological processes and therefore represents a valuable target for the treatment of several disorders. In addition to pain relief, opioids are used to treat itching, cough, addiction, mood disorders including depression, diarrhea, and opioid-induced side effects such as constipation [76,90-92].

The following two sections outline the current state of drug-induced receptor modulation in pain and depression treatment.

1.2.2.1. Opioids for Pain Treatment

Opioids are essential in the treatment of pain syndromes, especially severe pain [33]. Current opioid analgesics primarily target the MOR [48], which provides adequate pain relief, but also cause significant side effects (Table 1). These side effects reduce the clinical value of current opioids. Given the ongoing "opioid crisis" in the U.S. [50], the development of safer analgesics is of great pharmacological interest [93-95].

Several different strategies have been employed to obtain safer analgesics, such as targeting novel targets other than opioid receptors [52,93], development of abuse-deterrent formulations (ADFs) [41,96], design of G protein-biased opioid receptor ligands [33,48,95,97], discovery of peripherally restricted opioid receptor modulators [64,98-100], and design of bifunctional opioid receptor ligands [33,94,101,102]. These strategies are discussed in more detail below. By targeting non-opioid proteins involved in pain, opioid-related side effects can be avoided. Cannabinoid receptors, adrenergic receptors, chemokine receptors, TRPV1 channels, and other ion channels have been investigated for their potential in the development of safer analgesics, albeit with moderate success [52]. By switching targets, one exchanges the side effects of one target for another. As a result, many studies have observed adverse events or low efficacy, but some approaches are promising [52]. However, those are out of the scope of this dissertation.

Opioids have a high potential for abuse due to their addictive properties. ADFs have been developed to prevent opioid overdose-related hospitalizations and deaths. These formulations are designed to interfere with the reward of abuse. For example, ADFs combine agonists with antagonists that are only effective when abused, or include physical/chemical barriers that prevent crushing of solid doses in preparation for intravenous administration or inhalation [96]. Several ADFs have been approved by the FDA, but they do not prevent tampering [41]. Therefore, the other strategies discussed in this section are more promising for the design of safer analgesics.

Peripherally restricted opioids represent a promising approach for the development of safer analgesics with reduced risk of side effects [33,41,99,100]. Pain relief provided by peripheral opioid receptors strongly contributes to the analgesic properties of systematically applied opioids [54,100], while several opioid side effects are mediated centrally [41,52]. Thus, opioids with a peripheral mode of action are proposed to lack CNS side effects such as dysphoria, reward, respiratory depression, convulsion, and sedation which often limit the clinical value of opioids [41]. Peripherally acting opioids may also alleviate side effects that are at least partially mediated by the CNS, such as nausea and diuresis [64]. Experiments have confirmed that activation of peripheral opioid receptors alone provides sufficient pain relief [41,52,98-100] promoting the efforts to develop peripherally acting opioids with minimal or absent central

effects. The development of peripheral analgesics is based on four main approaches, in particular the restriction of ligand membrane permeability, the development of efflux pump substrates, the use of nanocarriers and the exploitation of pH-dependent opioid activation [64]. Limited blood-brain barrier (BBB) crossing is facilitated by hydrophilization of ligands or increased molecular weight [64]. Increased drug hydrophilicity can be achieved by quaternization of nitrogen atoms, the introduction of polar or ionizable substituents, and ligand glucuronidation [64]. The opioid modulator HS-731, discussed in Article A, is an example of a peripherally restricted ligand due to hydrophilization. HS-731 is a 6β-glycine substituted derivative of 14-O-methyloxymorphone where the introduction of the amino acid glycine results in a zwitterionic character preventing HS-731 from entering the CNS (Article A, Figure 1). The KOR-selective tetrapeptide CR845 (Difelikefalin) is another peripherally restricted KOR modulator with impaired membrane permeability due to hydrophilicity [103]. It has been studied in Phase II clinical trials for the treatment of post-operative pain (clinicaltrials.gov ID NCT01789476) and is already approved by the FDA for the treatment of pruritus associated with chronic kidney disease (CKD) in adults undergoing hemodialysis [67]. CR845 provides potent analgesia with only mild side effects and no dysphoria [99].

Despite significant BBB permeability, some opioid receptor ligands are unable to produce central nervous system effects due to rapid efflux from the brain facilitated by efflux pumps. Loperamide, a substrate of P-glycoprotein (P-gp) [104] is the most prominent member of this class. The MOR agonist is used clinically for the treatment of diarrhea, specifically targeting receptors in the gastrointestinal system, but higher doses of loperamide produce CNS effects by saturating P-gp [64]. Decreased loperamide efflux from the brain may also be due to drug interactions, either because loperamide competes with other pump substrates for P-gp or because a second compound inhibits the efflux pump. Thus, the design of peripheral activity should not solely dependent on active transport from the brain. KOR-selective asimadoline elicits low capacity for BBB crossing by a combination of its amphiphilic character and P-gp activation [64]. It was investigated as an analgesic but due to its difficult action profile and the lack of sufficient clinical efficacy at concentrations without side effects development of asimadoline as an analgesic was discontinued [41,99].

Inflammatory tissue is characterized by a decreased pH compared to healthy compartments. A new and interesting strategy to specifically target inflamed peripheral tissues is the pH-dependent activation of opioids. Typical opioids contain an amine moiety that participates in a salt bridge with D3.32 of opioid receptors, which is critical for receptor activation [13,42,105,106]. At physiological pH (7.4) the amine moiety of typical opioids ($pk_a > 7.5$) is charged leading to receptor activation in both healthy and inflamed tissue [107]. In contrast, ligands with a lower pk_a value would be selectively ionized in inflamed tissue with subsequent selective activation of opioid receptors within this inflamed tissue. Peripheral pain syndromes

are usually associated with inflammation and most pain syndromes originate in the periphery rendering pH-dependent ligand activation a promising strategy for the development of safer analgesics [64]. The MOR-selective fentanyl derivative NFEPP with a pk_a of 6.8 was shown to selectively cause analgesia in inflamed milieus without inducing respiratory depression, sedation, constipation, and addiction [108].

Drug-containing nanocarriers that release the ligand specifically at inflamed tissue represent another strategy to reduce opioid-related side effects [64,109]. The release of ligands from the carrier could be triggered by the low pH of the inflamed tissue. Morphine, which is known to cause several serious side effects when administered systematically, can provide analgesia without sedation and constipation in such a drug formulation [109].

Overall, peripheral opioid receptor agonists have been shown to combine sufficient analgesia with an improved safety profile. Nevertheless, the pharmacological profiles of these opioids still need to be improved, which rationalizes further efforts in this area.

The design of G protein-biased opioid receptor modulators that favor G protein recruitment over the recruitment of β-arrestin became promising for the development of safer analgesics when experiments with β-arrestin 2 knockout mice revealed maintained morphine-induced analgesia with reduced side effects [110-112]. These experiments suggest that opioid-related analgesia is mediated by activation of the G_i protein pathway, whereas β-arrestin recruitment mediates adverse events. Thus, G protein-biased opioid receptor agonists may represent potent analgesics with fewer side effects.

The development of G protein-biased agonists initially focused on the MOR with several G protein-biased ligands identified. TRV130 (oliceridine), PZM21, and SR-17018 are examples of proposed G protein-biased agonists at the MOR [113-115]. Studies support their improved safety profile, albeit not consistently [97]. TRV130 (oliceridine) has been approved by the FDA as an analgesic [116]. Nevertheless, the proposed correlation between β-arrestin and adverse events for the MOR is now questioned [117-121]. Phosphorylation-deficient mice that cannot recruit β-arrestin still suffer from typical MOR agonist-related side effects like respiratory depression and constipation [117] and the initial finding that β-arrestin 2 knockout mice treated with morphine did not suffer from respiratory depression was hardly reproducible [118]. Recent experiments suggest that both analgesia and side effects are dependent on the G protein pathway. [122]. Several proposed G protein-biased MOR agonists, including the aforementioned TRV130 (oliceridine), PZM21, and SR-17018, are ligands with low intrinsic efficacy rendering the partial agonism of these ligands an alternative mechanism for the *in vivo* profiles of these ligands [71,72].

Due to the limited success in developing safer analgesics with G protein-biased MOR agonists, interest in G protein-biased modulators shifted from MOR to the remaining opioid

receptors, with the greatest interest in the KOR. KOR activation provides analgesia without MOR-related side effects like respiratory depression and addiction [98], yet the clinical value of prototypic KOR agonists is limited due to dysphoria, motor incoordination, and sedation [48]. While biased MOR agonists are designed to separate analgesia from respiratory depression and tolerance, biased KOR agonists are designed to separate analgesia from aversion and sedation [66,95]. The therapeutically desired analgesic effect is likely G protein-dependent with analgesia retained in β-arrestin 2 knockout mice [123], while negative side effects such as aversion are correlated to β-arrestin induced p38 MAPK activation [83,124]. However, experiments by White and coworkers [123] based on β-arrestin 2 knockout mice suggest that unwanted aversion is possibly connected to G protein recruitment, which would hinder the separation of this side effect by G protein-biased KOR modulators. Nevertheless, tremendous efforts in the development of G protein-biased KOR agonists have resulted in several G protein-biased ligands with different scaffolds, potencies, and bias factors [48], such as nalfurafine, 22-thiocyanatosalvinorin A (RB-64), the diphenethylamines HS665 and HS666, and triazole 1.1, among others [70]. Many of the G protein-biased ligands show sufficient analgesia with reduced or absent aversion, and locomotor incoordination (a parameter for sedation) [48], yet some still induce aversion [123,125]. It is hypothesized, that mechanistic target of rapamycin (mTOR) signaling rather than β-arrestin signaling correlates with aversion as its inhibition eliminates this side effect [48].

While the influence of ligand bias on therapeutic effects at MOR and KOR have been extensively studied, DOR and NOP received much less attention [66]. Studies about ligand bias at DOR intend to separate analgesic effects from side effects (Table 1), foremost seizure liability [66]. DOR signals via β-arrestin 1 and β-arrestin 2 [97]. β-arrestin 1 appears to regulate seizure liability of DOR agonists acting as a negative regulator for convulsions while its therapeutic effects, particularly antidepressant and antihyperalgesic effects, are G protein-dependent [126]. In contrast, ligands promoting β-arrestin 2 recruitment rather than β-arrestin 1 recruitment are suggested to induce less tolerance and convulsions [97]. Several G protein-biased ligands with improved safety profiles were developed such as the G protein-biased DOR ligands KNT-127 and ARM390 that exhibit analgesia without convulsions [127].

The role of NOP in pain perception is complex and not fully understood [33]. Effects on pain transmission vary with ligands, pain states, and tissues [66]. Nevertheless, NOP modulators have therapeutic potential as analgesics, especially for chronic pain syndromes [66]. Ligand bias potentially reduces NOP-related sedative side effects while maintaining NOP analgesic effects [66]. However, a limited understanding of ligand bias-induced effects in the NOP system [66] hinders the development of NOP-related safer analgesics. In addition, doubts about the therapeutic potential of NOP bias arose. Azevedo Neto [128] and coworkers revealed that the therapeutic potential of NOP agonists as analgesics, i.e. the analgesia and

the locomotor impairment induced, was independent of their measured bias (G protein / β-arrestin 2).

Despite great efforts to develop new biased ligands for opioid receptors, the mechanism of bias itself is poorly understood. Linking *in vitro* ligand profiles to *in vivo* effects is a challenging process, further complicated by controversial experimental data and non-standardized assays [101]. Cell lines, experimental conditions, as well as the assay, especially its degree of signal amplification, strongly influence the calculated bias factor [101]. G protein signaling can be measured at the level of G protein recruitment (e.g. [^{35}S]GTPγS binding) or at the level of second messengers (e.g. cAMP production) encompassing different signal amplification levels. However, β-arrestin recruitment assays are not amplified. It is recommended to measure activity for the distinct signaling pathways at the same amplification level to avoid observation bias [129]. To simplify the comparison of bias experiments Kolb and coworkers [129] prepared guidelines for measuring and reporting bias.

Opioid receptors signal via several G proteins and both β-arrestins [95]. Preferences for individual G proteins likely contribute to distinct pharmacological profiles of G protein-biased opioid receptor modulators. Thus, further investigations are needed to address the question of which particular G protein is pharmacologically desirable.

In addition to problems of experimental comparability, the fundamental molecular mechanisms that trigger ligand bias at opioid receptors remain elusive. However, there are hypotheses regarding interactions or receptor conformational changes that may correlate with G protein bias. Uprety and coworkers [130] suggested that interactions between the ligand and upper portions of TM5 and ECL2 may be beneficial for G protein bias at KOR and MOR, while interactions with TM2 and TM3 likely promote β-arrestin recruitment. El Daibani and coworkers [53] recently published an X-ray crystal structure of the G protein-biased ligand nalfurafine bound to the KOR (PDB-ID: 7YIT). The authors proposed that the disruption of the intramolecular salt bridge between K227$^{5.39}$ and E297$^{6.58}$ is essential for nalfurafine's G protein bias. Stabilization of the Q115$^{2.60}$ conformation as observed in the crystal structure likely favors G protein bias while conformational rearrangements of W287$^{6.48}$ caused by the β-arrestin-biased modulator WMS-X600 may contribute to β-arrestin signaling, with both residues influencing the conformation of TM7 [53]. The frequent occurring 'occluded' KOR conformation in molecular dynamics (MD) simulations of the nalfurafine bound structure and its rare occurrence in simulations of KOR bound to neutral and β-arrestin-biased ligand suggest that this receptor conformation is associated with G protein bias [53]. The 'occluded' KOR conformation is characterized by clockwise rotation of the intracellular end of TM7 and a shift towards TM2 [53].

Notably, G protein-biased KOR modulators are chemical highly divers with differences in structural motifs, size, and charge [66,101]. Thus, it is possible that several mechanisms, rather than one single mechanism, can induce biased signaling.

Bifunctional opioids simultaneously target multiple opioid receptors and produce mixed pharmacological profiles. Simultaneous modulation of multiple opioid receptors may result in synergistic effects, allowing dose reductions to achieve adequate analgesia or attenuated side effect profiles [33]. The combined activation of KOR and MOR causes aversion and reward that may influence or balance each other out [101]. DOR agonists produce seizure and euphoria while KOR activation results in anticonvulsant and antiaddictive effects rendering the combined activation of KOR and DOR potentially beneficial [101]. Bifunctional opioids may additionally be biased at the targeted opioid receptors, which can improve their clinical profiles [33]. The bifunctional opioid Cebranopadol represents a full agonist at MOR and DOR and a partial agonist at KOR and NOP [101] with a G protein-biased signaling profile at the NOP [102]. Cebranopadol causes potent analgesia with a beneficial side effect profile without respiratory depression and motor incoordination [131] and was investigated in clinical trials for several indications related to pain [101] (Clinicaltrial.gov IDs: NCT01939366, NCT01964378, NCT05491785, NCT01709214). MP1208, a G protein-biased partial agonist at MOR and KOR, produces great antinociceptive effects with reduced liabilities for respiratory depression, addiction, and aversion in mice [130].

Despite the potential of multifunctional opioids as analgesics, the rational design of bi- or multifunctional opioid receptor ligands with improved pharmacological profiles is challenging due to the complex nature of GPCR pharmacology with strong receptor crosstalk. The same applies to the optimization of lead structures towards a desired receptor profile. Prior determination of the determinants of opioid receptor selectivity is essential for rational design of the desired receptor profile. In addition, targeting multiple opioid receptor subtypes at the same time can counteract only some, but not all, of the side effects associated with the different receptor subtypes.

So far, bi- or multifunctional opioids have been mainly discussed for other indications [132]. KOR/DOR bifunctional ligands have been investigated in the context of depression, KOR/MOR bifunctional ligands have been explored for substance use disorders, e.g. cocaine addiction, and DOR/NOP bifunctional ligands were suggested to improve the treatment of Parkinson disease [132].

A common feature of prototypical opioids is the presence of a basic moiety [133-135] that can form a salt bridge with D3.32 deep within the conserved orthosteric opioid receptor binding site. This basic moiety was thought to be critical for opioid receptor binding and activation

[13,42,105,106]. However, the discovery of SalA disproved this hypothesis. SalA is a diterpene natural product found in *Salvia divinorum* that contains no nitrogen atoms and lacks a basic moiety [136]. However, SalA was found to potently and selectively activate the KOR [134,137,138] without any affinity towards the remaining opioid receptors or a cassette of 50 human receptors, ion channels, and transporters, including 5-HT receptors [134,137-139].

Despite tremendous efforts to understand the reasons for SalA's KOR potency and outstanding selectivity profile, the binding mode of SalA at the KOR and thus the structural determinants of its activity profile remain elusive [13,134,140-146]. Many different and conflicting binding hypotheses of SalA were published [13,134,140-146] hindering the rational design of reasonable SalA derivatives and novel non-basic KOR agonists. To date, hundreds of SalA derivatives have been synthesized and tested, albeit being mostly inactive or much less active than SalA [147]. Due to the lack of a basic moiety in SalA, it is questionable whether SalA binds in the same binding pocket as described for prototypical basic opioids.

To date, a small number of other non-basic KOR opioid scaffolds have been described [148-152] but the vast majority of KOR opioids remain basic. There is very limited knowledge of the potential binding modes or activity and selectivity determinants of non-basic opioids. However, non-basic opioids hold the promise of selectively targeting the KOR, as most of the non-basic opioids discovered possess KOR selectivity [148-152]. Thus, non-basic opioids may circumvent MOR-associated side effects and act as safer analgesics. Unfortunately, SalA itself has poor pharmacokinetic properties and a strong hallucinogenic potential [136,153], which renders SalA clinically useless. However, SalA derivatives as well as novel scaffold non-basic KOR agonists remain promising for the development of safer analgesics. We believe that the elucidation of SalA's binding mode at the KOR is crucial for the rational design of such non-basic KOR ligands. This binding mode could rationalize the outstanding KOR selectivity of SalA and provide insights into the exact location of SalA within the KOR binding site. These findings may be generalizable to the design of non-basic opioids. Labor-intensive crystallization experiments and cryo-EM may lead to the determination of the binding mode of SalA. However, the already published experimental data on SalA and its derivatives provide a solid basis to investigate the binding mode of SalA at the KOR.

Overall, opioid receptor activation for the treatment of pain is well established, but safety issues remain. Despite the use of several different strategies to improve opioid side effect profiles, none has led to the successful pharmaceutical approval of a safe analgesic. There is still a lack of understanding of the influence of certain activation profiles on opioid safety profiles, such as G protein bias and partial agonism, and the structural determinants that induce them. Therefore, further research should prioritize this area. As MOR and DOR

agonism cause reward and therefore could lead to high abuse potential, KOR agonism seems to be more beneficial for further drug design efforts.

1.2.2.2. Opioids for Treatment of Depression

In addition to pain management, opioid receptor modulation is a valuable strategy in the treatment of depression [51,56,76,154]. All four opioid receptors (KOR, MOR, DOR, NOP) contribute to mood homeostasis [55,56] dysregulated in depression [76] and therefore represent valuable targets for the development of new antidepressants. MOR agonism was shown to provide mood-lifting effects [155-157]. Transient MOR agonism is likely to elicit antidepressant activity, but sustained stimulation results in counterproductive effects such as aversion [56]. MOR agonists further induce addiction and show a considerable abuse potential [96] rendering MOR agonism less favorable for the treatment of MDD considering the alternatives. Efforts to develop DOR agonists for the treatment of MDD have struggled with the separation of mood-enhancing effects from seizure liability and sedation [51]. In contrast, KOR antagonism has a high potential for the treatment of MDD and will be discussed below.

Non-selective and selective KOR modulators are differentiated in the treatment of MDD. Ongoing research focuses on the development of KOR selective antagonists, but repurposing of already known non-selective opioid receptor antagonists has also been explored. The non-selective opioid receptor antagonists buprenorphine and naltrexone, both already approved by the FDA for other indications, have received attention for repurposing in MDD therapy [158-160]. Buprenorphine, known as a MOR agonist and analgesic, modulates all four opioid receptors and exhibits KOR antagonistic efficacy [161]. In mood-related experiments, buprenorphine has shown potent antidepressant activity, rapid effectiveness with only 2-3 days for first symptom improvements, high rates of full symptom remission, and effectiveness against suicidal ideation [76]. Naltrexone purely antagonizes opioid receptor activity [162]. Naltrexone has been tested as an adjunct to the antidepressant buprenorphine, and the combined administration of naltrexone and buprenorphine has been shown to be synergistic [158,160].

The prototypical KOR-selective antagonists 5'-guanidinonaltrindole (GNTI), norbinaltorphimine (nor-BNI) and JDTic have been extensively studied for their clinical potential as antidepressants, but their clinical value is hampered by their delayed onset of effect, long duration of action, poor CNS accessibility and unfavorable side effect profiles [39,154,163]. In particular, the long-lasting signaling blockade, which can exceed one month after single-dose administration of nor-BNI [39] raised concerns about the applicability of KOR-selective antagonists as antidepressants [154]. Thus, considerable effort has been devoted to the development of KOR-selective, short-acting antagonists, resulting in several new ligands,

including Aticaprant (JNJ-67953964), PF-4455242, and zyklophin [39,154,164]. However, there are concerns about the toxicity of PF-4455242 [163] and the chemical space of short-acting KOR antagonists is limited. Only a small number of KOR selective antagonists entered clinical trials [76,154] and none of them got approved yet. Aticaprant represents the most promising drug candidate among the new short-acting antagonists, proven to be effective and well-tolerated in humans [76]. It is currently investigated in phase III clinical trials for MDD as adjunctive therapy (clinicaltrials.gov IDs: NCT05455684, NCT05518149, NCT05550532). The development of other promising selective KOR antidepressants with a short duration of action is hampered by unknown reasons for the long duration of receptor blockade.

Several studies confirmed that KOR antagonists are promising and effective in the treatment of MDD [39,51,154,163]. The rapid onset of antidepressant effects is a major advantage over traditional antidepressants, which typically take several weeks to show the desired effect [74]. However, the exact mechanism for the rapid effect remains elusive [51]. The development of KOR antagonists for the treatment of depression is still in its early stages [76], and further improvements are needed.

Overall, KOR antagonism represents a promising and novel strategy for the treatment of depression. However, the long-lasting receptor blockade of current KOR-selective antagonists combined with the lack of known KOR selectivity determinants hampers further drug design efforts.

1.2.2.3. Opioids in Structural Analyses

In articles A, B, and C structural analyses of two opioid receptor agonists and one antagonist were performed to rationalize their binding modes and subsequently define their determinants of selectivity and activity. These analyses addressed open questions regarding how different opioids exhibit affinity and potency at the opioid receptors, especially the KOR, as these mechanisms are currently poorly understood. A better understanding of these mechanisms would allow the rational design of optimized opioids such as partial agonists or KOR selective opioids. Each opioid under investigation holds promise for the development of safer analgesics or KOR-selective antidepressants.

HS-731 (Figure 6) represents a peripherally restricted opioid receptor agonist with partial agonism at the KOR and full agonism at MOR and DOR (Article A). Due to its morphinan-based scaffold, HS-731 was expected to bind similarly to other morphinan-based ligands deep within the conserved binding site. Thus, the study of HS-731 may reveal selectivity and affinity determinants that are generalizable to other opioid ligands binding in the same cavity. In addition, HS-731 is zwitterionic, a rare feature of opioids, and therefore the influence of the

additional negative charge was investigated. Opioid receptor partial agonism is suggested to improve opioid analgesic safety profiles [71,72]. As most KOR partial agonists were identified by serendipity, no structural determinants related to partial activation are available. HS-731 already combines several strategies for the design of safer analgesics. It is peripherally restricted and shows partial KOR agonism. However, only careful *in silico* studies can provide insight into the partial agonist properties of HS-731.
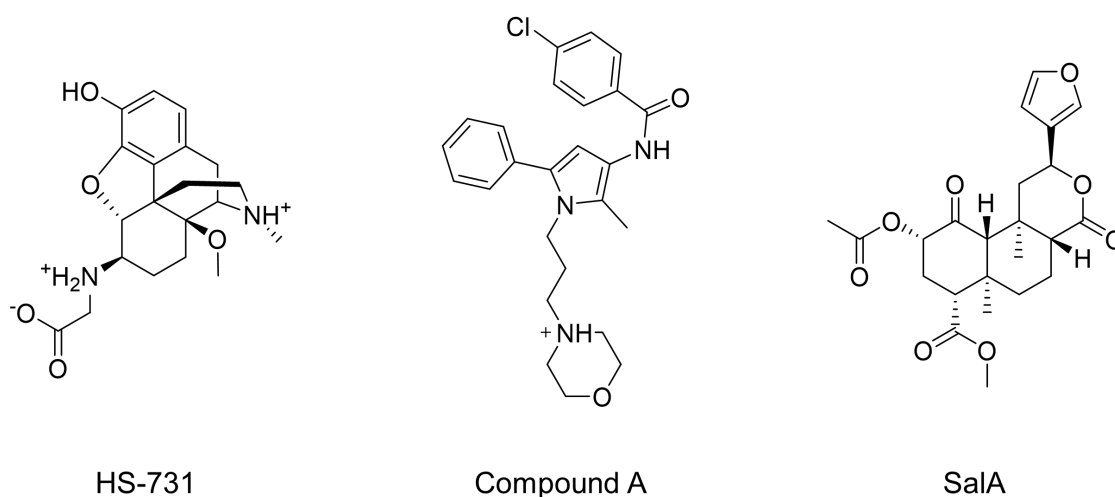

HS-731   Compound A   SalA

Figure 6. Chemical structures of opioids assessed in structural analyses.

Compound A (Figure 6) represents a dual KOR and MOR antagonist with KOR preference rendering it interesting as an antidepressant (Article B). Compound A is a novel scaffold and is therefore well suited for structural analysis. Any novel KOR antagonist scaffold promises to induce the clinically desired short-acting pharmacokinetic profile or to help understand the structural mechanisms behind the long-lasting receptor blockade. However, to further increase the chemical space of KOR-selective antagonists the prior elucidation of selectivity determinants for KOR antagonists is mandatory.

SalA (Figure 6) is a non-basic and potent KOR agonist with strong receptor selectivity (Article C). Very few non-basic opioid scaffolds are known, and even less information is available on the activity and selectivity determinants of non-basic opioids. At the beginning of the investigation, no crystal structure or cryo-EM structure of an opioid receptor with a non-basic opioid had been published. Elucidating how non-basic opioids possess activity at the KOR without the typical salt bridge to D3.32 would deepen our understanding of the KOR activation profile. SalA itself has no clinical value due to side effects and poor pharmacokinetic properties [136,153], but derivatives of SalA or other non-basic opioids promise increased clinical utility due to KOR selectivity that avoids MOR-related side effects. SalA is by far the most investigated non-basic opioid providing a good starting point for an *in silico* investigation of non-basic opioids [147]. To date, most SalA derivatives tested *in vitro* have been inactive

or have shown severely impaired activity [147]. Thus, the rationalization of the structure-activity relationship between SalA and its derivatives facilitates the rational drug design of SalA derivatives with improved KOR activation. The understanding of the binding mode of SalA would enable subsequent virtual screening campaigns for novel scaffold non-basic KOR agonists. The use of such a natural product-derived 3D pharmacophore as a virtual screening query in combination with natural product library searches increases the chances of successful identification of novel non-basic ligands, as natural products typically contain less charged compounds and are enriched in bioactivity due to evolutionary development [165].

1.2.3. Structural Basis for Computational Approaches at Opioid Receptors

Structure-based and Ligand-based drug design strongly depends on the availability of structural information about the receptor of interest and its ligands [166]. The more information available the more accurate hypotheses about ligand binding and receptor activation can be proposed [166].

There are several different opioid receptor ligand series, both agonists and antagonists, with thousands of entries in the ChEMBL database [167] for each human opioid receptor. The ChEMBL database represents an open-source database for ligand *in vitro* experimental data [167]. The available opioid receptor ligand information provides a suitable starting point for ligand-based *in silico* methods, structure-activity relationship (SAR) analysis, and determination of key protein-ligand interactions responsible for receptor activity [168]. The ligand set also allows for a sufficient validation of a 3D pharmacophore query used in virtual screenings via the generation of 'receiver operating characteristic' (ROC) curves [169]. The validation set used for this purpose in Article D was derived from the ChEMBL database.

To date, opioid receptor crystal structures and cryo-EM structures of all opioid receptor subtypes have been published (Table 2), including active state and inactive state structures for all receptor subtypes. However, when the *in silico* analysis of HS-731 was performed (Article A) no active state NOP structure was available. Thus, a homology model of the active state NOP needed to be generated using the active state KOR crystal structure as a template [13]. The opioid receptors share high sequential identity and similarity [55] rendering homology modeling suitable for structure prediction. Most structures within the set of published opioid receptor complexes contain a small molecule ligand, but several peptide-bound complexes exist as well. Several opioid receptor structures bound to G protein-biased ligands have been published, albeit only for the MOR and KOR and only in recent years. A receptor structure in complex with a β-arrestin-biased molecule is only available for the MOR [170].

Table 2. Experimentally solved structures of opioid receptors.

PDB-ID	Receptor subtype	Ligand	Conformational state	Year	Reference
4DJH	KOR	JDTic	Inactive	2012	[42]
4DKL	MOR	β-Funaltrexamine (β-FNA) - covalent	Inactive	2012	[45]
4EA3	NOP	C-24	Inactive	2012	[171]
4EJ4	DOR	Naltrindole	Inactive	2012	[172]
4N6H	DOR	Naltrindole	Inactive	2014	[44]
4RWA	DOR	Tetrapeptide H-Dmt-Tic-Phe-Phe-NH$_2$ (DIPP-NH$_2$)	Inactive	2015	[105]
4RWD	DOR	Tetrapeptide H-Dmt-Tic-Phe-Phe-NH$_2$ (DIPP-NH$_2$)	Inactive	2015	[105]
5C1M	MOR	BU72	Active	2015	[173]
5DHG	NOP	C-35	Inactive	2015	[47]
5DHH	NOP	SB-612111	Inactive	2015	[47]
6B73	KOR	MP1104	Active	2018	[13]
6DDE	MOR	DAMGO	Active	2018	[174]
6DDF	MOR	DAMGO	Active	2018	[174]
6PT2	DOR	KGCHM07 (peptide)	Active	2019	[175]
6PT3	DOR	DPI-287	Active	2019	[175]
6VI4	KOR	JDTic	Inactive	2020	[176]
7SBF	MOR	PMZ21 (G protein-biased)	Active	2022	[177]
7SCG	MOR	FH210	Active	2022	[177]
7T2G	MOR	Mitragynine pseudoindoxyl (G protein biased)	Active	2022	[170]
7T2H	MOR	Lofentanil (arrestin-biased)	Active	2022	[170]
7U2K	MOR	C6 guano (G-protein biased)	Active	2022	[178]
7U2L	MOR	C5 guano (G-protein biased)	Active	2022	[178]
7UL4	MOR	Alvimopan	Inactive	2022	[179]
7Y1F	KOR	Dynorphin A	Active	2023	[180]
7YIT	KOR	Nalfurafine (G-protein biased)	Active	2023	[53]
8DZP	KOR	momSalB (non-basic)	Active	2023	[181]
8DZQ	KOR	momSalB (non-basic)	Active	2023	[181]
8DZR	KOR	GR89,696	Active	2023	[181]
8DZS	KOR	GR89,696	Active	2023	[181]

8E0G	MOR	BU72	Active	2023	[182]
8EF5	MOR	Fentanyl	Active	2022	[46]
8EF6	MOR	Morphine	Active	2022	[46]
8EFB	MOR	Oliceridine / TRV130 (G protein-biased)	Active	2022	[46]
8EFL	MOR	SR17018 (G protein-biased)	Active	2022	[46]
8EFO	MOR	PMZ21 (G protein-biased)	Active	2022	[46]
8EFQ	MOR	DAMGO	Active	2022	[46]
8F7Q	MOR	β-Endorphin	Active	2023	[43]
8F7R	MOR	Endomorphin	Active	2023	[43]
8F7S	DOR	Deltorphin	Active	2023	[43]
8F7W	KOR	Dynorphin	Active	2023	[43]
8F7X	NOP	Nociceptin	Active	2023	[43]

Despite the existence of several crystal structures and cryo-EM structures of opioid receptors in complex with opioids, these cover only a small part of the chemical space of known opioids. Furthermore, most of them represent active state receptor conformations, which complicates the elucidation of activity and selectivity determinants for opioid antagonists. Opioid receptors share high structural similarity [55], especially in the orthosteric binding site, typically occupied by opioid ligands. This renders the rational design of ligands with subtype selectivity challenging. The first cryo-EM structure of an opioid receptor with a non-basic opioid was first published in 2023.

Overall, the available data on opioid receptors provide a solid foundation for ligand-based and structure-based drug design approaches. However, the binding mode of important ligand scaffolds remains elusive.

1.2.4. Pharmacological Evaluation of Opioid Drugs

Prospective *in silico* studies aiming for the prediction of new or optimized drug candidates are usually followed by comprehensive pharmacological assays to confirm the predicted drug features experimentally. Key experiments for testing new opioid drugs include *in vitro* binding and functional assays to assess drug affinity, potency, and efficacy [183,184] followed by *in vivo* experiments to evaluate the antinociceptive power [185,186], behavioral effects [187], as well as side effect profiles [188,189]. This section aims to provide an overview of *in vitro* assays used for the articles included in this dissertation.

The binding of ligands to opioid receptors is critical for influencing the activation profile of opioid receptors by opioids. Therefore, the first *in vitro* experiments performed for newly

developed opioids are *in vitro* binding studies. Typically, a radioligand binding competition assay is performed [183], also called displacement assay. Non-radioactive binding assays also exist, but the radioactive variety is highly sensitive and more common [190]. In this assay, a specific amount of receptor is incubated with a fixed amount of radioligand and varying concentrations of test ligand [191]. The radioligand used for the affinity measurement in the context of this dissertation was the small molecule KOR agonist [^{3}H]U69,593 [192]. After incubation, which facilitates equilibrium conditions, filtration and washing are performed to remove unbound radioligand from the receptors [191]. The radioactivity of the remaining receptor-bound radioligand is then measured by scintillation counting [192]. The measurement allows for determination of IC_{50} value, i.e. the concentration of test ligand necessary to inhibit 50% of radioligand binding [193]. Subsequently, the Cheng-Prusoff transformation allows the conversion of the IC_{50} value into K_i value, which is the equilibrium inhibitor constant of the test ligand [191]. The higher the affinity of the test ligand the smaller the K_i value and IC_{50} values [193]. Despite the widespread use of the assay, there are still some pitfalls to be aware of. The incubation time and conditions affect the precision and reliability of the assay and must be carefully adjusted as the calculations performed assume equilibrium conditions [190]. Adequate separation of bound and unbound radioligand is critical for accurate measurements [183]. Fiberglass is typically used for filtration, but centrifugation can be used instead [183]. The binding event measured in the assay is the combination of specific and non-specific binding of the radioligand, which must be corrected for accurate affinity predictions [190]. The amount of non-specific binding of the radioligand is determined by measuring radioligand binding in the presence of a high concentration of an unlabeled but high-affinity ligand to prevent radioligand binding to the receptor [191]. Under these conditions, radioligand binding may still occur to other parts of the assay such as the membrane, plastic, glass, or other materials or assay components. The non-specific binding value is then subtracted from the total binding value to obtain the specific binding value [190]. This assay is designed for competitive ligands, making it difficult to measure allosteric modulators. However, allosteric modulators can alter the affinity of the radioligand and are unable to completely inhibit ligand binding [190]. Noteworthy, radioligand binding assays cannot differentiate between agonists antagonists or inverse agonists [190]. Thus, the binding assay is often followed by *in vitro* functional assays.

The goal of *in vitro* functional assays is to characterize ligand-induced receptor signaling profiles for a specific pathway. For example, there are different functional assays for measuring activation of the G-protein and arrestin signaling pathways. Several functional assays have been developed for GPCRs, often based on second messenger concentrations, such as cAMP, Ca^{2+}, or IP_3, or on the measurement of protein-protein interactions [194]. However, not every assay is appropriate for every GPCR [194]. The [^{35}S]GTPγS assay

represents a typical functional assay to be performed to measure the G protein-dependent signaling for opioid receptors [130,195-197] and was used in the context of this dissertation. The [^{35}S]GTPγS assay measures the G protein activation resulting from agonist binding to the receptor [184]. Typically, GDP-bound heterotrimeric G proteins are activated after receptor binding by the exchange of GDP to GTP [198]. Subsequently, the complex dissociates into $G_α$-GTP and $G_{βγ}$ subunits and the GTPase activity of the $G_α$-subunit facilitates the rebinding of GDP to $G_α$ and the reformation of the inactive heterotrimeric G protein [199]. In contrast to natural GTP, [^{35}S]GTPγS ([^{35}S]guanosine-50-O-(3-thio)triphosphate) is poorly hydrolysable stabilizing the $G_α$-[^{35}S]GTPγS complex that accumulates in the membrane [198]. Usually, membranes expressing the receptor are incubated with [^{35}S]GTPγS, GDP, Mg^{2+}, and Na^+ ions, as well as a test compound followed by a filtration step to separate membrane-bound and free [^{35}S]GTPγS [184]. The amount of membrane-bound [^{35}S]GTPγS is then measured by scintillation [192]. Typically, the measurement takes place at a single time point per compound concentration [200]. Concentration-response curves can be generated to determine EC_{50} and E_{max} values [184] that represent the compound's potency and efficacy, respectively. The EC_{50} value describes the concentration of test compound required to achieve half of the maximum effect and the E_{max} value represents the concentration of compound of maximum effect. The assay is performed against a reference Compound and therefore provides relative efficacy values [184]. The [^{35}S]GTPγS assay allows for the differentiation between full agonists and partial agonists [200]. Preincubating the receptor with an agonist facilitates the measurement of antagonistic effects, which can be observed as a reduction in agonist effect [200]. The assay is characterized by a relatively simple workflow and low signal amplification level compared to other assays that measure downstream effects [184]. However, the assay conditions can heavily affect its performance [200], especially the concentrations of [^{35}S]GTPγS, GDP, and cations (Mg^{2+}, Na^+). In the articles included in this dissertation concentrations of these chemicals were used that are common for GPCR research [200], particularly 10mM $MgCl_2$ and 100mM NaCl, 0.05 nM [^{35}S]GTPγS, 10 μM GDP. The [^{35}S]GTPγS assay is most suitable for G_i-coupled GPCRs like the opioid receptors, as the nucleotide exchange rate for G_i is higher than for G_s and G_q [201]. However, the assay does not discriminate between different G_i subtypes present in the cell lines used for the experiment.

The radioligand binding assay and the [^{35}S]GTPγS assay are well-established experiments for the *in vitro* validation of opioids, that allow for the determination of opioid receptor affinity, potency, and efficacy. Thus, both methods were used to evaluate the ligands discussed in the included articles. The combined *in vitro* and *in silico* evaluation allows for conclusions about the structural mechanisms underlying the activity and to verify hypotheses generated *in silico*.

2. Aims and Objectives

Opioid receptor modulation is widely used in the treatment of pain and also holds great promise for the development of novel antidepressants. However, due to the severe side effects of current MOR agonists, the development of analgesics with improved safety profiles is highly desired. Efforts to improve opioid analgesics through selective KOR agonism have failed due to aversive side effects. Recent studies have suggested that KOR agonism in combination with low efficacy may be valuable. However, the structural mechanisms leading to partial agonism at the KOR are poorly understood and many ligands with these activation profiles have been found by serendipity. Therefore, structural studies of KOR partial agonists are needed.

KOR antagonists represent a novel class of antidepressants with a more rapid onset of antidepressant effects compared to standard medications and treatment of suicidal ideation. Current research is focused on KOR-selective antagonists. However, only a very limited number of KOR-selective antagonists are known and these mainly show problematic long-lasting receptor blockade. Thus, novel scaffold KOR antagonists need. However, to increase the chemical space of KOR-selective antagonists, prior knowledge about KOR selectivity determinants for antagonists is needed.

Despite extensive previous research, neither safe opioid analgesics nor approved selective KOR antagonists as antidepressants have reached approval for clinical use.

A common and major reason for the limited success in both indications is that rational drug design of safer opioid analgesics and KOR-selective antidepressants is hindered by the limited knowledge of the structural correlation between opioid scaffolds and *in vitro* measured opioid receptor activation and selectivity profiles. *In silico* studies can be used to elucidate this relationship. These studies provide atomic-level information that allows structural inferences to be made. Docking experiments determine binding modes faster than crystallization or cryo-EM experiments, thus larger chemical spaces can be investigated in a shorter amount of time. The dynamic study of binding modes allows a detailed examination of protein-ligand interactions and the conformational rearrangements they cause.

Opioids with different scaffolds, physicochemical properties, activity and selectivity profiles will be investigated. These opioids are of particular interest for the development of safer analgesics and KOR-selective antidepressants. In particular, these ligands are the peripherally restricted agonist HS-731, the novel scaffold antagonist Compound A, and the non-basic agonist SalA.

Despite their potential for the development of safer analgesics, non-basic opioids are currently understudied. Known non-basic opioid scaffolds were discovered by serendipity rather than rational drug design. Rational design of non-basic opioids is hampered by limited knowledge of how such opioids bind and activate the receptor and would greatly benefit from our structural investigation of SalA's binding mode and the structural determinants that define its *in vitro* activity and selectivity profile. New agonists would expand the currently very limited non-basic opioid chemical space and potentially have increased clinical value due to KOR selectivity. Therefore, we want to use the results from the structural investigation of SalA to develop new non-basic KOR agonists via a virtual screening campaign that allows for scaffold hopping. We want to screen natural product libraries because natural products usually contain fewer nitrogen atoms than synthetic library compounds and show enriched bioactivity due to evolutionary development.

Overall, this dissertation has three specific aims:

1) **Identification of opioid receptor subtype selectivity determinants via structural analyses for future drug design or drug optimization.**
   Binding mode elucidation, and rationalization of *in vitro* activity data for the different opioid receptor subtypes shall be performed for ligands that are valuable for the development of safer analgesics or novel antidepressants. These ligands are HS-731 (Article A), Compound A (Article B), and SalA (Article C).

2) **Identification of opioid receptor activity profile determinants via structural analyses for future drug design or drug optimization.**
   Analogously to the first aim, the binding mode for HS-731 (Article A), Compound A (Article B), and SalA (Article C) shall be investigated and mechanistically characterized, with subsequent SAR analysis and rationalization of *in vitro* activity data, including affinity, potency, and efficacy.

The results of the structural analyses performed for the first two aims could foster prospective opioid drug design. Thus, the third aim of this dissertation is:

3) **Design of novel, non-basic KOR agonists as potentially safer analgesics with KOR selectivity.**
   The binding mode of the potent, KOR selective, and non-basic natural product SalA from Article C shall serve as a starting point for a virtual screening campaign (Article D). Natural product libraries shall be screened to increase the chances for successful hit identification.

3. Computational Methods

This section provides an overview of the concepts underlying the *in silico* methods used extensively in this dissertation. The specific software parameters used can be found in the method sections of each included manuscript. All *in vitro* experiments included in this dissertation were conducted in collaboration in the research group of Prof. Mariana Spetea at the Institute of Pharmacy/Pharmaceutical Chemistry, University of Innsbruck, Austria. The theoretical background of these *in vitro* methods has already been introduced in section 1.2.4. The specific *in vitro* protocols can be found in each manuscript included later in this thesis.

3.1. Homology Modeling: Template-Based Protein Structure Prediction

In silico protein structure prediction methods are valuable when information on the 3D conformation of the protein of interest (target) is not available or insufficient. Two different approaches can be distinguished within *in silico* protein structure prediction, namely template-free and template-based structure prediction [202]. Template-based approaches aim to predict the protein structure of the protein of interest from the given structure of one or more similar proteins (templates), while template-free approaches use physics-based rules for protein folding [202]. Homology modeling (HM, also known as comparative modeling) is a template-based protein structure prediction method [203], while AlphaFold, which uses deep learning algorithms, is a template-free method [204,205].

HM was used within Article A. The method assumes that similar amino acid sequences of proteins cause similar 3D conformations [206]. Thus, HM utilized 3D conformations of proteins with high sequence identity or similarity to predict the 3D conformation of a query protein [203,206]. HM represents a valuable possibility to predict protein structures if no experimental data from X-ray crystallography, cryo-EM, or NMR spectroscopy is available [21].

HM is the most accurate *in silico* method for structure prediction if a suitable template structure exists [202,207]. After selecting a suitable template structure, the amino acid sequences of the target and template proteins are aligned. The alignment is of critical importance for the accuracy of the resulting homology model, while multi-sequence alignment is in general favorable over pairwise alignment [208,209]. Several different algorithms can be applied for sequence alignment, e.g. CLUSTALW [210] Clustal Omega [211], or MUSCLE [212]. HM is considered a reasonable approach if the sequence similarity after alignment is at a minimum of 30% [208]. After sequence alignment, the structural model of the target is generated based on the coordinates of the template structure. In this dissertation, Molecular Operating Environment (MOE) [213] was used to generate a NOP homology model after multi-sequence alignment (Article A) and therefore will be described in detail. Several additional software applications and web tools for HM exist such as I-TASSER [214], SWISS-MODEL [215], or

ROBETTA [216]. Within MOE's Homology Builder, the coordinates of all heavy atoms for identical residues between the target and template are copied into the homology model under construction. For non-identical residues, only the backbone coordinates are copied. Backbone conformations for residues not present in the template are obtained by collecting backbone fragments from a large high-resolution structural database. Loop regions and side-chain conformations are then constructed using an extensive rotamer library. The model then undergoes several minimization steps to relieve steric strains. According to this procedure, several individual models will be generated and the final homology model is selected based on the electrostatic solvation energy, calculated by the Generalized Born/Volume Integral (GB/VI) methodology [217], i.e. by the estimated free energy of hydration.

Once the homology model has been generated, the model must be validated and carefully checked manually. Structural parameters are investigated, such as atomic clashes, Ramachandran outliers [218], global fold, or protein family-specific structural features (e.g. disulfide bridges, characteristic secondary structure). If available, knowledge from mutational studies can be incorporated into model validation [203]. Further validation can be achieved by docking of known ligands to the active site of the protein [219,220].

3.2. Molecular Docking

Molecular docking is a computational method that predicts putative protein-ligand binding modes [221]. The resulting protein-ligand complexes facilitate the analysis of protein-ligand interactions valuable for drug discovery. The first docking algorithms were already developed in the 1980s [222]. Today, molecular docking is a well-established method in drug discovery, with a variety of docking software available, such as Gold [223], MOE Dock [224], Glide [225,226], AutoDock [227], and AutoDock Vina [228]. Critical determinants for docking program performance are the sampling algorithm and the scoring function used [229]. The sampling algorithm is responsible for the determination of plausible protein-ligand complex conformations. The scoring function ranks the ensemble of binding modes according to their energy values. Sampling algorithms can be roughly divided into five categories [230] (examples provided in brackets): Genetic algorithms (GOLD [223]), shape-based algorithms (DOCK [231]), incremental construction approaches (FlexX [232]), Monte Carlo simulations (LigandFit [233]), and systematic search techniques (Glide [225,226]). The three major classes of scoring functions consist of empirical (ChemScore [234]), knowledge-based (DrugScore [235]), and force field-based (GoldScore [236]) scoring functions [222,229].

The number of available sampling algorithms and scoring functions allows for a variety of different combinations that influence the prediction of the binding pose. Therefore, it is important to compare the reliability of docking program predictions. For this study, the docking

program GOLD [223] was chosen based on its excellent performance in comparison with several other docking programs [229,230,237]. GoldScore [236] was chosen as the docking score according to its great performance in the field of GPCRs [237].

GOLD, which stands for Genetic Optimization for Ligand Docking, is a genetic algorithm (GA) that attempts to mimic the process of evolution by constructing and optimizing an ensemble of data structures termed "chromosomes" [238]. In GOLD, chromosomes encode protein-ligand complex conformations and represent possible docking solutions. In the following, the GA of GOLD [238] is briefly explained: In the first step, a set of chromosomes ('parent chromosomes') is randomly generated. Subsequently, the set of chromosomes is improved by using the two genetic operators 'mutation' and 'crossover'. While the former combines chromosomes, the latter randomly disturbs chromosomes from the 'parent chromosomes'. The best-ranked chromosomes are more likely to be altered by the two genetic operators, introducing an evolutionary pressure into chromosome manipulation. The new chromosomes are ranked and added to the ensemble of chromosomes, displacing the worst-ranked chromosomes. The fitness of the chromosomes used for scoring is calculated by the number and strength of hydrogen bonds and the van der Waals energy within the protein-ligand complex. The iterative cycle of chromosome optimization and displacement ends when a specified number of GA runs have been performed. The final docking solution is selected from the last chromosome ensemble according to the highest fitness. Typically, multiple GA runs are performed for a ligand with newly randomized initial parameters for each run, resulting in multiple docking solutions. These are ranked according to the scoring functions implemented in the docking program. For Articles A, B and C in this dissertation, 30 different docking poses per ligand were generated. In Article D, 15 poses were generated, because more ligands had to be docked to the receptor.

Biomolecules undergo dynamic conformational changes. Thus, managing molecular flexibility is a critical aspect of molecular docking [229]. By treating the molecules rigidly, the docking process is computationally less demanding, but pharmacologically relevant conformations may be missed. On the other hand, introducing too much flexibility carries the risk of producing false positives. Unlike most docking programs that treat the protein as rigid by default during the docking process [230], GOLD performs docking with partial protein flexibility in the neighborhood of the protein active site [223]. GOLD also accounts for ligand flexibility by considering fully acyclic ligand flexibility and partially cyclic ligand flexibility [223].

Despite the establishment of docking as a valuable computational tool in drug discovery, it is important to mention the shortcomings of this method. While docking programs are capable of predicting useful and plausible protein-ligand complex conformations, they tend to fail to correctly score the putative docking solutions [221,222]. Therefore, alternative criteria should be used to select the putative pharmacologically relevant binding poses. In this dissertation,

the selection of pharmacologically relevant binding poses was independent of the score assigned by the scoring function. Instead, other criteria for pose selection like 3D pharmacophore overlap to a reference ligand [239], structural overlay with a reference ligand (Gaussian shape similarity score [240,241]), and agreement with mutational data and structure-activity-relationship (SAR) data were considered. Extensive visual inspection of docking poses was performed to further account for structural novelty, tautomers, interactions with specific residues, distorted ligand geometry, unsatisfied ligand heteroatoms, and many more. Visual inspection of docking poses is well established to improve the decisions made out of the docking experiments [242].

Molecular docking is prone to produce many false positives [242] as also inactive compounds will be placed into the protein binding site if they fit the size. Nonetheless, molecular docking was shown to sufficiently detect active compounds out of a set of decoys (putative inactive molecules) [221], which legitimates its broad use in virtual screening campaigns.

Docking performance can be improved by introducing knowledge about the protein-ligand system into the docking process by using constraints [221,237]. In the case of opioid receptors, it is feasible to apply a constraint that satisfies the need for a salt bridge between a positively charged moiety from the ligand and D3.32 of the protein whenever possible. This salt bridge is considered crucial for anchoring basic ligands and opioid receptor activation [13,42,105,106].

3.3. Molecular Dynamics Simulations

The static investigation of protein-ligand complexes according to the 'lock and key' hypothesis, in which both ligand and protein are considered rigid during complex formation, only represents a rough estimate of the actual biological state. It neglects the flexibility that is known to be inherent in small organic ligands and proteins [243]. Thus, the former 'lock and key' hypothesis of ligand recognition by proteins evolved into the current 'induced fit' hypothesis, in which both interacting partners undergo conformational changes during complex formation [243]. Protein-ligand complex conformations obtained from experimental structures in the PDB [21] represent only a single snapshot conformation out of an ensemble of protein-ligand complex conformations present in the particular biological context. Furthermore, these complexes could be biased towards the particular ligand bound to the protein. These characteristics illustrate the pitfall of missing relevant biological information by the sole investigation of static protein-ligand conformations. Introducing flexibility to the biological system by using molecular dynamics (MD) simulations allows for a more extensive *in silico* investigation of protein-ligand interactions over time, the prediction of cryptic pockets at the protein, the optimization of protein structures, and calculation of changes in free energy values

over an ensemble of conformations, among others [244,245]. The variety of possible applications renders MD simulations an important method in current drug discovery [246-249]. In MD simulations, atoms of molecules are treated as particles described by mass, coordinates, charge, and van der Waals (vdW) parameters [250]. Alterations of atom positions over time are then calculated based on the numeric integration of Newton's law of motion [251-253]. Newton's law of motion allows for the calculation of the acceleration of an atom after the application of a force. The acceleration in return facilitates the calculation of the atom velocity and the shift in coordinates of the atom. The initial position of each atom is defined by the static input conformation for the simulation, typically an experimental-derived structure or homology model. The initial velocities for the system are based on Maxwell-Boltzmann distribution at a given temperature [252]. The applied forces on the system per timestep are derived by the force field (FF) used [250]. The force field consists of a set of parameters that correlate the bonded and non-bonded interactions of the atom under consideration with the force acting on that atom [254]. Bond lengths, bond angles, and dihedrals are considered bonded terms while electrostatic (Coloumb) and vdW interactions are considered non-bonded interactions [250]. The parameters used in force fields represent approximations and thus are optimized to match experimental data and quantum-mechanical calculations [246]. Several different force fields have been developed so far, with AMBER [255], CHARMM [256], GROMOS [257], and OPLS [258] belonging to the most commonly used force field families for small molecule simulations [259]. The majority of force fields belong to the class of 'fixed-charge atomistic force fields' that assign each atom a fixed charge before the simulation starts [245,254,259]. Assigning dynamic partial charges would make the simulation of biological interactions more realistic, but at the cost of a significant increase in computational expenses [250]. A small number of polarizable force fields are available, yet only rarely used [260].

Minor differences in the velocities initially applied to the simulation system may result in large differences in atomic movements leading to diverse conformations at the end of the simulation time. To account for the statistical variance associated with multiple simulation runs, it is recommended that simulation replicates be performed, with five to ten replicates appearing to be sufficient. [261]. It is further preferable to perform several short MD simulations rather than one long simulation [261].

For modeling molecular movements, it is necessary to account for the fastest movements within molecular systems, i.e. bond length vibrations [262,263]. These bond length vibrations require very small time steps to be considered in molecular dynamics algorithms, greatly increasing the number of simulation steps and thus the computational cost and simulation time. As MD simulations usually aim to provide insights into biological processes on a larger time scale, it is common to apply bond constraints for simulations to increase the time step necessary for precise modeling [262]. The SHAKE method [264], heavily used in MD

simulations, removes bond fluctuations and allows for an increase in step size [262,263]. Yet, time steps around 1-2 femtoseconds (fs) are still necessary [247,265,266], which requires multiple simulation steps and large computational recourses for simulation.

The total simulation time of MD simulations depends on the aim of the project, the size of the system (number of atoms), and computational resources. With increasing atom number and simulation time the computational costs dramatically increase. At present, routine simulations only reach the microsecond (µs) time scale [254].

Before the MD simulation itself, the simulation system needs to be prepared, parametrized, and equilibrated. The simulation system typically includes the initial structure of interest (e.g. protein-ligand complex derived from docking), solvent, ions, and, in the case of GPCRs, a membrane. A distinction can be made between explicit and implicit water models [254,267]. Explicit solvation involves adding water molecules to the simulation system, while implicit solvation models compensate for the lack of water molecules by using dielectric constants that scale electrostatic force field contributions. [254]. While the first ones are more accurate the latter ones are computationally less demanding due to simulation system particle reduction [267]. Explicit water models, like TIP3P and TIP4P [268], are more common in classical MD simulations today [254], and were exclusively used within this dissertation. The addition of ions (Na^+, Cl^-) in a concentration of 1.5 M accounts for isotonic conditions during the simulation time. GPCRs are membrane proteins and therefore it is common to embed the protein into a phospholipid bilayer surrounded by water for simulation. The membrane can be placed according to the respective OPM database [269] entry for the considered GPCR or an entry of a similar GPCR in case the receptor of interest is not included in the database. Once the simulation system is prepared, an equilibration is performed before the actual simulation time starts. The aim of the equilibration is the reduction of steric strain and artifacts within the system [270]. A plethora of different simulation suites were developed such as AMBER [271], CHARMM [272], GROMACS [273], and NAMD [274].

During the MD simulation, a sequence of conformations of the simulation system is generated, typically referred to as frames. The evaluation of these frames depends on the project aim but frames could be compared to a reference conformation such as the first conformation of the simulation [53]. In general, possible assessment parameters could include atom movements, bond length or angle variations [53]. The calculation of the root mean square deviation (RMSD) or the root mean square fluctuation (RMSF) is popular within the MD simulation analysis to measure the similarity of three-dimensional structures [244]. While the first one calculates the atom deviation between two structures for the whole protein, the latter determines structural changes per residue [244]. In addition to assessment parameters solely focused on the geometry of the structure, differences in energy values throughout simulation time [244] or frequency of protein-ligand interactions [275] can be evaluated to link protein movements to
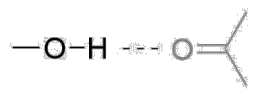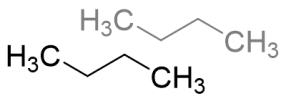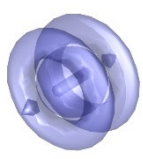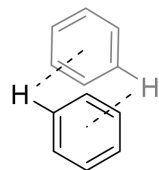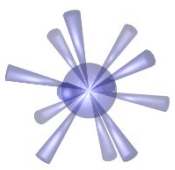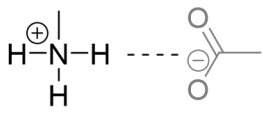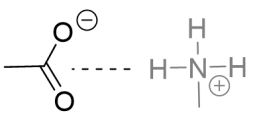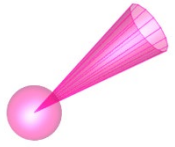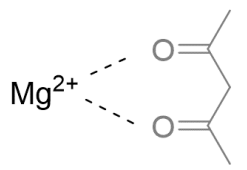
experimental observations. The frequency of protein-ligand interactions over time can be assessed utilizing dynamic 3D pharmacophores, so-called dynophores [275,276]. 3D pharmacophores and dynophores will be described comprehensively in the next section.

MD simulations are well established within drug design [254]. However, this method has its own limitations. First and foremost, the high computational costs [254] correlated with MD simulations hinder their usage for large datasets, huge simulation systems, or long timescales. With further improvements in computational hardware in the future, this limitation might be overcome. Secondly, the present force fields lack accuracy by neglection of quantum-mechanical effects by treating the atoms as single particles instead of a collection of atomic nuclei and electrons [244,245]. This approximation is currently needed due to excessive high computational costs to overcome this limitation.

3.4. Static and Dynamic Pharmacophores

3D pharmacophores (often only referred to as pharmacophores) consist of an ensemble of interaction features and steric features resembling protein-ligand interactions relevant to pharmacological response [277]. Within a 3D pharmacophore, interactions between ligand moieties and protein residues are abstracted into a small number of biologically relevant interaction feature classes, i.e. hydrogen bonds, hydrophobic contacts, aromatic interactions, charged interactions, metal coordination, and halogen bonds [278] (Table 3). Each interaction feature is defined by its interaction class, coordinates, spatial tolerance, weight, and possibly its directionality [278]. Besides information about the present protein-ligand interactions, 3D pharmacophores incorporate steric constraints, referred to as 'exclusion volumes', that account for the shape of the protein binding site [279].

Table 3. Overview of 3D pharmacophore features typically used in 3D pharmacophore modeling.

Feature	Representative Depiction	Example
Hydrogen Bond Donor		
Hydrogen Bond Acceptor		
Hydrophobic Contact		
Aromatic interaction		
Positive Ionizable		
Negative Ionizable		
Metal Coordination		
Halogen bond		

Feature depiction according to LigandScout [239,280].

Within the field of medicinal chemistry, the term 'pharmacophore' is often used by referring to chemical moieties, like carboxylic acids, guanidines, or chemical scaffolds, like steroids or flavonoids [277] possibly leading to confusion. To avoid any misunderstanding, it is therefore useful to use the term '3D pharmacophores' [278,281].

The process of generating 3D pharmacophores can be divided into two methods: ligand-based pharmacophore generation and structure-based 3D pharmacophore generation [278]. In ligand-based 3D pharmacophore generation, a set of compounds is aligned and analyzed according to their potential interactions with a protein. A consensus pharmacophore is then determined. Ligand-based approaches suffer from the dependence on accurate alignment of the active compounds without prior knowledge of the biologically active conformation [282]. The more diverse the scaffolds, the more difficult the alignment calculation. Since the actual binding modes are unknown, the risk of comparing ligands that bind to different sites on the protein is high [278]. Structure-based 3D pharmacophore generation calculates a 3D pharmacophore in the context of a protein environment. Both protein-ligand complexes and protein structures alone are suitable for 3D pharmacophore determination. When experimentally derived complex structures are available, structure-based methods are valuable because the bound ligand is already in its active conformation and knowledge of the spatial constraints of the binding site can be more accurately incorporated into the 3D pharmacophore model [279].

A variety of software suites for 3D pharmacophore generation are available, e.g. LigandScout [239,280], CATALYST [283], MOE [213], Phase [284], and Pharao [285] among others.

3D pharmacophores represent potential protein-ligand interactions statically, but as highlighted in the previous section on MD simulations, proteins, ligands, and their complexes exhibit dynamic behavior in biological systems. Therefore, a dynamic evaluation of 3D pharmacophores over time is of great interest. Dynamic pharmacophores, also called dynophores [275,276], illustrate interactions dynamically. They consist of probability density point clouds representing the interactions detected throughout MD simulations. The dynophore algorithm calculates the static 3D pharmacophores for each frame of the MD simulation and pools related interactions into superfeatures. Additionally, bar plots illustrating the occurrence frequency of detected interactions, are generated. Dynophores facilitate the temporal, spatial, and statistical analysis of detected interactions [278]. Bar plots allow for a time-resolved assessment of interaction appearance and statistical analysis by overall interaction frequency, while the feature cloud representation accounts for the spatial placement of interactions within the protein environment. The feature cloud representation also allows for an intuitive and quick evaluation of interaction stability over time by visual inspection of the 'blurriness' of the superfeature clouds. Dynophores were extensively used

within Articles A, B, and C where only the dynamic evaluation of protein-ligand interactions facilitated the rationalization of experimental results.

3D pharmacophores represent a valuable tool within computational drug design [281,286]. The strong abstraction level of 3D pharmacophore features allows for a broad and easy comparison between ligands and facilitates the determination of protein-ligand interactions favorable for ligand affinity [Articles A, B, and C]. 3D pharmacophores are also well suited for scaffold-hoping, i.e. the elucidation of new chemical scaffolds active at the protein of interest, due to their incorporated abstraction level [278]. 3D pharmacophore similarity calculations also provide a suitable method for selecting pharmacologically relevant docking poses. The Dynophore application allows the detection of key interactions by frequency of occurrence and the assessment of ligand binding mode stability by spatial fluctuations of the ligand in the binding site. Prospectively, 3D pharmacophores can serve as queries for virtual screening campaigns, which will be described in detail in the next section and was applied in Article D.

3.5. 3D-Pharmacophore-Based Virtual Screening

3D pharmacophores represent valuable tools for virtual screening campaigns [281]. The aim of *in silico* virtual screening campaigns is the identification of active molecules towards the protein of interest out of a database with molecules of unknown activity [287,288]. For this, a 3D pharmacophore query is screened against a multi-conformational molecule library, and molecules satisfying the query 3D pharmacophore are retrieved in a hit list [278,279]. Hit molecules can be docked to the protein of interest to further evaluate their potential for subsequent *in vitro* experimental evaluation [288]. Molecule databases used in virtual screenings often encompass millions of molecules. However, only a few of these molecules are likely to possess activity at the protein of interest. In addition, only a limited number of hit molecules can be assessed *in vitro*. The virtual screening sensitivity (retrieval of actives as hits) and specificity (exclusion of inactive molecules from the hit list) can be adjusted by modification of 3D pharmacophore feature tolerance and weight [278] as well as the number of 3D pharmacophore features within the query. The larger the number of 3D pharmacophore features and the smaller the allowed distance and angle deviations from the query 3D pharmacophore feature the lower the sensitivity and the higher the specificity of the virtual screening. Increasing the feature weight for more crucial protein-ligand interactions will prioritize more active molecules. Noteworthy, a balance between sensitivity and specificity needs to be found as these features negatively correlate with each other, which means that they cannot be optimized simultaneously [169].

Statistical validation of the virtual screening's predictive power is best facilitated by the retrospective screening of databases of known active and known inactive molecules with subsequent visualization of the virtual screening performance in a receiver operating characteristics (ROC) curve [169,279], that assesses if the model can include active compounds and exclude inactives. If inactive molecules are not available for validation, decoys can be used instead. Decoys represent computationally generated molecules of assumed inactivity that were designed to match the active molecules in terms of physicochemical properties, like number of rotatable bonds, molecular weight, or calculated logP, but differ in the 2D topology [289]. Active molecules correctly predicted as hit molecules represent true positives (TP), decoys excluded from the hit list true negatives (TN), actives incorrectly excluded from the hit list false negatives (FN), and decoys wrongly categorized as hit molecules false positives (FP) [169,279]. The ROC curve plots the true positive rate (sensitivity, y-axis) against the false-positive rate (1-specificity, x-axis) [169,279] (Figure 7). The ideal ROC curve goes straight to the upper left corner and then horizontally to the upper right corner (Figure 7, curve A). A diagonal line from the lower left to the upper right corner represents a random distribution of actives and decoys in the virtual screening (Figure 7, curve

C). A distribution superior to a random distribution is located above the random line (Figure 7, curve B). A curve below the random line indicates a systematic error in the distribution and the starting hypothesis for 3D pharmacophore generation should be re-evaluated (Figure 7, curve D). Another descriptor used to evaluate retrospective screening is the enrichment factor. The enrichment factor describes the improvement of the hit rate by the virtual screening compared to a random distribution [279,282].
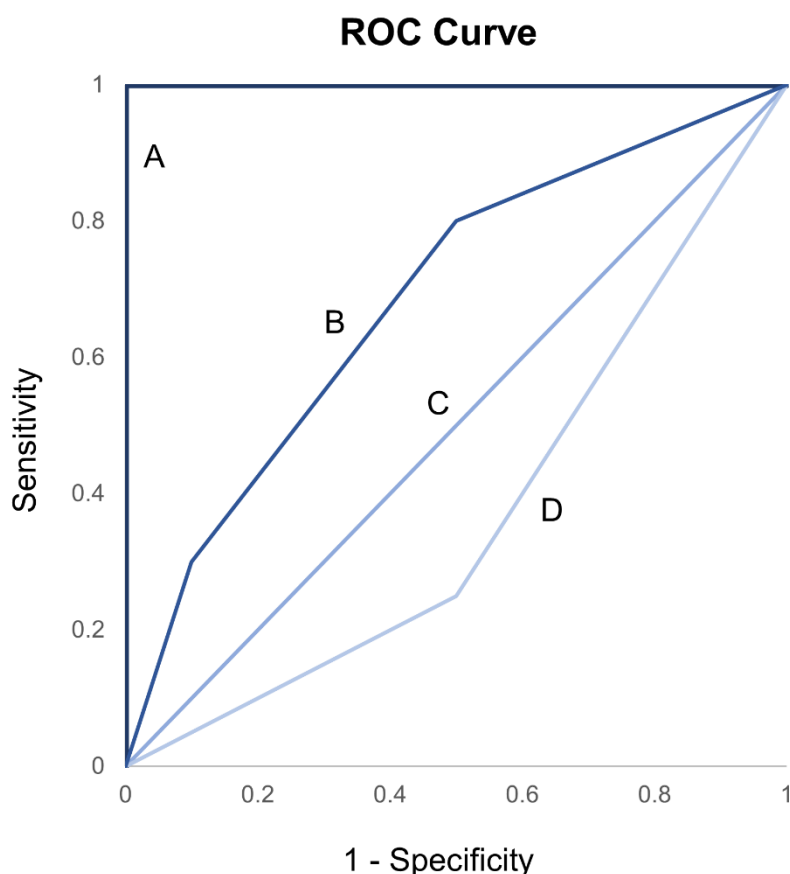
ROC Curve

Figure 7. Example of ROC curves. Curve A represents an ideal curve, curve B represents a valuable distribution compared to the random distribution shown in curve C. Curve D indicates a systematic error as the distribution is worse than random.

Virtual screening campaigns are widely used in drug design [281,282,288] as they serve as a filter to increase the hit rate for experimental testing and significantly reduce the costs compared to high-throughput screening (HTS) [287,290]. 3D pharmacophore-based virtual screening campaigns also have low computational costs and allow for easy scaffold hopping by retrieving bioisoteric ligands [282]. Given the potential patent protection of promising lead scaffolds in drug design, scaffold hopping is a highly valuable strategy for competing companies. In addition, new chemical scaffold ligands hold the promise of circumventing the

potential side effects of known lead compounds. Our recent review summarizes successful applications of 3D pharmacophore modeling in GPCR research [281].

In this dissertation (Article D), two 3D pharmacophore-based virtual screening methods were used. The first one includes protein-ligand interaction features as well as exclusion volume spheres in the virtual screening query and was performed in LigandScout [239,280]. The second one used the software ROCS (Rapid overlay on chemical structures) developed by Openeye [291,292], where a score for the similarity between a query ligand and a database ligand is calculated using 3D structural similarity via Gaussian functions and the chemical similarity via the overlap of pharmacophore features [293].

4. Results

4.1. Mechanistic Characterization of the Pharmacological Profile of HS-731, a Peripherally Acting Opioid Analgesic, at the μ-, δ-, κ-Opioid and Nociceptin Receptors [Article A]

The development of safer analgesics is highly desirable in light of the ongoing opioid crisis. One strategy to obtain such safer analgesics is the peripheral restriction of opioids. The zwitterionic HS-731 is a peripherally acting opioid showing full agonism at MOR and DOR, but partial agonism at KOR. The activity profile of HS-731 at the NOP remained elusive.

In this study, we demonstrated the lack of affinity of HS-731 at the NOP in *in vitro* experiments and performed a detailed *in silico* evaluation of HS-731 at the opioid receptors. In particular, we elucidated the binding mode of HS-731 at the classical opioid receptors and rationalized the affinity and potency profiles at the different opioid receptor subtypes in atomistic detail. We identified the conserved residue 5.39 (K) and the non-conserved residue 6.58 (MOR:K, DOR:W, and KOR:E) as responsible for the affinity differences at the classical opioid receptors. Y3.33 in NOP adopts a conformation pointing deeper into the binding side than in classical opioid receptors, preventing HS-731 from binding to NOP. Interactions between TM5 (K227$^{5.39}$) and TM6 (E297$^{6.58}$) in the KOR prevented intracellular TM6 outward movement directly related to KOR activation, correlating with the partial agonism observed for HS-731 at the KOR.

Contribution:

Conceptual design (75 %)

Computational experiments (100 %)

Visualization (80 %)

Manuscript preparation (75 %)

In vitro experiments were conducted at Mariana Spetea's lab. I planned and performed the *in silico* experiments and wrote the manuscript excluding the *in vitro* results.

Mechanistic Characterization of the Pharmacological Profile of HS-731, a Peripherally Acting Opioid Analgesic, at the μ-, δ-, κ-Opioid and Nociceptin Receptors

Kristina Puls [1], Helmut Schmidhammer [2], Gerhard Wolber [1,*] and Mariana Spetea [2,*]

[1] Department of Pharmaceutical Chemistry, Institute of Pharmcy, Freie Universität Berlin, Königin-Luise-Str. 2+4, D-14195 Berlin, Germany; kristina.puls@fu-berlin.de

[2] Department of Pharmaceutical Chemistry, Institute of Pharmacy and Center for Molecular Biosciences Innsbruck (CMBI), University of Innsbruck, Innrain 80-82, 6020 Innsbruck, Austria; helmut.schmidhammer@uibk.ac.at

* Correspondence: gerhard.wolber@fu-berlin.de (G.W.); mariana.spetea@uibk.ac.at (M.S.); Tel.: +49-30-838-52686 (G.W.); +43-512-507-58277 (M.S.)

Abstract: Accumulated preclinical and clinical data show that peripheral restricted opioids provide pain relief with reduced side effects. The peripherally acting opioid analgesic HS-731 is a potent dual μ-/δ-opioid receptor (MOR/DOR) full agonist, and a weak, partial agonist at the κ-opioid receptor (KOR). However, its binding mode at the opioid receptors remains elusive. Here, we present a comprehensive in silico evaluation of HS-731 binding at all opioid receptors. We provide insights into dynamic interaction patterns explaining the different binding and activity of HS-731 on the opioid receptors. For this purpose, we conducted docking, performed molecular dynamics (MD) simulations and generated dynamic pharmacophores (dynophores). Our results highlight two residues important for HS-731 recognition at the classical opioid receptors (MOR, DOR and KOR), particular the conserved residue 5.39 (K) and the non-conserved residue 6.58 (MOR: K, DOR: W and KOR: E). Furthermore, we assume a salt bridge between the transmembrane helices (TM) 5 and 6 via $K227^{5.39}$ and $E297^{6.58}$ to be responsible for the partial agonism of HS-731 at the KOR. Additionally, we experimentally demonstrated the absence of affinity of HS-731 to the nociceptin/orphanin FQ peptide (NOP) receptor. We consider the morphinan phenol $Y130^{3.33}$ responsible for this affinity lack. $Y130^{3.33}$ points deep into the NOP receptor binding pocket preventing HS-731 binding to the orthosteric binding pocket. These findings provide significant structural insights into HS-731 interaction pattern with the opioid receptors that are important for understanding the pharmacology of this peripheral opioid analgesic.

Keywords: GPCR; opioid receptor; HS-731; peripheral opioid agonist; analgesia; binding; selectivity; molecular docking; molecular dynamics simulations

1. Introduction

Opioid receptors are membrane-bound receptors belonging to the family of G protein-coupled receptors (GPCRs) [1]. There are four opioid receptor subtypes, including the three classical opioid receptors, μ (MOR), δ (DOR) and κ (KOR), and the more recently discovered nociceptin/orphanin FQ peptide (NOP) receptor [1]. The central role of the opioid system (opioid receptors and their endogenous and exogenous ligands) in pain treatment has been long recognized, with activation of each opioid receptor subtype leading to pain relief [2,3]. Because of their therapeutic relevance, the opioid receptors are among the few GPCRs determined in different activation states [4].

The most common strategy for the treatment of severe pain is by targeting the MOR [2,3,5]. Clinically used MOR agonists (e.g., morphine, oxycodone and fentanyl) are capable of producing potent and effective analgesia, but they also cause unwanted

and numerous side effects, such as respiratory depression, constipation, sedation, nausea, tolerance, dependence and addiction [2–4]. Opioid misuse and opioid-induced overdoses and death have become a global medical and socioeconomical issue leading to the ongoing opioid epidemic [6,7]. Recently, it was reported that the overdose deaths from opioids was increased to 56,064 in 2020 in the USA [8]. Therefore, the development of safer analgesics with lower or no abuse liability and other undesirable side effects is highly needed [9–11]. Diverse approaches in the design of safer analgesics include targeting multiple receptors simultaneously (bi- and multifunctional ligands) [11–13], functional selectivity at GPCRs (biased agonists) [11,14–16] and peripheralization of opioid receptor agonists [2,11,17,18].

Opioid receptors are expressed in the central and peripheral nervous systems (CNS and PNS), and various non-neuronal tissues (immune, neuroendocrine and ectodermal cells) [2,3,19,20]. Preclinical and clinical studies have shown that selective activation of peripheral opioid receptors leads to effective pain relief and reduced CNS-mediated side effects [2,17,18,21–23]. Increasing the hydrophilicity of opioids to limit their access to the CNS, and thus to minimize the incidence of undesirable CNS effects comprises diverse chemical modifications, such as incorporation of quaternary or amphiphilic molecules, which contain hydrophilic and hydrophobic components, pH-sensitive activation of analgesic compounds and synthesis of peptide-derived analgesics. The goal of achieving analgesia while avoiding CNS penetration has focused on both small molecules and peptides [2,17,18,21,22,24].

Among the first generation of peripherally restricted opioid compounds was the MOR agonist loperamide [25] (clinically used in the control of diarrhea), which is completely excluded from the CNS by the action of P-glycoprotein [18]. Asimadoline [26], an amphiphilic molecule, was the first peripherally selective agonist with activity at the KOR evaluated in humans for the treatment of peripheral pain. Unfortunately, asimadoline did not achieve clinically relevant efficacy at doses that lacked CNS adverse effects [17,21]. Through computer simulations at low pH, the fluorinated fentanyl analogue, NFEEP, was identified as a potent antinociceptive activating specifically the MOR in acidified peripheral tissues and to lack the typical opioid side effects in animals [18,21,27]. Peripheral restriction can also be achieved with peptidic agonists that produce analgesia by activating the MOR or KOR in the periphery [17,22,28]. The most advanced peripherally restricted KOR agonist under clinical development for acute postoperative pain and chronic pain is the tetrapeptide CR845 (also known as difelikefalin) [17,22].

Chemical and pharmacological work from our laboratory in the field of peripheral opioid analgesics from the class of opioid morphinans targeted the attachment of amino acid residues and dipeptides at the C6 position of the centrally acting MOR agonist 14-*O*-methyloxymorphone [29–37]. It was established that inclusion of an ionizable group, such as amino acid residues and sulfate conjugates, in morphinans leads to increased hydrophylicity and consequently reduced penetration into the CNS, by having greater selectivity towards peripheral tissues [31,32,34,35,37–40]. Inclusion of an ionizable group, such as amino acid residues, leads to increased hydrophylicity and consequently reduced penetration into the CNS, by having greater selectivity towards peripheral tissues. Several zwitterionic analogues were profiled as very potent MOR/DOR agonists producing antinociception after systemic administration in various pain models in rodents (mice and rats) via activation of peripheral opioid receptors [37]. A prominent representative of the series is HS-731, the 6β-glycine substituted derivative of 14-*O*-methyloxymorphone (Figure 1) [29], showing high affinity, potent and full agonism at the MOR and DOR, and a weak, partial agonism at the KOR (Table 1). In addition, HS-731 has been demonstrated to effectively induce peripheral opioid antinociception in a multitude of pain conditions, including acute nociception (tail-flick test) [31], visceral pain (acetic acid-induced writhing assay) [34,37], inflammatory pain (formalin test [31,33] and carrageenan-induced hyperalgesia [32]), neuropathic pain (sciatic nerve ligation) [33] and migraine pain (eye-wiping trigeminal nociceptive test) [36] in rodents. In acute thermal nociception, HS-731 was up to 200-fold more potent than morphine and had similar potencies to fentanyl when given systemically subcutaneous (s.c.), with considerably long-lasting antinociceptive effects. A

significant and prolonged duration of the antinociceptive effect (up to 4 h) with a peripheral site of action was shown after oral administration of HS-731 to rats with carrageenan-induced inflammatory pain [32]. Recent data were reported on the absence of analgesic tolerance for HS-731 in rats upon chronic s.c. treatment for 14 days [23].
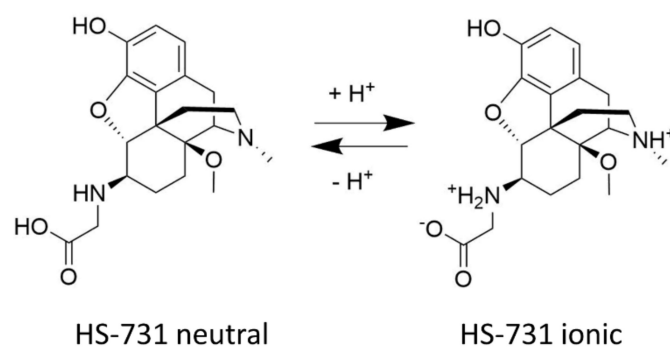

Figure 1. Structure of HS-731 and the acid-base equilibrium under physiological conditions.

Table 1. In vitro binding affinities and agonist activities of HS-731 at the opioid receptors.

Receptor	Rat Opioid Receptor	Human Opioid Receptor		
	Binding affinity K_i (nM)	Binding affinity K_i (nM)	Functional activity EC$_{50}$ (nM)	% stim.
MOR	0.83 ± 0.02 [a]	0.90 ± 0.14 [b]	3.78 ± 0.73 [b]	98 ± 9 [b]
DOR	7.86 ± 0.64 [a]	10.1 ± 2.7 [b]	7.92 ± 1.63 [b]	103 ± 7 [b]
KOR	44.8 ± 0.1 [a]	-	361 ± 154 [b]	82 ± 9 [b]
NOP	- [c]	>10,000	- [d]	- [d]

[a] Binding affinities (K_i, nM) to the opioid receptors in the rat brain were determined in competitive radioligand binding assays; data from [30]. [b] Binding affinities (K_i, nM) to the human opioid receptors expressed in CHO cells were determined in competitive radioligand binding assays; data from [35]. Potencies (EC$_{50}$, nM) and efficacies (% stimulation expressed as percentage relative to the maximum effect of a selective, full opioid agonist) to the human opioid receptors expressed in CHO cells were determined in the [^{35}S]GTPγS binding assays; data from [35]. [c]—denotes not determined. [d]—denotes not applicable. Values are means $\pm$ SEM ($n = 3$ independent experiments performed in duplicate).

In the present study, we present the first mechanistic in silico investigation of the binding mode and interaction mechanisms of HS-731 to the three classical opioid receptors and rationalize why HS-731 does not bind to the NOP receptor.

2. Results and Discussion

2.1. HS-731 Shows No Specific Binding to the NOP Receptor

We have reported previously on the specific binding of HS-731 to the three classical opioid receptors, MOR, DOR and KOR, in the rat brain and to the recombinant human receptors expressed in Chinese hamster ovary (CHO) cells (Table 1). HS-731 shows high binding affinities in the low nanomolar range to the MOR and DOR, and reduced affinity to the KOR [30,35]. In the present study, the first data on the binding affinity of HS-731 to the NOP receptor is reported. Competitive inhibition of [^{3}H]nociceptin binding by HS-731 to the NOP receptor was assessed using in vitro competitive radioligand binding assays with membranes of CHO cells expressing the human NOP receptor. HS-731 displayed no substantial binding to the NOP receptor up to a concentration of 10 μM. In the same assay, the reference nociceptin ligand had a very high binding affinity ($K_i = 0.17 \pm 0.04$ nM) to the NOP receptor (Figure 2 and Table 1).
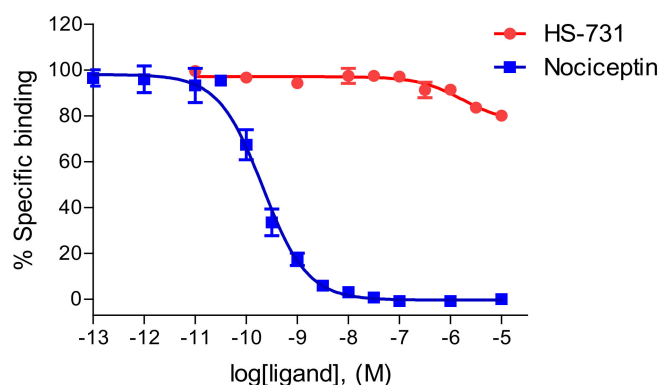
Figure 2. Binding curves of HS-731 to the human NOP receptor determined in the competitive radioligand binding assay. Concentration-dependent inhibition by HS-731 and nociceptin of [^{3}H]nociceptin binding to membranes from CHO cells stably expressing the human NOP receptor. Values are means ± SEM (*n* = 3 independent experiments performed in duplicate).

2.2. Homology Modeling Is Suitable to Predict the Active State Human Nociceptin Receptor

In order to characterize binding of HS-731 in a comprehensive way, an investigation of both the inactive conformation, but also the active conformation is necessary. Since no active-state crystal structure of the NOP receptor is available we modeled the active state human NOP structure using the crystal structure of the κ-opioid receptor (KOR, PDB-ID: 6B73 [41]). Model generation was carried out as described in the Section 3 and resulted in a model with a 0.7 Å root mean square deviation (RMSD) between the α-carbon atoms between NOP and active conformation KOR template, indicating a correct global fold. The NOP homology model contains no atom clashes and only two phi/psi angle outliers, suggesting a high-quality homology model (Figure 3, see Section 3 for details).
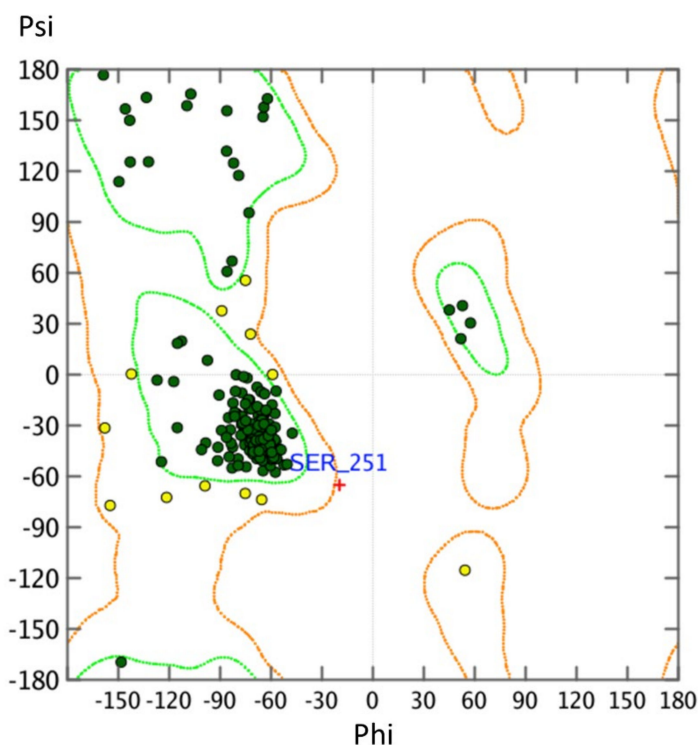

Figure 3. Ramachandran plot of the NOP homology model. Angles within the orange range angles are plausible (yellow spheres) and angles within the green space are optimal (green spheres).

2.3. Water Molecules Are Important for HS-731 Binding to the Opioid Receptors

Water-mediated hydrogen bonds between ligand and receptor are known to occur within opioid receptor crystal structures [41–43]. Both MOR and DOR x-ray crystal structures [42,43] contain crystal water molecules. In the MOR, three polar interactions between ligand and protein are mediated by water molecules, namely those to K233[5.39], H297[6.52] and Y148[3.33] (the numbering refers to the mouse MOR; the respective residues in the human MOR are K235[5.39], H299[6.52] and Y150[3.33], superscripts denote Ballesteros-Weinstein numbering [44]) were reported [42]. Mutagenesis studies have revealed all three residues to be involved in MOR binding and selectivity [45]. Therefore, the water molecules in the MOR structure were retained. The DOR structure with PDB-ID 6PT2 published by Claff et al. [43] contains three water molecules, which mediate interactions to K214[5.39] and Y129[3.33]. In mutagenesis studies, Y129[3.33] was shown to contribute to affinity and activity of DOR agonists [43,46], while K214[5.39] contributes to agonist binding and selectivity [47]. Therefore, all three water molecules were retained. For the KOR, no crystal waters are experimentally resolved. 'Interaction potential maps' implemented in MOE were therefore used to identify a single potential conserved water position. The same workflow was applied to the NOP homology model and the NOP inactive crystal structure. For all three structures water molecule between the transmembrane helices 5 and 6 (TM5/TM6) were identified that are capable to mediate interactions to the backbone carbonyl of K5.39, an interaction highlighted previously in opioid receptors [41–43]. The predicted water molecule in the KOR occupies the same coordinates as a preserved water molecule present in the MOR (PDB-ID: 5C1M).

2.4. Docking Reveals a Common Binding Mode for HS-731 to the Opioid Receptors

HS-731 contains the same morphinan scaffold (Figure 4) as the co-crystallized ligands of the active X-ray crystal structures used in this study (KOR co-crystalized with MP1104, PDB-ID: 6B73 [41], and MOR co-crystalized with BU72, PDB-ID: 5C1M [42], Figure 4). In contrast, the active state DOR structure used in this study contains a peptidic ligand [43]. Nevertheless, MP1104 is known to be a potent agonist at the MOR, DOR and KOR [41,48]. Thus, a maximal scaffold overlay of HS-731 and MP1104 or BU72, and additionally a common binding mode within the opioid receptors was aimed.
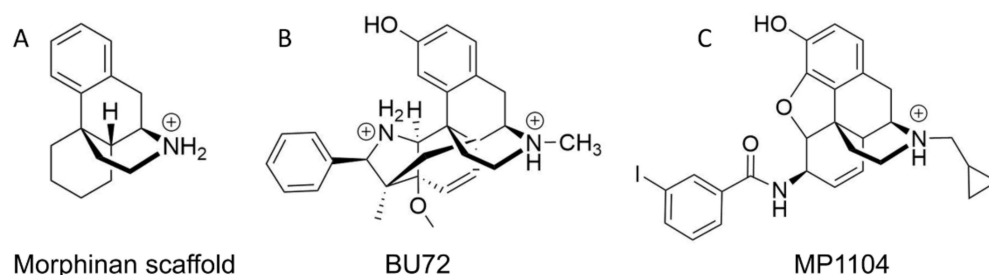

Figure 4. Chemical structures of (**A**) a morphinan scaffold and co-crystallized ligands (**B**) BU72 in MOR (PDB-ID: 5C1M) and (**C**) MP1104 in KOR (PDB-ID: 6B73) under physiological pH (7.4).

To obtain a common binding mode of HS-731 in all opioid receptors, we docked HS-731 into the prepared MOR, KOR, DOR x-ray crystal structures, as well as into the NOP active state homology model and the NOP inactive crystal structure. All protein structures contain water molecules in the TM5-6 region that is surmised to be important for ligand binding [41]. Docking revealed a common binding pose of HS-731 in the classical opioid receptors with the phenolic moiety establishing hydrogen bonding to the water molecules coordinating the K5.39 backbone carbonyl in TM5. The morphinan amine interacts with D3.32 via a salt bridge. The HS-731 carboxylate moiety points upwards to the extracellular domain (Figure 5A). An ionic interaction between the side chain of K5.39 and the carboxylate of HS-731 occurs in all the three classical opioid receptors. In the MOR, the carboxylate moiety also forms an ionic interaction with a second lysine positioned in

TM6 (K305$^{6.58}$). While K5.39 is conserved among the classical opioid receptors, residue 6.58 is not conserved, with the positively charged K305$^{6.58}$ in the MOR, neutral W284$^{6.58}$ in the DOR, and negatively charged E297$^{6.58}$ in the KOR. Thus, HS-731 is only able to form ionic interactions with both lysine residues in the MOR, explaining the highest affinity of HS-731 to this receptor. In contrast, HS-731 only can exhibit one ionic interaction to K5.39 in the KOR and DOR (Figure 5B–C).
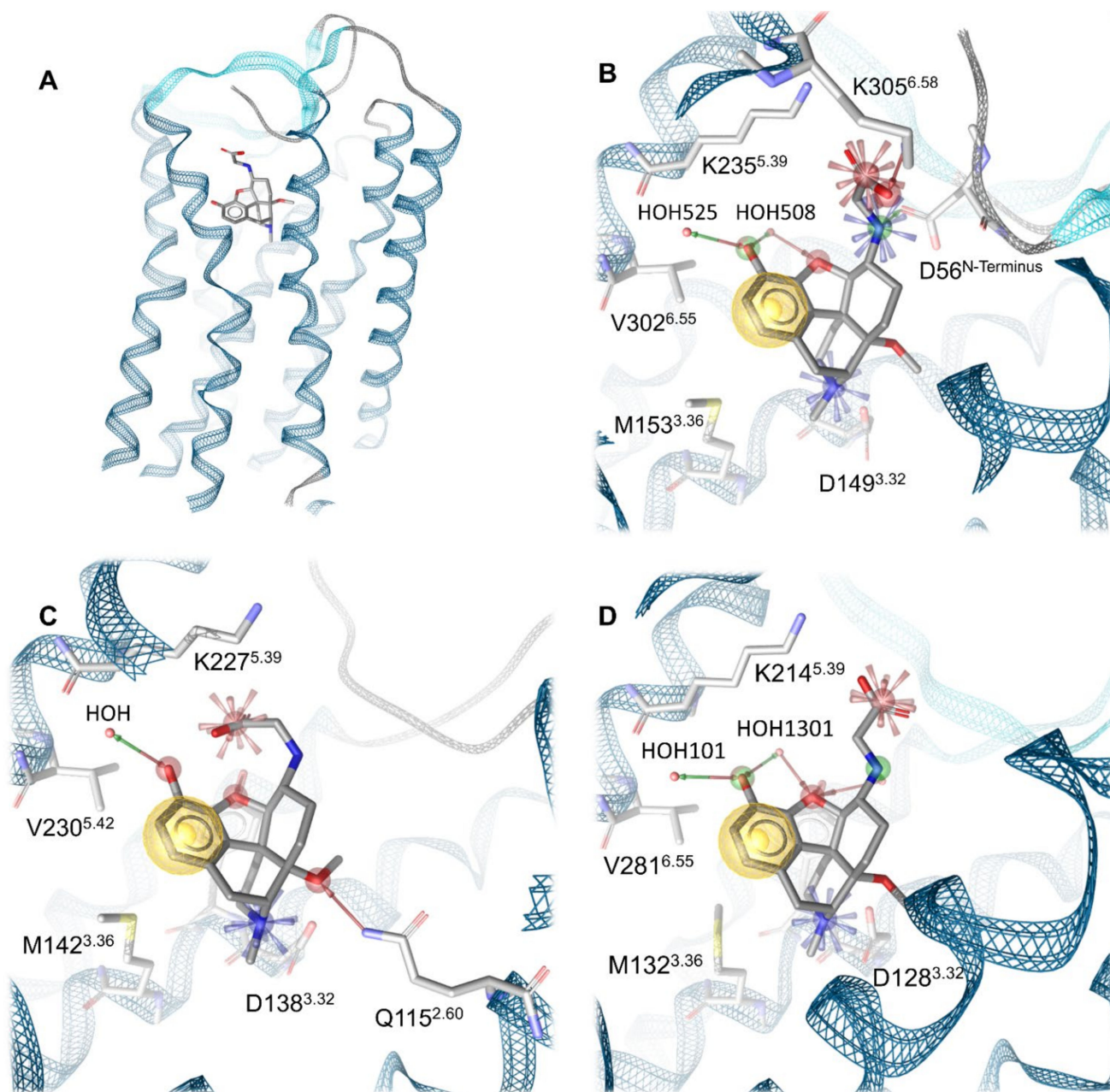

Figure 5. Binding modes of HS-731 to the classical opioid receptors. (**A**) Global view on the MOR binding pocket with docked HS-731. (**B**) Binding pocket of the MOR. Residues 297–303 and 322–325 are not shown for better visualization. (**C**) Binding pocket of the KOR. Residues 289–294 and 311–318 are not shown for better visualization. (**D**) Binding pocket of the DOR. Residues 275–282 are not shown for better visualization. Blue star indicates positive ionizable interactions, red stars negative ionizable interactions, yellow spheres lipophilic contacts, green arrow hydrogen bond donors and red arrows hydrogen bond acceptors. Water molecules are depicted as red spheres.

Even though residue 6.58 did not participate in an interaction with HS-731 in the KOR, it could have an influence on ligand binding. In the KOR, K227$^{5.39}$ and E297$^{6.58}$ could interact with each other in an ionic protein-protein-interaction. Subsequently the carboxylate of HS-731 would have to compete with E297$^{6.58}$ for K227$^{5.39}$ as interaction partner. This competition would likely weaken the strength of the ligand interaction to K227$^{5.39}$ and reduces HS-731's affinity to the KOR. The neutral W284$^{6.58}$ in the DOR cannot participate in an ionic interaction. Nonetheless, it could take part in a weaker π-cation interaction with K214$^{5.39}$. No geometrically plausible π-cation between W284$^{6.58}$ and K214$^{5.39}$ could be observed in our model. Subsequently, we surmise that W284$^{6.58}$ does not influence ligand binding resulting in a better affinity value compared to the KOR. Additionally the non-conserved residue 6.58 is a known selectivity-determinant at the classical opioid receptors [45,47,49], and therefore its influence on ligand binding could contribute to the affinity pattern of HS-731 at the opioid receptors.

A feature only visible in the binding hypothesis generated at the MOR is an ionic interaction between the secondary amine of HS-731 and D56 of the N-terminus. The MOR is currently the only solved opioid receptor crystal structure in which the N-terminus covers the binding site [42]. Thus, possible interactions between HS-731 and the N-terminus of the KOR or DOR were not detectable, even though the unresolved parts of the N-termini of both receptors contain negatively charged residues that could be oriented towards the binding pocket. Hence, the ionic interaction between the secondary amine of HS-731 and the N-terminus of the MOR was not investigated in this study.

Experimentally, HS-731 did not exhibit specific binding to the NOP receptor (Figure 2 and Table 1). Therefore, the generated binding hypothesis to the NOP receptor predominately served to give insights into the reasons for the lack of affinity to this receptor and to assess if HS-731 could be active in higher concentrations than experimentally tested. As there is no data about the activity profile of HS-731 at the NOP receptor available we conducted docking to the modeled active state NOP receptor as well as to the inactive state NOP receptor (crystal structure, PDB-ID: 5DGH). For the active state homology model no valid and plausible docking solution for the orthosteric binding pocket with the essential ionic interaction to D130$^{3.32}$ could be obtained. Residue Y130$^{3.33}$ is likely to cause this exclusion effect as it points deeper into the NOP receptor binding pocket than in the classical opioid receptors (Figure 6). A superimposition of NOP receptor with the classical opioid receptors in complex with HS-731 revealed atom clashes between the morphinan scaffold and Y130$^{3.33}$ (Figure 6). This steric hindrance precludes HS-731 from binding to the active state NOP receptor orthosteric binding pocket. Additionally, Akuzawa et al. [50] demonstrated abolished binding of the endogenous ligand nociceptin to the NOP receptor mutant Q280A, which indicates an important role of Q280 in anchoring NOP agonists. Residue Q280 is positioned deep in the orthosteric binding pocket; therefore, it could not mediate HS-731 binding to the active conformation of the NOP receptor. Also, for the inactive state NOP receptor (as obtained from the crystal structure with PDB-ID 5DGH), no reasonable binding mode could be obtained. The binding site in the inactive NOP receptor conformation is enlarged allowing HS-731 to bind to the lower part of the orthosteric binding pocket as does the co-crystallized antagonist C-35. However, HS-731 adopted a different orientation within the binding pocket and exhibited a distinct interaction pattern compared to known NOP antagonists [51,52] as no 3D pharmacophore overlay could be detected (Figure S2). Furthermore, HS-731 was not able to stabilize its two charged moieties outside the morphinan scaffold in ionic interactions resulting in an enthalpically unfavorable binding mode. Unlike endorphins, enkephalins and dynorphins, the endogenous NOP receptor ligand nociceptin contains FGGF instead of YGGF in its message domain [50,51,53]. The additional hydroxyl group is considered to function as a discriminator feature between classical opioid receptors and the NOP receptor [51] with dynorphin A (Y^{1}) showing no activity at the NOP receptor [54]. The phenyl group of nociceptin is considered to point deeply into the orthosteric binding pocket [51]. The discriminative hydroxyl group of HS-731 was similarly oriented further indicating an implausible binding mode for HS-731.
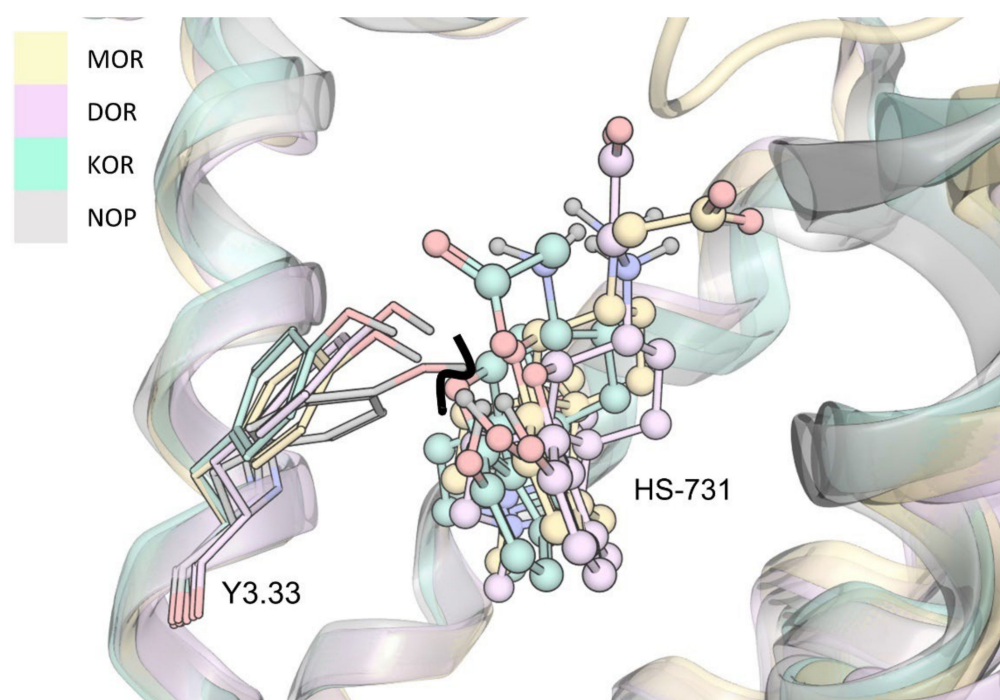
Figure 6. Superimposition of the NOP receptor and the classical opioid receptors in complex with HS-731. Atom clash is indicated by the bold black line.

Altogether, the absence of affinity of HS-731 to the NOP receptor is in line with reports indicating that NOP ligands often exhibit binding and activity patterns to the NOP receptor not observed in the classical opioid receptors [1]. Furthermore, the lack of plausible docking poses implies inactivity of HS-731 to the NOP receptor even for high ligand concentrations. Hence, the binding poses at the NOP receptor were not further assessed in MD simulations.

2.5. Molecular Dynamics Simulations Revealed Additional Interactions for HS-731 Binding to the Opioid Receptors

To obtain dynamic information for the opioid receptor-HS-731 complexes, we performed MD simulations and analyzed the interactions using the in-house developed Dynophore software [55], that calculates dynamic pharmacophores ('dynophores'). Table 2 shows the frequency of the ionic interactions between HS-731 and the three opioid receptors, MOR, DOR and KOR, during the simulations performed. Notably, the salt bridge between the morphinan amine and D3.32 that is known to be crucial for binding of positively charged ligands [56,57] occurred in 100% of the trajectory. In the case of the MOR, MD simulations resulted in the same four ionic interactions observed in the static model. The ionic interactions occurred with high frequencies, suggesting strong salt bridges between HS-731 and the MOR binding pocket (Table 2). Dynophore analysis obtained from the DOR and KOR complexes with HS-731 revealed additional, ionic interactions between the ligand and extracellular loops (DOR: R291[ECL3]; KOR: K200[ECL2]) that were not seen in the static model. The occurrence of ionic interactions with residues of the ECLs could be explained by a tilt of the loops towards the binding pocket during the simulations. Moreover, dynophore analysis revealed four stabilizing ionic interactions between ligand and protein in case of the KOR, but only three in case of the DOR (Table 2). Furthermore, the frequency of the ionic interaction between the morphinan amine and K5.39 is as frequent in the KOR as in the DOR, even though a lower frequency in case of the KOR was predicted due to possible intramolecular interaction between K227[5.39] and E297[6.58] as discussed in Section 2.4. The last two findings seem in disagreement with the higher affinity of HS-731 towards the DOR than to the KOR (Table 1). To explain these observations, we analyzed the geometry of

the stabilizing salt bridges between HS-731 and the opioid receptors residues (Table 2) as described in the next section.

Table 2. Ionic interaction occurrence between HS-731 and the three classical opioid receptors during MD simulations.

InteractionType	Interaction Partners			
	HS-731	MOR	DOR	KOR
Cationic interaction	morphinan amine	D149$^{3.32}$(100%)	D128$^{3.32}$ (100%)	D138$^{3.32}$ (100%)
Cationic interaction	secondary amine	D56$^{N\text{-}terminus}$ (73.7%)	Not present	E209^{ECL2} (12.5%)
Anionic interaction	Carboxylate	K235$^{5.39}$ (81.3%)	K214$^{5.39}$ (65.0%)	K227$^{5.39}$ (63.3%)
		K305$^{6.58}$ (75.0%)	R291^{ECL3} (9.2%)	K200^{ECL2} (15.7%)

The frequency is given as an average of five simulation replicates per system.

Detailed root-mean-square deviation (RMSD) plots of HS-731 and the protein backbone can be found in the Supplementary Materials (Figures S3–S8). Additionally, the supportive information provide a comparison of the binding modes of HS-731 at the end of the simulation time with the docking pose (Figures S9–S11).

2.6. Interaction Distance Assessment Confirms Binding Hypothesis

We measured the distances between the interaction partner atoms to examine the quality of the ionic interactions occurring during MD simulations. Ionic interactions are known to be strongly distance-dependent and the energy of ionic interactions is determined by an exponential term, i.e., the strength of the interaction decreases rapidly by increasing distance [58]. The distance measurement between the carboxylate moiety of HS-731 and K5.39 at the MOR revealed short distances throughout the majority of the MD simulation (Figure 7A). The large extent of strong interactions implies stable ligand binding over the simulation time and the higher amount compared to the other opioid receptors contributes to the superior affinity of around one order of magnitude exhibited at the MOR.

The corresponding distance assessment at the DOR and KOR revealed far more short-distance interactions at the DOR than at the KOR (Figure 7B). Thus, even though the interaction frequency at the DOR and KOR was very similar, the interaction was much stronger at the DOR, explaining the increased affinity of HS-731 at the DOR compared to the KOR (Table 1). Additional interactions between the carboxylate and the basic residues in the ECLs in both receptors (R291^{ECL3} in the DOR, K200^{ECL2} in the KOR) only occurred with low frequency and long interaction distances rendering their effect on ligand binding negligible (Figure S12A). The ionic interaction in the KOR between E209^{ECL2} and the secondary amine of HS-731 also only occurred with low frequency and again the distance assessment revealed mostly long distances, rendering its effect on ligand binding trivial (Figure S12B).

To explain the activity profile of HS-731 as a partial agonist at the KOR (Table 1), the possible interaction between K227$^{5.39}$ and E297$^{6.58}$ to the KOR was assessed. This is because a salt bridge between K227$^{5.39}$ and E297$^{6.58}$ at the KOR is assumed to hamper KOR activation in that the interaction between the TM5 and TM6 hinders TM6 from its outward movement [59]. At the same time, the translocation of TM6 is important for receptor activation at GPCRs like the opioid receptors [4,60] and interactions between TM5 and TM6 are considered to hamper activation in other GPCRs [61]. This hypothesis is supported by the fact that the salt bridge between K227$^{5.39}$ and E297$^{6.58}$ at the KOR only occurs in the inactive conformation (PDB-ID: 4DJH [56]), but was broken up in the active crystal structure (PDB ID: 6B73 [41]). The partial adoption of an intermediate state conformation with a less pronounced outward movement due to K227$^{5.39}$–E297$^{6.58}$ interaction would explain the partial agonism of HS-731 at the KOR. Our simulation shows that the two residues

interact with each other during 45.6% of the time indicating that the surmised intermediate state is indeed relevant. Furthermore, the proposed hindered TM6 outward movement at KOR was confirmed by a distance measurement between the alpha carbonyl atoms of the opposing residues 6.31 at the bottom of TM6 (MOR: R278[6.31], DOR: R257[6.31], KOR: R270[6.31]) and 4.40 at the bottom of TM4 (MOR: R184[4.40], DOR: A163[4.40], KOR: L173[4.40]) over the simulation time (Figure 8). Thus, the K227[5.39]–E297[6.58] interaction appears to induce a less active conformation at KOR explaining the observed partial agonism of HS-731 at the KOR. A comparison between the active state KOR (PDB-ID: 6B73) and one exemplary intermediate state conformation can be found in the Supplementary Materials (Figure S13).
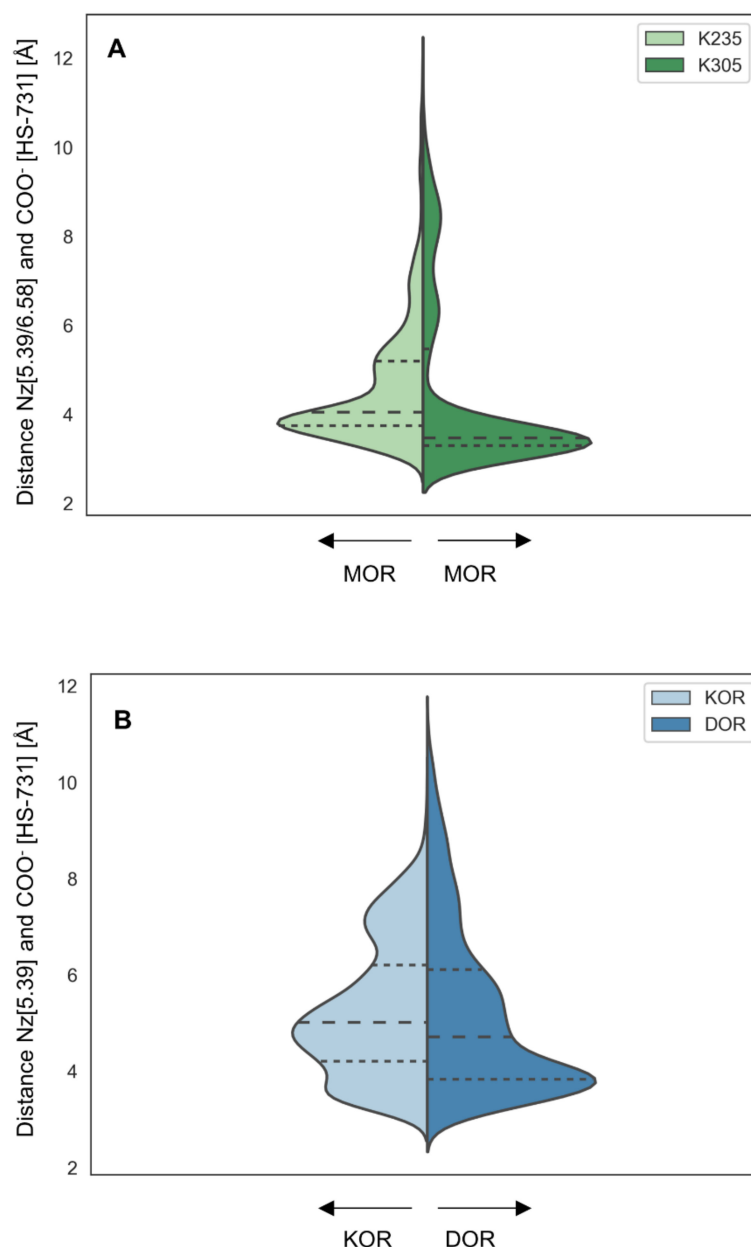

Figure 7. Ionic interaction distances. (**A**) Distances between K235[5.39] (Nz) or K305[6.58] (Nz) in the MOR and the carboxylate of HS-731. (**B**) Distances between K227[5.39] (KOR, Nz) or K214[5.39] (DOR, Nz) and the carboxylate moiety of HS-731. Dashed lines represent quantile. The width of the plot corresponds to the frequency of the measured distance.
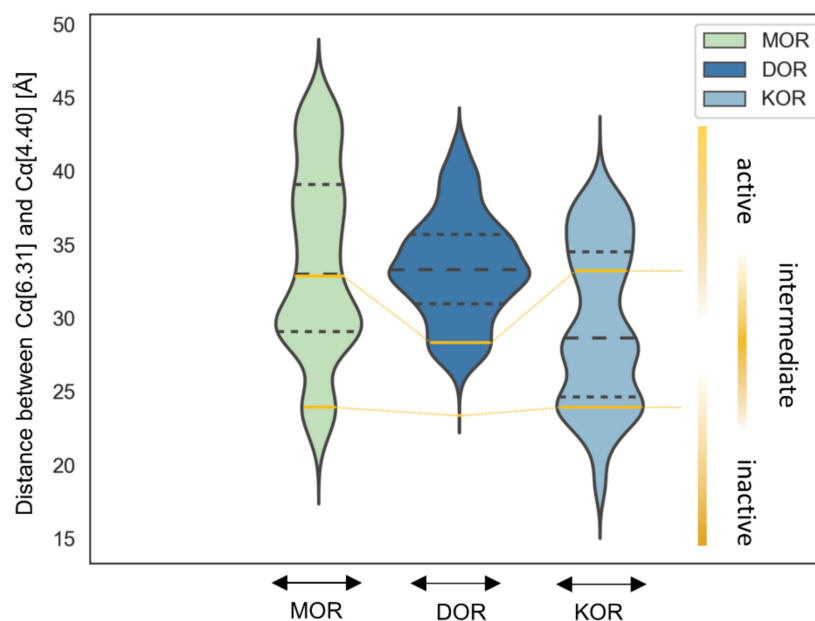
Figure 8. TM6 translocation. Measurement between the alpha carbon atoms of 6.31 at the bottom of TM6 (MOR: R278[6.31], DOR: R257[6.31], KOR: R270[6.31]) and 4.40 at the bottom of TM4 (MOR: R184[4.40], DOR: A163[4.40], KOR: L173[4.40]) over the simulation time. The width of the plot corresponds to the frequency of the measured distance. Dashed black lines represent quantile. Yellow solid lines indicate the analog measured distances at the active state crystal structures (PDB-ID: 5C1M for MOR, 6PT2 for DOR and 6B73 for KOR) and inactive state crystal structures (PDB-ID: 4DKL for MOR, 4N6H for DOR and 4DJH for KOR).

In the case of the MOR and DOR, which do not exhibit negatively charged residues in the upper half of TM6, no similar interaction occurred, in accordance with the HS-731 full agonism observed at these receptors (Table 1). To ensure that all influencing factors for TM5–TM6 interactions in the DOR were properly considered, the occurrence of cation–π-interactions between W284[6.58] and K214[5.39] were determined. As surmised this interaction was not detectable in MD simulations confirming the hypothesis of partial agonism in the presence of TM5–TM6 interactions. A comparison between the active state KOR (PDB-ID: 6B73) and one exemplary intermediate state conformation can be found in the Supplementary Materials (Figure S13).

Definition of the intermediate state for all opioid receptors based on the TM6 deflection measured between the alpha carbonyl atoms of the opposing residues 6.31 and 4.40 at the respective active state crystal structures (PDB-ID: 5C1M for MOR, 6PT2 for DOR and 6B73 for KOR) and inactive state crystal structures (PDB-ID: 4DKL for MOR, 4N6H for DOR and 4DJH for KOR) clearly indicates a maximum within the intermediate area for KOR, but also for MOR while DOR only very rarely adopts such a state (Figure 8). Nonetheless, the number of intermediate state conformations observed for all three opioid receptors during the simulation time reflects the order of activation potential measured in the [35S]GTPγS binding assay (Table 1). The KOR-HS-731 complex exhibits 51.9% of the time an intermediate state conformation corresponding to 82% stimulation in the [35S]GTPγS binding assay and partial agonism. The MOR-HS-731 complex in contrast only adopts an intermediate conformation in 44.6% of the simulation time correlating to 98% stimulation in the [35S]GTPγS binding assay and full agonism. The DOR-HS-731 complex reaches 103% stimulation in the [35S]GTPγS binding assay and full agonism with only 5.3% intermediate states.

3. Materials and Methods

3.1. Chemicals and Materials

HS-731 was prepared as previously described [29]. Radioligand [³H]nociceptin (119.4 Ci/mmol) was purchased from PerkinElmer (Boston, MA, USA). Tris(hydroxymethyl) aminomethane (Tris), bovine serum albumin (BSA) polyethylenimine (PEI) and nociceptin were obtained from Sigma-Aldrich Chemicals (St. Louis, MO, USA). Cell culture media and supplements were obtained from Sigma-Aldrich Chemicals (St. Louis, MO, USA). All other chemicals were of analytical grade and obtained from standard commercial sources. Test compounds were prepared as 1 mM stocks in water and further diluted to working concentrations in 50 mM Tris-HCl buffer (pH 7.4).

3.2. Cell Culture and Membrane Preparation

CHO cells stably expressing the human NOP receptor (CHO-hNOP cell line) was kindly provided by Dr. Lawrence Toll (SRI International, Menlo Park, CA, USA). CHO-hNOP cells were grown at 37 °C in Dulbecco's Modified Eagle's Medium (DMEM) culture medium supplemented with 10% fetal bovine serum (FBS), 0.1% penicillin/streptomycin, 2 mM L-glutamine and 0.4 mg/mL geneticin (G418). Cells were maintained in a humidified atmosphere of 95% air and 5% CO_2. Membranes from CHO-hNOP cells were prepared as described previously [62]. Briefly, CHO-hNOP cells grown at confluence were removed from the culture plates by scraping, homogenized in 50 mM Tris-HCl buffer (pH 7.7) using a Polytron homogenizer, then centrifuged once and washed by an additional centrifugation at 27,000× g for 15 min at 4 °C. The final pellet was resuspended in 50 mM Tris-HCl buffer (pH 7.7) and stored at –80 °C until use. Protein content of cell membrane preparations was determined by the method of Bradford using BSA as the standard [63].

3.3. [³H]NOP Receptor Binding Assay

Competitive binding assays at the human NOP receptor stably transfected into CHO cells were performed according to the published procedure [62]. Cell membranes (15 µg) were incubated in 50 mM Tris-HCl buffer (pH 7.4) with [³H]nociceptin (0.1 nM) and various concentrations of test compounds in a final volume of 1 mL, for 60 min at 25 °C. Non-specific binding was determined using 10 µM of unlabeled nociceptin. After incubation, reactions were terminated by rapid filtration through 0.5% PEI-soaked Whatman GF/C glass fiber filters. Filters were washed three times with 5 mL of ice-cold 50 mM Tris-HCl buffer (pH 7.4) using a Brandel M24R cell harvester (Brandel, Gaithersburg, MD, USA). Radioactivity retained on the filters was counted by liquid scintillation counting using a Beckman Coulter LS6500 (Beckman Coulter Inc., Fullerton, CA, USA). Inhibition constant (K_i, nM) values were determined by the method of Cheng and Prusoff [64] from concentration-response curves by nonlinear regression analysis using the GraphPad Prism 5.0 Software (GraphPad Prism Software Inc., San Diego, CA, USA). All experiments were performed in duplicate and repeated three times with independently prepared samples. Data are presented as means ± SEM.

3.4. Protein Preparation and Modeling of the KOR Active Conformation

For classical opioid receptors, X-ray crystal structures of the active state proteins are published and provided in the protein data bank (PDB [65]). The respective structures with PDB-IDs 5C1M for the MOR [42], 6PT2 for the DOR [43] and 6B73 for the KOR [41] were prepared using MOE v2020.0901 [66]. The X-ray crystal structure of the inactive state NOP receptor (PDB-ID: 5DGH) was prepared analog. Only the chain with the best resolution was processed. Fusion proteins (antibody fragment in MOR, thermostabilized cytochrome b562 (BRIL) in the DOR, nanobody in the KOR) and the unresolved parts of the N-terminus, as well as of the C-terminus of the opioid receptors were deleted. Thermostabilizing mutations in the DOR and KOR were subsequently reverted to the human wild-type sequence obtained from the UniProt-Databank [67] (human DOR: P41143, human KOR:

P41145). The MOR structure (PDB-ID: 5C1M) is of a murine receptor. Hence, the sequence was manually mutated to obtain the human wild-type MOR model

(UniProt-ID: P35372). The NOP receptor structure already contained the human sequence. Missing side chain atoms were automatically generated using the protein builder integrated in MOE. The unresolved parts of ECL2, ECL3 and ICL3 of the KOR and ICL2 of the NOP receptor were modeled using the loop modeler panel within MOE. To obtain high quality structures, Ramachandran outliers [68] and atom clashes were resolved using energy minimization with the OPLS-AA force field [69].

Homology modeling of the active state NOP receptor was performed using MOE v2020.0901 with default settings in a similar as described in [70]. The chain with the best resolution (3.10 Å) of the active KOR structure (PDB-ID: 6B73, sequence identity of 59% and sequence similarity of 73%) with the NOP receptor (Figure S1) served as a template. The protein target sequence (human NOP receptor) was obtained from the UniProt-Database (human NOP receptor P41146). Both Ramachandran outliers as shown in Figure 3 are located in flexible loops far away from the binding site (T206 of extracellular loop 2, ECL2, and S251 of intracellular loop 3, ICL3). Hence, we assume that these Ramachandran outliers are unlikely to influence ligand binding. Visual inspection revealed that the side chain orientations of the residues forming the orthosteric binding pocket, including D3.32 (number denote Ballesteros–Weinstein numbering [44]), responsible for the crucial ionic interaction between opioids and their receptors, show a similar orientation in the generated model as in the template.

'Interaction potential maps' as implemented in MOE v2020.0901 were used to determine putatively relevant water molecules inside the binding site of the KOR (resolution too low to determine co-crystallized waters) and the NOP receptor (homology model without water coordinates; too low resolution in the crystal structure). The interaction potential is an energy-based function that probes water molecules within the protein and calculates the interaction energy between water molecule and protein [66]. For this calculation the KOR binding site was defined as all residues within 4.5 Å around the crystalized ligand MP1104 in the KOR structure (PDB-ID: 6B73). Since the KOR and NOP receptor share a high sequence identity (59%) the same resides were used to define the NOP binding site in the active state homology model. For the NOP receptor crystal structure again, all residues within 4.5 Å around the crystalized ligand C-35 were used.

3.5. Protein-Ligand Docking

The starting conformation of HS-731 (IUPAC name: 2-[(4,5α-epoxy-3-hydroxy-14β-methoxy-17-methylmorphinan-6β-yl)amino]acetic acid) was generated using Corina v3.00 [71,72]. All five opioid receptor structures were protonated at a pH of 7.0 using the protonate 3D function [73] included in MOE (v2020.0901). GOLD v5.2 [74] was used for docking HS-731 into the receptors. The binding site was defined as a 20 Å sphere around the side chain carboxylate C (γC)-atom of D3.32 and restricted to the solvent-accessible surface. Pyramidal nitrogen atoms in the ligand were allowed to flip during the docking process. A total of 30 genetic algorithm runs per receptor structure were performed, generating diverse solutions (the root mean square deviation between docking poses was more than 1.5 Å). The generated binding hypotheses were scored using the GoldScore docking function [75,76]. The search efficiency was held at 100%. A constraint maintaining a maximum distance of 5.5 Å between the nitrogen in the morphinan scaffold and the γC-atom of D3.32 was set to ensure a crucial ionic interaction [41,56,57,77].

The obtained binding poses were energy-minimized in the protein environment using the MMFF94 force field [78] implemented in LigandScout v4.4.3 [79,80]. The binding poses of HS-731 in complex with the MOR, DOR and KOR were visually inspected and filtered according to the reported binding mode of the morphinan scaffold of opioid agonist BU72 co-crystallized with the MOR (PDB-ID: 5C1M [42]) and the morphinan scaffold of the opioid agonist MP1104 co-crystallized with the KOR (PDB-ID: 6B73 [41]). Additionally, MP1104-KOR interactions were used to score the DOR docking results as MP1104 also

exhibits full agonism at the DOR. The relevant interactions are summarized in Table 3. Rescoring of the MOR and KOR clearly identified one docking result as most plausible that was chosen for further evaluation. At the DOR however, several docking results were scored equal. Thus, the pose with the lowest distance between the positively charged nitrogen in the morphinan scaffold and the carboxylate of D3.32 out of the best scored docking results was chosen at the DOR.

Table 3. Ligand–receptor interactions used for rescoring of docking results.

| Interaction | BU72 | MP1104 | | |
	MOR	DOR	KOR	NOP
PI	D149$^{3.32}$	D128$^{3.32}$	D138$^{3.32}$	D130$^{3.32}$
HY	M153$^{3.36}$	M132$^{3.36}$	M142$^{3.36}$	M134$^{3.36}$
HY	V238$^{5.42}$	V217$^{5.42}$	V230$^{5.42}$	I219$^{5.42}$
HY	I298$^{6.51}$	-	-	-
HY	V302$^{6.55}$	V281$^{6.55}$	I294$^{6.55}$	283$^{6.55}$
HY	W320$^{7.35}$	-	-	-
HBA	-	Y129$^{3.33}$	Y139$^{3.33}$	-
HBA/HBD	HOH525/508	HOH101/1301/1302	HOH	HOH

PI, positive ionizable interaction; HY, hydrophobic interaction; HBA, hydrogen bond acceptor; HBD, hydrogen bond donor; HOH refers to water molecules.

None of the crystallized opioid ligands exhibit agonist activity to the NOP receptor, but due to high identity and similarity to the classical opioid receptors (Figure S1) a similar binding mode of HS-731 in all active state opioid receptors was assumed. MP1104 shares the morphinan scaffold of HS-731 and an alignment and superposition of the KOR crystal structure and the NOP receptor homology model revealed the same orientation of the residues that interact with MP1104 in the MP1104-KOR-complex and their NOP receptor equivalent, with the exception of Y131$^{3.33}$. Therefore, the binding poses were evaluated according to the geometry of the other interactions detected in the MP1104-KOR complex (Table 3). For the inactive state NOP receptor (PDB-ID: 5DGH) the orientation and interaction pattern of the cocrystallized ligand C-35 was used to evaluate the docking poses. C-35 only exhibit the crucial ionic interaction towards D130$^{3.32}$ as well as several hydrophobic interactions (to I127$^{3.29}$, I129$^{3.31}$, Y131$^{3.33}$, M134$^{3.36}$, V279$^{6.51}$, V283$^{6.55}$).

3.6. Molecular Dynamics Simulations and Analysis to Evaluate Docking Poses

Five replicates of molecular dynamics (MD) simulations of 100 ns were performed for each receptor-ligand complex. The systems were set up using Maestro v2020-4 [81] and parametrized using the OPLS 2005 force field [82,83]. The MD simulations were performed using Desmond v2020-4 [84]. The protein was placed in a cubic box with 10 Å padding either side to the protein surface filled with TIP4P water molecules [85] and ions (0.15 M NaCl), to ensure isotonic conditions, and was embedded in a 1-palmitoyl-2-oleoylphosphatidylcholine (POPC) bilayer. The membrane placement was carried out according the OPM database (PDB-ID: 5C1M for the MOR, 6PT2 for the DOR, 6B73 for the KOR). The simulation was performed under periodic boundary conditions as an NPγT ensemble, i.e., a constant number of particles, pressure (1.01325 bar), lateral surface tension (0 N/m) and temperature (300 K) throughout the simulation. Each simulation resulted in 1000 system conformations, according to a 100 ps recording interval. VMD v1.9.3 [86] was used to center the protein and to align the trajectory onto the backbone heavy atoms of the starting protein conformation.

For MD simulation analysis, dynamic pharmacophores, so called dynophores [55,87], were calculated. Dynamic pharmacophores encompass pharmacophoric information derived from an ensemble of protein conformations obtained from MD simulations. Interactions are grouped into feature groups according to their interaction type (e.g., lipophilic interaction, hydrogen bond acceptor, hydrogen bond donor). The interaction occurrence over the trajectory of each interaction group is statistically determined and reported as

percentages. The dynophore algorithm is implemented the ilib framework, on which also LigandScout [79,80] is based upon. To assess the quality of interactions occurring during the MD simulations distances between HS-731-COO-(C-atom)-KOR-K227$^{5.39}$ (Nz), HS-731-COO-(C-atom)-DOR-K214$^{5.39}$ (Nz), HS-731-COO-(C-atom)-MOR-K235$^{5.39}$ (Nz) and HS-731-COO-(C-atom)-MOR-K305$^{6.58}$ (Nz), HS-731-COO-(C-atom)–DOR-R291 (Cz), HS-731-COO-(C-atom)-KOR-K200, and HS-731-secundary amine-KOR-E209 (CD) were measured using VMD. The violin plots (Figure 7) representing the distribution of measured distances were generated using the python v3.8.5 [88] packages seaborn v0.11.2 [89] and matplotlib v3.4.3 [90].

4. Conclusions

In this study, we assessed the difference in binding affinity and activity values of the peripheral opioid antinociceptive, HS-731, at the opioid receptors, and generated a binding hypothesis at each opioid receptor subtype. HS-731 shows extensive ionic interactions with the classical opioid receptors, MOR, DOR and KOR, and the differences in the frequency and quality of those interactions mediate differences in the affinity and activity of HS-731 to these receptors. At the MOR, HS-731 forms four ionic interactions over the majority of the MD simulations. At the DOR and KOR, there were only two noteworthy ionic interactions present. A closer examination of the interaction quality facilitated by an interaction distance assessment revealed by far the strongest ionic interactions at the MOR followed by the DOR. The quality at the KOR was much weaker than at the DOR. A salt bridge between K227$^{5.39}$ and E297$^{6.58}$ was observed in about 50% in the case of the KOR. This interaction is likely to cause the KOR to adopt an intermediate-state conformation as supported by the decreased distance between the bottom of TM6 and TM4 as a surrogate parameter for the TM6 translocation and GPCR activation, and therefore could explain the partial agonism of HS-731 to the KOR. The MOR and DOR that did not exhibit TM5-TM6 ionic interactions, and thus were not forced to adopt an intermediate state conformation are able to be fully activated by the agonist HS-731.The present results highlight the importance of ionic interactions for the binding of the 6β-glycine substituted agonist HS-731 to the opioid receptors, and accentuate the non-conserved residue 6.58 and the N-terminus, as important selectivity determinants for the classical opioid receptors. We experimentally demonstrate that HS-731 displayed no substantial binding to the NOP receptor. We surmise that Y131$^{3.33}$ is responsible for this observation, in that it points further into the active state binding pocket than in the classical opioid receptors and prevents HS-731 binding within the orthosteric binding pocket. Furthermore, the hydroxyl group of HS-731 is likely to abolish ligand binding to the NOP receptor in that it mimics the tyrosine within the message address of endogenous peptides for the classical opioid receptors instead of the phenylalanine within the message address of the NOP receptor agonist nociceptin.

In conclusion, our findings offer significant structural insights into HS-731 interactions with the opioid receptors that are important for understanding the pharmacology of this peripheral opioid analgesic.

Supplementary Materials: The following are available online, Figure S1: Sequence identity and similarity among the opioid receptors, Figure S2: Docking pose of HS-731 to the inactive NOP receptor, Figure S3: Root mean square deviation of HS-731 in complex with the MOR over the simulation time, Figure S4: Root mean square deviation of the MOR backbone atoms in complex with HS-731 over the simulation time, Figure S5: Root mean square deviation of HS-731 in complex with the DOR over the simulation time., Figure S6: Root mean square deviation of the DOR backbone atoms in complex with HS-731 over the simulation time, Figure S7: Root mean square deviation of HS-731 in complex with the KOR over the simulation time, Figure S8: Root mean square deviation of the KOR backbone atoms in complex with HS-731 over the simulation time, Figure S9: Comparison of the binding modes of HS-731 at the MOR derived by docking and after MD simulations, Figure S10: Comparison of the binding modes of HS-731 at the DOR derived by docking and after MD simulations. Figure S11: Comparison of the binding modes of HS-731 at the KOR derived by docking

and after MD simulations. Figure S12: Ionic interaction distances. Figure S13: Comparison between the active state KOR and the intermediate state KOR.

References

1.　Waldhoer, M.; Bartlett, S.E.; Whistler, J.L. Opioid receptors. *Annu. Rev. Biochem.* **2004**, *73*, 953–990. [CrossRef] [PubMed]
2.　Stein, C. Opioid receptors. *Annu. Rev. Med.* **2016**, *67*, 433–451. [CrossRef] [PubMed]
3.　Corder, G.; Castro, D.C.; Bruchas, M.R.; Scherrer, G. Endogenous and exogenous opioids in pain. *Annu. Rev. Neurosci.* **2018**, *41*, 453–473. [CrossRef] [PubMed]
4.　Ribeiro, J.M.L.; Filizola, M. Insights From molecular dynamics simulations of a number of G-protein coupled receptor targets for the treatment of pain and opioid use disorders. *Front. Mol. Neurosci.* **2019**, *12*, 207. [CrossRef] [PubMed]
5.　Paul, A.K.; Smith, C.M.; Rahmatullah, M.; Nissapatorn, V.; Wilairatana, P.; Spetea, M.; Gueven, N.; Dietis, N. Opioid analgesia and opioid-induced adverse effects: A review. *Pharmaceuticals* **2021**, *14*, 1091. [CrossRef] [PubMed]
6.　Zierk, K.A. The real antidote: A critical review of U.S. and Canadian drug treatment courts and a call for public health prevention tools as a solution to the opioid epidemic. *Ind. Intl Comp. L. Rev.* **2019**, *29*, 185–217. [CrossRef]
7.　Sobczak, Ł.; Goryński, K. Pharmacological aspects of over-the-counter opioid drugs misuse. *Molecules* **2020**, *25*, 3905. [CrossRef]
8.　Centers for Disease Control and Prevention; National Center for Health Statistics; Office of Communication. Drug Overdose Deaths in the U.S. Top 100,000 Annually. Available online: https://www.cdc.gov/nchs/pressroom/nchs_press_releases/2021/20211117.htm (accessed on 29 November 2021).
9.　Volkow, N.D.; Blanco, C. The changing opioid crisis: Development, challenges and opportunities. *Mol. Psychiatry* **2021**, *26*, 218–233. [CrossRef]
10.　Obeng, S.; Hiranita, T.; León, F.; McMahon, L.R.; McCurdy, C.R. Novel approaches, drug candidates, and targets in pain drug discovery. *J. Med. Chem.* **2021**, *64*, 6523–6548. [CrossRef]
11.　Yekkirala, A.S.; Roberson, D.P.; Bean, B.P.; Woolf, C.J. Breaking barriers to novel analgesic drug development. *Nat. Rev. Drug Discov.* **2017**, *16*, 545–564. [CrossRef]
12.　Günther, T.; Dasgupta, P.; Mann, A.; Miess, E.; Kliewer, A.; Fritzwanker, S.; Steinborn, R.; Schulz, S. Targeting multiple opioid receptors–improved analgesics with reduced side effects? *Br. J. Pharmacol.* **2018**, *175*, 2857–2868. [CrossRef] [PubMed]
13.　Cunningham, C.W.; Elballa, W.M.; Vold, S.U. Bifunctional opioid receptor ligands as novel analgesics. *Neuropharmacology* **2019**, *151*, 195–207. [CrossRef] [PubMed]
14.　Mores, K.L.; Cummins, B.R.; Cassell, R.J.; van Rijn, R.M. A review of the therapeutic potential of recently developed G protein-biased kappa agonists. *Front. Pharmacol.* **2019**, *10*, 407. [CrossRef] [PubMed]
15.　Faouzi, A.; Varga, B.R.; Majumdar, S. Biased opioid ligands. *Molecules* **2020**, *25*, 4257. [CrossRef] [PubMed]
16.　Bermudez, M.; Nguyen, T.N.; Omieczynski, C.; Wolber, G. Strategies for the discovery of biased GPCR ligands. *Drug Discov. Today* **2019**, *24*, 1031–1037. [CrossRef]
17.　Albert-Vartanian, A.; Boyd, M.; Hall, A.; Morgado, S.; Nguyen, E.; Nguyen, V.; Patel, S.; Russo, L.; Shao, A.; Raffa, R. Will peripherally restricted kappa-opioid receptor agonists (pKORAs) relieve pain with less opioid adverse effects and abuse potential? *J. Clin. Pharm. Ther.* **2016**, *41*, 371–382. [CrossRef]

18. Martínez, V.; Abalo, R. Peripherally acting opioid analgesics and peripherally-induced analgesia. *Behav. Pharmacol.* **2020**, *31*, 136–158. [CrossRef]

19. Bidlack, J.M. Detection and function of opioid receptors on cells from the immune system. *Clin. Diagn. Lab.* **2000**, *7*, 719–723. [CrossRef] [PubMed]

20. Holzer, P. Opioids and opioid receptors in the enteric nervous system: From a problem in opioid analgesia to a possible new prokinetic therapy in humans. *Neurosci. Lett.* **2004**, *361*, 192–195. [CrossRef]

21. Machelska, H.; Celik, M.Ö. Advances in achieving opioid analgesia without side effects. *Front. Pharmacol.* **2018**, *9*, 1388. [CrossRef]

22. Beck, T.C.; Hapstack, M.A.; Beck, K.R.; Dix, T.A. Therapeutic potential of kappa opioid agonists. *Pharmaceuticals* **2019**, *12*, 95. [CrossRef] [PubMed]

23. Fürst, S.; Zádori, Z.S.; Zádor, F.; Király, K.; Balogh, M.; László, S.B.; Hutka, B.; Mohammadzadeh, A.; Calabrese, C.; Galambos, A.R. On the role of peripheral sensory and gut mu opioid receptors: Peripheral analgesia and tolerance. *Molecules* **2020**, *25*, 2473. [CrossRef] [PubMed]

24. DeHaven-Hudkins, D.L.; Dolle, R.E. Peripherally restricted opioid agonists as novel analgesic agents. *Curr. Pharm. Des.* **2004**, *10*, 743–757. [CrossRef] [PubMed]

25. Stokbroekx, R.A.; Vandenberk, J.; Van Heertum, A.H.; Van Laar, G.M.; Van der Aa, M.J.; Van Bever, W.F.; Janssen, P.A. Synthetic antidiarrheal agents. 2, 2-Diphenyl-4-(4′-aryl-4′-hydroxypiperidino) butyramides. *J. Med. Chem.* **1973**, *16*, 782–786. [CrossRef] [PubMed]

26. Barber, A.; Bartoszyk, G.; Bender, H.; Gottschlich, R.; Greiner, H.; Harting, J.; Mauler, F.; Minck, K.O.; Murray, R.; Simon, M. A pharmacological profile of the novel, peripherally-selective κ-opioid receptor agonist, EMD 61753. *Br. J. Pharmacol.* **1994**, *113*, 1317–1327. [CrossRef]

27. Spahn, V.; Del Vecchio, G.; Labuz, D.; Rodriguez-Gaztelumendi, A.; Massaly, N.; Temp, J.; Durmaz, V.; Sabri, P.; Reidelbach, M.; Machelska, H. A nontoxic pain killer designed by modeling of pathological receptor conformations. *Science* **2017**, *355*, 966–969. [CrossRef]

28. Schiller, P.W. Opioid peptide-derived analgesics. In *Drug Addiction*, 1st ed.; Rapaka, R.S., Sadée, W., Eds.; Springer: New York, NY, USA, 2008; pp. 357–366.

29. Schütz, J.; Brandt, W.; Spetea, M.; Wurst, K.; Wunder, G.; Schmidhammer, H. Synthesis of 6-amino acid Substituted derivatives of the highly potent analgesic 14-*O*-methyloxymorphone. *Helv. Chim. Acta* **2003**, *86*, 2142–2148. [CrossRef]

30. Spetea, M.; Friedmann, T.; Riba, P.; Schütz, J.; Wunder, G.; Langer, T.; Schmidhammer, H.; Fürst, S. In vitro opioid activity profiles of 6-amino acid substituted derivatives of 14-*O*-methyloxymorphone. *Eur. J. Pharmacol.* **2004**, *483*, 301–308. [CrossRef]

31. Fürst, S.; Riba, P.; Friedmann, T.; Tímar, J.; Al-Khrasani, M.; Obara, I.; Makuch, W.; Spetea, M.; Schütz, J.; Przewlocki, R. Peripheral versus central antinociceptive actions of 6-amino acid-substituted derivatives of 14-*O*-methyloxymorphone in acute and inflammatory pain in the rat. *J. Pharmacol. Exp. Ther.* **2005**, *312*, 609–618. [CrossRef]

32. Bileviciute-Ljungar, I.; Spetea, M.; Guo, Y.; Schütz, J.; Windisch, P.; Schmidhammer, H. Peripherally mediated antinociception of the mu-opioid receptor agonist 2-(4,5alpha-epoxy-3-hydroxy-14beta-methoxy-17-methylmorphinan-6beta-yl)aminoacetic acid (HS-731) after subcutaneous and oral administration in rats with carrageenan-induced hindpaw inflammation. *J. Pharmacol. Exp. Ther.* **2006**, *317*, 220–227. [CrossRef]

33. Obara, I.; Makuch, W.; Spetea, M.; Schütz, J.; Schmidhammer, H.; Przewlocki, R.; Przewlocka, B. Local peripheral antinociceptive effects of 14-*O*-methyloxymorphone derivatives in inflammatory and neuropathic pain in the rat. *Eur. J. Pharmacol.* **2007**, *558*, 60–67. [CrossRef] [PubMed]

34. Al-Khrasani, M.; Spetea, M.; Friedmann, T.; Riba, P.; Király, K.; Schmidhammer, H.; Furst, S. DAMGO and 6β-glycine substituted 14-*O*-methyloxymorphone but not morphine show peripheral, preemptive antinociception after systemic administration in a mouse visceral pain model and high intrinsic efficacy in the isolated rat vas deferens. *Brain Res. Bull.* **2007**, *74*, 369–375. [CrossRef] [PubMed]

35. Spetea, M.; Windisch, P.; Guo, Y.; Bileviciute-Ljungar, I.; Schütz, J.; Asim, M.F.; Berzetei-Gurske, I.P.; Riba, P.; Kiraly, K.; Fürst, S. Synthesis and pharmacological activities of 6-glycine substituted 14-phenylpropoxymorphinans, a novel class of opioids with high opioid receptor affinities and antinociceptive potencies. *J. Med. Chem.* **2011**, *54*, 980–988. [CrossRef]

36. Baillie, L.D.; Schmidhammer, H.; Mulligan, S.J. Peripheral μ-opioid receptor mediated inhibition of calcium signaling and action potential-evoked calcium fluorescent transients in primary afferent CGRP nociceptive terminals. *Neuropharmacology* **2015**, *93*, 267–273. [CrossRef]

37. Spetea, M.; Rief, S.B.; Haddou, T.B.; Fink, M.; Kristeva, E.; Mittendorfer, H.; Haas, S.; Hummer, N.; Follia, V.; Guerrieri, E. Synthesis, biological, and structural explorations of new zwitterionic derivatives of 14-*O*-methyloxymorphone, as potent μ/δ opioid agonists and peripherally selective antinociceptives. *J. Med. Chem.* **2019**, *62*, 641–653. [CrossRef] [PubMed]

38. Botros, S.; Lipkowski, A.; Larson, D.; Stark, P.; Takemori, A.; Portoghese, P.S. Opioid agonist and antagonist activities of peripherally selective derivatives of naltrexamine and oxymorphamine. *J. Med. Chem.* **1989**, *32*, 2068–2071. [CrossRef]

39. Mazak, K.; Noszal, B.; Hosztafi, S. Physicochemical and pharmacological characterization of permanently charged opioids. *Curr. Med. Chem.* **2017**, *24*, 3633–3648. [CrossRef]

40. Zádor, F.; Mohammadzadeh, A.; Balogh, M.; Zádori, Z.S.; Király, K.; Barsi, S.; Galambos, A.R.; László, S.B.; Hutka, B.; Váradi, A.; et al. Comparisons of in vivo and in vitro opioid effects of newly synthesized 14-methoxycodeine-6-*O*-sulfate and codeine-6-*O*-sulfate. *Molecules* **2020**, *25*, 1370. [CrossRef]

41. Che, T.; Majumdar, S.; Zaidi, S.A.; Ondachi, P.; McCorvy, J.D.; Wang, S.; Mosier, P.D.; Uprety, R.; Vardy, E.; Krumm, B.E.; et al. Structure of the nanobody-stabilized active state of the kappa opioid receptor. *Cell* **2018**, *172*, 55–67.e15. [CrossRef]

42. Huang, W.; Manglik, A.; Venkatakrishnan, A.J.; Laeremans, T.; Feinberg, E.N.; Sanborn, A.L.; Kato, H.E.; Livingston, K.E.; Thorsen, T.S.; Kling, R.C.; et al. Structural insights into μ-opioid receptor activation. *Nature* **2015**, *524*, 315–321. [CrossRef]

43. Claff, T.; Yu, J.; Blais, V.; Patel, N.; Martin, C.; Wu, L.; Han, G.W.; Holleran, B.J.; van der Poorten, O.; White, K.L.; et al. Elucidating the active δ-opioid receptor crystal structure with peptide and small-molecule agonists. *Sci. Adv.* **2019**, *5*, eaax9115. [CrossRef] [PubMed]

44. Ballesteros, J.A.; Weinstein, H. Integrated methods for the construction of three-dimensional models and computational probing of structure-function relations in G protein-coupled receptors. In *Methods in Neurosciences*; Academic Press: San Diego, USA; London, UK, 1995; Volume 25, pp. 366–428.

45. Chavkin, C.; McLaughlin, J.P.; Celver, J.P. Regulation of opioid receptor function by chronic agonist exposure: Constitutive activity and desensitization. *Mol. Pharmacol.* **2001**, *60*, 20–25. [CrossRef] [PubMed]

46. Befort, K.; Zilliox, C.; Filliol, D.; Yue, S.; Kieffer, B.L. Constitutive activation of the delta opioid receptor by mutations in transmembrane domains III and VII. *J. Biol. Chem.* **1999**, *274*, 18574–18581. [CrossRef] [PubMed]

47. Décaillot, F.M.; Befort, K.; Filliol, D.; Yue, S.; Walker, P.; Kieffer, B.L. Opioid receptor random mutagenesis reveals a mechanism for G protein-coupled receptor activation. *Nat. Struct. Biol.* **2003**, *10*, 629–636. [CrossRef]

48. Váradi, A.; Marrone, G.F.; Eans, S.O.; Ganno, M.L.; Subrath, J.J.; Le Rouzic, V.; Hunkele, A.; Pasternak, G.W.; McLaughlin, J.P.; Majumdar, S. Synthesis and characterization of a dual kappa-delta opioid receptor agonist analgesic blocking cocaine reward behavior. *ACS Chem. Neurosci.* **2015**, *6*, 1813–1824. [CrossRef]

49. Saleh, A.H.; Abdelwaly, A.; Darwish, K.M.; Eissa, A.A.H.M.; Chittiboyina, A.; Helal, M.A. Deciphering the molecular basis of the kappa opioid receptor selectivity: A molecular dynamics study. *J. Mol. Graph. Model.* **2021**, *106*, 107940. [CrossRef]

50. Akuzawa, N.; Takeda, S.; Ishiguro, M. Structural modelling and mutation analysis of a nociceptin receptor and its ligand complexes. *J. Biochem.* **2007**, *141*, 907–916. [CrossRef]

51. Thompson, A.A.; Liu, W.; Chun, E.; Katritch, V.; Wu, H.; Vardy, E.; Huang, X.-P.; Trapella, C.; Guerrini, R.; Calo, G.; et al. Structure of the nociceptin/orphanin FQ receptor in complex with a peptide mimetic. *Nature* **2012**, *485*, 395–399. [CrossRef]

52. Miller, R.L.; Thompson, A.A.; Trapella, C.; Guerrini, R.; Malfacini, D.; Patel, N.; Han, G.W.; Cherezov, V.; Caló, G.; Katritch, V.; et al. The importance of ligand-receptor conformational pairs in stabilization: Spotlight on the N/OFQ G protein-coupled receptor. *Structure* **2015**, *23*, 2291–2299. [CrossRef]

53. Mustazza, C.; Bastanzio, G. Development of nociceptin receptor (NOP) agonists and antagonists. *Med. Res. Rev.* **2011**, *31*, 605–648. [CrossRef]

54. Meunier, J.-C.; Mouledous, L.; Topham, C.M. The nociceptin (ORL1) receptor: Molecular cloning and functional architecture. *Peptides* **2000**, *21*, 893–900. [CrossRef]

55. Sydow, D. *Dynophores: Novel Dynamic Pharmacophores Implementation of Pharmacophore Generation Based on Molecular Dynamics Trajectories and Their Graphical Representation*; Freie Universität Berlin: Berlin, Germany, 2015.

56. Wu, H.; Wacker, D.; Mileni, M.; Katritch, V.; Han, G.W.; Vardy, E.; Liu, W.; Thompson, A.A.; Huang, X.-P.; Carroll, F.I.; et al. Structure of the human κ-opioid receptor in complex with JDTic. *Nature* **2012**, *485*, 327–332. [CrossRef] [PubMed]

57. Fenalti, G.; Zatsepin, N.A.; Betti, C.; Giguere, P.; Han, G.W.; Ishchenko, A.; Liu, W.; Guillemyn, K.; Zhang, H.; James, D.; et al. Structural basis for bifunctional peptide recognition at human δ-opioid receptor. *Nat. Struct. Mol. Biol.* **2015**, *22*, 265–268. [CrossRef] [PubMed]

58. Lee, K.K.; Fitch, C.A.; García-Moreno E., B. Distance dependence and salt sensitivity of pairwise, coulombic interactions in a protein. *Protein Sci.* **2002**, *11*, 1004–1016. [CrossRef]

59. Vardy, E.; Mosier, P.D.; Frankowski, K.J.; Wu, H.; Katritch, V.; Westkaemper, R.B.; Aubé, J.; Stevens, R.C.; Roth, B.L. Chemotype-selective modes of action of κ-opioid receptor agonists. *J. Biol. Chem.* **2013**, *288*, 34470–34483. [CrossRef] [PubMed]

60. Che, T.; English, J.; Krumm, B.E.; Kim, K.; Pardon, E.; Olsen, R.H.J.; Wang, S.; Zhang, S.; Diberto, J.F.; Sciaky, N.; et al. Nanobody-enabled monitoring of kappa opioid receptor states. *Nat. Commun.* **2020**, *11*, 1145. [CrossRef] [PubMed]

61. Wacker, D.; Wang, C.; Katritch, V.; Han, G.W.; Huang, X.-P.; Vardy, E.; McCorvy, J.D.; Jiang, Y.; Chu, M.; Siu, F.Y.; et al. Structural features for functional selectivity at serotonin receptors. *Science (New York, N.Y.)* **2013**, *340*, 615–619. [CrossRef]

62. Dumitrascuta, M.; Bermudez, M.; Trovato, O.; Neve, J.D.; Ballet, S.; Wolber, G.; Spetea, M. Antinociceptive efficacy of the μ-opioid/nociceptin peptide-based hybrid KGNOP1 in inflammatory pain without rewarding effects in mice: An experimental assessment and molecular docking. *Molecules* **2021**, *26*, 3267. [CrossRef] [PubMed]

63. Bradford, M.M. A rapid and sensitive method for the quantitation of microgram quantities of protein utilizing the principle of protein-dye binding. *Anal. Biochem.* **1976**, *72*, 248–254. [CrossRef]

64. Cheng, Y.-C.; Prusoff, W.H. Relationship between the inhibition constant (KI) and the concentration of inhibitor which causes 50 per cent inhibition (I50) of an enzymatic reaction. *Biochem. Pharmacol.* **1973**, *22*, 3099–3108. [CrossRef]

65. Berman, H.; Henrick, K.; Nakamura, H. Announcing the worldwide Protein Data Bank. *Nat. Struct. Biol.* **2003**, *10*, 980. [CrossRef] [PubMed]

66. Molecular Operating Environment (MOE). *Molecular Operating Environment (MOE), C.C.G.U.* Sherbooke St. West, Suite #910, Montreal, QC, Canada, H3A 2R7. 2021. Available online: https://www.chemcomp.com/Products.htm (accessed on 29 November 2021).

67. The UniProt Consortium. UniProt: The universal protein knowledgebase in 2021. *Nucleic Acids Res.* **2021**, *49*, D480–D489. [CrossRef] [PubMed]

68. Ramachandran, G.N.; Ramakrishnan, C.; Sasisekharan, V. Stereochemistry of polypeptide chain configurations. *J. Mol. Biol.* **1963**, *7*, 95–99. [CrossRef]

69. Zhu, S. Validation of the generalized force fields GAFF, CGenFF, OPLS-AA, and PRODRGFF by testing against experimental osmotic coefficient data for small drug-Like molecules. *J. Chem. Inf. Model.* **2019**, *59*, 4239–4247. [CrossRef] [PubMed]

70. Bermudez, M.; Rakers, C.; Wolber, G. Structural characteristics of the allosteric binding site represent a key to subtype selective modulators of muscarinic acetylcholine receptors. *Mol. Inform.* **2015**, *34*, 526–530. [CrossRef] [PubMed]

71. 3D Structure Generator CORINA Classic. Available online: https://mn-am.com/products/corina/ (accessed on 2 April 2021).

72. Gasteiger, J.; Rudolph, C.; Sadowski, J. Automatic generation of 3D-atomic coordinates for organic molecules. *Tetrahedron Comput. Methodol.* **1990**, *3*, 537–547. [CrossRef]

73. Labute, P. Protonate3D: Assignment of ionization states and hydrogen coordinates to macromolecular structures. *Proteins* **2009**, *75*, 187–205. [CrossRef]

74. Jones, G.; Willett, P.; Glen, R.C.; Leach, A.R.; Taylor, R. Development and validation of a genetic algorithm for flexible docking. *J. Mol. Biol.* **1997**, *267*, 727–748. [CrossRef]

75. Evers, A.; Hessler, G.; Matter, H.; Klabunde, T. Virtual screening of biogenic amine-binding G-protein coupled receptors: Comparative evaluation of protein- and ligand-based virtual screening protocols. *J. Med. Chem.* **2005**, *48*, 5448–5465. [CrossRef]

76. Verdonk, M.L.; Cole, J.C.; Hartshorn, M.J.; Murray, C.W.; Taylor, R.D. Improved protein-ligand docking using GOLD. *Proteins* **2003**, *52*, 609–623. [CrossRef]

77. Vo, Q.N.; Mahinthichaichan, P.; Shen, J.; Ellis, C.R. How μ-opioid receptor recognizes fentanyl. *Nat. Commun.* **2021**, *12*, 984. [CrossRef] [PubMed]

78. Halgren, T.A. Merck molecular force field. I. Basis, form, scope, parameterization, and performance of MMFF94. *J. Comput. Chem.* **1996**, *17*, 490–519. [CrossRef]

79. Wolber, G.; Dornhofer, A.A.; Langer, T. Efficient overlay of small organic molecules using 3D pharmacophores. *J. Comput. Aided Mol. Des.* **2006**, *20*, 773–788. [CrossRef] [PubMed]

80. Wolber, G.; Langer, T. LigandScout: 3-D pharmacophores derived from protein-bound ligands and their use as virtual screening filters. *J. Chem. Inf. Model.* **2005**, *45*, 160–169. [CrossRef]

81. *Schrödinger Release -4: Maestro, version Release -4*; Schrödinger, LLC: New York, NY, USA, 2020.

82. Jorgensen, W.L.; Maxwell, D.S.; Tirado-Rives, J. Development and Testing of the OPLS all-atom force field on conformational energetics and properties of organic liquids. *J. Am. Chem. Soc.* **1996**, *118*, 11225–11236. [CrossRef]

83. Ponder, J.W.; Case, D.A. Force fields for protein simulations. In *Advances in Protein Chemistry*; Academic Press: Cambridge, MA, USA, 2003; Volume 66, pp. 27–85.

84. Bowers, K.J.; Chow, E.; Xu, H.; Dror, R.O.; Eastwood, M.P.; Gregersen, B.A.; Klepeis, J.L.; Kolossvary, I.; Moraes, M.A.; Sacerdoti, F.D.; et al. Scalable algorithms for molecular dynamics simulations on commodity clusters. In Proceedings of the Proceedings of the ACM/IEEE Conference on Supercomputing (SC06), Tampa, FL, USA, 11–17 November 2006.

85. Jorgensen, W.L.; Chandrasekhar, J.; Madura, J.D.; Impey, R.W.; Klein, M.L. Comparison of simple potential functions for simulating liquid water. *J. Chem. Phys.* **1983**, *79*, 926–935. [CrossRef]

86. Humphrey, W.; Dalke, A.; Schulten, K. VMD: Visual molecular dynamics. *J. Mol. Graph.* **1996**, *14*, 33–38. [CrossRef]

87. Bock, A.; Bermudez, M.; Krebs, F.; Matera, C.; Chirinda, B.; Sydow, D.; Dallanoce, C.; Holzgrabe, U.; Amici, M.d.; Lohse, M.J.; et al. Ligand binding ensembles determine graded agonist efficacies at a G protein-coupled receptor. *J. Biol. Chem.* **2016**, *291*, 16375–16389. [CrossRef]

88. van Rossum, G.; Drake, F. *Python 3 Reference Manual*; CreateSpace: Scotts Valley, CA, USA, 2009.

89. Waskom, M. Seaborn: Statistical data visualization. *J. Open Source Softw.* **2021**, *6*, 3021. [CrossRef]

90. Hunter, J.D. Matplotlib: A 2D Graphics environment. *Comput. Sci. Eng.* **2007**, *9*, 90–95. [CrossRef]

Supplementary Materials

Mechanistic characterization of the pharmacological profile of HS-731, a peripherally acting opioid analgesic, at the μ-, δ-, κ-opioid and nociceptin receptors

Kristina Puls [1], Helmut Schmidhammer [2], Gerhard Wolber [1,*] and Mariana Spetea [2,*]

[1] Department of Pharmaceutical Chemistry, Institute of Pharmacy, Freie Universität Berlin; Königin-Luise-Str. 2+4, D-14195 Berlin, Germany; kristina.puls@fu-berlin.de (K.P.), gerhard.wolber@fu-berlin.de (G.W.)

[2] Department of Pharmaceutical Chemistry, Institute of Pharmacy and Center for Molecular Biosciences Innsbruck (CMBI), University of Innsbruck, Innrain 80-82, 6020 Innsbruck, Austria; mariana.spetea@uibk.ac.at (M.S.); helmut.schmidhammer@uibk.ac.at (H.S.)

* Correspondence: gerhard.wolber@fu-berlin.de (G.W.), Tel.: +49 30 838 52686; mariana.spetea@uibk.ac.at (M.S.), Tel.: +43 512 507 58277

Figure S1. Sequence identity and similarity among the opioid receptors (On the left identity, on the right similarity. Values were measured for the truncated sequences corresponding to residues 35 to 330 of the NOP receptor. The darker the box, the higher the identity or similarity.
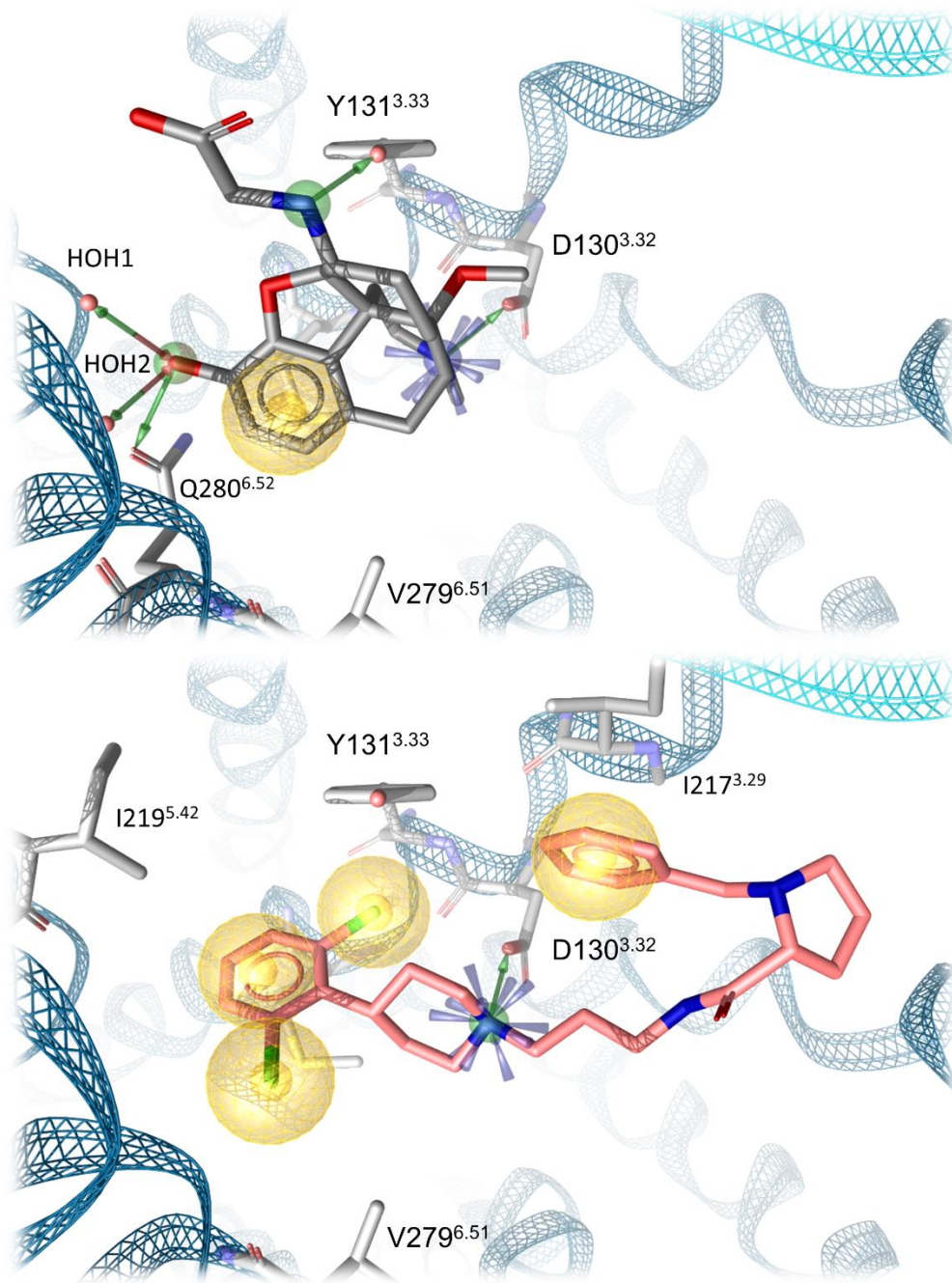
Figure S2: Docking of HS-731 to the inactive NOP receptor. Top: Implausible HS-731 conformation from unsuccessful docking experiments in PDB-ID 5DHG explaining experimental results. Bottom: Co-crystallized antagonist C-35 from 5DHG illustrating a plausible binding mode for this compound class for comparison. Blue stars indicate positive charge interactions, yellow spheres lipophilic contacts, green arrow hydrogen bond donors and red arrows hydrogen bond acceptors. Water molecules are depicted as red spheres.
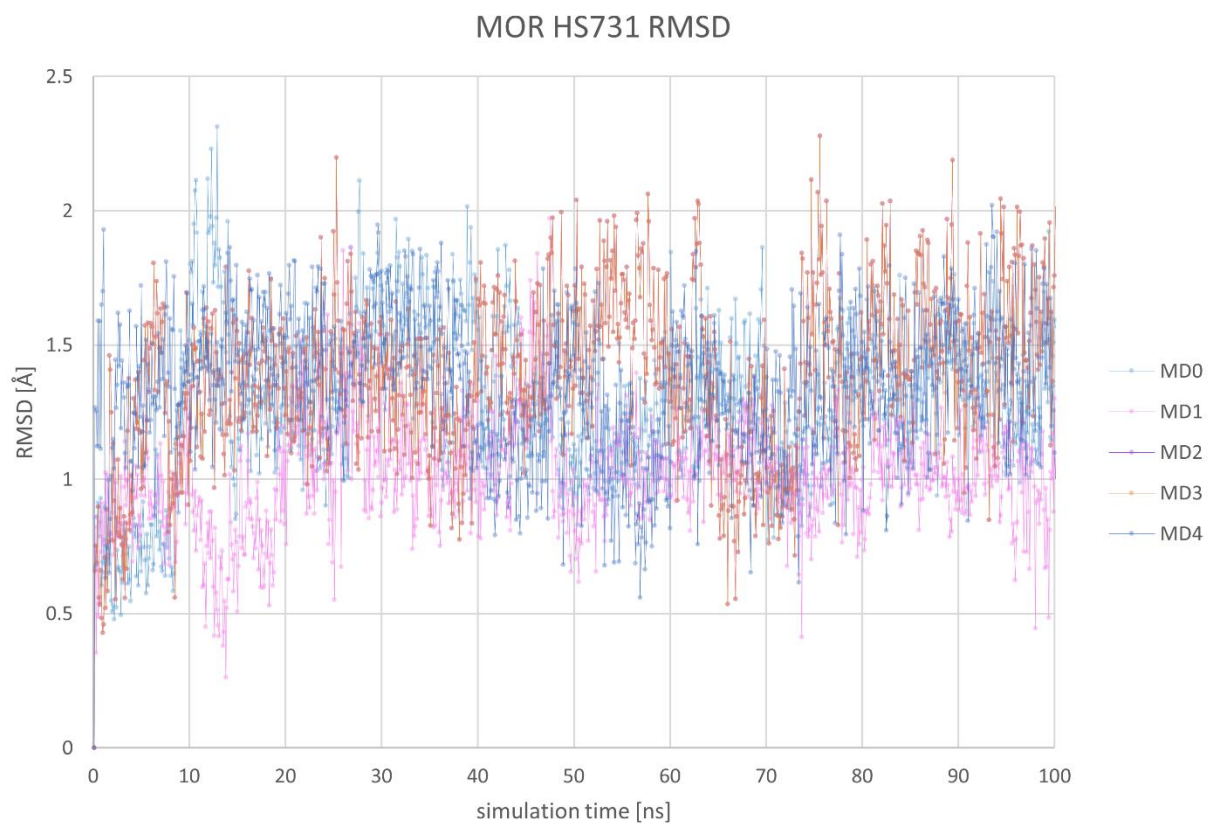
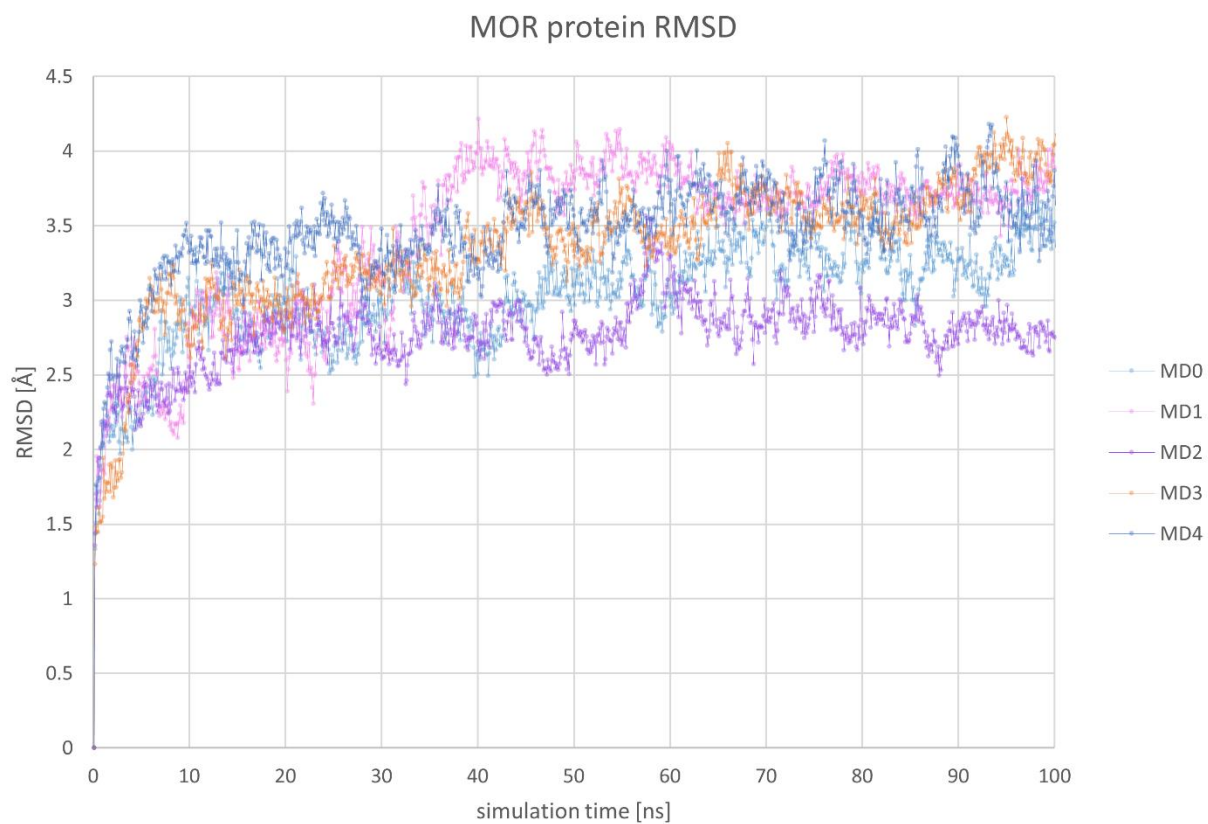**Figure S3.** Root mean square deviation of HS-731 in complex with the MOR over the simulation time.

Figure S4. Root mean square deviation of the MOR backbone atoms in complex with HS-731 over the simulation time.
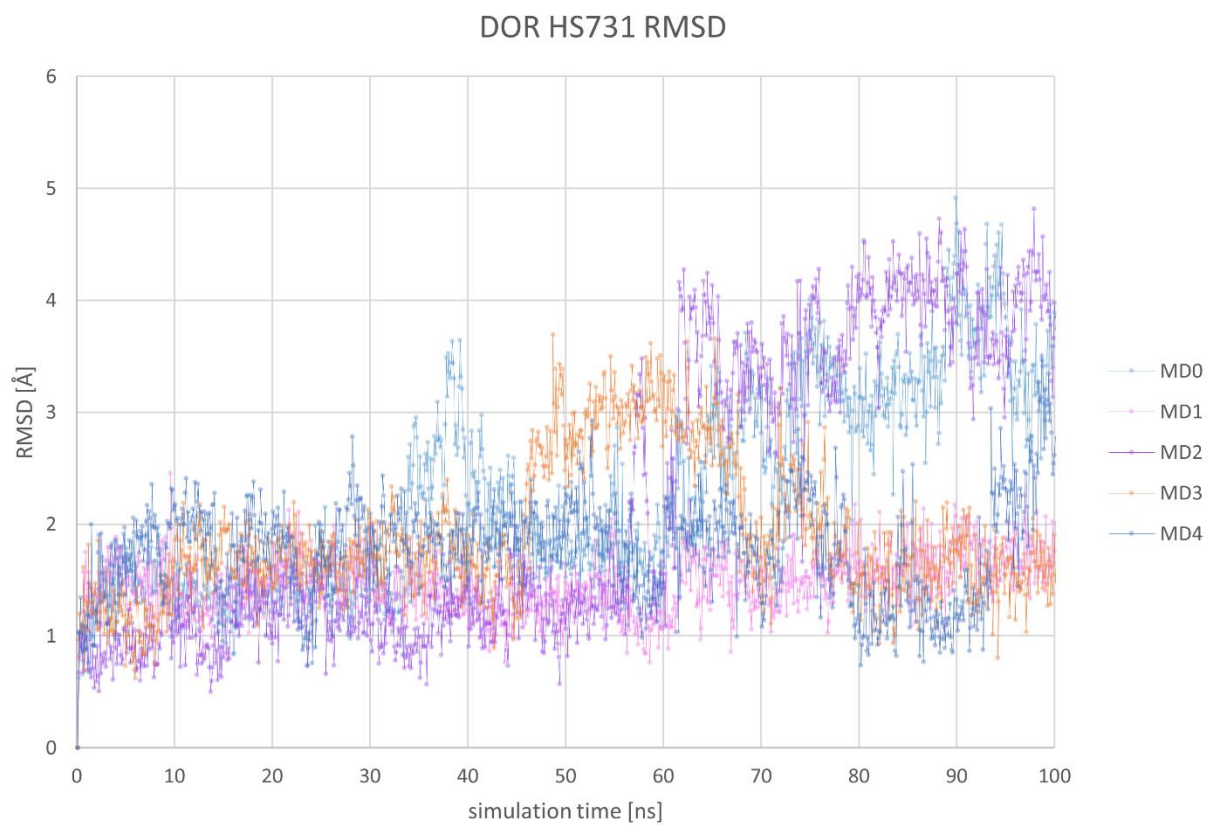
Figure S5. Root mean square deviation of HS-731 in complex with the DOR over the simulation time.
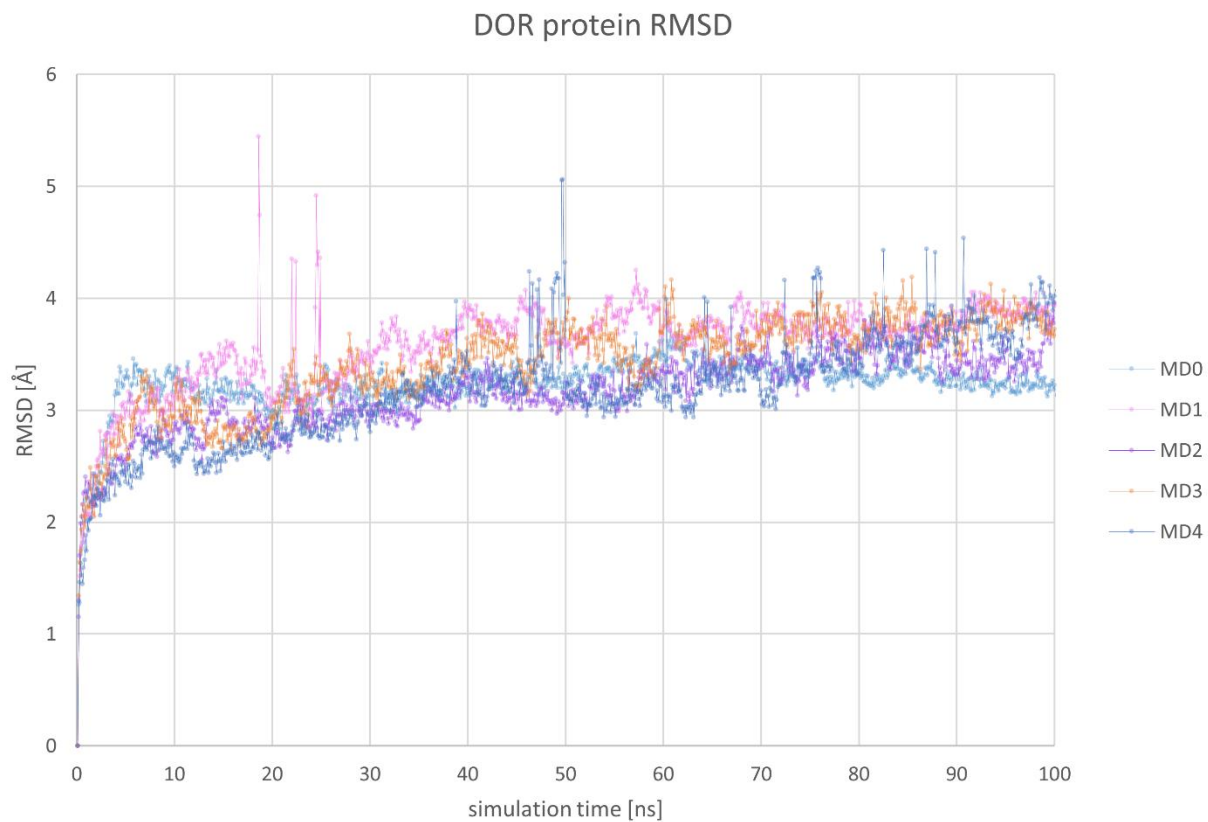
Figure S6. Root mean square deviation of the DOR backbone atoms in complex with HS-731 over the simulation time.
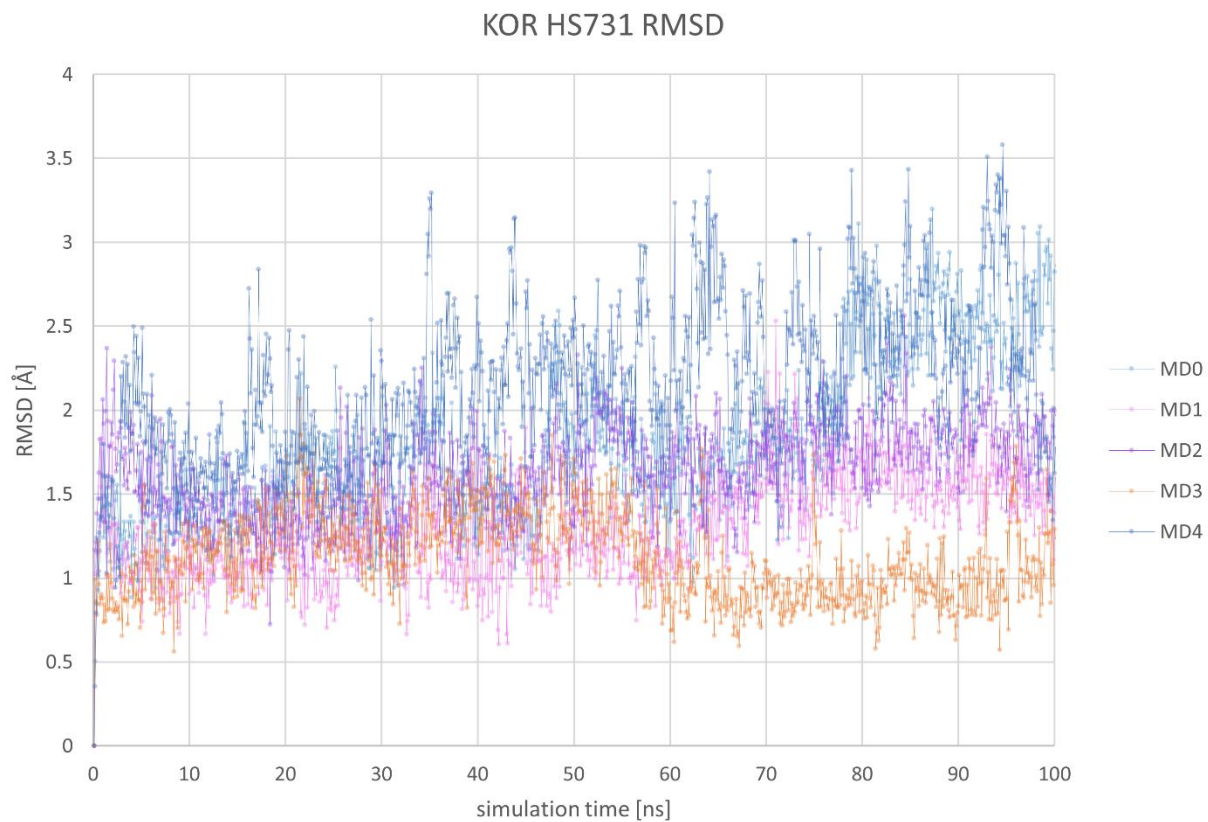
Figure S7. Root mean square deviation of HS-731 in complex with the KOR over the simulation time.
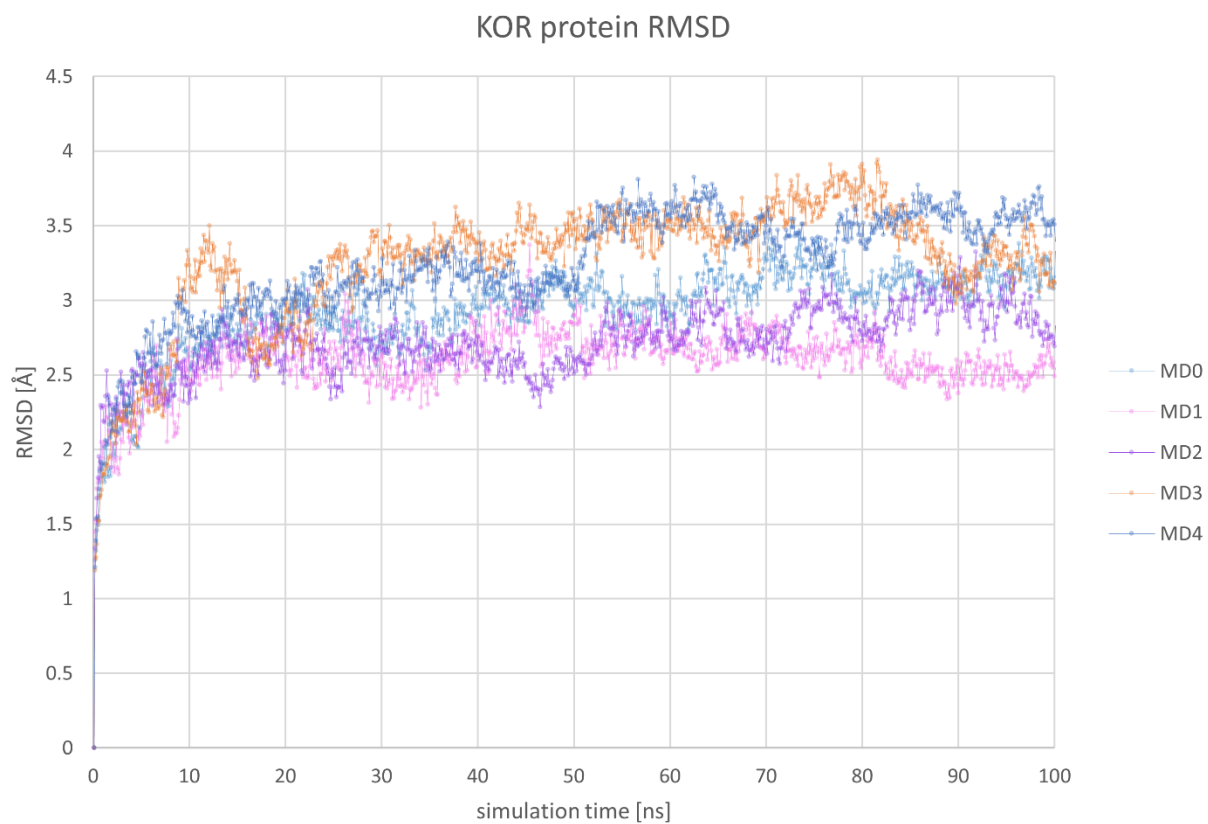
Figure S8. Root mean square deviation of the KOR backbone atoms in complex with HS-731 over the simulation time.

Figure S9. Comparison of the binding modes of HS-731 at the MOR derived by docking (A) and after molecular dynamics (MD) simulations (B-F). The order of the five MD simulation replicas is the following: (B) MD0, (C) MD1, (D) MD2, (E) MD3, and (F) MD4.

Figure S10. Comparison of the binding modes of HS-731 at the DOR derived by docking (A) and after molecular dynamics (MD) simulations (B-F). The order of the five MD simulation replicas is the following: (B) MD0, (C) MD1, (D) MD2, (E) MD3, and (F) MD4.
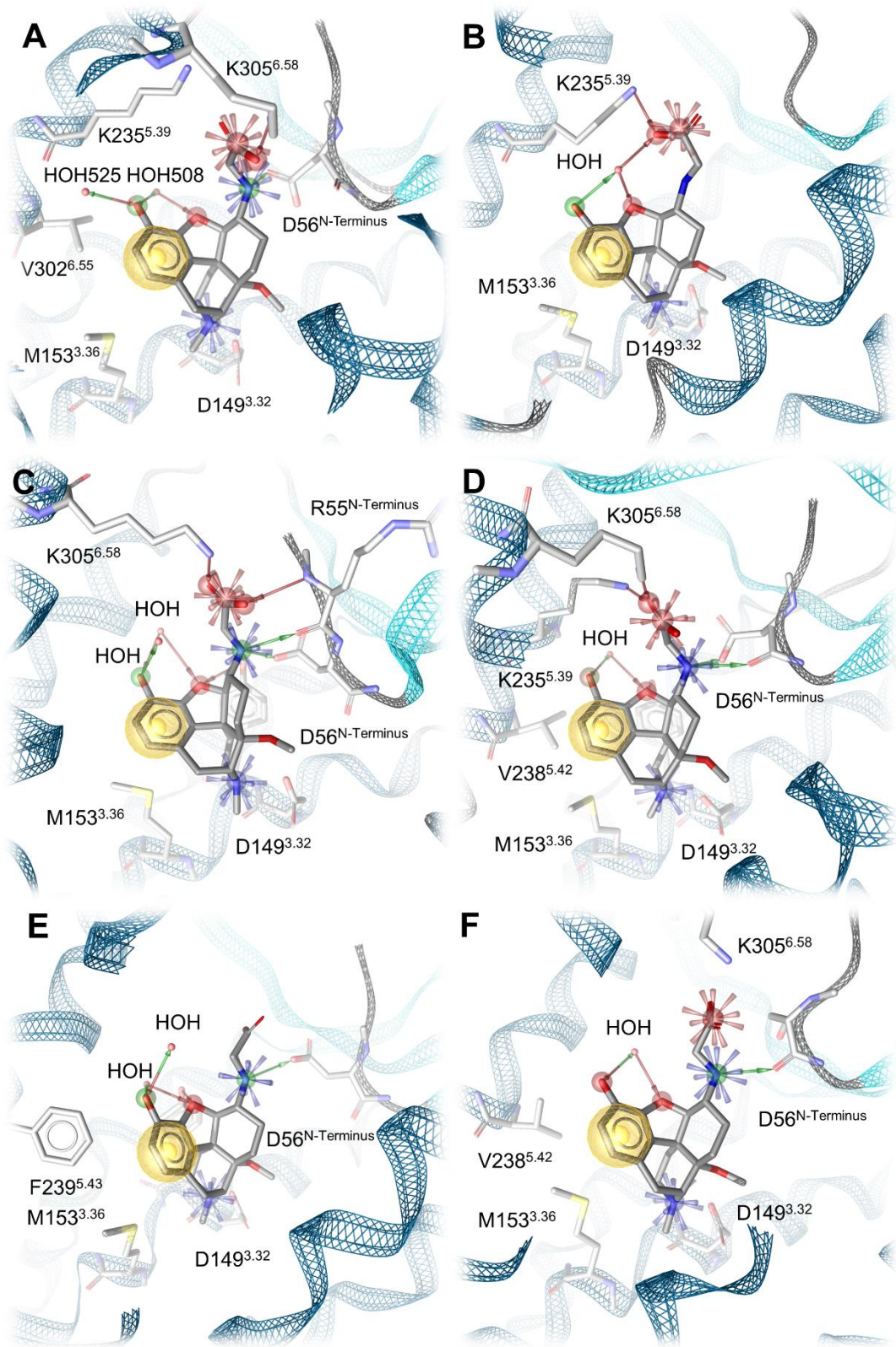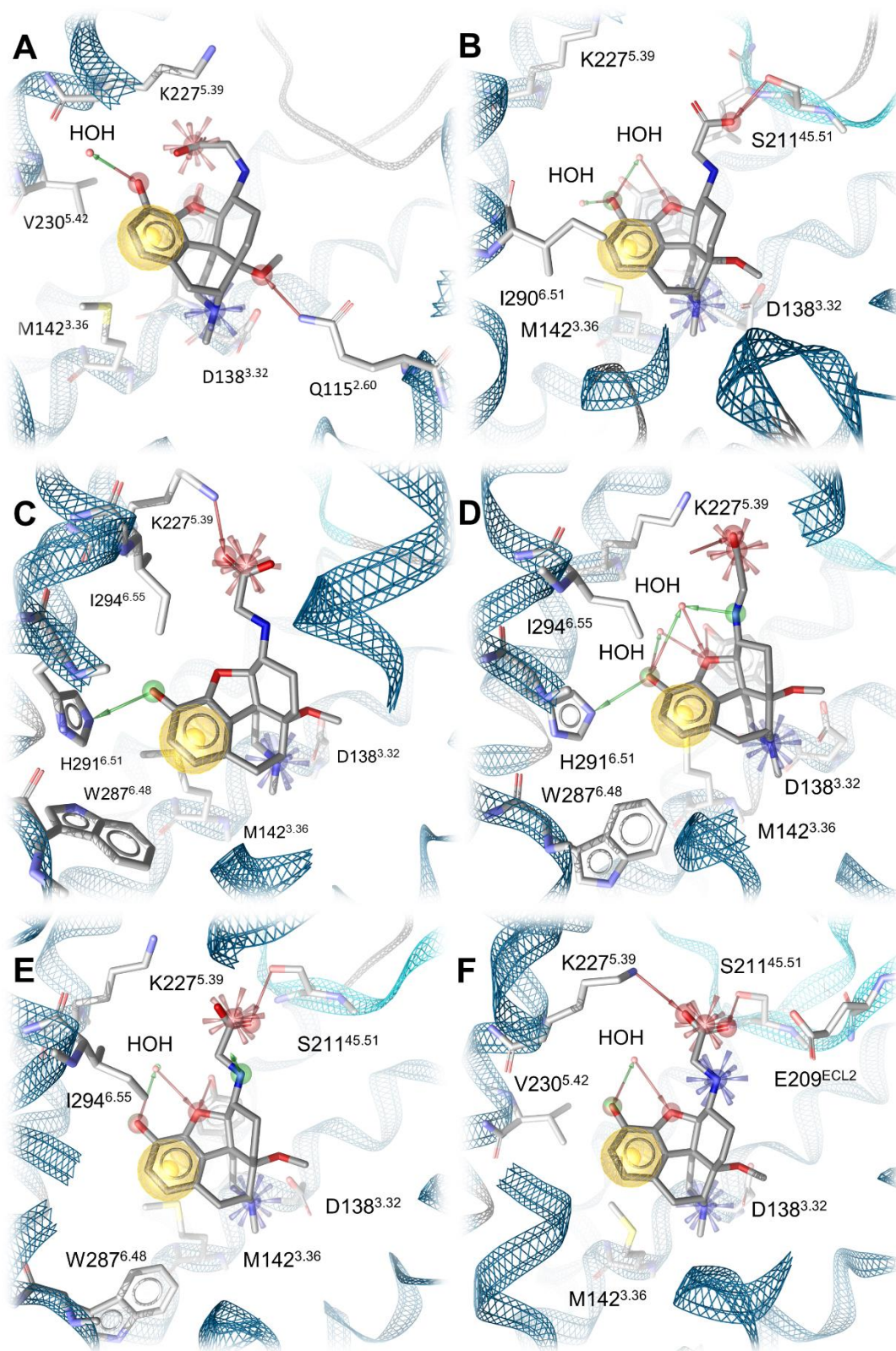
Figure S11. Comparison of the binding modes of HS-731 at the KOR derived by docking (A) and after molecular dynamics (MD) simulations (B-F). The order of the five MD simulation replicas is the following: (B) MD0, (C) MD1, (D) MD2, (E) MD3, and (F) MD4.
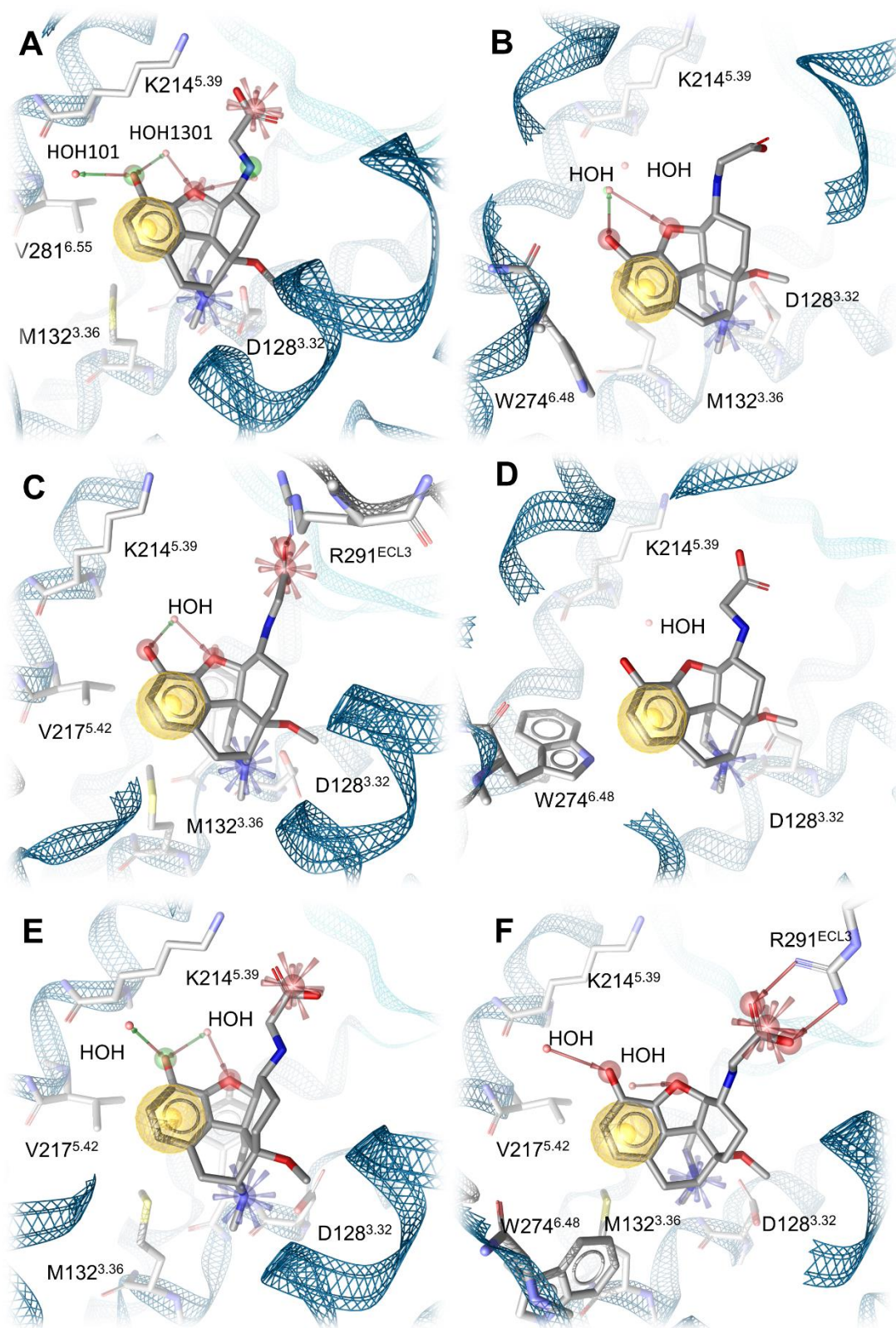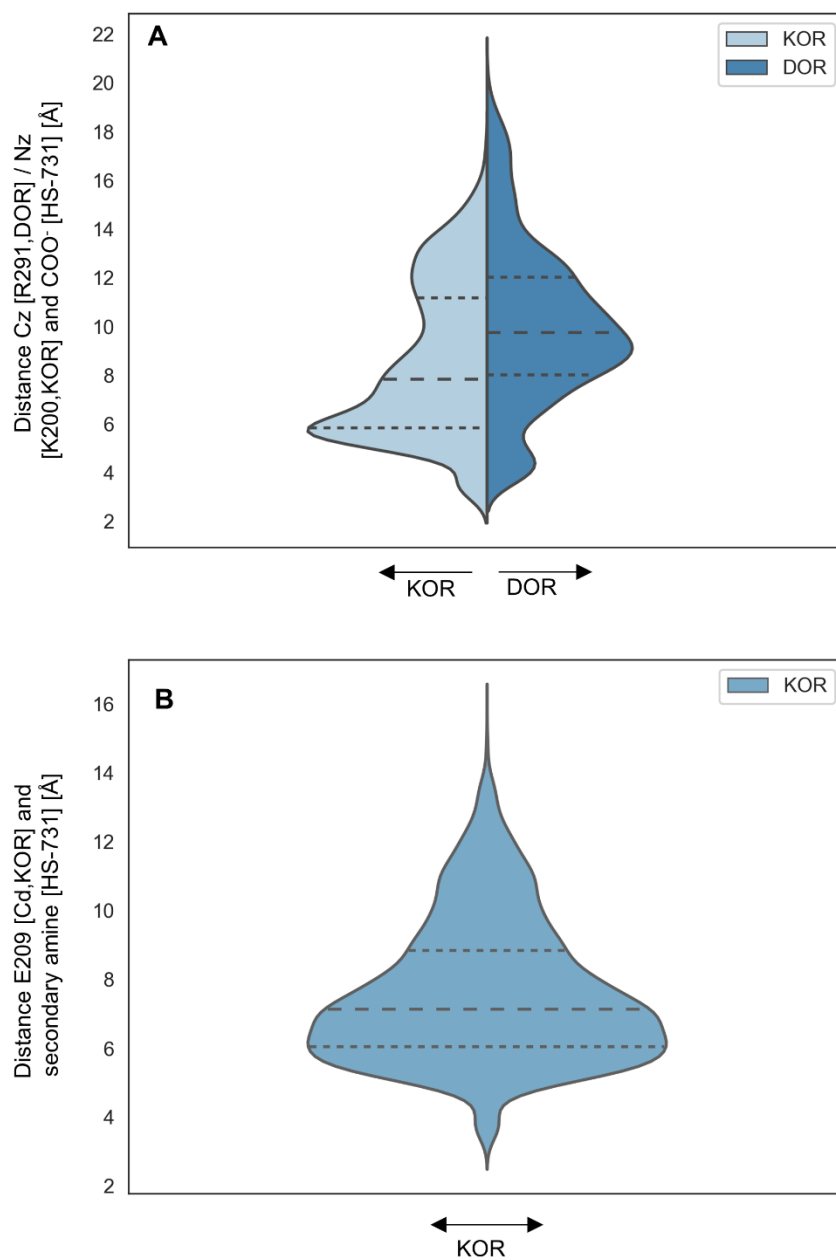
Figure S12. Ionic interaction distances. (A) Distances between R291[ECL3] (Cz, DOR) or K200[ECL2] (KOR) and the carboxylate moiety of HS-731. (B) Distances between E209 ECL2 (Cd, KOR) and the secondary amine of HS-731. Dashed lines represent quantile. The width of the plot corresponds to the frequency of the measured distance.
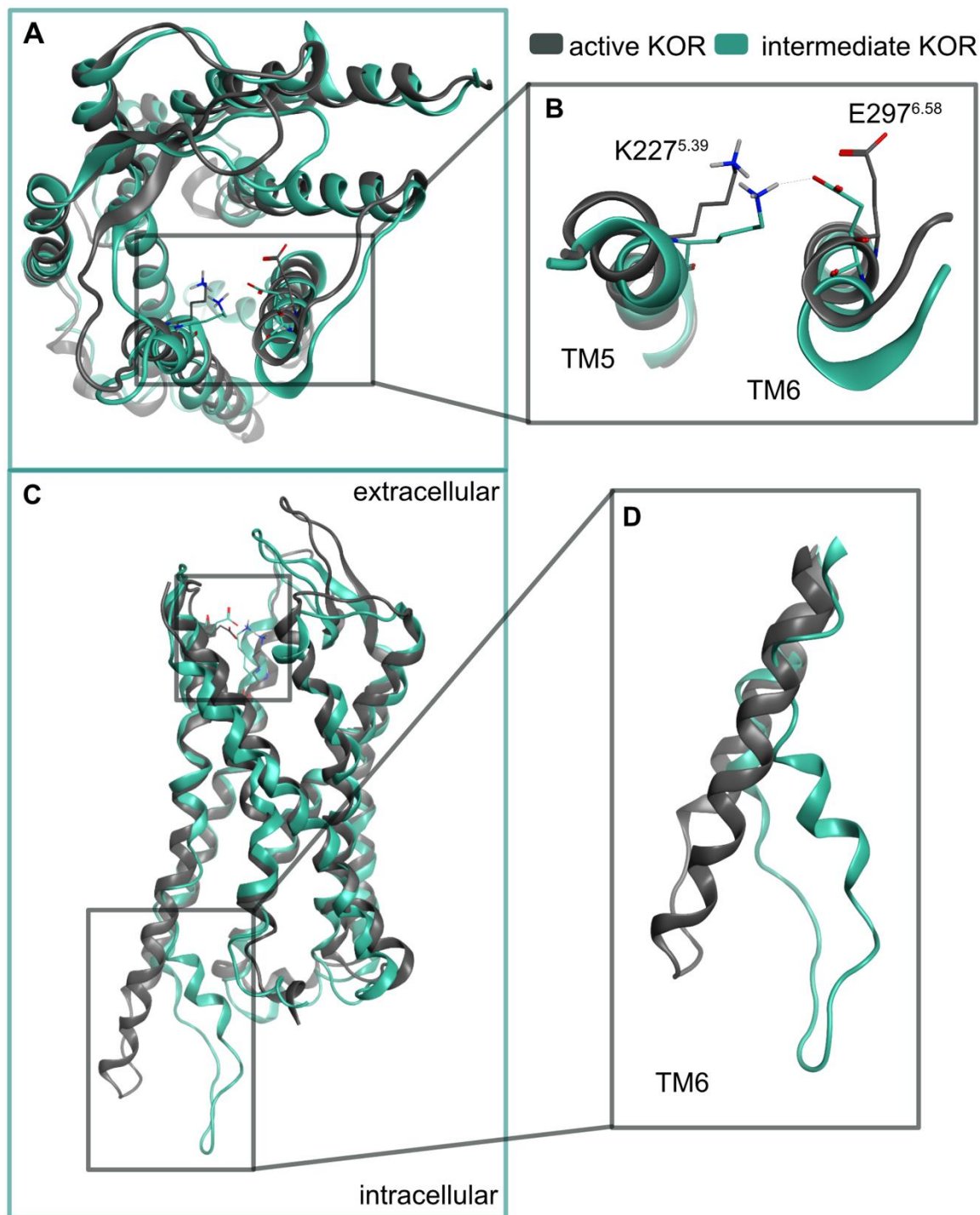
Figure S13. Comparison between the active state KOR (PDB-ID: 6B73, grey) and the intermediate state KOR (turquoise). An intermediate state KOR conformation shown is an example of an ensemble of intermediate state conformations. The intermediate state is characterized by a decreased TM6 outward movement. A) Extracellular view. B) Interaction between E297$^{6.58}$ and K227$^{5.39}$. An ionic interaction is only detectable in the intermediate state KOR but not in the active state KOR. C) Transmembrane view. Upper square depict the location of the ionic interaction also shown in B. D) The intermediate state KOR shows a pronounced inward movement of TM6 while the active state KOR exhibit a TM6 outward movement.

4.2. *In Vitro*, *In Vivo* and *In Silico* Characterization of a Novel Kappa-Opioid Receptor Antagonist [Article B]

Opioid receptors are involved in mood homeostasis. KOR antagonists represent interesting and promising novel therapeutics for the treatment of depression. However, the development of selective and short-acting KOR antagonists as antidepressants is still in its early stages. Compound A is a natural product found to be a MOR antagonist but its activation profile at the remaining opioid receptors remains elusive.

In this study, we conducted detailed *in vitro*, *in vivo*, and *in silico* analysis to reveal the pharmacological activation profile of Compound A at the KOR, and DOR and to explain the observed affinity differences at the classical opioid receptors (KOR, MOR; DOR). We found Compound A to be a KOR antagonist lacking affinity towards DOR. Docking experiments, MD simulations, and dynophore analysis revealed the formation of a halogen bond between Compound A and KOR which is missing the MOR to be responsible for the improved affinity at KOR compared to MOR. We identified the non-conserved residue K2.63 at DOR to prevent Compound A from binding in an analogous manner as in KOR and MOR. K2.63 in DOR is bulkier than V2.63 in KOR and N2.63 in MOR and points inside the binding side which in turn narrows the binding site volume.

Contribution:

Conceptual design (70 %)

Computational experiments (100 %)

Visualization (70 %)

Manuscript preparation (70 %)

In vitro experiments were conducted at Mariana Spetea's lab. I planned and performed the *in silico* experiments and wrote the manuscript excluding the *in vitro* results.

Article

In Vitro, In Vivo and In Silico Characterization of a Novel Kappa-Opioid Receptor Antagonist

Kristina Puls [1,†] , Aina-Leonor Olivé-Marti [2,†] , Szymon Pach [1] , Birgit Pinter [2], Filippo Erli [2], Gerhard Wolber [1,*] and Mariana Spetea [2,*]

[1] Department of Pharmaceutical Chemistry, Institute of Pharmacy, Freie Universität Berlin, Königin-Luise-Str. 2-4, 14195 Berlin, Germany; kristina.puls@fu-berlin.de (K.P.); s.pach@fu-berlin.de (S.P.)

[2] Department of Pharmaceutical Chemistry, Institute of Pharmacy and Center for Molecular Biosciences Innsbruck (CMBI), University of Innsbruck, Innrain 80-82, 6020 Innsbruck, Austria; aina-leonor.olive-marti@uibk.ac.at (A.-L.O.-M.); birgit-pinter@gmax.at (B.P.); f.erli@hotmail.it (F.E.)

* Correspondence: gerhard.wolber@fu-berlin.de (G.W.); mariana.spetea@uibk.ac.at (M.S.); Tel.: +49-30-838-52686 (G.W.); +43-512-507-58277 (M.S.)

† These authors contributed equally to this work.

Abstract: Kappa-opioid receptor (KOR) antagonists are promising innovative therapeutics for the treatment of the central nervous system (CNS) disorders. The new scaffold opioid ligand, Compound A, was originally found as a mu-opioid receptor (MOR) antagonist but its binding/selectivity and activation profile at the KOR and delta-opioid receptor (DOR) remain elusive. In this study, we present an in vitro, in vivo and in silico characterization of Compound A by revealing this ligand as a KOR antagonist in vitro and in vivo. In the radioligand competitive binding assay, Compound A bound at the human KOR, albeit with moderate affinity, but with increased affinity than to the human MOR and without specific binding at the human DOR, thus displaying a preferential KOR selectivity profile. Following subcutaneous administration in mice, Compound A effectively reverse the antinociceptive effects of the prototypical KOR agonist, U50,488. In silico investigations were carried out to assess the structural determinants responsible for opioid receptor subtype selectivity of Compound A. Molecular docking, molecular dynamics simulations and dynamic pharmacophore (dynophore) generation revealed differences in the stabilization of the chlorophenyl moiety of Compound A within the opioid receptor binding pockets, rationalizing the experimentally determined binding affinity values. This new chemotype bears the potential for favorable ADMET properties and holds promise for chemical optimization toward the development of potential therapeutics.

Keywords: GPCRs; kappa-opioid receptor; antagonists; binding affinity; selectivity; in vivo antagonism; molecular docking; molecular dynamics simulations; dynophores

1. Introduction

Opioid receptors belong to the large family of G protein-coupled receptors (GPCRs) [1]. GPCRs are membrane-embedded receptors that share a seven-transmembrane (7TM) helical structure and elicit a myriad of biological activities upon activation by endogenous or exogenous ligands [2–4]. Thus, GPCRs are widely addressed targets for drug development with around one-third of all approved drugs targeting GPCRs [5]. To date, the human opioid receptor family consists of four receptor subtypes, namely, the kappa-, mu- and delta-opioid receptors (KOR, MOR and DOR, respectively), and the non-classical nociceptin/orphanin FQ peptide (NOP) receptor [1,6]. Opioid receptors have a distinct expression pattern throughout the central and peripheral nervous systems (CNS and PNS) and are involved in the regulation of pain, response to stress, reward processing and regulation of mood states, among many other functions [1,6–9].

Over many years, the MOR has been the main pharmacological target for effective pain relief and treatment of other pathophysiological conditions, such as drug addiction

and gastrointestinal motility disorders [1,10–12]. However, the MOR is also the target of the most misused and abused opioid drugs, resulting in an ongoing and rapidly emerging opioid epidemic worldwide [13,14]. Therefore, the KOR has recently gained increased attention as a prominent GPCR in the pursuit of novel pharmacotherapies for a variety of human diseases, due to its role in mediating many physiological and pathophysiological responses [15]. Activation of the KOR is viewed as a promising strategy for the treatment of pain, itch and epilepsy, whereas receptor blockade is associated with potential therapeutic effects in mood (depression and anxiety) and addictive disorders [16–21]. Selective ligands for the KOR with diverse scaffolds—such as small molecules and peptides, natural products and synthetic molecules—and distinct pharmacology were designed [19–24]. Although targeting the KOR in drug discovery is very promising, the KOR is not devoid of detrimental side effects with receptor activation causing diuresis, dysphoria, sedation, psychotomimesis and anxiety in humans [15–17]. The small molecule with a morphinan scaffold, nalfurafine [25], and the peripherally acting peptide analogue, difelikephalin [26] (Figure 1), are two KOR agonists approved for clinical use as antipruritic drugs [27–29]. In addition, pain is a key clinical indication for KOR agonists, with experimental and clinical evidence that the KOR modulates pain processing in the CNS and PNS without the risk of physical dependence or abuse liability of MOR agonists [30–33].

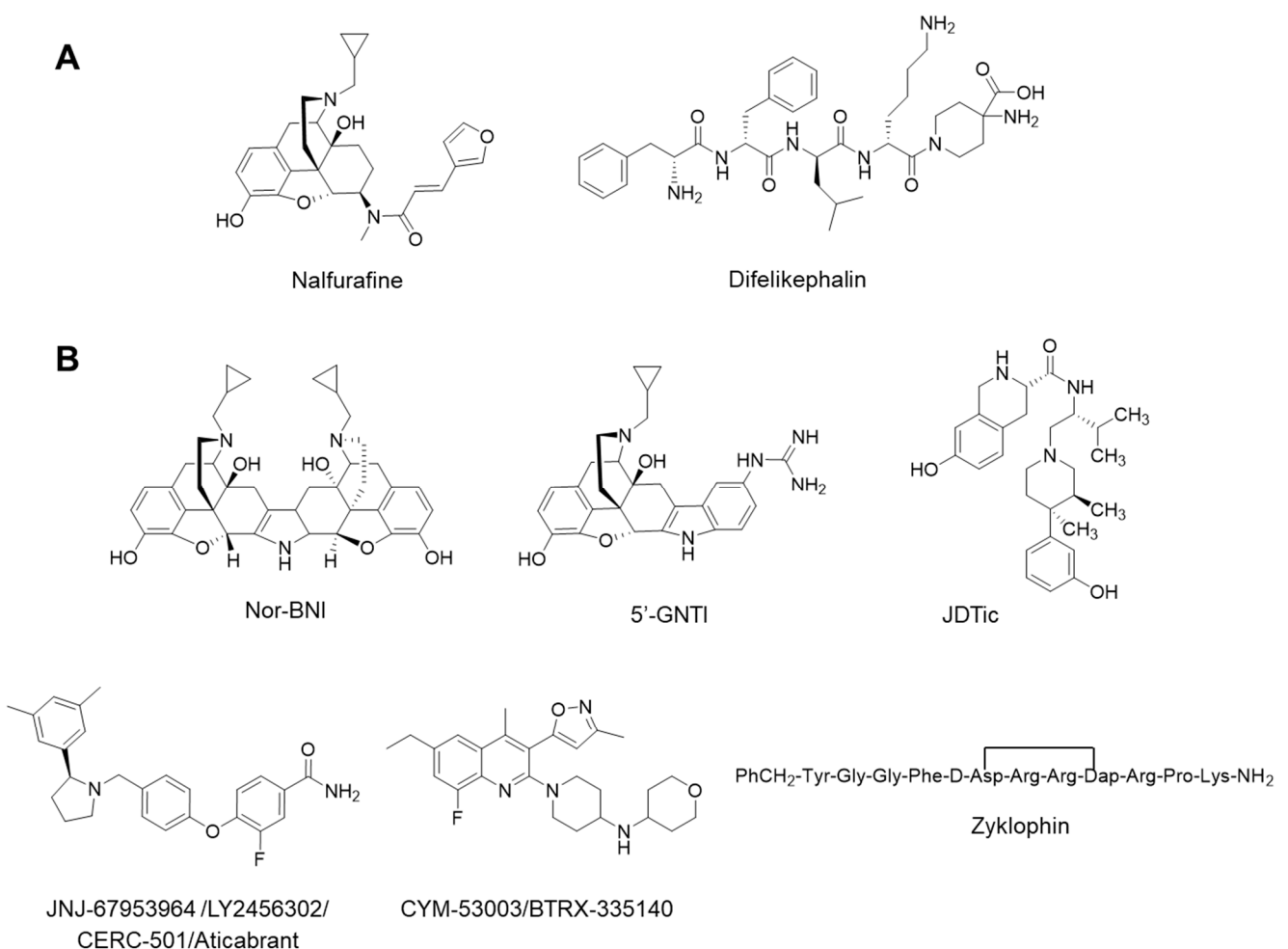**Figure 1.** Representative selective KOR ligands used in the clinics, as potential therapeutics or research tools. (**A**) KOR agonists; (**B**, **top**) long-acting KOR antagonists; (**B**, **bottom**) short-acting KOR antagonists.

Initially, KOR antagonists were widely used as pharmacological tools for studying the in vitro and in vivo actions upon KOR stimulation [19–21,28,34] The first selective KOR

antagonists included ligands with a morphinan scaffold structure, i.e., nor-binaltorphimine (nor-BNI) [35], 5′-guanidinonaltrindole (5′-GNTI) [36] and the 4′-phenylpiperidine derivative, JDTic [37] (Figure 1). Preclinical studies showed that KOR inhibition or receptor depletion in the brain resulted in attenuation of depressive, anxiogenic affective and addictive-like behaviors, thus encouraging the development of selective KOR antagonists for the treatment of mood and addictive disorders. JDTic was the first selective KOR antagonist tested in humans for the treatment of cocaine abuse. However, clinical development of JDTic was terminated after modest cardiac abnormalities and an unfavorable brain-to-plasma concentration ratio, indicating poor CNS penetration [38]. Although preclinical and clinical data provide evidence on the therapeutic potential of KOR antagonists for CNS disorders, some peculiarities limit their usefulness [35,36]. The main issue with prototypical KOR antagonists (i.e., nor-BNI, 5′-GNTI and JDTic) is their exceptionally long duration of action, with multi-week blockades of the KOR activity following systemic administration after a single minimal dose. At higher doses, the antagonism may be further prolonged as demonstrated by studies performed with nor-BNI [34,39,40]. Delayed onset of KOR antagonism and side effects given by transient interaction with other opioid receptors, such as MOR antagonism after nor-BNI administration, have also been reported [41]. However, their abnormal long duration of action is, at present, the main concern about the feasibility of archetypical KOR antagonists. These findings have led to the development of short-acting KOR antagonists, including the pyrrolidine derivative, JNJ-67953964 (also known as LY2456302, CERC501 and aticaprant) [42], the quinolone, pyranyl and piperidine containing small molecule CYM-53003/BTRX-335140 [43] and different peptidic structures (i.e., zyklophin [44]) [19–21,23,45] (Figure 1). JNJ-67953964 is the first short-acting selective KOR antagonist shown to be safe in humans after oral administration and as a monotherapy for the treatment of major depressive disorders and substance use disorders. CYM-53003/BTRX-335140 is a further short-duration KOR antagonist, currently undergoing a phase 2 clinical trial for major depressive disorders [20,21].

Because of its therapeutic significance, the KOR is among the few GPCRs of which the X-ray crystal structures were determined both in inactive (Protein Data Bank, PDB-ID: 4DJH) [46] and active states (PDB-ID: 6B73 [47]). More recently, another structure of inactive-state KOR was solved with JDTic in complex with a Nb6 antibody (PDB-ID: 6VI4 [48]). The structure elucidation of the KOR and continued development of computational tools provide novel opportunities for computational modeling studies of receptor dynamics and for structure-based ligand discovery [49].

In the present study, we report on the in vitro, in vivo and in silico characterization of a new ligand as a KOR antagonist (Compound A, Figure 2). In an earlier study, Kaserer et al. [50] performed a 3D pharmacophore-based virtual screening campaign using several structure-based and ligand-based 3D query pharmacophores to discover novel ligands at the MOR. Compound A (as 'compound 3' in [50], Figure 2) was originally found as an MOR antagonist with very low binding affinity in the micromolar range to the human MOR. We have undertaken a comprehensive evaluation of Compound A, where experimental pharmacological (binding and functional in vitro assays and behavioral nociceptive models) and computational (in silico methods) approaches were combined, and established Compound A as a novel KOR antagonist with a structurally distinct scaffold compared to the so far known KOR ligands. We determined the binding mode of Compound A in complex with the KOR, as well as the MOR and DOR, and the structural determinants responsible for subtype selectivity of Compound A by conducting molecular docking and molecular dynamics (MD) simulations with subsequent dynophore (dynamic pharmacophore) generation of Compound A bound to the three classical opioid receptors.
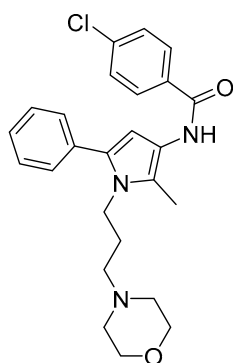
Figure 2. Structure of Compound A.

2. Results and Discussion

2.1. Compound A Binds at the KOR with Increased Affinity vs. MOR, Lacks Specific Binding at the DOR, and Displays KOR Antagonism In Vitro

Whereas Compound A was previously described to interact with the human MOR and to exhibit antagonist properties, albeit with a very reduced binding affinity (inhibition constant as K_i value of 10.7 μM) [50] (Table 1), its receptor binding/selectivity and activation profile at the KOR and DOR were not reported. In this study, the binding of Compound A to the human KOR was evaluated using in vitro radioligand competitive binding assays with membrane preparations from Chinese hamster ovary cells stably expressing the human KOR (CHO-hKOR cells) and the specific KOR radioligand [³H]U69,593, according to the published procedure [51]. As shown in Figure 3A, Compound A produced a concentration-dependent inhibition of [³H]U69,593 binding displaying relatively moderate affinity at the human KOR (K_i = 1.35 μM), while the reference KOR ligand, U69,593 had a very high affinity in the low nanomolar range (Table 1). Additionally, competitive inhibition by Compound A of [³H]diprenorphine binding at the human DOR was assessed using in vitro radioligand binding assays with membranes from CHO-hDOR cells. Compound A displayed no substantial binding at the DOR at the concentration of 10 μM (% inhibition = 0.31 ± 6.52, *n* = 4) (Table 1). In the same assay, the r standard DOR ligand, naltrindole presented a very high affinity (K_i = 0.81 ± 0.04 nM) at the human DOR. Based on the current in vitro competition binding results, Compound A binds at the human KOR with increased affinity than to the MOR (ca. 8-fold), and it is devoid of specific binding at the DOR, therefore, presenting a preferential KOR selectivity profile.

Table 1. In vitro binding affinities and functional activities of Compound A at the human KOR.

	Opioid Receptor Binding (K_i, μM) [a]			[³⁵S]GTPγS Binding, KOR [b]		
	KOR	**MOR**	**DOR**	**EC$_{50}$ (μM)**	**% stim.**	**K$_e$ (μM)**
Compound A	1.35 ± 0.32	10.7 ± 4.7 [c]	- [d]	- [e]	- [e]	1.53 ± 0.38
U69,593	0.0019 ± 0.0004	n.d.	n.d.	0.011 ± 0.004	100	n.a.

[a] Determined in radioligand competitive binding assays using membranes of CHO cell stably expressing the human KOR (CHO-hKOR). [b] Determined in the [³⁵S]GTPγS binding assay with membranes of CHO-hKOR cells. Efficacy (% stim.) is expressed as percentage stimulation relative to the maximum effect of the KOR full agonist U69,593 (as 100%). [c] Data from [50]. [d] No specific binding was detected at 10 μM in the radioligand binding assays using CHO-hDOR cell membranes. [e] No stimulation up to 10 μM. n.d. not determined. n.a. not applicable. Values are means ± SEM of at least three independent experiments performed in duplicate.
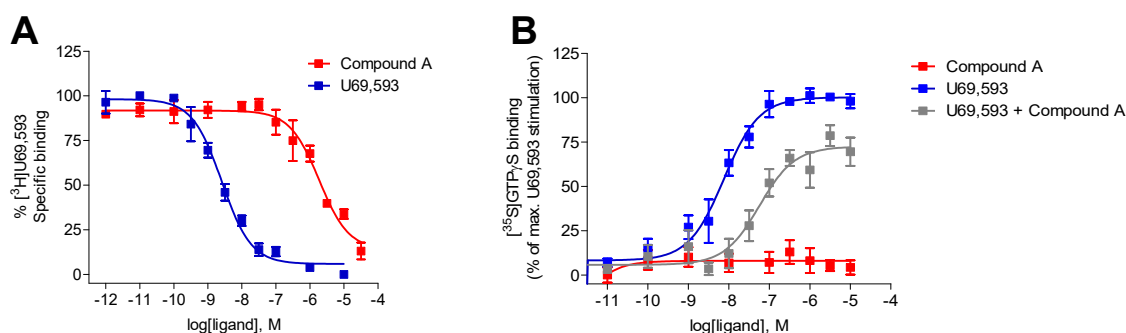
Figure 3. In vitro activity profile of Compound A at the human KOR. (**A**) Concentration-dependent inhibition by Compound A and U69,593 of [^{3}H]U69,593 binding to membranes from CHO-hKOR cells determined in radioligand competitive binding assays. (**B**) Concentration-dependent stimulation of [^{35}S]GTPγS binding by Compound A and U69,593, and effect of Compound A on U69,593-stimulated [^{35}S]GTPγS binding to membranes from CHO-hKOR cells determined in the [^{35}S]GTPγS binding assays. Values represent means ± SEM of at least 3 independent experiments performed in duplicate.

Next, we have evaluated the in vitro functional activity of Compound A at the human KOR in the guanosine-5′-O-(3-[^{35}S]thio)-triphosphate ([^{35}S]GTPγS) binding assay, which measures KOR-mediated G protein activation upon ligand binding to the receptor. Previously, Compound A was reported as an MOR antagonist [48], but its antagonist potency was not determined because of its extremely low affinity at the MOR (Table 1) [50]. In this study, the [^{35}S]GTPγS functional assay was performed with membranes from CHO cells, stably expressing the human KOR as described previously [51]. As shown in Figure 3B, Compound A did not increase the [^{35}S]GTPγS binding in membranes from CHO-hKOR cells, indicating an antagonist profile at the KOR, in contrast to the high potency and stimulatory effect shown by the prototypical KOR agonist U69,593 (Table 1). Additional investigations established the antagonist properties of Compound A at the KOR, based on the rightwards shift (ca. 13-fold) in the U69,593 concentration–response curve in the presence of 10 μM of Compound A (Figure 3B), thus giving an antagonist equilibrium constant (K_e) of 1.53 μM (Table 1). Our present results from the [^{35}S]GTPγS functional assay establish Compound A as a new KOR ligand with antagonist properties in vitro.

Compound A shows noticeable lower binding affinity and antagonist potency in the micromolar range to the KOR (Table 1) versus subnanomolar to nanomolar K_i and K_e values reported for known KOR antagonists (Table S1).

2.2. Subcutaneous Administration of Compound A Antagonized the KOR-Mediated Antinociception Induced by U50,488 in Mice

Based on the in vitro results, the KOR antagonist activity of Compound A was evaluated in vivo in mouse models of visceral pain (acetic acid-induced writhing assay) and inflammatory pain (the formalin test), according to previously described procedures [51,52]. To this aim, Compound A, administered to mice subcutaneously (s.c.), was assessed for its capability to antagonize the antinociceptive effect produced by the typical KOR agonist U50,488 in both pain models (Figure 4). When Compound A (10 mg/kg, 22.7 μmol/kg) was injected 15 min prior to U50,488 (2 mg/kg, s.c.) in the formalin assay, a significant and complete reversal of U50,488-induced inhibition of writhing behavior was measured (Figure 4A), demonstrating a KOR-mediate mechanism. Similarly, pretreatment of mice with the standard KOR antagonist nor-BNI (10 mg/kg, 13.6 μmol/kg, s.c.) for 24 h before U50,488 blocked the antinociceptive effect of the KOR agonist in the writhing assay (Figure 4A). Compound A was about twofold less potent than nor-BNI as a KOR antagonist in vivo. We further established that pretreatment of mice with Compound A (10 mg/kg, 22.7 μmol/kg s.c.) significantly antagonized the reduction of pain behaviors caused by U50,488 (1 mg/kg, s.c.) during the inflammatory phase of the formalin test, quantified by an increase in the amount of time each animal spent licking, biting, lifting and flinching the

formalin-injected paw (Figure 4B). Thus, we show in two pain models that Compound A after s.c. administration to mice behaves as a KOR antagonist in vivo.
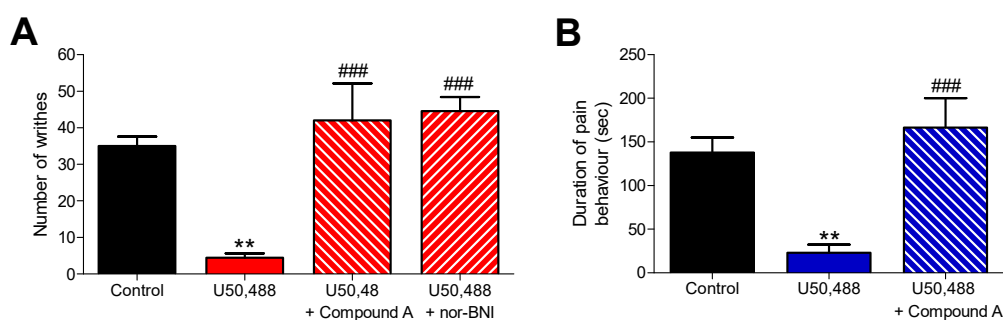

Figure 4. In vivo KOR antagonism of Compound A. Antagonism of U50,488-induced antinociception in mice by Compound A after s.c. administration in (**A**) the acetic acid-induced writing assay and (**B**) the formalin test. (**A**) In the writhing assay, groups of mice received s.c. control (vehicle), U50,488 (2 mg/kg) or were s.c. pre-treated with Compound A (10 mg/kg, −15 min) or nor-BNI (10 mg/kg, −24 h) before U50,488, and the number of writhes were counted for 10 min. Values represent means ± SEM (n = 5–6 mice per group). (**B**) In the formalin test, groups of mice received s.c. control (vehicle), U50,488 (1 mg/kg) or were s.c. pre-treated with Compound A (10 mg/kg, −15 min) before U50,488, and the duration of pain behavior (time spent licking, biting, lifting and flinching the formalin-injected paw) was counted for 15 min, starting 15 min after formalin injection. Values represent means ± SEM (n = 6–8 mice per group). ** $p < 0.01$ vs. control (vehicle) group; ### $p < 0.001$ vs. U50.488-treated group; one-way ANOVA with Tukey's post hoc test.

2.3. Modeling Inactive KOR Based on X-ray Crystal Structure 4DJH including Refinement of Transmembrane Helix 1

A comparison of the three inactive state X-ray crystal structures of the KOR, MOR and DOR (PDB-IDs: 4DJH [44], 4DKL [53], and 4N6H [54], respectively) reveals an overall similar global fold with the exception of the extracellular half of transmembrane helix (TM) 1. Although the MOR and DOR share a similar conformation of this helix, the extracellular half of TM1 is strongly bent outwards at the KOR (8.3 Å between the KOR and DOR, and 7.3 Å between the KOR and MOR; measured between Cα of residue 1.30 at the top of TM1 for each receptor pair). The inactive structure of the KOR (PDB-ID: 4DJH) was crystallized as a parallel dimer with the dimer interface consisting of TM1, 2 and 8 [46], i.e., the KOR TM1 conformation is likely influenced by the second receptor within the cell unit of the crystal structure. To ensure consistency with the global fold of the opioid receptors under investigation, and to remove potential artefacts from dimer crystallization, we remodeled the TM1 region of the KOR crystal structure. Thus, we modeled the upper half of TM1 (S55-V72) based on the DOR crystal structure (PDB-ID: 4N6H [54], 66.7% similarity within this region) as described in the Section 3. We thus obtained coordinates for the KOR that are based on the crystal structure but include a refined upper TM1 region.

2.4. Docking Reveals Stabilizing Interactions between the Chlorophenyl Moiety of Compound A and the KOR Responsible for the Highest Subtype Affinity

To investigate the mechanistic determinants of the different experimentally determined binding affinities of Compound A to the classical opioid receptor subtypes, we performed docking experiments of Compound A into the prepared crystal structures of the MOR (PDB-ID: 4DKL [53]), DOR (PDB-ID: 4N6H [54]) and the KOR model (based on PDB-ID: 4DJH [46]). We docked Compound A into the orthosteric binding pocket of the three opioid receptors as described in the Section 3. In our docking experiments, the morpholine group of Compound A deeply protrudes into the orthosteric binding pocket, establishing an ionic interaction between the positively charged nitrogen of the morpholine moiety and the carboxylate of $D^{3.32}$ (KOR: $D138^{3.32}$, MOR: $D149^{3.32}$ and DOR: $D128^{3.32}$, superscripts denote Ballesteros–Weinstein numbering [55]) that is known to be crucial for

ligand binding [46,47,56,57]. The phenyl group of Compound A points towards TM5 and TM6, establishing extensive lipophilic contacts to residues within TM3, TM5 and TM6, while the chlorophenyl moiety further extends toward the extracellular side and points toward TM2 and TM3 (Figure 5). The non-conserved residue K108[2.63] in TM2 in the DOR extends further into the binding pocket than the respective residues in the KOR (V118[2.63]) and MOR (N129[2.63]), causing a shift of Compound A toward TM5 and TM6 in the DOR compared to the KOR and MOR.
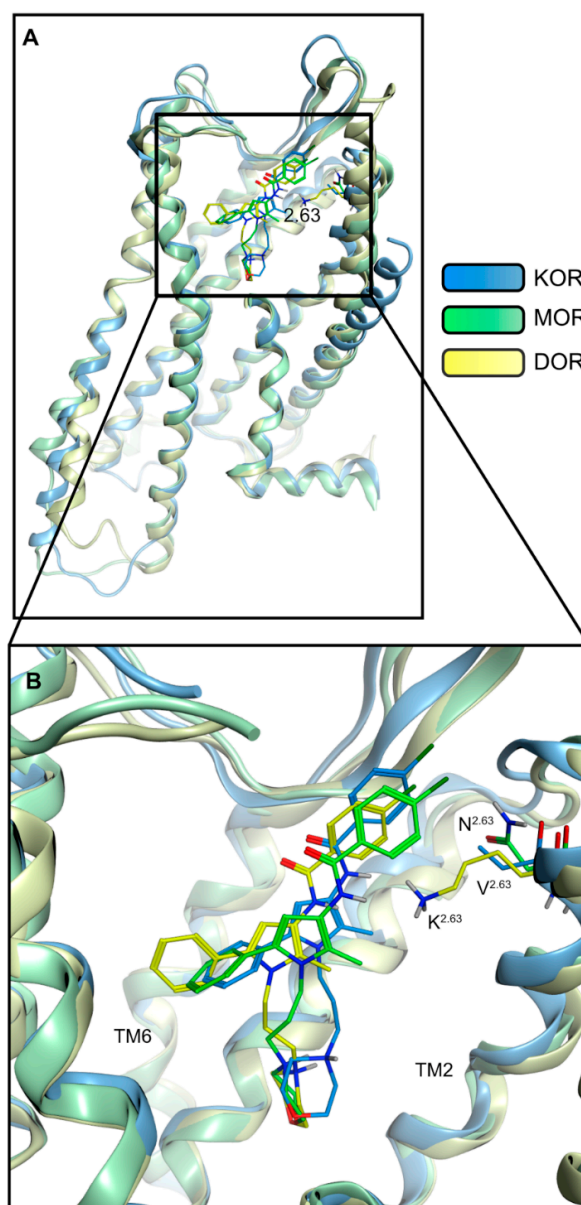
Figure 5. Binding mode of Compound A at the KOR, MOR and DOR. (**A**) Compound A binds within the orthosteric pocket in the extracellular half of the receptors. (**B**) Compound A shares an overall similar orientation within the receptors. The residues 7.28–7.41 are not shown for better visualization.

Development of 3D pharmacophores of the opioid receptor–Compound A complexes reveals a different number of interactions between the chlorophenyl moiety and the sub-pocket (residues 2.63, 2.67, 2.68, 2.69, 3.29, part of extracellular loop, ECL2) that accommodates this chlorophenyl moiety (Figure 6). The KOR establishes the most interactions, specifically three, followed by two interactions in the MOR and only one in the DOR (Table 2). In the KOR, the chlorophenyl moiety binds to the subpocket via two hydrophobic

contacts (V188$^{2.63}$, V207^{ECL2}) and a halogen bond towards N122$^{2.67}$. These interactions likely improve the affinity of Compound A at the KOR (K_i = 1.35 μM, Table 1). Conversely, at the MOR, the chlorophenyl moiety of Compound A is only stabilized by two hydrophobic contacts with a threonine side chain methyl group (T220$^{45.51/ECL2}$). This likely causes the decreased affinity of Compound A towards the MOR (K_i = 10.7 μM, Table 1) compared to the KOR. In the DOR, the positively charged K108$^{2.63}$ deeply points into the subpocket towards the chlorophenyl moiety of Compound A. The close proximity between the chlorophenyl moiety of Compound A and K108$^{2.63}$ (3.5 Å, measured between the primary amine nitrogen of K108$^{2.63}$ and the closest carbon of the chlorophenyl of Compound A) likely contributes to the absence of binding of Compound A in concentrations up to 10 μM to the DOR. Additionally, the phenyl ring of the chlorophenyl moiety of Compound A does not participate in any interactions with the DOR, in contrast to the KOR and MOR. Only the chlorine forms a hydrophobic contact with V197^{ECL2}. Table 2 shows all protein–ligand interactions from our docking experiments for comparison.
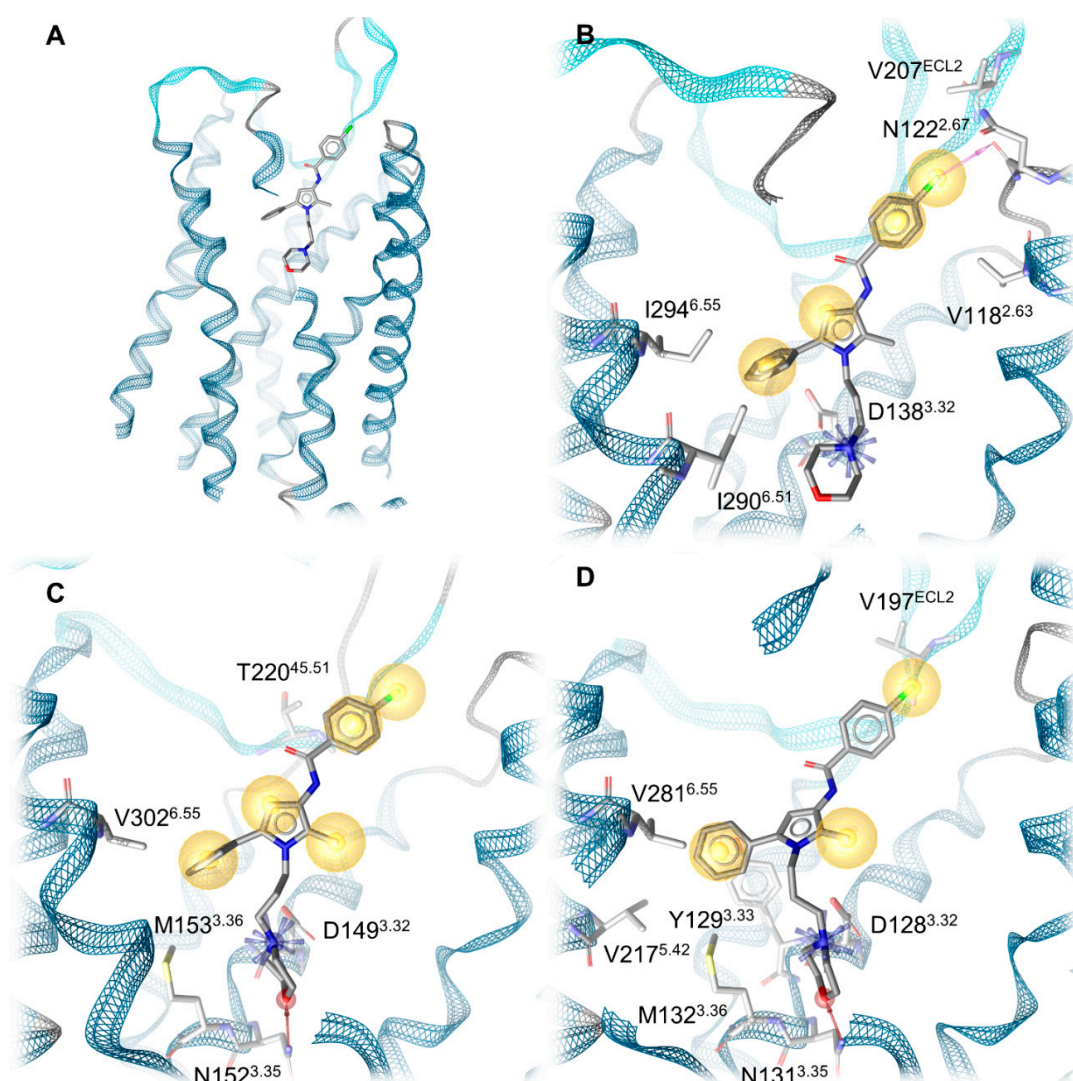
Figure 6. Protein–ligand interactions. (**A**) Global view of Compound A bound to the KOR. (**B**) Protein–ligand interactions at the KOR. (**C**) Protein–ligand interactions at the MOR. (**D**) Protein–ligand interactions at the DOR. Blue stars indicate positive charges, yellow spheres lipophilic contacts, pink arrows halogen bond donors and red arrows hydrogen bond acceptors. The residues 313–319 in the KOR, 314–327 in the MOR and 276–279 as well as 296–307 in the DOR are not shown for better visualization.

Table 2. Protein–ligand interactions between Compound A and the opioid receptors, KOR, MOR and DOR, derived from docking experiments.

Receptor	Interaction	Functional Group	Involved Residues
KOR	Ionic interaction Halogen bond Hydrophobic contacts	Morpholine nitrogen Chlorine Chlorophenyl 2-Methylpyrrole Phenyl moiety	D138$^{3.32}$ N122$^{2.67}$ V207^{ECL2} V118$^{2.63}$ Y312$^{7.35}$ I290$^{6.51}$ I294$^{6.55}$ I316$^{7.39}$
MOR	Ionic interaction Hydrogen bond Hydrophobic contacts	Morpholine nitrogen Morpholine oxygen Chlorophenyl 2-Methylpyrrole Phenyl moiety	D149$^{3.32}$ N152$^{3.35}$ T220$^{45.51/ECL2}$ I324$^{7.39}$ M153$^{3.36}$ V302$^{6.55}$ I324$^{7.39}$
DOR	Ionic interaction + hydrogen bond Hydrogen bond Hydrophobic contacts	Morpholine nitrogen Morpholine oxygen Chlorophenyl 2-Methylpyrrol Phenyl moiety	D128$^{3.32}$ N131$^{3.35}$ V197^{ECL2} V304$^{7.39}$ Y129$^{3.33}$ M132$^{3.36}$ V217$^{5.42}$ V281$^{6.55}$

Compound A is a weak opioid receptor binder with affinity values in the micromolar range (Table 1). To rationalize the low binding affinity, we performed a comparison of Compound A and the co-crystallized high-affinity ligands from the inactive crystal structures used for docking (KOR: JDTic, MOR: β-FNA, and DOR: naltrindole) in complex with the opioid receptors (Figure 7). This comparison reveals that the co-crystallized ligands are shifted toward TM5/TM6 in their corresponding complexes with respect to Compound A. Their bulky ring systems, containing a phenol group in all three ligands, are the moieties closest to TM5/TM6 and the hydroxyl groups of the phenol moieties take part in water-mediated hydrogen bonds connecting the co-crystallized ligands to TM3/TM5 and TM6 (KOR: Y139$^{3.33}$, K227$^{5.39}$ and H291$^{6.52}$; MOR: K235$^{5.39}$ and H299$^{6.52}$, DOR: Y129$^{3.33}$, K214$^{5.39}$ and H278$^{6.52}$). The phenyl group of Compound A does not participate in water-mediated hydrogen bonds as it does not point as far toward TM5/TM6 and contains no functional group capable of hydrogen bonding. A phenol moiety that interacts with TM5 is a common feature for opioids [47] and its absence in Compound A likely contributes to its low binding affinity. Additionally, it was previously reported that the presence of a phenol group is more important in the MOR than in the KOR [47], which is in accordance with the higher affinity of Compound A to the KOR compared to the MOR.
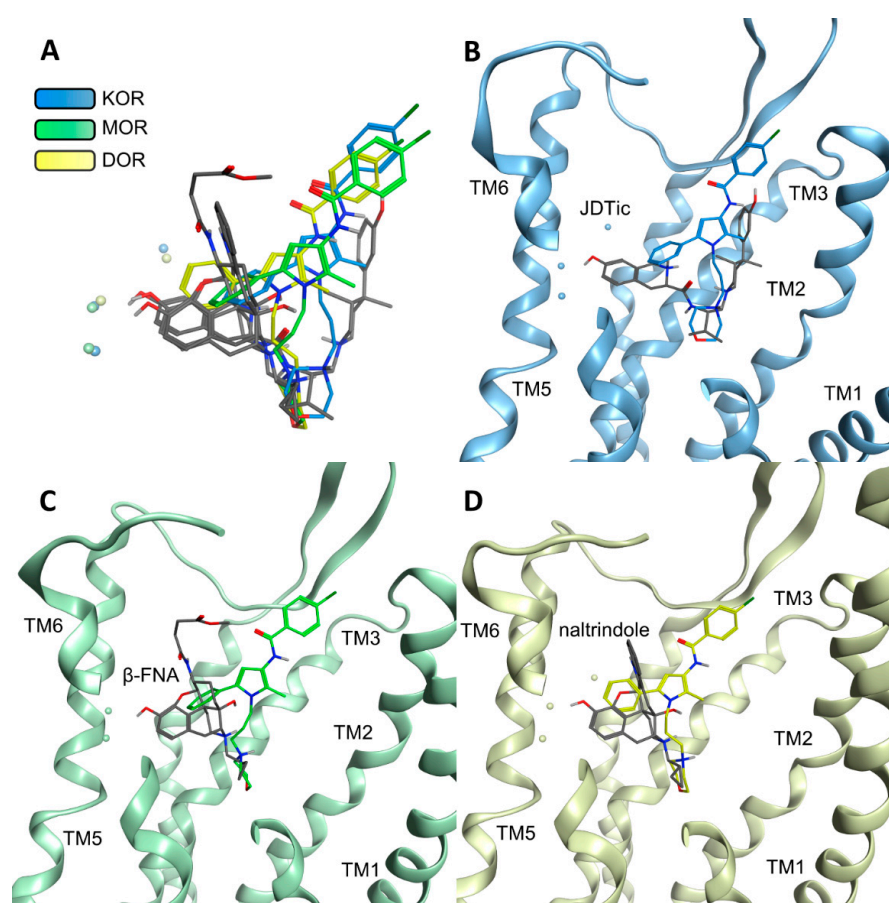
Figure 7. Comparison of the binding modes of Compound A and the binding modes of the co-crystallized ligands. (**A**) Overlay of all compared ligands. Co-crystallized ligands are depicted in gray. (**B**) JDTic and Compound A in the KOR. (**C**) β-FNA and Compound A in the MOR. (**D**) Naltrindole and Compound A in the DOR. Water molecules are shown as spheres without hydrogens.

2.5. Molecular Dynamics Simulations Reveal the Most Durable and Frequent Interaction Pattern of the Chlorophenyl Moiety of Compound A in the KOR Complex

To further investigate our static binding hypotheses, we performed molecular dynamics (MD) simulations and developed dynamic 3D pharmacophore models (dynophores [58]). The dynamic evaluation confirms our static hypothesis as it reveals the most durable and frequent interactions for the chlorophenyl moiety of Compound A in the KOR complex. The chlorophenyl moiety of Compound A participates in hydrophobic contacts in 99.1% and 98.4% (values for the chlorine and the chlorophenyl plane, respectively) of the simulation time (Table 3). Additionally, the chlorophenyl moiety is stabilized by a halogen bond in 13.3% of the simulation time that is not present in the complexes with the MOR and DOR (Table 3). These interaction patterns of the chlorophenyl moiety likely contribute to the affinity of Compound A measured at the KOR being the highest out of the three investigated complexes. In complex with the MOR, Compound A is also stabilized by hydrophobic contacts in the vast majority of the simulation time (99.8% and 99.2% for the chlorine and the chlorophenyl plane, respectively), but lacks the additional stabilization by halogen bonding (Table 3). The missing halogen bond appears to decrease the affinity of Compound A towards the MOR. At the DOR, Compound A does not only lack the halogen bond but also engages in less frequent hydrophobic contacts in total (100% and 83.2% for the chlorine and the chlorophenyl plane, respectively) compared to the KOR and MOR (Table 3), which likely explains the experimentally measured absence of affinity at the DOR. The difference in the stabilization of the chlorophenyl moiety at the opioid receptor complexes by hydrophobic contacts is even more pronounced when considering the total

number of hydrophobic contacts. In the KOR and MOR, a similar absolute number of hydrophobic contacts within the whole trajectories was counted (KOR: 4730, MOR: 5243), while there were fewer contacts detected in the DOR complex (3277, corresponding to 69.3% of the contact number counted at the KOR). This discrepancy further rationalizes the experimentally measured differences in the binding affinity of Compound A towards the three opioid receptor subtypes. The dynamic pharmacophores of Compound A within the opioid receptor complexes are shown in Figure 8.

Table 3. Frequency of interactions between the chlorophenyl ring of Compound A and the opioid receptors.

Receptor	Interaction	Functional Group	Mean Frequency (n = 3)
KOR	Hydrophobic contacts	Chloride	99.1%
	Halogen bond	Chloride	13.3%
	Hydrophobic contacts	Chlorophenyl	98.4%
MOR	Hydrophobic contacts	Chloride	99.8%
	Hydrophobic contacts	Chlorophenyl	99.2%
DOR	Hydrophobic contacts	Chloride	100%
	Hydrophobic contacts	Chlorophenyl	83.2%
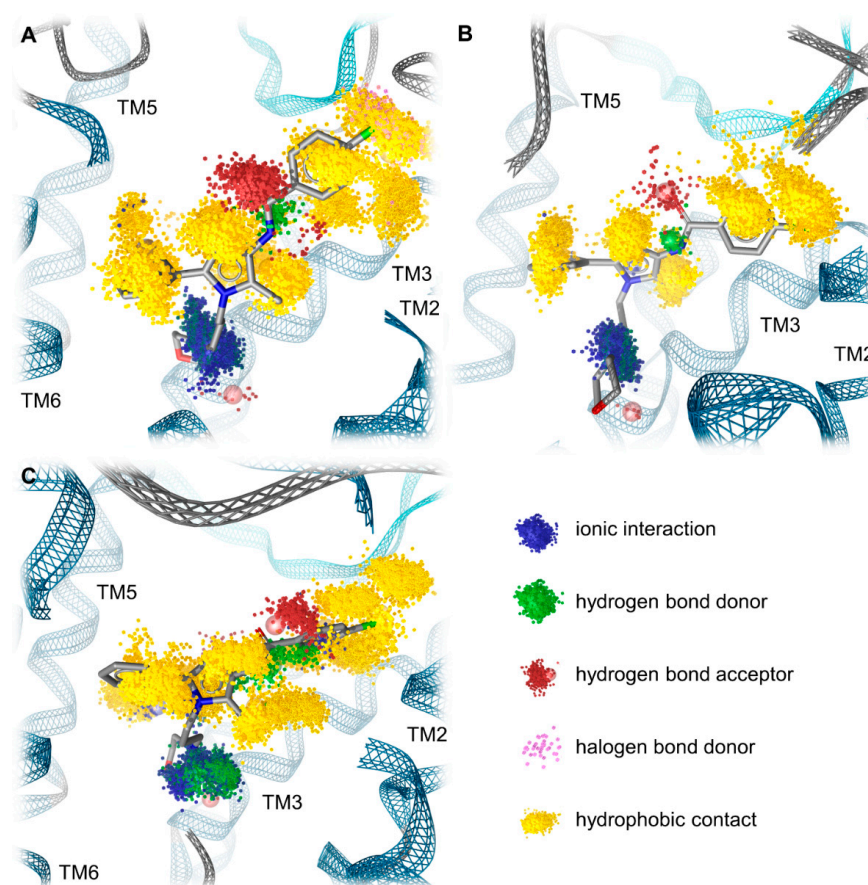
Figure 8. Dynamic 3D pharmacophores (dynophores) of Compound A–opioid receptor complexes. (**A**) KOR. (**B**) MOR. (**C**) DOR. Chemical feature clouds refer to interactions occurring over simulation time.

In order to address the protein and ligand conformational stability, we performed root mean square deviation (RMSD) calculations for the opioid receptors and Compound A, as well as heavy atom root mean square fluctuation (RMSF) calculations for the receptors

over the simulation time. The information is presented in the Supplementary Materials (Figures S1–S9). To track the receptor compactness along the simulations, we calculated the radius of gyration of the receptors over the simulation time (Figures S10–S12). The radius of gyration values remains stable over the trajectory, indicating steady receptor compactness. In order to monitor the correct protein folding over the course of the MD simulations, we calculated the solvent accessible surface areas (SASA) values of the receptors (Figures S13–S15). No strong increase in the SASA values was found, indicating that no protein unfolding processes could be observed.

2.6. Compound A Shows Favorable Physicochemical Properties and Is a CNS Penetrant KOR Antagonist

Evaluation of pharmacokinetic properties represents a key feature in today's drug discovery, particularly in predicting response profiles in vivo of bioactive molecules [59,60]. We have calculated and compared the partition coefficients ($c$logP) and distribution coefficients at pH 7.4 ($c$logD$_{7.4}$) of Compound A and various small molecules KOR antagonists (Table 4). In general, compounds with higher hydrophobicity, i.e., larger $c$logP and $c$logD$_{7.4}$ values, are expected to readily cross the blood–brain barrier [61]. According to the $c$logP and the $c$logD$_{7.4}$, Compound A shows favorable physicochemical features and a better capability to enter the CNS compared to the known KOR antagonists, that show increased hydrophilicity at physiological pH.

Table 4. Calculated logP and logD$_{7.4}$ of Compound A and various small molecules KOR antagonists.

Ligand	$c$logP [a]	$c$logD$_{7.4}$ [a]
Compound A	4.2	4.09
nor-BNI	3.13	1.55
5′-GNTI	1.72	−0.55
JDTic	3.43	1.78
JNJ-67953964	4.97	3.24
CYM-53003/BTRX-335140	3.82	2.37

[a] Calculated using Percepta software (version 2021, ACD/Labs, Toronto, Canada) [62].

Further calculations based on chemical properties of Compound A, including ADMET properties and bioavailability (BOILED-Egg plot [63]), are presented in the Supplementary Materials (Figure S16 and Figure S17, Table S2). The calculations were performed using the open access SwissADME web tool [64]. Compound A was predicted to have high gastrointestinal absorption and to readily pass the blood–brain barrier but also as a permeability–glycoprotein substrate.

3. Materials and Methods

3.1. Chemicals and Reagents

Radioligands [^{3}H]U69,593 (49.3 Ci/mmol), [^{3}H]diprenorphine (33.9 Ci/mmol) and [^{35}S]GTPγS (1250 Ci/mmol) were purchased from PerkinElmer (Boston, MA, USA). Guanosine diphosphate (GDP), GTPγS, U69,593, U50,488, diprenorphine, tris(hydroxymethyl) aminomethane (Tris), 2-[4-(2-hydroxyethyl)piperazin-1-yl]ethanesulfonic acid (HEPES), bovine serum albumin (BSA), formalin, nor-BNI and cell culture media and supplements were obtained from Sigma-Aldrich Chemicals (St. Louis, MO, USA). All other chemicals were of analytical grade and obtained from standard commercial sources. Compound A was obtained from Maybridge Chemical Co., Ltd. (Cornwall, UK) as in [50], and was prepared as 1 mM stock in 0.5% acetic acid solution and further diluted to working concentrations in the appropriate medium.

3.2. Cell Cultures and Cell Membrane Preparation

CHO cells stably expressing the human opioid receptors (CHO-hKOR and CHO-hDOR cell lines) were kindly provided by Lawrence Toll (SRI International, Menlo Park, CA).

CHO-hKOR cells were grown at 37 °C in Dulbecco's Modified Eagle's Medium (DMEM) culture medium and supplemented with 10% fetal bovine serum (FBS), 0.1% penicillin/streptomycin, 2 mM L-glutamine and 0.4 mg/mL geneticin (G418). CHO-hDOR cells were grown at 37 °C in DMEM/Ham's F12 culture medium and supplemented with 10% FBS, 0.1% penicillin/streptomycin, 2 mM L-glutamine and 0.4 mg/mL geneticin (G418). All cell cultures were maintained in a humidified atmosphere of 95% air and 5% CO_2. Membranes from CHO-hOR cells were prepared as previously described [51]. Briefly, CHO-hOR cells grown at confluence were removed from the culture plates by scraping, homogenized in 50 mM Tris-HCl buffer (pH 7.7) using a Dounce glass homogenizer, then centrifuged once and washed by an additional centrifugation at $27,000 \times g$ for 15 min at 4 °C. The final pellet was resuspended in 50 mM Tris-HCl buffer (pH 7.7) and stored at −80 °C until use. Protein content of cell membrane preparations was determined by the method of Bradford using BSA as the standard [65].

3.3. Competitive Radioligand Binding Assays

In vitro binding assays were conducted on human opioid receptors stably transfected into CHO cells according to the published procedures [51]. Assays were performed in 50 mM Tris-HCl buffer (pH 7.4) in a final volume of 1 mL. Cell membranes (20 µg) were incubated with various concentrations of test compounds of [^{3}H]U69,593 (0.4 nM) or [^{3}H]diprenorphine (0.2 nM) for labeling KOR or DOR, respectively, for 60 min at 25 °C. Non-specific binding was determined using 10 µM U69,593 or 1 µM diprenorphine. After incubation, reactions were terminated by rapid filtration through Whatman GF/C glass fiber filters. Filters were washed three times with 5 mL of ice-cold 50 mM Tris-HCl buffer (pH 7.4) using a Brandel M24R cell harvester (Brandel, Gaithersburg, MD, USA). Radioactivity retained on the filters was counted by liquid scintillation counting using a Beckman Coulter LS6500 (Beckman Coulter Inc., Fullerton, CA, USA). Inhibition constant (K_i, nM) values were determined by the method of Cheng and Prusoff [66] from concentration–response curves by nonlinear regression analysis using the GraphPad Prism 5.0 Software (GraphPad Prism Software Inc., San Diego, CA, USA). All experiments were performed in duplicate and repeated at least three times with independently prepared samples.

3.4. [^{35}S]GTPγS Binding Assays

Binding of [^{35}S]GTPγS to membranes from CHO stably expressing the human KOR was conducted according to the published procedure [51]. Cell membranes (15 µg) in 20 mM HEPES buffer (pH 7.4) supplemented with 10 mM $MgCl_2$ and 100 mM NaCl were incubated with 0.05 nM [^{35}S]GTPγS, 10 µM GDP and various concentrations of test compounds in a final volume of 1 mL for 60 min at 25 °C. Non-specific binding was determined using 10 µM GTPγS, and the basal binding was determined in the absence of test ligand. Samples were filtered over Whatman GF/B glass fiber filters and counted as described for competitive radioligand binding assays. The increase in [^{35}S]GTPγS binding above the basal activity was used to determine potency (EC_{50}, in nM) and efficacy (as % stimulation of maximum stimulation with respect to the reference KOR full agonist, U69,593, which was set as 100%) from concentration–response curves by nonlinear regression analysis using the GraphPad Prism 5.0 Software (GraphPad Prism Software Inc., San Diego, CA, USA). To determine the KOR antagonist potency of Compound A, the Schild analysis was performed, where a concentration–response curve for U69,593 was obtained by assessing the [^{35}S]GTPγS binding to CHO-hKOR cell membranes in the presence or absence of Compound A. The equilibrium dissociation constant (K_e) was calculated from the equation $K_e = [a]/(D − 1)$, where "a" is the concentration of antagonist, and DR is the ratio of EC_{50} values of U69,593 in the presence and absence of Compound A. All experiments were performed in duplicate and repeated at least three times with independently prepared samples.

3.5. Animals and Drug Administration

Experiments were performed in male CD1 mice (8–10 weeks old, 30–35 g body weight) purchased from Janvier Labs (Le Genest-Saint-Isle, France). All animal care and experimental procedures were in accordance with the ethical guidelines for the animal welfare standards of the European Communities Council Directive (2010/63/EU) and were approved by the Committee of Animal Care of the Austrian Federal Ministry of Science and Research. Mice were group-housed in a temperature-controlled specific pathogen free room with a 12 h light/dark cycle and with free access to food and water. U50,488 and nor-BNI were prepared in sterile physiological saline (0.9%). Compound A was prepared in 1% acetic acid solution in sterile physiological saline (0.9%). Test compounds or vehicle (saline) were administered s.c. in a volume of 10 μL/g body weight.

3.6. Acetic Acid-Induced Writhing Assay

Writhing was induced in mice by intraperitoneal (i.p.) injection of a 0.6% acetic acid aqueous solution as described previously [51]. Following a habituation period of 15 min to individual transparent observation chambers, mice were s.c. administered U50,488 (2 mg/kg) or control (vehicle), and after 25 min (5 min prior to testing) each animal received i.p. injection of acetic acid solution. The number of writhes was counted during a 10 min observation period. For the antagonism study, Compound A (10 mg/kg) and nor-BNI (10 mg/kg) were s.c. administered 15 min and 24 h, respectively, before U50,488 (2 mg/kg, s.c.), and writhing behavior was assessed as described above.

3.7. Formalin Test

The formalin test was performed as described previously [52]. Following a habituation period of 15 min to individual transparent observation chambers, mice were s.c. administered U50,488 (1 mg/kg) or control (vehicle), 5 min prior injection of 20 μL of 5% formalin aqueous solution to the plantar surface of the right hindpaw. The time (in s) each animal spent licking, biting, lifting and flinching the formalin-injected paw (pain behavior) was recorded in 5 min intervals between 15 and 30 min after the injection of formalin (Phase II reaction). For the antagonism study, Compound A (10 mg/kg) was s.c. administered 15 min before U50,488 (1 mg/kg, s.c.), and pain behavior was assessed as described above.

3.8. Data and Statistical Analysis

Experimental data were graphically processed and statistically analyzed using the GraphPad Prism Software (GraphPad Prism Software Inc., San Diego, CA, USA) and are presented as means ± SEM. Data were statistically evaluated using one-way ANOVA with Tukey's post hoc test for multiple comparisons between the treatment groups, with significance set at $p < 0.05$.

3.9. Protein Preparation

The inactive-state X-ray crystal structures of the three opioid receptors were retrieved from the protein data bank (PDB [67]) with PDB-ID: 4DJH for KOR [46], PDB-ID: 4DKL for MOR [53] and PDB-ID: 4N6H for DOR [53]). The structure preparation was carried out in a Molecular Operating Environment (MOE v2020.0901) [68] and focused on the chain with the better resolution out of the two chains in the KOR dimer (PDB-ID: 4DJH). Firstly, we deleted the unresolved parts of the chains as well as fusion proteins (T4 lysozyme in KOR and MOR, b562RIL (BRIL) in DOR). To restore the human receptors to wild-type we used the human wild-type sequence obtained from the UniProt-Databank [69] to revert thermostabilizing mutations in the DOR and KOR (human DOR: P41143, S37P; human KOR: P41145, L135I). The PDB-ID: 4DKL (MOR, [53]) encodes the mouse MOR. Thus, we reverted four mouse-specific residues in the MOR to the human wild-type MOR residues using the UniProt-ID: P35372 (V68I, N139T, V189I, I308V). Broken loops due to unresolved parts of ECL3 and ICL3 of the KOR as well as of ICL3 of the MOR were modeled using the loop modeler function while missing side chain atoms were generated using the protein

builder, both integrated into MOE. Subsequently, Ramachandran outliers [70] and atom clashes were resolved using energy minimization with the OPLS-AA force field [71].

Due to the dimerization of the KOR chains within a cell unit (PDB-ID: 4DJH), the extracellular portion of TM1 is bent outwards along the receptor's longitudinal axis. Hence, we restored the global fold of the KOR-TM1 structure during the protein preparation to achieve a conformation comparable to the global folds of the MOR and DOR. For this purpose, a homology model of the upper half of the KOR-TM1 (S55-V72 according to UniProt-ID P41145) was built using the homology modeling tool implemented in MOE (v2020.0901) [68] with the DOR (PDB-ID: 4N6H) serving as a template. Within the homology model generation ten intermediate models were built at 300 K using the OPLS-AA force field [71] and scored according their electrostatic solvation energy [72]. The best-scored model was chosen for further geometric refinement yielding in the final model used in this study. The homology model was subsequently fused to the KOR inactive X-ray crystal structure (PDB-ID: 4DJH). The geometric properties of the TM1 homology model (fused to the KOR X-ray crystal structure) and surrounding residues were again optimized using energy minimization with the OPLS-AA force field [71]. Furthermore, the conformations of neighboring $Y320^{7.46}$ and $Q115^{2.60}$ were aligned according to the respective conformations in the DOR ($Y308^{7.43}$, $Q105^{2.60}$), using the rotamer tool within MOE v2020.0901 [68].

At the MOR inactive crystal structure (PDB-ID: 4DKL), the residue $Y130^{2.64}$ adopts a conformation bend towards the TM1, which is not comparable to the DOR crystal structure (PDB-ID: 4N6H) and our KOR model. We surmise a single missing water molecule in the TM1 and TM2 region in the MOR crystal structure responsible for the conformation shift as the OH group in the corresponding $Y109^{2.64}$ establishes a water-mediated hydrogen bond to the hydroxyl group in $Y56^{1.39}$ at the high-resolution DOR crystal structure, which cannot be seen in the lower resolution MOR crystal structure. As we assume a similar water-mediated hydrogen bond in the MOR, supported by a weak electron density in the MOR structure that likely corresponds to a water molecule, we adjusted the orientation of the $Y130^{2.64}$ side chain in the MOR manually, according to the respective orientation in the DOR ($Y109^{2.64}$).

The protonate 3D function [73] implemented in MOE (v2020.0901) [68] was used to protonate all three opioid structures at pH 7 and temperature of 300 K.

All selected X-ray crystal structures contain some water molecules within the binding site. Only the water molecules HOH1303, HOH1307 and HOH1311 in case of the KOR, HOH718 and HOH719 in case of the MOR, and HOH1323, HOH1324 and HOH1336 in case of the DOR were retained for subsequent docking and MD simulations as they participate in water mediated interactions between the cocrystallized ligands and protein residues that are known to be involved in ligand binding and selectivity (KOR: $K227^{5.39}$, $H291^{6.52}$ and $Y139^{3.33}$ [74]; MOR: $K235^{5.39}$ and $H299^{6.52}$ [75]; DOR: $H278^{6.52}$, $K214^{5.39}$ and $Y129^{3.33}$ [76–78].

3.10. Protein-Ligand Docking Study

Corina v3.00 [79,80] was used to generate the 3D conformation of Compound A used for docking. The protonate 3D function [73] implemented in MOE (v2020.0901) [68] was conducted to protonate Compound A at a pH of 7 and a temperature of 300 K. Subsequent docking of Compound A into the orthosteric pocket of the opioid receptors was performed using GOLD v5.2 [81]. A 20 Å sphere with the side chain carboxylate carbon atom of $D^{3.32}$ (KOR: $D138^{3.32}$, MOR: $D149^{3.32}$ and DOR: $D128^{3.32}$) as its center defined the binding site of the receptors, which was limited to the solvent-accessible surface. For each opioid receptor structure, a total number of 30 genetic algorithm runs were performed, yielding diverse solutions (i.e., more than 1.5 Å RMSD between the binding hypotheses of each performed docking process). The search efficiency was set at 100%. To account for the physiological flexibility of pyramidal nitrogen atoms, these atoms were allowed to flip within the ligand throughout the docking process. All obtained docking poses were scored according the GoldScore docking function [82,83] implemented in GOLD v5.2 [81]. An ionic interaction

between the carboxylate of $D^{3.32}$ at the opioid receptors and a protonatable nitrogen of the ligand is known to be crucial for ligand binding [44,45,54,55]. Thus, we set a constraint of a maximum distance of 5.5 Å between the protonatable morpholine nitrogen of Compound A and the γC-atom of $D^{3.32}$.

After docking, the MMFF94 force field [84–88] incorporated in LigandScout v4.4.3 [89,90] was conducted to minimize the energy of the obtained binding hypotheses within the protein environment. The binding poses of Compound A in complex with the MOR, DOR and KOR were visually inspected and filtered according to the position of the positively charged morpholine nitrogen of Compound A within the receptor, essential for the opioid receptor activity [46,47,56,57], as well as the stabilization of Compound A via hydrophobic contacts to the receptors after generating 3D pharmacophores using LigandScout [89,90]. Hydrophobic contacts of Compound A towards TM2/TM3 region were preferred as they were already described for other non-morphinan antagonist, JDTic [46], and tetrapeptide DIPP-NH$_2$ [56].

3.11. Molecular Dynamics Simulations and Analysis

We performed three MD simulations of 100 ns length for each of the receptor–ligand complexes. We used Maestro v2020-4 [91] for system setup, OPLS 2005 force field [92,93] for system parametrization and Desmond v2020-4 [94] for performance of the MD simulations. For each system, we positioned the protein in a cubic box with 10 Å padding each side to the protein surface. A POPC (1-palmitoyl-2-oleoylphosphatidylcholine) bilayer was used to mimic the physiological membranes, and the proteins were embedded in these membranes according the OPM database [95] (PDB-ID: 4DJH for the KOR, 4DKL for the MOR, and 4N6H for the DOR). The remaining space in the box was subsequently filled with TIP4P water molecules [96] and ions (Na$^+$, Cl$^-$), leading to an isotonic solution (0.15 M NaCl). During the simulations, a constant number of particles, pressure (1.01325 bar), and a constant temperature (300 K) were maintained (NPT ensemble). The simulations were run for 100 ns each, resulting in 1000 distinct ligand–receptor conformations sampled per simulation. Centering of the protein and the alignment of the respective trajectories onto the backbone-heavy atoms of the first protein conformation sampled during the simulation were performed using VMD v1.9.3 [95].

For subsequent MD simulation analysis, we generated dynamic pharmacophores of Compound A over the simulation time using the Dynophore software (version 0.1, Gerhard Wolber, Berlin, Germany) [58,97]. Only interactions occurring for a minimum of 5% of the simulation time were considered for evaluation of MD simulations. Root mean square deviation (RMSD) and solvent accessible surface area (SASA) calculations of MD simulations were conducted using VMD v1.9.3 [98]. Root mean square fluctuation (RMSF) and radius of gyration calculations were performed using Maestro v2020-4 [91].

4. Conclusions

In conclusion, we reported on a comprehensive study aided by in vitro and in vivo assays and computational techniques where Compound A was characterized as a novel KOR antagonist. Our interesting observations from radioligand competitive binding and functional in vitro assays revealed Compound A to bind at the KOR, albeit with moderate affinity (in low micromolar range), but with increased affinity than to the MOR and to lack specific binding at the DOR, thus displaying a favorable KOR selectivity profile. Additionally, behavioral investigations in mice established the in vivo KOR antagonist properties of Compound A after s.c. administration, based on its ability to effectively reverse the antinociceptive effects of the prototypical KOR agonist, U50,488, in two pain models, the writhing assay and the formalin test.

At the in silico level, we performed molecular docking and MD simulations using the inactive state crystal structures of the KOR, MOR and DOR, in order to further assess the structural determinants responsible for receptor subtype selectivity of Compound A. Our molecular docking study on Compound A into the orthosteric site pocket of KOR, MOR and

DOR revealed distinct interaction patterns (pharmacophores) between the chlorophenyl moiety of Compound A and each opioid receptor subtype, which well correlated with the affinity (KOR > MOR >>>> DOR) of Compound A determined experimentally. The structure of the KOR exhibits two hydrophobic contacts (V207^{ECL2}, V118$^{2.63}$) and one halogen bond (N122$^{2.67}$) to Compound A, correlating with the highest binding affinity experimentally measured. The structure of the MOR exhibits only two contacts with the chlorophenyl moiety of Compound A (via T220^{ECL2}), leading to a binding affinity approximately one order of magnitude less compared to Compound A's affinity at the MOR. At the DOR, only the chloride is stabilized in a hydrophobic contact while the chlorophenyl plane does not take part in any interactions. This sparser interaction pattern, together with the bulky side chain K108$^{2.63}$ pointing into the binding site, thereby shifting Compound A out of the subpocket, likely contributes to the lack of binding of Compound A to the DOR, as determined experimentally. Furthermore, MD simulations of the opioid receptor–Compound A complexes revealed the strongest stabilization of Compound A's chlorophenyl moiety at the KOR with frequent hydrophobic contacts supported by halogen bonding. Although the ligand–MOR complex lacks the halogen bonding, the number of hydrophobic contacts at the DOR is decreased. Thus, the MD simulations confirmed our results obtained by docking.

Notably, Compound A shows a good capability to enter the CNS (based on the *c*logP and *c*logD$_{7.4}$), and it has a structurally distinct scaffold compared to the so far known KOR ligands (Figures 1 and 2). Although Compound A interacts with the KOR relatively weakly, this new chemotype shows promising KOR antagonist properties in vitro and in vivo. Thus, Compound A represents a valuable starting point for chemical optimization toward the development of innovative ligands as potential therapeutics for human conditions where the kappa opioid system has a key function.

References

1. Stein, C. Opioid Receptors. *Annu. Rev. Med.* **2016**, *67*, 433–451. [CrossRef] [PubMed]
2. Hilger, D.; Masureel, M.; Kobilka, B.K. Structure and dynamics of GPCR signaling complexes. *Nat. Struct. Mol. Biol.* **2018**, *25*, 4–12. [CrossRef] [PubMed]
3. Bock, A.; Bermudez, M. Allosteric coupling and biased agonism in G protein-coupled receptors. *FEBS J.* **2021**, *288*, 2513–2528. [CrossRef]
4. Qu, X.; Wang, D.; Wu, B. Progress in GPCR structure determination. In *GPCRs*; Jastrzebska, B., Park, P.S.H., Eds.; Academic Press: Cambridge, MA, USA; Elsevier: London, UK, 2020; pp. 3–22.
5. Sriram, K.; Insel, P.A. G Protein-coupled receptors as targets for approved drugs: How many targets and how many drugs? *Mol. Pharmacol.* **2018**, *93*, 251–258. [CrossRef] [PubMed]
6. Corder, G.; Castro, D.C.; Bruchas, M.R.; Scherrer, G. Endogenous and exogenous opioids in pain. *Annu. Rev. Neurosci.* **2018**, *41*, 453–473. [CrossRef] [PubMed]
7. Darcq, E.; Kieffer, B.L. Opioid receptors: Drivers to addiction? *Nat. Rev. Neurosci.* **2018**, *19*, 499–514. [CrossRef]
8. Paul, A.K.; Smith, C.M.; Rahmatullah, M.; Nissapatorn, V.; Wilairatana, P.; Spetea, M.; Gueven, N.; Dietis, N. Opioid analgesia and opioid-induced adverse effects: A review. *Pharmaceuticals* **2021**, *14*, 1091. [CrossRef]
9. Jacobson, M.L.; Browne, C.A.; Lucki, I. Kappa opioid receptor antagonists as potential therapeutics for stress-related disorders. *Annu. Rev. Pharmacol. Toxicol.* **2020**, *60*, 615–636. [CrossRef]
10. Spetea, M.; Faheem Asim, M.; Wolber, G.; Schmidhammer, H. The µ opioid receptor and ligands acting at the µ opioid receptor, as therapeutics and potential therapeutics. *Curr. Pharm. Des.* **2013**, *19*, 7415–7434. [CrossRef]
11. Pasternak, G.W.; Childers, S.R.; Pan, Y.-X. Emerging insights into mu opioid pharmacology. *Subst. Use Disord.* **2019**, *258*, 89–125. [CrossRef]
12. Pasternak, G.W.; Pan, Y.-X. Mu opioids and their receptors: Evolution of a concept. *Pharmacol. Rev.* **2013**, *65*, 1257–1317. [CrossRef] [PubMed]
13. Sobczak, Ł.; Goryński, K. Pharmacological aspects of over-the-counter opioid drugs misuse. *Molecules* **2020**, *25*, 3905. [CrossRef]
14. Volkow, N.D.; Blanco, C. The changing opioid crisis: Development, challenges and opportunities. *Mol. Psychiatry* **2021**, *26*, 218–233. [CrossRef] [PubMed]
15. Liu-Chen, L.-Y.; Inan, S. (Eds.) *The Kappa Opioid Receptor*; Springer International Publishing: Cham, Switzerland, 2021.
16. Lemos, J.C.; Chavkin, C. Kappa opioid receptor function. In *The Opiate Receptors*; Pasternak, G., Ed.; Humana Press: Totowa, NJ, USA, 2011; pp. 265–305.
17. Cahill, C.; Tejeda, H.A.; Spetea, M.; Chen, C.; Liu-Chen, L.Y. Fundamentals of the dynorphins/kappa opioid receptor system: From distribution to signaling and function. *Handb. Exp. Pharmacol.* **2022**, *271*, 3–21. [CrossRef] [PubMed]
18. Zangrandi, L.; Schwarzer, C. The kappa opioid receptor system in temporal lobe epilepsy. *Handb. Exp. Pharmacol.* **2022**, *271*, 379–400. [CrossRef] [PubMed]
19. Spetea, M.; Schmidhammer, H. Kappa opioid receptor ligands and pharmacology: Diphenethylamines, a class of structurally distinct, selective kappa opioid ligands. *Handb. Exp. Pharmacol.* **2022**, *271*, 163–195. [CrossRef]
20. Reed, B.; Butelman, E.R.; Kreek, M.J. Kappa opioid receptor antagonists as potential therapeutics for mood and substance use disorders. *Handb. Exp. Pharmacol.* **2022**, *271*, 473–491. [CrossRef]
21. Browne, C.A.; Wulf, H.; Lucki, I. Kappa Opioid receptors in the pathology and treatment of major depressive disorder. *Handb. Exp. Pharmacol.* **2022**, *271*, 493–524. [CrossRef]
22. Schmidhammer, H.; Erli, F.; Guerrieri, E.; Spetea, M. Development of diphenethylamines as selective kappa opioid receptor ligands and their pharmacological activities. *Molecules* **2020**, *25*, 5092. [CrossRef]
23. Aldrich, J.V.; McLaughlin, J.P. Peptide Kappa opioid receptor ligands and their potential for drug development. *Handb. Exp. Pharmacol.* **2022**, *271*, 197–220. [CrossRef]

24. Prisinzano, T.E. Neoclerodanes as Atypical opioid receptor ligands: 2012 David W. Robertson award for excellence in medicinal chemistry. *J. Med. Chem.* **2013**, *56*, 3435–3443. [CrossRef] [PubMed]

25. Nagase, H.; Hayakawa, J.; Kawamura, K.; Kawai, K.; Takezawa, Y.; Matsuura, H.; Tajima, C.; Endo, T. Discovery of a structurally novel opioid k-agonist derived from 4, 5-epoxymorphinan. *Chem. Pharm. Bull.* **1998**, *46*, 366–369. [CrossRef] [PubMed]

26. Vanderah, T.W.; Largent-Milnes, T.; Lai, J.; Porreca, F.; Houghten, R.A.; Menzaghi, F.; Wisniewski, K.; Stalewski, J.; Sueiras-Diaz, J.; Galyean, R. Novel D-amino acid tetrapeptides produce potent antinociception by selectively acting at peripheral κ-opioid receptors. *Eur. J. Pharmacol.* **2008**, *583*, 62–72. [CrossRef] [PubMed]

27. Deeks, E.D. Difelikefalin: First approval. *Drugs* **2021**, *81*, 1937–1944. [CrossRef] [PubMed]

28. Inan, S.; Cowan, A. Antipruritic effects of kappa opioid receptor agonists: Evidence from rodents to humans. *Handb. Exp. Pharmacol.* **2022**, *271*, 275–292. [CrossRef] [PubMed]

29. Miyamoto, Y.; Oh, T.; Aihara, E.; Ando, A. Clinical profiles of nalfurafine hydrochloride for the treatment of pruritus patients. *Handb. Exp. Pharmacol.* **2022**, *271*, 455–472. [CrossRef]

30. Albert-Vartanian, A.; Boyd, M.; Hall, A.; Morgado, S.; Nguyen, E.; Nguyen, V.; Patel, S.; Russo, L.; Shao, A.; Raffa, R. Will peripherally restricted kappa-opioid receptor agonists (pKORA s) relieve pain with less opioid adverse effects and abuse potential? *J. Clin. Pharm. Ther.* **2016**, *41*, 371–382. [CrossRef]

31. Lazenka, M.F. Antinociceptive Effects of kappa-opioid receptor agonists. *Handb. Exp. Pharmacol.* **2022**, *271*, 293–313. [CrossRef]

32. Paton, K.F.; Atigari, D.V.; Kaska, S.; Prisinzano, T.; Kivell, B.M. Strategies for Developing κ opioid receptor agonists for the treatment of pain with fewer side effects. *J. Pharmacol. Exp. Ther.* **2020**, *375*, 332–348. [CrossRef]

33. Kaski, S.W.; White, A.N.; Gross, J.D.; Siderovski, D.P. Potential for kappa-opioid receptor agonists to engineer nonaddictive analgesics: A narrative review. *Anesth. Analg.* **2021**, *132*, 406–419. [CrossRef]

34. Carroll, F.I.; Carlezon, W.A., Jr. Development of κ opioid receptor antagonists. *J. Med. Chem.* **2013**, *56*, 2178–2195. [CrossRef] [PubMed]

35. Portoghese, P.S.; Lipkowski, A.; Takemori, A. Binaltorphimine and nor-binaltorphimine, potent and selective k-opioid receptor antagonists. *Life Sci.* **1987**, *40*, 1287–1292. [CrossRef]

36. Jones, R.M.; Portoghese, P.S. 5′-Guanidinonaltrindole, a highly selective and potent κ-opioid receptor antagonist. *Eur. J. Pharmacol.* **2000**, *396*, 49–52. [CrossRef]

37. Thomas, J.B.; Atkinson, R.N.; Rothman, R.B.; Fix, S.E.; Mascarella, S.W.; Vinson, N.A.; Xu, H.; Dersch, C.M.; Lu, Y.-F.; Cantrell, B.E. Identification of the first trans-(3 R, 4 R)-dimethyl-4-(3-hydroxyphenyl) piperidine derivative to possess highly potent and selective opioid κ receptor antagonist activity. *J. Med. Chem.* **2001**, *44*, 2687–2690. [CrossRef] [PubMed]

38. Buda, J.J.; Carroll, F.I.; Kosten, T.R.; Swearingen, D.; Walters, B.B. A double-blind, placebo-controlled trial to evaluate the safety, tolerability, and pharmacokinetics of single, escalating oral doses of JDTic. *Neuropsychopharmacology* **2015**, *40*, 2059–2065. [CrossRef]

39. Munro, T.A.; Berry, L.M.; Van't Veer, A.; Béguin, C.; Carroll, F.; Zhao, Z.; Carlezon, W.A.; Cohen, B.M. Long-acting κ opioid antagonists nor-BNI, GNTI and JDTic: Pharmacokinetics in mice and lipophilicity. *BMC Pharmacol.* **2012**, *12*, 5. [CrossRef]

40. Black, S.L.; Chauvignac, C.; Grundt, P.; Miller, C.N.; Wood, S.; Traynor, J.R.; Lewis, J.W.; Husbands, S.M. Guanidino N-substituted and N,N-disubstituted derivatives of the kappa-opioid antagonist GNTI. *J. Med. Chem.* **2003**, *46*, 5505–5511. [CrossRef]

41. Endoh, T.; Matsuura, H.; Tanaka, C.; Nagase, H. Nor-binaltorphimine: A potent and selective kappa-opioid receptor antagonist with long-lasting activity in vivo. *Arch. Int. Pharmacodyn. Ther.* **1992**, *316*, 30–42.

42. Rorick-Kehn, L.M.; Witkin, J.M.; Statnick, M.A.; Eberle, E.L.; McKinzie, J.H.; Kahl, S.D.; Forster, B.M.; Wong, C.J.; Li, X.; Crile, R.S. LY2456302 is a novel, potent, orally-bioavailable small molecule kappa-selective antagonist with activity in animal models predictive of efficacy in mood and addictive disorders. *Neuropharmacology* **2014**, *77*, 131–144. [CrossRef]

43. Guerrero, M.; Urbano, M.; Kim, E.-K.; Gamo, A.M.; Riley, S.; Abgaryan, L.; Leaf, N.; Van Orden, L.J.; Brown, S.J.; Xie, J.Y. Design and synthesis of a novel and selective kappa opioid receptor (KOR) antagonist (BTRX-335140). *J. Med. Chem.* **2019**, *62*, 1761–1780. [CrossRef]

44. Patkar, K.A.; Yan, X.; Murray, T.F.; Aldrich, J.V. [N$^{\alpha}$-BenzylTyr ^{1},cyclo(d-Asp^5,Dap^8)]-dynorphin A-(1−11)NH$_2$ cyclized in the "Address" Domain is a novel κ-Opioid receptor antagonist. *J. Med. Chem.* **2005**, *48*, 4500–4503. [CrossRef] [PubMed]

45. Joshi, A.A.; Murray, T.F.; Aldrich, J.V. Structure-Activity relationships of the peptide kappa opioid receptor antagonist zyklophin. *J. Med. Chem.* **2015**, *58*, 8783–8795. [CrossRef] [PubMed]

46. Wu, H.; Wacker, D.; Mileni, M.; Katritch, V.; Han, G.W.; Vardy, E.; Liu, W.; Thompson, A.A.; Huang, X.-P.; Carroll, F. Structure of the human κ-opioid receptor in complex with JDTic. *Nature* **2012**, *485*, 327–332. [CrossRef] [PubMed]

47. Che, T.; Majumdar, S.; Zaidi, S.A.; Ondachi, P.; McCorvy, J.D.; Wang, S.; Mosier, P.D.; Uprety, R.; Vardy, E.; Krumm, B.E.; et al. Structure of the nanobody-stabilized active state of the kappa opioid receptor. *Cell* **2018**, *172*, 55–67.e15. [CrossRef] [PubMed]

48. Che, T.; English, J.; Krumm, B.E.; Kim, K.; Pardon, E.; Olsen, R.H.J.; Wang, S.; Zhang, S.; Diberto, J.F.; Sciaky, N.; et al. Nanobody-enabled monitoring of kappa opioid receptor states. *Nat. Commun.* **2020**, *11*, 1145. [CrossRef]

49. Zaidi, S.A.; Katritch, V. Structural Characterization of KOR Inactive and active states for 3D pharmacology and drug discovery. *Handb. Exp. Pharmacol.* **2022**, *271*, 41–64. [CrossRef]

50. Kaserer, T.; Lantero, A.; Schmidhammer, H.; Spetea, M.; Schuster, D. μ Opioid receptor: Novel antagonists and structural modeling. *Sci. Rep.* **2016**, *6*, 21548. [CrossRef]

51. Erli, F.; Guerrieri, E.; Ben Haddou, T.; Lantero, A.; Mairegger, M.; Schmidhammer, H.; Spetea, M. Highly Potent and selective new diphenethylamines interacting with the κ-opioid receptor: Synthesis, pharmacology, and structure-activity relationships. *J. Med. Chem.* **2017**, *60*, 7579–7590. [CrossRef]

52. Dumitrascuta, M.; Bermudez, M.; Trovato, O.; De Neve, J.; Ballet, S.; Wolber, G.; Spetea, M. Antinociceptive efficacy of the μ-opioid/nociceptin peptide-based hybrid KGNOP1 in inflammatory pain without rewarding effects in mice: An experimental assessment and molecular docking. *Molecules* **2021**, *26*, 3267. [CrossRef]

53. Manglik, A.; Kruse, A.C.; Kobilka, T.S.; Thian, F.S.; Mathiesen, J.M.; Sunahara, R.K.; Pardo, L.; Weis, W.I.; Kobilka, B.K.; Granier, S. Crystal structure of the μ-opioid receptor bound to a morphinan antagonist. *Nature* **2012**, *485*, 321–326. [CrossRef]

54. Fenalti, G.; Giguere, P.M.; Katritch, V.; Huang, X.-P.; Thompson, A.A.; Cherezov, V.; Roth, B.L.; Stevens, R.C. Molecular control of δ-opioid receptor signalling. *Nature* **2014**, *506*, 191–196. [CrossRef] [PubMed]

55. Ballesteros, J.A.; Weinstein, H. [19] Integrated methods for the construction of three-dimensional models and computational probing of structure-function relations in G protein-coupled receptors. In *Methods in Neurosciences*; Sealfon, S.C., Ed.; Academic Press: San Diego, CA, USA; London, UK, 1995; Volume 25, pp. 366–428.

56. Fenalti, G.; Zatsepin, N.A.; Betti, C.; Giguere, P.; Han, G.W.; Ishchenko, A.; Liu, W.; Guillemyn, K.; Zhang, H.; James, D.; et al. Structural basis for bifunctional peptide recognition at human δ-opioid receptor. *Nat. Struct. Mol. Biol.* **2015**, *22*, 265–268. [CrossRef] [PubMed]

57. Vo, Q.N.; Mahinthichaichan, P.; Shen, J.; Ellis, C.R. How μ-opioid receptor recognizes fentanyl. *Nat. Commun.* **2021**, *12*, 984. [CrossRef] [PubMed]

58. Sydow, D. *Dynophores: Novel Dynamic Pharmacophores Implementation of Pharmacophore Generation Based on Molecular Dynamics Trajectories and Their Graphical Representation*; Freie Universität Berlin: Berlin, Germany, 2015.

59. Avdeef, A.; Testa, B. Physicochemical profiling in drug research: A brief survey of the state-of-the-art of experimental techniques. *Cell. Mol. Life Sci.* **2002**, *59*, 1681–1689. [CrossRef] [PubMed]

60. Faller, B. Physicochemical profiling in early drug discovery: New challenges at the age of high-throughput screen and combinatorial chemistry. In *Chemistry and Molecular Aspects of Drug Design and Action*; Rekka, E.A., Kourounakis, P.N., Eds.; CRC Press: Boca Raton, FL, USA, 2008; pp. 303–312.

61. Habgood, M.; Begley, D.; Abbott, N. Determinants of passive drug entry into the central nervous system. *Cell. Mol. Neurobiol.* **2000**, *20*, 231–253. [CrossRef]

62. *ACD/Percepta*, Version 2021; Advanced Chemistry Development (ACD/Labs), Inc.: Toronto, ON, Canada, 2021. Available online: https://www.acdlabs.com/products/percepta/ (accessed on 3 May 2022).

63. Daina, A.; Zoete, V. A boiled-egg to predict gastrointestinal absorption and brain penetration of small molecules. *ChemMedChem* **2016**, *11*, 1117–1121. [CrossRef]

64. Daina, A.; Michielin, O.; Zoete, V. SwissADME: A free web tool to evaluate pharmacokinetics, drug-likeness and medicinal chemistry friendliness of small molecules. *Sci. Rep.* **2017**, *7*, 42717. [CrossRef]

65. Bradford, M.M. A rapid and sensitive method for the quantitation of microgram quantities of protein utilizing the principle of protein-dye binding. *Anal. Biochem.* **1976**, *72*, 248–254. [CrossRef]

66. Cheng, Y.-C.; Prusoff, W.H. Relationship between the inhibition constant (KI) and the concentration of inhibitor which causes 50 per cent inhibition (I50) of an enzymatic reaction. *Biochem. Pharmacol.* **1973**, *22*, 3099–3108. [CrossRef]

67. Berman, H.; Henrick, K.; Nakamura, H. Announcing the worldwide Protein Data Bank. *Nat. Struct. Biol.* **2003**, *10*, 980. [CrossRef]

68. Molecular Operating Environment (MOE), C.C.G.U., Sherbooke St. West, Suite #910, Montreal, QC, Canada, H3A 2R7, 2021. Available online: https://www.chemcomp.com/Products.htm (accessed on 24 January 2022).

69. The UniProt Consortium. UniProt: The universal protein knowledgebase in 2021. *Nucleic Acids Res.* **2021**, *49*, D480–D489. [CrossRef] [PubMed]

70. Ramachandran, G.N.; Ramakrishnan, C.; Sasisekharan, V. Stereochemistry of polypeptide chain configurations. *J. Mol. Biol.* **1963**, *7*, 95–99. [CrossRef]

71. Zhu, S. Validation of the Generalized Force Fields GAFF, CGenFF, OPLS-AA, and PRODRGFF by Testing Against Experimental Osmotic Coefficient Data for Small Drug-Like Molecules. *J. Chem. Inf. Model.* **2019**, *59*, 4239–4247. [CrossRef] [PubMed]

72. Labute, P. The generalized Born/volume integral implicit solvent model: Estimation of the free energy of hydration using London dispersion instead of atomic surface area. *J. Comput. Chem.* **2008**, *29*, 1693–1698. [CrossRef] [PubMed]

73. Labute, P. Protonate3D: Assignment of ionization states and hydrogen coordinates to macromolecular structures. *Proteins* **2009**, *75*, 187–205. [CrossRef]

74. Vardy, E.; Mosier, P.D.; Frankowski, K.J.; Wu, H.; Katritch, V.; Westkaemper, R.B.; Aubé, J.; Stevens, R.C.; Roth, B.L. Chemotype-selective modes of action of κ-opioid receptor agonists. *J. Biol. Chem.* **2013**, *288*, 34470–34483. [CrossRef]

75. Chavkin, C.; McLaughlin, J.P.; Celver, J.P. Regulation of opioid receptor function by chronic agonist exposure: Constitutive activity and desensitization. *Mol. Pharmacol.* **2001**, *60*, 20–25. [CrossRef]

76. Claff, T.; Yu, J.; Blais, V.; Patel, N.; Martin, C.; Wu, L.; Han, G.W.; Holleran, B.J.; van der Poorten, O.; White, K.L.; et al. Elucidating the active δ-opioid receptor crystal structure with peptide and small-molecule agonists. *Sci. Adv.* **2019**, *5*, eaax9115. [CrossRef]

77. Befort, K.; Zilliox, C.; Filliol, D.; Yue, S.; Kieffer, B.L. Constitutive activation of the delta opioid receptor by mutations in transmembrane domains III and VII. *J. Biol. Chem.* **1999**, *274*, 18574–18581. [CrossRef]

78. Décaillot, F.M.; Befort, K.; Filliol, D.; Yue, S.; Walker, P.; Kieffer, B.L. Opioid receptor random mutagenesis reveals a mechanism for G protein-coupled receptor activation. *Nat. Struct. Biol.* **2003**, *10*, 629–636. [CrossRef]

79. 3D Structure Generator CORINA Classic. Molecular Networks GmbH, Nuremberg, Germany. Available online: https://mn-am.com/products/corina/ (accessed on 3 February 2022).

80. Gasteiger, J.; Rudolph, C.; Sadowski, J. Automatic generation of 3D-atomic coordinates for organic molecules. *Tetrahedron Comput. Methodol.* **1990**, *3*, 537–547. [CrossRef]

81. Jones, G.; Willett, P.; Glen, R.C.; Leach, A.R.; Taylor, R. Development and validation of a genetic algorithm for flexible docking. *J. Mol. Biol.* **1997**, *267*, 727–748. [CrossRef] [PubMed]

82. Evers, A.; Hessler, G.; Matter, H.; Klabunde, T. Virtual screening of biogenic amine-binding G-protein coupled receptors: Comparative evaluation of protein- and ligand-based virtual screening protocols. *J. Med. Chem.* **2005**, *48*, 5448–5465. [CrossRef] [PubMed]

83. Verdonk, M.L.; Cole, J.C.; Hartshorn, M.J.; Murray, C.W.; Taylor, R.D. Improved protein-ligand docking using GOLD. *Proteins* **2003**, *52*, 609–623. [CrossRef]

84. Halgren, T.A. Merck molecular force field. I. Basis, form, scope, parameterization, and performance of MMFF94. *J. Comput. Chem.* **1996**, *17*, 490–519. [CrossRef]

85. Halgren, T.A. Merck molecular force field. II. MMFF94 van der Waals and electrostatic parameters for intermolecular interactions. *J. Comput. Chem.* **1996**, *17*, 520–552. [CrossRef]

86. Halgren, T.A. Merck molecular force field. III. Molecular geometries and vibrational frequencies for MMFF94. *J. Comput. Chem.* **1996**, *17*, 553–586. [CrossRef]

87. Halgren, T.A.; Nachbar, R.B. Merck molecular force field. IV. Conformational energies and geometries for MMFF94. *J. Comput. Chem.* **1996**, *17*, 587–615. [CrossRef]

88. Halgren, T.A. Merck molecular force field. V. Extension of MMFF94 using experimental data, additional computational data, and empirical rules. *J. Comput. Chem.* **1996**, *17*, 616–641. [CrossRef]

89. Wolber, G.; Dornhofer, A.A.; Langer, T. Efficient overlay of small organic molecules using 3D pharmacophores. *J. Comput. Aided Mol. Des.* **2006**, *20*, 773–788. [CrossRef]

90. Wolber, G.; Langer, T. LigandScout: 3-D pharmacophores derived from protein-bound ligands and their use as virtual screening filters. *J. Chem. Inf. Model.* **2005**, *45*, 160–169. [CrossRef] [PubMed]

91. *Schrödinger Release-4: Maestro*, Version 2020-4; Schrödinger LLC.: New York, NY, USA, 2020.

92. Jorgensen, W.L.; Schyman, P. Treatment of Halogen Bonding in the OPLS-AA Force Field: Application to Potent Anti-HIV Agents. *J. Chem. Theory Comput.* **2012**, *8*, 3895–3901. [CrossRef] [PubMed]

93. Ponder, J.W.; Case, D.A. Force Fields for protein simulations. In *Advances in Protein Chemistry*; Academic Press: Cambridge, MA, USA, 2003; Volume 66, pp. 27–85.

94. Bowers, K.J.; Chow, D.E.; Xu, H.; Dror, R.O.; Eastwood, M.P.; Gregersen, B.A.; Klepeis, J.L.; Kolossvary, I.; Moraes, M.A.; Sacerdoti, F.D.; et al. Scalable Algorithms for Molecular Dynamics Simulations on Commodity Clusters. In Proceedings of the ACM/IEEE Conference on Supercomputing (SC06), Tampa, FL, USA, 11–17 November 2006.

95. Lomize, M.A.; Pogozheva, I.D.; Joo, H.; Mosberg, H.I.; Lomize, A.L. OPM database and PPM web server: Resources for positioning of proteins in membranes. *Nucleic Acids Res.* **2012**, *40*, D370–D376. [CrossRef] [PubMed]

96. Jorgensen, W.L.; Chandrasekhar, J.; Madura, J.D.; Impey, R.W.; Klein, M.L. Comparison of simple potential functions for simulating liquid water. *J. Chem. Phys.* **1983**, *79*, 926–935. [CrossRef]

97. Bock, A.; Bermudez, M.; Krebs, F.; Matera, C.; Chirinda, B.; Sydow, D.; Dallanoce, C.; Holzgrabe, U.; Amici, M.d.; Lohse, M.J.; et al. Ligand binding ensembles determine graded agonist efficacies at a G protein-coupled receptor. *J. Biol. Chem.* **2016**, *291*, 16375–16389. [CrossRef]

98. Humphrey, W.; Dalke, A.; Schulten, K. VMD: Visual molecular dynamics. *J. Mol. Graph.* **1996**, *14*, 33–38. [CrossRef]

Supporting Materials

In vitro, *in vivo* and *in silico* characterization of a novel kappa-opioid receptor antagonist

Kristina Puls[1], Aina-Leonor Olivé-Marti[2], Szymon Pach[1], Birgit Pinter[2], Filippo Erli[2], Gerhard Wolber[1]*, Mariana Spetea[2]*

[1]Department of Pharmaceutical Chemistry, Institute of Pharmacy, Freie Universität Berlin; Königin-Luise-Str. 2+4, D-14195 Berlin, Germany; kristina.puls@fu-berlin.de (K.P.), s.pach@fu-berlin.de (S.P.), gerhard.wolber@fu-berlin.de (G.W.)
[2]Department of Pharmaceutical Chemistry, Institute of Pharmacy and Center for Molecular Biosciences Innsbruck (CMBI), University of Innsbruck, Innrain 80-82, 6020 Innsbruck, Austria; aina-leonor.olive-marti@uibk.ac.at (A-L.O-M.), birgit-pinter@gmax.at (B.P.), f.erli@hotmail.it (F.E.), mariana.spetea@uibk.ac.at (M.S.)

*Correspondence: gerhard.wolber@fu-berlin.de (G.W.), Tel.: +49-30-838-52686; mariana.spetea@uibk.ac.at (M.S.), Tel.: +43-512-507-58277
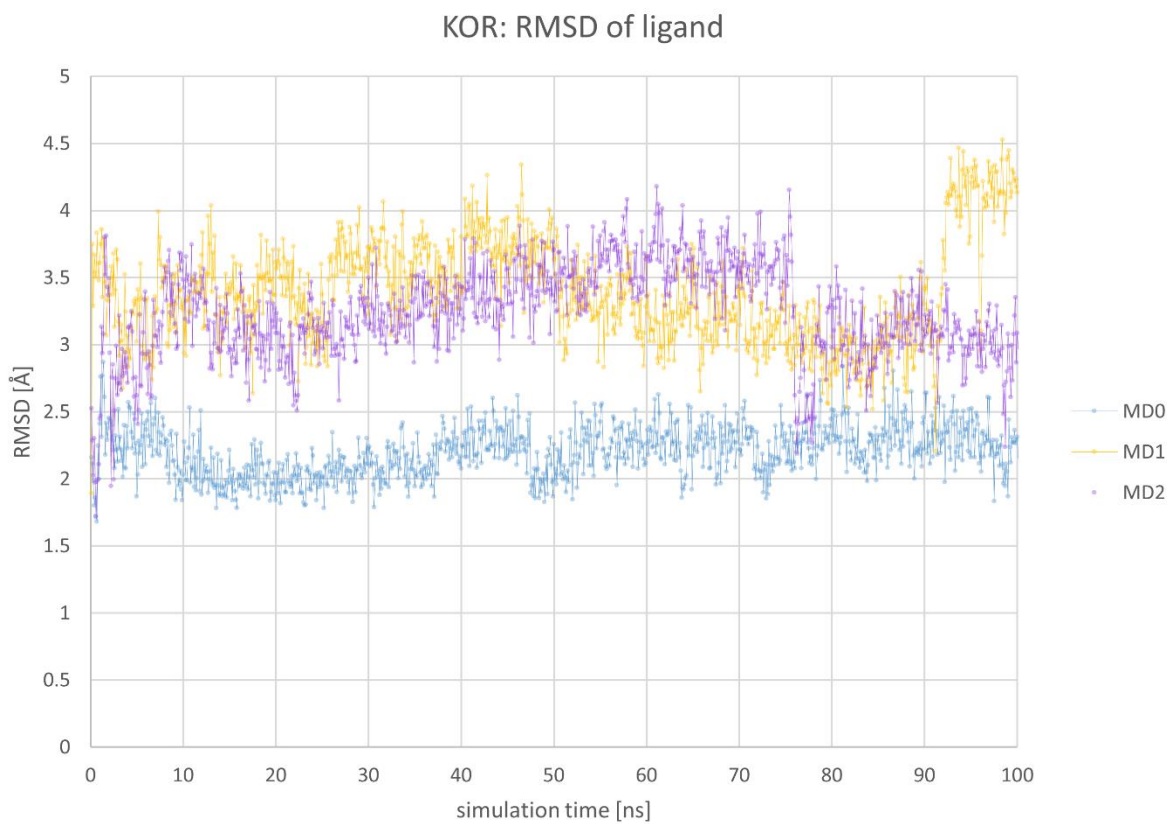
Figure S1. Root mean square deviation of Compound A in complex with the KOR over the simulation time.
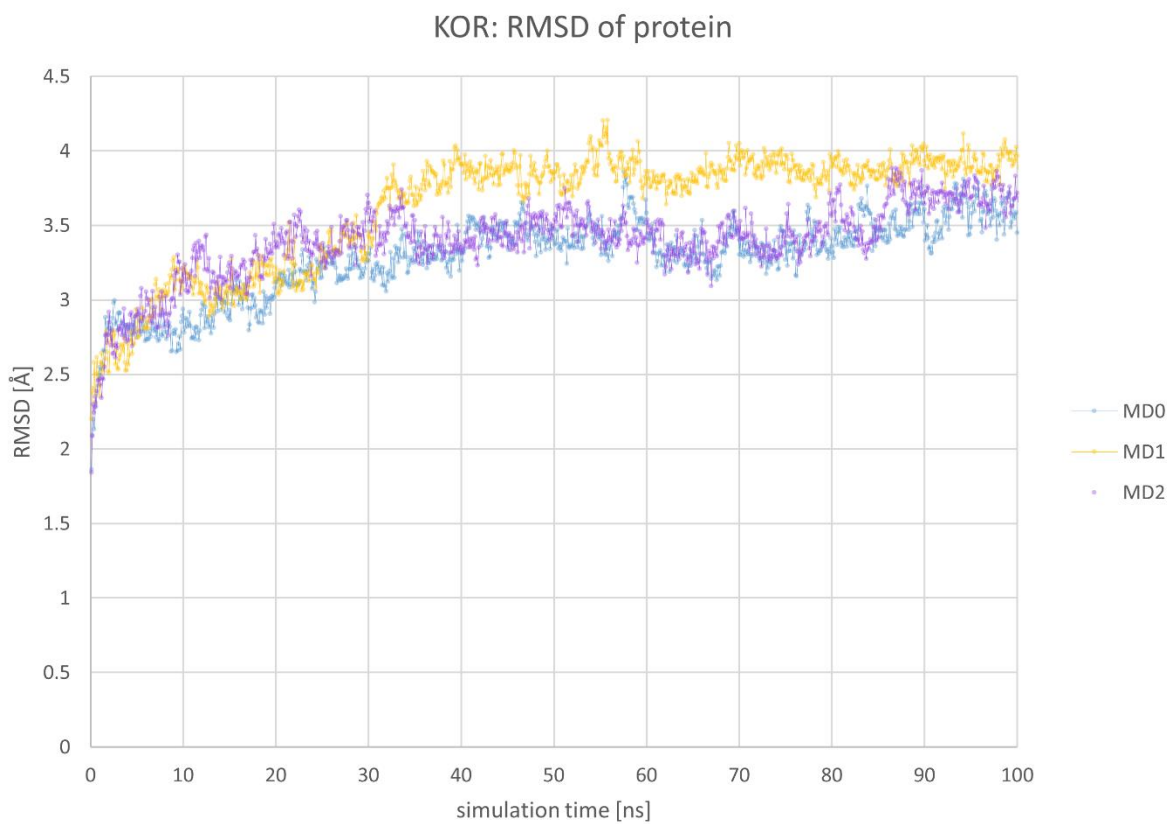
Figure S2. Root mean square deviation of the KOR backbone atoms in complex with Compound A over the simulation time.

Figure S3. Root mean square deviation of Compound A in complex with the MOR over the simulation time.

Figure S4. Root mean square deviation of the MOR backbone atoms in complex with Compound A over the simulation time.

Figure S5. Root mean square deviation of Compound A in complex with the DOR over the simulation time.

Figure S6. Root mean square deviation of the DOR backbone atoms in complex with Compound A over the simulation time.

KOR: RMSF of heavy atoms
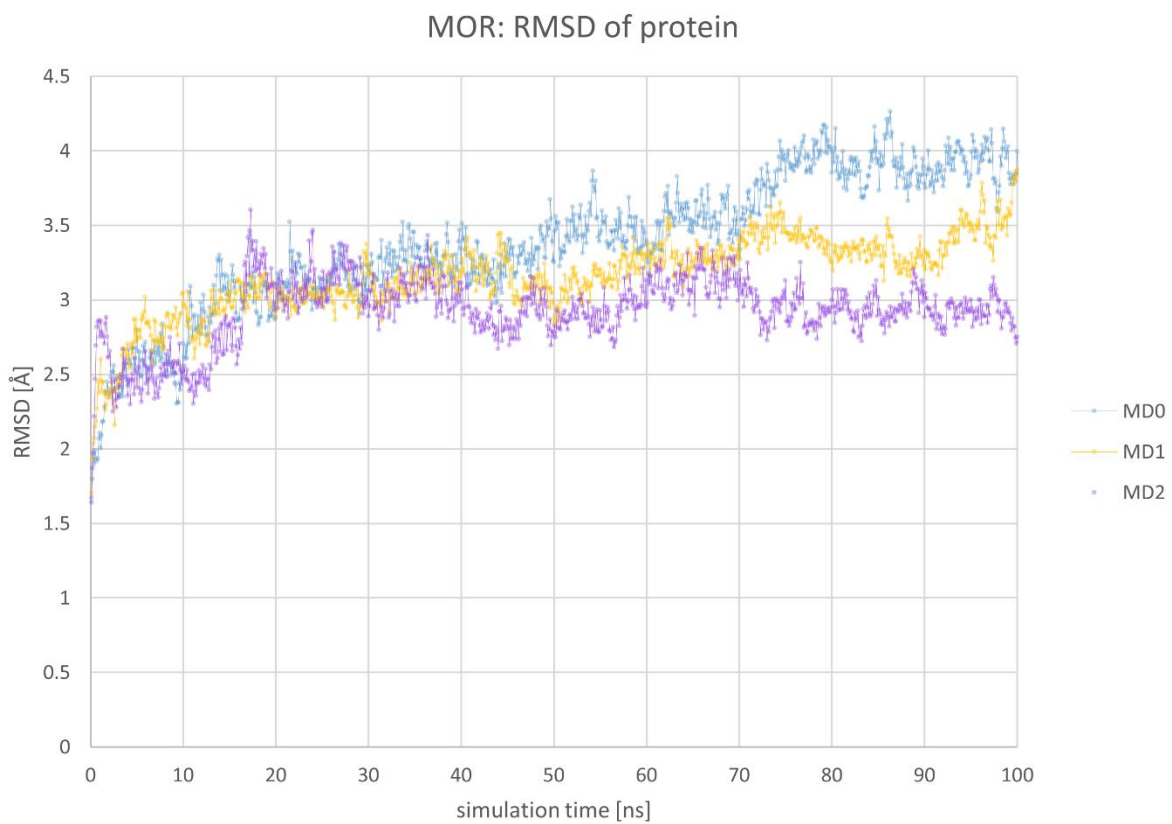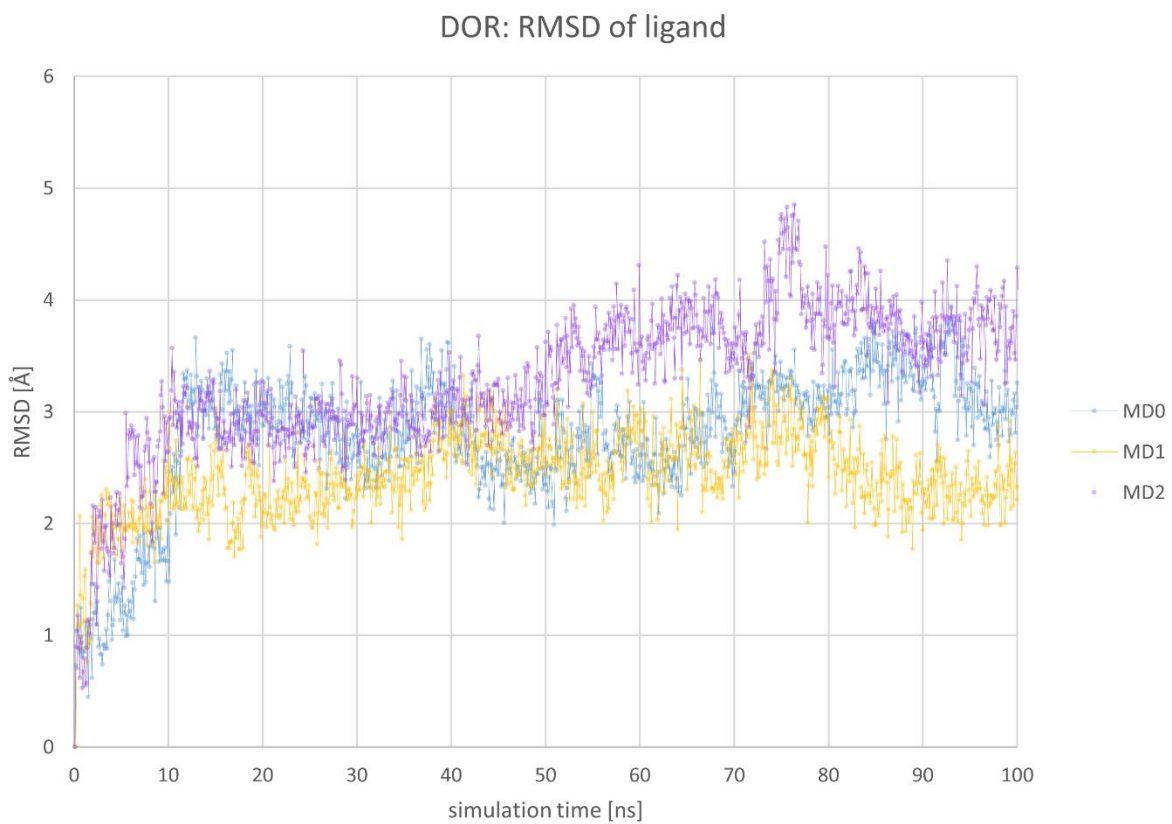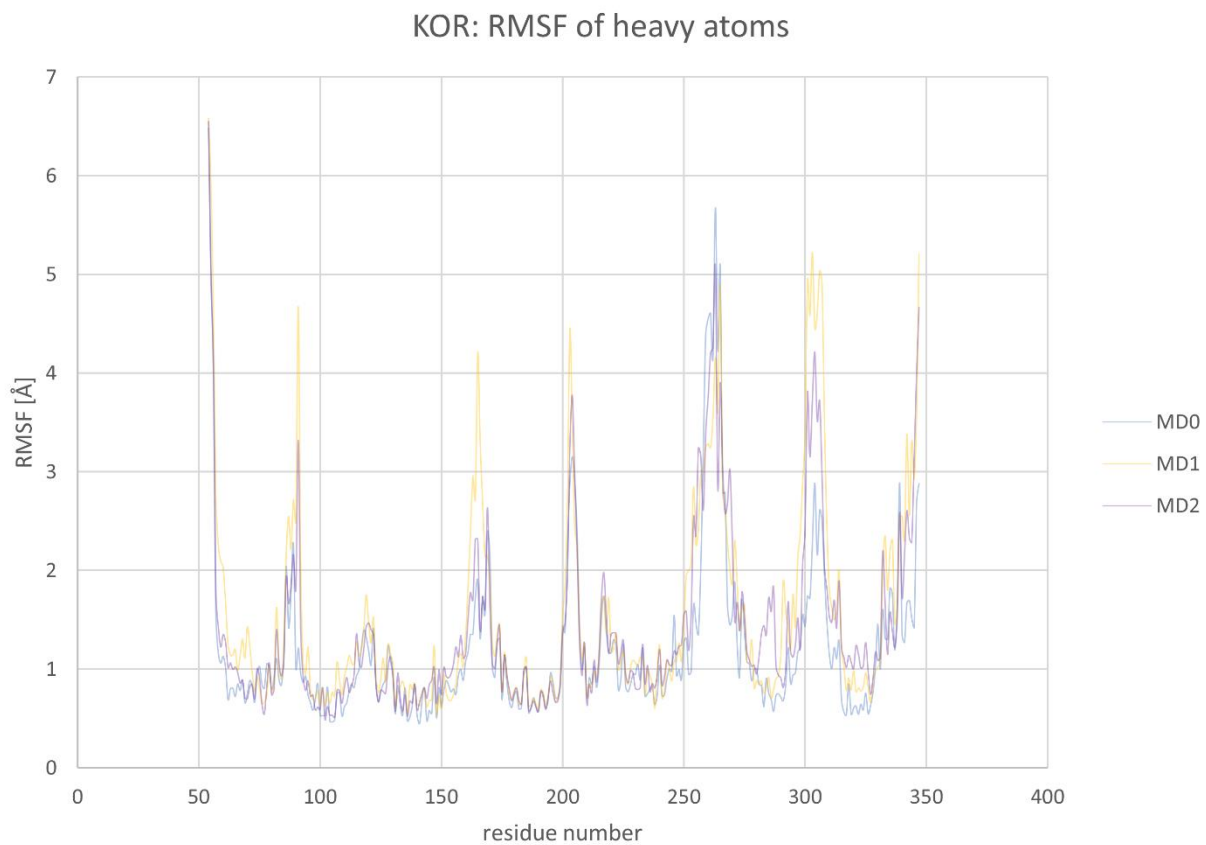
Figure S7. Root mean square fluctuation (RMSF) of KOR heavy atoms within MD simulations.
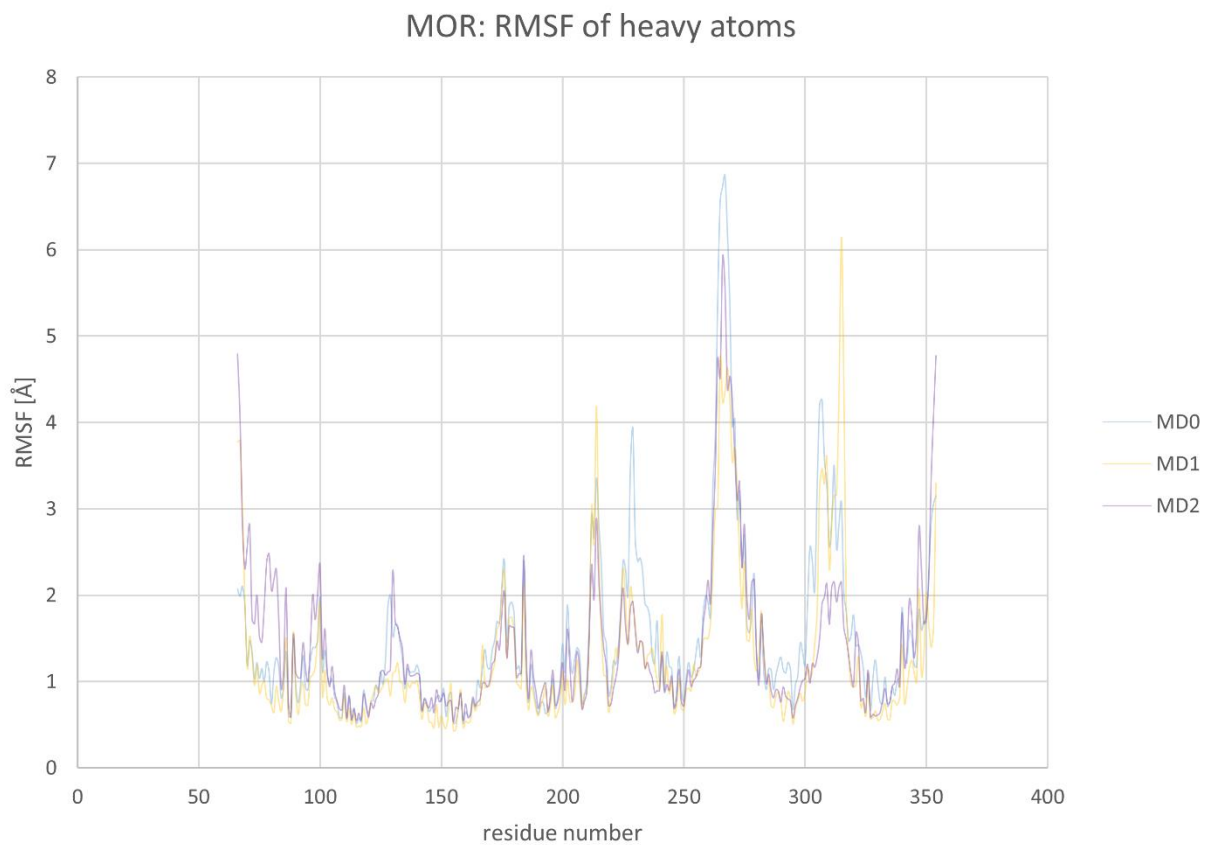
Figure S8. Root mean square fluctuation (RMSF) of MOR heavy atoms within MD simulations.
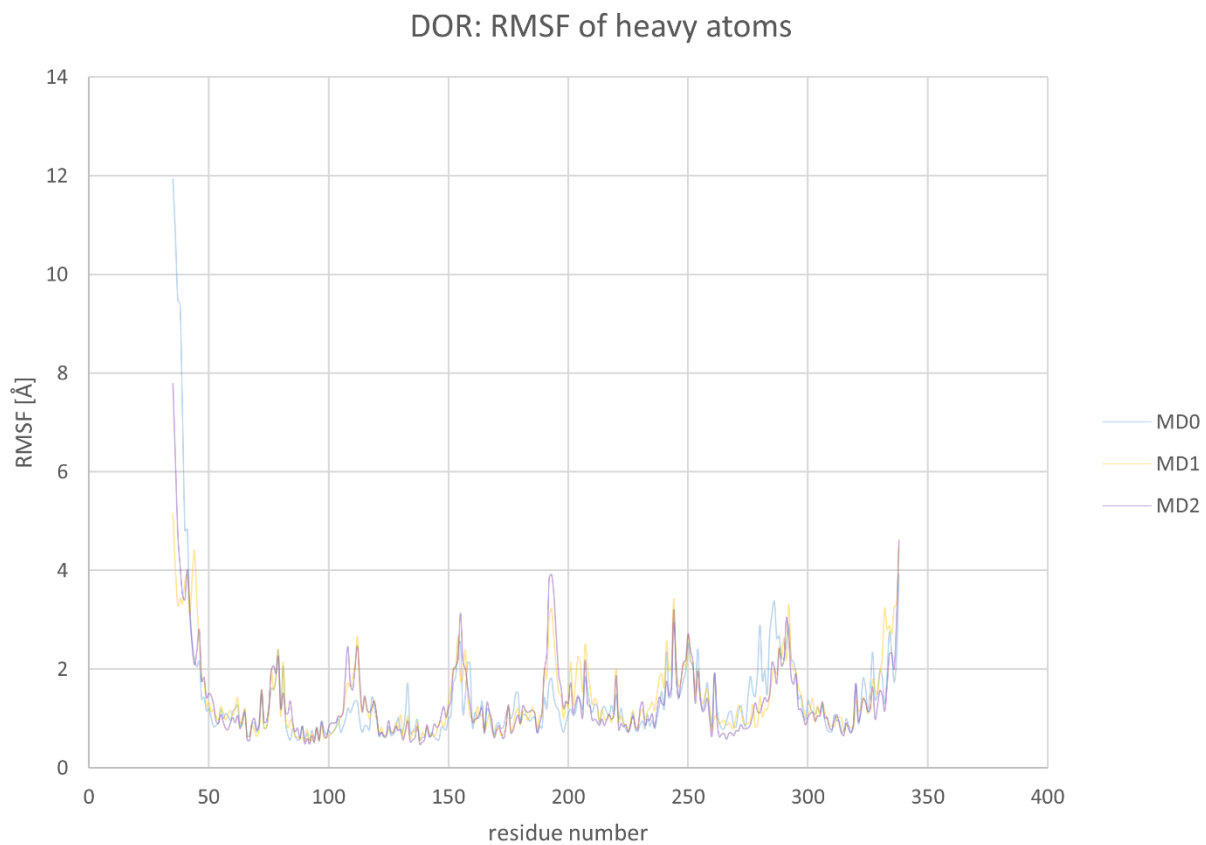
Figure S9. Root mean square fluctuation (RMSF) of DOR heavy atoms within MD simulations.
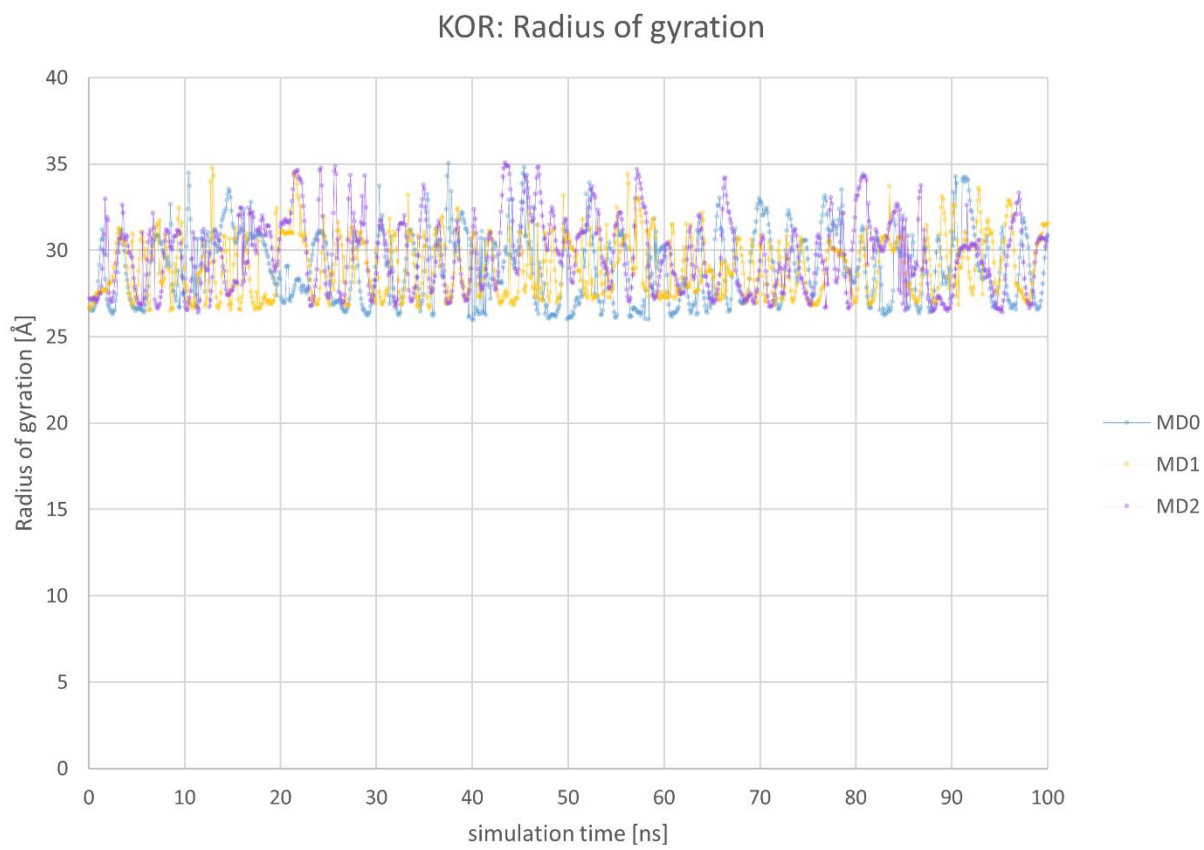
Figure S10. Radius of gyration of the KOR in complex with Compound A over the simulation time. The radius of gyration values remain stable over the simulation time corresponding to a similar KOR compactness along the MD simulations.
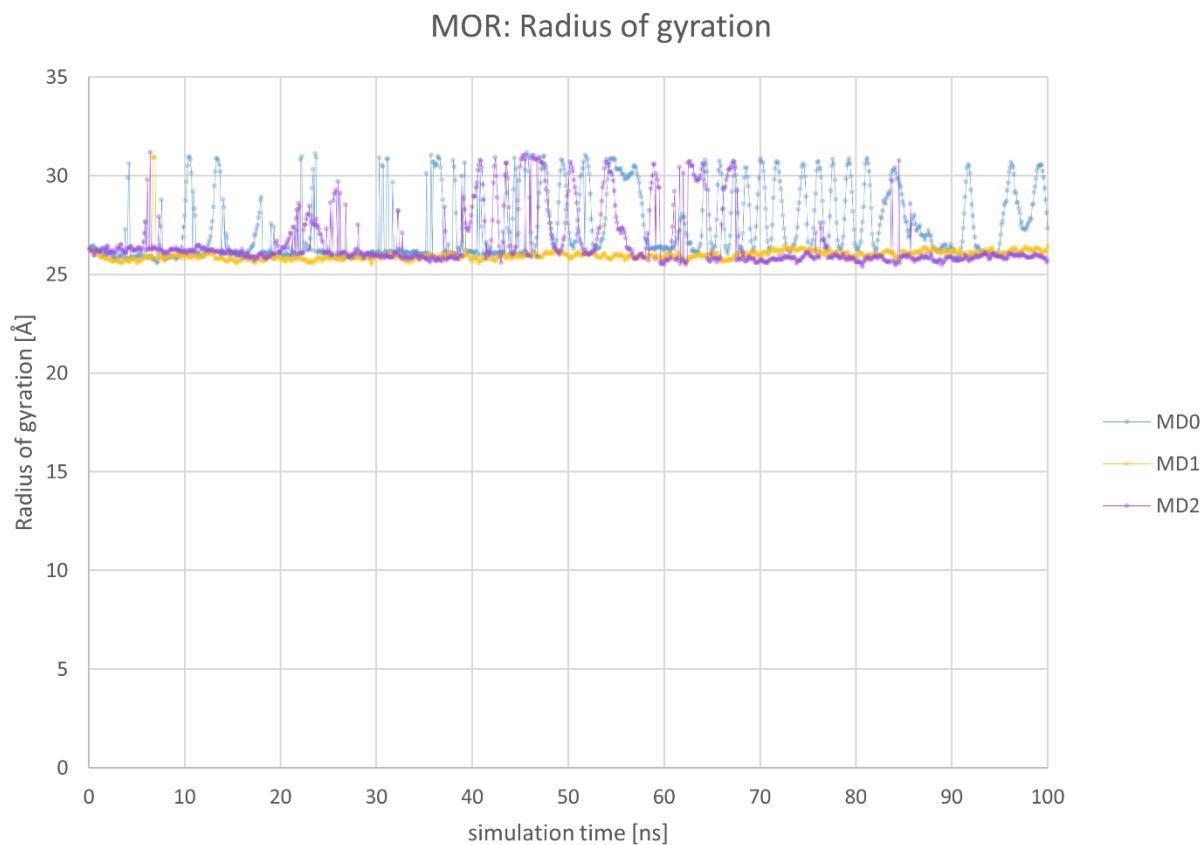
Figure S11. Radius of gyration of the MOR in complex with Compound A over the simulation time. The radius of gyration values remain stable over the simulation time corresponding to a similar MOR compactness along the MD simulations.
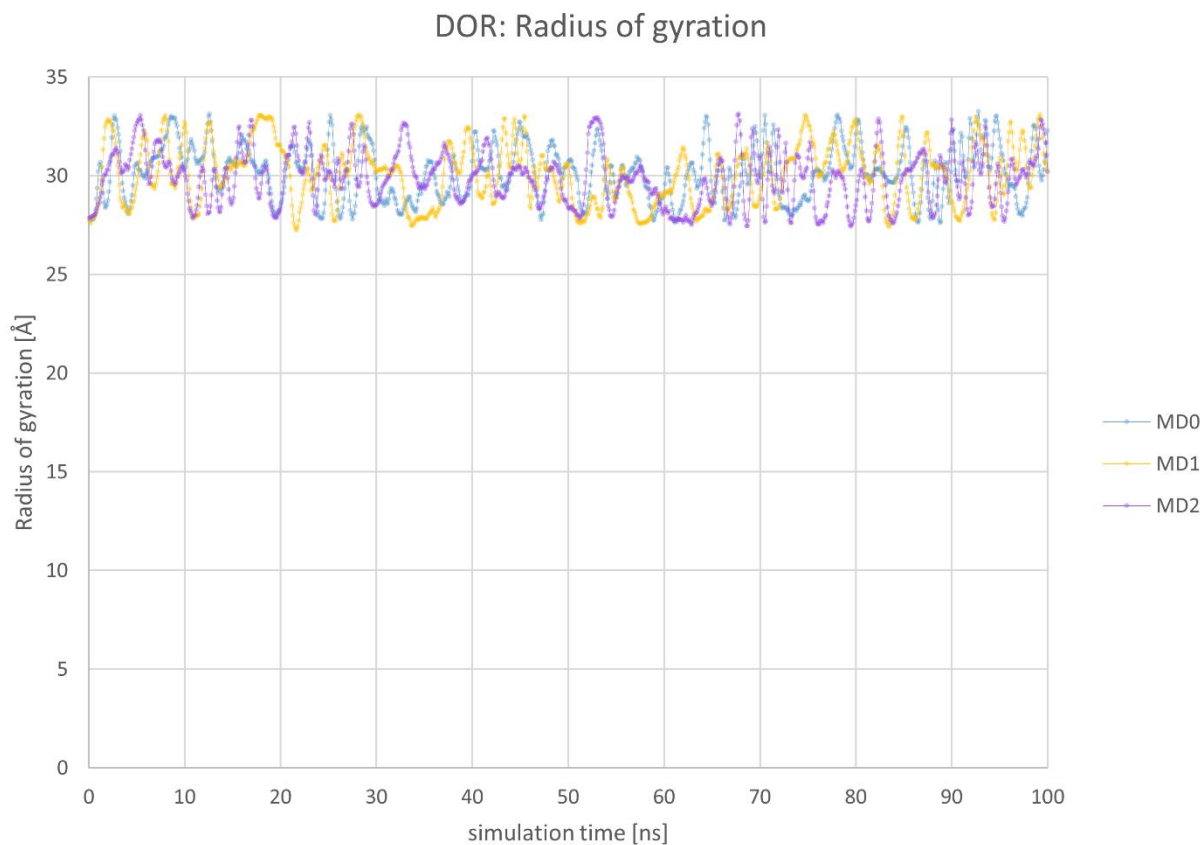
Figure S12. Radius of gyration of the DOR in complex with Compound A over the simulation time. The radius of gyration values remain stable over the simulation time corresponding to a similar DOR compactness along the MD simulations.
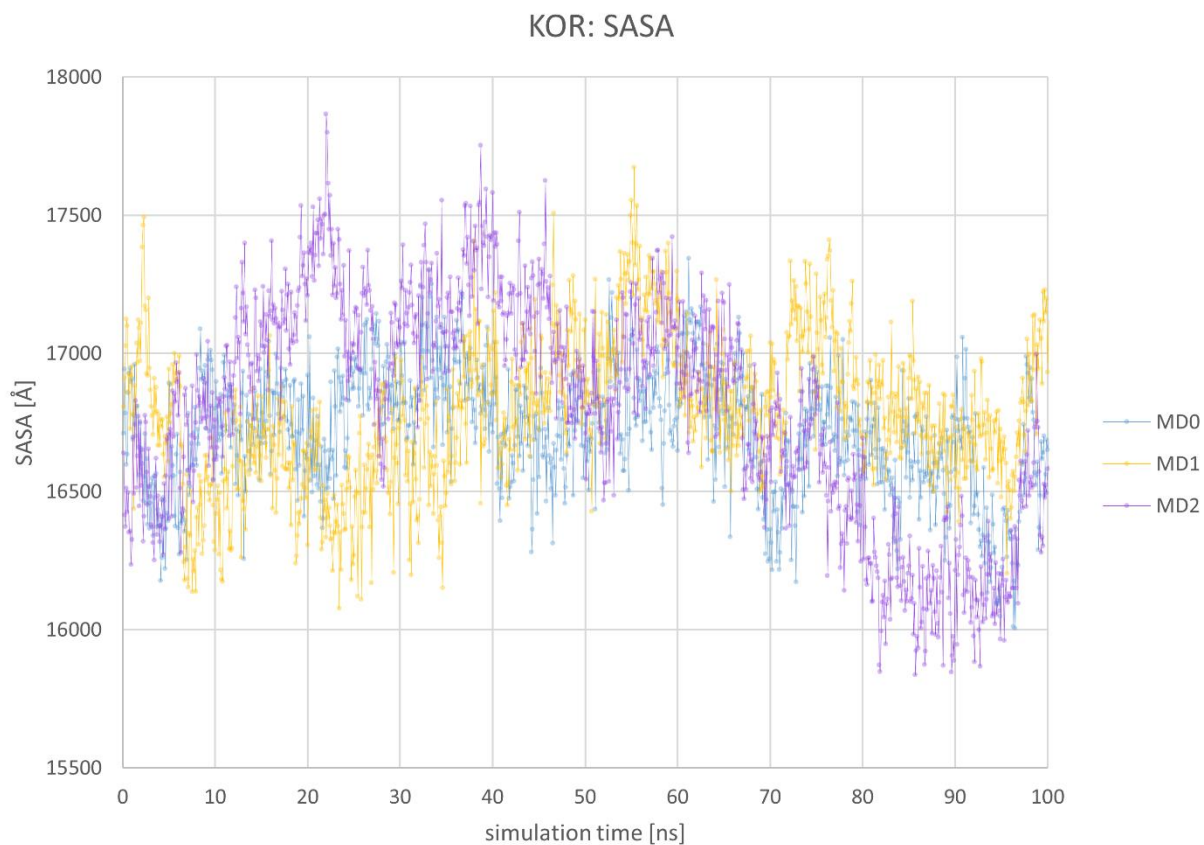
Figure S13. Solvent accessible surface area (SASA) of KOR in complex with Compound A over the simulation time. No strong increase in SASA was observed correlating with stable receptor folding.
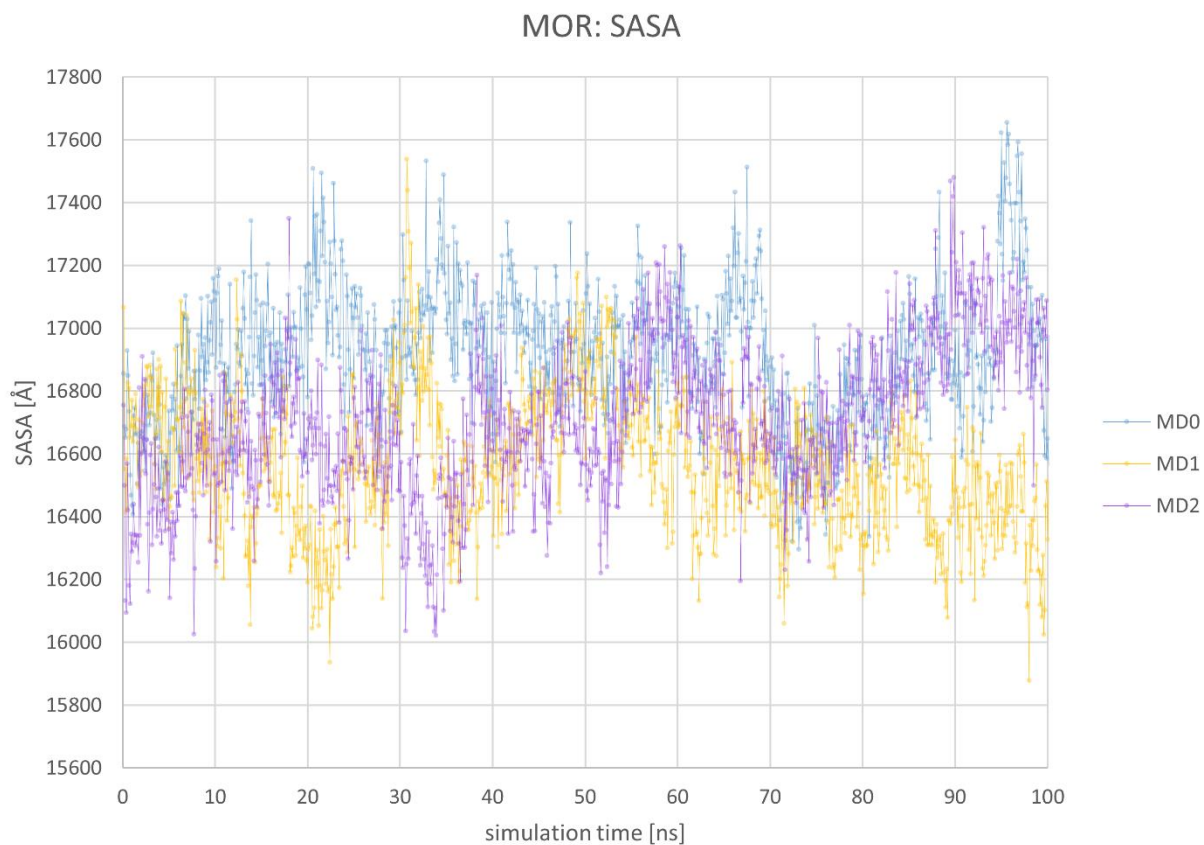
Figure S14. Solvent accessible surface area (SASA) of MOR in complex with Compound A over the simulation time. No strong increase in SASA was observed correlating with stable receptor folding.
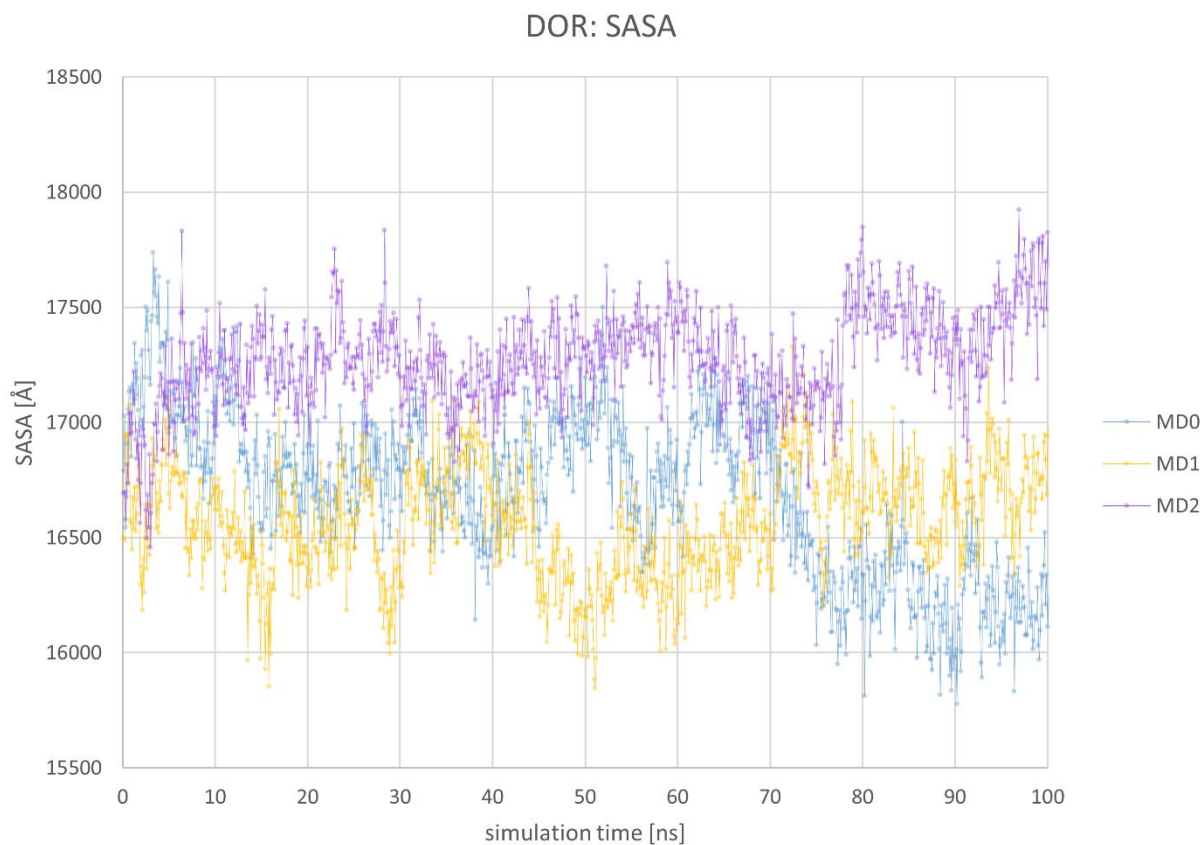
Figure S15. Solvent accessible surface area (SASA) of DOR in complex with Compound A over the simulation time. No strong increase in SASA was observed correlating with stable receptor folding.
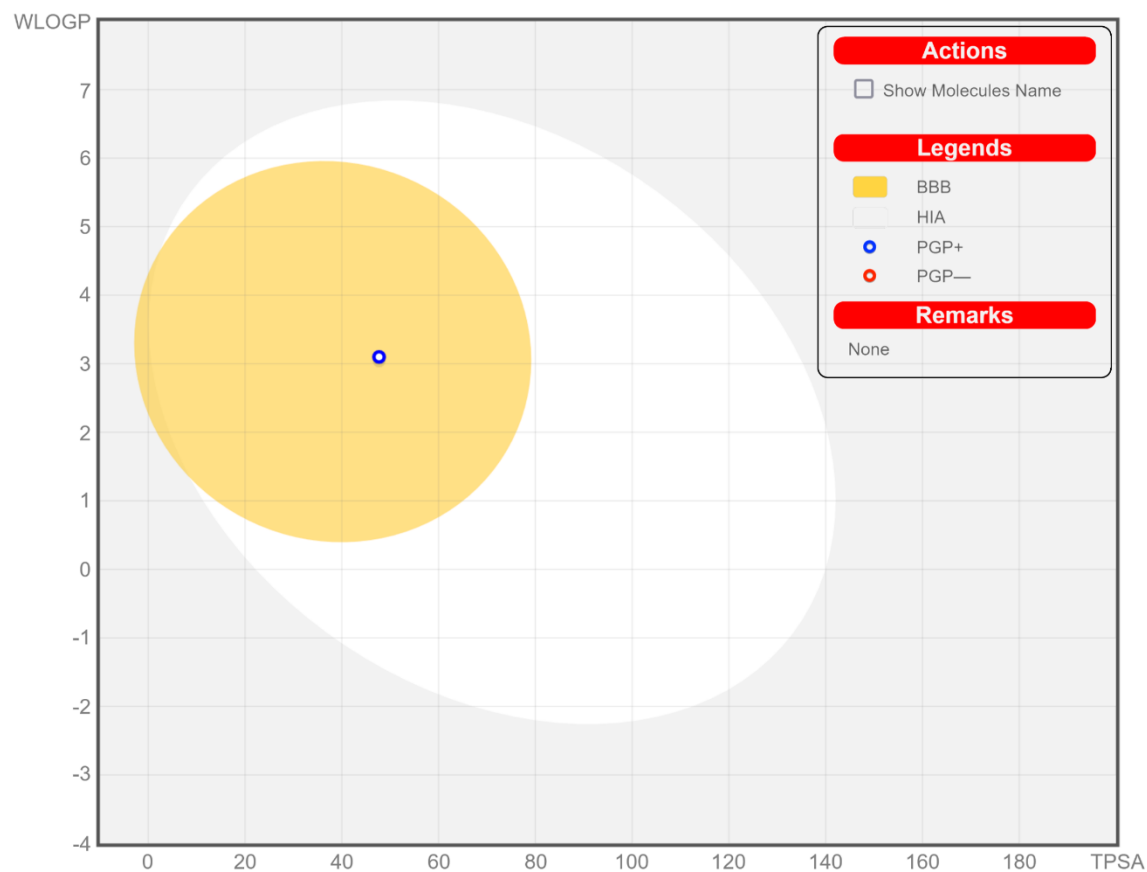
Figure S16. BOILED-Egg plot of Compound A calculated using SwissADME web tool [1]. The BOILED-Egg method (Brain or IntestinaL EstimateD permeation method) calculated lipophilicity (WLOGP, a logP method developed by Wildman and Crippen) and polarity (topological polar surface area, TPSA) to estimate the permeation capabilities of small molecules [2]. Compound A was predicted to have high gastrointestinal absorption and to readily pass the brain- barrier barrier, but also as a permeability-glycoprotein substrate. These findings are in accordance with the previous hypothesis of Compound A being a CNS penetrant. Abbreviations: HIA: passive human gastrointestinal absorption, PGP: Permeability glycoprotein.
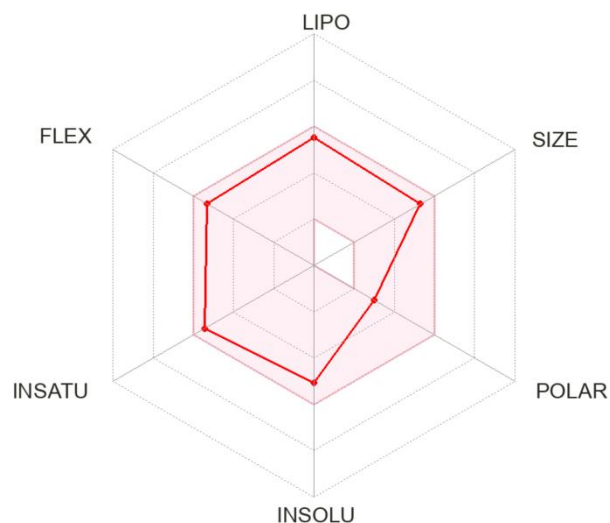
Figure S17. Bioavailability radar of Compound A. The bioavailability radar includes information about Compound A's lipophilicity (LIPO), molecular weight (SIZE), polarity (POLAR), solubility (INSOLU), flexibility (FLEX), and saturation (INSATU), all calculated using the SwissADME web tool [1]. Compound A is predicted orally available as all calculated physicochemical properties are within the optimal range (LIPO: 0.7 < XLOGP3 < +5.0; SIZE: 150 g/mol < MV < 500 g/mol; POLAR: 20Å^2 < TPSA < 130 Å^2; INSOLU: -6 < Log S (ESOL) < 0; INSATU: 0.25 < Fraction Csp3 < 1; FLEX: 0 < No. of rotatable bonds < 9) indicated in pink.

Table S1. Binding affinities and antagonist potencies at the KOR of Compound A and known KOR antagonists.

Ligand	Binding affinity[a] K_i	Antagonist activity[b] K_e	Reference
Compound A	1.53 μM	1.53 μM	
nor-BNI	0.153 nM	0.798 nM	[3]
5'-GNTI	0.18 nM	0.04 nM	[4]
JDTic	0.031 nM	0.098 nM	[3]
JNJ-67953964/LY2456302	0.807 nM	0.813 nM	[3]
CYM-53003/BTRX-335140	-[c]	0.8 nM[d]	[5]
Zyklophin	95.2 nM	336 nM	[6]

[a]Determined in the radioligand binding assay using recombinant cells expressing the human KOR; [b]Determined in the [^{35}S]GTPγS binding assay using recombinant cells expressing the human KOR. [c]- Not reported. [d]Reported as IC_{50} value.

Table S2. Calculated physicochemical properties of Compound A[a] to predict its bioavailability.

Physicochemical property	Parameter	Predicted value[b]
Lipophilicity (LIPO)	Log $P_{o/w}$ (XLOGP3)	4.14
Molecular weight (SIZE)	Molecular weight	438.97 g/mol
Polarity (POLAR)	TPSA	47.70 Å^2
Solubility (INSOLU)	Log S (ESOL)	-5.05
Flexibility (FLEX)	Fraction Csp3	0.32
Saturation (INSATU)	Number of rotatable bonds	8

[a]For Compound A in the protonated state. [b]Calculated using SwissADME web tool [1]. Abbreviations: TPSA: topological polar surface area, ESOL: estimated solubility, log S: decimal logarithm of the molar solubility in water, Csp3: total carbon count of the molecule.

References

1. Daina, A.; Michielin, O.; Zoete, V. SwissADME: a free web tool to evaluate pharmacokinetics, drug-likeness and medicinal chemistry friendliness of small molecules. *Sci. Rep.* **2017**, *7*, 42717.

2. Daina, A.; Zoete, V. A boiled-egg to predict gastrointestinal absorption and brain penetration of small molecules. *ChemMedChem* **2016**, *11*, 1117-1121.

3. Rorick-Kehn, L. M.; Witkin, J. M.; Statnick, M. A.; Eberle, E. L.; McKinzie, J. H.; Kahl, S. D.; Forster, B. M.; Wong, C. J.; Li, X.; Crile, R. S.; Shaw, D. B.; Sahr, A. E.; Adams, B. L.; Quimby, S. J.; Diaz, N.; Jimenez, A.; Pedregal, C.; Mitch, C. H.; Knopp, K. L.; Anderson, W. H.; Cramer, J.W.; McKinzie, D. L. LY2456302 is a novel, potent, orally-bioavailable small molecule kappa-selective antagonist with activity in animal models predictive of efficacy in mood and addictive disorders. *Neuropharmacology* **2014**, *77*, 131-144.

4. Black, S. L.; Chauvignac, C.; Grundt, P.; Miller, C. N.;Wood, S.; Traynor, J. R.; Lewis, J. W.; Husbands, S. M. (2003). Guanidino N-substituted and N,N-disubstituted derivatives of the kappa-opioid antagonist GNTI. *J. Med. Chem.*, **2003**, *46*, 5505-5511.

5. Guerrero, M.; Urbano, M.; Kim, E.-K.; Gamo, A.M.; Riley, S.; Abgaryan, L.; Leaf, N.; Van Orden, L.J.; Brown, S.J.; Xie, J.Y. Design and synthesis of a novel and selective kappa opioid receptor (KOR) antagonist (BTRX-335140). *J. Med. Chem.* **2019**, *62*, 1761-1780.

6. Joshi, A. A.; Murray, T. F.; Aldrich, J. V. Structure-Activity relationships of the peptide kappa opioid receptor antagonist zyklophin. *J. Med. Chem.*, **2015**, *58*, 8783-8795.

4.3. Solving an Old Puzzle: Elucidation and Evaluation of the Binding Mode of Salvinorin A at the Kappa Opioid Receptor [Article C]

Prototypical opioids share a basic amine moiety within their scaffolds. The natural product SalA was the first discovered opioid without such a basic moiety showing high KOR selectivity and strong KOR potency. Despite great interest in the mechanisms by which SalA achieves its unique activation profile its binding mode at the KOR remained elusive. However, several mutagenesis studies with SalA were performed and a plethora of SalA derivatives tested provided experimental data for the generation of a knowledge-based binding mode prediction. In this study, we comprehensively evaluated the structure-activity relationship (SAR) data and mutational data published for SalA and its derivatives to generate a putative binding mode for SalA at the KOR. We further evaluated our binding hypothesis by extensive molecular dynamics simulations and identified relevant structural opioid receptor subtype selectivity determinants (V118$^{2.63}$, Y312$^{7.35}$, and Y313$^{7.36}$). SalA binds above the conserved binding site occupied by prototypical basic opioids in a less conserved part of the receptor allowing for extraordinary KOR selectivity.

Contribution:
Conceptual design (90 %)
Computational experiments (100 %)
Visualization (90 %)
Manuscript preparation (80 %)

I initialized the project, planned and performed the *in silico* experiments, and wrote the manuscript.

Solving an Old Puzzle: Elucidation and Evaluation of the Binding Mode of Salvinorin A at the Kappa Opioid Receptor

Kristina Puls [ID] and Gerhard Wolber *[ID]

Department of Biology, Chemistry and Pharmacy, Institute of Pharmacy, Freie Universität Berlin, Königin-Luise-Str. 2+4, 14195 Berlin, Germany
* Correspondence: gerhard.wolber@fu-berlin.de; Tel.: +49-30-838-52686

Abstract: The natural product Salvinorin A (SalA) was the first nitrogen-lacking agonist discovered for the opioid receptors and exhibits high selectivity for the kappa opioid receptor (KOR) turning SalA into a promising analgesic to overcome the current opioid crisis. Since SalA's suffers from poor pharmacokinetic properties, particularly the absence of gastrointestinal bioavailability, fast metabolic inactivation, and subsequent short duration of action, the rational design of new tailored analogs with improved clinical usability is highly desired. Despite being known for decades, the binding mode of SalA within the KOR remains elusive as several conflicting binding modes of SalA were proposed hindering the rational design of new analgesics. In this study, we rationally determined the binding mode of SalA to the active state KOR by in silico experiments (docking, molecular dynamics simulations, dynophores) in the context of all available mutagenesis studies and structure-activity relationship (SAR) data. To the best of our knowledge, this is the first comprehensive evaluation of SalA's binding mode since the determination of the active state KOR crystal structure. SalA binds above the morphinan binding site with its furan pointing toward the intracellular core while the C2-acetoxy group is oriented toward the extracellular loop 2 (ECL2). SalA is solely stabilized within the binding pocket by hydrogen bonds (C210^{ECL2}, Y312$^{7.35}$, Y313$^{7.36}$) and hydrophobic contacts (V118$^{2.63}$, I139$^{3.33}$, I294$^{6.55}$, I316$^{7.39}$). With the disruption of this interaction pattern or the establishment of additional interactions within the binding site, we were able to rationalize the experimental data for selected analogs. We surmise the C2-substituent interactions as important for SalA and its analogs to be experimentally active, albeit with moderate frequency within MD simulations of SalA. We further identified the non-conserved residues 2.63, 7.35, and 7.36 responsible for the KOR subtype selectivity of SalA. We are confident that the elucidation of the SalA binding mode will promote the understanding of KOR activation and facilitate the development of novel analgesics that are urgently needed.

Keywords: GPCRs; kappa opioid receptor; Salvinorin A; natural products; docking; molecular dynamics simulations; dynophores

1. Introduction

Proper pain management is an ongoing issue in medicine [1–4]. Efficient, strong, and safe analgesics for severe pain treatment are highly needed as currently available pain medications suffer from clinical drawbacks, like side effects, addiction, and overdose-related deaths [1,3,5]. Today, the most important drugs for severe pain treatment are opioids that mainly target the μ-opioid receptor (MOR) [5,6]. These drugs exhibit a high liability for drug abuse and elicit a myriad of side effects like respiratory depression, addiction, and constipation among others [5,7–9]. To overcome the current issue of insufficient severe pain medication the research focus shifts toward alternative targets [1]. The κ-opioid receptor (KOR) is a subtype of the opioid receptor (OR) family, belonging to the large class of membrane-embedded G protein-coupled receptors (GPCRs) [5]. Activation of the KOR provides strong analgesia without addiction and respiratory depression turning the KOR

into a promising target for the development of new analgesics with an improved safety profile [6,10].

Nature hosts a plethora of diverse chemical scaffolds, many of which exhibit biological effects rendering natural products a promising source for the search for new drug candidates [11,12]. One such natural product, Salvinorin A (SalA, Figure 1), gained attention as an untypical, novel-scaffold KOR ligand [13–15]. SalA is a diterpene from the medicinal plant *Salvia divinorum* (Lamiaceae) endemic to Mexico [13,14,16]. *Salvia divinorum* was traditionally used by the Mazatecans for religious but also medicinal purposes like pain treatment, rheumatism, and inflammatory diseases [13,16]. In higher concentrations, SalA and *Salvia divinorum* products elicit strong hallucinogenic effects which led to the recreational use of SalA-containing products recently [13,14,16,17].
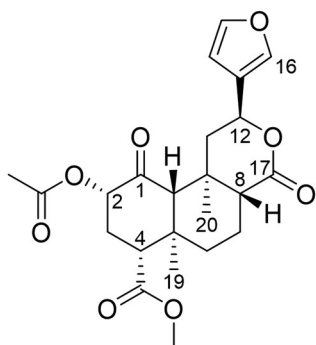
Figure 1. Chemical structure of Salvinorin A (SalA).

Due to its diterpene structure, SalA lacks the nitrogen atom typical for small molecules OR ligands, like morphine, fentanyl, and buprenorphine, which are mainly alkaloids [16,18]. An ionic interaction between the positively charged nitrogen of the ligand and the carboxylate of $D^{3.32}$ (Superscripts denote Ballesteros-Weinstein numbering [19]) was believed to be crucial for OR affinity and activity of small molecule OR ligands thereby serving as an anchor point for the ligand [20–23]. SalA was the first nitrogen-lacking OR ligand discovered [14] underlying its unique character. Furthermore, SalA shows high selectivity for the KOR acting as a potent agonist without binding towards the MOR and the DOR (δ-opioid receptor) [24–27]. A broad screen of SalA against 50 transporters and receptors revealed no substantial activation besides its KOR activity [13,28]. Of note, SalA does not modulate the 5-HT$_{2A}$-receptor which is commonly targeted by hallucinogens [13,27]. Nonetheless, Dopamin2 receptor modulation, allosteric MOR modulation, and allosteric modulation of cannabinoid type 1 receptors are discussed [13,14].

The potential of SalA as a new analgesic is not only supported by its high KOR selectivity, but also by its overall low toxicity with no severe adverse outcomes reported [13,16]. Despite its hallucinogenic character and its recreational usage SalA does not cause addiction [13,14] in contrast to typical opioids [5]. Nonetheless, reports about typical KOR-mediated side effects like anhedonia, locomotor impairment, and aversion caused by SalA but also its hallucinogenic effects may hinder SalA's clinical usefulness [14,27,29,30]. SalA's clinical usefulness is further impaired by bad pharmacokinetic properties with rapid gastrointestinal degradation, quick metabolic inactivation, and fast elimination [16,31–36]. At the oral route of administration, drug absorbance can only occur within the mouth mucosa by holding the SalA-containing product in the mouth for several minutes [16,36]. Vaporization or smoking of Salvia divinorum leaves or extracts with subsequent inhalation is a more efficient administration route and is often used by recreational users [16,17]. After bioabsorption, SalA quickly enters the central nervous system eliciting its clinical effects but leaving the CNS just as quickly [15,17]. SalA is metabolized by esterases, glucuronidases, and CYP enzymes [16,31–33] with fast elimination [34,35]. Especially blood esterases rapidly metabolize SalA via C2-ester cleavage to the main metabolite Salvinorin B (SalB) that is inactive at the KOR [15,16,35]. Of note sex differences in metabolism and

elimination were observed with females showing slower metabolism and excretion [35]. As a result, SalA exhibits a short duration of effect [16,17,35], which likely contributes to SalA's low toxicity but also hinders its usage as an analgesic drug.

To overcome SalA's clinical drawbacks, a plethora of analogs were synthesized and tested [15,37], which led to the development of agonists [15,37–40], partial agonists [37,38,40,41] and antagonists [37,40,42,43] of the KOR and even to MOR modulators [37,44–48]. Despite a large number of around 600 available analogs the majority of these exhibit alterations at the C2 position or modifications of the furan ring [15] which resulted in fewer diverse ligand sets than desired. The rational design of new analogs is further hindered by the still unknown binding mode of SalA at the KOR which also hinders the understanding of the structure-activity relationship (SAR). Furthermore, most of the derivatives exhibit less affinity or activity than SalA itself [15]. The comparison of different analog series is hampered by the different assays used, the choice of different cell lines, and the reference ligand used. Due to the focus on KOR affinity and activity and the lack of in vivo experiments of analogs, it is hard to evaluate the safety profiles, hallucinogenic effects, addictive properties, and therefore the misuse potential of almost all analogs.

The rational design of new analogs to explore the chemical space around SalA is hampered by the still unknown binding mode of SalA at the KOR. Several different and conflicting binding modes for SalA at the KOR were proposed [22,25,49–55]. For example, Vardy and coworkers [49] as well as Roach and coworkers [50] postulated binding modes in which the furan moiety of SalA points upwards towards the extracellular portion of the KOR while Che and coworkers [22] and Kane and coworkers [25] postulated the opposed orientation. In contrast to the mostly vertical orientation of SalA within the KOR binding site, Vortherms and coworkers [53] predicted a horizontal orientation of SalA. The discrepancies within these results are partially caused by the lack of an active-state crystal structure of the KOR until 2018 [22]. SalA was then docked into KOR homology models [50,52,54] or active-like structures [49,51] derived from the inactive KOR crystal structure published in 2012 [20], which differs from the active-state crystal structure.

To solve the confusion about the SalA binding mode a comprehensive evaluation of SalA within the active-state KOR crystal structure with respect to available mutagenesis studies and SAR data is needed. In this paper, we carefully and rationally elucidate the binding mode of SalA to the active-state KOR taking into account available mutational and SAR data. We rationalize determinants for SalA receptor subtype selectivity as well as effects of ligand modifications for experimental measured affinity and activity at the KOR by using docking experiments, molecular dynamics simulations, and dynophore [56,57] analysis.

2. Results

2.1. Salvinorin A Binds above the Morphinan Binding Pocket of the Kappa Opioid Receptor

To elucidate the binding mode of Salvinorin A (SalA) at the kappa opioid receptor (KOR) we performed docking experiments of SalA to the KOR binding cavity of the prepared active-state KOR crystal structure (PDB-ID: 6B73 [22]). SalA binds above the morphinan binding site at the extracellular part of the KOR binding cavity with its C4-methyl ester interacting with the extracellular loop 2 (ECL2) while its furan moiety points downwards to the morphinan binding pocket (Figure 2). Unlike typical KOR ligands that always establish an ionic interaction with D138$^{3.32}$ (superscript denotes Ballesteros–Weinstein numbering [19]) at the bottom of the morphinan binding site [20–23], SalA is solely stabilized in its position by hydrophobic contacts and hydrogen bonds (Table 1). The C4-methyl ester forms hydrogen bonds to E210^{ECL2}, the C1-carbonyl moiety to Y312$^{7.35}$, and the C2-acetoxy group to Y313$^{7.36}$. The furan moiety is stabilized via hydrophobic contacts with Y139$^{3.33}$ and I294$^{6.55}$, while C19 and C20 (both methyl groups) form lipophilic contacts with V118$^{2.63}$, Y313$^{7.36}$, or I316$^{7.39}$, respectively. SalA sterically fits into the binding pocket shape with perfect complementarity.
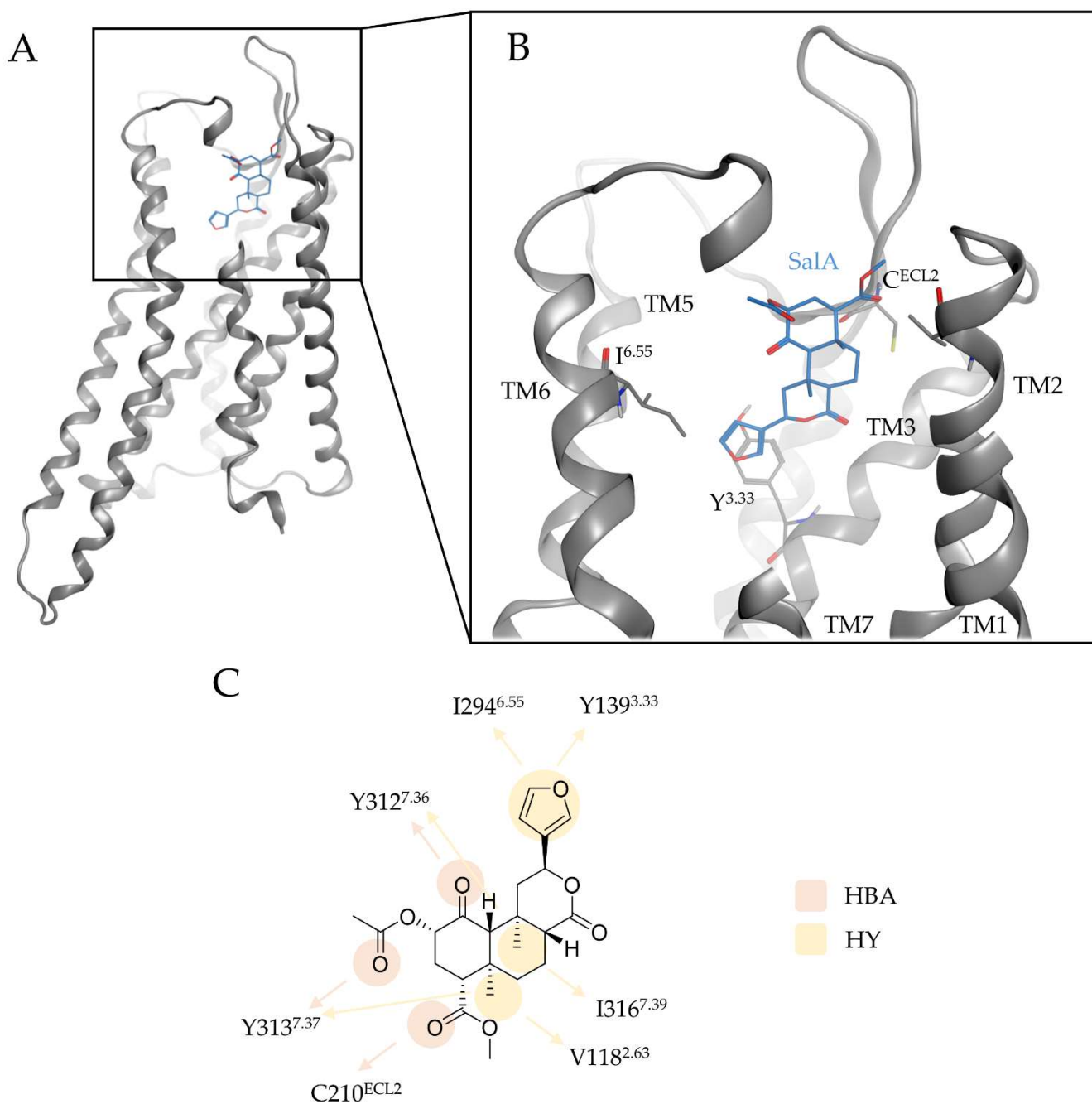
Figure 2. Binding mode of SalA at the KOR. (**A**) shows the overall architecture of KOR bound to SalA while (**B**) highlights the binding pocket of SalA at the KOR. (**C**) depicts the protein-ligand interactions between SalA and KOR. $Y^{3.33}$ denotes to $Y139^{3.33}$, C^{ECL2} to $C210^{ECL2}$, and $I^{6.55}$ to $I294^{6.55}$. TM denotes to transmembrane helices, HBA to hydrogen bond acceptor, and HY to hydrophobic contact.

Table 1. Protein-ligand interactions between SalA and the KOR.

Interaction	Functional Group	Residue
Hydrogen bond	C1-carbonyl	$Y312^{7.35}$
Hydrogen bond	C2-carbonyl	$Y313^{7.36}$
Hydrogen bond	C4-carbonyl	$C210^{ECL2}$
Hydrophobic contact	C19	$V118^{2.63}$, $Y313^{7.36}$
Hydrophobic contact	C20	$I316^{7.39}$
Hydrophobic contact	Furan	$I294^{6.55}$; $Y139^{3.33}$

Our proposed binding mode is in accordance with previous published mutational data: Several mutagenesis studies highlight the detrimental role of Y312[7.35] and [25,49,54] and Y313[7.36] [6,25,49] for SalA affinity and activity; in our model both residues anchor SalA in the KOR binding cavity. Participation of the ECL2 loop in SalA binding was proposed based on binding studies with chimeric opioid receptors [25], which agrees with C210[ECL2] interacting with the C4 methyl ester of SalA via hydrogen bonding. V118[2.63] and Y139[3.33] were also proposed to affect SalA affinity [25,26,49] and stabilize SalA by hydrophobic contacts in the KOR binding site.

Despite the indisputable importance of mutagenesis studies for experimental validation of a proposed binding mode we need to carefully check whether the underlying studies were performed probe-dependently or probe-independently. Several studies found a strong decrease in the affinity and activity of SalA in a Y320[7.43]A KOR mutant [25,49,54] suggesting a SalA binding mode in which the ligand binds as deep in the orthosteric binding site as morphinan ligands do. Nonetheless, this phenomenon seems to be independent of the ligand tested albeit with strong differences in the chemical ligand space (SalA, nitrogen-containing small molecules, peptides) [49]. Thus, we surmise a ligand-independent conformational change of the KOR Y320[7.43]A mutant that led to the decreased affinities and activities experimentally measured. Indeed, Y320[7.43] is in close proximity to W287[6.48], a residue believed to play an important role in KOR activation as it directly interacts with F283[6.44] of the conserved PIF-motif [22] and therefore the truncated side chain in the Y320[7.43]A mutant likely alters the orientation of W287[6.48] and indirectly the KOR activation.

The Q115[2.60]A KOR mutant was found to strongly decrease SalA affinity and activity [25,49]. We did not observe interactions of SalA with Q115[2.60] in our binding model but Q115[2.60] is in close proximity to the C17-carbonyl of SalA. We, therefore, investigated the potential interaction of SalA with Q115[2.60] through molecular dynamics simulations.

2.2. Molecular Dynamics Simulations Confirm Salvinorin A Binding Mode Obtained by Docking Experiments but Revealed Additional Interaction with Q115

To evaluate our SalA binding mode found in docking experiments and to assess whether Q115[2.60] contributes to SalA binding in a dynamic investigation we performed molecular dynamics (MD) simulations of SalA bound to the KOR crystal structure and subsequent calculated dynamic pharmacophores (dynophores, Figure 3) [56,57]. Dynophores represent interactions dynamically. They consist of probability density point clouds representing the interactions detected over the course of MD simulations. MD simulations confirm our putative binding mode for SalA with an average ligand root mean square deviation (RMSD) of 2.9 Å over the five replica simulations (200 ns each). Detailed information about the RMSD of SalA and the KOR can be found in the Supplementary Materials (Figures S1 and S2). SalA is stabilized within the binding pocket by highly frequent hydrophobic contacts and several hydrogen bonds (Table 2).

Table 2. Interactions between SalA and the KOR during MD simulations.

Interaction	Functional Group	Residue	Frequency (%)
Hydrogen bond	C2-carbonyl	Y312[7.35], Y313[7.36]	17.6
Hydrogen bond	C4-carbonyl	C210[ECL2]	94.1
Hydrogen bond	C1-carbonyl	Y312[7.35]	79.0
Hydrogen bond	C17-carbonyl	Q115[2.60]	54.0
Hydrophobic contact	C19	V118[2.63], Y313[7.36]	97.3
Hydrophobic contact	C20	I316[7.39], Y312[7.35]	76.0
Hydrophobic contact	Furan	I135[3.29], L212[ECL2]; Y139[3.33]	99.5

We observed a tendency for SalA to very slightly shift towards the TM2 over the course of the simulation and a tendency for Q115[2.60] to reorient towards the C17-carbonyl of SalA facilitating hydrogen bonding (54.0%). This hydrogen bonding was not observed within

the static docking results but agrees with previously published mutagenesis studies that showed decreased affinity and activity values for SalA with Q115[2.60]A KOR mutants [25,49].
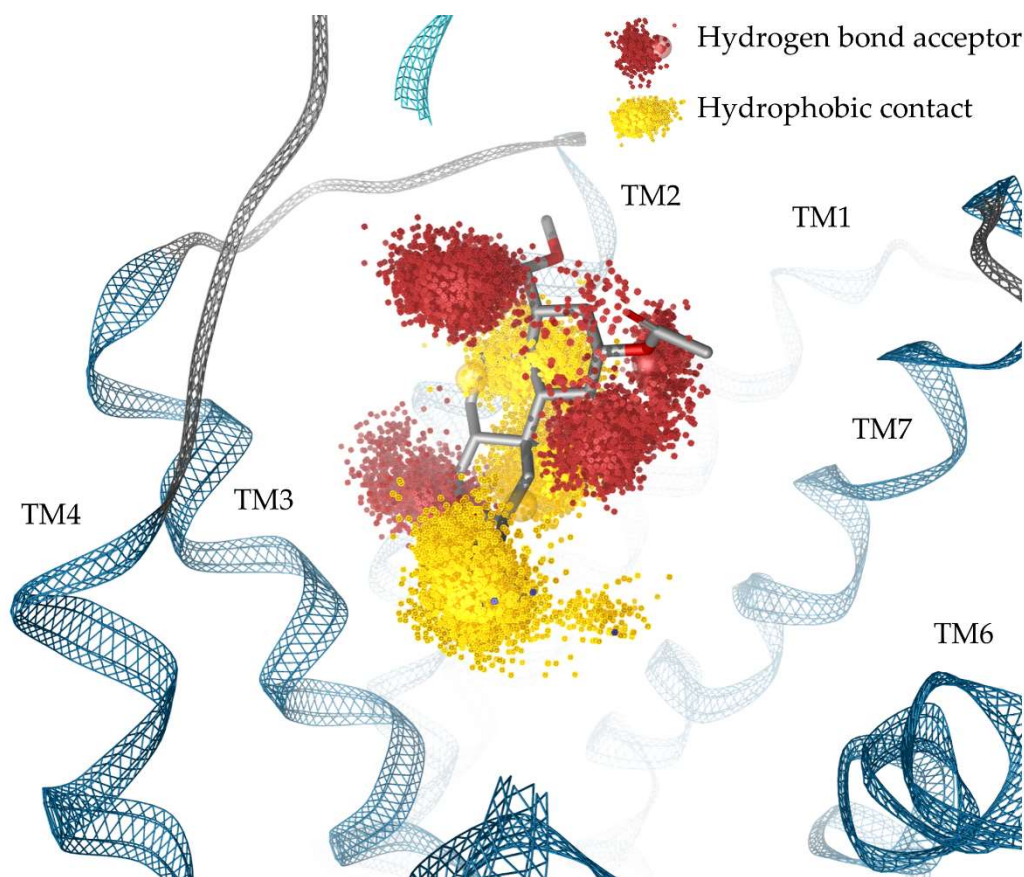
Figure 3. Dynamic pharmacophores (dynophores) of protein-ligand interactions between SalA and KOR (probability density point cloud representation). TM denotes to transmembrane helices.

All carbonyl groups of SalA participate in hydrogen bonding. Hydrogen bonding between the C4 methyl ester and C210[ECL2] occurred in 94.1% of MD simulations. This most frequent hydrogen bonding interaction is likely important for SalA's affinity as alterations in the C4-substituent mostly induce affinity and activity drops [15,58,59]. The C1-carbonyl group participates in highly frequent hydrogen bonding (79.0%) with Y312[7.35]. We detected weak hydrogen bonding between the C2-acetoxy group and KOR along MD simulations (17.6% to Y312[7.35], Y313[7.36]). SalB, the main metabolite of SalA, exhibiting a C2-hydroxy group instead of a C2-acetoxy group is inactive at the KOR [15,16,35] rendering the C2-acetoxy group interaction of SalA important for SalA's potency. Thus, the low frequency of the C2-acetoxy group interactions was unexpected. However, the absolute frequency of a particular interaction is less meaningful than the ratio of these interactions between analogs. Despite overall low occurrence, this interaction could still play a key role in the binding and activation of KOR by SalA. Off note, both residues that interact with the C2-substituent of SalA are non-conserved which likely contributes to the strong selectivity of SalA.

The hydrophobic contact between the furan moiety of SalA and L212[ECL2] was not observed in static docking but agrees with the observation of poor binding of SalA to the L212[ECL2]A mutant [20].

The dynamic interaction analysis agrees with the results obtained by static docking with the addition of C17-carbonyl hydrogen bonding due to the reorientation of Q115[2.60] and additional hydrophobic contacts to L212[ECL2]. Thus, the results are in accordance with mutagenesis studies too. Figure 3 shows the dynophore model (probability density point cloud representation of protein-ligand interactions) of the SalA-KOR complex.

2.3. Non-Conserved Residues Harboring Salvinorin A at the Kappa Opioid Receptor Lead to Receptor Subtype Selectivity of Salvinorin A

SalA is characterized by its strong KOR subtype selectivity without affinity towards the MOR, DOR, and the fourth OR called the nociceptin/orphanin FQ peptide (NOP) receptor [24–26]. Thus, SalA mediates its analgesic effect solely by KOR activation avoiding classical MOR side effects like respiratory depression, addiction, and constipation [5,7–9].

The three classical OR receptors (KOR, MOR, and DOR) share high overall sequence identity and similarity values that hamper subtype selectivity (Identity KOR/MOR = 56.3%; Identity KOR/DOR = 56.3%; Similarity KOR/MOR = 70.5; Similarity KOR/DOR = 68.2; all values for full sequence comparison, Figure S3). Especially the orthosteric binding site is highly conserved. This holds true for the GPCR class A family in general. On the contrary, the extracellular parts of these receptors are more diverse with several non-conserved residues. Thus, selective orthosteric ligands often additionally target extracellular regions of GPCRs to facilitate their subtype selectivity [60,61]. The recently discovered NOP is more distinct from the three classical ORs but still exhibits significant sequence identity and similarity values (Identity KOR/NOP = 48.9%; Similarity KOR/NOP = 62.6%; values for full sequence comparison). The less conserved structure leads to marked differences in the binding and activation profile of OR ligands binding to the NOP compared to binding to the classical ORs [62].

Docking experiments show that SalA binds above the morphinan binding site, the deepest part of the orthosteric binding site, within a less conserved site of the KOR. The residues $V118^{2.63}$, $I294^{6.55}$, $Y312^{7.35}$, $Y313^{7.36}$, and $I316^{7.39}$ that participate in protein-ligand interactions with SalA in the KOR-SalA complex vary among the different OR subtypes and therefore likely influence SalA's selectivity profile. While $I316^{7.39}$ differs in the NOP but is conserved within the classical ORs the remaining before-mentioned residues vary within the classical ORs. Table 3 provides a comprehensive list of the non-conserved residues participating in SalA binding at the KOR.

Table 3. Non-conserved residues within the opioid receptor family participating in SalA binding.

Residue	KOR	MOR	DOR	NOP
2.63	V118	N129	K108	D110
6.55	I294	V302	V281	V283
7.35	Y312	W320	L300	L301
7.36	Y313	H321	H301	R302
7.39	I316	I324	I304	T305

In order to rationalize the determinants for SalA's outstanding selectivity, we evaluated the impact of non-conserved residues within the SalA binding site for OR subtype selectivity. In order to account for the orientation of the non-conserved residues within the binding pocket, we superimposed the KOR-SalA complex according to its transmembrane region (OPM-Database entry: 6B73) with the active-state structures of MOR (PDB-ID: 5C1M [63]), DOR (PDB-ID: 6PT2 [64]) and NOP (Figure 4). Since there is no experimentally derived active-state NOP structure available, we used a homology model based on the active-state KOR crystal structure (PDB-ID: 6B73 [22]) already described in one of our previous publications [65].

$V118^{2.63}$ at the top of KOR-TM2 forms hydrophobic contacts with C19 (methyl moiety between Rings A and B) of SalA. While nonpolar in the KOR, this region is polar in the remaining three receptors (MOR: N, DOR: K, NOP: D) and therefore would be unable to maintain this interaction with SalA in these receptors. The ionic character in DOR and NOP likely even pushes the lipophilic SalA scaffold away.

$Y313^{7.36}$ establishes hydrogen bonding to SalA's C2-acetoxy moiety in the KOR-SalA complex as well as hydrophobic contacts to C19 of SalA (methyl moiety between Ring A and B). The respective residues in the remaining ORs (MOR: H, DOR: H, NOP: R) are able to facilitate hydrogen bonding, but only if they are correctly oriented. The histidines in

MOR and DOR are too far away to establish hydrogen bonds (MOR: 6.2 Å, DOR: 6.4 Å; distance measured between NE2 of histidines and C2-acetoxy carbonyl oxygen atom of SalA) and also to form hydrophobic contacts (MOR: 6.5 Å, DOR: 6.9 Å; distance measured between CE1 of histidines and C19 of SalA). They therefore cannot facilitate the interactions possible at KOR. In our NOP homology model, the arginine was predicted to point away from the ligand binding site towards E295$^{7.29}$ at the top of TM7. Thus, it likely would not contribute to SalA binding towards the NOP.
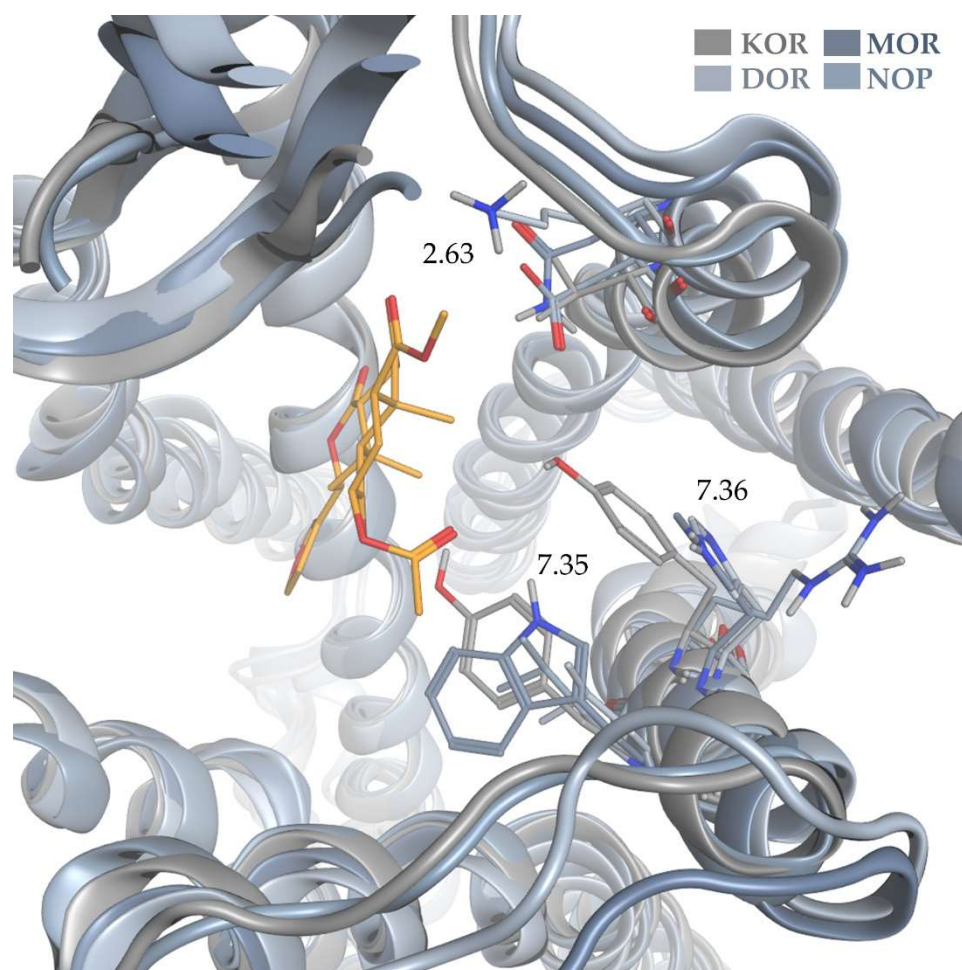
Figure 4. Superimposition of SalA bound to the KOR and the active-state crystal structures of MOR and DOR as well as the active-state homology model of NOP.

The C1-carbonyl moiety of SalA forms hydrophobic contacts to Y312$^{7.35}$. From the three remaining ORs (MOR: W, DOR: L, NOP: L) only tryptophan in the MOR could form hydrogen bonds if positioned correctly within the binding pocket. The receptor superimposition revealed that the tryptophan in MOR is too distant for hydrogen bonding analog in the KOR-SalA complex (5.2 Å between NE1 of W320$^{7.35}$ and C1-carbonyl oxygen atom). Thus, none of the ORs can mimic the interactions of Y312$^{7.35}$ to SalA in KOR.

The furan moiety of SalA is stabilized by hydrophobic contact with the conserved Y139$^{3.33}$ and the non-conserved I294$^{6.55}$. The respective residues for I294$^{6.55}$ in the remaining receptors (V for all three receptors) are all hydrophobic as well and only differ from I294$^{6.55}$ in the truncation of one methyl group. Within the receptor superimposition, all residues are within the range of 5.9 Å for hydrophobic contacts set as the default range in Ligandscout 4.4.3 (Inte:Ligand, Vienna, Austria) [66,67] albeit scarce (MOR: 5.4 Å, DOR: 5.9 Å, NOP: 4.6 Å, measured between C15 of SalA and CG2 of valine in MOR and DOR and

CG1 of valine in NOP). We surmise that I294[6.55] hardly contributes to SalA selectivity. The effect of the beforementioned residues is more pronounced.

The position 7.39 participates in hydrophobic contacts with C20 (methyl moiety between Ring B and C) at the KOR-SalA complex and is conserved within the classical ORs (KOR: I316[7.39], MOR: I324[7.39], DOR: I304[7.39]) and only differs in the NOP structure (T305[7.39]). The isoleucine is positioned similarly in all three classical ORs with all residues capable to facilitate hydrophobic contacts. Despite being rather polar the side chain methyl group of the threonine in the NOP homology model is oriented in that it can participate in hydrophobic contacts, albeit scarce again (5.9 Å betweenCG2 of T305 and C20 of SalA). The non-conserved residue 7.39 therefore likely has a minor role in SalA KOR selectivity.

After careful evaluation of non-conserved residues participating in SalA binding at the KOR, we surmise positions 2.63, 7.35, and 7.36 are responsible for SalA selectivity as the interactions within the KOR complex cannot be mimicked by the remaining receptors.

To date, the active-state MOR crystal structure (PDB-ID: 5C1M [63]) is the only experimental solved OR structure with longer parts of the flexible extracellular N-terminus solved. In the superimposition of the KOR-SalA complex and MOR, a clash of SalA (Ring A, C2-acetoxy group, C4-methyl ester) and the N-terminus of MOR is observed. As the MOR structure was derived with a morphinan-based orthosteric ligand binding deeper in the receptor and due to the flexible character of the N-terminus the consequence of this potential clash cannot be fully evaluated. Furthermore, as the N-termini of KOR, DOR and NOP are not solved and therefore their respective positions are unknown the impact of the N-terminus position of the binding and selectivity profile of SalA cannot be estimated.

2.4. Salvinorin A Binding Mode Is in Agreement with Previous Published Structure-Activity-Relationship Data

Next, we evaluated our binding hypothesis in the context of available structure-activity relationship (SAR) data. Due to around 600 experimental tested analogs [15] of SalA (**1**) being available, sufficient data is available to evaluate and further assess our model. Thus, we carefully selected several analogs of SalA to explain the general effects of specific substitution patterns on the affinity and activity of SalA analogs. Most SalA alterations lead to strong affinity and activity drops and only a little number of analogs with improved properties are known [15,39,68–71]. Figure 5 shows the structures of all ligands discussed in this section while Table 4 lists the respective experimental data.

Table 4. Experimental data for binding of SalA and all analogs discussed within this section measured in radioligand binding assays.

Ligand	Affinity (K_i) [nM]	K_i [ligand]/K_i [SalA]	Reference
	155 ± 23 [c]	119	[38]
	>10,000 [a]	-	[72]
2 (SalB)	111 ± 12 [c]	85	[71]
	155 ± 23 [c]	119	[73]
	280 ± 20 [d]	147	[47]
	>10,000 [b]	-	[68]
3	>10,000 [a]	-	[72]
4	>10,000 [a]	-	[72]
	>10,000 [c]	-	[71]
5	17.6 ± 3.1 [c]	14	[73]
6	0.32 ± 0.02 [c]	0.133	[69]
	3.13 ± 0.40 [b]	0.423	[70]
	0.59 ± 0.21 [b]	0.328	[55]
7 (RB-64)	39 ± 11 [c]	2	[55]
	0.6 ± 0.2 [b]	0.097	[68]
	>10,000 [c]	-	[74]
8	>1000 [c]	-	[58]
	>1000 [c]	-	[59]

Table 4. *Cont.*

Ligand	Affinity (K_i) [nM]	K_i [ligand]/K_i [SalA]	Reference
9	>10,000 [c]	-	[73]
10	28.5 ± 0.9 [c]	22	[58]
11	>1000 [c]	-	[58]
12	3400 ± 150 [d]	1789	[42]
13	55 ± 23 [c]	22	[41]
14	40 ± 1 [b]	5	[75]
15	2.9 ± 0.3 [c]	1	[41]
	3.0 ± 0.2 [d]	2	[42]
16	>8000 [b]	-	[76]
17	6 ± 1 [b]	2	[77]
18	18 ± 2 [b]	5	[77]
19	1125 ± 365 [b]	281	[77]

[a] K_i determined against [^{3}H]bremazocine. [b] K_i determined against [^{3}H]U69,593. [c] K_i determined against [^{3}H]diprenorphine. [d] K_i determined against [^{125}I]IOXY.
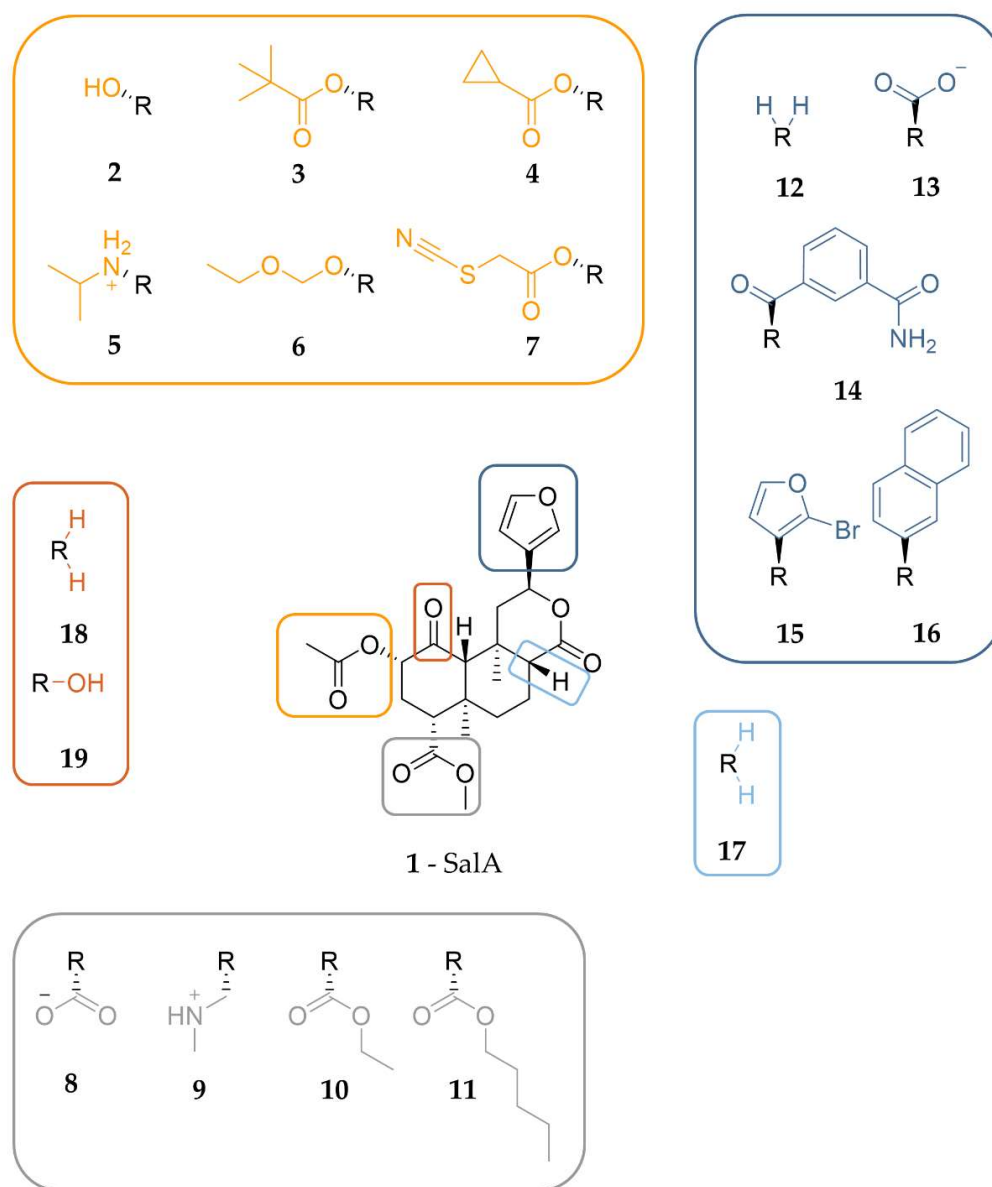
Figure 5. Chemical structure of SalA-analogs discussed to evaluate the proposed binding mode of SalA.

2.4.1. C2-Analogs of SalA

The majority of available SalA analogs host alterations of the C2-acetoxy group of SalA [15]. Several ester analogs including ethers, amides, amines, and carbamates are known and others are available [15,38,68,70,73].

The common metabolic inactivation of SalA represents the C2-acetoxy group cleavage leading to SalB (**2**) with a C2-bound hydroxy group [16]. Despite the wide acceptance of SalB as the inactive metabolite of SalA conflicting experimental data were measured with K_i values between 111 nM and >10,000 nM [15,38,47,68,71–73] and EC_{50} values between 2.4 nM and 492 nM [71,78]. However, compared to SalA, SalB binds to the KOR in a much weaker way. Docking of SalB into the KOR binding cavity reveals an almost identical binding mode of SalB compared to SalA (Steric overlap of 87%) with almost identical interactions, albeit the lack of any C2-hydroxy group interactions (Figure S4). This finding renders the C2-acetoxy hydrogen bonding an important requirement for KOR affinity and activity of SalA despite its moderate frequency in MD simulations (17.6%).

Several authors postulate a size restriction hypothesis for the C2-substituent with spacious lipophilic groups resulting in affinity drop [14,41,79]. We replaced the acetoxy group at C2 of SalA with a more spacious pivaloxy moiety (**3**) [72] or a cyclopropanecarboxylic moiety (**4**) [71,72] as both analogs were measured to have an abolished affinity towards KOR [15,71,72] and docked both analogs into the KOR. Docking experiments show reduced interactions for both analogs with **4** lacking both hydrogen bonds at the C1-carbonyl moiety and at the carbonyl oxygen of the C2-cyclopropanecarboxylic moiety while its cyclopropyl moiety does not form any hydrophobic contacts (Figure S5C,D). The pivaloxy-analog **3** is capable of stabilizing its C2-rest in hydrophobic contacts with $I294^{6.55}$, but lacks the C1- and C2-hydrogen bonds as well (Figure S5A,B). The C1-carbonyl hydrogen bonding occurred in SalA MD simulations with high frequency (79.0%) and therefore likely contributes to SalA's experimental activity. Its lack of both analogs likely diminishes affinity. The hydrogen bond at the C2-acetoxy group of SalA was detected with lower frequency in SalA MD simulations (17.6%), but due to its important role in SalA metabolic inactivation, it is considered important as well. The combined lack of both interactions likely rationalizes the completely abolished affinity of the two analogs. According to the docking poses of the analogs, the C2-substituents are positioned in the middle of the central binding cavity pointing towards TM6. Within this region, there are only a few lipophilic residues present (mainly $I294^{6.55}$) but several charged residues ($E297^{6.58}$, $K227^{5.39}$, $E209^{ECL2}$). Additionally, the C2-substituents would be surrounded by water filling the empty parts of the binding cavity. Together, this explains the experimentally measured loss of affinity by substituting the C2-acetoxy group of SalA with bulkier lipophilic moieties as they hardly can form interactions resulting in enthalpically unfavorable binding poses. A size restriction rule due to a small pocket that only can accommodate a limited number of atoms cannot be applied.

An outstanding feature of SalA is its nitrogenless structure, but several studies tested the effect of nitrogen introduction at different positions of SalA [15,38,39,41,58,73,80–82]. At C2 the introduction of a positively charged nitrogen often led to strong decreases in KOR affinity and activity but some analogs tolerate the introduction of the positive charge [15,38,39,73,80,81]. This finding agrees with the C2-acetoxy group of SalA being oriented towards a region with multiple negatively charged ligands ($E297^{6.58}$, $E209^{ECL2}$) that could interact with positive amines.

Beguin and co-workers [73] tested a series of alkyl amines at the C2-position with **5** being the best-tolerated amine (K_i 17.6 nM, about 14-fold diminished affinity compared to SalA) with an isopropylamine moiety at C2. Compared to the binding mode of SalA, **5** is shifted towards TM5 establishing charge interactions with $E297^{6.58}$ and $E209^{ECL2}$, but loses hydrogen bonding at the C4 position (Figure S6). The isopropyl moiety at the amine is likewise surrounded by the negative residues and does not take place in any hydrophobic contacts. The lack of the hydrogen bond at C4 combined with the overall shift within the binding pocket likely caused the decrease in affinity, but the ionic interactions stabilizing **5** from two sides seem to rescue its affinity towards KOR.

Although the alteration of the SalA structure mostly leads to impaired affinity and activity values measured in experiments, several examples of analogs with improved properties are known. One of such improved analogs is **6** with an ethoxymethyl ether at C2 [15,69,70] being the most affine ligand of a series of alkoxymethyl ether derivates tested by Munro and coworkers [69]. Docking of **6** to KOR revealed an extended interaction pattern when compared to the KOR-SalA complex (Figure S7). The oxygen atoms of the ethoxymethyl ether establish hydrogen bonding to Y312[7.35] and Y313[7.36] and the ethyl group is stabilized by hydrophobic contacts to Y312[7.35] and L309[7.32]. Hydrogen bonding to Q115[2.60] that was not seen in the static investigation of SalA but in MD simulations (79.0% frequency) occurred also in the KOR-**6** complex (to C1-carbonyl moiety of **6**). The new interactions while maintaining the SalA interaction pattern rationalizing the increased affinity values measured for **6**.

22-thiocyanato-SalA, also called RB-64 (**7**, RB-64), is one of the most prominent SalA analogs as it shows G protein bias and therefore represents a potential analgesic compound with an improved safety profile [6,83]. RB-64 (**7**) was originally designed by Yan and coworkers [55] as a covalent KOR agonist, but the postulated covalent binding mode with C315[7.38] is poorly supported by experimental data. The experimental data for the wash-resistant readout in the binding assay is not shown within the publication, the experiments were conducted under unphysiological conditions with a huge amount of ligand (10 h and 20 μM, 4 °C), and the postulated covalent bond between RB-64 and C315[7.38] is quite large (4.9 Å). However, White and coworkers postulate a non-covalent binding mechanism for RB-64 administered in vivo [83]. The experimentally measured affinity of RB-64 towards KOR differs in a probe-dependent manner. RB-64 (**7**) shows improved affinity compared to SalA in [^{3}H]U69,593 competition assay [55,68] but slightly impaired affinity in [^{3}H]diprenorphine competition assay [55].

We performed non-covalent docking of RB-64 into the active state KOR crystal structure as we doubt the covalent binding mode proposed by Yan and coworkers [55] and due to the lack of a free cysteine residue around the C2-acetoxy group of SalA. Our non-covalent docking experiments reveal a highly similar binding mode of RB-64 compared to SalA, but with lacking interactions at the C2-substituent (Figure S8). The absence of C2-substituent interactions is questionable as RB-64 shows improved affinity compared to SalA in certain experiments. We, therefore, performed 1 μs (five replicas à 200 ns) of MD simulations for the RB-64-KOR complex to investigate the interactions in a dynamic fashion. The MD simulations reveal highly similar interactions between the RB-64-KOR complex and the SalA-KOR complex, but with the exception of slightly increased C2-substituent interactions in the case of RB-64 (Table 5). The thiocyanate of the C2-substituent only weakly participates in hydrogen bonding (8.6%) but probably serves as an anchor to stabilize the position of the carbonyl moiety of C2. Compared to SalA the interaction frequency of the C2-carbonyl moiety is increased by around 5% to 22.2% in total. As mentioned earlier, the absolute frequency is less meaningful than the frequency shift between close derivatives in order to explain affinity differences obtained in experiments. Therefore, the small increase in the interaction frequency observed in MD simulations can explain the improved affinity of RB-64 in certain experiments. Information about the RMSD von RB-64 and the protein-heavy atoms can be found in Figures S9 and S10.

We further performed several relative binding free energy (RBFE) calculations based on the docking poses of SalA and RB-64 (FEP in Maestro [84,85], openfe [86]) and absolute binding free energy calculations of both complexes (Yank [87]). All methods predicted the binding of RB-64 at KOR more favorable than the binding of SalA to KOR. More information about the energy calculations can be found in the Supplementary Material (Table S1) and the Section 4.

Table 5. Interactions between RB-64 (**7**) and the KOR during MD simulations.

Interaction	Functional Group	Residue	Frequency (%)
Hydrogen bond	C2-carbonyl	Y313[7.36] (Y312[7.35])	22.2
Hydrogen bond	C2-thiocyanate	Y313[7.36]	8.6
Hydrogen bond	C4-carbonyl	C210[ECL2]	93.9
Hydrogen bond	C1-carbonyl	Y312[7.35]	80.1
Hydrogen bond	C17-carbonyl	Q115[2.60]	57.4
Hydrophobic contact	C19	V118[2.63]	94.4
Hydrophobic contact	C20	I316[7.39]	51.7
Hydrophobic contact	Furan	I135[3.29], L212[ECL2]; Y139[3.33]	99.9

2.4.2. C4-Analogs of SalA

In contrast to C2, charges at C4 are not tolerated in SalA and lead to drastically reduced affinity values [15,58,59,73,74]. The C4-substituent of SalA is positioned near ECL1 and ECL2 without any charged residues in reach and with a space restriction that only allows growing to the extracellular side. Thus, the introduction of a charge at C4 likely introduces an unfavorable negative repulsion that forces the ligand to adopt a new orientation resulting in reduced affinity compared to SalA. We docked one analog with a negative charge at C4 (carboxylate moiety, **8** [58,59,74]) and one with a positive charge (methylaminomethyl moiety, **9** [73]) both without any measurable affinity at 10 μM concentration to the KOR. As expected, we found no reasonable docking poses for both compounds. In order to fulfill charge interactions, both compounds adopt orientations completely dissimilar from SalA with scaffold reorientations (Figure S11). The absence of a rational binding pose explains the lack of experimentally measured affinities for compounds containing a charge at C4.

Lee and coworkers [58] tested a series of alkyl esters at the C4 position and found a complete loss of affinity by any extension of the methyl group. Even the addition of one methyl group (ethyl ester) led to an absence of any affinity. Thus, we investigated a possible size exclusion effect of the C4 moiety. Docking of the ethyl ester (**10**) [58] as the smallest alkyl ester with abolished affinity and the bulkier pentyl ester (**11**) [58] cause ligand shifts within the KOR binding site towards TM5 to accommodate the C4-substituent within a more lipophilic pocket at TM2/3 (T111[2.56], V118[2.63], W124[23.50], V134[3.28], I135[3.29]) instead of the hydrophilic environment of ECL1/ECL2, where the methyl ester of SalA is positioned (Figure S12). The ligand shift towards TM5 causes the loss of all hydrogen bonds in the case of the ethyl ester, while the pentyl ester can at least rescue hydrogen bonding at the C1-carbonyl position with Y312[7.35]. The strongly diminished interaction pattern with loss of C2- and C4-hydrogen bonding in both cases and the additional C1-hydrogen bonding loss in case of **10** rationalizes the observed affinity lack for all alkyl esters except the methyl ester of SalA.

2.4.3. C12-Analogs of SalA (Furan-Analogs)

The furan moiety at C12 of SalA is positioned the deepest in the KOR binding cavity and is stabilized by hydrophobic contacts with Y139[3.33] and I294[6.55]. Simpson and coworkers [42] found that the omission of the C12-substituent (**12**) results in a 1789-fold decrease in binding affinity. At the same time, the replacement of the furan by a carboxylic moiety (**13**) only causes a small affinity drop (22-fold) [41]. Thus, we surmise the furan to be an anchor point for the ligand with establishing favorable but not necessarily hydrophobic contacts.

To rationalize how SalA tolerates the replacement of the furan by a carboxylic moiety we docked **13** into the KOR binding site (Figure S13). **13** takes place in extensive protein-ligand interactions with establishing hydrogen bonds to six interaction partners (C210[ECL2], S211[ECL2], L212[ECL2], K200[ECL2], K227[5.39], Y312[7.35]) and ionic interactions with two residues (K200[ECL2], K227[5.39]). The C4-methyl ester does not participate in the interaction pattern. The carboxylate shifted towards TM5 and is positioned more extracellularly than the furan of SalA. The furan serves as an anchor for the remaining ligand scaffold without establishing crucial interactions. Thus, the C12-substituent shift is likely tolerated and

the centration between the two lysines anchors the remaining ligand scaffold of **13** in a conformation with hydrogen bonding to almost all residues also attacked by SalA with only interactions to Y313[7.36] missing. Keeping crucial interactions from SalA with additional hydrogen bonding and anchoring ionic interactions illuminates the moderate toleration of a carboxylate in a C12 position. Of note, **5** (isopropylamine at C2) is anchored between two opposing charged residues (E297[6.58], E209[ECL2]) with no C4-interactions and moderately tolerated as well (14-fold diminished affinity compared to SalA). Thus, the deficit of the C4-substituent interactions seems to be less severe in cases where the C1- and C2-substituent interactions are maintained.

There is no clear correlation between the size or polarity of C12-alterations and affinity. Besides the small polar carboxylate substituent at C12 in **13** being tolerated the bulky m-carboxamidobenzoyl moiety in **14** [75] is tolerated as well with only a 5-fold affinity drop. The bromination of C16 in **15** [41,42,88] at the furan ring increasing steric size and hydrophobicity does not influence binding to KOR at all while the replacement by bulky greasy naphthalene in **16** [76] diminishes affinity completely. Docking of **14** and **15** to the KOR revealed almost identical binding poses and the maintenance of all interactions was also detected in the KOR-SalA complex but with additional interactions respectively (Figure S14). The m-carboxamidobenzoyl moiety of **14** participates in hydrogen bonding to D138[3.32] with its carboxamide substructure and to Y139[3.33] with its benzoyl substructure while the bromine atom of **15** established hydrophobic contacts to Y139[3.33]. The almost identical binding modes of these two analogs with the one of SalA rationalizing the toleration of both substitution patterns according to KOR affinity. In contrast, docking of **16** resulted in the loss of all hydrogen bonds except the interaction of the C1-carbonyl moiety with Y313[7.36] while the naphthalene moiety is shifted towards TM5 (Figure S15). These docking results illustrate the difficulty of rationally designing newly tailored SalA-analogs without prior knowledge about the actual binding mode of SalA within the KOR by only taking physicochemical properties into account. The combination of favorable physicochemical properties and the right orientation within the binding pocket facilitates improved affinity while only one requirement satisfied can still result in no binding at all.

2.4.4. SalA Derivatives with Modified Scaffolds

Most alterations of the SalA structure focus on the adaption of the C2-, C4, and C12-substituents [15,37]. Nonetheless, some SalA-analogs with alterations within the SalA-ring-system are known including reduction of the carbonyl moieties at positions 1 and 17 as well as ring-opening [15,42,43,71,77,78,81,89].

The complete reduction of the C17-carbonyl moiety in **17** has almost no effect on KOR affinity [77] rendering the C17-carbonyl interactions favorable but dispensable. Docking of **17** into the KOR shows an almost identical binding mode compared to SalA with the same interactions as detected in the KOR-SalA complex and thus explains the almost unaltered biological data (Figure S16).

The effect of omitting moieties at C1 is contradictory. While the complete omission of substituents (**18**) only shows a small impact on KOR affinity and activity [43,77], the change of the carbonyl moiety to a hydroxyl group (**19**) leads to a 281-fold affinity drop [43,77]. When docking **18** and **19** into the KOR we observed similar docking poses compared to SalA, but with slight differences (Figure S17). **18** forms the same protein-ligand interactions as SalA with only the C1 interaction missing, while **19** shows altered interactions. **19** lacks the C2-interaction to Y313[7.36] as its C2-acetoxy group is differently oriented and establishes a hydrogen bond to Y312[7.35] with its C1-hydroxyl group instead. The fact that the complete loss of the C2-substituent abolishes KOR activity completely [78] rationalizes the strong affinity drop for **19**. As **18** mainly differs in the interaction pattern for C1 and was shown less critical for affinity [43,77] it can rescue its affinity in experiments.

3. Discussion

In this study, we presented a putative binding mode for SalA bound to the KOR active-state crystal structure (PDB-ID: 6B73 [22]). To the best of our knowledge, this is the first paper where the binding mode of SalA is systematically modeled within the active-state KOR crystal structure available since 2018. We comprehensively evaluated the structure-activity relationship and mutational data available to generate our model. We further elucidated our binding hypothesis by extensive molecular dynamics simulations and identified relevant structural OR subtype selectivity determinants.

In previous publications, a variety of different binding modes for SalA (and close derivatives) bound to the KOR were postulated but with conflicting orientations [20,22,25, 49–55] causing confusion within the community. The binding poses were guided by mutational data available for SalA at the KOR rather than SAR data. Most studies [22,25,49–52] predicted a vertical orientation of SalA within the KOR binding pocket to account for the far distance between the residues highlighted as important for SalA's affinity and potency at KOR in mutagenesis studies (from Y320[7.43] at the mid of TM7 to residues belonging to ECL2). However, horizontal binding modes were proposed as well [53,54]. The majority of studies evaluating SalA's binding mode were conducted before the publication of the active-state KOR structure (PDB-ID: 6B73 [22]) in 2018. Homology models based on other active-state GPCR structures (like rhodopsin [52] or MOR [50]) or active-like KOR models [20,49,51] based on the inactive-state KOR crystal structure (PDB-ID: 4DJH [20]) were used instead. Those KOR models differ in overall receptor architecture as well as side-chain orientations from the experimentally solved active state X-ray KOR crystal structure used by Che and coworkers [22] and within this study. These differences in the KOR model are used to contribute to the different binding modes proposed for SalA. Yan and coworkers [54] for example generated a KOR model based on the inactive-state rhodopsin crystal structure with Y119[2.64] pointing towards the binding site while Y312[7.35] and Y313[7.36] are oriented more outward ending up with a rather horizontal SalA binding mode to agree with mutagenesis studies. In the active-state crystal structure, the orientations of Y119[2.64], Y312[7.35], and Y313[7.36] are opposed rendering a horizontal binding mode of SalA implausible.

Results of mutagenesis studies should be treated with caution. The effects can be divided into probe-dependent and probe-independent or direct and indirect. Mutations can affect ligand binding and receptor activation by direct interactions with the ligand but also due to alterations in conformations of neighboring residues. Y320[7.43] and Y119[2.64] were both highlighted as important for SalA affinity/activity based on mutagenesis studies [25,49,54]. Y119[2.64] is oriented outward the binding cavity in the active-state X-ray KOR crystal structure which renders direct protein-ligand interactions doubtful. The strong decrease in KOR activity by Y320[7.43]A mutation occurs not only for the nitrogen lacking SalA but also for chemically distinct nitrogen-containing ligands and opioid peptides turning the effect likely probe-independent. The impact of both mutations consists probably of influencing neighboring residues, particularly Y313[7.36] in the case of Y119[2.64] and W287[6.48] which in turn influences the conserved PIF motif in the case of Y320[7.43]. Thus, the evaluation of a binding mode solely by mutational data is less valuable than taking SAR data additionally into account.

Several studies postulate a binding mode in which the furan of SalA points towards the extracellular side of KOR [49–51], which is in contrast to our binding mode and those of several other publications [22,25,52]. Roach and coworkers [50] for example used docking of SalA into the active-state KOR homology model based on the active-state MOR crystal structure (PDB-ID: 5C1M [63]) resulting in a binding mode in which the furan points upwards the receptor cavity while the C2-acetoxy and C4-methyl ester of SalA is positioned deep in the receptor orthosteric binding site. The C4-methyl ester moiety of SalA points towards the negatively charged D138[3.32]. However, experimental testing of SalA analogs revealed the intolerance of positively charged amino groups at the C4 position [15,58,59,73,74] rendering the close proximity of the C4 group to D138[3.32] implausible.

Vardy and coworkers [49] used flexible docking into the inactive-state KOR crystal structure (PDB-ID: 4DJH [20]) and obtained a similar binding mode as Roach and coworkers with the furan pointing upwards the binding cavity but with a permutation of the C2-acetoxy and the C4-methyl ester groups so that the C2-moiety directly interacts with D138$^{3.32}$. This binding mode is supported by the fact that positively charged amino substitutions at the C2 position could be tolerated [73]. However, the D138$^{3.32}$A mutation does not affect the binding of SalA to the KOR [25]. Additionally, cystein-substitution analysis and CoMFA analysis gave hints to the proximity of C2-substituents to E297$^{6.58}$ [52,54] which agrees with our postulated binding mode but conflicts with any binding modes having the furan oriented extracellular and the C2-acetoxy group intracellular.

In 2018 Che and coworkers [22] published the active-state KOR X-ray crystal structure and postulated a binding mode for SalA, albeit without any validation. The published binding mode is similar to our proposed binding mode. In their model, SalA is positioned vertically in the KOR binding cavity with its furan moiety pointing intracellular interacting with Y139$^{3.33}$ while the C1-carbonyl moiety, the C2-acetoxy moiety, and the C4-methyl ester group point upwards interacting with Y312$^{7.35}$ (C1, C2) and C210^{ECL2} (C4). Despite the high similarity between their binding mode and the binding mode of SalA described within this study Che and coworkers did not provide any validation of their putative binding hypothesis. Thus, the confusion within the community about the correct orientation of SalA in the KOR binding site still hold on and kept the need for this study up.

Of note, even after the elucidation of the SalA binding mode, the rational design of SalA analogs with improved clinical usefulness as analgesics is hampered by the lack of data according to the side effects of SalA analogs, first of all, their hallucinogenic properties, but also the common KOR related side effects like anhedonia, sedation, and locomotor incoordination. The side effect profile of SalA analogs needs to receive more attention and should be considered in further studies. G-protein-biased KOR agonists are promising safer analgesics as they likely sow an improved safety profile [6]. Some G-protein-biased SalA analogs are already known, including RB-64 (22-Thiocyanatosalvinorin A), and further attempts at understanding and utilization of G-protein bias may occur in SalA analogs with desired clinical properties.

4. Materials and Methods

4.1. Protein Preparation

All used receptor structures within this study were originally retrieved from the Protein data bank (PDB) [90] and subsequently processed using MOE 2020.0901 [91]. The respective PDB entries for the active-state X-ray crystal structures are 6B73 for KOR, 5C1M for MOR, and 6PT2 for DOR [22,63,64]. In the case of 6B73 (KOR) and 6PT2 (DOR) which were solved as dimeric receptors only the monomeric chain with the better resolution was processed while the remaining one was deleted. All fusion proteins (KOR: nanobody, MOR: antibody fragment, DOR: thermostabilized cytochromeb562 (BRIL)), cocrystallized lipids, and solvent molecules were deleted. To restore the human wild-type receptor sequence the receptor sequences were remutated according to the respective UniProt-Databank entries [92] (UniProt-IDs: P41145 for KOR, P35372 for MOR, and P41143 for DOR). The loop modeler implemented in MOE was conducted to model partially missing loop structures (ECL2, ECL3, ICL3) of KOR and missing side chains of all receptor structures. Improved geometric properties of the receptor structures were facilitated by careful energy minimization of atom clashes and Ramachandran outliers [93] using the OPLS-AA force field [94]. Finally, the receptor structures were protonated at 300 K and a pH of 7 using the Protonate3D application [95] implemented in MOE.

4.2. Docking

The structure of Salvinorin A (SalA) was retrieved from the PubChem database [96] and protonated using the Protonate3D application [95] within MOE. Docking experiments of SalA into the receptor structures were performed by conducting GOLD v5.2 [97]. The

binding site was defined by a 30Å sphere around D3.32-γC (KOR: D138, MOR: D149, DOR: D128) encompassing the hole extracellular half of the receptors. 30 docking runs per experiment were performed resulting in 30 diverse solutions. 'Diverse solution' means that the calculated poses exhibit a root mean square deviation of at least 1.5 Å. The docking solutions were scored according to the GoldScore docking function [98,99]. The search efficiency was set to 200% and pyramidal nitrogen atoms were allowed to flip during the calculations. For docking of SalA into the KOR structure, a distance constraint between C20 of SalA and the phenolic oxygen atom of Y313$^{7.36}$ (maximum 4 Å) was set to ensure binding of SalA around the putative binding site derived by mutagenesis studies.

The generated docking poses were subsequently energy minimized within their protein environment using the MMFF94 force field implemented in LigandScout [66,67] and visually inspected. The final binding hypothesis of SalA was selected according to the geometric properties of SalA within the binding pocket, the number of interactions, and according to information derived from mutagenesis studies as well as experimental testing from SalA analog series. In particular, the residues Q115$^{2.60}$, V118$^{2.63}$, Y119$^{2.64}$, Y139$^{3.33}$, Y312$^{7.35}$, and Y313$^{7.36}$ as well as residues from the ECL2 were considered as putative binding site residues [25,26,49,54] and the C4-methyl ester group must not point towards TM5/TM6 region, i.e., towards several charged residues as neither positive nor negative substituents at the C4-position are tolerated [15,58,59,73,74]. The putative binding poses of SalA analogs were selected according to the Gaussian shape similarity score [100,101] towards SalA measured in LigandScout and the number of interactive features.

4.3. Molecular Dynamics Simulations and Generation of Dynophores

Molecular dynamics (MD) simulations of SalA and RB-64 were prepared with Maestro v2020 [102] and performed with Desmond v2020-4 [85] in five replicates of 200 ns each. The Ligand-KOR complex was put in a rectangular simulation box that spans 10 Å to each receptor side and subsequently embedded in a POPC (1-palmitoyl-2-oleoylphosphatidylcholine) membrane according to the OPM database [103] entry for the active KOR structure (PDB-ID: 6B73). The remaining space within the simulation box was filled up with TIP3P water molecules [104] and ions (Na$^+$, CL$^-$) in an isotonic mixture (0.15 M). For system parametrization, the Charmm36 force field [105] was implemented into Maestro-setup using viparr-ffpublic [106,107]. The simulation run under NPT ensemble conditions, i.e., with a constant number of particles, constant pressure (1.01325 bar), and constant temperature (300 K).

For subsequent simulation analysis, the protein was centered and the trajectory (1000 frames) was aligned onto the backbone heavy atoms of the first sampled protein conformation using VMD v1.9.3 [108]. Additional to the visual inspection of the MD simulations dynamic pharmacophores (dynophores) were calculated with the in-house developed Dynophore tool [56,57]. Dynophores can be visualized within LigandScout as the dynophore algorithm is implemented in the same ilib framework as LigandScout. Only interactions occurring in at least 5% of the simulation time were considered for evaluation.

4.4. Energy Calculations

We performed several different energy calculations implemented in different software applications for calculating the relative binding free energy (RBFE) and absolute binding free energy (ABFE) of SalA and Rb-64 bounded to KOR. We used the docking poses for calculations.

Openfe [86] is an open-source python package (https://github.com/OpenFreeEnergy/openfe, accessed on 1 December 2022) that uses alchemical transformation together with replica exchange simulations to predict RBFE values. The software utilizes OpenMM [109] for conducting the simulation of 5 ns with NPT conditions and additional 2 ns equilibration. The protein was embedded in the TIP3P water model [104,110] with 0.15 M NaCL. The default 'RelativeLigandTransformSettings' were used encompassing 11 λ windows, 1 bar

pressure, and 298.15 Kelvin as temperature among others. For the protein the amber99sb forcefield [111] and for the ligand, the openff-2.0.0 forcefield [112] was applied.

The Ligand FEP panel only implemented in the academic version of Desmond, obtained from D. E. Shaw Research [84,85], uses free energy perturbation calculations for the prediction of the RBFE. 11 replicates of 11 λ-intervals each are performed. The simulations of 5 ns each with an additional equilibration time beforehand are conducted under NPT conditions and the SPC water model [113]. The OPLS2005 forcefield [114,115] was applied.

The open-source python package YANK [87] (https://github.com/choderalab/yank, accessed on 1 December 2022) predicts absolute binding free energy values by conducting alchemical free energy calculations. The whole thermodynamic cycle with its solvent phase (ligand and receptor separated and solvated where the ligand is coupled or decoupled) and the complex phase (ligand bound to the receptor where ligand interacts with protein or is decoupled but restrained in a harmonic manner not to move too far from the binding site) are calculated. We performed calculations with explicit water (TIP4P-EW water model [116]). For accurate long-range treatment of electrostatic interactions particle mesh ewald (PME) method [117,118] was applied with a cutoff at 9 Å. For simulations, the ff14SB forcefield [119] for the protein and the gaff2 forcefield [120] for the ligand were applied.

5. Conclusions

In this study we present the binding mode of SalA to the active-state KOR crystal structure, discuss and present this carefully elucidated binding mode using available mutational and structure-activity data of SalA derivates, and investigate SalA binding using extensive molecular dynamics simulations. The consistency of the binding conformations led to the identification of selectivity determinants towards the other OR subtypes.

SalA adopts a vertically binding mode within the KOR binding site with its furan moiety pointing towards the receptor center while its C2- and C4-substituents span towards the extracellular site. The SalA-KOR complex is stabilized by extensive hydrogen bonding and hydrophobic contacts. Based on this binding mode we rationalize the affinity and activity data of several analogs of SalA. We surmise the C2-substituent interactions as important for SalA and its analogs to be experimentally active, albeit with moderate frequency within MD simulations of SalA. Protein-ligand-interactions at the C17-carbonyl group are rendered less important than those involving C1-, C2-, and C4-substituents as the complete reduction of the former moiety does not alter the affinity of the analog compared to SalA. The furan moiety likely serves as an anchor point for the ligand as modification of this group mostly decreases affinity but the replacement by a negatively charged carboxylate group is somehow tolerated.

SalA interacts with several non-conserved residues in the KOR binding site. We surmise the non-conserved residues 2.63, 7.35, and 7.36 are responsible for SalA's excellent OR subtype selectivity with no binding to MOR, DOR, and NOP. The respective residues in the MOR, DOR, and NOP are unlikely to maintain the interactions observed at the SalA-KOR complex.

We discussed our proposed binding mode of SalA in light of former publications that postulate a majority of different binding hypotheses for SalA at the KOR. We highlighted the difficulty of choosing the right KOR model for subsequent docking studies, the necessity to consider possible probe-independent effects within mutational studies, and the need for SAR data to be considered to determine a binding mode in silico. We show that SalA needs to adopt a vertical binding mode with the C2- and C4-moieties pointing toward the extracellular side instead of the central core of KOR. We are confident that the new insights in the binding mode of SalA at the KOR will facilitate rational design of new analogs with improved properties and therefore promote the development of clinically useful analgesics based on SalA.

Supplementary Materials: The following supporting information can be downloaded at: https://www.mdpi.com/article/10.3390/molecules28020718/s1, Figure S1. Root mean square deviation of

SalA (**1**) in complex with the KOR over the simulation time, Figure S2. Root mean square deviation of the KOR backbone atoms in complex with SalA (**1**) over the simulation time, Figure S3. Sequence identity and similarity of the full sequence of KOR, MOR, DOR, and NOP, Figure S4. Protein-ligand interactions and binding mode of **2** at the KOR in comparison to SalA, Figure S5. Protein-ligand interactions and binding mode of **3** and **4** at the KOR in comparison to SalA, Figure S6. Protein-ligand interactions and binding mode of **5** at the KOR in comparison to SalA, Figure S7. Protein-ligand interactions and binding mode of **6** at the KOR in comparison to SalA, Figure S8. Protein-ligand interactions and binding mode of **7** at the KOR in comparison to SalA, Figure S9: Root mean square deviation of RB-64 (**7**) in complex with the KOR over the simulation time, Figure S10: Root mean square deviation of the KOR backbone atoms in complex with RB-64 (**7**) over the simulation time, Table S1. Energy calculations performed for the docking poses of SalA and RB64 bounded to the KOR, Figure S11. Protein-ligand interactions and binding mode of **8** and **9** at the KOR in comparison to SalA, Figure S12. Protein-ligand interactions and binding mode of **10** and **11** at the KOR in comparison to SalA, Figure S13. Protein-ligand interactions and binding mode of **13** at the KOR in comparison to SalA, Figure S14. Protein-ligand interactions and binding mode of **14** and **15** at the KOR in comparison to SalA, Figure S15. Protein-ligand interactions and binding mode of **16** at the KOR in comparison to SalA, Figure S16. Protein-ligand interactions and binding mode of **17** at the KOR in comparison to SalA, Figure S17. Protein-ligand interactions and binding mode of **18** and **19** at the KOR in comparison to SalA.

Author Contributions: Conceptualization, K.P. and G.W.; methodology, K.P.; validation, K.P.; formal analysis, K.P.; investigation, K.P.; resources, G.W.; writing—original draft preparation, K.P.; writing—review and editing, K.P. and G.W.; visualization, K.P.; supervision, G.W.; funding acquisition, G.W. All authors have read and agreed to the published version of the manuscript.

Institutional Review Board Statement: The study did not require ethical approval.

Data Availability Statement: Data is available from the authors upon reasonable request.

Conflicts of Interest: The authors declare no conflict of interest. The funders had no role in the design of the study; in the collection, analyses, or interpretation of data; in the writing of the manuscript, or in the decision to publish the results.

References

1. Yekkirala, A.S.; Roberson, D.P.; Bean, B.P.; Woolf, C.J. Breaking barriers to novel analgesic drug development. *Nat. Rev. Drug Discov.* **2017**, *16*, 545–564. [CrossRef] [PubMed]
2. Pierce, M.; van Amsterdam, J.; Kalkman, G.A.; Schellekens, A.; van den Brink, W. Is Europe facing an opioid crisis like the United States? An analysis of opioid use and related adverse effects in 19 European countries between 2010 and 2018. *Eur. Psychiatry* **2021**, *64*, e47. [CrossRef]
3. Zierk, K.A. The Real Antidote: A Critical Review of U.S. and Canadian Drug Treatment Courts and a Call for Public Health Prevention Tools as a Solution to the Opioid Epidemic. *Indiana Int. Comp. Law Rev.* **2019**, *29*, 185–217. [CrossRef]
4. Sobczak, Ł.; Goryński, K. Pharmacological aspects of over-the-counter opioid drugs misuse. *Molecules* **2020**, *25*, 3905. [CrossRef]
5. Stein, C. Opioid Receptors. *Annu. Rev. Med.* **2016**, *67*, 433–451. [CrossRef] [PubMed]
6. Mores, K.L.; Cummins, B.R.; Cassell, R.J.; van Rijn, R.M. A review of the therapeutic potential of recently developed G protein-biased kappa agonists. *Front. Pharmacol.* **2019**, *10*, 407. [CrossRef]
7. Corder, G.; Castro, D.C.; Bruchas, M.R.; Scherrer, G. Endogenous and exogenous opioids in pain. *Annu. Rev. Neurosci.* **2018**, *41*, 453–473. [CrossRef] [PubMed]
8. Ribeiro, J.M.L.; Filizola, M. Insights from molecular dynamics simulations of a number of G-protein coupled receptor targets for the treatment of pain and opioid use disorders. *Front. Mol. Neurosci.* **2019**, *12*, 207. [CrossRef]
9. Chou, R.; Fanciullo, G.J.; Fine, P.G.; Adler, J.A.; Ballantyne, J.C.; Davies, P.; Donovan, M.I.; Fishbain, D.A.; Foley, K.M.; Fudin, J.; et al. Clinical guidelines for the use of chronic opioid therapy in chronic noncancer pain. *J. Pain* **2009**, *10*, 113–130. [CrossRef]
10. Albert-Vartanian, A.; Boyd, M.; Hall, A.; Morgado, S.; Nguyen, E.; Nguyen, V.; Patel, S.; Russo, L.; Shao, A.; Raffa, R. Will peripherally restricted kappa-opioid receptor agonists (pKORA s) relieve pain with less opioid adverse effects and abuse potential? *J. Clin. Pharm. Ther.* **2016**, *41*, 371–382. [CrossRef]

11. Atanasov, A.G.; Zotchev, S.B.; Dirsch, V.M.; Supuran, C.T. Natural products in drug discovery: Advances and opportunities. *Nat. Rev. Drug Discov.* **2021**, *20*, 200–216. [CrossRef]

12. Harvey, A.L.; Edrada-Ebel, R.; Quinn, R.J. The re-emergence of natural products for drug discovery in the genomics era. *Nat. Rev. Drug Discov.* **2015**, *14*, 111–129. [CrossRef] [PubMed]

13. Coffeen, U.; Pellicer, F. Salvia divinorum: From recreational hallucinogenic use to analgesic and anti-inflammatory action. *J. Pain Res.* **2019**, *12*, 1069–1076. [CrossRef]

14. Zjawiony, J.K.; Machado, A.S.; Menegatti, R.; Ghedini, P.C.; Costa, E.A.; Pedrino, G.R.; Lukas, S.E.; Franco, O.L.; Silva, O.N.; Fajemiroye, J.O. Cutting-edge search for safer opioid pain relief: Retrospective review of salvinorin A and its analogs. *Front. Psychiatry* **2019**, *10*, 157. [CrossRef] [PubMed]

15. Roach, J.J.; Shenvi, R.A. A review of salvinorin analogs and their kappa-opioid receptor activity. *Bioorg. Med. Chem. Lett.* **2018**, *28*, 1436–1445. [CrossRef] [PubMed]

16. Brito-da-Costa, A.M.; Dias-da-Silva, D.; Gomes, N.G.; Dinis-Oliveira, R.J.; Madureira-Carvalho, Á. Pharmacokinetics and Pharmacodynamics of Salvinorin A and Salvia divinorum: Clinical and Forensic Aspects. *Pharmaceuticals* **2021**, *14*, 116. [CrossRef]

17. Hooker, J.M.; Xu, Y.; Schiffer, W.; Shea, C.; Carter, P.; Fowler, J.S. Pharmacokinetics of the potent hallucinogen, salvinorin A in primates parallels the rapid onset and short duration of effects in humans. *NeuroImage* **2008**, *41*, 1044–1050. [CrossRef]

18. Butelman, E.R.; Fry, R.S.; Kimani, R.; Reed, B.; Kreek, M.J. Neuroendocrine effects of naltrexone versus nalmefene in humans. *Hum. Psychopharmacol. Clin. Exp.* **2020**, *35*, e2726. [CrossRef]

19. Ballesteros, J.A.; Weinstein, H. Integrated methods for the construction of three-dimensional models and computational probing of structure-function relations in G protein-coupled receptors. In *Methods in Neurosciences*; Sealfon, S.C., Ed.; Academic Press: San Diego, CA, USA; London, UK, 1995; Volume 25, pp. 366–428.

20. Wu, H.; Wacker, D.; Mileni, M.; Katritch, V.; Han, G.W.; Vardy, E.; Liu, W.; Thompson, A.A.; Huang, X.-P.; Carroll, F. Structure of the human κ-opioid receptor in complex with JDTic. *Nature* **2012**, *485*, 327–332. [CrossRef]

21. Fenalti, G.; Zatsepin, N.A.; Betti, C.; Giguere, P.; Han, G.W.; Ishchenko, A.; Liu, W.; Guillemyn, K.; Zhang, H.; James, D.; et al. Structural basis for bifunctional peptide recognition at human δ-opioid receptor. *Nat. Struct. Mol. Biol.* **2015**, *22*, 265–268. [CrossRef]

22. Che, T.; Majumdar, S.; Zaidi, S.A.; Ondachi, P.; McCorvy, J.D.; Wang, S.; Mosier, P.D.; Uprety, R.; Vardy, E.; Krumm, B.E.; et al. Structure of the nanobody-stabilized active state of the kappa opioid receptor. *Cell* **2018**, *172*, 55–67.e15. [CrossRef]

23. Vo, Q.N.; Mahinthichaichan, P.; Shen, J.; Ellis, C.R. How μ-opioid receptor recognizes fentanyl. *Nat. Commun.* **2021**, *12*, 984. [CrossRef]

24. Wang, Y.; Tang, K.; Inan, S.; Siebert, D.; Holzgrabe, U.; Lee, D.Y.; Huang, P.; Li, J.-G.; Cowan, A.; Liu-Chen, L.-Y. Comparison of pharmacological activities of three distinct κ ligands (salvinorin A, TRK-820 and 3FLB) on κ opioid receptors in vitro and their antipruritic and antinociceptive activities in vivo. *J. Pharmacol. Exp. Ther.* **2005**, *312*, 220–230. [CrossRef] [PubMed]

25. Kane, B.E.; Nieto, M.J.; McCurdy, C.R.; Ferguson, D.M. A unique binding epitope for salvinorin A, a non-nitrogenous kappa opioid receptor agonist. *FEBS J.* **2006**, *273*, 1966–1974. [CrossRef] [PubMed]

26. Vortherms, T.A.; Mosier, P.D.; Westkaemper, R.B.; Roth, B.L. Differential helical orientations among related G protein-coupled receptors provide a novel mechanism for selectivity: Studies with salvinorin A and the κ-opioid receptor. *J. Biol. Chem.* **2007**, *282*, 3146–3156. [CrossRef] [PubMed]

27. Butelman, E.R.; Kreek, M.J. Salvinorin A, a kappa-opioid receptor agonist hallucinogen: Pharmacology and potential template for novel pharmacotherapeutic agents in neuropsychiatric disorders. *Front. Pharmacol.* **2015**, *6*, 190. [CrossRef]

28. Roth, B.L.; Baner, K.; Westkaemper, R.; Siebert, D.; Rice, K.C.; Steinberg, S.; Ernsberger, P.; Rothman, R.B. Salvinorin A: A potent naturally occurring nonnitrogenous kappa opioid selective agonist. *Proc. Natl. Acad. Sci. USA* **2002**, *99*, 11934–11939. [CrossRef]

29. MacLean, K.A.; Johnson, M.W.; Reissig, C.J.; Prisinzano, T.E.; Griffiths, R.R. Dose-related effects of salvinorin A in humans: Dissociative, hallucinogenic, and memory effects. *Psychopharmacology* **2012**, *226*, 381–392. [CrossRef]

30. Kivell, B.M.; Ewald, A.W.; Prisinzano, T.E. Salvinorin A analogs and other kappa-opioid receptor compounds as treatments for cocaine abuse. *Adv. Pharmacol.* **2014**, *69*, 481–511. [CrossRef]

31. Tsujikawa, K.; Kuwayama, K.; Miyaguchi, H.; Kanamori, T.; Iwata, Y.; Inoue, H. In vitro stability and metabolism of salvinorin A in rat plasma. *Xenobiotica* **2009**, *39*, 391–398. [CrossRef]

32. Schmidt, M.S.; Prisinzano, T.E.; Tidgewell, K.; Harding, W.; Butelman, E.R.; Kreek, M.J.; Murry, D.J. Determination of Salvinorin A in body fluids by high performance liquid chromatography–atmospheric pressure chemical ionization. *J. Chromatogr. B* **2005**, *818*, 221–225. [CrossRef] [PubMed]

33. Teksin, Z.S.; Lee, I.J.; Nemieboka, N.N.; Othman, A.A.; Upreti, V.V.; Hassan, H.E.; Syed, S.S.; Prisinzano, T.E.; Eddington, N.D. Evaluation of the transport, in vitro metabolism and pharmacokinetics of Salvinorin A, a potent hallucinogen. *Eur. J. Pharm. Biopharm.* **2009**, *72*, 471–477. [CrossRef] [PubMed]

34. McCurdy, C.R.; Sufka, K.J.; Smith, G.H.; Warnick, J.E.; Nieto, M.J. Antinociceptive profile of salvinorin A, a structurally unique kappa opioid receptor agonist. *Pharmacol. Biochem. Behav.* **2006**, *83*, 109–113. [CrossRef] [PubMed]

35. Schmidt, M.D.; Schmidt, M.S.; Butelman, E.R.; Harding, W.W.; Tidgewell, K.; Murry, D.J.; Kreek, M.J.; Prisinzano, T.E. Pharma-cokinetics of the plant-derived κ-opioid hallucinogen salvinorin A in nonhuman primates. *Synapse* **2005**, *58*, 208–210. [CrossRef]

36. Siebert, D.J. Salvia divinorum and salvinorin A: New pharmacologic findings. *J. Ethnopharmacol.* **1994**, *43*, 53–56. [CrossRef] [PubMed]

37. Prisinzano, T.E.; Rothman, R.B. Salvinorin A analogs as probes in opioid pharmacology. *Chem. Rev.* **2008**, *108*, 1732–1743. [CrossRef]

38. Béguin, C.; Richards, M.R.; Wang, Y.; Chen, Y.; Liu-Chen, L.-Y.; Ma, Z.; Lee, D.Y.; Carlezon, W.A., Jr.; Cohen, B.M. Synthesis and in vitro pharmacological evaluation of salvinorin A analogues modified at C (2). *Bioorg. Med. Chem. Lett.* **2005**, *15*, 2761–2765. [CrossRef]

39. Beguin, C.; Potter, D.N.; DiNieri, J.A.; Munro, T.A.; Richards, M.R.; Paine, T.A.; Berry, L.; Zhao, Z.; Roth, B.L.; Xu, W. N-methylacetamide analog of salvinorin A: A highly potent and selective κ-opioid receptor agonist with oral efficacy. *J. Pharmacol. Exp. Ther.* **2008**, *324*, 188–195. [CrossRef]

40. Erli, F.; Guerrieri, E.; Ben Haddou, T.; Lantero, A.; Mairegger, M.; Schmidhammer, H.; Spetea, M. Highly potent and selective new diphenethylamines interacting with the κ-opioid receptor: Synthesis, pharmacology, and structure-activity relationships. *J. Med. Chem.* **2017**, *60*, 7579–7590. [CrossRef] [PubMed]

41. Béguin, C.; Duncan, K.K.; Munro, T.A.; Ho, D.M.; Xu, W.; Liu-Chen, L.-Y.; Carlezon, W.A., Jr.; Cohen, B.M. Modification of the furan ring of salvinorin A: Identification of a selective partial agonist at the kappa opioid receptor. *Biorg. Med. Chem.* **2009**, *17*, 1370–1380. [CrossRef]

42. Simpson, D.S.; Katavic, P.L.; Lozama, A.; Harding, W.W.; Parrish, D.; Deschamps, J.R.; Dersch, C.M.; Partilla, J.S.; Rothman, R.B.; Navarro, H. Synthetic studies of Neoclerodane diterpenes from Salvia divinorum: Preparation and opioid receptor activity of Salvinicin analogues. *J. Med. Chem.* **2007**, *50*, 3596–3603. [CrossRef]

43. Holden, K.G.; Tidgewell, K.; Marquam, A.; Rothman, R.B.; Navarro, H.; Prisinzano, T.E. Synthetic studies of neoclerodane diterpenes from Salvia divinorum: Exploration of the 1-position. *Bioorg. Med. Chem. Lett.* **2007**, *17*, 6111–6115. [CrossRef] [PubMed]

44. Harding, W.W.; Schmidt, M.; Tidgewell, K.; Kannan, P.; Holden, K.G.; Gilmour, B.; Navarro, H.; Rothman, R.B.; Prisinzano, T.E. Synthetic studies of Neoclerodane diterpenes from Salvia divinorum: Semisynthesis of Salvinicins A and B and other chemical transformations of Salvinorin A. *J. Nat. Prod.* **2006**, *69*, 107–112. [CrossRef] [PubMed]

45. Bikbulatov, R.V.; Stewart, J.; Jin, W.; Yan, F.; Roth, B.L.; Ferreira, D.; Zjawiony, J.K. Short synthesis of a novel class of salvinorin A analogs with hemiacetalic structure. *Tetrahedron Lett.* **2008**, *49*, 937–940. [CrossRef] [PubMed]

46. Crowley, R.S.; Riley, A.P.; Alder, A.F.; Anderson III, R.J.; Luo, D.; Kaska, S.; Maynez, P.; Kivell, B.M.; Prisinzano, T.E. Synthetic studies of neoclerodane diterpenes from salvia divinorum: Design, synthesis, and evaluation of analogues with improved potency and G-protein activation bias at the μ-opioid receptor. *ACS Chem. Neurosci.* **2020**, *11*, 1781–1790. [CrossRef] [PubMed]

47. Tidgewell, K.; Groer, C.E.; Harding, W.W.; Lozama, A.; Schmidt, M.; Marquam, A.; Hiemstra, J.; Partilla, J.S.; Dersch, C.M.; Rothman, R.B. Herkinorin analogues with differential β-arrestin-2 interactions. *J. Med. Chem.* **2008**, *51*, 2421–2431. [CrossRef] [PubMed]

48. Keasling, A.W.; Pandey, P.; Doerksen, R.J.; Pedrino, G.R.; Costa, E.A.; da Cunha, L.C.; Zjawiony, J.K.; Fajemiroye, J.O. Salvindolin elicits opioid system-mediated antinociceptive and antidepressant-like activities. *J. Psychopharm.* **2019**, *33*, 865–881. [CrossRef] [PubMed]

49. Vardy, E.; Mosier, P.D.; Frankowski, K.J.; Wu, H.; Katritch, V.; Westkaemper, R.B.; Aubé, J.; Stevens, R.C.; Roth, B.L. Chemotype-selective modes of action of κ-opioid receptor agonists. *J. Biol. Chem.* **2013**, *288*, 34470–34483. [CrossRef]

50. Roach, J.J.; Sasano, Y.; Schmid, C.L.; Zaidi, S.; Katritch, V.; Stevens, R.C.; Bohn, L.M.; Shenvi, R.A. Dynamic strategic bond analysis yields a ten-step synthesis of 20-nor-Salvinorin A, a potent κ-OR agonist. *ACS Cent. Sci.* **2017**, *3*, 1329–1336. [CrossRef]

51. Polepally, P.R.; Huben, K.; Vardy, E.; Setola, V.; Mosier, P.D.; Roth, B.L.; Zjawiony, J.K. Michael acceptor approach to the design of new salvinorin A-based high affinity ligands for the kappa-opioid receptor. *Eur. J. Med. Chem.* **2014**, *85*, 818–829. [CrossRef]

52. McGovern, D.L.; Mosier, P.D.; Roth, B.L.; Westkaemper, R.B. CoMFA analyses of C-2 position Salvinorin A analogs at the kappa-opioid receptor provides insights into epimer selectivity. *J. Mol. Graph. Model.* **2010**, *28*, 612–625. [CrossRef] [PubMed]

53. Vortherms, T.A.; Roth, B.L. Salvinorin A. *Mol. Interv.* **2006**, *6*, 257. [CrossRef]

54. Yan, F.; Mosier, P.D.; Westkaemper, R.B.; Stewart, J.; Zjawiony, J.K.; Vortherms, T.A.; Sheffler, D.J.; Roth, B.L. Identification of the molecular mechanisms by which the diterpenoid salvinorin A binds to κ-opioid receptors. *Biochemistry* **2005**, *44*, 8643–8651. [CrossRef]

55. Yan, F.; Bikbulatov, R.V.; Mocanu, V.; Dicheva, N.; Parker, C.E.; Wetsel, W.C.; Mosier, P.D.; Westkaemper, R.B.; Allen, J.A.; Zjawiony, J.K. Structure-based design, synthesis, and biochemical and pharmacological characterization of novel salvinorin A analogues as active state probes of the κ-opioid receptor. *Biochemistry* **2009**, *48*, 6898–6908. [CrossRef] [PubMed]

56. Bock, A.; Bermudez, M.; Krebs, F.; Matera, C.; Chirinda, B.; Sydow, D.; Dallanoce, C.; Holzgrabe, U.; Amici, M.d.; Lohse, M.J.; et al. Ligand binding ensembles determine graded agonist efficacies at a G protein-coupled receptor. *J. Biol. Chem.* **2016**, *291*, 16375–16389. [CrossRef]

57. Sydow, D. *Dynophores: Novel Dynamic Pharmacophores Implementation of Pharmacophore Generation Based on Molecular Dynamics Trajectories and Their Graphical Representation*; Freie Universität Berlin: Berlin, Germany, 2015.

58. Lee, D.Y.; He, M.; Kondaveti, L.; Liu-Chen, L.-Y.; Ma, Z.; Wang, Y.; Chen, Y.; Li, J.-G.; Beguin, C.; Carlezon, W.A., Jr. Synthesis and in vitro pharmacological studies of C (4) modified salvinorin A analogues. *Bioorg. Med. Chem. Lett.* **2005**, *15*, 4169–4173. [CrossRef]

59. Lee, D.Y.; He, M.; Liu-Chen, L.-Y.; Wang, Y.; Li, J.-G.; Xu, W.; Ma, Z.; Carlezon, W.A., Jr.; Cohen, B. Synthesis and in vitro pharmacological studies of new C (4)-modified salvinorin A analogues. *Bioorg. Med. Chem. Lett.* **2006**, *16*, 5498–5502. [CrossRef]

60. Egyed, A.; Kelemen, Á.A.; Vass, M.; Visegrády, A.; Thee, S.A.; Wang, Z.; de Graaf, C.; Brea, J.; Loza, M.I.; Leurs, R. Controlling the selectivity of aminergic GPCR ligands from the extracellular vestibule. *Bioorg. Chem.* **2021**, *111*, 104832. [CrossRef]

61. Tröger, T.; Langenberg, M.; Zhong, S.; Ambrosini, D.; Enzensperger, C. Fishing for accessory binding sites at GPCRs with 'Loop-Hooks'–An approach towards selectivity? Part I. *Chem. Biodivers.* **2014**, *11*, 197–208. [CrossRef] [PubMed]

62. Waldhoer, M.; Bartlett, S.E.; Whistler, J.L. Opioid receptors. *Annu. Rev. Biochem.* **2004**, *73*, 953–990. [CrossRef]

63. Huang, W.; Manglik, A.; Venkatakrishnan, A.J.; Laeremans, T.; Feinberg, E.N.; Sanborn, A.L.; Kato, H.E.; Livingston, K.E.; Thorsen, T.S.; Kling, R.C.; et al. Structural insights into μ-opioid receptor activation. *Nature* **2015**, *524*, 315–321. [CrossRef]

64. Claff, T.; Yu, J.; Blais, V.; Patel, N.; Martin, C.; Wu, L.; Han, G.W.; Holleran, B.J.; van der Poorten, O.; White, K.L.; et al. Elucidating the active δ-opioid receptor crystal structure with peptide and small-molecule agonists. *Sci. Adv.* **2019**, *5*, eaax9115. [CrossRef]

65. Puls, K.; Schmidhammer, H.; Wolber, G.; Spetea, M. Mechanistic characterization of the pharmacological profile of HS-731, a peripherally acting opioid analgesic, at the μ-, δ-, κ-opioid and nociceptin receptors. *Molecules* **2022**, *27*, 919. [CrossRef] [PubMed]

66. Wolber, G.; Langer, T. LigandScout: 3-D pharmacophores derived from protein-bound ligands and their use as virtual screening filters. *J. Chem. Inf. Model.* **2005**, *45*, 160–169. [CrossRef]

67. Wolber, G.; Dornhofer, A.A.; Langer, T. Efficient overlay of small organic molecules using 3D pharmacophores. *J. Comput. Aided Mol. Des.* **2006**, *20*, 773–788. [CrossRef]

68. Polepally, P.R.; White, K.; Vardy, E.; Roth, B.L.; Ferreira, D.; Zjawiony, J.K. Kappa-opioid receptor-selective dicarboxylic ester-derived salvinorin A ligands. *Bioorg. Med. Chem. Lett.* **2013**, *23*, 2860–2862. [CrossRef]

69. Munro, T.A.; Duncan, K.K.; Xu, W.; Wang, Y.; Liu-Chen, L.-Y.; Carlezon, W.A., Jr.; Cohen, B.M.; Béguin, C. Standard protecting groups create potent and selective κ opioids: Salvinorin B alkoxymethyl ethers. *Biorg. Med. Chem.* **2008**, *16*, 1279–1286. [CrossRef] [PubMed]

70. Prevatt-Smith, K.M.; Lovell, K.M.; Simpson, D.S.; Day, V.W.; Douglas, J.T.; Bosch, P.; Dersch, C.M.; Rothman, R.B.; Kivell, B.; Prisinzano, T.E. Potential drug abuse therapeutics derived from the hallucinogenic natural product salvinorin A. *MedChemComm* **2011**, *2*, 1217–1222. [CrossRef] [PubMed]

71. Lee, D.Y.; Karnati, V.V.; He, M.; Liu-Chen, L.-Y.; Kondaveti, L.; Ma, Z.; Wang, Y.; Chen, Y.; Beguin, C.; Carlezon, W.A., Jr. Synthesis and in vitro pharmacological studies of new C (2) modified salvinorin A analogues. *Bioorg. Med. Chem. Lett.* **2005**, *15*, 3744–3747. [CrossRef] [PubMed]

72. Chavkin, C.; Sud, S.; Jin, W.; Stewart, J.; Zjawiony, J.K.; Siebert, D.J.; Toth, B.A.; Hufeisen, S.J.; Roth, B.L. Salvinorin A, an active component of the hallucinogenic sage Salvia divinorum is a highly efficacious κ-opioid receptor agonist: Structural and functional considerations. *J. Pharmacol. Exp. Ther.* **2004**, *308*, 1197–1203. [CrossRef]

73. Béguin, C.; Richards, M.R.; Li, J.-G.; Wang, Y.; Xu, W.; Liu-Chen, L.-Y.; Carlezon, W.A., Jr.; Cohen, B.M. Synthesis and in vitro evaluation of salvinorin A analogues: Effect of configuration at C (2) and substitution at C (18). *Bioorg. Med. Chem. Lett.* **2006**, *16*, 4679–4685. [CrossRef]

74. Munro, T.A.; Duncan, K.K.; Staples, R.J.; Xu, W.; Liu-Chen, L.-Y.; Béguin, C.; Carlezon, W.A., Jr.; Cohen, B.M. 8-epi-Salvinorin B: Crystal structure and affinity at the κ opioid receptor. *Beilstein J. Org. Chem.* **2007**, *3*, 1. [CrossRef]

75. Lovell, K.M.; Vasiljevik, T.; Araya, J.J.; Lozama, A.; Prevatt-Smith, K.M.; Day, V.W.; Dersch, C.M.; Rothman, R.B.; Butelman, E.R.; Kreek, M.J. Semisynthetic neoclerodanes as kappa opioid receptor probes. *Biorg. Med. Chem.* **2012**, *20*, 3100–3110. [CrossRef] [PubMed]

76. Lozama, A.; Cunningham, C.W.; Caspers, M.J.; Douglas, J.T.; Dersch, C.M.; Rothman, R.B.; Prisinzano, T.E. Opioid receptor probes derived from cycloaddition of the hallucinogen natural product salvinorin A. *J. Nat. Prod.* **2011**, *74*, 718–726. [CrossRef]

77. Munro, T.A.; Rizzacasa, M.A.; Roth, B.L.; Toth, B.A.; Yan, F. Studies toward the pharmacophore of salvinorin A, a potent κ opioid receptor agonist. *J. Med. Chem.* **2005**, *48*, 345–348. [CrossRef]

78. Sherwood, A.M.; Crowley, R.S.; Paton, K.F.; Biggerstaff, A.; Neuenswander, B.; Day, V.W.; Kivell, B.M.; Prisinzano, T.E. Addressing structural flexibility at the A-ring on salvinorin A: Discovery of a potent kappa-opioid agonist with enhanced metabolic stability. *J. Med. Chem.* **2017**, *60*, 3866–3878. [CrossRef] [PubMed]

79. Lee, D.Y.; Yang, L.; Xu, W.; Deng, G.; Guo, L.; Liu-Chen, L.-Y. Synthesis and biological evaluation of C-2 halogenated analogs of salvinorin A. *Bioorg. Med. Chem. Lett.* **2010**, *20*, 5749–5752. [CrossRef] [PubMed]

80. Fichna, J.; Lewellyn, K.; Yanc, F.; Roth, B.L.; Zjawiony, J.K. Synthesis and biological evaluation of new salvinorin A analogues incorporating natural amino acids. *Bioorg. Med. Chem. Lett.* **2011**, *21*, 160–163. [CrossRef] [PubMed]

81. Crowley, R.S.; Riley, A.P.; Sherwood, A.M.; Groer, C.E.; Shivaperumal, N.; Biscaia, M.; Paton, K.; Schneider, S.; Provasi, D.; Kivell, B.M. Synthetic studies of neoclerodane diterpenes from salvia divinorum: Identification of a potent and centrally acting μ opioid analgesic with reduced abuse liability. *J. Med. Chem.* **2016**, *59*, 11027–11038. [CrossRef]

82. Simpson, D.S.; Lovell, K.M.; Lozama, A.; Han, N.; Day, V.W.; Dersch, C.M.; Rothman, R.B.; Prisinzano, T.E. Synthetic studies of neoclerodane diterpenes from Salvia divinorum: Role of the furan in affinity for opioid receptors. *Org. Biomol. Chem.* **2009**, *7*, 3748–3756. [CrossRef]

83. White, K.L.; Robinson, J.E.; Zhu, H.; DiBerto, J.F.; Polepally, P.R.; Zjawiony, J.K.; Nichols, D.E.; Malanga, C.; Roth, B.L. The G protein–biased κ-opioid receptor agonist RB-64 is analgesic with a unique spectrum of activities in vivo. *J. Pharmacol. Exp. Ther.* **2015**, *352*, 98–109. [CrossRef] [PubMed]

84. D E Shaw Research. *Desmond Molecular Dynamics System*; 2022–1; D E Shaw Research: New York, NY, USA, 2022.

85. Bowers, K.J.; Chow, D.E.; Xu, H.; Dror, R.O.; Eastwood, M.P.; Gregersen, B.A.; Klepeis, J.L.; Kolossvary, I.; Moraes, M.A.; Sacerdoti, F.D.; et al. Scalable algorithms for molecular dynamics simulations on commodity clusters. In Proceedings of the ACM/IEEE Conference on Supercomputing (SC06), Tampa, FL, USA, 11–17 November 2006.

86. Gowers, R.J.; Alibay, I.; Swenson, D.W.H.; Henry, M.M. *Open Free Energy (OpenFE)*; Version 0.21. 2022.

87. Rizzi, A.; Grinaway, P.B.; Parton, D.L.; Shirts, M.R.; Wang, K.; Eastman, P.; Friedrichs, M.; Pande, V.S.; Branson, K.; Mobley, D.L.; et al. YANK: A GPU-Accelerated Platform for Alchemical Free Energy Calculations. Available online: http://getyank.org/latest/ (accessed on 1 December 2022).

88. Riley, A.P.; Groer, C.E.; Young, D.; Ewald, A.W.; Kivell, B.M.; Prisinzano, T.E. Synthesis and κ-opioid receptor activity of furan-substituted salvinorin A analogues. *J. Med. Chem.* **2014**, *57*, 10464–10475. [CrossRef] [PubMed]

89. Harding, W.W.; Tidgewell, K.; Byrd, N.; Cobb, H.; Dersch, C.M.; Butelman, E.R.; Rothman, R.B.; Prisinzano, T.E. Neoclerodane diterpenes as a novel scaffold for μ opioid receptor ligands. *J. Med. Chem.* **2005**, *48*, 4765–4771. [CrossRef] [PubMed]

90. Berman, H.; Henrick, K.; Nakamura, H. Announcing the worldwide Protein Data Bank. *Nat. Struct. Biol.* **2003**, *10*, 980. [CrossRef]

91. *Molecular Operating Environment (MOE)*; Chemical Computing Group: Montreal, QC, Canada, 2021; Available online: https://www.chemcomp.com/Products.htm (accessed on 10 April 2022).

92. The UniProt Consortium. UniProt: The universal protein knowledgebase in 2021. *Nucleic Acids Res.* **2021**, *49*, D480–D489. [CrossRef] [PubMed]

93. Ramachandran, G.N.; Ramakrishnan, C.; Sasisekharan, V. Stereochemistry of polypeptide chain configurations. *J. Mol. Biol.* **1963**, *7*, 95–99. [CrossRef]

94. Zhu, S. Validation of the generalized force fields GAFF, CGenFF, OPLS-AA, and PRODRGFF by testing against experimental osmotic coefficient data for small drug-like molecules. *J. Chem. Inf. Model.* **2019**, *59*, 4239–4247. [CrossRef]

95. Labute, P. Protonate3D: Assignment of ionization states and hydrogen coordinates to macromolecular structures. *Proteins* **2009**, *75*, 187–205. [CrossRef]

96. Kim, S.; Chen, J.; Cheng, T.; Gindulyte, A.; He, J.; He, S.; Li, Q.; Shoemaker, B.A.; Thiessen, P.A.; Yu, B. PubChem in 2021: New data content and improved web interfaces. *Nucleic Acids Res.* **2021**, *49*, D1388–D1395. [CrossRef]

97. Jones, G.; Willett, P.; Glen, R.C.; Leach, A.R.; Taylor, R. Development and validation of a genetic algorithm for flexible docking. *J. Mol. Biol.* **1997**, *267*, 727–748. [CrossRef]

98. Evers, A.; Hessler, G.; Matter, H.; Klabunde, T. Virtual screening of biogenic amine-binding G-protein coupled receptors: Comparative evaluation of protein- and ligand-based virtual screening protocols. *J. Med. Chem.* **2005**, *48*, 5448–5465. [CrossRef]

99. Verdonk, M.L.; Cole, J.C.; Hartshorn, M.J.; Murray, C.W.; Taylor, R.D. Improved protein-ligand docking using GOLD. *Proteins* **2003**, *52*, 609–623. [CrossRef] [PubMed]

100. Kumar, A.; Zhang, K.Y.J. Advances in the development of shape similarity methods and their application in drug discovery. *Front. Chem.* **2018**, *6*, 315. [CrossRef] [PubMed]

101. Grant, J.A.; Pickup, B. A Gaussian description of molecular shape. *J. Phys. Chem.* **1995**, *99*, 3503–3510. [CrossRef]

102. *Schrödinger Release-4: Maestro*, version 2020-4; Schrödinger LLC.: New York, NY, USA, 2020.

103. Lomize, M.A.; Pogozheva, I.D.; Joo, H.; Mosberg, H.I.; Lomize, A.L. OPM database and PPM web server: Resources for positioning of proteins in membranes. *Nucleic Acids Res.* **2012**, *40*, D370–D376. [CrossRef]

104. Boonstra, S.; Onck, P.R.; van der Giessen, E. CHARMM TIP3P water model suppresses peptide folding by solvating the unfolded state. *J. Phys. Chem. B* **2016**, *120*, 3692–3698. [CrossRef] [PubMed]

105. Huang, J.; MacKerell, A.D., Jr. CHARMM36 all-atom additive protein force field: Validation based on comparison to NMR data. *J. Comput. Chem.* **2013**, *34*, 2135–2145. [CrossRef]

106. Tucker, M.R.; Piana, S.; Tan, D.; LeVine, M.V.; Shaw, D.E. Development of force field parameters for the simulation of single-and double-stranded DNA molecules and DNA–protein complexes. *J. Phys. Chem. B* **2022**, *126*, 4442–4457. [CrossRef]

107. Gullingsrud, J. DEShawResearch. Viparr-Ffpublic. Available online: https://github.com/DEShawResearch/viparr-ffpublic (accessed on 8 August 2022).

108. Humphrey, W.; Dalke, A.; Schulten, K. VMD: Visual molecular dynamics. *J. Mol. Graph.* **1996**, *14*, 33–38. [CrossRef]

109. Eastman, P.; Pande, V. OpenMM: A hardware-independent framework for molecular simulations. *Comput. Sci. Eng.* **2010**, *12*, 34–39. [CrossRef]

110. Jorgensen, W.L.; Chandrasekhar, J.; Madura, J.D.; Impey, R.W.; Klein, M.L. Comparison of simple potential functions for simulating liquid water. *J. Chem. Phys.* **1983**, *79*, 926–935. [CrossRef]

111. Showalter, S.A.; Brüschweiler, R. Validation of molecular dynamics simulations of biomolecules using NMR spin relaxation as benchmarks: Application to the AMBER99SB force field. *J. Chem. Theory Comput.* **2007**, *3*, 961–975. [CrossRef]

112. Boothroyd, S.; Behara, P.K.; Madin, O.; Hahn, D.; Jang, H.; Gapsys, V.; Wagner, J.; Horton, J.; Dotson, D.; Thompson, M. Development and benchmarking of open force field 2.0.0—The sage small molecule force field. In preparation. [CrossRef]

113. Zielkiewicz, J. Structural properties of water: Comparison of the SPC, SPCE, TIP4P, and TIP5P models of water. *J. Chem. Phys.* **2005**, *123*, 104501. [CrossRef] [PubMed]

114. Jorgensen, W.L.; Maxwell, D.S.; Tirado-Rives, J. Development and testing of the OPLS all-atom force field on conformational energetics and properties of organic liquids. *J. Am. Chem. Soc.* **1996**, *118*, 11225–11236. [CrossRef]

115. Ponder, J.W.; Case, D.A. Force fields for protein simulations. *Adv. Protein Chem.* **2003**, *66*, 27–85. [PubMed]

116. Horn, H.W.; Swope, W.C.; Pitera, J.W.; Madura, J.D.; Dick, T.J.; Hura, G.L.; Head-Gordon, T. Development of an improved four-site water model for biomolecular simulations: TIP4P-Ew. *J. Chem. Phys.* **2004**, *120*, 9665–9678. [CrossRef]

117. Essmann, U.; Perera, L.; Berkowitz, M.L.; Darden, T.; Lee, H.; Pedersen, L.G. A smooth particle mesh Ewald method. *J. Chem. Phys.* **1995**, *103*, 8577–8593. [CrossRef]

118. Toukmaji, A.Y.; Board, J.A., Jr. Ewald summation techniques in perspective: A survey. *Comput. Phys. Commun.* **1996**, *95*, 73–92. [CrossRef]

119. Maier, J.A.; Martinez, C.; Kasavajhala, K.; Wickstrom, L.; Hauser, K.E.; Simmerling, C. ff14SB: Improving the accuracy of protein side chain and backbone parameters from ff99SB. *J. Chem. Theory Comput.* **2015**, *11*, 3696–3713. [CrossRef]

120. He, X.; Man, V.H.; Yang, W.; Lee, T.-S.; Wang, J. A fast and high-quality charge model for the next generation general AMBER force field. *J. Chem. Phys.* **2020**, *153*, 114502. [CrossRef]

Supporting Materials

Solving an Old Puzzle: Elucidation and Evaluation of the Binding Mode of Salvinorin A at the Kappa Opioid Receptor

Kristina Puls and Gerhard Wolber*

Department of Biology, Chemistry and Pharmacy, Institute of Pharmacy, Freie Universität Berlin; Königin-Luise-Str. 2+4, 14195 Berlin, Germany

*Correspondence: gerhard.wolber@fu-berlin.de (G.W.), Tel.: +49-30-838-52686
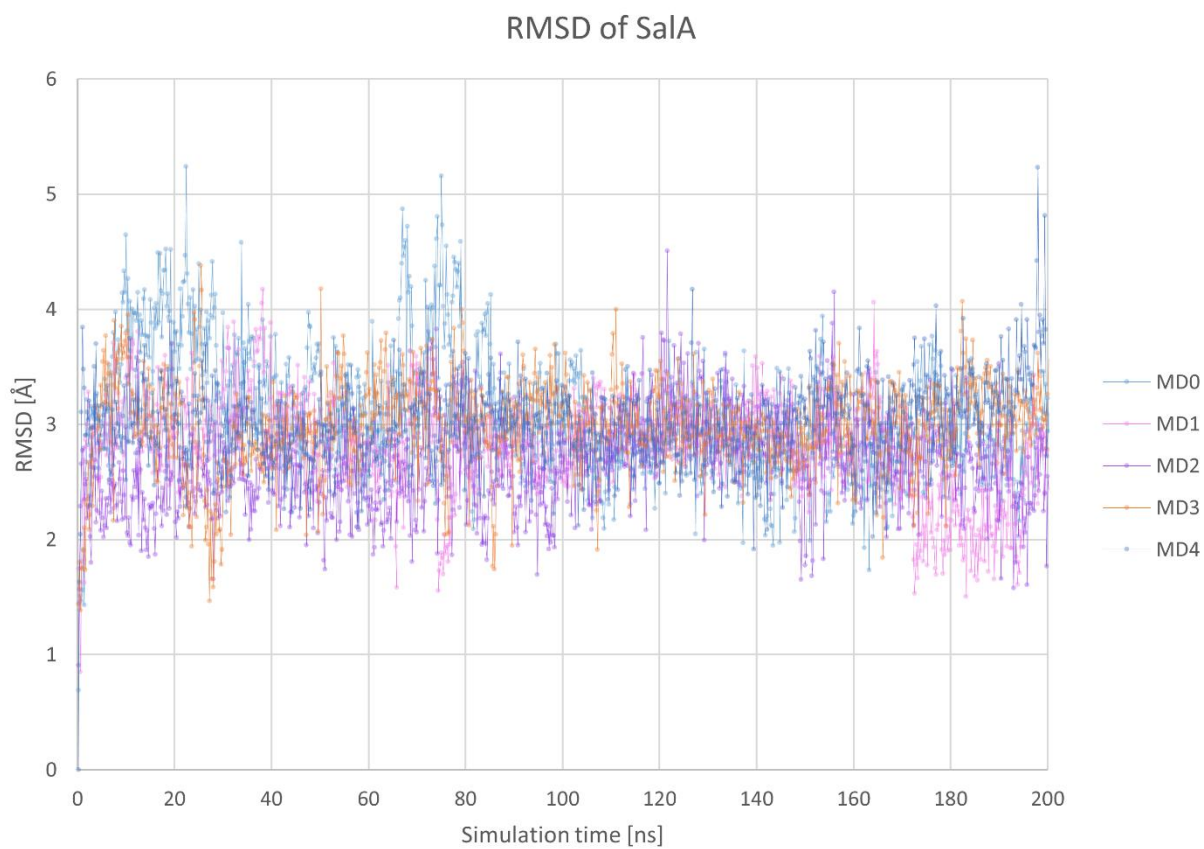
Figure S1. Root mean square deviation of SalA (**1**) in complex with the kappa opioid receptor (KOR) over the simulation time.
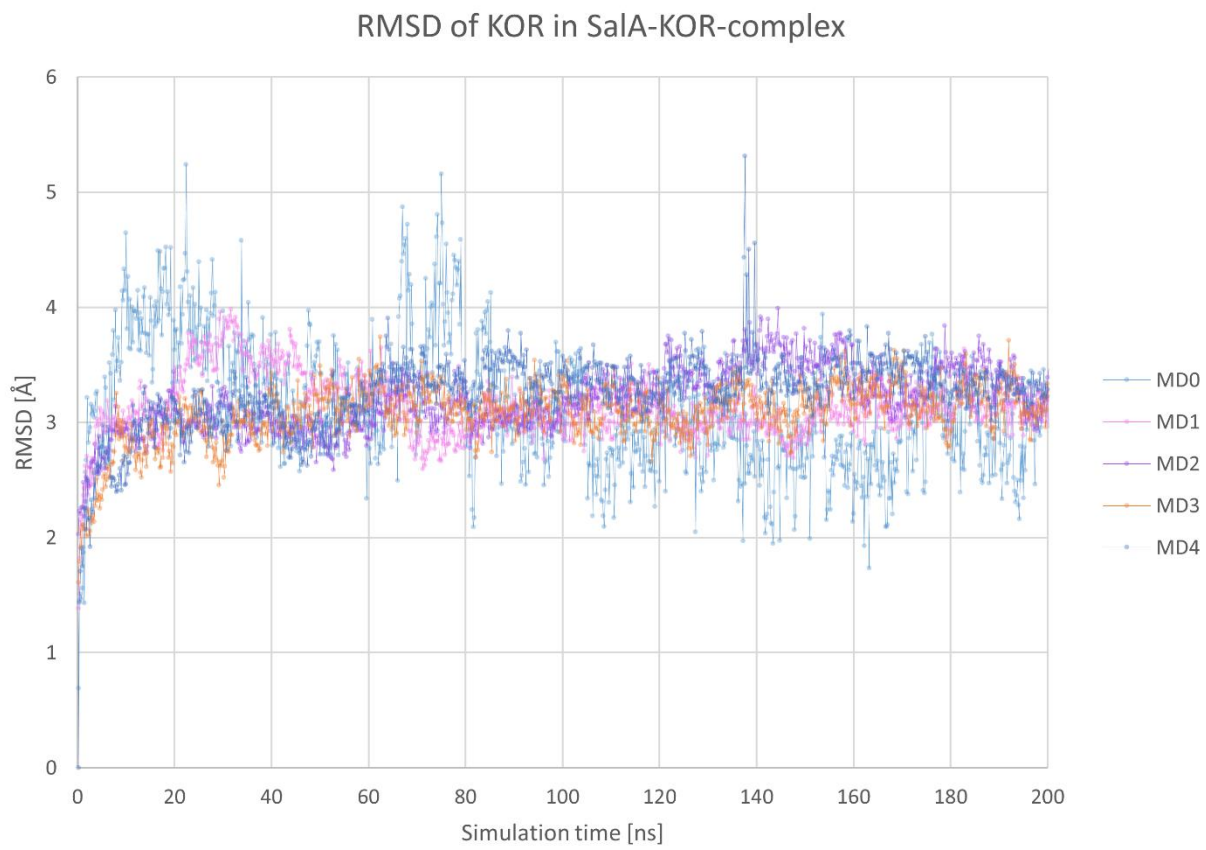
Figure S2. Root mean square deviation of the KOR backbone atoms in complex with SalA (**1**) over the simulation time.

Identity

	1.	2.	3.	4.
1. hKOR		53.5	57.4	50.3
2. hMOR	56.3		60.5	50.3
3. hDOR	56.3	56.2		50.0
4. hNOP	48.9	46.5	49.7	

Similarity

	1.	2.	3.	4.
1. hKOR		67.0	69.6	64.3
2. hMOR	70.5		70.7	63.8
3. hDOR	68.2	65.8		62.4
4. hNOP	62.6	59.0	62.1	

Figure S3. Sequence identity and similarity of the full sequence of KOR, MOR, DOR, and NOP.

Figure S4. Protein-ligand interactions (A) and binding mode (B) of **2** (orange) at the KOR in comparison to SalA (blue). $Y^{3.33}$ denotes to $Y139^{3.33}$, C^{ECL2} to $C210^{ECL2}$, and $I^{6.55}$ to $I294^{6.55}$. Interactions types are abbreviated with HBA for hydrogen bond acceptor and HY for hydrophobic contact.

Figure S5. Protein-ligand interactions and binding mode of **3** (A, B, orange) and **4** (C, D, orange) at the KOR in comparison to SalA (blue). Y[3.33] denotes to Y139[3.33], C[ECL2] to C210[ECL2], and I[6.55] to I294[6.55]. Interactions types are abbreviated with HBA for hydrogen bond acceptor and HY for hydrophobic contact.

Figure S6. Protein-ligand interactions (A) and binding mode (B) of **5** (orange) at the KOR in comparison to SalA (blue). $Y^{3.33}$ denotes to $Y139^{3.33}$, C^{ECL2} to $C210^{ECL2}$, and $I^{6.55}$ to $I294^{6.55}$. Interactions types are abbreviated with HBA for hydrogen bond acceptor, HY for hydrophobic contact, HBD for hydrogen bond donor, and PI for positive charged interaction.

Figure S7. Protein-ligand interactions (A) and binding mode (B) of **6** (orange) at the KOR in comparison to SalA (blue). $Y^{3.33}$ denotes to $Y139^{3.33}$, C^{ECL2} to $C210^{ECL2}$, and $I^{6.55}$ to $I294^{6.55}$. Interactions types are abbreviated with HBA for hydrogen bond acceptor and HY for hydrophobic contact.
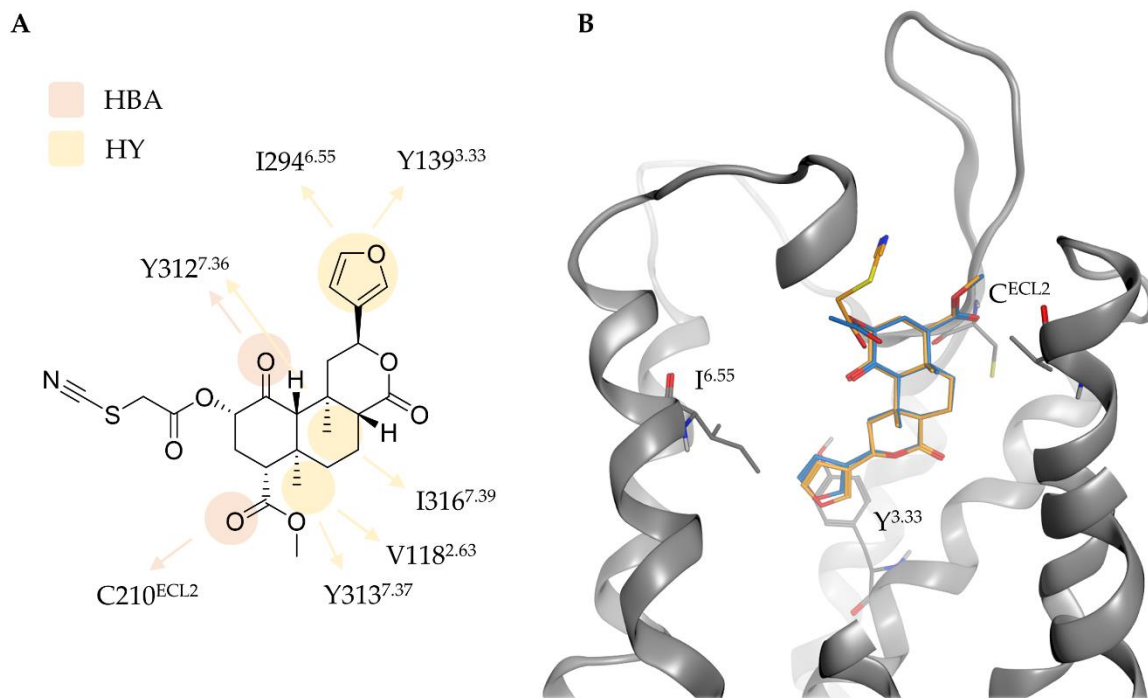
Figure S8. Protein-ligand interactions (A) and binding mode (B) of **7** (orange) at the KOR in comparison to SalA (blue). $Y^{3.33}$ denotes to $Y139^{3.33}$, C^{ECL2} to $C210^{ECL2}$, and $I^{6.55}$ to $I294^{6.55}$. Interactions types are abbreviated with HBA for hydrogen bond acceptor and HY for hydrophobic contact.

Figure S9. Root mean square deviation of RB-64 (**7**) in complex with the KOR over the simulation time.

Figure S10. Root mean square deviation of the KOR backbone atoms in complex with RB-64 (**7**) over the simulation time.

Table S1. Energy calculations performed for the docking poses of SalA and RB64 bounded to the KOR.

RBFE				
Software	**Calculation**	**ΔG complex (kcal/mol)**	**ΔG solvent (kcal/mol)**	**RBFE (kcal/mol)**
Openfe [1]	Alchemical transformation of SalA into RB-64 bound to KOR	-27.273 ± 0.379	-25.059 ± 0.016	-2.214 ± 0.395
Schrödinger Ligand FEP [2,3]	Free energy perturbation turning RB-64 to SalA bound to KOR, respectively	-2.020 ± 0.202	-2.519 ± 0.214	0.499 ± 0.416
ABFE				
Software	**Calculation**	**ABFE (kcal/mol)**	**Difference in ABFE (kcal/mol)**	
YANK [4]	Binding free energy of SalA bound to KOR	-16.637 ± 0.961	|ABFE(SalA)| − |ABFE(RB-64)| = -3.817 ± 2.03	
	Binding free energy of RB-64 bound to KOR	-20.454 ± 1.069		

The abbreviations RBFE and ABFE refer to relative and absolute binding free energy. All methods predicted the binding of RB-64 to the active state KOR crystal structure (PDB-ID 6B73 [5]) favorable over the binding of SalA. The negative RBFE value in the case of openfe, where SalA is alchemically transformed into Rb-64, indicates that the latter (Rb-64) is favored over the first (SalA). The positive RBFE value in the case of Schrödinger Ligand FEP, where RB-64 is transformed into SalA, indicates the favorable binding of the first (RB-64) over the latter (SalA). In the case of YANK the absolute binding free energy of the two complexes, SalA or RB-64 bound to KOR, was calculated and compared. The more negative value for the RB-64 bound complex indicates an energetic improvement of the RB-64 bound state over the SalA-bound state.
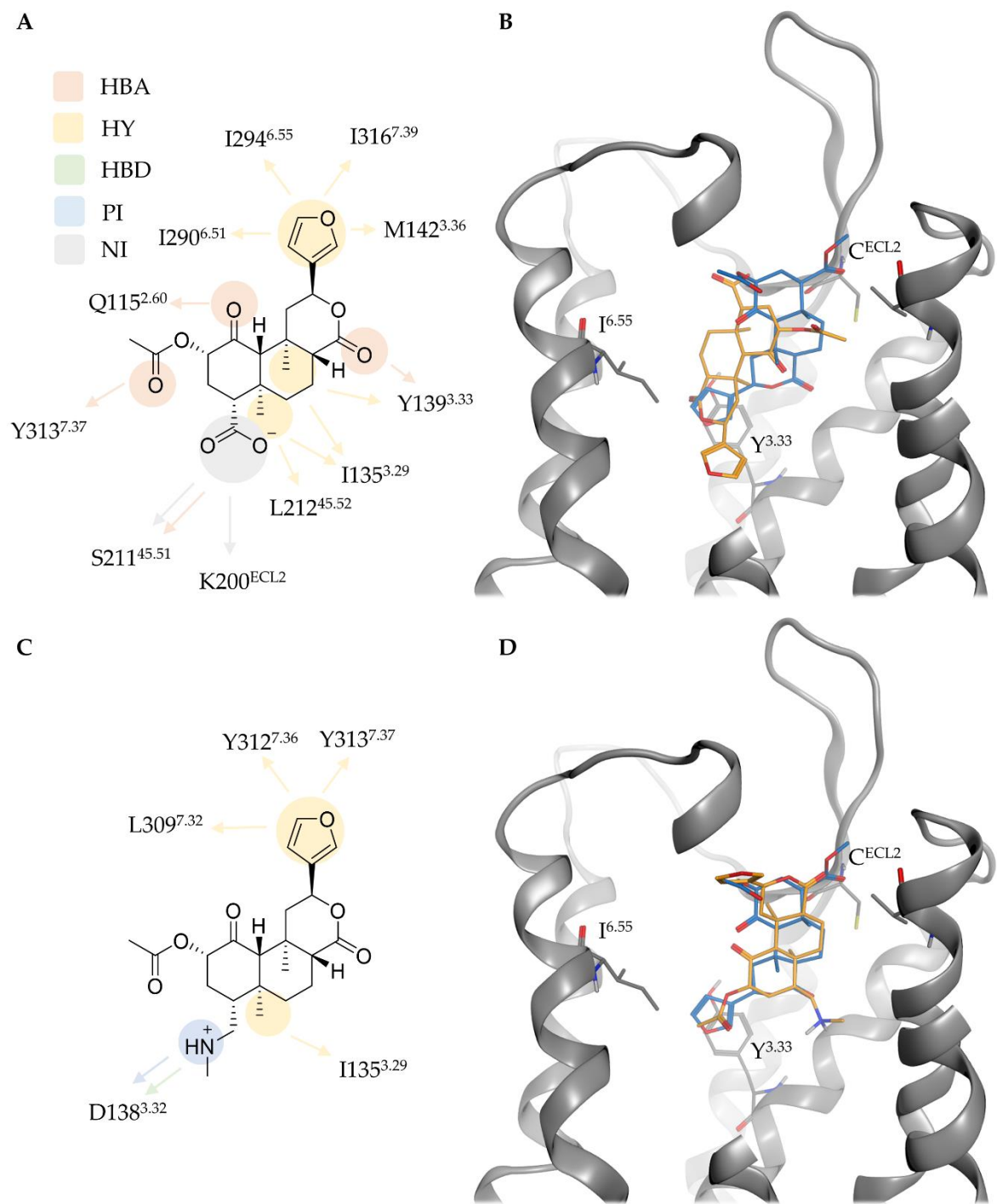
Figure S11. Protein-ligand interactions and binding mode of **8** (A, B, orange) and **9** (C, D, orange) at the KOR in comparison to SalA (blue). **8** is shifted in the binding side and shows an alternative Y139[3.33], C[ECL2] to C210[ECL2], and I[6.55] to I294[6.55]. Interactions types are abbreviated with HBA for hydrogen scaffold orientation while **9** shows a reversed orientation compared to SalA. Y[3.33] denotes to bond acceptor, HY for hydrophobic contact, HBD for hydrogen bond donor, NI for negative charged interaction, and PI for positive charged interaction.
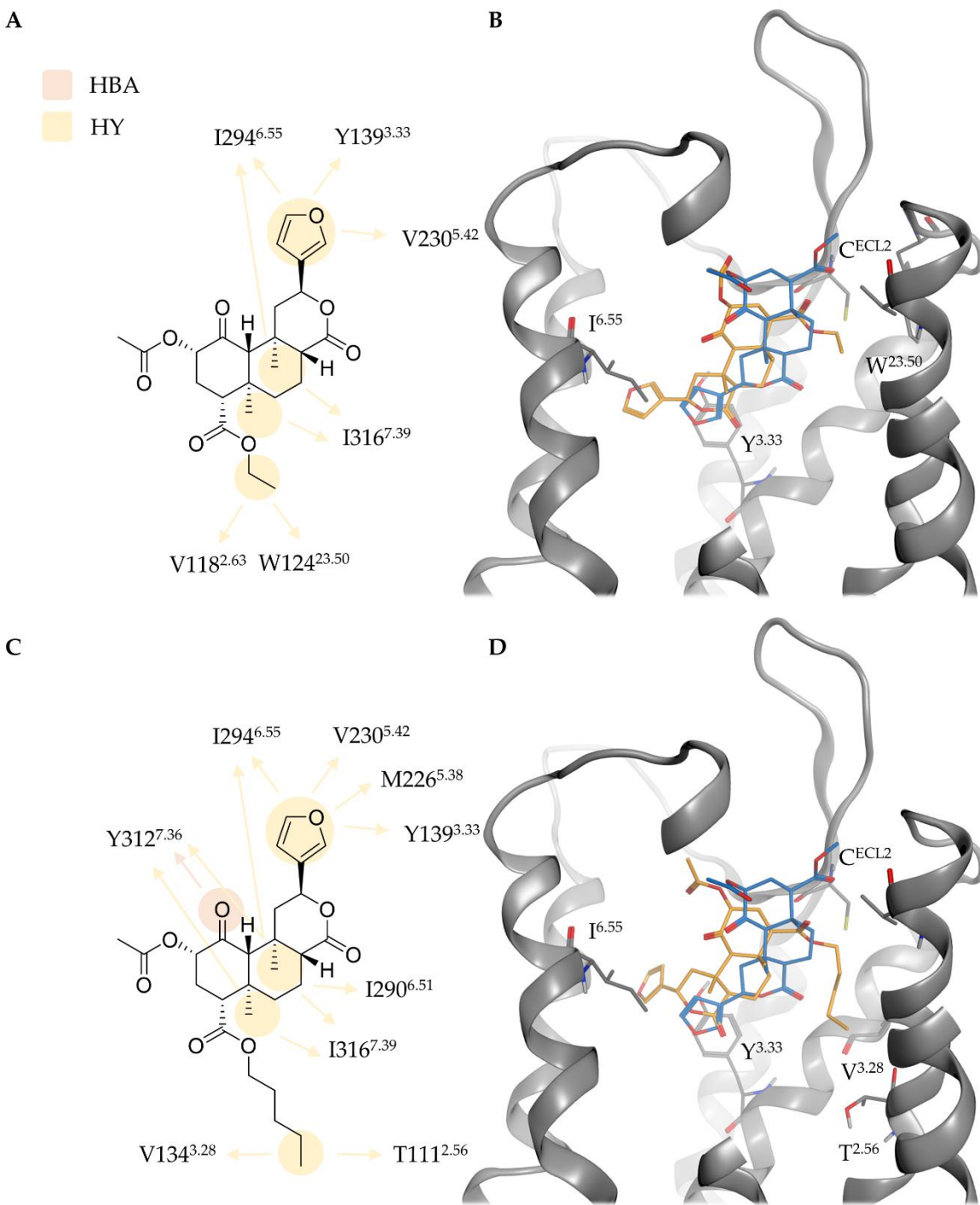
Figure S12. Protein-ligand interactions and binding mode of **10** (A, B, orange) and **11** (C, D, orange) at the KOR in comparison to SalA (blue). $Y^{3.33}$ denotes to $Y139^{3.33}$, C^{ECL2} to $C210^{ECL2}$, and $I^{6.55}$ to $I294^{6.55}$. Interactions types are abbreviated with HBA for hydrogen bond acceptor and HY for hydrophobic contact.
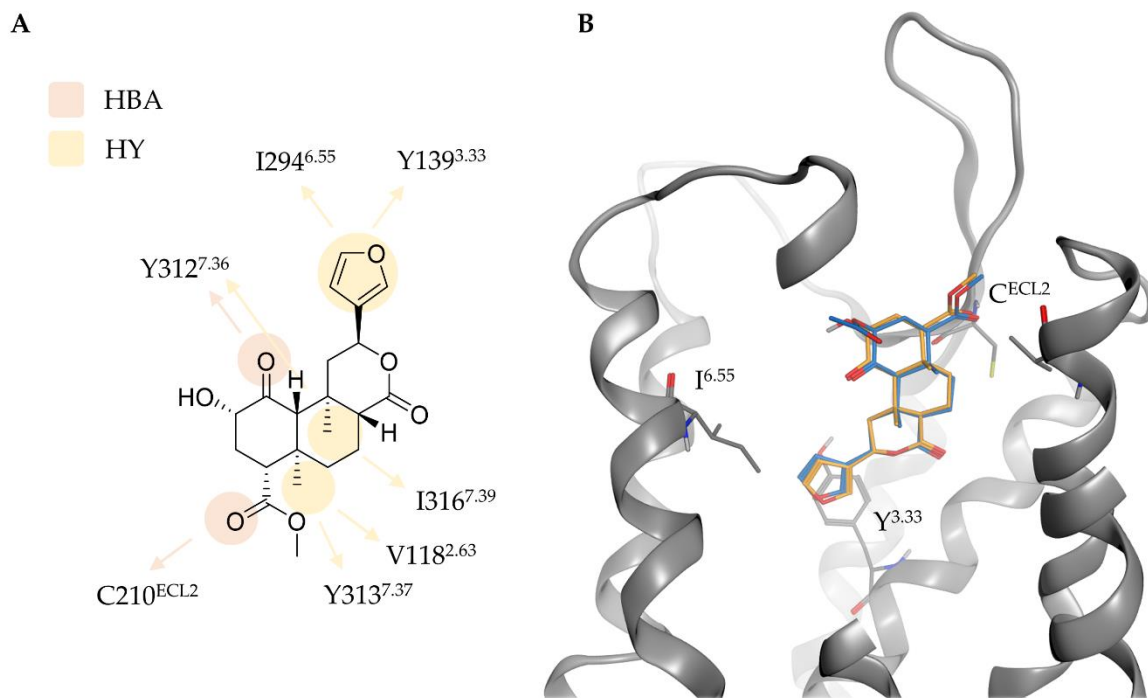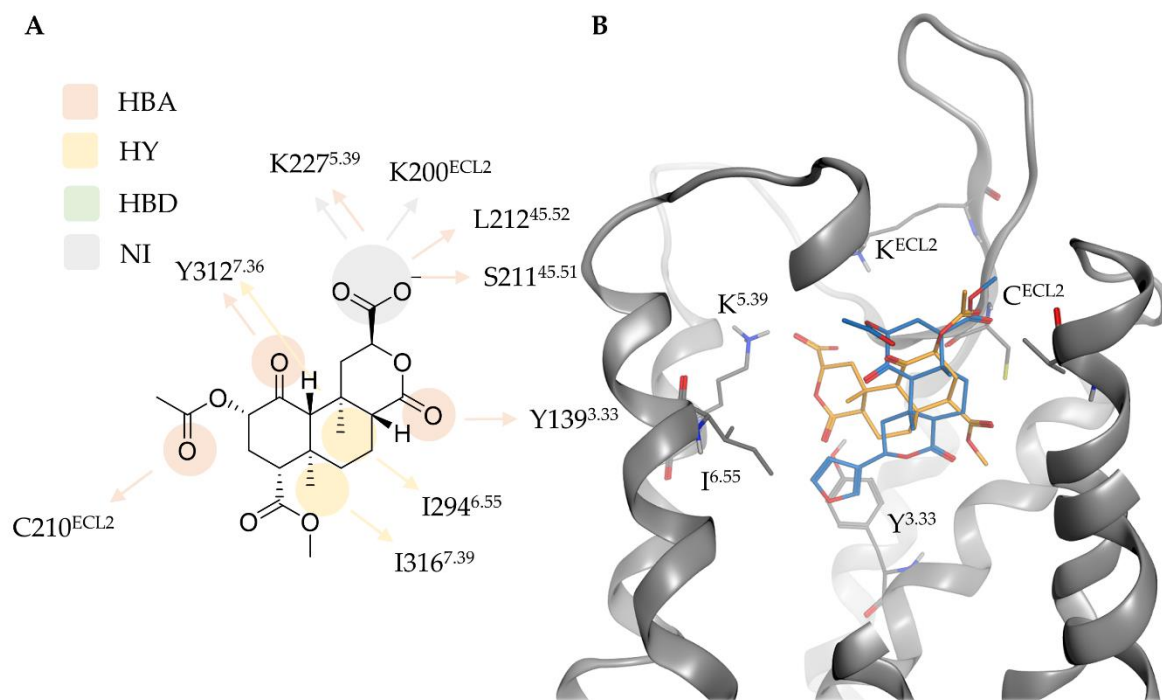
Figure S13. Protein-ligand interactions (A) and binding mode (B) of **13** (orange) at the KOR in comparison to SalA (blue). $Y^{3.33}$ denotes to $Y139^{3.33}$, C^{ECL2} to $C210^{ECL2}$, and $I^{6.55}$ to $I294^{6.55}$. Interactions types are abbreviated with HBA for hydrogen bond acceptor, HY for hydrophobic contact, HBD for hydrogen bond donor, and NI for negative charged interaction.
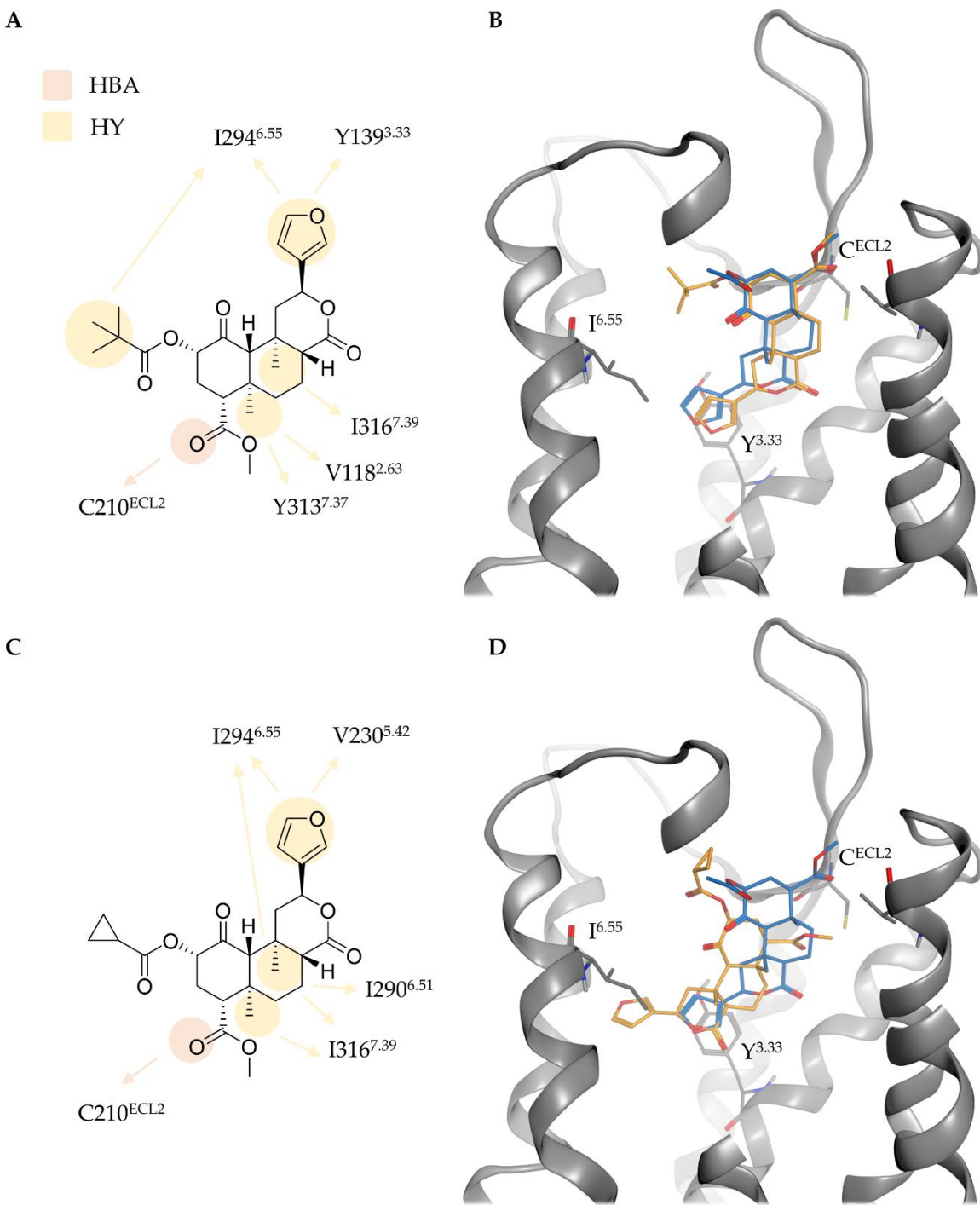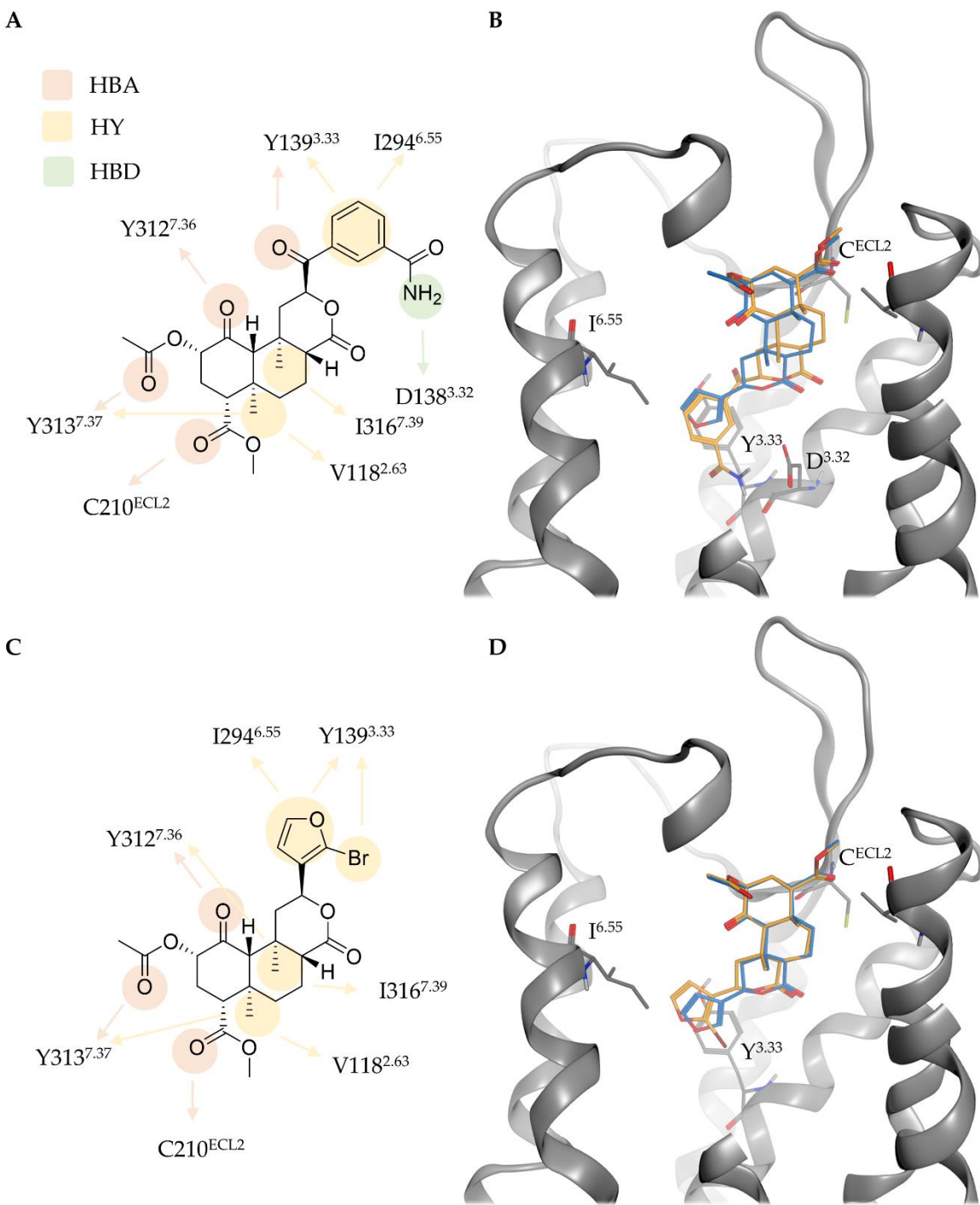
Figure S14. Protein-ligand interactions and binding mode of **14** (A, B, orange) and **15** (C, D, orange) at the KOR in comparison to SalA (blue). $Y^{3.33}$ denotes to Y139[3.33], C^{ECL2} to C210[ECL2], and $I^{6.55}$ to I294[6.55]. Interactions types are abbreviated with HBA for hydrogen bond acceptor and HY for hydrophobic contact.
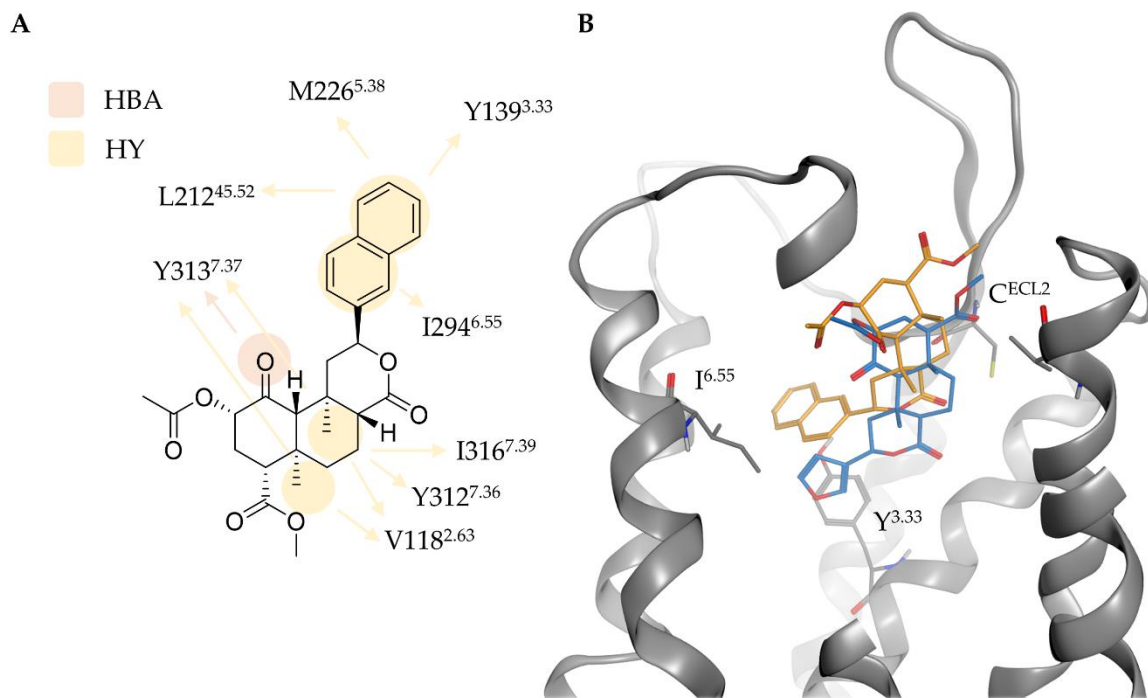
Figure S15. Protein-ligand interactions (A) and binding mode (B) of **16** (orange) at the KOR in comparison to SalA (blue). $Y^{3.33}$ denotes to $Y139^{3.33}$, C^{ECL2} to $C210^{ECL2}$, and $I^{6.55}$ to $I294^{6.55}$. Interactions types are abbreviated with HBA for hydrogen bond acceptor and HY for hydrophobic contact.
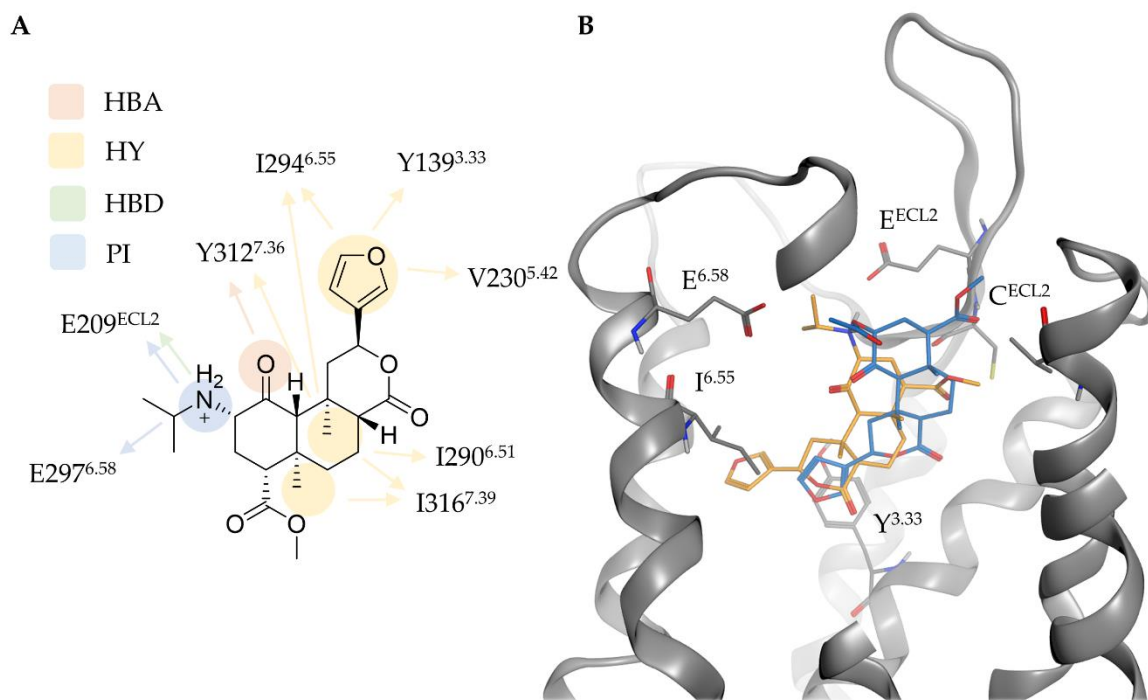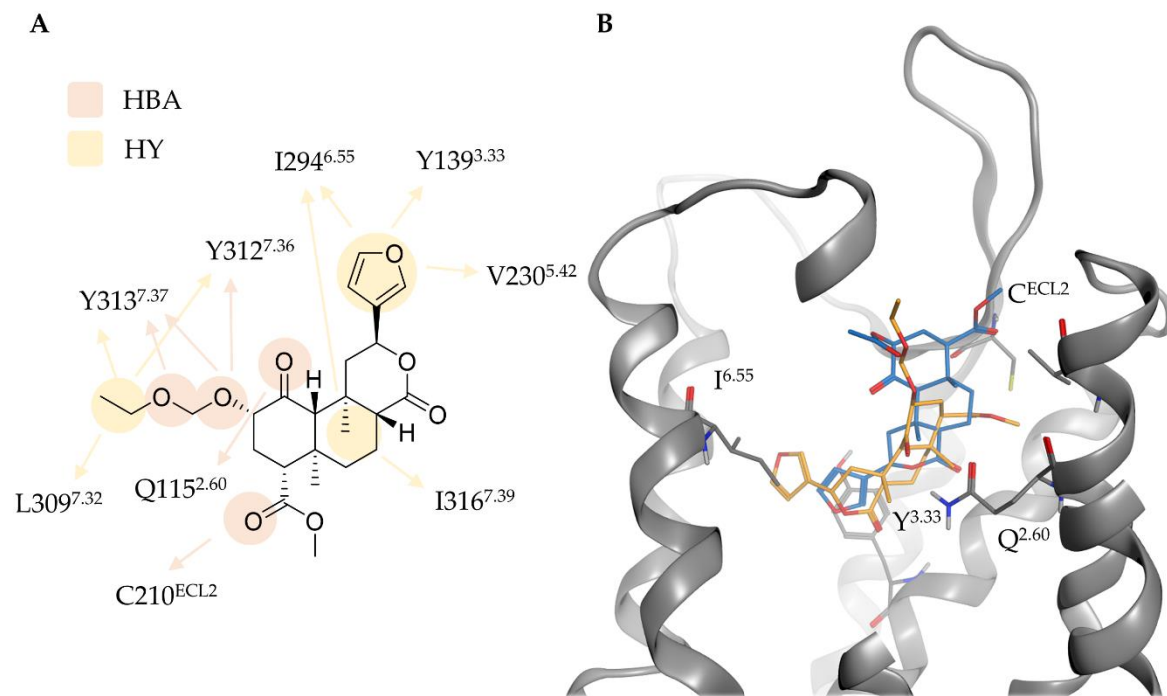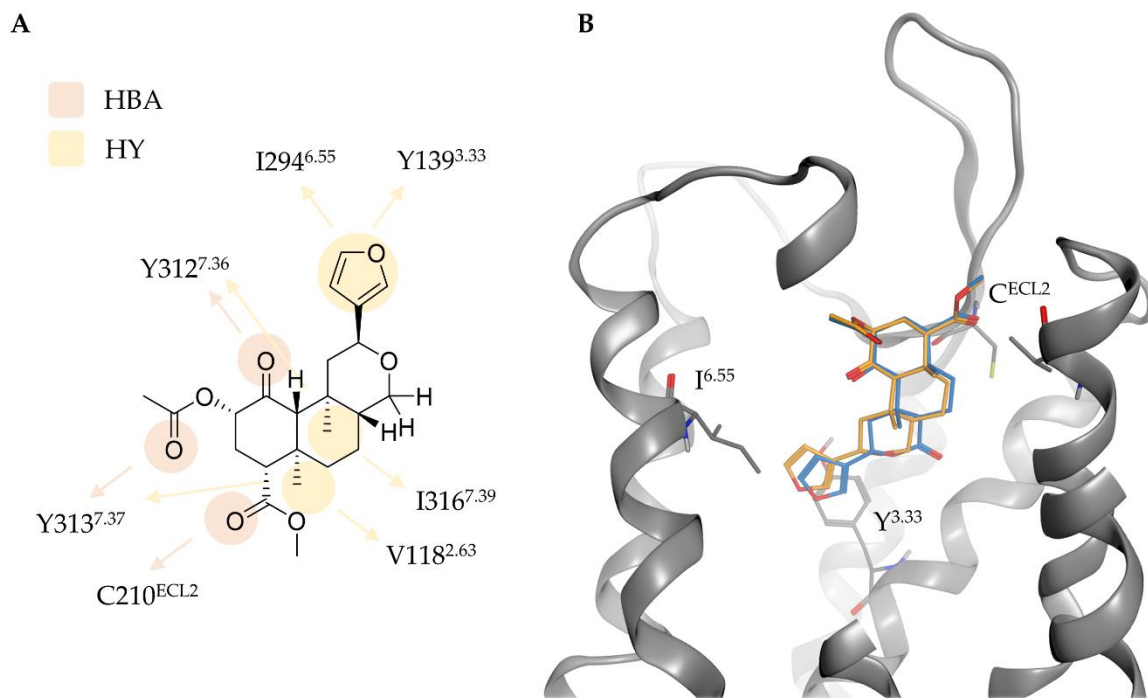
Figure S16. Protein-ligand interactions (A) and binding mode (B) of **17** (orange) at the KOR in comparison to SalA (blue). $Y^{3.33}$ denotes to $Y139^{3.33}$, C^{ECL2} to $C210^{ECL2}$, and $I^{6.55}$ to $I294^{6.55}$. Interactions types are abbreviated with HBA for hydrogen bond acceptor and HY for hydrophobic contact.
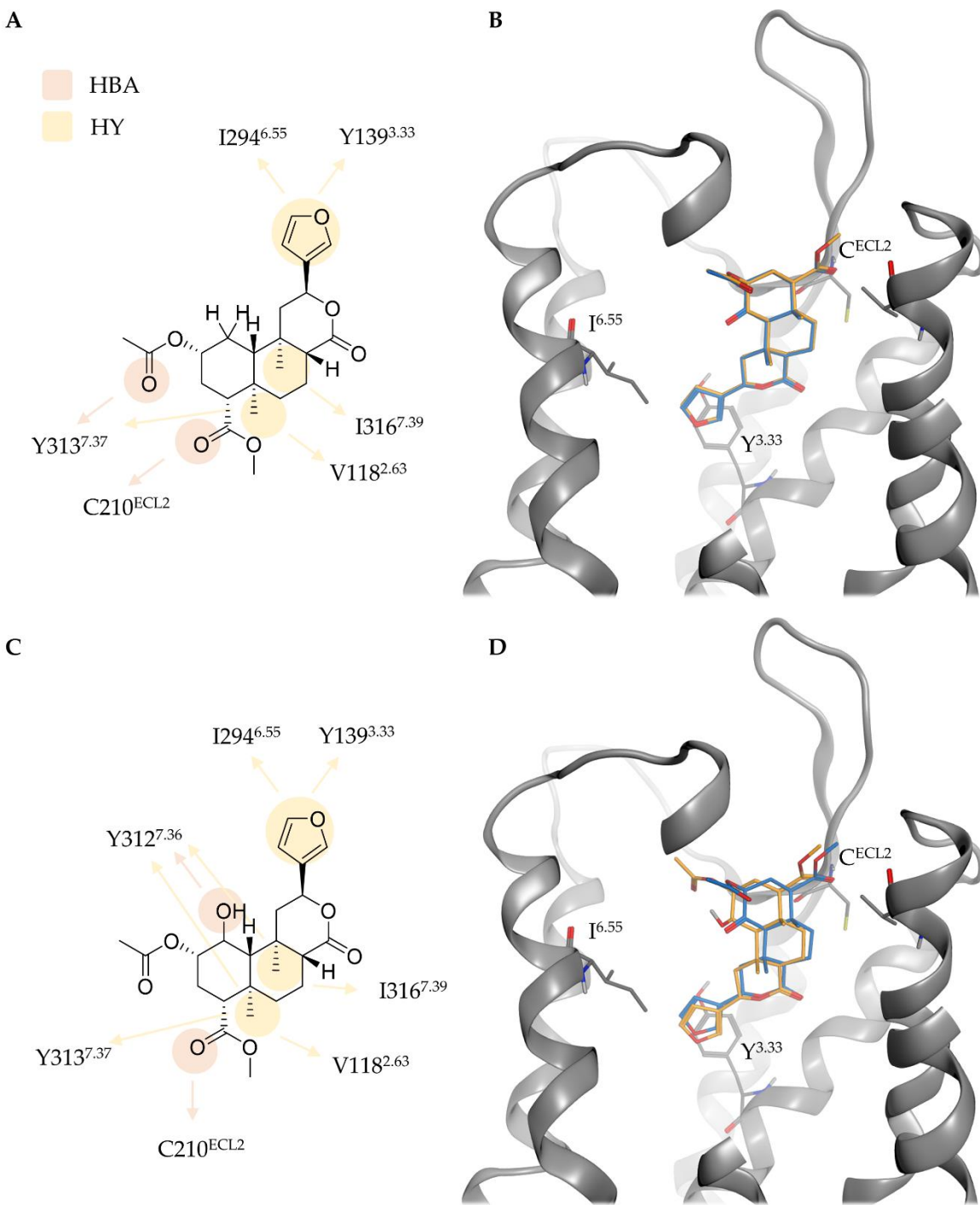
Figure S17. Protein-ligand interactions and binding mode of **18** (A, B, orange) and **19** (C, D, orange) at the KOR in comparison to SalA (blue $Y^{3.33}$ denotes to $Y139^{3.33}$, C^{ECL2} to $C210^{ECL2}$, and $I^{6.55}$ to $I294^{6.55}$. Interactions types are abbreviated with HBA for hydrogen bond acceptor and HY for hydrophobic contact.
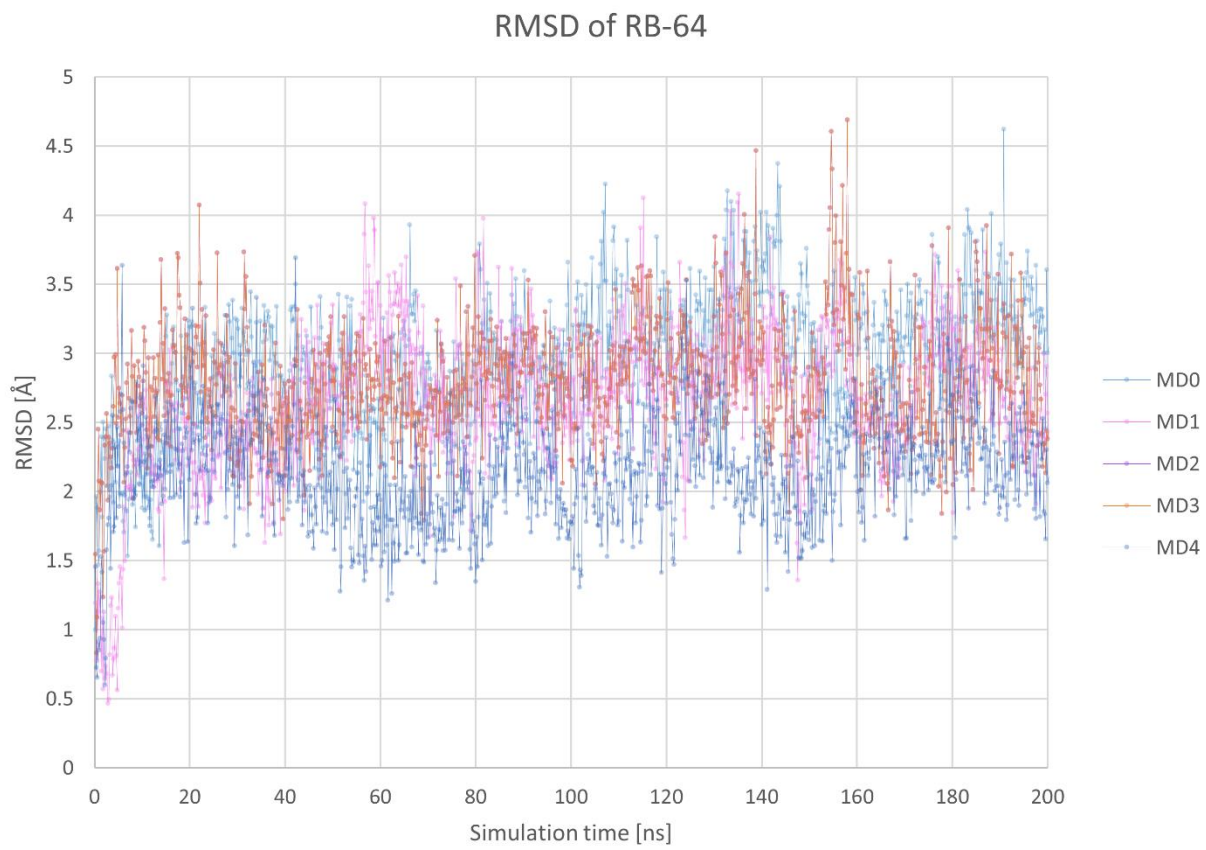
References:

1. Gowers, R.J.; Alibay, I.; Swenson, D.W.H.; Henry, M.M. *Open Free Energy (openfe)*, version 0.21; 2022.
2. D E Shaw Research. *Desmond Molecular Dynamics System*, 2022-1; D E Shaw Research: New York, NY, USA, 2022.
3. Bowers, K.J.; Chow, D.E.; Xu, H.; Dror, R.O.; Eastwood, M.P.; Gregersen, B.A.; Klepeis, J.L.; Kolossvary, I.; Moraes, M.A.; Sacerdoti, F.D.; et al. Scalable algorithms for molecular dynamics simulations on commodity clusters. In Proceedings of the Proceedings of the ACM/IEEE Conference on Supercomputing (SC06), Tampa, FL, USA, 11-17 November 2006.
4. Rizzi A; Grinaway P.B.; Parton D.L.; Shirts M.R.; Wang K.; Eastman P.; Friedrichs M.; Pande V.S.; Branson K.; Mobley D.L.; et al. YANK: A GPU-accelerated platform for alchemical free energy calculations. http://getyank.org/latest/, accessed on December 1, 2022.
5. Che, T.; Majumdar, S.; Zaidi, S.A.; Ondachi, P.; McCorvy, J.D.; Wang, S.; Mosier, P.D.; Uprety, R.; Vardy, E.; Krumm, B.E.; et al. Structure of the nanobody-stabilized active state of the kappa opioid receptor. Cell **2018**, 172, 55-67.e15, doi:10.1016/j.cell.2017.12.011.

4.4. Discovery of Novel, Selective, and Non-basic Agonists for the Kappa-Opioid Receptor Determined by Salvinorin A-Based Virtual Screening [Article D]

The number of basic opioid scaffolds exceeds the number of known non-basic opioids by far. Known non-basic ligands have been discovered through serendipity rather than rational drug design. To the best of our knowledge, no virtual screening campaign has been conducted to identify new non-basic KOR ligands. However, non-basic ligands offer an opportunity to selectively target the KOR.

The elucidation of a putative binding mode of SalA at the KOR, described in Article C, facilitates the performance of a 3D pharmacophore-based virtual screening campaign aiming for novel-scaffold, potent, and selective KOR agonists without basic moieties. We performed two 3D pharmacophore-based virtual screening methods in parallel and identified a novel spiro moiety-containing ligand scaffold for the KOR as well as two new ligands. These ligands exhibit desired high affinity, potency, and selectivity for the KOR *in vitro*.

Contribution:

Conceptual design (80 %)

Computational experiments (100 %)

Visualization (80 %)

Manuscript preparation (75 %)

All *in vitro* experiments were conducted at the lab of Mariana Spetea. I planned and performed the *in silico* experiments and wrote the manuscript excluding the *in vitro* results.

The manuscript was submitted to the Journal of Medicinal Chemistry at 11.03.2024.

Discovery of Novel, Selective, and Non-basic Agonists for the Kappa-Opioid Receptor Determined by Salvinorin A-Based Virtual Screening

Kristina Puls[1], Aina-Leonor Olivé-Marti[2], David Lamp[2], Mariana Spetea[2*] and Gerhard Wolber[1*]

[1]Department of Pharmaceutical Chemistry, Institute of Pharmacy, Freie Universität Berlin, Königin-Luise-Str. 2-4, 14195 Berlin, Germany; kristina.puls@fu-berlin.de (K.P.) gerhard.wolber@fu-berlin.de

[2]Department of Pharmaceutical Chemistry, Institute of Pharmacy and Center for Molecular Biosciences Innsbruck (CMBI), University of Innsbruck, Innrain 80-82, 6020 Innsbruck, Austria; aolive.marti@gmail.com (A.-L.O.-M) davidlamp42@gmail.com (D.L.) mariana.spetea@uibk.ac.at (M.S.)

*Correspondence: gerhard.wolber@fu-berlin.de (G.W.); mariana.spetea@uibk.ac.at (M.S.); Tel.: +49-30-838-52686 (G.W.); +43-512-507-58277 (M.S.)

ABSTRACT: The kappa-opioid receptor (KOR) modulation is a promising strategy for treating multiple human diseases. KOR agonists show potential for treating pain, pruritus, and epilepsy, while KOR antagonists show potential for treating depression, anxiety, and addiction. The natural product (NP) Salvinorin A (SalA) is a potent and selective KOR agonist. Unlike prototypical opioids, SalA does not contain a basic nitrogen. The discovery of SalA led to the idea of targeting KOR selectively with non-basic ligands. Nevertheless, only a limited number of non-basic KOR ligands have been identified to date. This study utilized the 3D pharmacophore of SalA bound to the KOR to conduct a virtual screening campaign with the aim of discovering novel, non-basic, potent and selective KOR agonists. Pharmacological *in vitro* studies identified two hit compounds, **SalA-VS-07** and **SalA-VS-08**, to be highly selective for the KOR and to show KOR agonist activity. Both KOR ligands are NP derivatives sharing a novel spiro-moiety containing and non-basic scaffold. Our results may represent significant starting points for future chemical optimization towards the development of therapeutics for the treatment of pain and other clinical conditions where the KOR plays a central role.

Introduction.

Pain medications have been in use for a long time[1], but the safe and effective treatment of pain is still an area of unmet medical need. Approved opioids are mu-opioid receptor (MOR) agonists that provide strong analgesia. However, they also cause serious side effects, such as respiratory depression, constipation, sedation, analgesic tolerance, physical dependence and addiction[2,3]. Opioids are currently indispensable for the treatment of severe pain conditions[2,4]. As a result of promiscuous opioid prescribing, the opioid crisis has emerged in the United States, with thousands of opioid-related deaths and hospitalizations each year[5]. This crisis emphasized the critical need for safer pain medications. In addition to the MOR, there are the kappa- (KOR) and the delta-opioid receptors (DOR), and the non-classical opioid receptor nociceptin/orphanin FQ peptide (NOP) receptor[6]. All opioid receptor types belong to the family of G protein-coupled receptors (GPCRs) with seven transmembrane domains[7]. Opioid receptor activation can provide analgesia, but with different side effect profiles[2,4,8]. The knowledge that activation of the KOR, opposite to the MOR, does not produce euphoria, respiratory depression or risk of overdose[9] has stimulated the interest in discovering

drugs acting on the KOR as potential pain therapeutics[10-16]. Overall, modulation of KOR signaling is a promising strategy for developing pharmacotherapies for several human diseases, either by activating (treatment of pain[13,16], pruritus[16] and epilepsy[17]) or blocking (treatment of depression[13,18], anxiety[13,18] and addiction[13]) the receptor. However, the generation of selective KOR agonists is challenging due to the strong binding site similarity of the opioid receptor subtypes.

Salvinorin A (SalA) is a natural product (NP) of *Salvia divinorum*[19] (Figure 1). SalA was the first naturally-occurring non-nitrogenous KOR agonist to be discovered[19], having high affinity and selectivity for the KOR[19-22]. Notably, SalA lacks the basic amine function found in prototypic opioids, which was previously believed to be essential for the interaction with opioid receptors[23-26]. SalA was the first non-basic opioid to be discovered, and much effort has been devoted to examining its exceptional KOR potency and selectivity profile. However, the lack of an active-state KOR crystal structure until 2018 (PDB-ID: 6B73[24]), and the numerous conflicting proposed binding modes of SalA at the KOR[20,24,27-33] have hindered the elucidation of SalA's selectivity determinants to the KOR. In addition, the potential

clinical use of SalA is severely limited due to its unfavorable pharmacokinetics and strong hallucinogenic properties[34,35]. However, the discovery of SalA has led to the idea of selectively targeting the KOR using non-basic ligands.

Despite the pharmacological potential, the number of known basic KOR ligands surpasses the number of reported non-basic ligands by far, with only a small number of non-basic ligand scaffolds identified. Frankowski and coworkers[36] reported a series of isoquinoline derivatives (N-alkyl-octahydroisoquinolin-1-one-8-carboxamides) as novel, potent, non-basic, and KOR-selective ligands with **1xx** (Figure 1) being the lead compound. These compound series showed good off-target selectivity against 38 non-opioid GPCRs. Two years later, Frankowski and coworkers[37] published two new non-basic KOR agonists obtained by a high throughput screening campaign, particularly the N-[1-(cyclohexylcarbamoyl)cyclohexyl]-N-(thiophen-2-ylmethyl)pyridine-2-carboxamide chemotype and the a 1,2,4-triazol scaffold (Figure 1). In an attempt to identify small molecules mimicking β-turn conformations, Whitby and coworkers[38] discovered the non-basic trans-pyrrolidine-3,4-dicarboxamide scaffold (Figure 1). Gupta and coworkers identified collybolide (Figure 1), a sesquiterpene from the mushroom *Collybia masculata* as a potent and selective non-basic KOR agonist[39]. Collybolide shares the furyl-δ-lactone core with SalA. Bedini and coworkers[40] identified the cyclic tetrapeptide LOR17 (c[Phe-Gly-(Ala)-DTrp], Figure 1) to be a selective KOR agonist that displays favorable G protein bias with an improved safety profile compared to prototypical KOR agonists). To date, SalA remains the most extensively studied non-basic scaffold. Approximately 600 derivatives of SalA have been synthesized and tested in KOR affinity or functional assays, albeit often with moderate or absent activity[41-43]. Despite the extensive SAR around SalA, there is little information on the in vivo pharmacology of SalA derivatives. However, in a previous study[40], we have reviewed the extensive published experimental data around SalA and its derivatives, and predicted a putative binding mode of SalA at the KOR.

Historically, NPs have made a major contribution to pharmacotherapy[44]. Despite a decline in interest in NPs in the 1990s and the exploration of synthetic databases, NP-based drug development is experiencing a revival[45]. Between January 1981 and September 2019, 1881 drugs have been approved by the United States Food and Drug Administration (FDA) or comparable organizations, of which about a quarter are unaltered NPs, defined mixtures of NPs, or (semisynthetic) derivatives of NPs[46]. If only small molecules (n = 1394) are considered, the proportion rises to one third[46]. NPs exhibit some advantages over synthetic compounds, but also bring some challenges[45]. They typically differ from synthetic compounds by greater rigidity, more sp3 hybridized carbon and oxygen atoms but fewer nitrogen and halogen atoms, more chiral centers, greater molecular mass, larger hydrophilicity, and a higher number of hydrogen bond acceptors and donors[45,46]. Overall, NPs cover a wider chemical space than synthetic compounds[47]. In addition, NPs possess an enriched bioactivity due to evolutionary development[45]. Frequent problems in NP-based drug discovery are labor-intensive synthesis or extraction processes, problems with the cultivation or extraction of sufficient

product from the original source, or the complex elucidation of the molecular mechanisms behind effects in phenotypic screening assays[45]. However, the exploration of the chemical space around NPs is useful for the development of novel drug candidates. Thus, our putative KOR-SalA binding mode represents a valuable starting point for a virtual screening to search for new non-basic opioids. Virtual screening has already been proven to be a suitable method for the discovery of novel GPCR ligands[48-50].

In this study, we conducted a 3D pharmacophore-based virtual screening campaign amining to discover novel, non-basic, and selective KOR agonists as potential therapeutics. We employed our recently published binding mode of SalA at the KOR[51] as a starting point for the 3D pharmacophore generation. Selected virtual screening hits were subjected to pharmacological *in vitro* evaluation resulting in the discovery of two new non-basic KOR agonists with nanomolar affinity and potency, as well as very good selectivity for the KOR over the other opioid receptor subtypes, MOR and DOR. We identified **SalA-VS-07** as a partial agonist at the KOR, while **SalA-VS-08** shows a full agonist profile at the KOR. Both hit compounds are NP derivatives that share a novel scaffold containing a spiro moiety.

Results.

SalA-Based Virtual Screening. Identification of Novel NP Derived KOR Ligands. We used structure-based virtual screening to search for non-basic KOR ligands. Two virtual screening workflows were implemented using LigandScout[52,53] (Inte:Ligand, Vienna, Austria) and ROCS (OpenEye/Cadence Molecular Sciences, Santa Fe, NM). The first workflow was based on structure-based 3D pharmacophores developed with LigandScout, while the second workflow was based on three-dimensional shape and chemical feature similarity using ROCS. Due to the absence of an experimentally determined structure of the SalA-KOR complex at the start of the study, we utilized our previously published binding hypothesis of SalA at the KOR[51] to generate both of our virtual screening queries (Figure 2). Further details about the query generation can be found in the Experimental Section.

Before conducting the virtual screening campaign, we validated and fine-tuned the SalA 3D pharmacophore query using receiver operating characteristic (ROC) curves[54] to ensure optimal performance in virtual screening. A set of 82 non-basic KOR agonists, obtained from the ChEMBL database[55], was used as active compounds. A number of 4100 decoys were generated using DUD-E[56] yielding in a ratio of actives to decoys of 1:50. The dataset only includes non-basic KOR agonists, primarily SalA analogues, due to the limited number of different non-basic KOR ligand scaffolds known. Basic agonists were excluded because a similar binding mode of basic and non-basic KOR ligands cannot be assumed. Several mutational studies suggest that residues above the morphinan binding site are crucial for SalA, including $Y312^{7.35}$, $Y313^{7.36}$, $Y119^{2.64}$ as well as extracellular loop 2[20,27,32]. Our previously published binding mode of SalA at the KOR suggests a distinct SalA binding site as well[51]. Additional information regarding the database curation process can be found in the Experimental Section. The initial 3D pharmacophore of SalA bound to the KOR comprises three hydrophobic contact features (HY) and three hydrogen
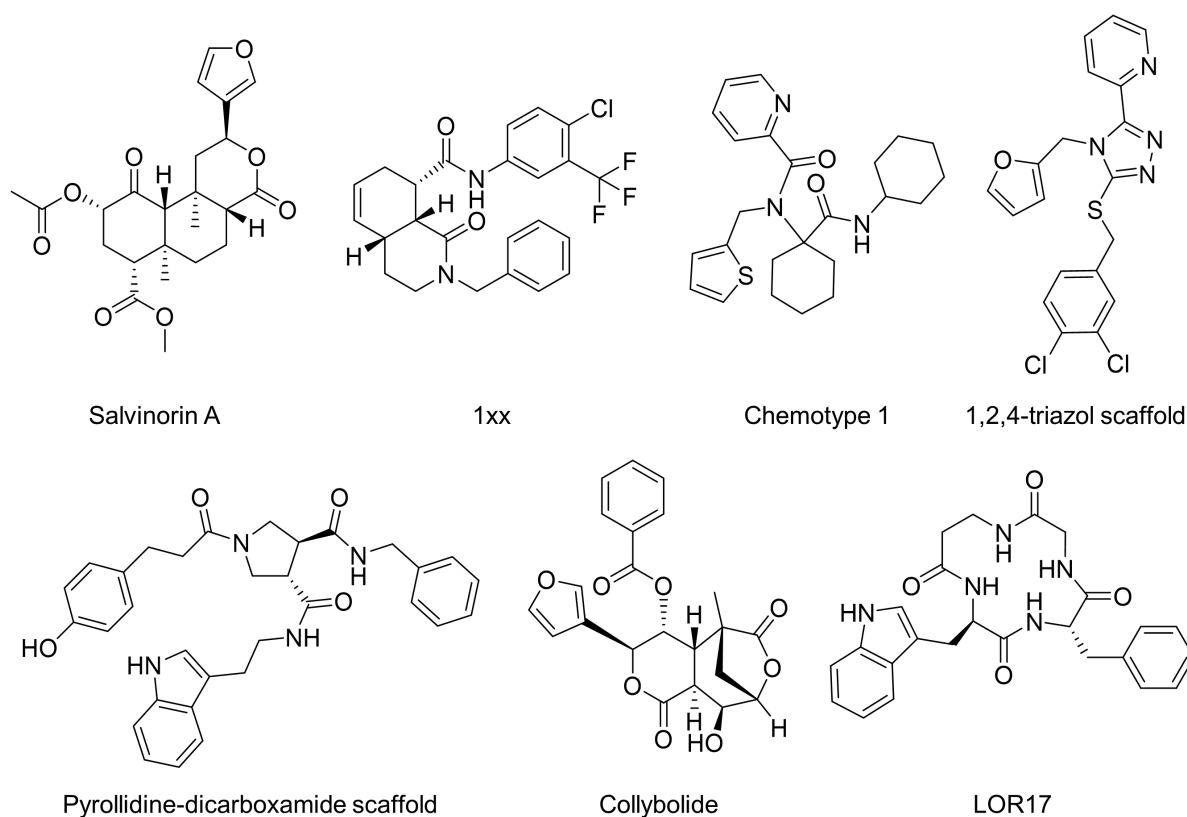
Figure 1. Non-basic ligand scaffolds with reported activity at the KOR.

bond acceptor features (HBA)[51]. ROC curve evaluation indicated that the omission of the SalA-C2 HBA yields better virtual screening performance, in particular for the virtual screening workflow performed in LigandScout (Figure 2). Both 3D pharmacophores in the ROCS screening perform similarly. However, we omitted the SalA-C2 HBA feature, which slightly improved early enrichment. For the sake of conformity, we performed the virtual screening with the reduced pharmacophore for both methods. The optimized queries yielded the following results: The LigandScout 3D pharmacophore screening achieved a sensitivity of 68% (56 out of 82 actives) with a total of 67 hits (11 false positives, FP). The area under the curve (AUC) is 0.85. In the ROCS screening 79 out of the 82 active compounds were ranked within the top 87 molecules with the first decoy at position 59, followed by positions 67, 74, 79, and 83-86. The remaining three active compounds were ranked at positions 702, 848, and 1476. The AUC is 0.99.

The screened molecule libraries include both NP libraries and synthetic compound libraries (Table 1). NPs typically contain fewer nitrogen atoms than synthetic compounds, and their library size is much smaller. The screened NP or NP-derived databases were Analyticon's NATx and MEGx libraries[57], as well as Selleckchem's NP library[58]. The Enamine database, which comprises Enamine's advanced, functional, HTS, and premium collections, was screened for synthetic compounds[59]. Both virtual screening methods were used in parallel to screen a total of around 3 million molecules.

The virtual screening workflow is illustrated in Figure 3. The LigandScout screening resulted in 250 hits, while the ROCS screening resulted in 2000 hits. The hit lists were combined, and charged ligands were filtered out using RDKit v2022.03.3[60] and KNIME v4.5.2[61], resulting in 1821 non-basic hits. These hits were then docked into the active state KOR x-ray crystal structure (PDB-ID: 6B73[24]) to generate plausible binding modes. To evaluate the initial docking, we calculated the 3D pharmacophore score in LigandScout towards the starting binding mode of SalA. The docking poses were scored based on their ability to fulfill the query pharmacophore features, and only those with a score greater than zero were kept for further evaluation. We then visually inspected the remaining docking poses and carefully selected the best fitting molecules for experimental testing. The manual selection criteria primarily include high 3D pharmacophore scores and high Gaussian shape similarity scores[62,63] towards SalA. Additionally, good physicochemical properties of the hit compounds were considered, such as a low number of rotatable bonds (≤10, with one exception) and a molecular weight of ≤500 Da. Criteria from our previous SalA investigation[51] were also included, assuming similar binding modes for our non-basic hit compounds compared to the non-basic starting ligand SalA. Docking poses that interacted with residues highlighted as crucial for SalA affinity and potency in mutagenesis studies
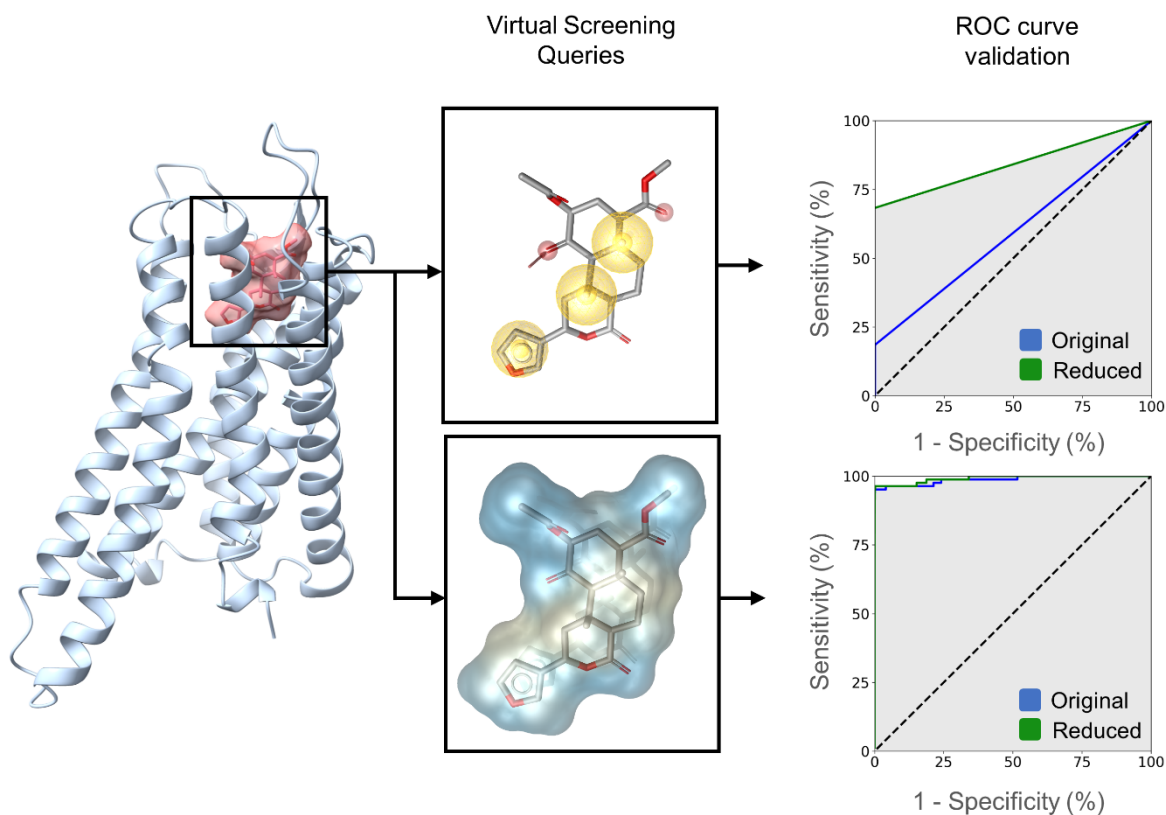
Figure 2. Virtual screening queries and validation. Previously published binding mode of SalA at the KOR used for query generation is shown on the left side. At the top, the 3D pharmacophore information used as query for the screening in LigandScout is depicted. Exclusion volume spheres are not shown for the sake of clarity. At the bottom, the shape information used as query for the ROCS screening is shown. ROCS additionally takes 3D pharmacophore features into account. On the right sight the respective receiver operating characteristic (ROC) curves are shown. The queries derived from the original 3D pharmacophore of the KOR-SalA complex (blue) are compared with the reduced 3D pharmacophore queries missing the SalA-C2 HBA feature (green). The dashed black line on both sides indicates the random line. Grey area shows the area under the curve for the reduced 3D pharmacophore query.

Table 1. Composition of the screened compound databases.

Natural Product Library	Synthetic Compound Library	Number of Molecules	Percent
NATx (Analyticon)		33,717	
MEGx (Analyticon)		6,541	1.44%
Natural product library (Selleckchem)		2,724	
	Advanced Collection (Enamine)	640,219	
	functional Collection (Enamine)	119,088	98.46%
	HTS Collection (Enamine)	2,146,100	
	Premium Collection (Enamine)	41,281	
		Total: 2,989,670	100%

(Y312[7.35], Y313[7.36], V118[2.63], Y139[3.33], Q115[2.60])[3,20,21,27,32] were prioritized. We selected docking poses that align with the SAR data of SalA, particularly those that have an HBA at the position of SalA's C2-acetoxy carbonyl group. This HBA is crucial for SalA's potency to the KOR, as its primary metabolite Salvinorin B (SalB), which has a hydroxy group at its C2 position, is inactive[34,35]. We further validated experimentally the 15 best molecules selected (Figure 4). It is worth noting that 14 out of the 15 hit molecules were obtained through ROCS screening, with 6 molecules derived from the synthetic Enamine database and 9 molecules from NP libraries. This indicates that our developed 3D interaction model shows a clear preference for NP or NP derivatives.

Pharmacological Evaluation. Identification of SalA-VS-07 and SalA-VS-08, Two NP Derivatives, as Novel, Selective KOR Agonists. In the quest for the identification of novel, selective ligands at the KOR, the seven NP derivatives, **SalA-VS-1** to **SalA-VS-13**, selected from the virtual screening campaign, were provided by AnalytiCon for experimental testing. The initial biological screening was performed using a competitive radioligand binding assay at the human KOR. The ability of the test compounds and the reference KOR ligands, SalA[19] and HS665[64], all tested at 10 μM, to inhibit binding of the specific KOR radioligand [^{3}H]U69,593 was assessed with membranes from Chinese hamster ovary (CHO) cells stably expressing the human KOR (CHO-hKOR), according to the described procedure[65]. Among the tested compounds, **SalA-VS-07** and **SalA-VS-08** inhibited [^{3}H]U69,593 binding at the KOR by >50% (Figure 5). Therefore, they were selected for further investigations of their *in vitro* KOR activities. Both compounds produced concentration-dependent inhibition of [^{3}H]U69,593 binding (Figure 6A), displaying good binding affinities (defined by the K_i value) in the nanomolar range at the human KOR (Table 2). **SalA-VS-08** showed about 6-fold increased affinity at the KOR than **SalA-VS-07**. The parent KOR ligand SalA, as expected, exhibited high binding affinity, in the low nanomolar range, at the human KOR (K_i = 2.66 nM). To assess selectivity of **SalA-VS-07** and **SalA-VS-08** for the KOR, competitive radioligand binding studies were performed with membranes from CHO cells stably expressing the human MOR or DOR, and using [^{3}H]DAMGO and [^{3}H]DPDPE as specific MOR and DOR radioligands, respectively. As shown in Figure 7, **SalA-VS-07** and **SalA-VS-08** showed no substantial binding at the MOR and DOR at a concentration of 10 μM. In the same assays, the reference MOR and DOR ligands, morphine and HS378[66], respectively, showed significant binding at the specific opioid receptors (Figure 7).

Next, we have evaluated the *in vitro* functional activity of **SalA-VS-07** and **SalA-VS-08** at the human KOR in the guanosine-5'-O-(3-[^{35}S]thio)-triphosphate ([^{35}S]GTPγS) binding assay with CHO-hKOR cell membranes as described previously[65]. Their *in vitro* KOR activity was compared to the reference KOR agonists, SalA and U69,593 (Figure 6B). Agonist potencies (EC$_{50}$, nM) and efficacies (E$_{max}$, %) are listed in Table 2. Both **SalA-VS-07** and **SalA-VS-08** produced concentration-dependent increase in the [^{35}S]GTPγS binding in CHO-hKOR cell membranes although with distinct activation profiles. Whereas **SalA-VS-08** showed full efficacy (108% of U69,593) in inducing KOR-mediated G-protein

activation, **SalA-VS-07** displayed partial agonism based on reduced efficacy (48% of U69,593). Notable is also the observation on the 5-fold lower agonist potency at the KOR of **SalA-VS-08** compared to **SalA-VS-07**. Experimentally, we established that **SalA-VS-07** displays a more potent KOR activation despite lower binding affinity compared to **SalA-VS-08** (Table 2).

Both **SalA-VS-07**, **SalA-VS-08**, as well as the inactive **SalA-VS-09** (Figure 4) share the same common scaffold only differing at the aromatic substitution at the benzamide function. **SalA-VS-07** contains a 4-chlorobenzamide, **SalA-VS-08** a 3-fluorobenzamide, and **SalA-VS-09** a pyridine-4-carboxamide structure. The corresponding experimental data provides first insights into the SAR of our newly developed 2-methylspiro[6H-pyrazolo[1,5-a]pyrimidine-7,4'-piperidine]-5-one scaffold series. The introduction of a halogen moiety in para or meta position of the benzamide substructure facilitates KOR activity as its absence in **SalA-VS-09** represent an interesting activity cliff.

Discussion.

Based on our recently reported binding hypothesis of SalA at the KOR[51], 3D pharmacophore-based virtual screening discovered two NP derivatives as novel, selective, and non-basic KOR agonists. This is the first time that new non-basic opioids have been rationally rather than serendipitously discovered. These new KOR agonists, **SalA-VS-07** and **SalA-VS-08**, share the 2-methylspiro[6H-pyrazolo[1,5-a]pyrimidine-7,4'-piperidine]-5-one scaffold (Figure 4). Both **SalA-VS-07** and **SalA-VS-08** were highly selective for the KOR and showed KOR agonist activity *in vitro*.

To assess the novelty of our new spiro moiety-containing scaffold (Figure 4), we conducted a thorough literature review. A few studies have already reported on spiro moiety-containing opioids[67-79]. However, these compounds only share limited similarity to **SalA-VS-07** and **SalA-VS-08**. Moreover, the previously reported compounds were primarily developed for the NOP receptor[67,68,72-76,78,79] and DOR[70,71], and often do not report activity values for the KOR[68,74,77]. **SalA-VS-07** and **SalA-VS-08** contain a spiro-piperidine substructure. Spiro-piperidine opioids have already been reported for the DOR and NOP receptor[67,68,70,71,73,76,78,79]. However, unlike **SalA-VS-07** and **SalA-VS-08** many of the spiro compounds found in the literature possess a spiro group of a 6-membered ring connected to a 5-membered ring[67,68,73,76,78,79] or pyrans or oxidated pyrans[69-71,74,75]. Only Mustazza and co-workers reported a spiro moiety encompassing two nitrogen containing 6-membered rings similar to our discovered scaffold[72]. Despite this similarity, the molecules contain a quinazoline substructure dissimilar to our hit compounds[72]. The structure-activity relationship (SAR) data provided by Mustazza and co-workers indicates all compounds far less potent at the KOR (micromolar range) compared to our newly discovered lead compounds (nanomolar range). Additionally, most of their compounds are less KOR selective. Unlike **SalA-VS-07** and **SalA-VS-08**, all spiro opioids found in the literature contain a basic amine. From the results of our literature review we concluded that our spiro moiety-containing scaffold is indeed novel for opioid receptor modulation.
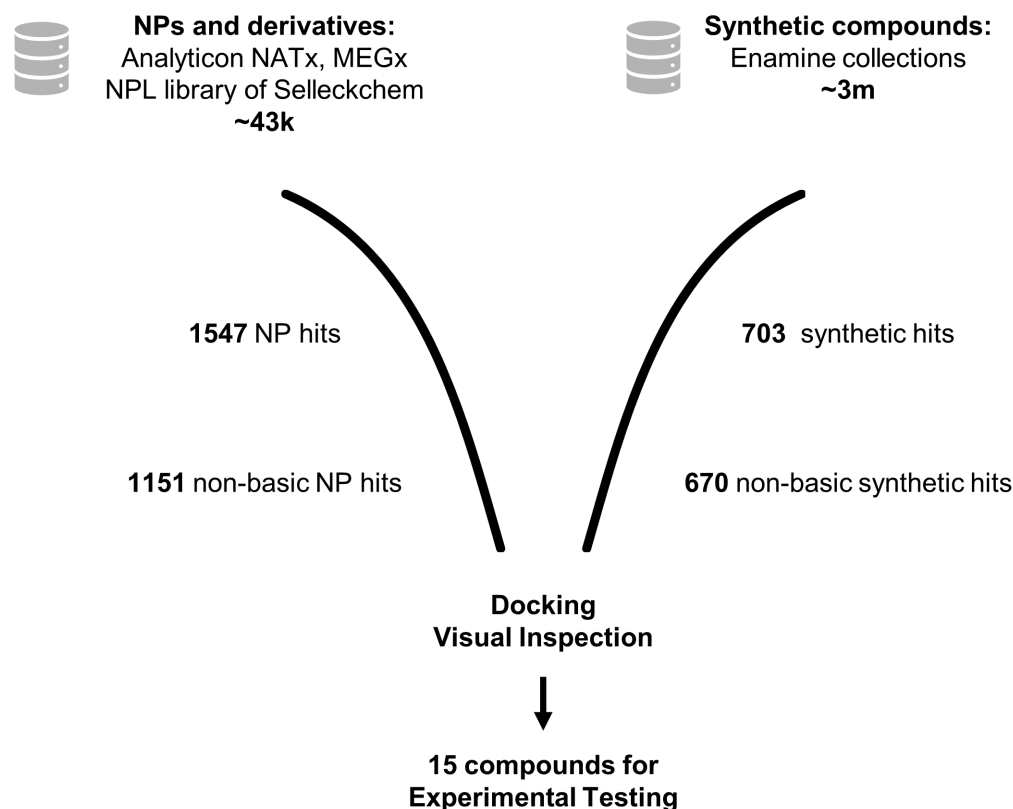
Figure 3. Schematic workflow of the virtual screening campaign including the number of data points per step. Hits were summarized for both virtual screening methods. By default, ROCS retrieves the 500 best fitting compounds. Abbreviations: NPL = Natural product library of Selleckchem. Enamine databases screened were advanced, functional, HTS, and premium collections.

Despite the much larger size of the synthetic libraries screened only five (**SalA-VS-01** - **SalA-VS-05**) of the thirteen substances for experimental validation were derived from the synthetic Enamine databases. The remaining eight substances belong to NP or NP-derived libraries. In particular, **SalA-VS-06** originates from Selleckchem's NPL, **SalA-VS-10** - **SalA-VS-13** from Analyticon's MEGx and **SalA-VS-07** – **SalA-VS-09** from Analyticon's NATx. Thus, **SalA-VS-07** and **SalA-VS-08** represent NP derived compounds. There is a long history of modulating the opioid receptor system using NPs. Besides the well-known morphine[44,80] and already discussed SalA and collybolide, kratom alkaloids such as mitragynine, 7-OH mitragynine, and mitragynine pseudoindoxyl modulate MOR and KOR[81] (Figure S1). Further NP-opioids are the naturally occurring peptides rubiscolin-5 (YPLDL) and rubiscolin-6 (YPLDLF)[82] (Figure S1). Our lead compounds, **SalA-VS-07** and **SalA-VS-08**, represent a novel chemical category within natural compounds demonstrated to be active at the KOR.

SalA-VS-07 and **SalA-VS-08** are non-basic KOR ligands with agonist profile at the KOR, but with different efficacy in inducing activation of the KOR. While **SalA-VS-08** shows a full agonistic profile compared to the prototypical KOR agonist U69,593, **SalA-VS-07** exhibits partial agonistic properties at the KOR. Recent reports point out to the potential clinical value of opioids with reduced efficacy, partial agonists, as effective and safer pain therapeutics[15,83,84].

This study relied on the previously docked KOR-SalA complex as the foundation for our virtual screening campaign[51]. At the time of the virtual screening, no experimental structure of SalA or its derivatives at the KOR was available. Therefore, the proposed KOR-SalA complex represented the best available binding hypothesis, as it agrees with mutagenesis data and SAR around SalA. However, in the course of our project, cryo-EM structures of KOR bound to methoxymethyl-salvinorin B (momSalB), a derivative of SalA, were published (PDB-IDs: 8DZP, 8DZQ)[85]. MomSalB differs from SalA by containing a methoxymethyl ether moiety at the C2 position instead of a C2-acetoxy moiety. Analogous to SalA, momSalB shows strong KOR affinity and potency together with high KOR selectivity[20,86]. Within the cryo-EM structures, momSalB binds deep in the orthosteric binding site, similar to morphinan-based opioids, and adopts a flipped conformation compared to our *in silico* prediction
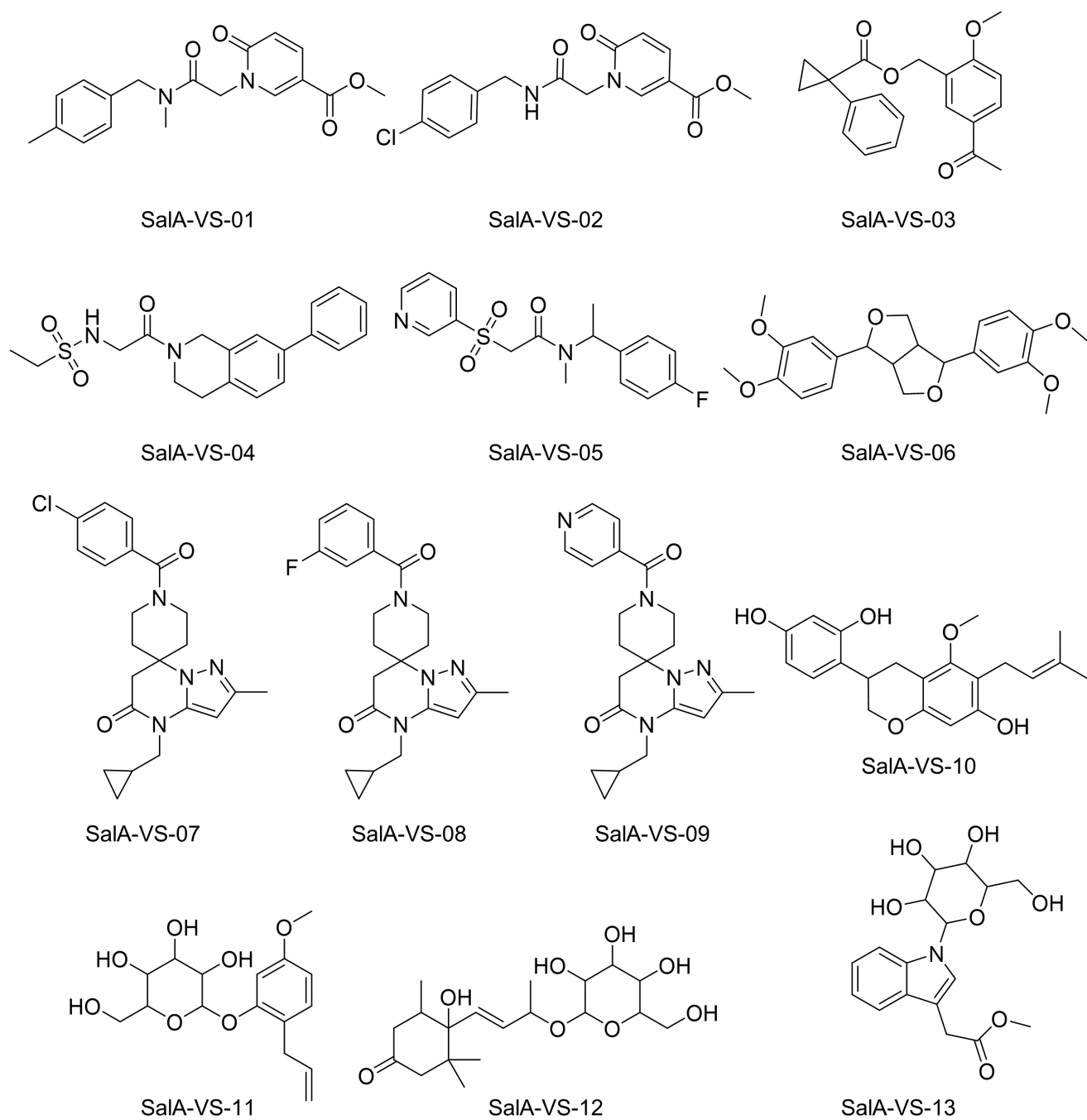
Figure 4. Chemical structures of selected virtual hit molecules for experimental testing.
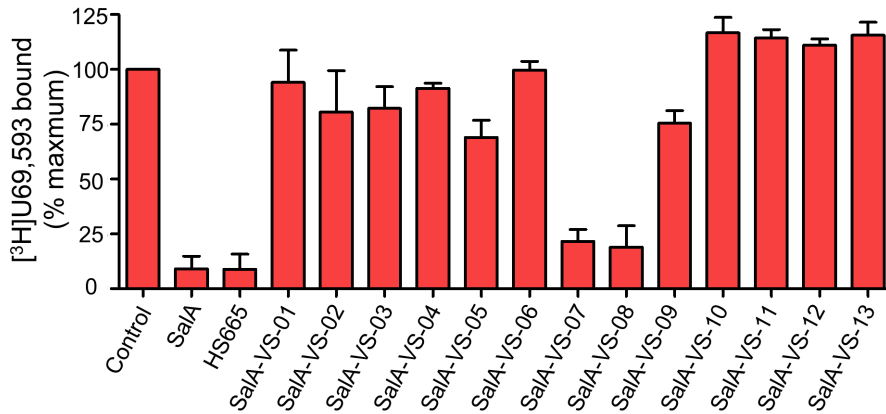
Figure 5. Screening of **SalA-VS** compounds for binding at the human KOR. Competitive inhibition of [³H]U69,593 binding by **SalA-VS** compounds and reference KOR ligands, SalA and HS665, at the human KOR was measured in radioligand binding assays. Membranes from CHO cells stably expressing the human KOR were incubated with [³H]U69,593 in the absence (control) or presence of test compounds (10 μM). Values represent the mean ± SEM (n=3).
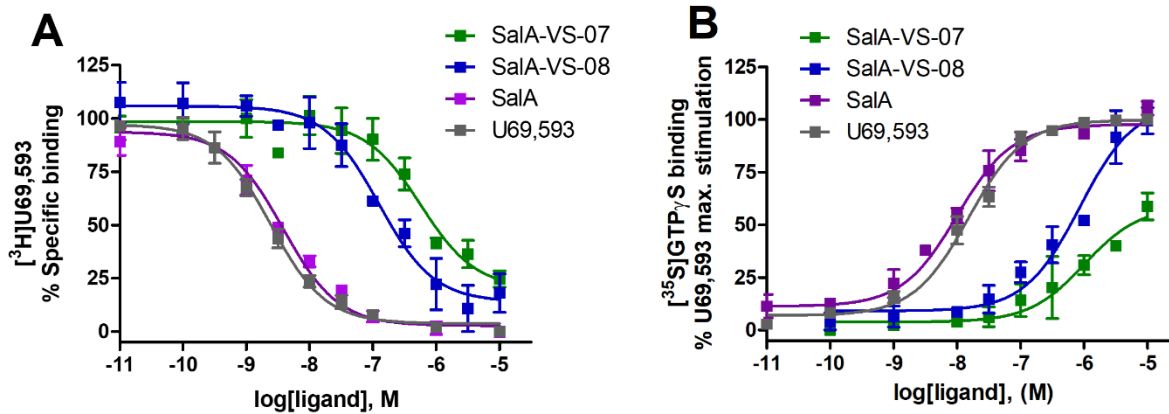
Figure 6. *In vitro* activity profile of **SalA-VS-07** and **SalA-VS-08** at the human KOR. (A) Concentration-dependent inhibition by **SalA-VS-07**, **SalA-VS-08**, SalA and U69,593 of [³H]U69,593 binding to membranes from CHO-hKOR cells determined in the radioligand competitive binding assay. (B) Concentration-dependent stimulation of [³⁵S]GTPγS binding by **SalA-VS-07**, **SalA-VS-08**, SalA and U69,593 in the [³⁵S]GTPγS binding assay using membranes from CHO-hKOR cells. [³⁵S]GTPγS binding data are presented as percentage stimulation relative to the maximum effect of the reference KOR agonist U69,593. Values represent the mean ± SEM (n=3-4).
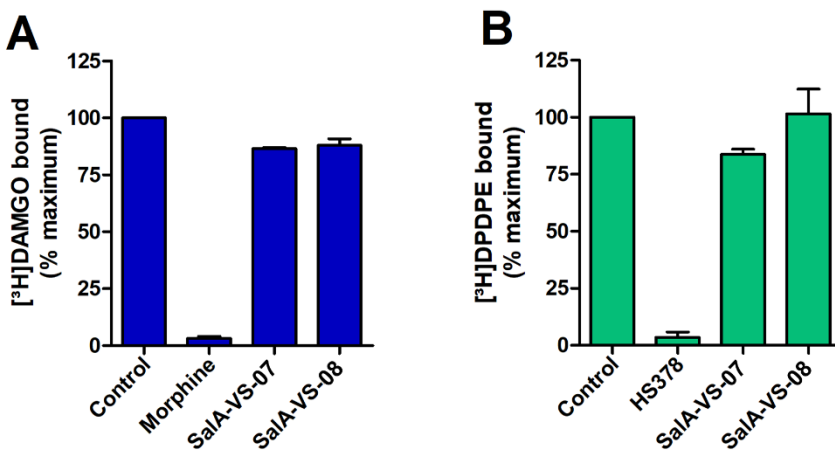
Figure 7. Binding of **SalA-VS-07** and **SalA-VS-08** at the human MOR and DOR determined in radioligand binding assays. Membranes from CHO cells stably expressing the human MOR or DOR were incubated with (A) the specific MOR radioligand [³H]DAMGO or (B)

the specific DOR radioligand [³H]DPDPE in the absence (control) or presence of test compounds (10 μM). Morphine (10 μM) and HS378 (10 μM) were used as reference MOR and DOR ligands, respectively. Values represent the mean ± SEM (n=3).

Table 2. Binding affinities and functional activities of **SalA-VS-07** and **SalA-VS-08** at the human KOR

Ligand	Binding affinity[a]	Agonist activity[b]	
	K_i (nM)	EC_{50} (nM)	E_{max} (%)
SalA-VS-07	423 ± 97	181 ± 49	48 ± 7
SalA-VS-08	68.5 ± 5.5	854 ± 60	108 ± 8
SalA	2.66 ± 0.75	11.8 ± 3.5	100 ± 1
U69,593	1.56 ± 0.34	16.3 ± 3.5	100

[a]Determined in the radioligand competitive binding assays using membranes from CHO cells stably expressing the human KOR. [b]Determined in the [³⁵S]GTPγS binding assays using membranes from CHO cells stably expressing the human KOR. E_{max} (%) values represent the percentage relative to the maximal effect of U69,593 (as 100%).Values represent the mean ± SEM (n=3-4).

(Figure 8). The methoxymethyl ether moiety of momSalB is oriented down towards the receptor core while its furan moiety points between the transmembrane domains (TM) 2 and 3. The binding mode of momSalB nicely overlaps with the morphinan derivative MP1104 co-crystallized in the active-state KOR x-ray crystal structure published in 2018 (PDB-ID: 6B73[24], Figure S2).

The elucidation of the binding mode of momSalB at the KOR may raise doubts about the usefulness of our virtual screening starting from the binding mode of SalA. However, identifying two novel scaffold non-basic KOR agonists justified utilizing this binding hypothesis as a starting point for virtual screening. Furthermore, there is uncertainty about the generalizability of the momSalB binding mode for SalA: Limited information about the KOR-momSalB cryo-EM structure generation are stated in the publication[85] (Figure S3), especially about the conformational sampling procedures, leaving the possibility for alternative ligand conformations. The published cryo-EM structures neither explain the outstanding KOR selectivity of SalA nor do they agree with the main SAR or mutagenesis data of SalA. MomSalB occupies a pocket highly conserved among the opioid receptors. However, superimposition of KOR-momSalB (PDB-ID: 8DZQ) with MOR (PDB-ID: 5C1M[87]) and DOR (PDB-ID: 6PT2[88]) does not reveal any potential steric clashes or selectivity determinants that would rationalize the strong subtype selectivity (Figure S4). SalA undergoes a rapid metabolic transformation to SalB, which is inactive at the KOR[35]. SalB differs from SalA by a hydroxy group at C2 instead of a C2-acetoxy group (Figure S5). Thus, the C2-acetoxy moiety of SalA is crucial for the KOR activity and therefore the C2-substituents of active SalA derivatives should participate in receptor-ligand interactions. However, the methoxymethyl moiety of momSalB does not interact with the KOR neither in the static cryo-EM structures (Figure 9) nor in molecular dynamics (MD) simulations (Figure S5). Additionally, the SAR of SalA indicates hydrogen bonding between SalA's C2- and C4 substituents and the KOR as important for affinity[41], yet momSalB barely participates in such interactions (Figure S5). Furthermore, momSalB strongly moves within the binding site in several MD simulations with RMSD values up to 9.5 Å (Figure S6). Within the cryo-EM structures momSalB only interacts with few residues highlighted as

important in mutagenesis data[20,27,32], particularly only Y312[7.35] and I316[7.39] (Figure S7).

Considering the aforementioned discrepancies, it would be conceivable that SalA exhibits dynamic ligand binding at the KOR or that momSalB and SalA prefer different orientations at the KOR. The concept of 'dynamic ligand binding' describes that a ligand can adopt multiple distinct conformations at the same protein[89]. This phenomenon was already described for ligands of the estrogen receptor (ER)[90], muscarinic M_2 receptor[89,91], and cytochrome P450 3A4 (CYP3A4)[92]. Additionally, closely related compounds that adopt different orientations at the same receptor[93-95] have been described for the soluble epoxide hydrolase[95] (Figure S8, panel A), and PPARγ[96]. There is also an example of different binding modes observed for the same ligand at closely related proteins, particularly the ERα and ERβ[97] (Figure S8, panel B).

In summary, the newly developed cryo-EM structures of momSalB bound to the KOR provide new insights in potential receptor recognition of SalA and its derivatives but requires further detailed evaluation considering existing experimental data of SalA and its analogs. In this study, both hit compounds, **SalA-VS-07** and **SalA-VS-08**, were retrieved by virtual screening that strongly focus on shape similarity. This possibly contributed to successful hit identification despite uncertainty about the correct binding mode of SalA.

Conclusion.

In this study, we conducted a virtual screening campaign aiming for new, potent, selective, and non-basic KOR agonists as potential candidates for therapeutic use as safer analgesics among others parthologies. We performed two 3D pharmacophore-based virtual screening methods in parallel and searched both NP libraries and synthetic compound libraries. Experimental evaluation of selected hit compounds revealed two ligands at the KOR, namely **SalA-VS-07** and **SalA-VS-08**. Both compounds show affinity and potency at the KOR in the nanomolar range, with **SalA-VS-07** being a partial agonist at the KOR and **SalA-VS-08** a full agonist at the KOR. *In vitro* radioligand competition binding studies demonstrated both new ligands to be KOR selective.
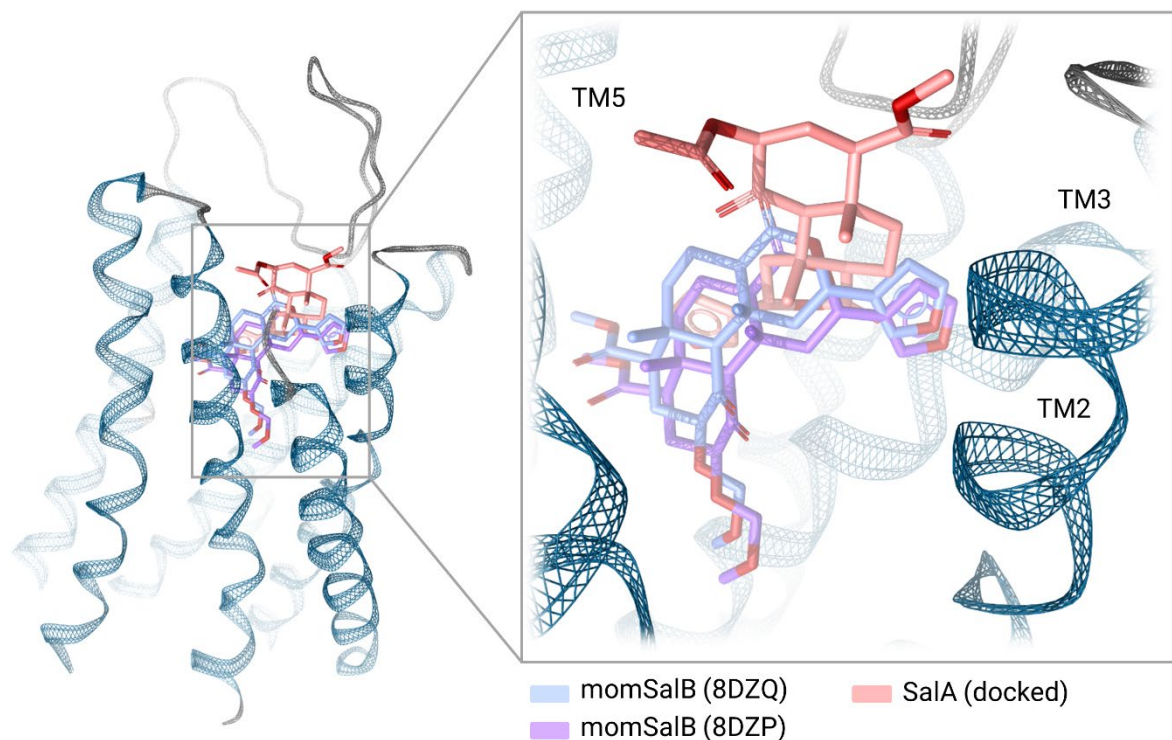
Figure 8. Comparison of momSalB binding mode at the KOR (PDB-IDs: 8DZQ, 8DZP), and previously docked SalA used for virtual screening query 3D pharmacophore generation.

Sal-VS-08 and **Sal-VS-09** share a common 2-methyl-spiro[6H-pyrazolo[1,5-a]pyrimidine-7,4'-piperidine]-5-one scaffold that was never reported as opioid scaffold before. Altogether, our findings indicate that the applied KOR pharmacophore models and virtual screening workflows have a clear potential for the discovery of novel bioactive molecules at the KOR. The new chemotypes **Sal-VS-08** and **Sal-VS-09,** as NP, represent a valuable starting point for chemical optimization towards the development of therapeutics for pain and other human disorders by selective targeting the KOR.

Experimental Section.

Virtual Screening. Two virtual screening methods were conducted in parallel. The first one is a classical 3D pharmacophore-based virtual screening performed in LigandScout[52,98], the second one is a ROCS v3.4.3.0 screening implemented in OpenEye[99,100].

Query Generation for Virtual Screening. The 3D pharmacophore-based queries for virtual screening were obtained from the previously published binding hypothesis of SalA at the KOR[51]. In particular the 3D pharmacophore of this binding complex was generated in LigandScout v.4.4.3[52,98] with an additional exclusion volume coat. As the 3D pharmacophore validation indicated the omission of the C2-hydrogen bond acceptor (HBA) feature meaningful this feature was deleted to retrieve the final query 3D pharmacophore for the LigandScout screening. For the ROCS screening SalA was extracted from the complex and loaded

into the graphical user interface of ROCS v3.4.3.0[99,100] of OpenEye. The automatically generated 3D pharmacophore features were manually corrected to resemble those of the initial binding complex. In particular the HBA features of the furan and the C17-carbonyl group were deleted. Again, the HBA feature of the C2-acetoxy group was deleted after 3D pharmacophore validation to retrieve the final screening query.

Query Validation. The virtual screening queries were evaluated for their ability to separate active molecules from decoys and receiver operating characteristic (ROC) curves were generated for visualization of results. For this, databases of known actives and assumed inactives (decoys) were screened in analogous way as later on the screening libraries of unknown activity. The active dataset was generated from the ChEMBL database[55]. In particular, all entries of the human KOR with any EC_{50} values measured in cell-based assays and a molecular weight of 300-500 Da were retrieved. Subsequently, all entries without exact EC_{50} values, missing EC_{50} values, or other units than nM for their EC_{50} values were deleted. Only those entries measured in the [^{35}S]GTPγS assays were kept. Entries uncharged at pH 7 were separated and their duplicates deleted leading to 82 uncharged KOR ligands with EC_{50} values from the pM range up to 5740 nM. Decoys of the active dataset were generated by DUD-E webserver[56] resulting in 4100 decoys. Thus, the active-decoy ratio is 1:50.

Protein and Ligand Preparation. The human KOR model used for docking experiments is identical with those
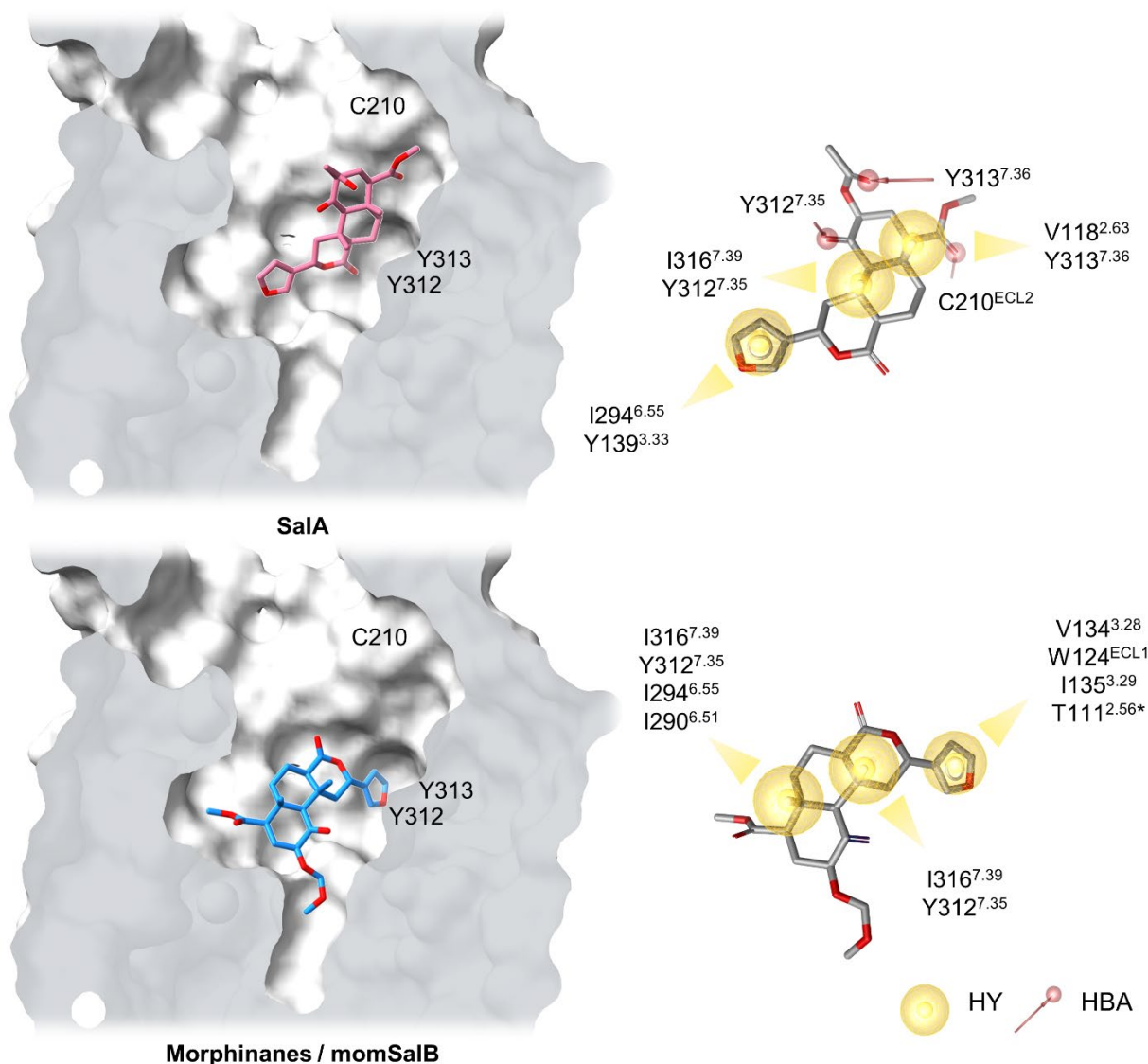
Figure 9. 3D pharmacophore models of momSalB at KOR according the cryo-EM structures (PDB-IDs: 8DZQ, 8DZP) and previously docked SalA used for virtual screening query 3D pharmacophore generation. The momSalB cryo-EM structure 8DZQ is shown, but the binding mode of momSalB in 8DZP is correspondingly the same. The only altered interaction is the hydrophobic contact to T111, which is only present in 8DZP (marked with *). MomSalB only participates in hydrophobic contacts (HY) in both cryo-EM structures while the docked SalA additionally shows three hydrogen bond acceptor (HBA) features. Other abbreviations used: ECL = extracellular loop.

described in detail in the methods section of our previous publication[51]. For MD simulations of momSalB the respective cryo-EM structures were prepared as followed using MOE 2020.0901[101]: The PDB-IDs 8DZP and 8DZQ were downloaded and the intracellular bound G protein was deleted. Missing side chains were added and broken loops closed using the loop modeler panel implemented in MOE. Particularly, in 8DZP the residues 203-205 in ECL2 were closed while in 8DZQ the residues 203-204 and 215-219 of ECL2 as well as 300-302 of ECL3 were modeled. The KOR wildtype sequence was restored by re-mutation of L135 to I135 according the UniProt-ID P41145[102]. The protein geometry was optimized by solving Ramachandran plot outliers[103] and atom clashes by careful side chain optimization and minimization using the OPLS-AA force field[104]. The

Protonate3D application[105] implemented in MOE was used to assign ionization states at the pH of 7 and 300 K.

Protein-Ligand Docking. Protein-ligand docking experiments were conducted to position the virtual screening hit compounds in the binding site of the active state KOR x-ray crystal structure (PDB-ID: 6B73[24]) prepared as described above. All docking experiments were conducted in Gold v5.2[106]. The KORbinding site was defined by a sphere of 15 Å radius around the terminal carbon atom (CD) of E209 and limited to solvent accessible space. For each ligand 15 separate and diverse docking hypothesis were generated, i.e. the root mean square deviation (RMSD) between the docking hypothesis must be ≥1.5 Å. During pose generation pyramidal nitrogens were allowed to flip. The experiments run with 100% search efficiency. Generated poses were

scored by GoldScore[107,108]. To promote binding modes with interactions indicated important by SAR studies a pharmacophore constraint was applied. Poses with hydrogen bond acceptor (HBA) features at analogues positions as for SalA's carbonyl groups at its C1-, C2-, and C4-substituents received higher scoring and were therefore favorably generated. These HBA features of SalA were indicated important in SAR studies[41,51]. After docking pose generation all poses were locally minimized in their protein environment by the MMFF94 force field implemented in LigandScout v.4.4.3[52,98]. Gaussian shape similarity scores and 3D pharmacophore scores of docking poses were generated in LigandScout with the SalA binding mode as reference pose.

Molecular Dynamics (MD) Simulations. MD simulations were prepared in Maestro v2020[109] and conducted using Desmond v2020-4[110]. The protein-ligand complex models of momSalB (PDB-IDs: 8DZQ, 8DZP) were placed in a rectangular box with at least 10 Å distance between the receptor and the box edges and embedded in a POPC (1-palmitoyl-2-oleoylphosphatidylcholine) bilayer according to the OPM database[111] entry of the active state KOR (PDB-ID: 6B73). The remaining space was filled by TIP3P water[112] and 1.5 M Na^+ and Cl^- ions for isotonic conditions. For system parametrization, the Charmm36 force field was implemented into Maestro-setup using viparr-ffpublic[113,114]. Five replicates of 200 ns each were performed per simulations system with 1000 sampled conformations per simulation run (in total 5000 per simulation system). The simulations were conducted with NPT ensemble conditions, i.e. with a constant number of particles, constant pressure (1.01325 bar), and constant temperature (300 K). After simulation the protein was centered and the trajectories aligned according the backbone heavy atoms of the first conformation of the simulation using VMD v1.9.3[115]. For MD simulation analysis Dynophores were generated with the in-house developed Dynophore tool[53,91,116]. Only interactions occurring in at least 5% of the simulation time were considered for evaluation. Of note, the MD simulations of SalA in complex with KOR were used from[51] with the same setting as described above

Drugs and Chemicals. Radioligands [³H]U69,593 (49.3 Ci/mmol), [³H]DAMGO (51.7 Ci/mmol), [³H]DPDPE (47.4 Ci/mmol) and [³⁵S]GTPγS (1250 Ci/mmol) were purchased from PerkinElmer (Boston, MA, USA). Guanosine diphosphate (GDP), GTPγS, DAMGO, DPDPE, U69,593, Salvinorin A, tris(hydroxymethyl) aminomethane (Tris), 2-[4-(2-hydroxyethyl)piperazin-1-yl]ethanesulfonic acid (HEPES), bovine serum albumin (BSA), and cell culture media and supplements were obtained from Sigma-Aldrich Chemicals (St. Louis, MO, USA). HS665 and HS378 were kindly provided by Dr. Helmut Schmidhammer (University of Innsbruck, Innsbruck, Austria). Morphine hydrochloride was obtained from Gatt-Koller GmbH (Innsbruck, Austria). **SalA-VS-1** to **SalA-VS-13** were obtained from AnalytiCon Discovery GmbH (Potsdam, Germany), and were prepared as 10 mM stock in DMSO and further diluted to working concentrations in the appropriate medium. All other chemicals were of analytical grade and obtained from standard commercial sources. All thirteen tested compounds from the virtual screening campaign are >95% pure by HPLC analysis. HPLC data can be found in the Supportive Information (SI-section 09).

Cell Cultures and Membrane Preparation. CHO cells stably expressing the human opioid receptors (CHO-hKOR, CHO-hMOR, and CHO-hDOR) were kindly provided by Dr. Lawrence Toll (SRI International, Menlo Park, CA). CHO-hKOR cells were cultured in Dulbecco's Modified Eagle's Medium (DMEM) culture medium supplemented with 10% fetal bovine serum (FBS), 0.1% penicillin/streptomycin, 2 mM L-glutamine and 0.4 mg/ml geneticin (G418). CHO-hMOR and CHO-hDOR cells were cultured in DMEM/Ham's F12 culture medium supplemented with 10% FBS, 0.1% penicillin/streptomycin, 2 mM L-glutamine and 0.4 mg/mL geneticin (G418). All cell cultures were grown at 37°C in a humidified atmosphere of 95% air and 5% CO_2. Membranes from CHO-hOR cells were prepared as previously described[65]. Briefly, cells grown at confluence were removed from the culture plates by scraping, homogenized in 50 mM Tris-HCl buffer (pH 7.7) using a Dounce glass homogenizer, then centrifuged once and washed by an additional centrifugation at 27,000 x g for 15 min at 4°C. The final pellet was resuspended in 50 mM Tris-HCl buffer (pH 7.7) and stored at –80°C until use. Protein content of cell membrane preparations was determined by the method of Bradford using BSA as the standard[117].

Radioligand Competitive Binding Assays for Opioid Receptors. Competitive binding assays were conducted on human opioid receptors stably transfected into CHO cells according to the published procedures[65]. Binding assays were performed using [³H]U69,593 (1 nM), [³H]DAMGO (1 nM) or [³H]DPDPE (1 nM), for labelling KOR, MOR, or DOR, respectively. Non-specific binding was determined using 10 µM of the unlabeled counterpart of each radioligand. Assays were performed in 50 mM Tris-HCl buffer (pH 7.4) in a final volume of 1 ml. Cell membranes (15-20 µg) were incubated with test compounds and the appropriate radioligand for 60 min at 25°C. After incubation, reactions were terminated by rapid filtration through Whatman GF/C glass fiber filters. Filters were washed three times with 5 ml of ice-cold 50 mM Tris-HCl buffer (pH 7.4) using a Brandel M24R cell harvester (Gaithersburg, MD, USA). Radioactivity retained on the filters was counted by liquid scintillation counting using a Beckman Coulter LS6500 (Beckman Coulter Inc., Fullerton, CA, USA). All experiments were performed in duplicate and repeated three times with independently prepared samples.

[³⁵S]GTPγS binding assay for the KOR. Binding of [³⁵S]GTPγS to membranes from CHO cells stably expressing the human KOR (CHO-hKOR) was conducted according to the published procedure[65]. Cell membranes (10-15 µg) in Buffer A (20 mM HEPES, 10 mM $MgCl_2$ and 100 mM NaCl, pH 7.4) were incubated with 0.05 nM [³⁵S]GTPγS, 10 µM GDP and test compounds in a final volume of 1 ml, for 60 min at 25°C. Non-specific binding was determined using 10 µM GTPγS, and the basal binding was determined in the absence of test compound. Samples were filtered over Whatman GF/B glass fiber filters using a Brandel M24R cell harvester (Brandel, Gaithersburg, MD, USA). Radioactivity retained on the filters was counted by liquid scintillation counting using a Beckman Coulter LS6500 (Beckman Coulter Inc., Fullerton, CA, USA). All experiments were performed in duplicate and repeated three times with independently prepared samples.

Data and Statistical Analysis. Experimental data were graphically processed and statistically analyzed using the GraphPad Prism Software (GraphPad Prism Software Inc., San Diego, CA). In *in vitro* binding assays, inhibition constant (K_i, nM), potency (EC_{50}, nM), and efficacy (E_{max}, %) values were determined from concentration-response curves by nonlinear regression analysis. The K_i values were determined by the method of Cheng and Prusoff[118]. In the [^{35}S]GTPγS binding assays, efficacy was determined relative to the reference KOR full agonist, U69,593. All data are presented as the mean ± SEM.

ASSOCIATED CONTENT

Supporting Information. Figure S1. Chemical structures of NPs which modulate opioid receptors. Figure S2. Binding mode comparison between momSalB, docked SalA and morphinan agonist MP1104. Figure S3. Cryo-EM map of momSalB bound to KOR. Figure S4. Interaction pattern of momSalB with non-conserved residues of KOR and whether they can be maintained in MOR or DOR. Figure S5. Dynamic protein-Ligand interaction patterns of SalA and momSalB. Figure S6. Ligand root mean square deviation (RMSD) in MD simulations. Figure S7. Interactions of SalA and momSalB to KOR residues highlighted as important in mutagenesis studies. Figure S8. Examples for similar ligands that bind differently at the same protein or the same ligand that exhibits distinct binding modes at closely related receptors. Section 09. Purity data for virtual screening hits. This material is available free of charge via the Internet at http://pubs.acs.org.

AUTHOR INFORMATION

Corresponding Authors

Gerhard Wolber - Department of Pharmaceutical Chemistry, Institute of Pharmacy, Freie Universität Berlin, Königin-Luise-Str. 2-4, 14195 Berlin, Germany; Email: gerhard.wolber@fu-berlin.de (G.W.)

Mariana Spetea - Department of Pharmaceutical Chemistry, Institute of Pharmacy and Center for Molecular Biosciences Innsbruck (CMBI), University of Innsbruck, Innrain 80-82, 6020 Innsbruck, Austria; Email: mariana.spetea@uibk.ac.at (M.S.)

Authors

Kristina Puls - Department of Pharmaceutical Chemistry, Institute of Pharmacy, Freie Universität Berlin, Königin-Luise-Str. 2-4, 14195 Berlin, Germany; Email: kristina.puls@fu-berlin.de (K.P.)

Aina-Leonor Olivé-Marti - Department of Pharmaceutical Chemistry, Institute of Pharmacy and Center for Molecular Biosciences Innsbruck (CMBI), University of Innsbruck, Innrain 80-82, 6020 Innsbruck, Austria; Email: aolive.marti@gmail.com (A.-L.O.-M)

David Lamp - Department of Pharmaceutical Chemistry, Institute of Pharmacy and Center for Molecular Biosciences Innsbruck (CMBI), University of Innsbruck, Innrain 80-82, 6020 Innsbruck, Austria; Email: davidlamp42@gmail.com (D.L.)

Author Contributions

Conceptualization, K.P., M.S. and G.W.; methodology, K.P., A.-L.O.-M., D.L.; formal analysis, K.P., A.-L.O.-M., D.L.; investigation, K.P., A.-L.O.-M., D.L.; resources, G.W. and M.S.; writing - original draft preparation, K.P.; writing - review and editing, K.P., M.S.

and G.W.; supervision, M.S. and G.W.; funding acquisition, M.S. and G.W. All authors have given approval to the final version of the manuscript.

Notes

The authors declare no competing financial interest.

ABBREVIATIONS

AUC, area under the curve; CHO, Chinese hamster ovary; DAMGO, [D-Ala^2,N-Me-Phe^4,Gly-ol^5]enkephalin; DOR, delta-opioid receptors; DPDPE, [D-Pen^2,D-Pen^5]encephalin; ER, estrogen receptor; GPCRs, G protein-coupled receptors; HBA, hydrogen bond acceptor feature; HY, hydrophobic contact feature; KOR, kappa-opioid receptor; MD, molecular dynamics; MOR, mu-opioid receptor; NOP, nociceptin/orphanin FQ peptide; NP, natural product; PDB, protein data base; RMSD, root mean square deviation; ROC, receiver operating characteristic; SalA, Salvinorin A; SalB, Salvinorin B; [^{35}S]GTPγS, guanosine-5'-O-(3-[^{35}S]thio)-triphosphate; U69,593, N-methyl-2-phenyl-N-[(5R,7S,8S)-7-(pyrrolidin-1-yl)-1-oxaspiro[4.5]dec-8-yl]acetamide

REFERENCES

(1) Bourke, J. *The Story of Pain - From Prayer to Painkillers*; Oxford University Press, 2014.

(2) Paul, A. K.; Smith, C. M.; Rahmatullah, M.; Nissapatorn, V.; Wilairatana, P.; Spetea, M.; Gueven, N.; Dietis, N. Opioid analgesia and opioid-induced adverse effects: A review. *Pharmaceuticals* **2021**, *14*, 1091. DOI: 10.3390/ph14111091.

(3) Mores, K. L.; Cummins, B. R.; Cassell, R. J.; van Rijn, R. M. A review of the therapeutic potential of recently developed G protein-biased kappa agonists. *Front. Pharmacol.* **2019**, *10*, 407. DOI: 10.3389/fphar.2019.00407 PubMed.

(4) Laycock, H.; Bantel, C. Opioid mechanisms and opioid drugs. *Anaesth. Intensive Care Med.* **2019**, *20*, 450-455. DOI: 10.1016/j.mpaic.2019.05.009.

(5) Lyden, J.; Binswanger, I. A. The united states opioid epidemic. In *Seminars in perinatology*, 2019; Elsevier: Vol. 43, pp 123-131. DOI: 10.1053/j.semperi.2019.01.001.

(6) Corder, G.; Castro, D. C.; Bruchas, M. R.; Scherrer, G. Endogenous and exogenous opioids in pain. *Annu. Rev. Neurosci.* **2018**, *41*, 453-473. DOI: 10.1146/annurev-neuro-080317-061522.

(7) Fredriksson, R.; Lagerström, M. C.; Lundin, L.-G.; Schiöth, H. B. The G-protein-coupled receptors in the human genome form five main families. Phylogenetic analysis, paralogon groups, and fingerprints. *Mol. Pharmacol.* **2003**, *63*, 1256-1272. DOI: 10.1124/mol.63.6.1256.

(8) Mustazza, C.; Pieretti, S.; Marzoli, F. Nociceptin/orphanin FQ peptide (NOP) receptor modulators: an update in structure-
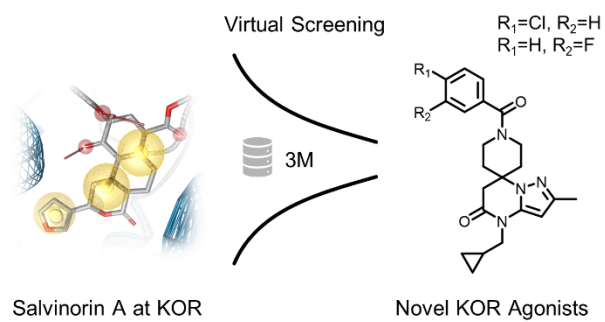
activity relationships. *Curr. Med. Chem.* **2018**, *25*, 2353-2384. DOI: 10.2174/0929867325666180111095458.

(9) Brust, T. F.; Morgenweck, J.; Kim, S. A.; Rose, J. H.; Locke, J. L.; Schmid, C. L.; Zhou, L.; Stahl, E. L.; Cameron, M. D.; Scarry, S. M. Biased agonists of the kappa opioid receptor suppress pain and itch without causing sedation or dysphoria. *Sci Signal.* **2016**, *9*, ra117. DOI: 10.1126/scisignal.aai8441.

(10) Albert-Vartanian, A.; Boyd, M.; Hall, A.; Morgado, S.; Nguyen, E.; Nguyen, V.; Patel, S.; Russo, L.; Shao, A.; Raffa, R. Will peripherally restricted kappa-opioid receptor agonists (pKORA s) relieve pain with less opioid adverse effects and abuse potential? *J. Clin. Pharm. Ther.* **2016**, *41*, 371-382. DOI: 10.1111/jcpt.12404.

(11) Paton, K. F.; Atigari, D. V.; Kaska, S.; Prisinzano, T.; Kivell, B. M. Strategies for Developing κ Opioid Receptor Agonists for the Treatment of Pain with Fewer Side Effects. *J. Pharmacol. Exp. Ther.* **2020**, *375*, 332–348. DOI: 10.1124/jpet.120.000134 PubMed.

(12) Aldrich, J. V.; McLaughlin, J. P. Peptide Kappa Opioid Receptor Ligands and Their Potential for Drug Development. In *The Kappa Opioid Receptor*, Liu-Chen, L., Inan, S. Eds.; Springer, Cham, Switzerland, 2021; pp 197-220.

(13) Khan, M. I. H.; Sawyer, B. J.; Akins, N. S.; Le, H. V. A systematic review on the kappa opioid receptor and its ligands: New directions for the treatment of pain, anxiety, depression, and drug abuse. *Eur. J. Med. Chem.* **2022**, *243*, 114785. DOI: 10.1016/j.ejmech.2022.114785.

(14) Spetea, M.; Schmidhammer, H. Kappa Opioid Receptor Ligands and Pharmacology: Diphenethylamines, a Class of Structurally Distinct, Selective Kappa Opioid Ligands. In *The Kappa Opioid Receptor*, Chen, L., Inan, S. Eds.; Springer, Cham, Switzerland, 2021.

(15) Santino, F.; Gentilucci, L. Design of κ-Opioid Receptor Agonists for the Development of Potential Treatments of Pain with Reduced Side Effects. *Molecules* **2023**, *28*, 346. DOI: 10.3390/molecules28010346.

(16) Dalefield, M. L.; Scouller, B.; Bibi, R.; Kivell, B. M. The kappa opioid receptor: A promising therapeutic target for multiple pathologies. *Front. Pharmacol.* **2022**, *13*, 837671. DOI: 10.3389/fphar.2022.837671.

(17) Zangrandi, L.; Schwarzer, C. The Kappa Opioid Receptor System in Temporal Lobe Epilepsy. *Handb. Exp. Pharmacol.* **2022**, *271*, 379-400. DOI: 10.1007/164_2021_444.

(18) Browne, C. A.; Lucki, I. Targeting opioid dysregulation in depression for the development of novel therapeutics. *Pharmacol. Ther.* **2019**, *201*, 51-76. DOI: 10.1016/j.pharmthera.2019.04.009.

(19) Roth, B. L.; Baner, K.; Westkaemper, R.; Siebert, D.; Rice, K. C.; Steinberg, S.; Ernsberger, P.; Rothman, R. B. Salvinorin A: a potent naturally occurring nonnitrogenous κ opioid selective agonist. *PNAS* **2002**, *99*, 11934-11939. DOI: 10.1073/pnas.182234399.

(20) Kane, B. E.; Nieto, M. J.; McCurdy, C. R.; Ferguson, D. M. A unique binding epitope for salvinorin A, a non-nitrogenous kappa opioid receptor agonist. *The FEBS journal* **2006**, *273*, 1966-1974. DOI: 10.1111/j.1742-4658.2006.05212.x.

(21) Vortherms, T. A.; Mosier, P. D.; Westkaemper, R. B.; Roth, B. L. Differential helical orientations among related G protein-coupled receptors provide a novel mechanism for selectivity: studies with salvinorin A and the κ-opioid receptor. *J. Biol. Chem.* **2007**, *282*, 3146-3156. DOI: 10.1074/jbc.M609264200.

(22) Wang, Y.; Tang, K.; Inan, S.; Siebert, D.; Holzgrabe, U.; Lee, D. Y.; Huang, P.; Li, J.-G.; Cowan, A.; Liu-Chen, L.-Y. Comparison of pharmacological activities of three distinct κ ligands (salvinorin A, TRK-820 and 3FLB) on κ opioid receptors in vitro and their antipruritic and antinociceptive activities in vivo. *J. Pharmacol. Exp. Ther.* **2005**, *312*, 220-230. DOI: 10.1124/jpet.104.073668.

(23) Fenalti, G.; Zatsepin, N. A.; Betti, C.; Giguere, P.; Han, G. W.; Ishchenko, A.; Liu, W.; Guillemyn, K.; Zhang, H.; James, D.; et al. Structural basis for bifunctional peptide recognition at human δ-opioid receptor. *Nat. Struct. Mol. Biol.* **2015**, *22*, 265–268. DOI: 10.1038/nsmb.2965 PubMed.

(24) Che, T.; Majumdar, S.; Zaidi, S. A.; Ondachi, P.; McCorvy, J. D.; Wang, S.; Mosier, P. D.; Uprety, R.; Vardy, E.; Krumm, B. E.; et al. Structure of the nanobody-stabilized active state of the kappa opioid receptor. *Cell* **2018**, *172*, 55-67.e15. DOI: 10.1016/j.cell.2017.12.011 PubMed.

(25) Vo, Q. N.; Mahinthichaichan, P.; Shen, J.; Ellis, C. R. How μ-opioid receptor recognizes fentanyl. *Nat. Commun.* **2021**, *12*, 984. DOI: 10.1038/s41467-021-21262-9 PubMed.

(26) Wu, H.; Wacker, D.; Mileni, M.; Katritch, V.; Han, G. W.; Vardy, E.; Liu, W.; Thompson, A. A.; Huang, X.-P.; Carroll, F. Structure of the human κ-opioid receptor in complex with JDTic. *Nature* **2012**, *485*, 327-332. DOI: 10.1038/nature10939.

(27) Vardy, E.; Mosier, P. D.; Frankowski, K. J.; Wu, H.; Katritch, V.; Westkaemper, R. B.; Aubé, J.; Stevens, R. C.; Roth, B. L. Chemotype-selective modes of action of κ-opioid receptor agonists. *J. Biol. Chem.* **2013**, *288*, 34470–34483. DOI: 10.1074/jbc.M113.515668 PubMed.

(28) Roach, J. J.; Sasano, Y.; Schmid, C. L.; Zaidi, S.; Katritch, V.; Stevens, R. C.; Bohn, L. M.; Shenvi, R. A. Dynamic strategic bond analysis yields a ten-step synthesis of 20-nor-Salvinorin A, a potent κ-OR agonist. *ACS central science* **2017**, *3*, 1329-1336. DOI: 10.1021/acscentsci.7b00488.

(29) Polepally, P. R.; Huben, K.; Vardy, E.; Setola, V.; Mosier, P. D.; Roth, B. L.; Zjawiony, J. K. Michael acceptor approach to the design of new salvinorin A-based high affinity ligands for the kappa-opioid receptor. *Eur. J. Med. Chem.* **2014**, *85*, 818-829. DOI: 10.1016/j.ejmech.2014.07.077.

(30) McGovern, D. L.; Mosier, P. D.; Roth, B. L.; Westkaemper, R. B. CoMFA analyses of C-2 position Salvinorin A analogs at the kappa-opioid receptor provides insights into epimer selectivity. *J. Mol. Graph. Model.* **2010**, *28*, 612-625. DOI: 10.1016/j.jmgm.2009.12.008.

(31) Vortherms, T. A.; Roth, B. L. Salvinorin A. *Molecular interventions* **2006**, *6*, 257. DOI: 10.1124/mi.6.5.7.

(32) Yan, F.; Mosier, P. D.; Westkaemper, R. B.; Stewart, J.; Zjawiony, J. K.; Vortherms, T. A.; Sheffler, D. J.; Roth, B. L. Identification of the molecular mechanisms by which the diterpenoid salvinorin A binds to κ-opioid receptors. *Biochemistry* **2005**, *44*, 8643-8651. DOI: 10.1021/bi050490d.

(33) Yan, F.; Bikbulatov, R. V.; Mocanu, V.; Dicheva, N.; Parker, C. E.; Wetsel, W. C.; Mosier, P. D.; Westkaemper, R. B.; Allen, J. A.; Zjawiony, J. K. Structure-based design, synthesis, and biochemical and pharmacological characterization of novel salvinorin A analogues as active state probes of the κ-opioid receptor. *Biochemistry* **2009**, *48*, 6898-6908. DOI: 10.1021/bi900605n.

(34) Coffeen, U.; Pellicer, F. Salvia divinorum: from recreational hallucinogenic use to analgesic and anti-inflammatory action. *J. Pain Res.* **2019**, *12*, 1069-1076. DOI: 10.2147%2FJPR.S188619.

(35) Brito-da-Costa, A. M.; Dias-da-Silva, D.; Gomes, N. G.; Dinis-Oliveira, R. J.; Madureira-Carvalho, Á. Pharmacokinetics and Pharmacodynamics of Salvinorin A and Salvia divinorum: Clinical and Forensic Aspects. *Pharmaceuticals* **2021**, *14*, 116. DOI: 10.3390/ph14020116.

(36) Frankowski, K. J.; Ghosh, P.; Setola, V.; Tran, T. B.; Roth, B. L.; Aubé, J. N-alkyl-octahydroisoquinolin-1-one-8-carboxamides: selective and nonbasic κ-opioid receptor ligands. *ACS Med. Chem. Lett.* **2010**, *1*, 189-193. DOI: 10.1021/ml100040t.

(37) Frankowski, K. J.; Hedrick, M. P.; Gosalia, P.; Li, K.; Shi, S.; Whipple, D.; Ghosh, P.; Prisinzano, T. E.; Schoenen, F. J.; Su, Y. Discovery of small molecule kappa opioid receptor agonist and antagonist chemotypes through a HTS and hit refinement strategy. *ACS Chem. Neurosci.* **2012**, *3*, 221-236. DOI: 10.1021/cn200128x.

(38) Whitby, L. R.; Ando, Y.; Setola, V.; Vogt, P. K.; Roth, B. L.; Boger, D. L. Design, synthesis, and validation of a β-turn mimetic library targeting protein–protein and peptide–receptor interactions. *J. Am. Chem. Soc.* **2011**, *133*, 10184-10194. DOI: 10.1021/ja201878v.

(39) Gupta, A.; Gomes, I.; Bobeck, E. N.; Fakira, A. K.; Massaro, N. P.; Sharma, I.; Cavé, A.; Hamm, H. E.; Parello, J.; Devi, L. A.

Collybolide is a novel biased agonist of κ-opioid receptors with potent antipruritic activity. *PNAS* **2016**, *113*, 6041-6046. DOI: 10.1073/pnas.1521825113.

(40) Bedini, A.; Di Cesare Mannelli, L.; Micheli, L.; Baiula, M.; Vaca, G.; De Marco, R.; Gentilucci, L.; Ghelardini, C.; Spampinato, S. Functional selectivity and antinociceptive effects of a novel KOPr agonist. *Front. Pharmacol.* **2020**, *11*, 188. DOI: 10.3389/fphar.2020.00188.

(41) Roach, J. J.; Shenvi, R. A. A review of salvinorin analogs and their kappa-opioid receptor activity. *Bioorg. Med. Chem. Lett.* **2018**, *28*, 1436-1445. DOI: 10.1016/j.bmcl.2018.03.029.

(42) Hill, S.; Dao, N.; Dang, V.; Stahl, E.; Bohn, L.; Shenvi, R. A route to potent, selective, and biased salvinorin chemical space. *ACS Central Science* **2023**, *9*, 1567-1574. DOI: 10.1021/acscentsci.3c00616.

(43) Sherwood, A. M.; Crowley, R. S.; Paton, K. F.; Biggerstaff, A.; Neuenswander, B.; Day, V. W.; Kivell, B. M.; Prisinzano, T. E. Addressing structural flexibility at the A-ring on salvinorin A: discovery of a potent kappa-opioid agonist with enhanced metabolic stability. *J. Med. Chem.* **2017**, *60*, 3866-3878. DOI: 10.1021/acs.jmedchem.7b00148.

(44) Bharate, S. S.; Mignani, S.; Vishwakarma, R. A. Why are the majority of active compounds in the CNS domain natural products? A critical analysis. *J. Med. Chem.* **2018**, *61*, 10345-10374. DOI: 10.1021/acs.jmedchem.7b01922.

(45) Atanasov, A. G.; Zotchev, S. B.; Dirsch, V. M.; Supuran, C. T. Natural products in drug discovery: advances and opportunities. *Nat. Rev. Drug Discovery* **2021**, *20*, 200-216. DOI: 10.1038/s41573-020-00114-z.

(46) Newman, D. J.; Cragg, G. M. Natural products as sources of new drugs over the nearly four decades from 01/1981 to 09/2019. *J. Nat. Prod.* **2020**, *83*, 770-803. DOI: 10.1021/acs.jnatprod.9b01285.

(47) Young, R. J.; Flitsch, S. L.; Grigalunas, M.; Leeson, P. D.; Quinn, R. J.; Turner, N. J.; Waldmann, H. The time and place for nature in drug discovery. *JACS Au* **2022**, *2*, 2400-2416. DOI: 10.1021/jacsau.2c00415.

(48) Noonan, T.; Denzinger, K.; Talagayev, V.; Chen, Y.; Puls, K.; Wolf, C. A.; Liu, S.; Nguyen, T. N.; Wolber, G. Mind the Gap—Deciphering GPCR Pharmacology Using 3D Pharmacophores and Artificial Intelligence. *Pharmaceuticals* **2022**, *15*, 1304.

(49) Spetea, M.; Faheem Asim, M.; Noha, S.; Wolber, G.; Schmidhammer, H. Current κ Opioid Receptor Ligands and Discovery of a New Molecular Scaffold as a κ Opioid Receptor Antagonist Using Pharmacophore-Based Virtual Screening. *Curr. Pharm. Des.* **2013**, *19*, 7362–7372.

(50) Schaller, D.; Wolber, G. PyRod Enables Rational Homology Model-based Virtual Screening Against MCHR1. *Mol. Inform.* **2020**, *39*, 2000020. DOI: 10.1002/minf.202000020.

(51) Puls, K.; Wolber, G. Solving an old puzzle: Elucidation and evaluation of the binding mode of Salvinorin A at the kappa opioid receptor. *Molecules* **2023**, *28*, 718. DOI: 10.3390/molecules28020718.

(52) Wolber, G.; Langer, T. LigandScout: 3-D pharmacophores derived from protein-bound ligands and their use as virtual screening filters. *J. Chem. Inf. Model.* **2005**, *45*, 160–169. DOI: 10.1021/ci049885e PubMed.

(53) Schaller, D.; Šribar, D.; Noonan, T.; Deng, L.; Nguyen, T. N.; Pach, S.; Machalz, D.; Bermudez, M.; Wolber, G. Next generation 3D pharmacophore modeling. *WIREs Comput Mol Sci.* **2020**, *10*, e1468. DOI: 10.1002/wcms.1468 CrossRef.

(54) Triballeau, N.; Acher, F.; Brabet, I.; Pin, J.-P.; Bertrand, H.-O. Virtual screening workflow development guided by the "receiver operating characteristic" curve approach. Application to high-throughput docking on metabotropic glutamate receptor subtype 4. *J. Med. Chem.* **2005**, *48*, 2534–2547. DOI: 10.1021/jm049092j PubMed.

(55) Mendez, D.; Gaulton, A.; Bento, A. P.; Chambers, J.; De Veij, M.; Félix, E.; Magariños, M. P.; Mosquera, J. F.; Mutowo, P.; Nowotka, M. ChEMBL: towards direct deposition of bioassay data. *Nucleic Acids Res.* **2019**, *47*, D930-D940. DOI: 10.1093/nar/gky1075.

(56) Mysinger, M. M.; Carchia, M.; Irwin, J. J.; Shoichet, B. K. Directory of useful decoys, enhanced (DUD-E): better ligands and decoys for better benchmarking. *J. Med. Chem.* **2012**, *55*, 6582-6594. DOI: 10.1021/jm300687e.

(57) *AnalytiCon Discovery*. https://ac-discovery.com/ (accessed 19.09.2022).

(58) *Selleckchem*. https://www.selleckchem.com/screening/natural-product-library.html (accessed 14.11.2022).

(59) *Enamine Screening Collection*. https://enamine.net/compound-collections/screening-collection (accessed 17.03.2022).

(60) *RDKit: Open-source cheminformatics*; https://www.rdkit.org" (accessed.

(61) Berthold, M. R.; Cebron, N.; Dill, F.; Gabriel, T. R.; Kötter, T.; Meinl, T.; Ohl, P.; Sieb, C.; Thiel, K.; Wiswedel, B. KNIME: The Konstanz Information Miner. In *31st Annual Conference of the Gesellschaft für Klassifikation e.V.*, Berlin, Heidelberg, 2008; Springer Berlin Heidelberg: pp 319-326.

(62) Kumar, A.; Zhang, K. Y. J. Advances in the development of shape similarity methods and their application in drug discovery. *Front. Chem.* **2018**, *6*, 315. DOI: 10.3389/fchem.2018.00315 PubMed.

(63) Grant, J. A.; Pickup, B. A Gaussian description of molecular shape. *J. Phys. Chem.* **1995**, *99*, 3503-3510. DOI: 10.1021/j100011a016.

(64) Spetea, M.; Berzetei-Gurske, I. P.; Guerrieri, E.; Schmidhammer, H. Discovery and pharmacological evaluation of a diphenethylamine derivative (HS665), a highly potent and selective κ opioid receptor agonist. *J. Med. Chem.* **2012**, *55*, 10302–10306. DOI: 10.1021/jm301258w PubMed.

(65) Erli, F.; Guerrieri, E.; Ben Haddou, T.; Lantero, A.; Mairegger, M.; Schmidhammer, H.; Spetea, M. Highly potent and selective new diphenethylamines interacting with the κ-opioid receptor: Synthesis, pharmacology, and structure-activity relationships. *J. Med. Chem.* **2017**, *60*, 7579–7590. DOI: 10.1021/acs.jmedchem.7b00981 PubMed.

(66) Spetea, M.; Harris, H. E.; Berzetei-Gurske, I. P.; Klareskog, L.; Schmidhammer, H. Binding, pharmacological and immunological profiles of the δ-selective opioid receptor antagonist HS 378. *Life Sci.* **2001**, *69*, 1775-1782. DOI: 10.1016/S0024-3205(01)01271-1.

(67) Bignan, G. C.; Connolly, P. J.; Middleton, S. A. Recent advances towards the discovery of ORL-1 receptor agonists and antagonists. *Expert Opin. Ther. Pat.* **2005**, *15*, 357-388. DOI: 10.1517/13543776.15.4.357.

(68) Guerrini, R.; Carra', G.; Calo', G.; Trapella, C.; Marzola, E.; Rizzi, D.; Regoli, D.; Salvadori, S. Nonpeptide/peptide chimeric ligands for the nociceptin/orphanin FQ receptor: design, synthesis and in vitro pharmacological activity. *The Journal of peptide research* **2004**, *63*, 477-484. DOI: 10.1111/j.1399-3011.2004.00157.x.

(69) Kronenberg, E.; Weber, F.; Brune, S.; Schepmann, D.; Almansa, C.; Friedland, K.; Laurini, E.; Pricl, S.; Wünsch, B. Synthesis and Structure–Affinity Relationships of Spirocyclic Benzopyrans with Exocyclic Amino Moiety. *J. Med. Chem.* **2019**, *62*, 4204-4217. DOI: 10.1021/acs.jmedchem.9b00449.

(70) Le Bourdonnec, B.; Windh, R. T.; Leister, L. K.; Zhou, Q. J.; Ajello, C. W.; Gu, M.; Chu, G.-H.; Tuthill, P. A.; Barker, W. M.; Koblish, M. Spirocyclic delta opioid receptor agonists for the treatment of pain: discovery of N, N-diethyl-3-hydroxy-4-(spiro [chromene-2, 4'-piperidine]-4-yl) benzamide (ADL5747). *J. Med. Chem.* **2009**, *52*, 5685-5702. DOI: 10.1021/jm900773n.

(71) Nozaki, C.; Le Bourdonnec, B.; Reiss, D.; Windh, R. T.; Little, P. J.; Dolle, R. E.; Kieffer, B. L.; Gavériaux-Ruff, C. δ-Opioid mechanisms for ADL5747 and ADL5859 effects in mice: analgesia,

locomotion, and receptor internalization. *J. Pharmacol. Exp. Ther.* **2012**, *342*, 799-807. DOI: 10.1124/jpet.111.188987.

(72) Mustazza, C.; Borioni, A.; Sestili, I.; Sbraccia, M.; Rodomonte, A.; Ferretti, R.; Del Giudice, M. R. Synthesis and evaluation as NOP ligands of some spiro [piperidine-4, 2′(1′ H)-quinazolin]-4′(3′ H)-ones and spiro [piperidine-4, 5′(6′ H)-[1, 2, 4] triazolo [1, 5-c] quinazolines]. *Chem. Pharm. Bull.* **2006**, *54*, 611-622. DOI: 10.1248/cpb.54.611.

(73) Röver, S.; Wichmann, J.; Jenck, F.; Adam, G.; Cesura, A. M. ORL1 receptor ligands: Structure–activity relationships of 8-cycloalkyl-1-phenyl-1, 3, 8-triaza-spiro [4.5] decan-4-ones. *Bioorg. Med. Chem. Lett.* **2000**, *10*, 831-834. DOI: 10.1016/S0960-894X(00)00111-6.

(74) Schunk, S.; Linz, K.; Hinze, C.; Frormann, S.; Oberbörsch, S.; Sundermann, B.; Zemolka, S.; Englberger, W.; Germann, T.; Christoph, T. Discovery of a potent analgesic NOP and opioid receptor agonist: cebranopadol. *ACS Med. Chem. Lett.* **2014**, *5*, 857-862. DOI: 10.1021/ml500117c.

(75) Schunk, S.; Linz, K.; Frormann, S.; Hinze, C.; Oberbörsch, S.; Sundermann, B.; Zemolka, S.; Englberger, W.; Germann, T.; Christoph, T. Discovery of spiro [cyclohexane-dihydropyrano [3, 4-b] indole]-amines as potent NOP and opioid receptor agonists. *ACS Med. Chem. Lett.* **2014**, *5*, 851-856. DOI: 10.1021/ml500116x.

(76) Thomsen, C.; Hohlweg, R. (8-Naphthalen-1-ylmethyl-4-oxo-1-phenyl-1, 3, 8-triaza-spiro [4.5] dec-3-yl)-acetic acid methyl ester (NNC 63-0532) is a novel potent nociceptin receptor agonist. *Br. J. Pharmacol.* **2000**, *131*, 903-908. DOI: 10.1038/sj.bjp.0703661.

(77) Váradi, A.; Marrone, G. F.; Palmer, T. C.; Narayan, A.; Szabó, M. R.; Le Rouzic, V.; Grinnell, S. G.; Subrath, J. J.; Warner, E.; Kalra, S. Mitragynine/corynantheidine pseudoindoxyls as opioid analgesics with mu agonism and delta antagonism, which do not recruit β-arrestin-2. *J. Med. Chem.* **2016**, *59*, 8381-8397. DOI: 10.1021/acs.jmedchem.6b00748.

(78) Wichmann, J.; Adam, G.; Röver, S.; Cesura, A. M.; Dautzenberg, F. M.; Jenck, F. 8-acenaphthen-1-yl-1-phenyl-1, 3, 8-triaza-spiro [4.5] decan-4-one derivatives as orphanin FQ receptor agonists. *Bioorg. Med. Chem. Lett.* **1999**, *9*, 2343-2348. DOI: 10.1016/S0960-894X(99)00385-6.

(79) Wichmann, J.; Adam, G.; Röver, S.; Hennig, M.; Scalone, M.; Cesura, A. M.; Dautzenberg, F. M.; Jenck, F. Synthesis of (1S, 3aS)-8-(2, 3, 3a, 4, 5, 6-hexahydro-1H-phenalen-1-yl)-1-phenyl-1, 3, 8-triaza-spiro [4.5] decan-4-one, a potent and selective orphanin FQ (OFQ) receptor agonist with anxiolytic-like properties. *Eur. J. Med. Chem.* **2000**, *35*, 839-851. DOI: 10.1016/S0223-5234(00)00171-9.

(80) Zhuang, Y.; Wang, Y.; He, B.; He, X.; Zhou, X. E.; Guo, S.; Rao, Q.; Yang, J.; Liu, J.; Zhou, Q. Molecular recognition of morphine and fentanyl by the human μ-opioid receptor. *Cell* **2022**, *185*, 4361-4375. e4319. DOI: 10.1016/j.cell.2022.09.041.

(81) Chakraborty, S.; Majumdar, S. Natural products for the treatment of pain: chemistry and pharmacology of salvinorin A, mitragynine, and collybolide. *Biochemistry* **2021**, *60*, 1381-1400. DOI: 10.1021/acs.biochem.0c00629.

(82) Perlikowska, R.; Janecka, A. Rubiscolins-highly potent peptides derived from plant proteins. *Mini Rev. Med. Chem.* **2018**, *18*, 104-112. DOI: 10.2174/1389557517666170426160703.

(83) Azevedo Neto, J.; Costanzini, A.; De Giorgio, R.; Lambert, D. G.; Ruzza, C.; Calò, G. Biased versus partial agonism in the search for safer opioid analgesics. *Molecules* **2020**, *25*, 3870. DOI: 10.3390/molecules25173870.

(84) Gress, K.; Charipova, K.; Jung, J. W.; Kaye, A. D.; Paladini, A.; Varrassi, G.; Viswanath, O.; Urits, I. A comprehensive review of partial opioid agonists for the treatment of chronic pain. *Best Pract. Res. Clin. Anaesthesiol.* **2020**, *34*, 449-461. DOI: 10.1016/j.bpa.2020.06.003.

(85) Han, J.; Zhang, J.; Nazarova, A. L.; Bernhard, S. M.; Krumm, B. E.; Zhao, L.; Lam, J. H.; Rangari, V. A.; Majumdar, S.; Nichols, D. E. Ligand and G-protein selectivity in the κ-opioid receptor. *Nature* **2023**, 1-9. DOI: 10.1038/s41586-023-06030-7.

(86) Wang, Y.; Chen, Y.; Xu, W.; Lee, D. Y.; Ma, Z.; Rawls, S. M.; Cowan, A.; Liu-Chen, L.-Y. 2-Methoxymethyl-salvinorin B is a potent κ opioid receptor agonist with longer lasting action in vivo than salvinorin A. *J. Pharmacol. Exp. Ther.* **2008**, *324*, 1073-1083. DOI: 10.1124/jpet.107.132142.

(87) Huang, W.; Manglik, A.; Venkatakrishnan, A. J.; Laeremans, T.; Feinberg, E. N.; Sanborn, A. L.; Kato, H. E.; Livingston, K. E.; Thorsen, T. S.; Kling, R. C.; et al. Structural insights into μ-opioid receptor activation. *Nature* **2015**, *524*, 315–321. DOI: 10.1038/nature14886 PubMed.

(88) Claff, T.; Yu, J.; Blais, V.; Patel, N.; Martin, C.; Wu, L.; Han, G. W.; Holleran, B. J.; van der Poorten, O.; White, K. L.; et al. Elucidating the active δ-opioid receptor crystal structure with peptide and small-molecule agonists. *Sci. Adv.* **2019**, *5*, eaax9115. DOI: 10.1126/sciadv.aax9115 PubMed.

(89) Bock, A.; Chirinda, B.; Krebs, F.; Messerer, R.; Bätz, J.; Muth, M.; Dallanoce, C.; Klingenthal, D.; Tränkle, C.; Hoffmann, C. Dynamic ligand binding dictates partial agonism at a G protein–coupled receptor. *Nat. Chem. Biol.* **2014**, *10*, 18-20. DOI: 10.1038/nchembio.1384.

(90) Bruning, J. B.; Parent, A. A.; Gil, G.; Zhao, M.; Nowak, J.; Pace, M. C.; Smith, C. L.; Afonine, P. V.; Adams, P. D.; Katzenellenbogen, J. A. Coupling of receptor conformation and ligand orientation determine graded activity. *Nat. Chem. Biol.* **2010**, *6*, 837-843. DOI: 10.1038/nchembio.451.

(91) Bock, A.; Bermudez, M.; Krebs, F.; Matera, C.; Chirinda, B.; Sydow, D.; Dallanoce, C.; Holzgrabe, U.; Amici, M. d.; Lohse, M. J.; et al. Ligand binding ensembles determine graded agonist efficacies at a G protein-coupled receptor. *J. Biol. Chem.* **2016**, *291*, 16375–16389. DOI: 10.1074/jbc.m116.735431 PubMed.

(92) Ekroos, M.; Sjögren, T. Structural basis for ligand promiscuity in cytochrome P450 3A4. *PNAS* **2006**, *103*, 13682-13687. DOI: 10.1073/pnas.0603236103.

(93) Kim, K. H. Outliers in SAR and QSAR: 2. Is a flexible binding site a possible source of outliers? *J. Comput. Aided Mol. Des.* **2007**, *21*, 421-435. DOI: 10.1007/s10822-007-9126-y.

(94) Maximciuc, A. A.; Putkey, J. A.; Shamoo, Y.; MacKenzie, K. R. Complex of calmodulin with a ryanodine receptor target reveals a novel, flexible binding mode. *Structure* **2006**, *14*, 1547-1556. DOI: 10.1016/j.str.2006.08.011.

(95) Gomez, G. A.; Morisseau, C.; Hammock, B. D.; Christianson, D. W. Human soluble epoxide hydrolase: structural basis of inhibition by 4-(3-cyclohexylureido)-carboxylic acids. *Protein Sci.* **2006**, *15*, 58-64. DOI: 10.1110/ps.051720206.

(96) Bruning, J. B.; Chalmers, M. J.; Prasad, S.; Busby, S. A.; Kamenecka, T. M.; He, Y.; Nettles, K. W.; Griffin, P. R. Partial agonists activate PPARγ using a helix 12 independent mechanism. *Structure* **2007**, *15*, 1258-1271. DOI: 10.1016/j.str.2007.07.014.

(97) Norman, B. H.; Dodge, J. A.; Richardson, T. I.; Borromeo, P. S.; Lugar, C. W.; Jones, S. A.; Chen, K.; Wang, Y.; Durst, G. L.; Barr, R. J. Benzopyrans are selective estrogen receptor β agonists with novel activity in models of benign prostatic hyperplasia. *J. Med. Chem.* **2006**, *49*, 6155-6157. DOI: 10.1021/jm060491j.

(98) Wolber, G.; Dornhofer, A. A.; Langer, T. Efficient overlay of small organic molecules using 3D pharmacophores. *J. Comput. Aided Mol. Des.* **2006**, *20*, 773–788. DOI: 10.1007/s10822-006-9078-7 PubMed.

(99) *ROCS 3.4.3.0: OpenEye Scientific Software*; Santa Fe, NM., http://www.eyesopen.com (accessed.

(100) Hawkins, P. C.; Skillman, A. G.; Nicholls, A. Comparison of shape-matching and docking as virtual screening tools. *J. Med. Chem.* **2007**, *50*, 74-82. DOI: 10.1021/jm0603365.

(101) Molecular Operating Environment (MOE), C. C. G. U., Sherbooke St. West, Suite #910, Montreal, QC, Canada, H3A 2R7, 2021. https://www.chemcomp.com/Products.htm (accessed 01.03.2022).

(102) The UniProt Consortium. UniProt: the universal protein knowledgebase in 2021. *Nucleic Acids Res.* **2021**, *49*, D480-D489. DOI: 10.1093/nar/gkaa1100.

(103) Ramachandran, G. N.; Ramakrishnan, C.; Sasisekharan, V. Stereochemistry of polypeptide chain configurations. *J. Mol. Biol.* **1963**, *7*, 95–99. DOI: 10.1016/s0022-2836(63)80023-6 CrossRef.

(104) Zhu, S. Validation of the generalized force fields GAFF, CGenFF, OPLS-AA, and PRODRGFF by testing against experimental osmotic coefficient data for small drug-like molecules. *J. Chem. Inf. Model.* **2019**, *59*, 4239–4247. DOI: 10.1021/acs.jcim.9b00552 PubMed.

(105) Labute, P. Protonate3D: assignment of ionization states and hydrogen coordinates to macromolecular structures. *Proteins* **2009**, *75*, 187–205. DOI: 10.1002/prot.22234 PubMed.

(106) Jones, G.; Willett, P.; Glen, R. C.; Leach, A. R.; Taylor, R. Development and validation of a genetic algorithm for flexible docking. *J. Mol. Biol.* **1997**, *267*, 727–748. DOI: 10.1006/jmbi.1996.0897 PubMed.

(107) Evers, A.; Hessler, G.; Matter, H.; Klabunde, T. Virtual screening of biogenic amine-binding G-protein coupled receptors: comparative evaluation of protein- and ligand-based virtual screening protocols. *J. Med. Chem.* **2005**, *48*, 5448–5465. DOI: 10.1021/jm050090o PubMed.

(108) Verdonk, M. L.; Cole, J. C.; Hartshorn, M. J.; Murray, C. W.; Taylor, R. D. Improved protein-ligand docking using GOLD. *Proteins* **2003**, *52*, 609–623. DOI: 10.1002/prot.10465 PubMed.

(109) Schrödinger Release -4: Maestro; 2020-4, v.; Schrödinger; LLC; New York; NY; USA. 2020.

(110) Bowers, K. J.; Chow, D. E.; Xu, H.; Dror, R. O.; Eastwood, M. P.; Gregersen, B. A.; Klepeis, J. L.; Kolossvary, I.; Moraes, M. A.; Sacerdoti, F. D.; et al. Scalable algorithms for molecular dynamics simulations on commodity clusters. In *Proceedings of the ACM/IEEE Conference on Supercomputing (SC06)*, Tampa, Florida, USA, 11–17 November, 2006; Bowers, K. J., Chow, E., Xu, H., Dror, R. O., Eastwood, M. P., Gregersen, B. A., Klepeis, J. L., Kolossvary, I., Moraes, M. A., Sacerdoti, F. D., et al., Eds.

(111) Lomize, M. A.; Pogozheva, I. D.; Joo, H.; Mosberg, H. I.; Lomize, A. L. OPM database and PPM web server: resources for positioning of proteins in membranes. *Nucleic Acids Res.* **2012**, *40*, D370-D376. DOI: 10.1093/nar/gkr703.

(112) Boonstra, S.; Onck, P. R.; van der Giessen, E. CHARMM TIP3P water model suppresses peptide folding by solvating the unfolded state. *J. Phys. Chem. B* **2016**, *120*, 3692-3698. DOI: 10.1021/acs.jpcb.6b01316.

(113) Gullingsrud, J. *DEShawResearch. viparr-ffpublic*. https://github.com/DEShawResearch/viparr-ffpublic (accessed 2022 08.08.2022).

(114) Tucker, M. R.; Piana, S.; Tan, D.; LeVine, M. V.; Shaw, D. E. Development of force field parameters for the simulation of single- and double-stranded DNA molecules and DNA–protein complexes. *J. Phys. Chem. B* **2022**, *126*, 4442-4457. DOI: 10.1021/acs.jpcb.1c10971.

(115) Humphrey, W.; Dalke, A.; Schulten, K. VMD: Visual molecular dynamics. *J. Mol. Graph.* **1996**, *14*, 33–38. DOI: 10.1016/0263-7855(96)00018-5 CrossRef.

(116) Sydow, D. *Dynophores: Novel dynamic pharmacophores implementation of pharmacophore generation based on molecular dynamics trajectories and their graphical representation*; Freie Universität Berlin, 2015.

(117) Bradford, M. M. A rapid and sensitive method for the quantitation of microgram quantities of protein utilizing the principle of protein-dye binding. *Anal. Biochem.* **1976**, *72*, 248-254. DOI: 10.1016/0003-2697(76)90527-3.

(118) Cheng, Y.-C.; Prusoff, W. H. Relationship between the inhibition constant (KI) and the concentration of inhibitor which causes 50 per cent inhibition (I50) of an enzymatic reaction. *Biochem. Pharmacol.* **1973**, *22*, 3099-3108. DOI: 10.1016/0006-2952(73)90196-2.

Insert Table of Contents artwork here

Virtual Screening

R_1=Cl, R_2=H
R_1=H, R_2=F

3M

Salvinorin A at KOR

Novel KOR Agonists

Discovery of Novel, Selective, and Non-basic Agonists for the Kappa-Opioid Receptor Determined by Salvinorin A-Based Virtual Screening

Kristina Puls[1], Aina-Leonor Olivé-Marti[2], David Lamp[2], Mariana Spetea[2]* and Gerhard Wolber[1]*

[1]Department of Pharmaceutical Chemistry, Institute of Pharmacy, Freie Universität Berlin, Königin-Luise-Str. 2-4, 14195 Berlin, Germany; kristina.puls@fu-berlin.de (K.P.) gerhard.wolber@fu-berlin.de

[2]Department of Pharmaceutical Chemistry, Institute of Pharmacy and Center for Molecular Biosciences Innsbruck (CMBI), University of Innsbruck, Innrain 80-82, 6020 Innsbruck, Austria; aolive.marti@gmail.com (A.-L.O.-M) davidlamp42@gmail.com (D.L.) mariana.spetea@uibk.ac.at (M.S.)

*Correspondence: gerhard.wolber@fu-berlin.de (G.W.); mariana.spetea@uibk.ac.at (M.S.); Tel.: +49-30-838-52686 (G.W.); +43-512-507-58277 (M.S.)

Table of Contents

1. Natural Products with Opioid Activity

Morphine

Mitragynine (R = H)
7-OH Mitragynine (R = OH)

Mitragynine pseudoindoxyl

Rubiscolin-5
(YPLDL)

Rubiscolin-6
(YPLDLF)

Figure S1. Chemical structures of natural products with reported activity at the opioid receptors.

2. Binding Mode of SalA, MomSalB, and MP1104 at the KOR
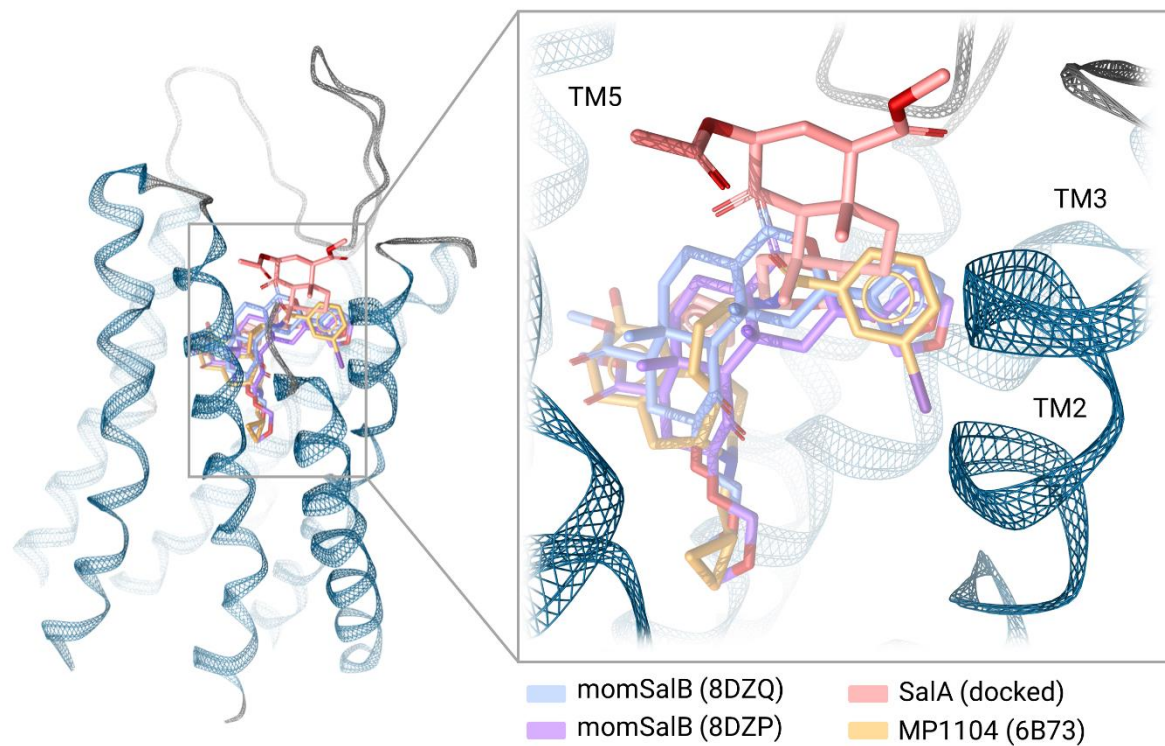
Figure S2. Binding mode comparison between momSalB (PDB-IDs: 8DZQ, 8DZP), docked SalA[1] and morphinan agonist MP1104 at the KOR (PDB-ID: 6B73). MomSalB binds deep into the orthosteric binding site analog morphinan ligands and nicely overlaps with the co-crystallized agonist MP1104. However, momSalB occupies a pocket highly conserved among the opioid receptors that disagrees with the outstanding KOR selectivity of momSalB.

3. Cryo-EM Map of KOR-MomSalB Complex
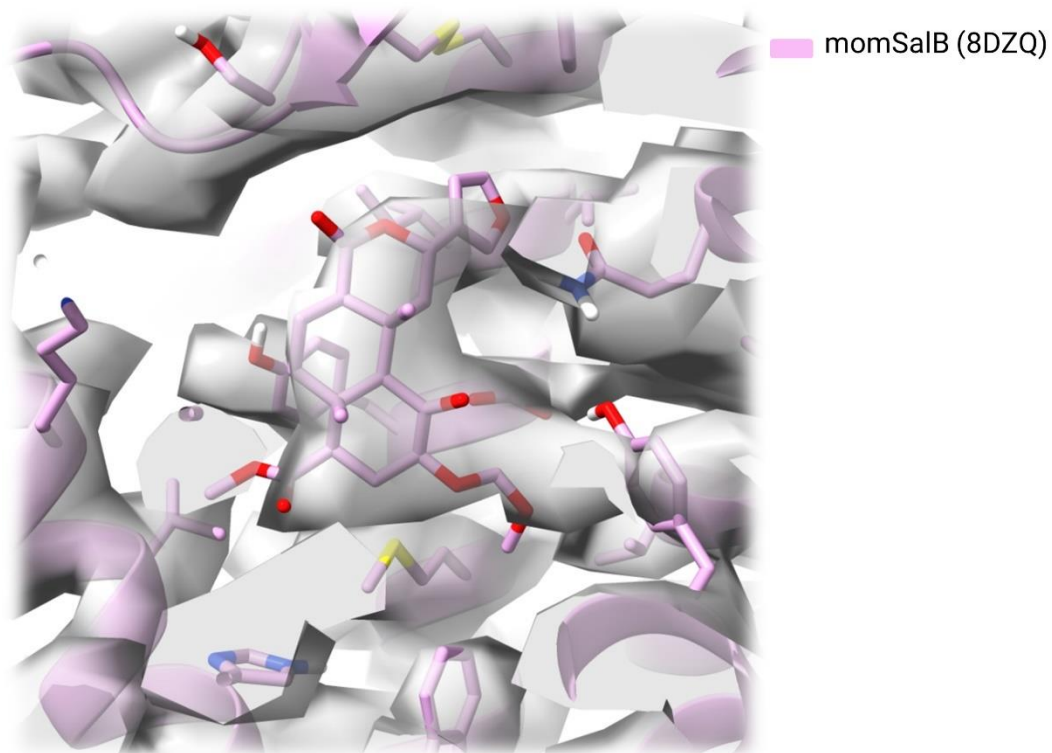
momSalB (8DZQ)

Figure S3. Cryo-EM map of momSalB bound to the KOR (PDB-ID: 8DZQ). The cryo-EM map supports the binding mode of momSalB at the KOR. However, limited information about the clustering and selection procedures of conformational states are given in the publication[2]. Usually only a small fraction of particles of the cryo-EM experiment are evaluated for the final model leaving the potential for alternative ligand conformations. Cryo-EM experiments were conducted with 10 µM ligand concentration.

4.Superimposition of KOR-MomSalB with MOR and DOR
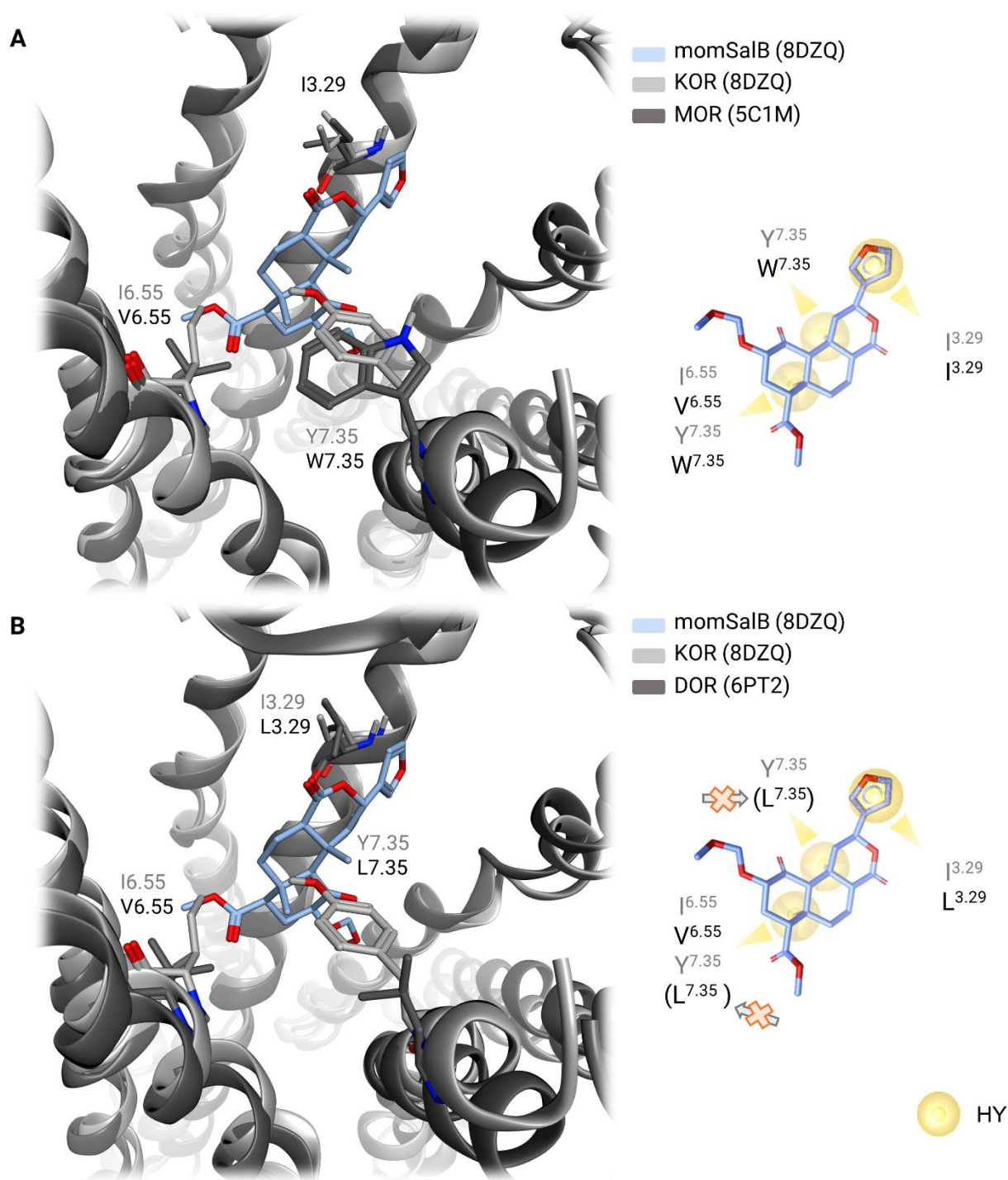
Figure S4. Interaction pattern of momSalB with non-conserved residues of the KOR and whether they can be maintained in the MOR or DOR. MomSalB participates in hydrophobic contacts (HY) to three residues of KOR that are not conserved within the three classical receptor subtypes (I3.29, I6.55, Y7.35). Panel A shows an overlay of momSalB bound to the active state KOR (PDB-ID: 8DZQ) and the active state MOR (PDB-ID: 5C1M) while panel B shows the overlay with the active state DOR (PDB-ID: 6PT2). In the MOR all interactions could be maintained while in the DOR all interactions except the hydrophobic contacts to residue 7.35 could be maintained. The maintenance of

interaction patterns in the MOR and DOR contrasts with the strong KOR selectivity of momSalB. No potential atom clashes with any residues within 4.5 Å around momSalB could be identified.

5. SalA-SAR and Dynamic Investigation of KOR-SalA and KOR-MomSalB

A

Ligand	C2-substituent
SalA	R—O—acetyl
SalB	R—OH
momSalB	R—O—O—

B

C2-substituent	C4-substituent
R—Cl	R—O—
R—H	R—O—
R—Br	

C Hydogen bonding frequency within MD simulations.

Substi-tuent	8DZQ mom SalB	8DZP mom SalB	SalA dock
C1	15.7%	25.6%	79.0%
C2	<5%	<5%	17.6%
C4	25.8%	6.7%	94.1%
C17	37.7%	13.9%	54.0%

D

E

F
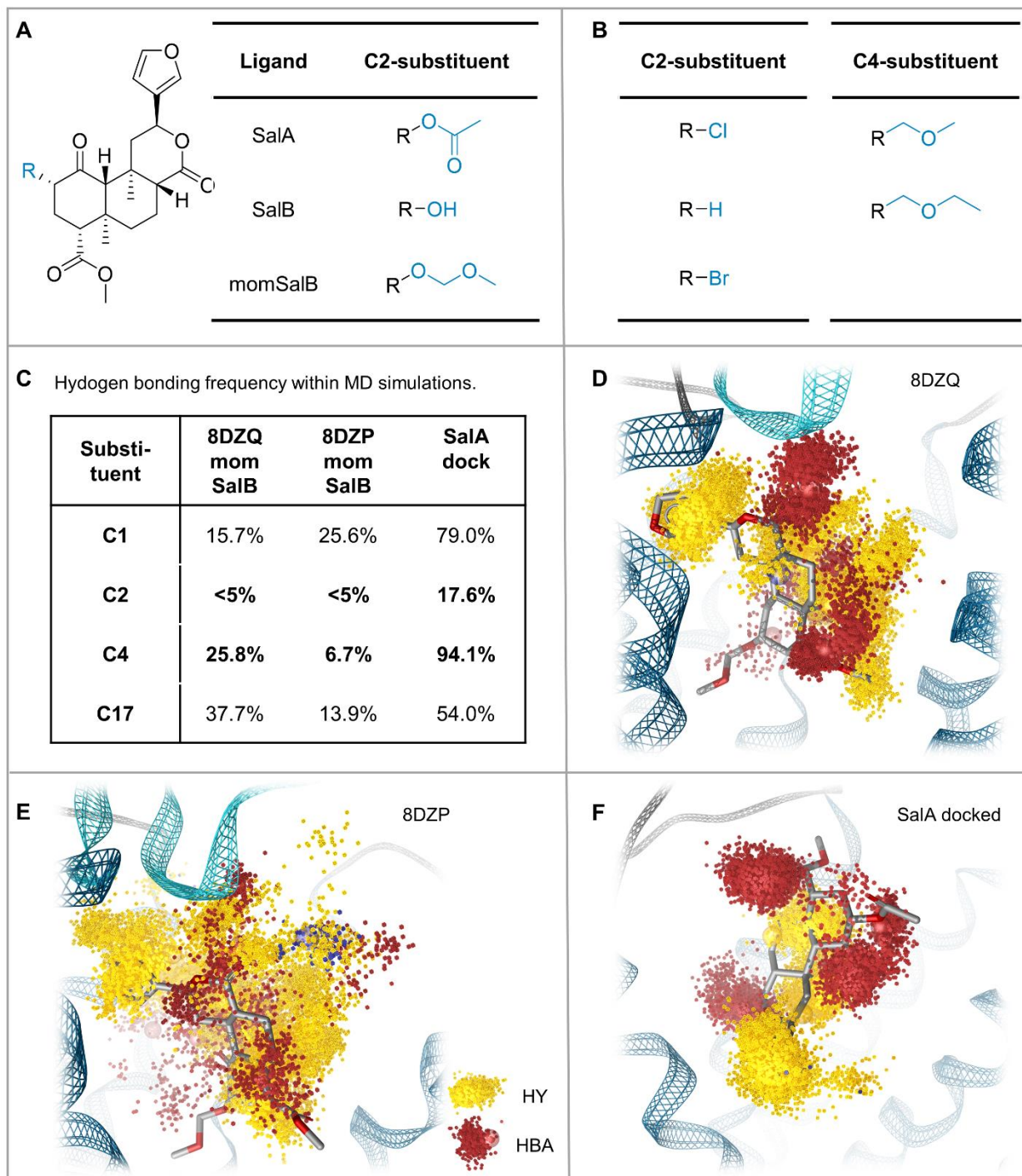
Figure S5. Dynamic protein-ligand interaction patterns of SalA and momSalB at the KOR. A) Chemical structure of SalA, momSalB and inactive metabolite SalB. B) SalA derivatives with strongly reduced affinity and activity[3] that together with SalB indicate a crucial role for hydrogen bonds for SalA's activity at KOR. C) Hydrogen bond acceptor frequency detected in MD simulations. MomSalB barely participates in hydrogen bonding and lacks crucial C2-interactions. The most frequent hydrogen bonding for momSalB is detected for its C17-carbonyl moiety. However, this interaction is neglectable for affinity as the complete reduction of the carbonyl moiety in SalA did not affect the

affinity[3]. D-F) Dynophore (dynamic pharmacophore) representation of protein-ligand interactions detected during MD simulations. The blurrier the feature clouds, the more movement of the ligand.

6. MD Simulations of KOR-SalA and KOR-MomSalB

Ligand RMSD during MD simulations
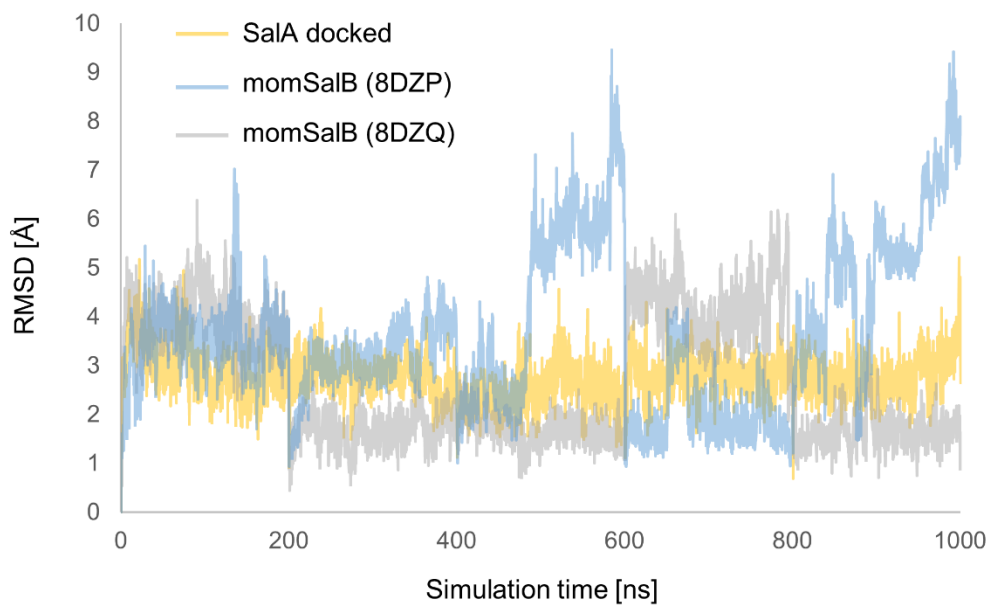
Figure S6. Ligand root mean square deviation (RMSD) in MD simulations at the KOR. Each ligand-KOR complex was modeled in five replicates of 200 ns each or 1000 ns in total. The MD simulations of SalA were used from[1] performed with the same settings as for momSalB. In several replicates of momSalB in both complexes the ligand moves strongly within the binding site.

7. KOR-Ligand Interactions of SalA and MomSalB to Important Residues from Mutagenesis Studies

Residue	MomSalB	SalA
Q115[2.60]	-	HBA (MDs)
Y312[7.35]	HY	HBA/HY
Y313[7.36]	-	HBA/HY
I316[7.39]	HY	HY
Y119[7.42]	-	-
Y320[7.43]	-	-

■ momSalB (8DZQ)   ■ SalA (docked)
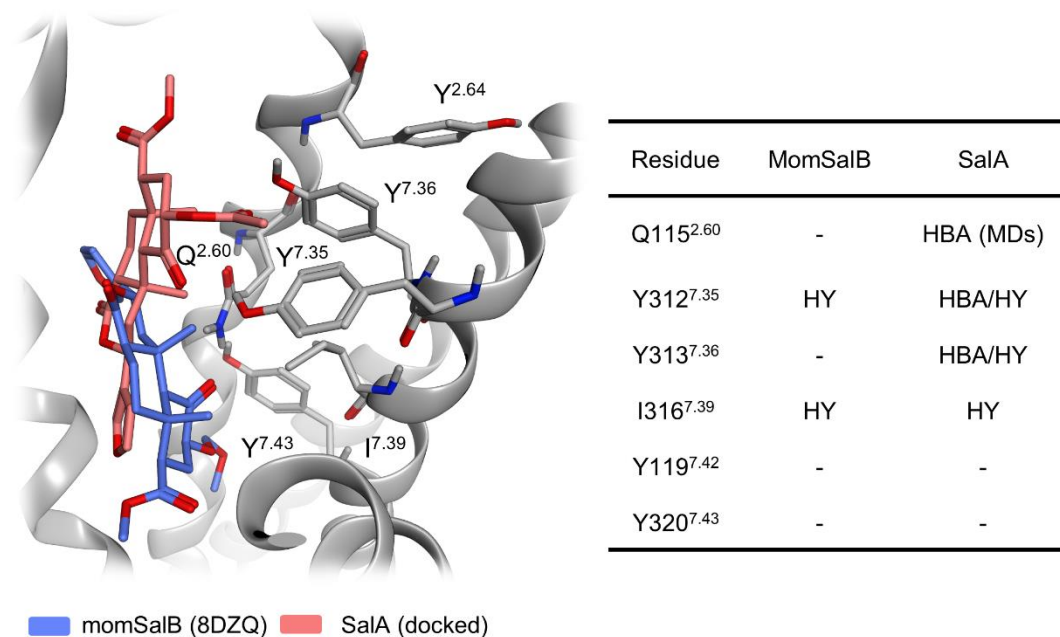
Figure S7. Interactions of SalA and momSalB (PDB-IDs: 8DZQ, 8DZP) to the KOR residues highlighted as important in mutagenesis studies[4-6]. SalA from[1] interacts with four out of six amino acids of which hydrogen bonding to Q115[2.60] only occurs within the dynamic investigation. In contrast, momSalB only participates in hydrophobic contacts to two residues in both cryo-EM models in the static and dynamic investigation. For the sake of clarity only momSalB from 8DZQ is shown in the left part, but the discussed interaction pattern is true for both cryo-EM models. As discussed in[1] Y119[7.42] does not point towards the binding site. Thus, direct interactions to the ligand are rather doubtful and its importance for SalA's activity likely results from its influence on adjacent residues like Y313[7.36]. Similarly, Y320[7.43], that was shown to affect KOR activation for peptides, small molecules, basic ligands, and non-basic ligands, likely exhibits its effects by influencing adjacent W287[6.48] of the conserved CWxP motif involved in receptor activation. Abbreviations used: HY = hydrophobic contact, HBA = Hydrogen bond acceptor.

8. Binding Mode Differences of Similar Ligands or for Closely Related Proteins
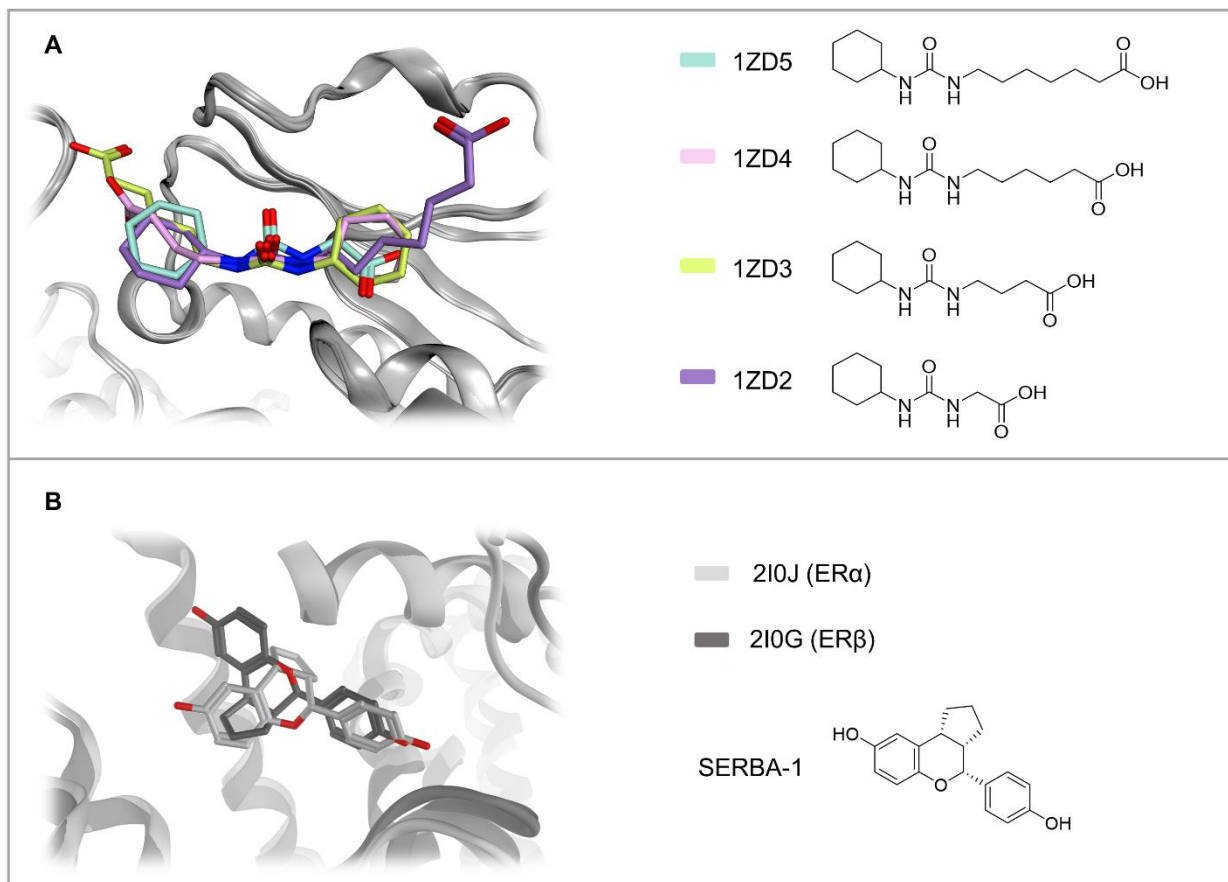
Figure S8 Examples for similar ligands that bind differently at the same protein (A) or the same ligand that exhibits distinct binding modes at closely related receptors (B). A) A ligand series shows inverse binding modes at the soluble epoxide hydrolases[7]. B) The ligand SERBA-1 adopts flipped conformations in estrogen receptor subtypes α and β[8].

9. HPLC Data for Virtual Screening Hits with Experimental Validation

SalA-VS-01

Data file:	2023-03-16 11-37-23+01-00-28.dx		
Sequence Name:	HPLC-UV-2023-03-16 04-50-04+01-00	**Project Name:**	Wahlpflicht_HPLC_WS22_23
Sample name:	K1	**Operator:**	SYSTEM (SYSTEM)
Instrument:	HPLC-UV	**Injection date:**	2023-03-16 11:38:07+01:00
Inj. volume:	2.000 µL	**Location:**	73
Acq. method:	AG_Wolber_C18_95_5.amx	**Type:**	Sample
Processing method:	*Auswertung_Purity_Wolber.pmx	**Sample amount:**	0.00
Manually modified:	None		

* DAD1A,Sig=254,4 Ref=360,100 [b]
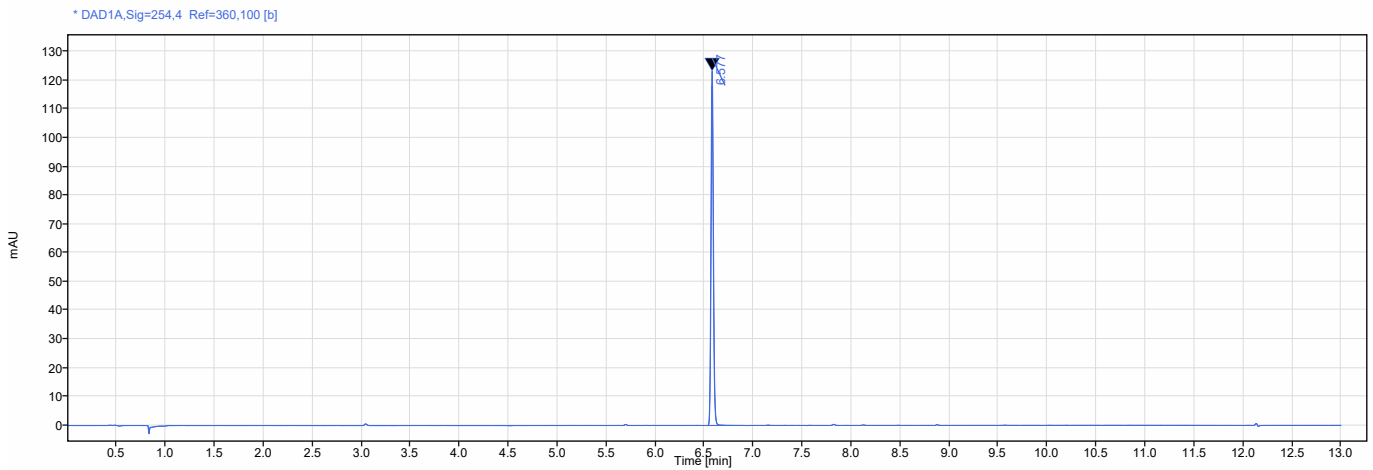
Signal: * DAD1A,Sig=254,4 Ref=360,100 [b]

RT [min]	Type	Width [min]	Area	Height	Area%	Name
6.577	BV	0.18	205.15	123.19	100.00	
		Sum	**205.15**			

SalA-VS-02

Data file:	2023-03-16 12-07-55+01-00-30.dx		
Sequence Name:	HPLC-UV-2023-03-16 04-50-04+01-00	**Project Name:**	Wahlpflicht_HPLC_WS22_23
Sample name:	K3	**Operator:**	SYSTEM (SYSTEM)
Instrument:	HPLC-UV	**Injection date:**	2023-03-16 12:08:39+01:00
Inj. volume:	2.000 µL	**Location:**	75
Acq. method:	AG_Wolber_C18_95_5.amx	**Type:**	Sample
Processing method:	*Auswertung_Purity_Wolber.pmx	**Sample amount:**	0.00
Manually modified:	None		
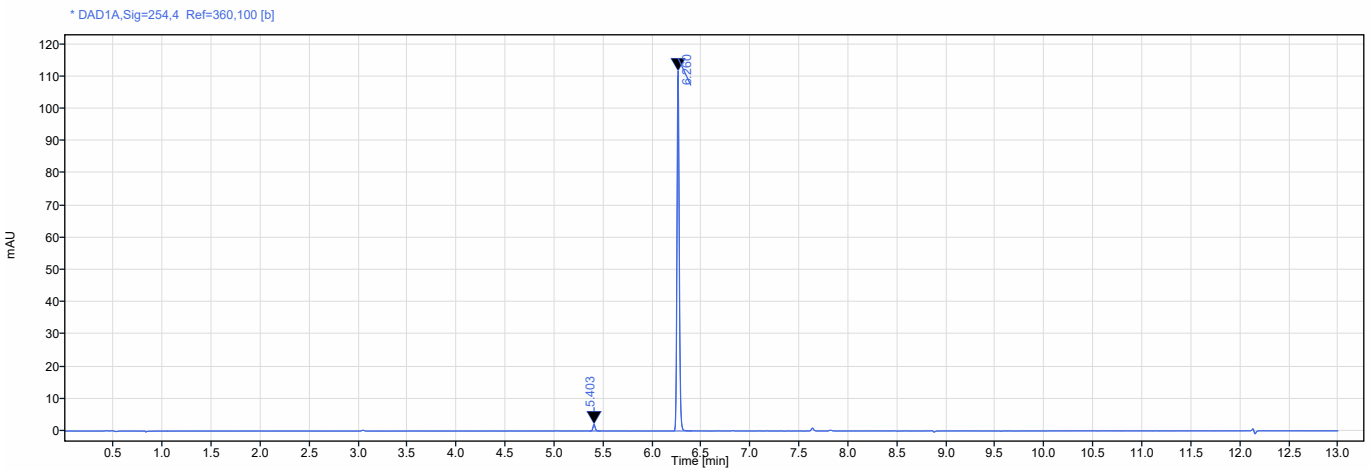
Signal: * DAD1A,Sig=254,4 Ref=360,100 [b]

RT [min]	Type	Width [min]	Area	Height	Area%	Name
5.403	BV	0.11	3.29	2.02	1.80	
6.260	BV	0.19	179.24	111.56	98.20	
		Sum	**182.53**			

SalA-VS-03

Data file:	2023-03-16 12-23-10+01-00-31.dx		
Sequence Name:	HPLC-UV-2023-03-16 04-50-04+01-00	**Project Name:**	Wahlpflicht_HPLC_WS22_23
Sample name:	K4	**Operator:**	SYSTEM (SYSTEM)
Instrument:	HPLC-UV	**Injection date:**	2023-03-16 12:23:54+01:00
Inj. volume:	2.000 µL	**Location:**	76
Acq. method:	AG_Wolber_C18_95_5.amx	**Type:**	Sample
Processing method:	*Auswertung_Purity_Wolber.pmx	**Sample amount:**	0.00
Manually modified:	None		

* DAD1A,Sig=254,4 Ref=360,100 [b]
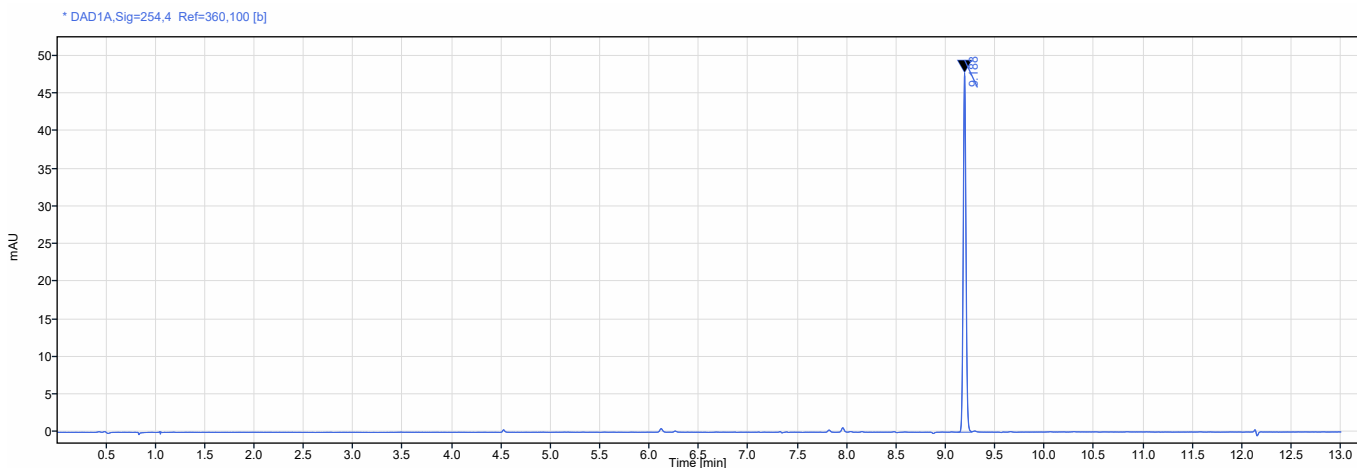
Signal: * DAD1A,Sig=254,4 Ref=360,100 [b]

RT [min]	Type	Width [min]	Area	Height	Area%	Name
9.188	BV	0.15	92.18	47.67	100.00	
		Sum	**92.18**			

SalA-VS-04

Agilent

Data file:	2023-03-16 12-38-27+01-00-32.dx		
Sequence Name:	HPLC-UV-2023-03-16 04-50-04+01-00	**Project Name:**	Wahlpflicht_HPLC_WS22_23
Sample name:	K5	**Operator:**	SYSTEM (SYSTEM)
Instrument:	HPLC-UV	**Injection date:**	2023-03-16 12:39:12+01:00
Inj. volume:	2.000 µL	**Location:**	77
Acq. method:	AG_Wolber_C18_95_5.amx	**Type:**	Sample
Processing method:	*Auswertung_Purity_Wolber.pmx	**Sample amount:**	0.00
Manually modified:	None		

* DAD1A,Sig=254,4 Ref=360,100 [b]
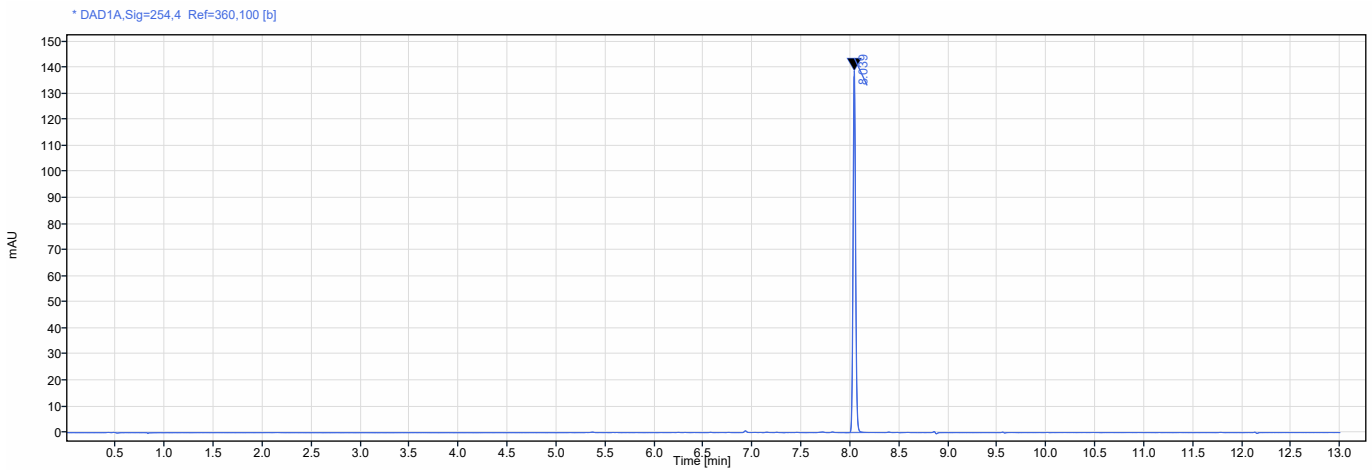
Signal: * DAD1A,Sig=254,4 Ref=360,100 [b]

RT [min]	Type	Width [min]	Area	Height	Area%	Name
8.039	BV	0.25	246.49	138.55	100.00	
		Sum	**246.49**			

SalA-VS-05

<table>
<tr><td>Data file:</td><td>2023-03-16 12-53-45+01-00-33.dx</td><td></td><td></td></tr>
<tr><td>Sequence Name:</td><td>HPLC-UV-2023-03-16 04-50-04+01-00</td><td>Project Name:</td><td>Wahlpflicht_HPLC_WS22_23</td></tr>
<tr><td>Sample name:</td><td>K6-A</td><td>Operator:</td><td>SYSTEM (SYSTEM)</td></tr>
<tr><td>Instrument:</td><td>HPLC-UV</td><td>Injection date:</td><td>2023-03-16 12:54:28+01:00</td></tr>
<tr><td>Inj. volume:</td><td>2.000 µL</td><td>Location:</td><td>78</td></tr>
<tr><td>Acq. method:</td><td>AG_Wolber_C18_95_5.amx</td><td>Type:</td><td>Sample</td></tr>
<tr><td>Processing method:</td><td>*GC_LC Area Percent_DefaultMethod.pmx</td><td>Sample amount:</td><td>0.00</td></tr>
<tr><td>Manually modified:</td><td>Manual Integration</td><td></td><td></td></tr>
</table>
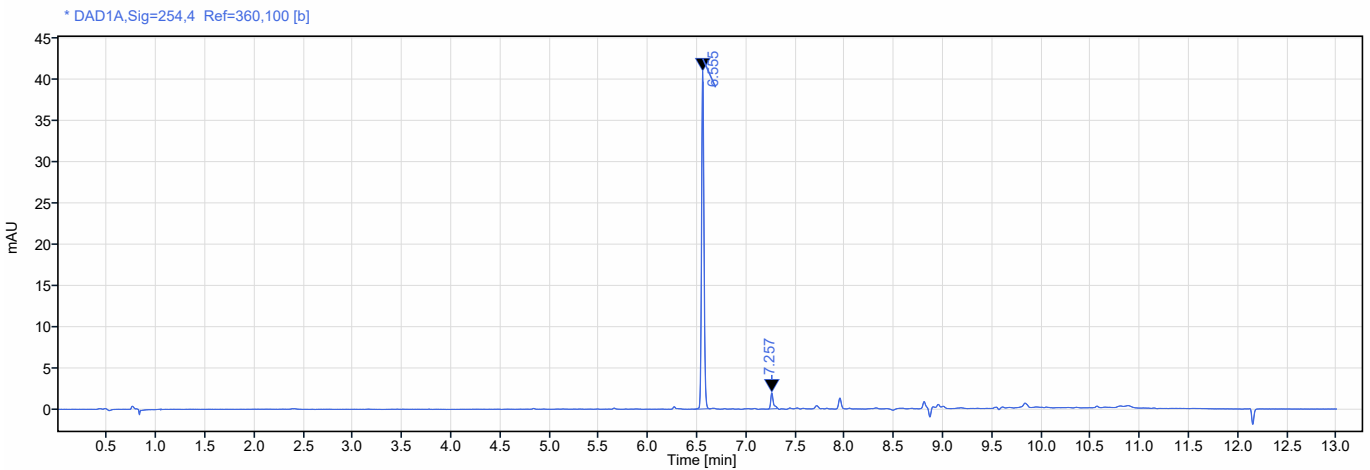
Signal: * DAD1A,Sig=254,4 Ref=360,100 [b]

RT [min]	Type	Width [min]	Area	Height	Area%	Name
6.555	VM m	0.18	69.72	40.85	95.11	
7.257	MM m	0.10	3.58	1.93	4.89	
		Sum	**73.31**			

SalA-VS-06

Single Injection Report

Agilent

Data file:	2023-03-16 13-24-19+01-00-35.dx			
Sequence Name:	HPLC-UV-2023-03-16 04-50-04+01-00	**Project Name:**	Wahlpflicht_HPLC_WS22_23	
Sample name:	K7	**Operator:**	SYSTEM (SYSTEM)	
Instrument:	HPLC-UV	**Injection date:**	2023-03-16 13:25:04+01:00	
Inj. volume:	2.000 µL	**Location:**	80	
Acq. method:	AG_Wolber_C18_95_5.amx	**Type:**	Sample	
Processing method:	*Auswertung_Purity_Wolber.pmx	**Sample amount:**	0.00	
Manually modified:	None			
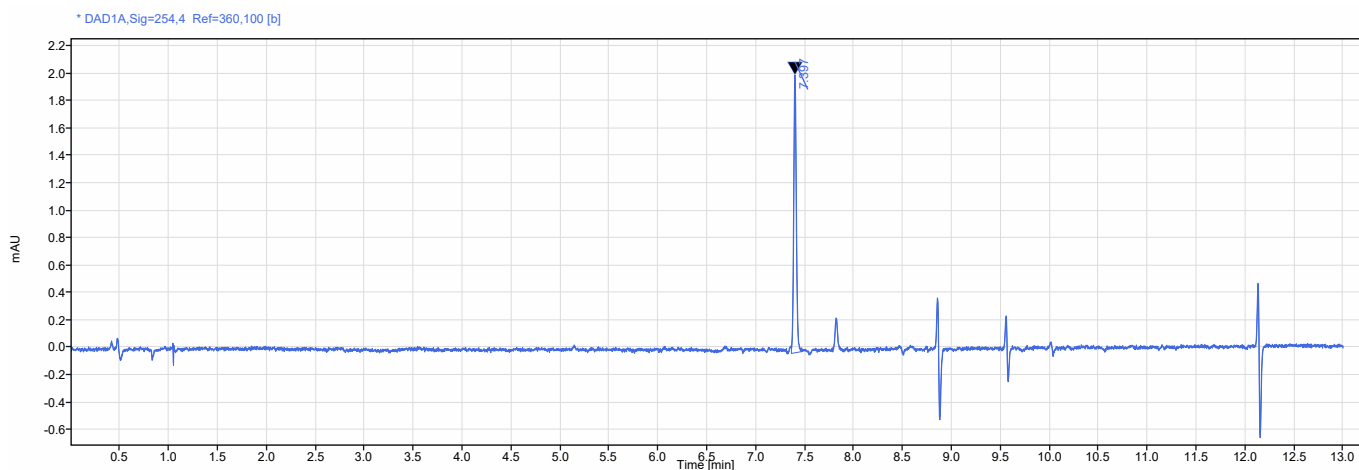
Signal: * DAD1A,Sig=254,4 Ref=360,100 [b]

RT [min]	Type	Width [min]	Area	Height	Area%	Name
7.397	VB	0.11	3.72	2.02	100.00	
		Sum	**3.72**			

SalA-VS-07

Sample name: 7135_1F1

Analysis method: ACDFINAL.M

Injection volume: 0.100

Injection date: 8/14/2019 1:54:57 PM

Acq. operator: chemist

Instrument: uHPLC Agilent 1290 Infinity

Description: Column: ACQUITY UHPLC BEH C18 (1.7μm) 2.1mmx50mm T40°C Detection: DAD + 6120 Quadrupole Flow: 1.2mL/min. SolventA: Water+0.1% formic acid SolventB:MeCN+0.1% formic acid;Gradient:0min.2%B;0.2min.2%B;2.0min.98% B;2.2min.98%B., 2.21min.2%B;2.5min.2%B;200-300nm+215nm

DAD1 A, Sig=250,100 Ref=off

1.501

1.352 1.442 1.466 1.837

DAD1 C, Sig=215,4 Ref=off

1.501

1.356 1.836

MSD1 SPC, MM-ES+APCI

RT= 1.542 min

413
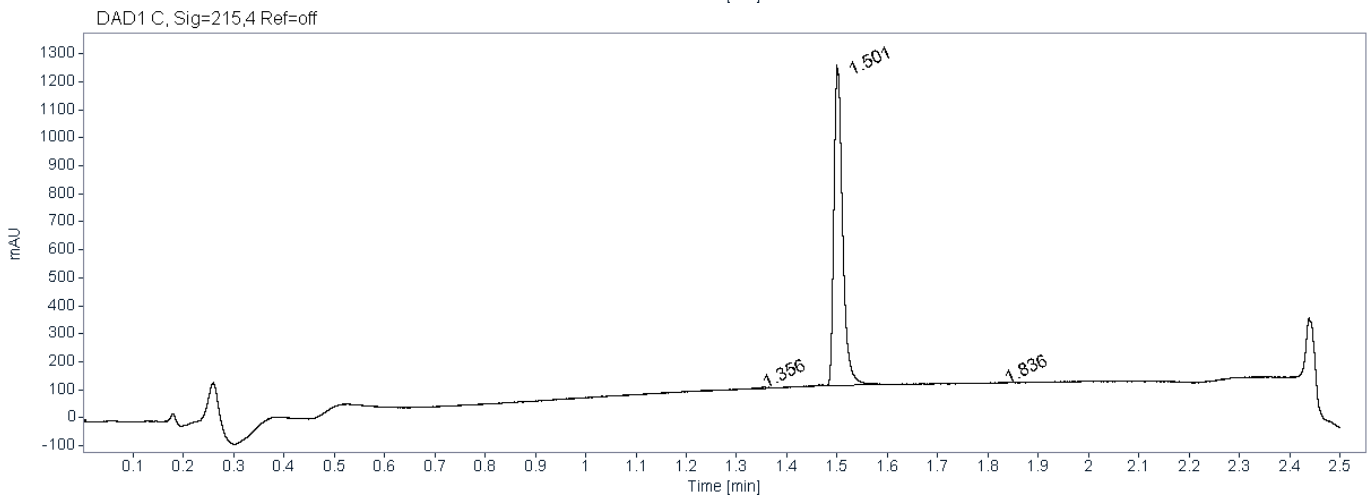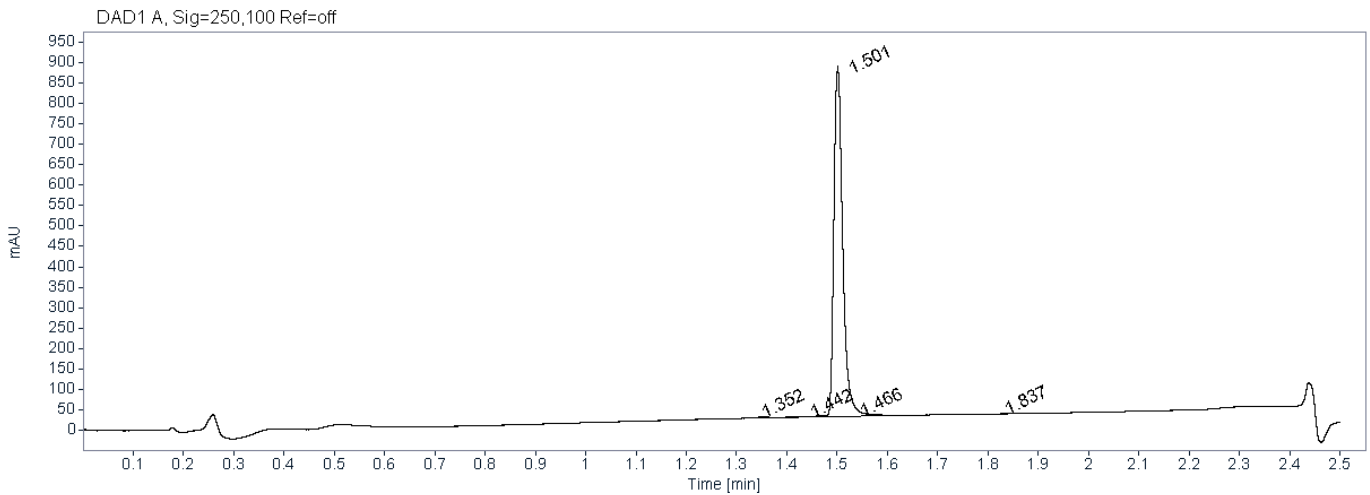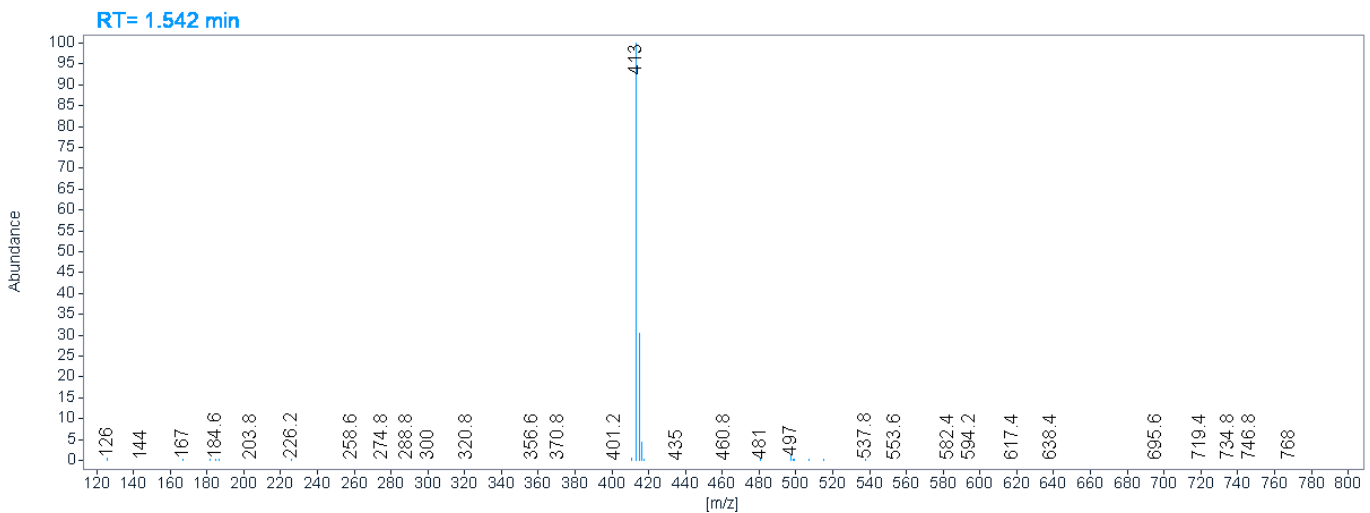
Signal: DAD1 A, Sig=250,100 Ref=off

RT [min]	Peak Area Percent
1.352	0.29
1.442	0.27
1.466	0.37
1.501	98.75
1.837	0.32

Signal: DAD1 C, Sig=215,4 Ref=off

RT [min]	Peak Area Percent
1.356	0.44
1.501	99.17
1.836	0.39

SalA-VS-08

DAD1 A, Sig=250,100 Ref=off

DAD1 C, Sig=215,4 Ref=off

MSD1 SPC, MM-ES+APCI

RT= 1.461 min
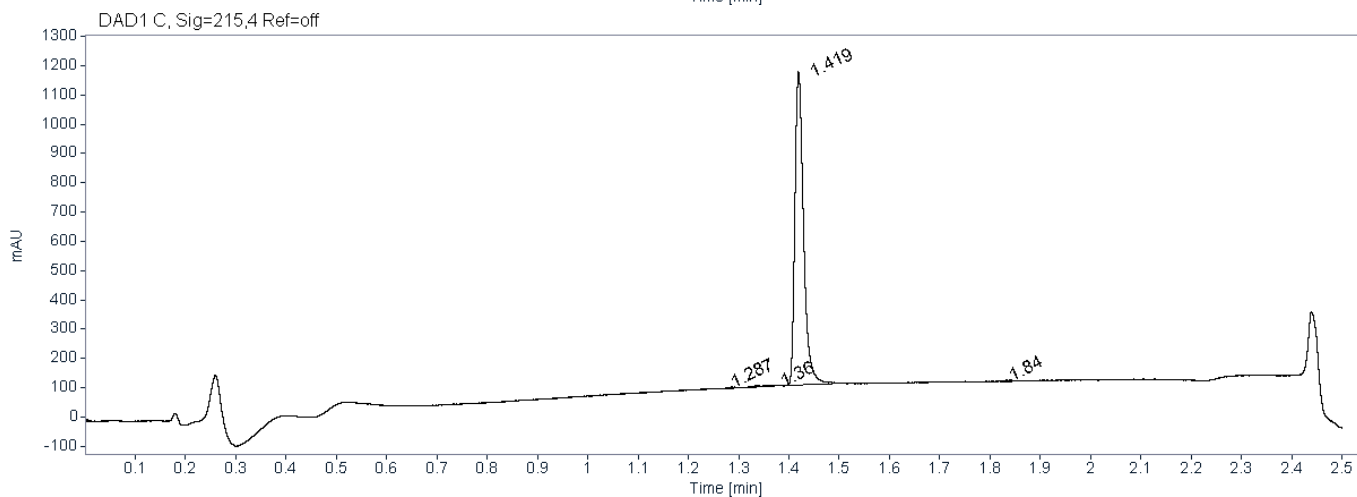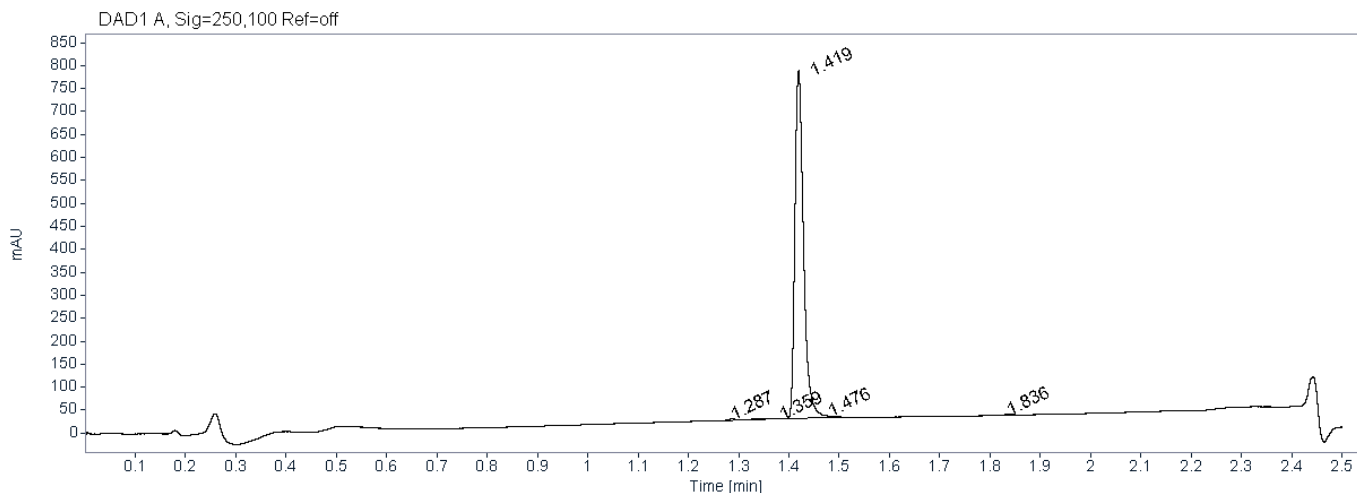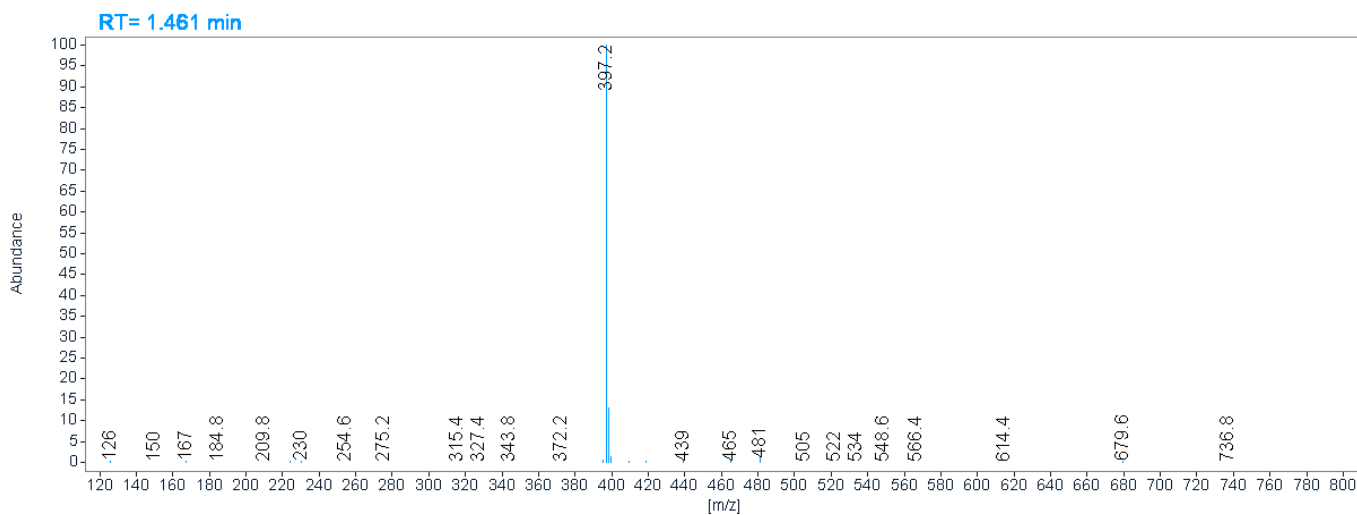
Signal: DAD1 A, Sig=250,100 Ref=off

RT [min]	Peak Area Percent
1.287	0.34
1.359	0.62
1.419	98.09
1.476	0.67
1.836	0.29

Signal: DAD1 C, Sig=215,4 Ref=off

RT [min]	Peak Area Percent
1.287	0.30
1.360	0.71
1.419	98.66
1.840	0.33

SalA-VS-09

Sample name: 7120_1F1

Analysis method: ACDFINAL.M

Injection volume: 0.500

Injection date: 11/5/2019 11:27:39 PM

Acq. operator: chemist

Instrument: uHPLC Agilent 1290 Infinity

Description: Column: ACQUITY UHPLC BEH C18 (1.7µm) 2.1mmx50mm T40°C Detection: DAD + 6120 Quadrupole Flow: 1.2mL/min. SolventA: Water+0.1% formic acid SolventB:MeCN+0.1% formic acid;Gradient:0min.2%B;0.2min.2%B;2.0min.98% B;2.2min.98%B., 2.21min.2%B;2.5min.2%B;200-300nm+215nm

DAD1 A, Sig=250,100 Ref=off

DAD1 C, Sig=215,4 Ref=off

MSD1 SPC, MM-ES+APCI

RT= 1.108 min
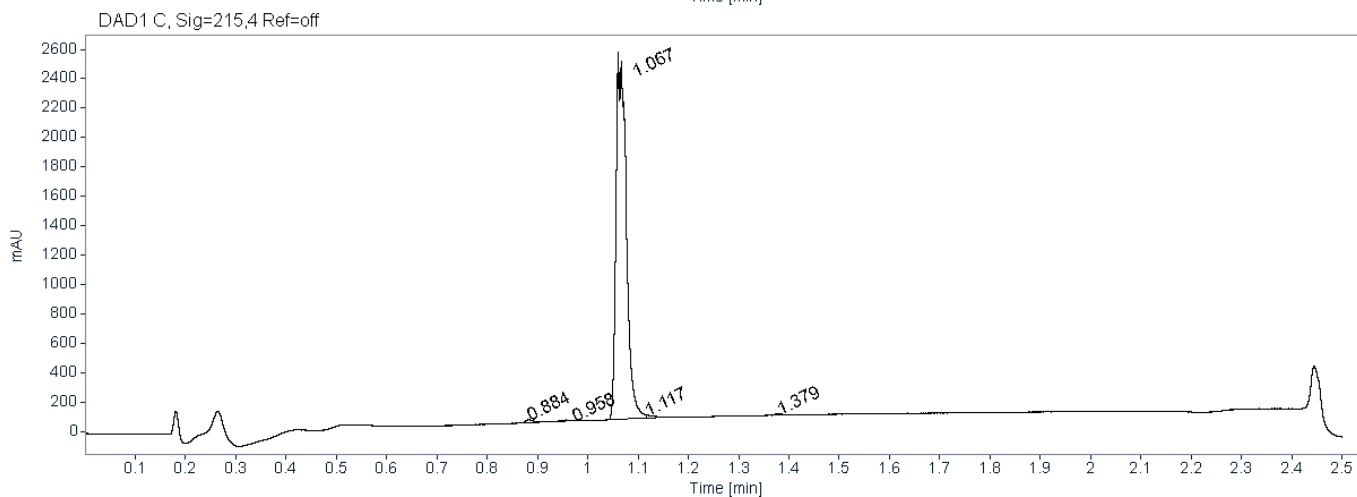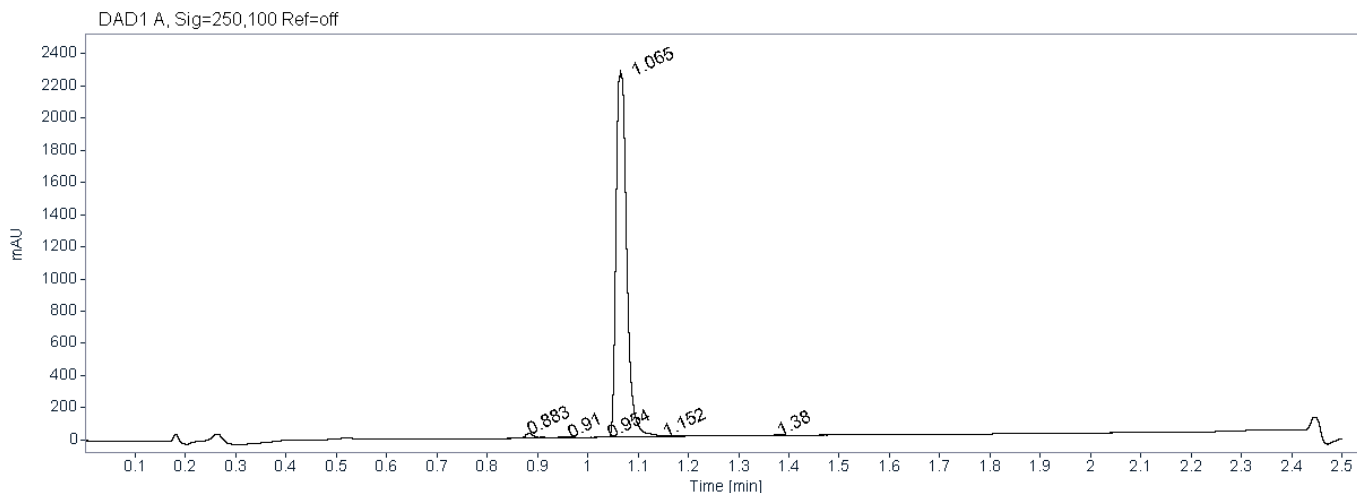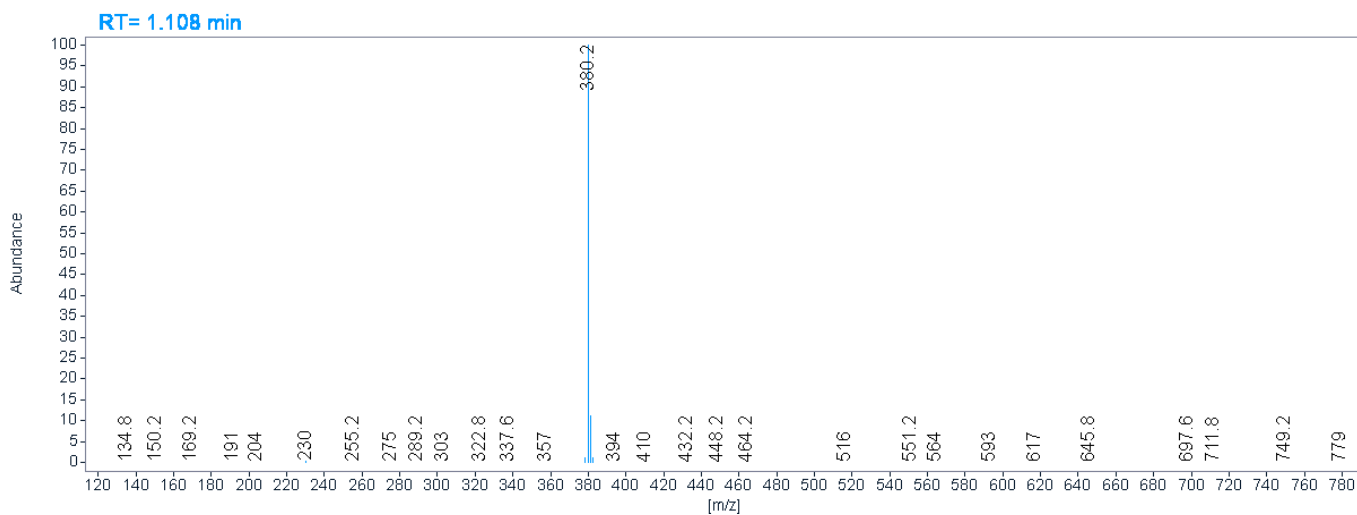
Signal: DAD1 A, Sig=250,100 Ref=off

RT [min]	Peak Area Percent
0.883	0.91
0.910	0.12
0.954	0.25
1.065	98.13
1.152	0.35
1.380	0.24

Signal: DAD1 C, Sig=215,4 Ref=off

RT [min]	Peak Area Percent
0.884	0.63
0.958	0.36
1.067	98.07
1.117	0.56
1.379	0.38

Manager Report

D-7000 HPLC System Manager Report

Analyzed:	31.10.20 11:19	**Reported:**	4. November 2020
System Name:	Sys 1	**HPLC Method:**	HPLC-Megdex (kurz) Kurz-Gradient, Megdex mittels ELSD + evtl. UV-Detektion
Proc. Method:	C-3357-H		
Application:	Extrabolite	**Series:**	6433
Vial Number:	47	**Sample Name:**	C-3357-H-D11
Vial Type:	UNK	**Volume:**	17,0 ul
Injection from vial:	1 of 1	**Sample Description:**	

Channel 1

Chrom Type: HPLC Channel : 1

HPLC System: Anlage 9 (kurz)
Detection: ELSD
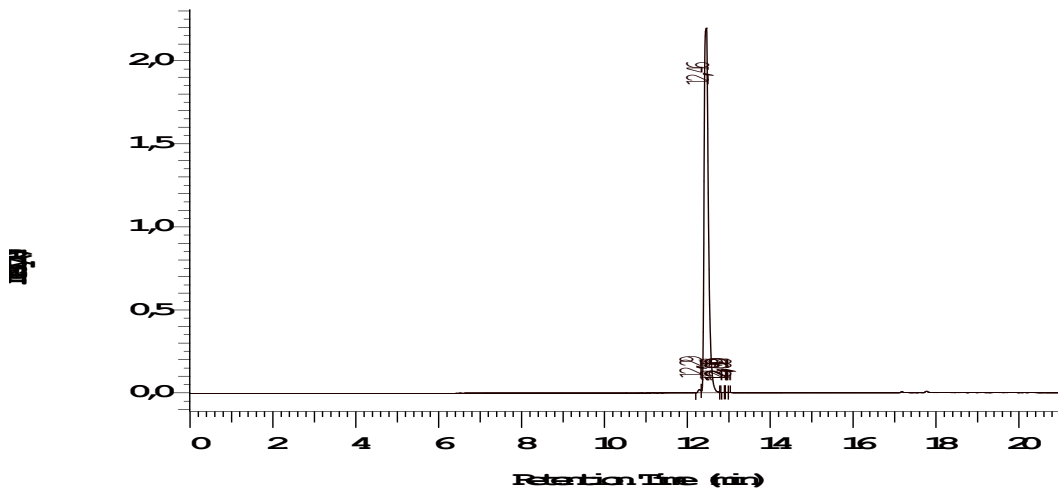
No.	RT	Area	Height	Area %
1	12,29	44.154	9598	0,577
2	12,46	7.586.203	1097593	99,212
3	12,78	1.594	1109	0,021
4	12,89	5.177	1660	0,068
5	12,9	1.467	1668	0,019
6	12,92	6.190	1675	0,081
7	13	1.645	772	0,022
		7.646.430	1114075	100

Segment#1

Intensity
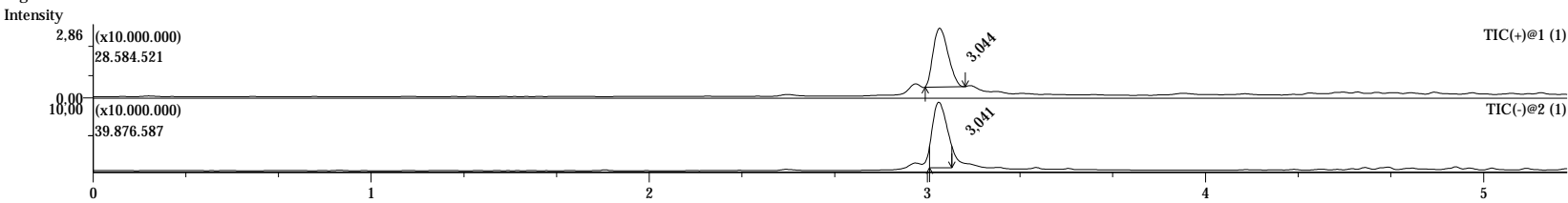
Peak#	Ret. Time	Area	Area%
1	2,965	61715	1,507
2	3,051	4029419	98,408
3	4,265	3457	0,084
Total		4094590	100,000

PDA Ch1 215nm

Peak#	Ret. Time	Area	Area%
Total			

ELSD

V

AU

1 PDA Multi 1 215nm,4nm

Positive3,044

Negative3,042

SalA-VS-11

Intensity

10,00 (x10.000.000)
30.713.986

TIC(+)@1

5.079

2,64 (x10.000.000)
26.361.538

TIC(-)@2

5.078

1,00

0   1   2   3   4   5   6   7   8   9   10   11   12   13
min

ELSD

V

0,50

5.047

0,25

5.551

0,00

4.429 4.748 5.472

0   1   2   3   4   5   6   7   8   9   10   11   12   13
min

Positive5,072

4000000

343,8

3000000

2000000

164,7

1000000

205,6 290,7   406,9   502,1 579,2   675,3 705,5   835,8 888,2   998,7 1097,3 1178,5 1228,9   1365,4   1445,6   1552,3

100   200   300   400   500   600   700   800   900   1000   1100   1200   1300   1400   1500

Negative5,074

371,1

10000000

162,7   324,8   428,9 478,1   601,2   697,2 776,9   908,7 985,1 1030,5 1102,9   1217,5   1350,7 1428,5   1523,7

100   200   300   400   500   600   700   800   900   1000   1100   1200   1300   1400   1500

Peak Table MEGx_Box_0408_G11_210121
AD2

Peak#	Ret. Time	Area	Area%
1	4,429	3387	0,153
2	4,748	10533	0,475
3	5,047	2125897	95,919
4	5,472	40315	1,819
5	5,551	36204	1,633
Total		2216336	100,000

SalA-VS-12

Segment#1
Intensity

TIC(+)@1 (1)

(x10.000.000)
16.566.194

7,146

TIC(-)@2 (1)

(x10.000.000)
11.944.679

7,149

ELSD

V

7,073

Positive7,139

406,0

152,8 208,9 250,0 371,0 467,0 560,7 602,2 715,3 794,6 832,1 888,4 1003,1 1071,9 1183,6 1277,4 1376,9 1468,1

Negative7,144

433,0

224,8 379,1 486,9 540,7 635,2 775,2 821,1 901,3 998,5 1091,4 1216,3 1331,1 1385,6
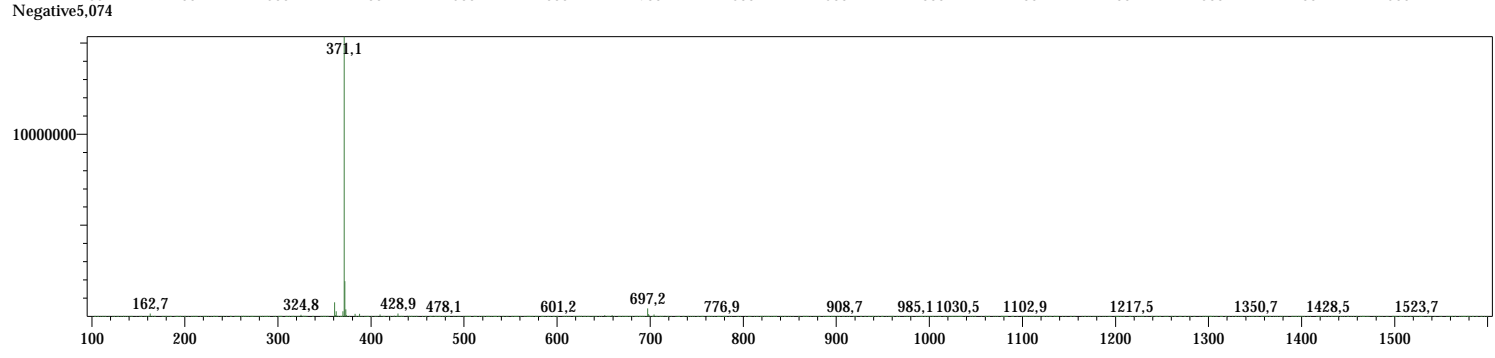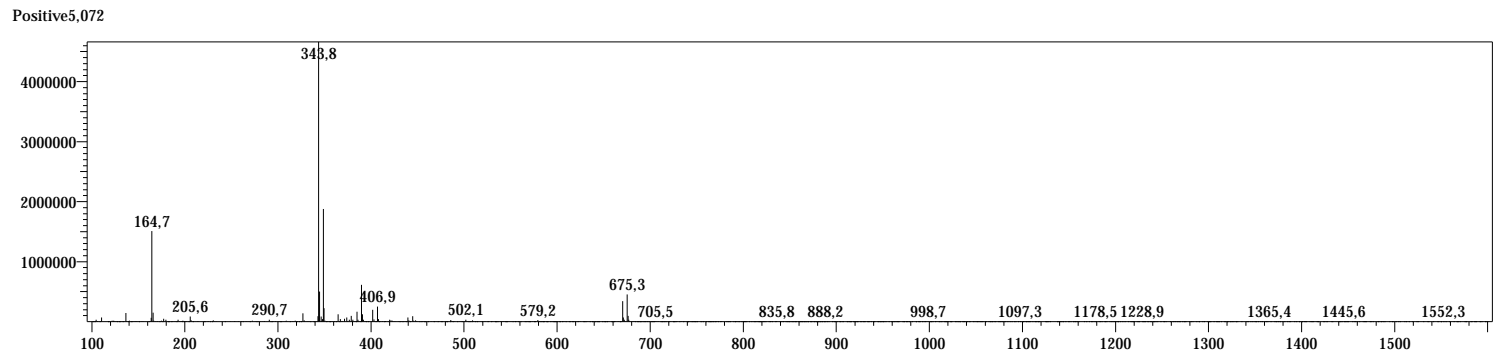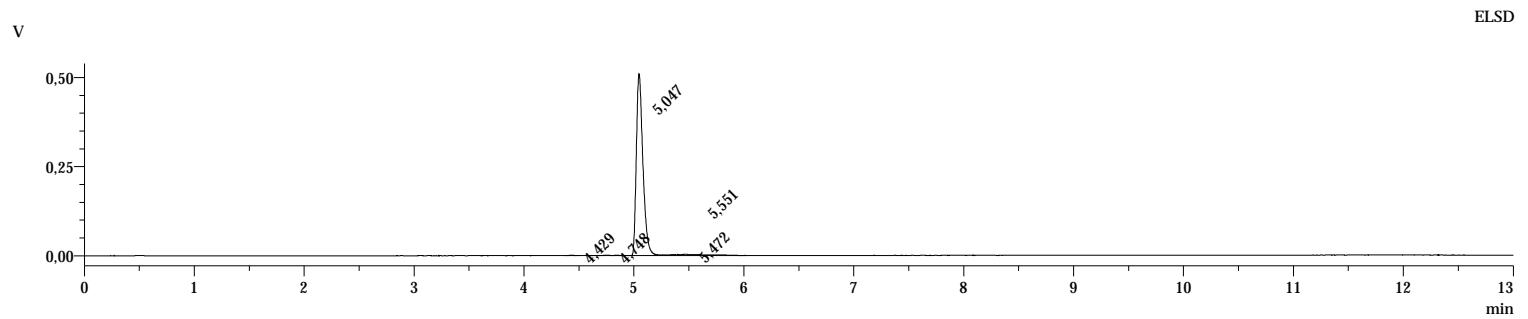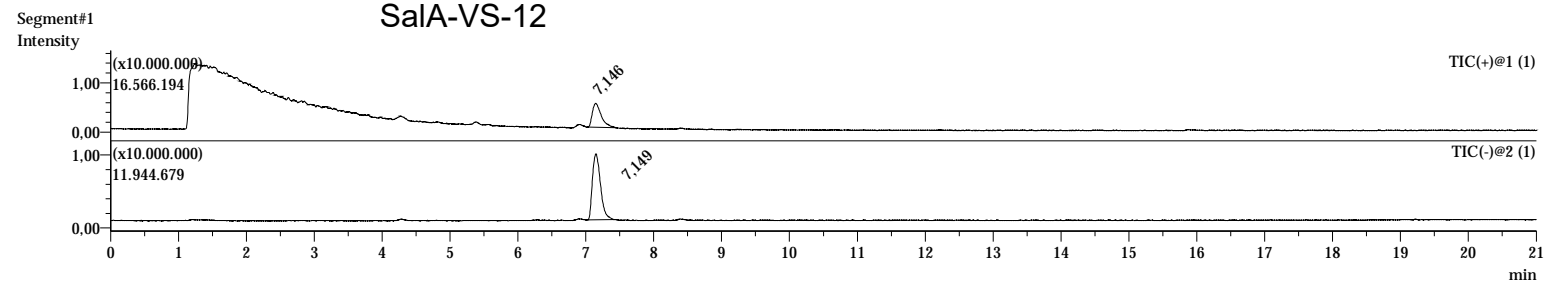
Peak Table MEGx_Store_MTP-1577_F12_190313
AD2

Peak#	Ret. Time	Area	Area%
1	7,073	1123968	100,000
Total		1123968	100,000
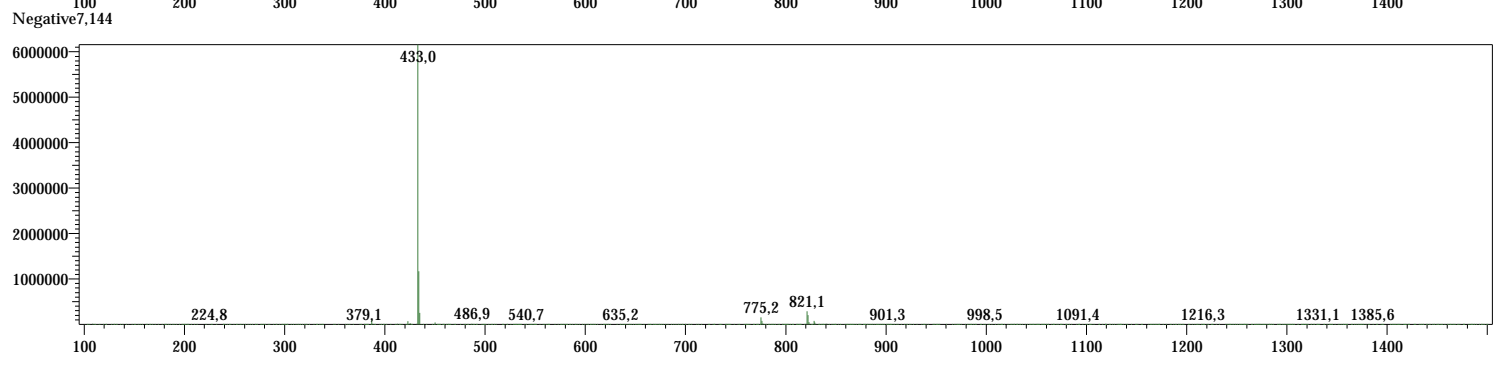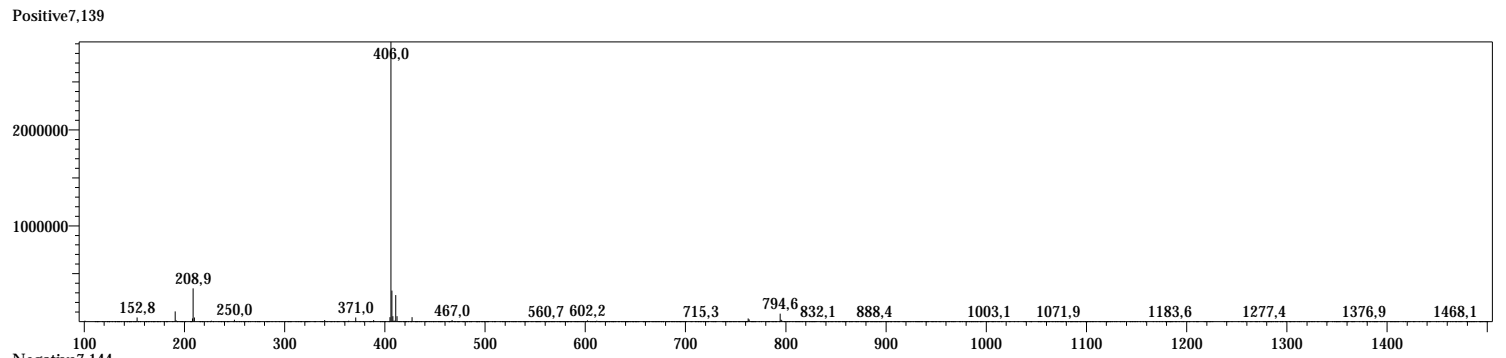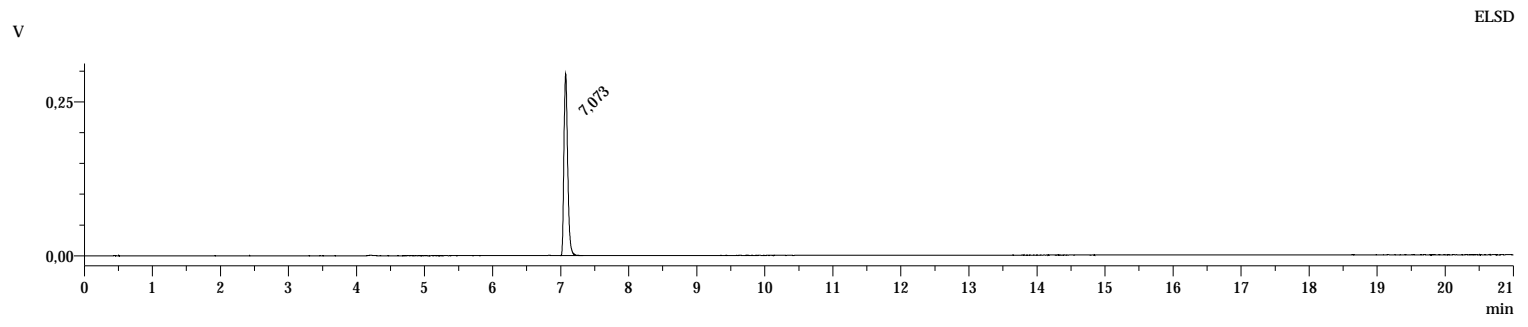
D-7000 HPLC System Manager Report

Analyzed:	9.1.21 9:19	**Reported:**	11. Januar 2021
System Name:	Sys 1	**HPLC Method:**	HPLC-Megdex (kurz)
			Kurz-Gradient, Megdex mittels ELSD + evtl. UV-Detektion
Proc. Method:	H-2192-G		
Application:	Intrabolite	**Series:**	6525
Vial Number:	44	**Sample Name:**	H-2192-G-D08
Vial Type:	UNK	**Volume:**	14,0 ul
Injection from vial:	1 of 1	**Sample Description:**	

Channel 1

Chrom Type: HPLC Channel : 1	**HPLC System:**	Anlage 9 (kurz)
	Detection:	ELSD

No.	RT	Area	Height	Area %
1	7,36	2.568.283	436275	100
		2.568.283	436275	100

Segment#1
Intensity

TIC(+)@1 (1)

(x10.000.000)
17.771.080

TIC(-)@2 (1)

(x10.000.000)
22.785.468

ELSD

1,959

1,579   2,095

AU

1 PDA Multi 1 215nm,4nm
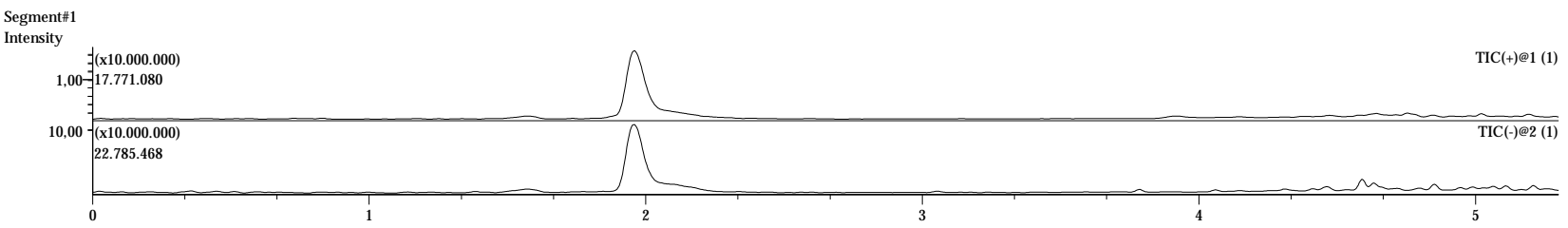
Peak Table H-2192-G-D08
AD2

Peak#	Ret. Time	Area	Area%
1	1,579	4420	0,176
2	1,959	2442569	97,336
3	2,095	62420	2,487
Total		2509409	100,000

PDA Ch1 215nm

Peak#	Ret. Time	Area	Area%
Total			

Positive1,956

369,0

5000000

129,9   189,8   273,9   412,9   531,2 569,1   701,4   849,0   963,6   1051,1 1109,6   1185,4 1240,0   1375,1   1524,5

Negative1,958

10000000

396,0

5000000

169,1   270,9   413,0   492,7   579,9   699,2   747,2   814,9   917,2   984,4   1060,5 1105,4   1213,7 1257,4   1359,6   1521,1
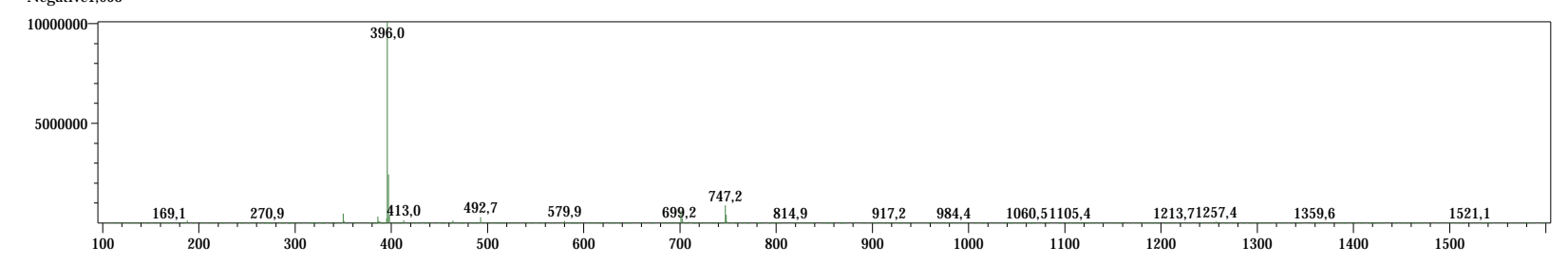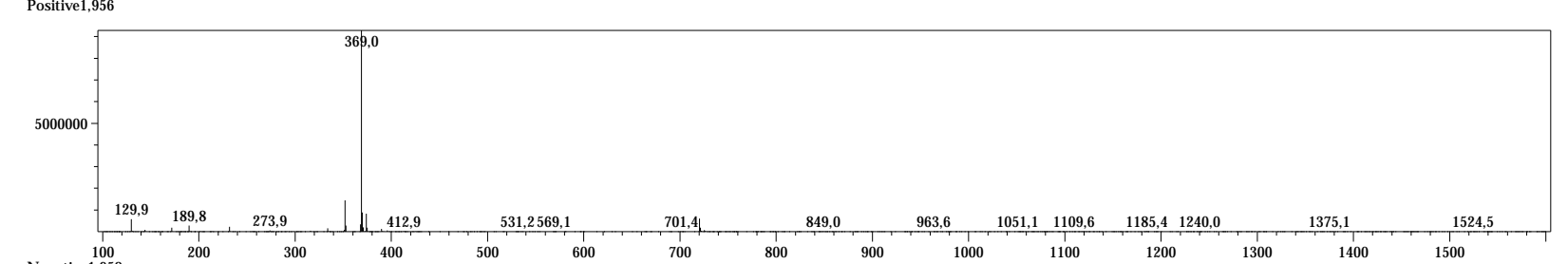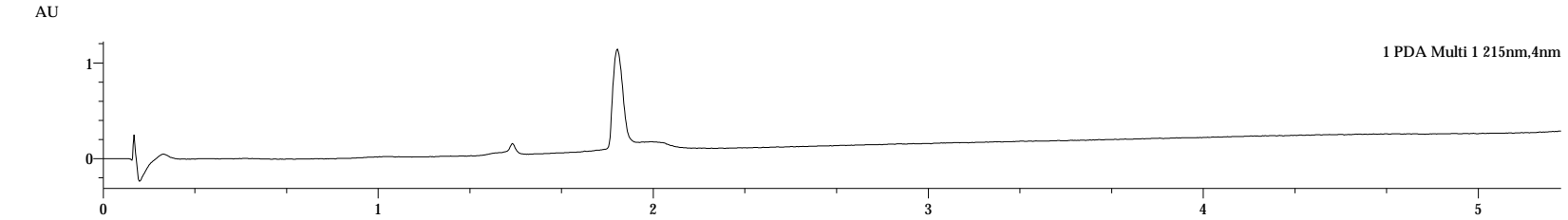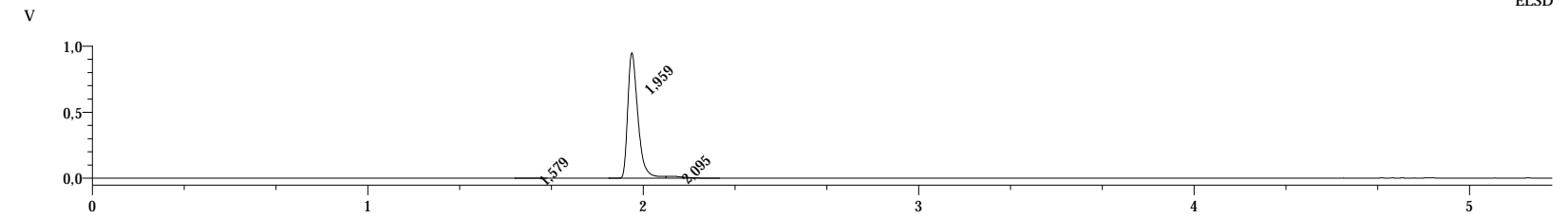
References

(1) Puls, K.; Wolber, G. Solving an old puzzle: Elucidation and evaluation of the binding mode of Salvinorin A at the kappa opioid receptor. *Molecules* **2023**, *28*, 718. DOI: 10.3390/molecules28020718.

(2) Han, J.; Zhang, J.; Nazarova, A. L.; Bernhard, S. M.; Krumm, B. E.; Zhao, L.; Lam, J. H.; Rangari, V. A.; Majumdar, S.; Nichols, D. E. Ligand and G-protein selectivity in the κ-opioid receptor. *Nature* **2023**, 1-9. DOI: 10.1038/s41586-023-06030-7.

(3) Roach, J. J.; Shenvi, R. A. A review of salvinorin analogs and their kappa-opioid receptor activity. *Bioorg. Med. Chem. Lett.* **2018**, *28*, 1436-1445. DOI: 10.1016/j.bmcl.2018.03.029.

(4) Kane, B. E.; Nieto, M. J.; McCurdy, C. R.; Ferguson, D. M. A unique binding epitope for salvinorin A, a non-nitrogenous kappa opioid receptor agonist. *The FEBS journal* **2006**, *273*, 1966-1974. DOI: 10.1111/j.1742-4658.2006.05212.x.

(5) Vardy, E.; Mosier, P. D.; Frankowski, K. J.; Wu, H.; Katritch, V.; Westkaemper, R. B.; Aubé, J.; Stevens, R. C.; Roth, B. L. Chemotype-selective modes of action of κ-opioid receptor agonists. *J. Biol. Chem.* **2013**, *288*, 34470–34483. DOI: 10.1074/jbc.M113.515668 PubMed.

(6) Yan, F.; Mosier, P. D.; Westkaemper, R. B.; Stewart, J.; Zjawiony, J. K.; Vortherms, T. A.; Sheffler, D. J.; Roth, B. L. Identification of the molecular mechanisms by which the diterpenoid salvinorin A binds to κ-opioid receptors. *Biochemistry* **2005**, *44*, 8643-8651. DOI: 10.1021/bi050490d.

(7) Gomez, G. A.; Morisseau, C.; Hammock, B. D.; Christianson, D. W. Human soluble epoxide hydrolase: structural basis of inhibition by 4-(3-cyclohexylureido)-carboxylic acids. *Protein Sci.* **2006**, *15*, 58-64. DOI: 10.1110/ps.051720206.

(8) Norman, B. H.; Dodge, J. A.; Richardson, T. I.; Borromeo, P. S.; Lugar, C. W.; Jones, S. A.; Chen, K.; Wang, Y.; Durst, G. L.; Barr, R. J. Benzopyrans are selective estrogen receptor β agonists with novel activity in models of benign prostatic hyperplasia. *J. Med. Chem.* **2006**, *49*, 6155-6157. DOI: 10.1021/jm060491j.

5. Discussion

After decades of opioid receptor research, safe opioid analgesics and approved opioid antidepressants are still lacking. The urgent need for safer analgesics for pain management is highlighted by the current opioid crisis in the United States [50]. The high non-response rate to standard antidepressants, combined with their slow onset of antidepressant effect, underscores the need for the approval of opioid antidepressants [51]. The rational design of desired opioid drugs is hampered by the limited understanding of how ligand binding to opioid receptors structurally leads to *in vitro* measured affinity and selectivity profiles. Therefore, this section highlights how the structural investigation of HS-731, Compound A, and SalA supports our concept of ligand-induced receptor selectivity and activity, and how the newly gained knowledge supports rational drug design in the field of currently understudied non-basic opioids.

5.1. Structural Analyses of Opioid Receptor-Ligand Complexes

Rational design of KOR-selective ligands may lead to improved analgesics and novel antidepressants. Selective KOR antagonists as antidepressants avoid the dysphoric effects of MOR and DOR antagonists [56]. KOR-selective agonists as analgesics avoid the negative side effects associated with MOR and DOR agonism, such as respiratory depression and seizures (Table 1). However, opioid receptors share a common binding site that is highly conserved across receptor subtypes, which hinders the rational design of KOR-selective ligands. The understanding of how different opioid ligands mediate receptor subtype selectivity is limited. Therefore, we hypothesize that the identification of opioid receptor selectivity determinants is important for further rational drug design of KOR-selective ligands. This dissertation therefore aims to identify the selectivity determinants of three promising opioids, namely HS-731, Compound A, and SalA, by structural analysis.

The clinical value of opioids strongly depends on their receptor activity profile, in particular their affinity, potency and efficacy. The binding of opioids is a prerequisite for the induction of potency and efficacy at the receptors. Thus, elucidation of binding modes, identification of important protein-ligand interactions, and rationalization of determinants responsible for affinity differences between opioids provide important insights for further drug design. Partial agonism is an activation profile considered useful in opioid analgesic research [71,72]. Thus, the rational design of KOR-selective partial agonists may be promising for the development of safer analgesics to reduce KOR-associated side effects like aversion [48,294]. However, partial agonists have been found rather by serendipity and the structural determinants responsible for the induction of KOR partial agonism are largely unknown. Therefore, one aim

of this dissertation was to elucidate the activity profile defining determinants for the three promising opioids HS-731, Compound A, and SalA by *in silico* structural analyses.

5.1.1. Binding Mode, Selectivity Determinants and Activity Rationalization of HS-731

In Article A the pharmacological profile of the peripherally restricted opioid HS-731 was characterized and rationalized *in silico*. The experimental *in vitro* evaluation at the classical opioid receptors (KOR, MOR, DOR) was already available from a previous study by Spetea and coworkers [295]. HS-731 is a peripherally restricted opioid that acts as a potent MOR (EC_{50} = 3.8 nM) and DOR (EC_{50} = 7.9 nM) full agonist, but a weak KOR partial agonist (EC_{50} = 361 nM). In our study, the *in vitro* validation was performed at the NOP, showing no affinity to the NOP at concentrations up to 10 µM.

We developed a new model for the binding mode of HS-731 at all opioid receptor isoforms using *in silico* docking experiments. Subsequently, we rationalized the experimental observations using molecular dynamics simulations, dynamic pharmacophore (dynophore) analysis, and interaction distance analysis. We identified the non-conserved residue 6.58 located in TM6 as a selectivity determinant for HS-731 at the classical opioid receptors. This residue is positively charged in MOR ($K305^{6.58}$), neutral in DOR ($W284^{6.58}$), and negatively charged in KOR ($E297^{6.58}$). Residue 6.58 shows selectivity through its interaction with the conserved lysine residue K5.39, which alters protein-ligand interactions. This selectivity is not due to size exclusion effects. In the MOR, K5.39 and K6.58 can both participate in ionic interactions with the carboxylate moiety of HS-731, which correlates with the highest affinity. In the DOR, no interaction between K5.39 and W6.58 can be detected and K5.39 still participates in ionic interactions with HS-731. The establishment of only one stable ionic interaction between K5.39 and HS-731 at the DOR results in a reduced affinity for the DOR compared to the MOR. At the KOR, E6.58 participates in ionic interactions with K5.39, weakening the ionic interactions between HS-731 and K5.39 and thus the ligand affinity towards the KOR. Notably, the detrimental effect of the ionic interaction between E6.58 and K5.39 at KOR was not significant based on the interaction frequencies alone, but on a detailed statistical interaction distance analysis. The residue $E297^{6.58}$ has already been described as a selectivity determinant for the opioid receptor antagonist nor-BNI and its derivatives [296]. Nor-BNI binds the KOR (E6.58) better than the MOR (K6.58), but swapping mutations (E6.58K in KOR, K6.58E in MOR) reverses the result. However, no atomistic explanation for this observation has been described.

At the time of this study, no experimentally solved structure of the active state NOP was available. Thus, we determined the structural selectivity determinants responsible for the

absent NOP affinity of HS-731 based on a homology model. The active state KOR crystal structure (PDB-ID: 6B73 [13]) served as a template for the NOP homology model generation due to high receptor identity and similarity (sequence identity of 59%, sequence similarity of 73%). Residues responsible for receptor selectivity are often not conserved between receptor subtypes. However, in this case, the conserved residue Y3.33, located deep within the conserved opioid binding site, was predicted to prevent HS-731 from binding to NOP. In the homology model of NOP, this residue points deeper into the binding side than in classical opioid receptors, thereby narrowing the width of the NOP binding site. The bulky morphinan scaffold containing HS-731 cannot be accommodated by this reduced binding site, which correlates with its lack of NOP affinity. The different orientations of the conserved parts of the receptor are caused by the complex conformational interplay of all amino acids of the protein, including the non-conserved ones. Of note, Wang and coworkers recently published a cryo-EM structure of active state NOP bound to its native ligand nociceptin in 2023 (PDB-ID: 8F7X [43]), which supports our hypothesis. Within the crystal structure, Y3.33 adopts an orientation similar to that predicted by our homology model, pointing deep into the binding site.

HS-731 shows a partial agonist profile at KOR which is considered favorable in terms of opioid safety [294,297,298]. However, structural determinants that define ligand functionality at the KOR, including full and partial agonistic profiles, are still lacking. Thus, the rational design of partial agonists remains challenging. We were able to rationalize the formation of HS-731's partial agonism at the KOR in agreement with the maintenance of full agonistic profiles at MOR and DOR. The salt bridge between $K227^{5.39}$ and $E297^{6.58}$ at the KOR hinders KOR activation in that the interaction between TM5 and TM6 prevents TM6 from moving outward [140,299]. The outward movement of TM6 is directly linked to the activation of GPCRs [176,300]. The salt bridge hypothesis is supported by the observation that the salt bridge between $K227^{5.39}$ and $E297^{6.58}$ at the KOR is present only in the inactive conformation (PDB-ID: 4DJH). $K227^{5.39}$ and $E297^{6.58}$ interact with each other in about half of the MD simulation time and distance measurements at the intracellular part of KOR confirmed the adoption of an intermediate activation state KOR conformation with less pronounced TM6 outward movement. A similar interaction between TM5 and TM6 is not observed at MOR and DOR, which correlates with HS-731 having a full agonist profile at these receptor subtypes. Our results are consistent with previous *in silico* experiments of 6'-GNTI and 5'-GNTI at the KOR, which indicated a critical role of $E297^{6.58}$ in TM6 translocation [301]. Sharma and coworkers [302] also correlated the transition from the KOR antagonist 5'-GNTI to the KOR agonist 6'-GNTI with $E297^{6.58}$ interactions that may lead to rotation of TM6. In addition, El Daibani and coworkers [53] who published a crystal structure of the G protein-biased ligand nalfurafine bound to the KOR, also linked the activation profile of nalfurafine to the salt bridge between $K227^{5.39}$ and $E297^{6.58}$. However, there are no *in vitro* data to support our partial agonism

hypothesis. Therefore, we propose to perform a mutagenesis study in which E297 is mutated to an alanine (E297A) or lysine (E297K) analog of the MOR. If our hypothesis is correct, HS-731 would show full agonism at these mutant receptors. This structural insight into the partial activation of KOR should facilitate future efforts to develop safer opioid analgesics.

HS-731 consists of a morphinan backbone linked to the amino acid glycine. This makes HS-731 zwitterionic at physiological pH and therefore unable to enter the brain, i.e. HS-731 is peripherally restricted. As mentioned before, peripheral restriction of KOR agonists is a promising strategy for the development of safer analgesics [33,41,54,64,98-100]. As discussed above, HS-731 also exhibits partial agonism at the KOR, which is likely to further enhance its safety profile. These new insights into the structural selectivity determinants of HS-731, together with the known selectivity descriptors and those described in Article B could be used to derivatize HS-731 to increase its KOR selectivity. For example, modifying the carboxylate moiety of HS-731 to interact only with the conserved K5.39 but not the non-conserved K6.58 in MOR would likely decrease MOR affinity. This could be facilitated by steric constraint of the carboxylate moiety. The introduction of a steric clash between an HS-731 derivative and the bulky, non-conserved residue K2.63 in DOR would likely decrease DOR affinity. The new HS-731 derivatives could then combine three strategies for the development of safer analgesics, namely partial agonism, peripheral restriction, and KOR selectivity, increasing their potential for clinical use. Notably, El Daibani and coworkers [53] proposed the disruption of the intramolecular salt bridge between K227[5.39] and E297[6.58] essential for nalfurafine's G protein bias. As HS-731 also disrupts this salt bridge, HS-731 may already have a G-protein bias, further increasing its clinical value.

To further evaluate the functional profiles and clinical values of HS-731 and its derivatives, an *in vitro* assessment of arrestin recruitment followed by an *in vivo* evaluation of their side effect profiles could be performed. The *in vivo* analgesic potential of HS-731 has already been evaluated [303] revealing significant pain relief. However, this study did not assess potential side effects of HS-731.

Taken together, we determined the binding mode of HS-731 at the classical opioid receptors, identified subtype selectivity descriptors rationalizing the measured experimental affinity of HS-731, and explained the observed partial agonistic profile of HS-731 at the KOR. Our findings promote our understanding of KOR activity and selectivity, which may facilitate future efforts in designing safer and more effective opioid analgesics.

5.1.2. Binding Mode, Selectivity Determinants, and Activity Rationalization of Compound A

Article B includes an *in vitro* and *in vivo* characterization of the novel scaffold ligand Compound A at the classical opioid receptors as well as an *in silico* evaluation revealing its binding mode, activity determinants, and selectivity determinants. In previous *in vitro* studies [304], Compound A has been described as a weak MOR antagonist. In this study, we found Compound A to be a moderately potent KOR antagonist. In addition, we demonstrated that Compound A has no affinity for DOR at concentrations up to 10 μM as determined by radioligand binding assay. *In vivo* mouse models of visceral pain (acetic acid-induced writhing assay) and inflammatory pain (the formalin test) confirmed the KOR antagonist activity of Compound A. To rationalize the selectivity profile of Compound A, we performed docking experiments and MD simulations followed by dynophore analysis to determine the binding mode and protein-ligand interaction patterns of Compound A. Our investigation revealed that the non-conserved residue 2.63 (DOR: K, MOR: N, KOR: V) prevents Compound A from binding to DOR. K2.63 at DOR is bulkier than N2.63 and V2.63 at MOR and KOR and is located deep within the binding site, preventing Compound A from binding.

The differences in affinity between KOR and MOR can be rationalized by a halogen bond between Compound A and the KOR extracellular loop 1 and 2 residues (S123, W124, I208), which is absent in the MOR. The overall moderate affinity of Compound A at KOR and MOR can be further rationalized by its position in the binding site. Compared to the potent co-crystallized morphinan-based opioid receptor antagonists JDTic, β-FNA, and naltrindole, Compound A is shifted away from TM5 towards TM2/TM3. In addition, Compound A lacks the possibility for interactions with conserved water molecules potentially involved in morphinan opioid binding, as it contains only a phenyl group instead of a phenol moiety. These findings can be used for further ligand optimization towards stronger KOR potency.

Compound A represents a novel scaffold KOR antagonist with KOR preference but no KOR selectivity. The presented novel insights into the selectivity descriptors of Compound A provide an opportunity to optimize the KOR selectivity of Compound A. The new KOR selective derivative could undergo *in vivo* experiments to assess its pharmacokinetic profile. A short KOR blockade would be desirable, but even a long duration of action could provide further understanding of how this unfavorable behavior arises.

In conclusion, we have demonstrated that Compound A is a dual KOR/MOR antagonist with KOR preference and moderate activity at KOR. We evaluated the binding mode of Compound A and elucidated receptor subtype selectivity descriptors. Our findings will facilitate the rational design of novel, selective KOR antagonists and Compound A derivatives with improved clinical profiles.

5.1.3. Binding Mode Elucidation and SAR Analysis of SalA at the KOR

In Article C we carefully evaluated the existing experimental data about SalA and its derivatives to determine the binding mode of SalA at the KOR *in silico*. We combined mutagenesis data for SalA, structure-activity relationship (SAR) data of SalA derivatives, and affinity data for SalA at all opioid receptors to define a binding hypothesis that rationalizes these experimental results. We employed docking experiments, MD simulations, and dynophore analysis to generate and evaluate the binding mode. SalA binds above the binding pocket described for morphinans in a less conserved part of the KOR. Its furan moiety points toward the receptor center, while its C2 and C4 substituents span toward the extracellular site. SalA interacts with several non-conserved residues and we propose that the non-conserved residues 2.63, 7.35 and 7.36 are responsible for the exceptional subtype selectivity of SalA. Protein-ligand interactions between SalA and these residues are not observed for the remaining opioid receptors. We evaluated our SalA binding hypothesis by rationalization of affinity differences between SalA and 18 close derivatives. Retention or disruption of the protein-ligand interaction pattern observed for SalA in the binding mode of its derivatives revealed that some interactions are more important than others for KOR affinity. Interactions of the C2 substituent of SalA seem to be most crucial, followed by interactions of its C1 and C4 substituents. The interactions of its C17 carbonyl group are less important in our model.

Several attempts have been made to discover the SalA binding mode using *in silico* methods, resulting in the publication of several conflicting binding hypotheses [13,134,140-146]. The active state KOR crystal structure (PDB-ID: 6B73 [13]) was published in 2018, but many studies were conducted before. For example, most researchers used KOR models based on the inactive KOR structure (PDB-ID: 4DJH [42]) or active-like models based on other GPCR structures that significantly differ from the published active state KOR crystal structure. In addition, most researchers relied on mutagenesis data only without incorporating SAR data into the binding pose generation process. To the best of our knowledge, our study was the first comprehensive analysis of all experimental data around SalA and its derivatives since the publication of the active state crystal structure.

During the pharmacological evaluation of our hits from the SalA-based virtual screening campaign described in Article D, cryo-EM structures of KOR bound to the SalA analog methoxymethyl-salvinorin B (momSalB) were published (PDB-IDs: 8DZP, 8DZQ [181]). The structural difference between momSalB and SalA is the presence of a methoxymethyl ether moiety at the C2 position in momSalB instead of a C2-acetoxy moiety present in SalA. Similar to SalA, momSalB shows high affinity and selectivity for the KOR acting as a full agonist [305]. Unexpectedly, momSalB adopts a different binding pose at the KOR compared to our *in silico* prediction (Article D, Figure 8). MomSalB binds to the morphinan-binding pocket deep inside the KOR instead of the more extracellularly located pocket predicted for SalA. This

experimentally determined binding mode of momSalB might raise doubts about our model. Therefore, we further analyzed the plausibility of our model compared to the binding mode of momSalB at the KOR as shown in the cryo-EM structure. First, the publication provides limited information on the generation of the deposited KOR-momSalB cryo-EM structures, particularly on the conformational sampling procedures. This leaves open the possibility of alternative ligand conformations. Second, the published binding mode of momSalB is not consistent with the experimental data published for SalA. In the cryo-EM structures, momSalB occupies a binding pocket strongly conserved among the opioid receptors and an overlay of the cryo-EM structures with the active state MOR (PDB-ID: 5C1M) and active state DOR (PDB-ID: 6PT2) does not reveal any potential steric clashes. These findings conflict with the experimental measured strong KOR subtype selectivity of SalA [305]. The physiological cleavage of SalA's C2-acetoxy group to a mere hydroxy group causes inactivation at the KOR [136]. However, although the C2-moiety is crucial for KOR activity, the C2-methoxymethyl group of momSalB does not participate in protein-ligand interactions, as revealed by both static and dynamic analyses (Article D Figure 9 and S5). Additionally, in several MD simulations, momSalB strongly moves within the binding site (Article D Figure S6). The KOR-momSalB complexes do not rationalize the effect of several residues highlighted as important in SalA mutagenesis studies on KOR binding [134,140,145]. However, they contain a protein-ligand interaction with an unnatural residue (I135L) potentially biasing momSalB's binding mode.

Despite the issues with the compatibility of the momSalB cryo-EM binding mode and *in vitro* experimental results of SalA, it does not necessarily mean that the momSalB binding mode is incorrect. It could also mean that momSalB binds in a different way than SalA. SalA and its derivatives may adopt multiple distinct conformations at the same receptor, a phenomenon called 'dynamic ligand binding' [306]. Dynamic ligand binding was already observed for the estrogen receptor [307], muscarinic M2 receptor [275,306], and CYP enzymes [308]. It would also be possible that SalA and momSalB adopt different orientations in the same receptor despite their structural similarity. This phenomenon was already described for closely related ligands at PPARγ [309] and p38α [310].

Although a crystallization-based or cryo-EM-based structural determination of SalA's binding mode is currently not available, using the *in silico* determined SalA binding mode as a starting point for virtual screening led to the discovery of two novel non-basic KOR agonists (Article D). This suggests that the binding mode of SalA described in our model may be useful for future drug design.

In summary, we have determined a putative binding mode of SalA at the KOR through an extensive evaluation of available mutagenesis and SAR data as well as the use of *in silico* methods including docking, MD simulations, and dynophore analysis. The new binding mode is consistent with experimental data on SalA. The binding mode and insights from the

rationalization of SAR data will promote future efforts in designing non-basic KOR ligands. The discovered protein-ligand interaction pattern between KOR and SalA was used to conduct a virtual screening campaign aiming for novel non-basic KOR ligands (Article D).

5.1.4. Insights from the Structural Analyses

The aforementioned structural analyses of HS-731, Compound A, and SalA successfully identified their binding modes as well as selectivity and activity determinants. This section discusses how these findings will foster future drug design efforts.

In the structural analysis of HS-731, we identified the conserved residue Y3.33 as a selectivity determinant, because this residue sterically prevents HS-731 from binding to the NOP. This residue is located deep within the conserved binding site where most opioids bind. Therefore, this selectivity determinant can be utilized for the design of opioids with selectivity for the classical opioid receptors (KOR; MOR; DOR) over the NOP by introducing a steric clash with NOP.

In our analysis of Compound A, we described the selectivity-inducing effect of the non-conserved residue 2.63 (DOR: K, MOR: N, KOR: V) due to size exclusion and differences in polarity. The polar and bulky K108[2.63] of DOR is located at the top of TM2. Morphinan ligands typically bind deep within the conserved receptor pocket and smaller morphinan ligands such as naltrindole do not reach far enough toward TM2 to interact with residue 2.63 (PDB-ID: 4N6H [44]). Thus, residue 2.63 can only be used for the rational design of opioids that favor or disfavor DOR if these ligands reach the TM2 region. However, several opioids fulfill this requirement. We surmise that ligands with longer, hydrophobic substituents reaching towards TM2 show KOR preference due to the small and greasy nature of V2.63 at KOR which is different from MOR and DOR.

HS-731 achieves selectivity through the interplay of the conserved residue K5.39 and the non-conserved residue 6.58 (KOR: E, MOR: K, DOR: W), which can be modified by HS-731. However, this selectivity determinant is likely to be rather difficult to exploit for future rational drug design, at least if KOR selectivity is desired. Opioid receptors that interact with both residues, such as HS-731, are likely to favor the MOR. Thus, decreased MOR affinity could be achieved by preventing ligands from interacting with the non-conserved K6.58. However, increasing KOR affinity would be more difficult to achieve because these ligands would likely require an additional positive charge to interact with E6.58. These ligands would then contain three charges which is highly un-drug-like. However, it would be feasible to use this selectivity determinant to reduce the MOR affinity of negatively charged opioids while using other selectivity determinants, such as residue 2.63, to favor KOR affinity.

In the structural analysis of SalA, we identified a potential new binding site with high diversity between the opioid receptor subtypes that can be used to rationally design KOR-selective ligands. The non-conserved residues 2.63, 7.35, and 7.36 were identified as selectivity determinants for SalA and if non-basic opioids bind to the same binding site at KOR, then these selectivity determinants would be generalizable to non-basic opioids. In addition, if typical basic opioids are large enough to reach the binding pocket of SalA, then these selectivity determinants would also apply to basic ligands. This is already shown for Compound A, which shares the selectivity determinant 2.63 with SalA.

If non-basic opioids bind the KOR in a similar manner to SalA, not only selectivity determinants, but also activity determinants would be generalizable for non-basic opioids. Thus, not only the elucidation of the binding mode, but also the results of our comprehensive SAR analysis of SalA and its derivatives could likely facilitate future drug design approaches. For example, the SAR analysis highlighted interactions of the C2 and C4 substituents of SalA as more important than other interactions evaluated. Thus, rational-designed ligands forming hydrogen bonds to Y313$^{7.36}$ and C210^{ECL2} are likely to show increased KOR affinity.

We have identified the occurrence of the salt bridge between K227$^{5.39}$ and E297$^{6.58}$ at the KOR to prevent KOR activation. Since HS-731 disturbs this salt bridge in around 50% of the simulation time it results in partial agonism. In general, the better the ligands disturb this salt bridge the higher the KOR activation should be. By taking advantage of this factor, KOR ligands with tailor-made efficacy can be designed in a rational way. To the best of our knowledge, this is the first time that such an efficacy-regulating mechanism usable for rational drug design has been proposed for the KOR.

Overall, the findings of our structural analysis are likely to promote the optimization of the evaluated ligands themselves and enable the rational design of new tailored modulators of the KOR. However, the insights gained from our structural analysis cannot cover all the mechanisms responsible for selectivity and activity. Further research on the structural correlation of opioids and their selectivity and activity profiles is needed to promote the rational drug design of optimized opioid ligands.

5.2. Rational Drug Design of Novel, Non-Basic KOR Agonists

Non-basic opioids are currently understudied with only a small number of non-basic scaffolds known. The development of new non-basic ligands would be desirable as they promise to show KOR selectivity or at least KOR preference [148-152]. However, the mechanism by which non-basic opioids bind to the KOR and facilitate receptor subtype selectivity remains unclear. Our structural analysis of SalA has shed light on this issue. Our proposed binding mode of SalA at the KOR and the rationalization of SalA's SAR allow for subsequent rational

drug design of either SalA derivatives with improved clinical usability or the discovery of novel non-basic ligands via virtual screening campaigns. The latter allows for easy scaffold hopping, thus expanding the chemical space of non-basic opioids. Novel non-basic opioid scaffolds bear the promise to circumvent the unfavorable properties associated with SalA, i.e. its poor pharmacokinetic properties, difficult synthesis, fast metabolism, and hallucinogenic properties [136,147,153]. Therefore, we assume that a 3D pharmacophore-based virtual screening campaign based on the SalA is more promising than the derivatization of SalA for the development of non-basic KOR ligands. Therefore, the aim of this dissertation was to perform such a virtual screening campaign for the identification of novel non-basic opioids with chemistry different from SalA.

5.2.2. Virtual Screening for Novel Non-Basic KOR Agonists

In this study, a 3D pharmacophore-based virtual screening campaign was conducted to identify novel scaffold, selective, and non-basic KOR agonists as potential safer analgesics. We performed two separate 3D pharmacophore-based virtual screening techniques in parallel, namely a classical 3D pharmacophore-based virtual screening performed in LigandScout and a rapid overlay of chemical structures (ROCS) screening. The former relies solely on 3D pharmacophore features including exclusion volume spheres and is generally more restrictive. The latter focuses on the shape similarity between a query ligand and the molecules in the database, while also considering 3D pharmacophore features. We used the KOR-SalA complex model, which was developed in Article C, for virtual screening query definition. Multiple databases of natural products, natural product derivatives, and synthetic compounds - approximately 3 million molecules in total - have been screened. After docking experiments and visual inspection, 13 non-basic hit molecules were selected for experimental evaluation *in vitro*. Two out of these 13 molecules showed promising results in a radioligand binding-based pre-screening and therefore were selected for further experimental characterization. *In vitro* radioligand binding assays and *in vitro* GTPγS functional assays revealed that both hit molecules, **7** and **8**, show affinity and potency values in the nanomolar concentration range. In particular, **7** binds to the KOR with a K_i value of 423 ± 97 nM and activates the KOR with an EC_{50} value of 181 ± 49 nM. **8** shows a K_i value of 68.5 ± 5.5 nM and an EC_{50} value of 854 ± 60 nM. **8** exhibits a full agonistic profile at KOR (108 ± 8%), while **7** shows partial agonism with 48 ± 7% stimulation compared to the full agonist reference molecule U69,593. Both compounds show KOR selectivity as indicated by radioligand binding assays conducted at DOR and MOR.

Our two hit molecules share a common spiro-scaffold (2-methylspiro[6H-pyrazolo[1,5-a]pyrimidine-7,4'-piperidine]-5-one scaffold) that was never described for KOR ligands before

(Article D, Figure 4). **9**, selected for in vitro evaluation was found to be inactive. This ligand shares the same spiro-scaffold as our novel agonists, enabling a preliminary SAR analysis. The two hit compounds **7** and **8** only differ in the halogen substitution of a benzamide substituent and are both active while the inactive **9** lacks the halogen-substituted benzamide and possesses a 4-pyridineamide instead. Thus, the halogen-substituted benzamide seems to be crucial for KOR activity. However, whether halogen substituents could be replaced by other bulky hydrophobic substituents remains elusive. A literature search showed that other opioids with spiro moieties have been described. However, all of them differ from our scaffold and contain a basic moiety that is not desired for this study. Therefore, we consider our spiro scaffold to be novel. Although the concept of selective targeting of the KOR by non-basic opioids is well-established, only a few non-basic scaffolds for KOR ligands have been identified so far [147-152]. Thus, the discovery of our new non-basic spiro-scaffold with KOR activity broadens the non-basic chemical space of opioids promoting the development of safer analgesics.

We currently perform a ligand optimization study. Eight analogs of our hit compounds, sharing the same novel spiro-scaffold are currently under pharmacological evaluation at the lab of Mariana Spetea. The analogs differ from our lead structures mainly by their halogen substitution, but also by the replacement of the cyclopropyl moiety by heteroaromatics, the introduction of sulfonamide moieties, and the omission of the methyl substituent. One derivative even possesses a basic nitrogen atom to confirm our binding hypothesis. We aim to improve the understanding of protein-ligand interactions important for our novel ligands and to enhance their affinity and potency to make them safer analgesics. It is worth mentioning that **7** and **8** already exhibit sufficient activity, but there is still room for improvement.

An interesting feature of our lead structures is the inverse relationship between affinity and potency. While **7** has the lower affinity but higher potency **8** shows the opposite. The reason for this phenomenon is currently unknown. It is possible that there is a bias for the G protein signaling pathway measured in the conducted [^{35}S]GTPγS assay performed. However, this is speculative at this point. Therefore, we recommend follow-up *in vitro* evaluation of potentially biased signaling.

Partial agonist opioids may be safer than full agonist opioids [97,294,297]. **7** exhibits such partial agonism combined with KOR selectivity, both of which are likely to increase the therapeutic value of **7**. Although the results are encouraging, the present study only includes an *in vitro* evaluation of our hits. A detailed follow-up *in vivo* evaluation of **7** and **8** is necessary to assess their analgesic potentials and side effect profiles, in particular their hallucinogenic potential. SalA shows a strong hallucinogenic potential that is atypical for opioids. Although the opioid collybolide found in the mushroom *Collybia masculata* shares the furyl-δ-lactone substructure with SalA, there are no reports of hallucinogenic effects associated with Collybia

masculata [151]. Therefore, the psychedelic effects of SalA seem to be highly dependent on SalA's chemical scaffold. Thus, we are optimistic that our hits will avoid this severe side effect because they have less structural similarity to SalA.

For future derivatization, it would be desirable to aim for the inclusion of a peripheral restriction or G protein bias as both strategies likely improve the therapeutic value. However, whether or not these modifications are necessary will depend on the results of the *in vivo* evaluation of our lead compounds and the ongoing optimization campaign.

Overall, we have identified two novel-scaffold, potent, selective, and non-basic KOR ligands through a virtual screening campaign based on SalA's 3D pharmacophore. Both compounds share a novel spiro scaffold. Promising *in vitro* experimental results render our hit compounds potentially interesting for later clinical use. One of the hit compounds, **7**, shows a partial agonist profile at KOR potentially increasing its therapeutic value. However, the side effect profiles of our lead compounds remain to be evaluated. Our findings expand the limited knowledge about non-basic opioids and should facilitate future efforts to design safer analgesics by circumventing MOR side effects with KOR-selective non-basic opioids. Thus, the third aim of this thesis could be addressed in a successful manner.

5.3. Limitations and Usefulness of *In Silico* Methods

This section discusses the limitations, uncertainties, and usefulness of *in silico* methods in drug discovery. Computational methods usually handle simplified biological systems to compute results in a reasonable time: Many algorithms for HM, docking, and virtual screening treat the receptor or ligand rather rigid [203,230,278], despite the flexible nature of biological systems. Computation of any potential movements would cause the calculation time to explode [311,312]. MD simulations that account for biological flexibility are computationally highly demanding and therefore limited to short time scales [254]. Additionally, the structure of MD simulation systems is simplified. In the MD simulations used in this dissertation, the protein-ligand complex was modeled without intracellular G protein bound to minimize the number of atoms and was embedded in a membrane consisting only of 1-palmitoyl-2-oleoylphosphatidylcholine (POPC) despite the more complex construction of biological membranes. Intermolecular and intramolecular interactions that determine the energy of the complex conformation as well as the forces within the system are calculated by the force fields [250]. Force field parameters are approximations even though they have been optimized to match experimental data and quantum-mechanical calculations [246]. Entropic terms are usually omitted [313]. HM assumes that the same sequence would result in the same protein conformation [206]. However, proteins are flexible and can adapt to interaction partners like

bound ligands thereby altering the conformation of the binding site essentially for the drug design process. GPCRs further switch between active and inactive states. Consideration of only one conformation therefore represents a strong simplification [203].

The system simplifications mentioned above result in uncertainties that could accumulate during drug discovery. Static crystal structure conformations could contain artifacts [314,315] resulting from insufficient density maps, inaccurate fitting, or not generalizable conformational adaptions to the bound ligand among others. Analogously, artifacts can be introduced into protein conformations obtained with HM by insufficient sequence alignment or inaccurate template structures [208]. In the case of GPCRs, the N-termini, C-termini, and loops may be unresolved in experimentally solved structures [2,10] and not modeled due to missing templates. Thus, potential influences of these receptor parts on the protein-ligand complex are neglected. Docking is known to produce false positives [242] and scoring functions used in docking fail to correctly score the putative docking solutions [221,222]. 3D pharmacophores represent interactions abstractly [278] therefore risking false positive hits in a virtual screening. In a workflow of crystal structure preparation followed by protein-ligand docking, 3D pharmacophore generation, and 3D pharmacophore-based virtual screening as performed in Articles C and D, it would be conceivable that artifacts within the crystal structure bias the docking results, that the 3D pharmacophore of the chosen docking pose would not represent the biologically active interaction pattern, and that the virtual screening hits would all be false positives. However, the uncertainties associated with *in silico* techniques can be reduced by meaningful validation of the results of each method before proceeding with the next method [169,203,242].

To increase the accuracy of protein prediction methods such as HM, model generation is followed by a validation that should include the incorporation of available information about the protein. In the case of the NOP homology model in Article A a geometric validation as well as a visual inspection of the NOP model was performed with special interest at D3.32 and the side chain orientation of the binding site residues. To avoid the selection of false positive docking poses in all included articles the scoring of the poses by the docking score was neglected and a visual inspection was performed. Alternative criteria for docking pose selection encompass 3D pharmacophore overlap to a reference ligand, Gaussian shape similarity score, agreement with mutational data and SAR studies, structural novelty, tautomers, interactions with specific residues, distorted ligand geometry, unsatisfied ligand heteroatoms among others. Furthermore, docking constraints favoring the generation of plausible docking poses were incorporated. Prior to the virtual screening in Article D, a validation of the predictive power of the 3D pharmacophore query was performed using ROC curves. The accuracy of virtual screenings can further be improved by consideration of sufficient ligand conformations to avoid missing potential hit conformations [316].

Although *in silico* methods are associated with system simplifications and uncertainties, they have become established methods in drug design and significantly contributed to the discovery of new drugs and the mechanistic understanding of biological processes [281,286,317].

In silico methods allow for the investigation of biological events hardly observed in classical experiments [318] such as the interplay of HS-731, K5.39, and the non-conserved residue 6.58 in Article A. *In silico* methods like virtual screenings are very time-effective and cost-effective and yield higher rates of active compounds compared to classical methods like High Throughput Screening [169,312,318,319]. 3D pharmacophore-based virtual screening further allows for scaffold-hopping often desired in drug discovery [278].

Overall, *in silico* methods are highly useful for drug discovery purposes and represent a useful expansion of the drug discovery toolkit. *In silico* methods have benefits as well as limitations but contributed to the discovery of many active compounds. The meaningful combination of *in silico* methods with each other and with classical experimental methods reduces their drawbacks and further increases the usefulness of *in silico* methods.

6. Conclusion

In this dissertation, comprehensive *in silico* studies were performed to address current questions in opioid research. A variety of *in silico* techniques such as docking and MD simulations combined with dynophore analysis were used to better understand the relationship between structural ligand or receptor motifs and pharmacological effects. This task is particularly challenging due to the complexity of opioid receptor signaling. In addition, a virtual screening campaign was conducted for the development of new opioid ligands.

The four opioid receptor subtypes share a high degree of structural similarity. At the same time, our understanding of the determinants of opioid receptor selectivity is limited, hampering the rational drug design of subtype-selective opioids. However, such selective opioids are highly desired. Selective KOR agonists are promising as safer analgesics, while selective KOR antagonists may represent novel antidepressants. In addition, partial agonism is considered beneficial for opioid analgesics. However, the mechanisms underlying partial agonism remain elusive. This dissertation includes three articles in which we performed structural analyses and identified the binding modes of opioid ligands with subsequent elucidation of the subtype selectivity determinants and the activity-determining protein-ligand interactions. The first investigated opioid ligand was HS-731, representing a peripherally restricted opioid receptor agonist. The second assessed ligand was Compound A, an opioid antagonist with a novel scaffold. The third ligand was SalA, a non-basic KOR agonist. The affinity differences of HS-731 between the opioid receptor subtypes mainly depend on the interaction interplay of residues 5.39 and 6.58 with each other and with the ligand as well as on the steric hindrance at NOP via Y3.33. The partial agonism of HS-731 at the KOR is due to the partial occurrence of a salt bridge between K227$^{5.39}$ and E297$^{6.58}$. The lack of affinity of Compound A for DOR is due to steric hindrance of the non-conserved K$^{2.63}$ in DOR, while its preference for KOR over MOR correlates with the presence of an additional halogen bond at KOR. SalA occupies a novel binding site above the typical morphinan binding site, which is highly non-conserved providing a plausible explanation for SalA's exceptional KOR selectivity. In all cases, the findings can be used to improve the clinical value of the aforementioned opioids, can be transferred to other opioid ligands and can be used for the design of novel opioids with tailored signaling profiles.

Typical opioids contain a basic moiety that forms a salt bridge to the opioid receptor. Very few opioids without this basic moiety are known. These non-basic opioids are mostly KOR selective. Thus, non-basic opioids hold great promise for the development of analgesics with improved safety profiles because they bypass the MOR-associated side effects. However, our knowledge about how these non-basic opioids bind to the KOR is very limited. In the fourth article included in this dissertation, the putative binding mode of non-basic SalA was used in

a virtual screening to identify novel non-basic opioids. Two non-basic compounds from the virtual screening were experimentally confirmed to be potent and selective KOR agonists with nanomolar affinity and potency. Both compounds share a novel non-basic scaffold containing a spiro moiety.

We have demonstrated that *in silico* techniques are useful and effective tools for the study of opioid receptors and the identification of new opioids. We are confident that the results of our studies will stimulate further efforts to design and optimize opioid drugs for clinical use.

Ideally, in the next step, an *in vivo* evaluation of the new spiro lead compounds will be performed to assess the side effects and clinical value of these new non-basic compounds combined with the establishment of a SAR to optimize ligand affinity, potency, and efficacy. In addition, the SAR data may be used to predict the binding mode of the spiro scaffold to subsequently evaluate the possibility of a common binding mode of non-basic opioids. In addition, mutagenesis studies of residues 5.39 and 6.58 can be performed to confirm the KOR partial agonism hypothesis established in the structural analysis of HS-731 (Article A), which could then be used for the rational design of KOR partial agonists as safer analgesics.

7. References

1. Munk, C.; Isberg, V.; Mordalski, S.; Harpsøe, K.; Rataj, K.; Hauser, A.; Kolb, P.; Bojarski, A.; Vriend, G.; Gloriam, D. GPCRdb: the G protein-coupled receptor database – an introduction. *Br. J. Pharmacol.* **2016**, *173*, 2195-2207, doi:10.1111/bph.13509.
2. Qu, X.; Wang, D.; Wu, B. Progress in GPCR structure determination. In *GPCRs: Structure, Function, and Drug Discovery*, Jastrzebska, B., Park, P.S.H., Eds.; Academic Press: London, United Kingdom, 2020; pp. 3–22.
3. Fredriksson, R.; Lagerström, M.C.; Lundin, L.-G.; Schiöth, H.B. The G-protein-coupled receptors in the human genome form five main families. Phylogenetic analysis, paralogon groups, and fingerprints. *Mol. Pharmacol.* **2003**, *63*, 1256-1272, doi:10.1124/mol.63.6.1256.
4. Koch, C.; Engele, J. Functions of the CXCL12 Receptor ACKR3/CXCR7—What Has Been Perceived and What Has Been Overlooked. *Mol. Pharmacol.* **2020**, *98*, 577-585, doi:10.1124/molpharm.120.000056.
5. Heng, B.C.; Aubel, D.; Fussenegger, M. An overview of the diverse roles of G-protein coupled receptors (GPCRs) in the pathophysiology of various human diseases. *Biotechnol. Adv.* **2013**, *31*, 1676-1694, doi:10.1016/j.biotechadv.2013.08.017.
6. Yang, D.; Zhou, Q.; Labroska, V.; Qin, S.; Darbalaei, S.; Wu, Y.; Yuliantie, E.; Xie, L.; Tao, H.; Cheng, J. G protein-coupled receptors: structure-and function-based drug discovery. *Signal. Transduct. Target Ther.* **2021**, *6*, 7, doi:10.1038/s41392-020-00435-w.
7. Kolakowski Jr, L.F. GCRDb: a G-protein-coupled receptor database. *Receptors Channels* **1994**, *2*, 1-7.
8. Lin, H.-H. G-protein-coupled receptors and their (Bio) chemical significance win 2012 Nobel Prize in Chemistry. *Biomed. J.* **2013**, *36*, 118-124, doi:10.4103/2319-4170.113233.
9. Palczewski, K.; Kumasaka, T.; Hori, T.; Behnke, C.A.; Motoshima, H.; Fox, B.A.; Trong, I.L.; Teller, D.C.; Okada, T.; Stenkamp, R.E. Crystal structure of rhodopsin: A G protein-coupled receptor. *Science* **2000**, *289*, 739-745, doi:10.1126/science.289.5480.739.
10. García-Nafría, J.; Tate, C.G. Structure determination of GPCRs: cryo-EM compared with X-ray crystallography. *Biochem. Soc. Trans.* **2021**, *49*, 2345-2355, doi:10.1042/BST20210431.
11. Rasmussen, S.G.; Choi, H.-J.; Rosenbaum, D.M.; Kobilka, T.S.; Thian, F.S.; Edwards, P.C.; Burghammer, M.; Ratnala, V.R.; Sanishvili, R.; Fischetti, R.F. Crystal structure of the human β2 adrenergic G-protein-coupled receptor. *Nature* **2007**, *450*, 383-387, doi:10.1038/nature06325.
12. Cherezov, V.; Rosenbaum, D.M.; Hanson, M.A.; Rasmussen, S.G.; Thian, F.S.; Kobilka, T.S.; Choi, H.-J.; Kuhn, P.; Weis, W.I.; Kobilka, B.K. High-resolution crystal structure of an engineered human β2-adrenergic G protein–coupled receptor. *Science* **2007**, *318*, 1258-1265, doi:10.1126/science.1150577.
13. Che, T.; Majumdar, S.; Zaidi, S.A.; Ondachi, P.; McCorvy, J.D.; Wang, S.; Mosier, P.D.; Uprety, R.; Vardy, E.; Krumm, B.E.; Han, G.W.; Lee, M.-Y.; Pardon, E.; Steyaert, J.; Huang, X.-P.; Strachan, R.T.; Tribo, A.R.; Pasternak, G.W.; Carroll, F.I.; Stevens, R.C.; Cherezov, V.; Katritch, V.; Wacker, D.; Roth, B.L. Structure of the nanobody-stabilized active state of the kappa opioid receptor. *Cell* **2018**, *172*, 55-67.e15, doi:10.1016/j.cell.2017.12.011.
14. Vuister, G.W.; Fogh, R.H.; Hendrickx, P.M.; Doreleijers, J.F.; Gutmanas, A. An overview of tools for the validation of protein NMR structures. *J. Biomol. NMR* **2014**, *58*, 259-285, doi:10.1007/s10858-013-9750-x.
15. Stollar, E.J.; Smith, D.P. Uncovering protein structure. *Essays Biochem.* **2020**, *64*, 649-680, doi:10.1042/EBC20190042.

16. Liang, Y.-L.; Khoshouei, M.; Radjainia, M.; Zhang, Y.; Glukhova, A.; Tarrasch, J.; Thal, D.M.; Furness, S.G.; Christopoulos, G.; Coudrat, T. Phase-plate cryo-EM structure of a class B GPCR–G-protein complex. *Nature* **2017**, *546*, 118-123, doi:10.1038/nature22327.

17. Kato, H.E.; Zhang, Y.; Hu, H.; Suomivuori, C.-M.; Kadji, F.M.N.; Aoki, J.; Krishna Kumar, K.; Fonseca, R.; Hilger, D.; Huang, W. Conformational transitions of a neurotensin receptor 1–Gi1 complex. *Nature* **2019**, *572*, 80-85, doi:10.1038/s41586-019-1337-6.

18. Fan, X.; Wang, J.; Zhang, X.; Yang, Z.; Zhang, J.-C.; Zhao, L.; Peng, H.-L.; Lei, J.; Wang, H.-W. Single particle cryo-EM reconstruction of 52 kDa streptavidin at 3.2 Angstrom resolution. *Nat. Commun.* **2019**, *10*, 2386, doi:10.1038/s41467-019-10368-w.

19. Zhang, K.; Wu, H.; Hoppe, N.; Manglik, A.; Cheng, Y. Fusion protein strategies for cryo-EM study of G protein-coupled receptors. *Nat. Commun.* **2022**, *13*, 4366, doi:10.1038/s41467-022-32125-2.

20. Jakowiecki, J.; Miszta, P.; Niewieczerzal, S.; Filipek, S. Structural diversity in ligand recognition by GPCRs. In *GPCRs: Structure, function, and drug discovery*, Jastrzebska, B., Park, P.S.H., Eds.; Academic Press: London, United Kingdom, 2020; pp. 43–63.

21. Burley, S.K.; Berman, H.M.; Kleywegt, G.J.; Markley, J.L.; Nakamura, H.; Velankar, S. Protein Data Bank (PDB): the single global macromolecular structure archive. *Methods Mol Biol.* **2017**, *1607*, 627-641, doi:10.1007/978-1-4939-7000-1_26.

22. Ballesteros, J.A.; Weinstein, H. Integrated methods for the construction of three-dimensional models and computational probing of structure-function relations in G protein-coupled receptors. In *Methods in neurosciences*, Sealfon, S.C., Ed.; Academic Press: San Diego, CA, U.S.; London, United Kingdom, 1995; Volume 25, pp. 366–428.

23. Kurose, H.; Kim, S.G. Pharmacology of antagonism of GPCR. *Biol. Pharm. Bull.* **2022**, *45*, 669-674, doi:10.1248/bpb.b22-00143.

24. Seifert, R.; Wenzel-Seifert, K. Constitutive activity of G-protein-coupled receptors: cause of disease and common property of wild-type receptors. *Naunyn-Schmiedeberg's Arch. Pharmacol.* **2002**, *366*, 381-416, doi:10.1007/s00210-002-0588-0.

25. Tsutsumi, N.; Maeda, S.; Qu, Q.; Vögele, M.; Jude, K.M.; Suomivuori, C.-M.; Panova, O.; Waghray, D.; Kato, H.E.; Velasco, A. Atypical structural snapshots of human cytomegalovirus GPCR interactions with host G proteins. *Sci. Adv.* **2022**, *8*, eabl5442, doi:10.1126/sciadv.abl5442.

26. Bock, A.a.B., M. Allosteric coupling and biased agonism in G protein-coupled receptors *FEBS J.* **2021**, *288*, 2513-2528, doi:10.1111/febs.15783.

27. Olsen, R.H.; English, J.G. Advancements in G protein-coupled receptor biosensors to study GPCR-G protein coupling. *Br. J. Pharmacol.* **2022**, 1-11, doi:10.1111/bph.15962.

28. McCudden, C.; Hains, M.; Kimple, R.; Siderovski, D.; Willard, F. G-protein signaling: back to the future. *Cell. Mol. Life Sci.* **2005**, *62*, 551-577, doi:10.1007/s00018-004-4462-3.

29. Zheng, K.; Kibrom, A.; Viswanathan, G.; Rajagopal, S. Arrestin-mediated signaling at GPCRs. In *GPCRs: Structure, Function, and Drug Discovery*, Jastrzebska, B., Park, P.S.H., Eds.; Academic Press: London, United Kingdom, 2020; pp. 243–255.

30. Gurevich, V.V.; Gurevich, E.V. GPCR signaling regulation: the role of GRKs and arrestins. *Front. Pharmacol.* **2019**, *10*, 125, doi:10.3389/fphar.2019.00125.

31. Hur, E.-M.; Kim, K.-T. G protein-coupled receptor signalling and cross-talk: achieving rapidity and specificity. *Cell. Signal.* **2002**, *14*, 397-405, doi:10.1016/S0898-6568(01)00258-3.

32. Bermudez, M.; Nguyen, T.N.; Omieczynski, C.; Wolber, G. Strategies for the discovery of biased GPCR ligands. *Drug Discov. Today* **2019**, *24*, 1031–1037, doi:10.1016/j.drudis.2019.02.010.

33. De Neve, J.; Barlow, T.M.; Tourwé, D.; Bihel, F.; Simonin, F.; Ballet, S. Comprehensive overview of biased pharmacology at the opioid receptors: biased ligands and bias factors. *RSC Med. Chem.* **2021**, *12*, 828-870, doi:10.1039/D1MD00041A.

34. Filipek, S. Molecular switches in GPCRs. *Curr. Opin. Struct. Biol.* **2019**, *55*, 114-120, doi:10.1016/j.sbi.2019.03.017.

35. Alhosaini, K.; Azhar, A.; Alonazi, A.; Al-Zoghaibi, F. GPCRs: The most promiscuous druggable receptor of the mankind. *Saudi Pharm. J.* **2021**, *29*, 539-551, doi:10.1016/j.jsps.2021.04.015.

36. Sriram, K.; Insel, P.A. G protein-coupled receptors as targets for approved drugs: how many targets and how many drugs? *Mol. Pharmacol.* **2018**, *93*, 251-258, doi:10.1124/mol.117.111062.

37. Wang, J.; Bhattarai, A.; Ahmad, W.I.; Farnan, T.S.; John, K.P.; Miao, Y. Computer-aided GPCR drug discovery. In *GPCRs: Structure, Function, and Drug Discovery*, Jastrzebska, B., Park, P.S.H., Eds.; Academic Press: London, United Kingdom, 2020; pp. 283–293.

38. Waldhoer, M.; Bartlett, S.E.; Whistler, J.L. Opioid receptors. *Annu. Rev. Biochem.* **2004**, *73*, 953–990, doi:10.1146/annurev.biochem.73.011303.073940.

39. Carlezon Jr, W.A.; Krystal, A.D. Kappa-opioid antagonists for psychiatric disorders: From bench to clinical trials. *Depress. Anxiety* **2016**, *33*, 895-906, doi:10.1002/da.22500.

40. Laycock, H.; Bantel, C. Opioid mechanisms and opioid drugs. *Anaesth. Intensive Care Med.* **2019**, *20*, 450-455, doi:10.1016/j.mpaic.2019.05.009.

41. Machelska, H.; Celik, M.Ö. Advances in achieving opioid analgesia without side effects. *Front. Pharmacol.* **2018**, *9*, 1388, doi:10.3389/fphar.2018.01388.

42. Wu, H.; Wacker, D.; Mileni, M.; Katritch, V.; Han, G.W.; Vardy, E.; Liu, W.; Thompson, A.A.; Huang, X.-P.; Carroll, F. Structure of the human κ-opioid receptor in complex with JDTic. *Nature* **2012**, *485*, 327-332, doi:10.1038/nature10939.

43. Wang, Y.; Zhuang, Y.; DiBerto, J.F.; Zhou, X.E.; Schmitz, G.P.; Yuan, Q.; Jain, M.K.; Liu, W.; Melcher, K.; Jiang, Y. Structures of the entire human opioid receptor family. *Cell* **2023**, *186*, 413-427. e417, doi:10.1016/j.cell.2022.12.026.

44. Fenalti, G.; Giguere, P.M.; Katritch, V.; Huang, X.-P.; Thompson, A.A.; Cherezov, V.; Roth, B.L.; Stevens, R.C. Molecular control of δ-opioid receptor signalling. *Nature* **2014**, *506*, 191–196, doi:10.1038/nature12944.

45. Manglik, A.; Kruse, A.C.; Kobilka, T.S.; Thian, F.S.; Mathiesen, J.M.; Sunahara, R.K.; Pardo, L.; Weis, W.I.; Kobilka, B.K.; Granier, S. Crystal structure of the μ-opioid receptor bound to a morphinan antagonist. *Nature* **2012**, *485*, 321–326, doi:10.1038/nature10954.

46. Zhuang, Y.; Wang, Y.; He, B.; He, X.; Zhou, X.E.; Guo, S.; Rao, Q.; Yang, J.; Liu, J.; Zhou, Q. Molecular recognition of morphine and fentanyl by the human μ-opioid receptor. *Cell* **2022**, *185*, 4361-4375. e4319, doi:10.1016/j.cell.2022.09.041.

47. Miller, R.L.; Thompson, A.A.; Trapella, C.; Guerrini, R.; Malfacini, D.; Patel, N.; Han, G.W.; Cherezov, V.; Caló, G.; Katritch, V.; Stevens, R.C. The importance of ligand-receptor conformational pairs in stabilization: Spotlight on the N/OFQ G protein-coupled receptor. *Structure* **2015**, *23*, 2291–2299, doi:10.1016/j.str.2015.07.024.

48. Mores, K.L.; Cummins, B.R.; Cassell, R.J.; van Rijn, R.M. A review of the therapeutic potential of recently developed G protein-biased kappa agonists. *Front. Pharmacol.* **2019**, *10*, 407, doi:10.3389/fphar.2019.00407.

49. Chou, R.; Fanciullo, G.J.; Fine, P.G.; Adler, J.A.; Ballantyne, J.C.; Davies, P.; Donovan, M.I.; Fishbain, D.A.; Foley, K.M.; Fudin, J.; Gilson, A.M.; Kelter, A.; Mauskop, A.; O'Connor, P.G.; Passik, S.D.; Pasternak, G.W.; Portenoy, R.K.; Rich, B.A.; Roberts, R.G.; Todd, K.H.; Miaskowski, C. Clinical guidelines for the use of chronic opioid therapy in chronic noncancer pain. *J. Pain* **2009**, *10*, 113–130, doi:10.1016/j.jpain.2008.10.008.

50. Lyden, J.; Binswanger, I.A. The united states opioid epidemic. In Proceedings of the Semin. Perinatol., 2019; pp. 123-131.

51. Browne, C.A.; Jacobson, M.L.; Lucki, I. Novel targets to treat depression: opioid-based therapeutics. *Harv. Rev. Psychiatry* **2020**, *28*, 40-59, doi:10.1097/HRP.0000000000000242.

52. Yekkirala, A.S.; Roberson, D.P.; Bean, B.P.; Woolf, C.J. Breaking barriers to novel analgesic drug development. *Nat. Rev. Drug Discov.* **2017**, *16*, 545–564, doi:10.1038/nrd.2017.87.

53. El Daibani, A.; Paggi, J.M.; Kim, K.; Laloudakis, Y.D.; Popov, P.; Bernhard, S.M.; Krumm, B.E.; Olsen, R.H.; Diberto, J.; Carroll, F.I. Molecular mechanism of biased signaling at the kappa opioid receptor. *Nat. Commun.* **2023**, *14*, 1338, doi:10.1038/s41467-023-37041-7.

54. Stein, C. Opioid Receptors. *Annu. Rev. Med.* **2016**, *67*, 433–451, doi:10.1146/annurev-med-062613-093100.

55. Ubaldi, M.; Cannella, N.; Borruto, A.M.; Petrella, M.; Micioni Di Bonaventura, M.V.; Soverchia, L.; Stopponi, S.; Weiss, F.; Cifani, C.; Ciccocioppo, R. Role of nociceptin/orphanin FQ-NOP receptor system in the regulation of stress-related disorders. *Int. J. Mol. Sci.* **2021**, *22*, 12956, doi:10.3390/ijms222312956.

56. Lutz, P.-E.; Kieffer, B.L. Opioid receptors: distinct roles in mood disorders. *Trends Neurosci.* **2013**, *36*, 195-206, doi:10.1016/j.tins.2012.11.002.

57. Raja, S.N.; Carr, D.B.; Cohen, M.; Finnerup, N.B.; Flor, H.; Gibson, S.; Keefe, F.; Mogil, J.S.; Ringkamp, M.; Sluka, K.A. The revised IASP definition of pain: Concepts, challenges, and compromises. *Pain* **2020**, *161*, 1976-1982, doi:10.1097/j.pain.0000000000001939.

58. Sneddon, L.U. Comparative physiology of nociception and pain. *Physiology* **2017**, *33*, 63-73, doi:10.1152/physiol.00022.2017.

59. Aziz, Q.; Giamberardino, M.A.; Barke, A.; Korwisi, B.; Baranowski, A.P.; Wesselmann, U.; Rief, W.; Treede, R.-D. The IASP classification of chronic pain for ICD-11: chronic secondary visceral pain. *Pain* **2019**, *160*, 69-76, doi:10.1097/j.pain.0000000000001362.

60. Yam, M.F.; Loh, Y.C.; Tan, C.S.; Khadijah Adam, S.; Abdul Manan, N.; Basir, R. General pathways of pain sensation and the major neurotransmitters involved in pain regulation. *Int. J. Mol. Sci.* **2018**, *19*, 2164, doi:10.3390/ijms19082164.

61. Mustazza, C.; Pieretti, S.; Marzoli, F. Nociceptin/orphanin FQ peptide (NOP) receptor modulators: an update in structure-activity relationships. *Curr. Med. Chem.* **2018**, *25*, 2353-2384, doi:10.2174/0929867325666180111095458.

62. Tuteja, N. Signaling through G protein coupled receptors. *Plant signaling & behavior* **2009**, *4*, 942-947, doi:10.4161/psb.4.10.9530.

63. Browne, C.A.; Lucki, I. Targeting opioid dysregulation in depression for the development of novel therapeutics. *Pharmacol. Ther.* **2019**, *201*, 51-76, doi:10.1016/j.pharmthera.2019.04.009.

64. Martínez, V.; Abalo, R. Peripherally acting opioid analgesics and peripherally-induced analgesia. *Behav. Pharmacol.* **2020**, *31*, 136-158, doi:10.1097/FBP.0000000000000558.

65. McDonald, J.; Lambert, D.G. Opioid mechanisms and opioid drugs. *Anaesth. Intensive Care Med.* **2016**, *17*, 464-468, doi:10.1016/j.mpaic.2016.06.012.

66. Faouzi, A.; Varga, B.R.; Majumdar, S. Biased opioid ligands. *Molecules* **2020**, *25*, 4257, doi:10.3390/molecules25184257.

67. Deeks, E.D. Difelikefalin: First Approval. *Drugs* **2021**, *81*, 1937-1944, doi:10.1007/s40265-021-01619-6.

68. Seyedabadi, M.; Gharghabi, M.; Gurevich, E.V.; Gurevich, V.V. Receptor-arrestin interactions: the GPCR perspective. *Biomolecules* **2021**, *11*, 218, doi:10.3390/biom11020218.

69. Kim, K.; Chung, K.Y. Many faces of the GPCR-arrestin interaction. *Arch. Pharm. Res.* **2020**, *43*, 890-899, doi:10.1007/s12272-020-01263-w.

70. Brust, T.F. Biased ligands at the kappa opioid receptor: fine-tuning receptor pharmacology. In *The Kappa opioid receptor. Handbook of experimental pharmacology*, Inan, S., Ed.; Springer: Liu-Chen, LY, 2020; Volume 271, pp. 115-135.

71. Gillis, A.; Kliewer, A.; Kelly, E.; Henderson, G.; Christie, M.J.; Schulz, S.; Canals, M. Critical assessment of G protein-biased agonism at the µ-opioid receptor. *Trends Pharmacol. Sci.* **2020**, *41*, 947–959, doi:10.1016/j.tips.2020.09.009.

72. Gillis, A.; Gondin, A.B.; Kliewer, A.; Sanchez, J.; Lim, H.D.; Alamein, C.; Manandhar, P.; Santiago, M.; Fritzwanker, S.; Schmiedel, F. Low intrinsic efficacy for G protein activation can explain the improved side effect profiles of new opioid agonists. *Sci Signal.* **2020**, *13*, eaaz3140, doi:10.1126/scisignal.aaz3140.

73. Reed, B.; Butelman, E.R.; Kreek, M.J. Kappa opioid receptor antagonists as potential therapeutics for mood and substance use disorders. In *The Kappa Opioid Receptor*, Liu-Chen, L., Inan, S., Eds.; Springer: Cham, Switzerland, 2020; pp. 473-491.

74. Perez-Caballero, L.; Torres-Sanchez, S.; Romero-López-Alberca, C.; González-Saiz, F.; Mico, J.; Berrocoso, E. Monoaminergic system and depression. *Cell Tissue Res.* **2019**, *377*, 107-113, doi:10.1007/s00441-018-2978-8.

75. Gutiérrez-Rojas, L.; Porras-Segovia, A.; Dunne, H.; Andrade-González, N.; Cervilla, J.A. Prevalence and correlates of major depressive disorder: a systematic review. *Braz. J. Psychiatr.* **2020**, *42*, 657-672, doi:10.1590/1516-4446-2020-0650.

76. Jacobson, M.L.; Browne, C.A.; Lucki, I. Kappa opioid receptor antagonists as potential therapeutics for stress-related disorders. *Annu. Rev. Pharmacol. Toxicol.* **2020**, *60*, 615–636, doi:10.1146/annurev-pharmtox-010919-023317.

77. Browne, C.A.; Wulf, H.; Lucki, I. Kappa opioid receptors in the pathology and treatment of major depressive disorder. In *The kappa opioid receptor*, Liu-Chen, L., Inan, S., Eds.; Springer: Cham, Switzerland, 2021; pp. 493-524.

78. Knoll, A.T.; Carlezon Jr, W.A. Dynorphin, stress, and depression. *Brain Res.* **2010**, *1314*, 56-73, doi:10.1016/j.brainres.2009.09.074.

79. Cordonnier, L.; Sanchez, M.; Roques, B.; Noble, F. Facilitation of enkephalins-induced delta-opioid behavioral responses by chronic amisulpride treatment. *Neuroscience* **2005**, *135*, 1-10, doi:10.1016/j.neuroscience.2005.06.006.

80. Zhuang, Y.; Xu, P.; Mao, C.; Wang, L.; Krumm, B.; Zhou, X.E.; Huang, S.; Liu, H.; Cheng, X.; Huang, X.-P. Structural insights into the human D1 and D2 dopamine receptor signaling complexes. *Cell* **2021**, *184*, 931-942. e918, doi:10.1016/j.cell.2021.01.027.

81. Seki, K.; Yoshida, S.; Jaiswal, M.K. Molecular mechanism of noradrenaline during the stress-induced major depressive disorder. *Neural Regen Res.* **2018**, *13*, 1159, doi:10.4103%2F1673-5374.235019.

82. Galeotti, N.; Ghelardini, C. Regionally selective activation and differential regulation of ERK, JNK and p38 MAP kinase signalling pathway by protein kinase C in mood modulation. *Int. J. Neuropsychopharmacol.* **2012**, *15*, 781-793, doi:10.1017/S1461145711000897.

83. Bruchas, M.R.; Land, B.B.; Aita, M.; Xu, M.; Barot, S.K.; Li, S.; Chavkin, C. Stress-induced p38 mitogen-activated protein kinase activation mediates κ-opioid-dependent dysphoria. *J. Neurosci.* **2007**, *27*, 11614-11623, doi:10.1523/JNEUROSCI.3769-07.2007.

84. Ehrich, J.M.; Messinger, D.I.; Knakal, C.R.; Kuhar, J.R.; Schattauer, S.S.; Bruchas, M.R.; Zweifel, L.S.; Kieffer, B.L.; Phillips, P.E.; Chavkin, C. Kappa opioid receptor-induced aversion requires p38 MAPK activation in VTA dopamine neurons. *J. Neurosci.* **2015**, *35*, 12917-12931, doi:10.1523/JNEUROSCI.2444-15.2015.

85. Eisch, A.J.; Harburg, G.C. Opiates, psychostimulants, and adult hippocampal neurogenesis: Insights for addiction and stem cell biology. *Hippocampus* **2006**, *16*, 271-286, doi:10.1002/hipo.20161.

86. Torregrossa, M.M.; Isgor, C.; Folk, J.E.; Rice, K.C.; Watson, S.J.; Woods, J.H. The δ-opioid receptor agonist (+) BW373U86 regulates BDNF mRNA expression in rats. *Neuropsychopharmacol.* **2004**, *29*, 649-659, doi:10.1038/sj.npp.1300345.

87. Zhang, H.; Shi, Y.-G.; Woods, J.H.; Watson, S.J.; Ko, M.-C. Central κ-opioid receptor-mediated antidepressant-like effects of nor-Binaltorphimine: Behavioral and BDNF mRNA expression studies. *Eur. J. Pharmacol.* **2007**, *570*, 89-96, doi:10.1016/j.ejphar.2007.05.045.

88. Gomes, I.; Sierra, S.; Lueptow, L.; Gupta, A.; Gouty, S.; Margolis, E.B.; Cox, B.M.; Devi, L.A. Biased signaling by endogenous opioid peptides. *PNAS* **2020**, *117*, 11820-11828, doi:10.1073/pnas.2000712117.

89. Meyrath, M.; Szpakowska, M.; Zeiner, J.; Massotte, L.; Merz, M.P.; Benkel, T.; Simon, K.; Ohnmacht, J.; Turner, J.D.; Krüger, R. The atypical chemokine receptor ACKR3/CXCR7 is a broad-spectrum scavenger for opioid peptides. *Nat. Commun.* **2020**, *11*, 3033, doi:10.1038/s41467-020-16664-0.

90. Coppes, O.M.; Sang, C.N. Indications for opioid antagonists. *Curr. Pain Headache Rep.* **2017**, *21*, 30, doi:10.1007/s11916-017-0630-z.

91. Bolser, D.C.; Davenport, P.W. Codeine and cough: an ineffective gold standard. *Curr. Opin. Allergy Clin. Immunol.* **2007**, *7*, 32-36, doi:10.1097/ACI.0b013e3280115145.

92. De Schepper, H.; Cremonini, F.; Park, M.I.; Camilleri, M. Opioids and the gut: pharmacology and current clinical experience. *Neurogastroenterol. Motil.* **2004**, *16*, 383-394, doi:10.1111/j.1365-2982.2004.00513.x.

93. Obeng, S.; Hiranita, T.; León, F.; McMahon, L.R.; McCurdy, C.R. Novel approaches, drug candidates, and targets in pain drug discovery. *J. Med. Chem.* **2021**, *64*, 6523-6548, doi:10.1021/acs.jmedchem.1c00028.

94. Varga, B.R.; Streicher, J.M.; Majumdar, S. Strategies towards safer opioid analgesics—A review of old and upcoming targets. *Br. J. Pharmacol.* **2021**, *180*, 975-993, doi:10.1111/bph.15760.

95. Che, T.; Dwivedi-Agnihotri, H.; Shukla, A.K.; Roth, B.L. Biased ligands at opioid receptors: Current status and future directions. *Sci Signal.* **2021**, *14*, eaav0320, doi:10.1126/scisignal.aav0320.

96. Carinci, A.J. Abuse-deterrent opioid analgesics: a guide for clinicians. *Pain Management* **2020**, *10*, 55-62, doi:10.2217/pmt-2019-0052.

97. Kelly, E.; Conibear, A.; Henderson, G. Biased agonism: lessons from studies of opioid receptor agonists. *Annu. Rev. Pharmacol. Toxicol.* **2023**, *63*, 491-515, doi:10.1146/annurev-pharmtox-052120-091058.

98. Beck, T.C.; Hapstack, M.A.; Beck, K.R.; Dix, T.A. Therapeutic potential of kappa opioid agonists. *Pharmaceuticals* **2019**, *12*, 95, doi:10.3390/ph12020095.

99. Albert-Vartanian, A.; Boyd, M.; Hall, A.; Morgado, S.; Nguyen, E.; Nguyen, V.; Patel, S.; Russo, L.; Shao, A.; Raffa, R. Will peripherally restricted kappa-opioid receptor agonists (pKORA s) relieve pain with less opioid adverse effects and abuse potential? *J. Clin. Pharm. Ther.* **2016**, *41*, 371-382, doi:10.1111/jcpt.12404.

100. Stein, C.; Machelska, H. Modulation of peripheral sensory neurons by the immune system: implications for pain therapy. *Pharmacol. Rev.* **2011**, *63*, 860–881, doi:10.1124/pr.110.003145.

101. Paton, K.F.; Atigari, D.V.; Kaska, S.; Prisinzano, T.; Kivell, B.M. Strategies for developing κ opioid receptor agonists for the treatment of pain with fewer side effects. *J. Pharmacol. Exp. Ther.* **2020**, *375*, 332–348, doi:10.1124/jpet.120.000134.

102. Cunningham, C.W.; Elballa, W.M.; Vold, S.U. Bifunctional opioid receptor ligands as novel analgesics. *Neuropharmacology* **2019**, *151*, 195-207, doi:10.1016/j.neuropharm.2019.03.006.

103. Fishbane, S.; Jamal, A.; Munera, C.; Wen, W.; Menzaghi, F. A phase 3 trial of difelikefalin in hemodialysis patients with pruritus. *N. Engl. J. Med.* **2020**, *382*, 222-232, doi:10.1056/NEJMoa1912770.

104. Vandenbossche, J.; Huisman, M.; Xu, Y.; Sanderson-Bongiovanni, D.; Soons, P. Loperamide and P-glycoprotein inhibition: assessment of the clinical relevance. *J. Pharm. Pharmacol.* **2010**, *62*, 401-412, doi:10.1211/jpp.62.04.0001.

105. Fenalti, G.; Zatsepin, N.A.; Betti, C.; Giguere, P.; Han, G.W.; Ishchenko, A.; Liu, W.; Guillemyn, K.; Zhang, H.; James, D.; Wang, D.; Weierstall, U.; Spence, J.C.H.; Boutet,

S.; Messerschmidt, M.; Williams, G.J.; Gati, C.; Yefanov, O.M.; White, T.A.; Oberthuer, D.; Metz, M.; Yoon, C.H.; Barty, A.; Chapman, H.N.; Basu, S.; Coe, J.; Conrad, C.E.; Fromme, R.; Fromme, P.; Tourwé, D.; Schiller, P.W.; Roth, B.L.; Ballet, S.; Katritch, V.; Stevens, R.C.; Cherezov, V. Structural basis for bifunctional peptide recognition at human δ-opioid receptor. *Nat. Struct. Mol. Biol.* **2015**, *22*, 265–268, doi:10.1038/nsmb.2965.

106. Vo, Q.N.; Mahinthichaichan, P.; Shen, J.; Ellis, C.R. How μ-opioid receptor recognizes fentanyl. *Nat. Commun.* **2021**, *12*, 984, doi:10.1038/s41467-021-21262-9.

107. Spahn, V.; Del Vecchio, G.; Rodriguez-Gaztelumendi, A.; Temp, J.; Labuz, D.; Kloner, M.; Reidelbach, M.; Machelska, H.; Weber, M.; Stein, C. Opioid receptor signaling, analgesic and side effects induced by a computationally designed pH-dependent agonist. *Sci. Rep.* **2018**, *8*, 8965, doi:10.1038/s41598-018-27313-4.

108. Spahn, V.; Del Vecchio, G.; Labuz, D.; Rodriguez-Gaztelumendi, A.; Massaly, N.; Temp, J.; Durmaz, V.; Sabri, P.; Reidelbach, M.; Machelska, H. A nontoxic pain killer designed by modeling of pathological receptor conformations. *Science* **2017**, *355*, 966-969, doi:10.1126/science.aai8636.

109. González-Rodríguez, S.; Quadir, M.A.; Gupta, S.; Walker, K.A.; Zhang, X.; Spahn, V.; Labuz, D.; Rodriguez-Gaztelumendi, A.; Schmelz, M.; Joseph, J. Polyglycerol-opioid conjugate produces analgesia devoid of side effects. *eLife* **2017**, *6*, e27081, doi:10.7554/eLife.27081.

110. Bohn, L.M.; Lefkowitz, R.J.; Gainetdinov, R.R.; Peppel, K.; Caron, M.G.; Lin, F.-T. Enhanced morphine analgesia in mice lacking β-arrestin 2. *Science* **1999**, *286*, 2495-2498, doi:10.1126/science.286.5449.2495.

111. Bohn, L.M.; Gainetdinov, R.R.; Lin, F.-T.; Lefkowitz, R.J.; Caron, M.G. μ-Opioid receptor desensitization by β-arrestin-2 determines morphine tolerance but not dependence. *Nature* **2000**, *408*, 720-723, doi:10.1038/35047086.

112. Raehal, K.M.; Walker, J.K.; Bohn, L.M. Morphine side effects in β-arrestin 2 knockout mice. *J. Pharmacol. Exp. Ther.* **2005**, *314*, 1195-1201, doi:10.1124/jpet.105.087254.

113. Fossler, M.J.; Sadler, B.M.; Farrell, C.; Burt, D.A.; Pitsiu, M.; Skobieranda, F.; Soergel, D.G. Oliceridine (TRV130), a novel G protein–biased ligand at the μ-opioid receptor, demonstrates a predictable relationship between plasma concentrations and pain relief. I: Development of a pharmacokinetic/pharmacodynamic model. *J. Clin. Pharmacol.* **2018**, *58*, 750-761, doi:10.1002/jcph.1076.

114. Manglik, A.; Lin, H.; Aryal, D.K.; McCorvy, J.D.; Dengler, D.; Corder, G.; Levit, A.; Kling, R.C.; Bernat, V.; Hübner, H. Structure-based discovery of opioid analgesics with reduced side effects. *Nature* **2016**, *537*, 185-190, doi:10.1038/nature19112.

115. Stahl, E.L.; Schmid, C.L.; Acevedo-Canabal, A.; Read, C.; Grim, T.W.; Kennedy, N.M.; Bannister, T.D.; Bohn, L.M. G protein signaling–biased mu opioid receptor agonists that produce sustained G protein activation are noncompetitive agonists. *PNAS* **2021**, *118*, e2102178118, doi:10.1073/pnas.2102178118.

116. Lambert, D.; Calo, G. Approval of oliceridine (TRV130) for intravenous use in moderate to severe pain in adults. *Br. J. Anaesth.* **2020**, *125*, e473-e474, doi:10.1016/j.bja.2020.09.021.

117. Kliewer, A.; Schmiedel, F.; Sianati, S.; Bailey, A.; Bateman, J.; Levitt, E.; Williams, J.; Christie, M.; Schulz, S. Phosphorylation-deficient G-protein-biased μ-opioid receptors improve analgesia and diminish tolerance but worsen opioid side effects. *Nat. Commun.* **2019**, *10*, 367, doi:10.1038/s41467-018-08162-1.

118. Kliewer, A.; Gillis, A.; Hill, R.; Schmiedel, F.; Bailey, C.; Kelly, E.; Henderson, G.; Christie, M.J.; Schulz, S. Morphine-induced respiratory depression is independent of β-arrestin2 signalling. *Br. J. Pharmacol.* **2020**, *177*, 2923-2931, doi:10.1111/bph.15004.

119. Altarifi, A.A.; David, B.; Muchhala, K.H.; Blough, B.E.; Akbarali, H.; Negus, S.S. Effects of acute and repeated treatment with the biased mu opioid receptor agonist TRV130 (oliceridine) on measures of antinociception, gastrointestinal function, and abuse

liability in rodents. *J. Psychopharm.* **2017**, *31*, 730-739, doi:10.1177/0269881116689257.

120. Hill, R.; Disney, A.; Conibear, A.; Sutcliffe, K.; Dewey, W.; Husbands, S.; Bailey, C.; Kelly, E.; Henderson, G. The novel μ-opioid receptor agonist PZM21 depresses respiration and induces tolerance to antinociception. *Br. J. Pharmacol.* **2018**, *175*, 2653-2661, doi:10.1111/bph.14224.

121. Zamarripa, C.A.; Edwards, S.R.; Qureshi, H.N.; John, N.Y.; Blough, B.E.; Freeman, K.B. The G-protein biased mu-opioid agonist, TRV130, produces reinforcing and antinociceptive effects that are comparable to oxycodone in rats. *Drug Alcohol Depend.* **2018**, *192*, 158-162, doi:10.1016/j.drugalcdep.2018.08.002.

122. Montandon, G.; Ren, J.; Victoria, N.C.; Liu, H.; Wickman, K.; Greer, J.J.; Horner, R.L. G-protein–gated inwardly rectifying potassium channels modulate respiratory depression by opioids. *Anesthesiology* **2016**, *124*, 641-650, doi:10.1097/ALN.0000000000000984.

123. White, K.L.; Robinson, J.E.; Zhu, H.; DiBerto, J.F.; Polepally, P.R.; Zjawiony, J.K.; Nichols, D.E.; Malanga, C.; Roth, B.L. The G protein–biased κ-opioid receptor agonist RB-64 is analgesic with a unique spectrum of activities in vivo. *J. Pharmacol. Exp. Ther.* **2015**, *352*, 98-109, doi:10.1124/jpet.114.216820.

124. Bruchas, M.R.; Chavkin, C. Kinase cascades and ligand-directed signaling at the kappa opioid receptor. *Psychopharmacology* **2010**, *210*, 137–147, doi:10.1007/s00213-010-1806-y.

125. Spetea, M.; Eans, S.O.; Ganno, M.L.; Lantero, A.; Mairegger, M.; Toll, L.; Schmidhammer, H.; McLaughlin, J.P. Selective κ receptor partial agonist HS666 produces potent antinociception without inducing aversion after i.c.v. administration in mice. *Br. J. Pharmacol.* **2017**, *174*, 2444–2456, doi:10.1111/bph.13854.

126. Dripps, I.J.; Boyer, B.T.; Neubig, R.R.; Rice, K.C.; Traynor, J.R.; Jutkiewicz, E.M. Role of signalling molecules in behaviours mediated by the δ opioid receptor agonist SNC80. *Br. J. Pharmacol.* **2018**, *175*, 891-901, doi:10.1111/bph.14131.

127. Bertels, Z.; Witkowski, W.D.; Asif, S.; Siegersma, K.; van Rijn, R.M.; Pradhan, A.A. A non-convulsant delta-opioid receptor agonist, KNT-127, reduces cortical spreading depression and nitroglycerin-induced allodynia. *Headache* **2021**, *61*, 170-178, doi:10.1111/head.14019.

128. Azevedo Neto, J.; Ruzza, C.; Sturaro, C.; Malfacini, D.; Pacifico, S.; Zaveri, N.T.; Calò, G. Functional selectivity does not predict antinociceptive/locomotor impairing potencies of NOP receptor agonists. *Front. Neurosci.* **2021**, *15*, 657153, doi:10.3389/fnins.2021.657153.

129. Kolb, P.; Kenakin, T.; Alexander, S.P.; Bermudez, M.; Bohn, L.M.; Breinholt, C.S.; Bouvier, M.; Hill, S.J.; Kostenis, E.; Martemyanov, K.A. Community guidelines for GPCR ligand bias: IUPHAR review 32. *Br. J. Pharmacol.* **2022**, *179*, 3651-3674, doi:10.1111/bph.15811.

130. Uprety, R.; Che, T.; Zaidi, S.A.; Grinnell, S.G.; Varga, B.R.; Faouzi, A.; Slocum, S.T.; Allaoa, A.; Varadi, A.; Nelson, M. Controlling opioid receptor functional selectivity by targeting distinct subpockets of the orthosteric site. *eLife* **2021**, *10*, e56519, doi:10.7554/eLife.56519.

131. Linz, K.; Christoph, T.; Tzschentke, T.M.; Koch, T.; Schiene, K.; Gautrois, M.; Schröder, W.; Kögel, B.Y.; Beier, H.; Englberger, W.; Schunk, S.; Vry, J.d.; Jahnel, U.; Frosch, S. Cebranopadol: a novel potent analgesic nociceptin/orphanin FQ peptide and opioid receptor agonist. *J. Pharmacol. Exp. Ther.* **2014**, *349*, 535–548, doi:10.1124/jpet.114.213694.

132. Anand, J.P.; Montgomery, D. Multifunctional opioid ligands. In *Delta opioid receptor pharmacology and therapeutic applications. Handbook of experimental pharmacology*, Jutkiewicz, E.M., Ed.; Springer: Cham, Switzerland, 2018; Volume 247, pp. 21-51.

133. Zjawiony, J.K.; Machado, A.S.; Menegatti, R.; Ghedini, P.C.; Costa, E.A.; Pedrino, G.R.; Lukas, S.E.; Franco, O.L.; Silva, O.N.; Fajemiroye, J.O. Cutting-edge search for

safer opioid pain relief: retrospective review of salvinorin A and its analogs. *Front. Psychiatry* **2019**, *10*, 157, doi:10.3389/fpsyt.2019.00157.

134.   Kane, B.E.; Nieto, M.J.; McCurdy, C.R.; Ferguson, D.M. A unique binding epitope for salvinorin A, a non-nitrogenous kappa opioid receptor agonist. *The FEBS journal* **2006**, *273*, 1966-1974, doi:10.1111/j.1742-4658.2006.05212.x.

135.   Butelman, E.R.; Kreek, M.J. Salvinorin A, a kappa-opioid receptor agonist hallucinogen: pharmacology and potential template for novel pharmacotherapeutic agents in neuropsychiatric disorders. *Front. Pharmacol.* **2015**, *6*, 190, doi:10.3389/fphar.2015.00190.

136.   Brito-da-Costa, A.M.; Dias-da-Silva, D.; Gomes, N.G.; Dinis-Oliveira, R.J.; Madureira-Carvalho, Á. Pharmacokinetics and pharmacodynamics of Salvinorin A and Salvia divinorum: Clinical and forensic aspects. *Pharmaceuticals* **2021**, *14*, 116, doi:10.3390/ph14020116.

137.   Vortherms, T.A.; Mosier, P.D.; Westkaemper, R.B.; Roth, B.L. Differential helical orientations among related G protein-coupled receptors provide a novel mechanism for selectivity: studies with salvinorin A and the κ-opioid receptor. *J. Biol. Chem.* **2007**, *282*, 3146-3156, doi:10.1074/jbc.M609264200.

138.   Wang, Y.; Tang, K.; Inan, S.; Siebert, D.; Holzgrabe, U.; Lee, D.Y.; Huang, P.; Li, J.-G.; Cowan, A.; Liu-Chen, L.-Y. Comparison of pharmacological activities of three distinct κ ligands (salvinorin A, TRK-820 and 3FLB) on κ opioid receptors in vitro and their antipruritic and antinociceptive activities in vivo. *J. Pharmacol. Exp. Ther.* **2005**, *312*, 220-230, doi:10.1124/jpet.104.073668.

139.   Roth, B.L.; Baner, K.; Westkaemper, R.; Siebert, D.; Rice, K.C.; Steinberg, S.; Ernsberger, P.; Rothman, R.B. Salvinorin A: a potent naturally occurring nonnitrogenous κ opioid selective agonist. *PNAS* **2002**, *99*, 11934-11939, doi:10.1073/pnas.182234399.

140.   Vardy, E.; Mosier, P.D.; Frankowski, K.J.; Wu, H.; Katritch, V.; Westkaemper, R.B.; Aubé, J.; Stevens, R.C.; Roth, B.L. Chemotype-selective modes of action of κ-opioid receptor agonists. *J. Biol. Chem.* **2013**, *288*, 34470–34483, doi:10.1074/jbc.M113.515668.

141.   Roach, J.J.; Sasano, Y.; Schmid, C.L.; Zaidi, S.; Katritch, V.; Stevens, R.C.; Bohn, L.M.; Shenvi, R.A. Dynamic strategic bond analysis yields a ten-step synthesis of 20-nor-Salvinorin A, a potent κ-OR agonist. *ACS central science* **2017**, *3*, 1329-1336, doi:10.1021/acscentsci.7b00488.

142.   Polepally, P.R.; Huben, K.; Vardy, E.; Setola, V.; Mosier, P.D.; Roth, B.L.; Zjawiony, J.K. Michael acceptor approach to the design of new salvinorin A-based high affinity ligands for the kappa-opioid receptor. *Eur. J. Med. Chem.* **2014**, *85*, 818-829, doi:10.1016/j.ejmech.2014.07.077.

143.   McGovern, D.L.; Mosier, P.D.; Roth, B.L.; Westkaemper, R.B. CoMFA analyses of C-2 position Salvinorin A analogs at the kappa-opioid receptor provides insights into epimer selectivity. *J. Mol. Graph. Model.* **2010**, *28*, 612-625, doi:10.1016/j.jmgm.2009.12.008.

144.   Vortherms, T.A.; Roth, B.L. Salvinorin A. *Molecular interventions* **2006**, *6*, 257, doi:10.1124/mi.6.5.7.

145.   Yan, F.; Mosier, P.D.; Westkaemper, R.B.; Stewart, J.; Zjawiony, J.K.; Vortherms, T.A.; Sheffler, D.J.; Roth, B.L. Identification of the molecular mechanisms by which the diterpenoid salvinorin A binds to κ-opioid receptors. *Biochemistry* **2005**, *44*, 8643-8651, doi:10.1021/bi050490d.

146.   Yan, F.; Bikbulatov, R.V.; Mocanu, V.; Dicheva, N.; Parker, C.E.; Wetsel, W.C.; Mosier, P.D.; Westkaemper, R.B.; Allen, J.A.; Zjawiony, J.K. Structure-based design, synthesis, and biochemical and pharmacological characterization of novel salvinorin A analogues as active state probes of the κ-opioid receptor. *Biochemistry* **2009**, *48*, 6898-6908, doi:10.1021/bi900605n.

147. Roach, J.J.; Shenvi, R.A. A review of salvinorin analogs and their kappa-opioid receptor activity. *Bioorg. Med. Chem. Lett.* **2018**, *28*, 1436-1445, doi:10.1016/j.bmcl.2018.03.029.

148. Frankowski, K.J.; Ghosh, P.; Setola, V.; Tran, T.B.; Roth, B.L.; Aubé, J. N-alkyl-octahydroisoquinolin-1-one-8-carboxamides: selective and nonbasic κ-opioid receptor ligands. *ACS Med. Chem. Lett.* **2010**, *1*, 189-193, doi:10.1021/ml100040t.

149. Frankowski, K.J.; Hedrick, M.P.; Gosalia, P.; Li, K.; Shi, S.; Whipple, D.; Ghosh, P.; Prisinzano, T.E.; Schoenen, F.J.; Su, Y. Discovery of small molecule kappa opioid receptor agonist and antagonist chemotypes through a HTS and hit refinement strategy. *ACS Chem. Neurosci.* **2012**, *3*, 221-236, doi:10.1021/cn200128x.

150. Whitby, L.R.; Ando, Y.; Setola, V.; Vogt, P.K.; Roth, B.L.; Boger, D.L. Design, synthesis, and validation of a β-turn mimetic library targeting protein–protein and peptide–receptor interactions. *J. Am. Chem. Soc.* **2011**, *133*, 10184-10194, doi:10.1021/ja201878v.

151. Gupta, A.; Gomes, I.; Bobeck, E.N.; Fakira, A.K.; Massaro, N.P.; Sharma, I.; Cavé, A.; Hamm, H.E.; Parello, J.; Devi, L.A. Collybolide is a novel biased agonist of κ-opioid receptors with potent antipruritic activity. *PNAS* **2016**, *113*, 6041-6046, doi:10.1073/pnas.1521825113.

152. Bedini, A.; Di Cesare Mannelli, L.; Micheli, L.; Baiula, M.; Vaca, G.; De Marco, R.; Gentilucci, L.; Ghelardini, C.; Spampinato, S. Functional selectivity and antinociceptive effects of a novel KOPr agonist. *Front. Pharmacol.* **2020**, *11*, 188, doi:10.3389/fphar.2020.00188.

153. Coffeen, U.; Pellicer, F. Salvia divinorum: from recreational hallucinogenic use to analgesic and anti-inflammatory action. *J. Pain Res.* **2019**, *12*, 1069-1076, doi:10.2147%2FJPR.S188619.

154. Khan, M.I.H.; Sawyer, B.J.; Akins, N.S.; Le, H.V. A systematic review on the kappa opioid receptor and its ligands: New directions for the treatment of pain, anxiety, depression, and drug abuse. *Eur. J. Med. Chem.* **2022**, *243*, 114785, doi:10.1016/j.ejmech.2022.114785.

155. Tejedor-Real, P.; Mico, J.; Maldonado, R.; Roques, B.; Gibert-Rahola, J. Implication of endogenous opioid system in the learned helplessness model of depression. *Pharmacol. Biochem. Behav.* **1995**, *52*, 145-152, doi:10.1016/0091-3057(95)00067-7.

156. Yang, Q.-Z.; Lu, S.-S.; Tian, X.-Z.; Yang, A.-M.; Ge, W.-W.; Chen, Q. The antidepressant-like effect of human opiorphin via opioid-dependent pathways in mice. *Neurosci. Lett.* **2011**, *489*, 131-135, doi:10.1016/j.neulet.2010.12.002.

157. Berrocoso, E.; Ikeda, K.; Sora, I.; Uhl, G.R.; Sánchez-Blázquez, P.; Mico, J.A. Active behaviours produced by antidepressants and opioids in the mouse tail suspension test. *Int. J. Neuropsychopharmacol.* **2013**, *16*, 151-162, doi:10.1017/S1461145711001842.

158. Gerra, G.; Fantoma, A.; Zaimovic, A. Naltrexone and buprenorphine combination in the treatment of opioid dependence. *J. Psychopharm.* **2006**, *20*, 806-814, doi:10.1177/0269881106060835.

159. Serafini, G.; Adavastro, G.; Canepa, G.; De Berardis, D.; Valchera, A.; Pompili, M.; Nasrallah, H.; Amore, M. The efficacy of buprenorphine in major depression, treatment-resistant depression and suicidal behavior: a systematic review. *Int. J. Mol. Sci.* **2018**, *19*, 2410, doi:10.3390/ijms19082410.

160. Mischoulon, D.; Hylek, L.; Yeung, A.S.; Clain, A.J.; Baer, L.; Cusin, C.; Ionescu, D.F.; Alpert, J.E.; Soskin, D.P.; Fava, M. Randomized, proof-of-concept trial of low dose naltrexone for patients with breakthrough symptoms of major depressive disorder on antidepressants. *J. Affect. Disord.* **2017**, *208*, 6-14, doi:10.1016/j.jad.2016.08.029.

161. Tröster, A.; Ihmsen, H.; Singler, B.; Filitz, J.; Koppert, W. Interaction of fentanyl and buprenorphine in an experimental model of pain and central sensitization in human volunteers. *Clin. J. Pain* **2012**, *28*, 705-711, doi:10.1097/AJP.0b013e318241d948.

162. Toljan, K.; Vrooman, B. Low-dose naltrexone (LDN)—review of therapeutic utilization. *Med. Sci.* **2018**, *6*, 82, doi:10.3390/medsci6040082.

163. Urbano, M.; Guerrero, M.; Rosen, H.; Roberts, E. Antagonists of the kappa opioid receptor. *Bioorg. Med. Chem. Lett.* **2014**, *24*, 2021–2032, doi:10.1016/j.bmcl.2014.03.040.

164. Jacobson, M.L.; Wulf, H.A.; Browne, C.A.; Lucki, I. The kappa opioid receptor antagonist aticaprant reverses behavioral effects from unpredictable chronic mild stress in male mice. *Psychopharmacology* **2020**, *237*, 3715-3728, doi:10.1007/s00213-020-05649-y.

165. Atanasov, A.G.; Zotchev, S.B.; Dirsch, V.M.; Supuran, C.T. Natural products in drug discovery: advances and opportunities. *Nat. Rev. Drug Discovery* **2021**, *20*, 200-216, doi:10.1038/s41573-020-00114-z.

166. Sharma, V.; Wakode, S.; Kumar, H. Structure-and ligand-based drug design: Concepts, approaches, and challenges. In *Chemoinformatics and bioinformatics in the pharmaceutical sciences*, Sharma, N., Ojha, H., Raghav, P.K., Goyal, R.K., Eds.; Academic Press: Cambridge, Massachusetts, 2021; pp. 27-53.

167. Mendez, D.; Gaulton, A.; Bento, A.P.; Chambers, J.; De Veij, M.; Félix, E.; Magariños, M.P.; Mosquera, J.F.; Mutowo, P.; Nowotka, M. ChEMBL: towards direct deposition of bioassay data. *Nucleic Acids Res.* **2019**, *47*, D930-D940, doi:10.1093/nar/gky1075.

168. Hassan Baig, M.; Ahmad, K.; Roy, S.; Mohammad Ashraf, J.; Adil, M.; Haris Siddiqui, M.; Khan, S.; Amjad Kamal, M.; Provazník, I.; Choi, I. Computer aided drug design: success and limitations. *Curr. Pharm. Des.* **2016**, *22*, 572-581, doi:10.2174/1381612822666151125000550.

169. Triballeau, N.; Acher, F.; Brabet, I.; Pin, J.-P.; Bertrand, H.-O. Virtual screening workflow development guided by the "receiver operating characteristic" curve approach. Application to high-throughput docking on metabotropic glutamate receptor subtype 4. *J. Med. Chem.* **2005**, *48*, 2534–2547, doi:10.1021/jm049092j.

170. Qu, Q.; Huang, W.; Aydin, D.; Paggi, J.M.; Seven, A.B.; Wang, H.; Chakraborty, S.; Che, T.; DiBerto, J.F.; Robertson, M.J. Insights into distinct signaling profiles of the µOR activated by diverse agonists. *Nat. Chem. Biol.* **2023**, *19*, 423-430, doi:10.1038/s41589-022-01208-y.

171. Thompson, A.A.; Liu, W.; Chun, E.; Katritch, V.; Wu, H.; Vardy, E.; Huang, X.-P.; Trapella, C.; Guerrini, R.; Calo, G.; Roth, B.L.; Cherezov, V.; Stevens, R.C. Structure of the nociceptin/orphanin FQ receptor in complex with a peptide mimetic. *Nature* **2012**, *485*, 395–399, doi:10.1038/nature11085.

172. Granier, S.; Manglik, A.; Kruse, A.C.; Kobilka, T.S.; Thian, F.S.; Weis, W.I.; Kobilka, B.K. Structure of the δ-opioid receptor bound to naltrindole. *Nature* **2012**, *485*, 400–404, doi:10.1038/nature11111.

173. Huang, W.; Manglik, A.; Venkatakrishnan, A.J.; Laeremans, T.; Feinberg, E.N.; Sanborn, A.L.; Kato, H.E.; Livingston, K.E.; Thorsen, T.S.; Kling, R.C.; Granier, S.; Gmeiner, P.; Husbands, S.M.; Traynor, J.R.; Weis, W.I.; Steyaert, J.; Dror, R.O.; Kobilka, B.K. Structural insights into µ-opioid receptor activation. *Nature* **2015**, *524*, 315–321, doi:10.1038/nature14886.

174. Koehl, A.; Hu, H.; Maeda, S.; Zhang, Y.; Qu, Q.; Paggi, J.M.; Latorraca, N.R.; Hilger, D.; Dawson, R.; Matile, H.; Schertler, G.F.X.; Granier, S.; Weis, W.I.; Dror, R.O.; Manglik, A.; Skiniotis, G.; Kobilka, B.K. Structure of the µ-opioid receptor-Gi protein complex. *Nature* **2018**, *558*, 547–552, doi:10.1038/s41586-018-0219-7.

175. Claff, T.; Yu, J.; Blais, V.; Patel, N.; Martin, C.; Wu, L.; Han, G.W.; Holleran, B.J.; van der Poorten, O.; White, K.L.; Hanson, M.A.; Sarret, P.; Gendron, L.; Cherezov, V.; Katritch, V.; Ballet, S.; Liu, Z.-J.; Müller, C.E.; Stevens, R.C. Elucidating the active δ-opioid receptor crystal structure with peptide and small-molecule agonists. *Sci. Adv.* **2019**, *5*, eaax9115, doi:10.1126/sciadv.aax9115.

176. Che, T.; English, J.; Krumm, B.E.; Kim, K.; Pardon, E.; Olsen, R.H.J.; Wang, S.; Zhang, S.; Diberto, J.F.; Sciaky, N.; Carroll, F.I.; Steyaert, J.; Wacker, D.; Roth, B.L. Nanobody-enabled monitoring of kappa opioid receptor states. *Nat. Commun.* **2020**, *11*, 1145, doi:10.1038/s41467-020-14889-7.

177. Wang, H.; Hetzer, F.; Huang, W.; Qu, Q.; Meyerowitz, J.; Kaindl, J.; Hübner, H.; Skiniotis, G.; Kobilka, B.K.; Gmeiner, P. Structure-based evolution of G protein-biased μ-opioid receptor agonists. *Angew. Chem. Int. Ed.* **2022**, *61*, e202200269, doi:10.1002/anie.202200269.

178. Faouzi, A.; Wang, H.; Zaidi, S.A.; DiBerto, J.F.; Che, T.; Qu, Q.; Robertson, M.J.; Madasu, M.K.; El Daibani, A.; Varga, B.R. Structure-based design of bitopic ligands for the μ-opioid receptor. *Nature* **2023**, *613*, 767-774, doi:10.1038/s41586-022-05588-y.

179. Robertson, M.J.; Papasergi-Scott, M.M.; He, F.; Seven, A.B.; Meyerowitz, J.G.; Panova, O.; Peroto, M.C.; Che, T.; Skiniotis, G. Structure determination of inactive-state GPCRs with a universal nanobody. *Nat. Struct. Mol. Biol.* **2022**, 1188–1195, doi:10.1038/s41594-022-00859-8.

180. Chen, Y.; Chen, B.; Wu, T.; Zhou, F.; Xu, F. Cryo-EM structure of human κ-opioid receptor-Gi complex bound to an endogenous agonist dynorphin A. *Protein & Cell* **2023**, *14*, 464-468, doi:10.1093/procel/pwac033.

181. Han, J.; Zhang, J.; Nazarova, A.L.; Bernhard, S.M.; Krumm, B.E.; Zhao, L.; Lam, J.H.; Rangari, V.A.; Majumdar, S.; Nichols, D.E. Ligand and G-protein selectivity in the κ-opioid receptor. *Nature* **2023**, 1-9, doi:10.1038/s41586-023-06030-7.

182. Munro, T.A. Reanalysis of a μ opioid receptor crystal structure reveals a covalent adduct with BU72. *BMC Biol.* **2023**, *21*, 213, doi:10.1186/s12915-023-01689-w.

183. Khoramjouy, M.; Ahmadi, F.; Faizi, M.; Shahhosseini, S. Optimization binding studies of opioid receptors, saturation and competition, using [3 H]-DAMGO. *Pharmacol. Rep.* **2021**, *73*, 1390-1395, doi:10.1007/s43440-021-00265-9.

184. Harrison, C.; Traynor, J. The [35S] GTPγS binding assay: approaches and applications in pharmacology. *Life Sci.* **2003**, *74*, 489-508, doi:10.1016/j.lfs.2003.07.005.

185. Hunskaar, S.; Berge, O.-G.; Hole, K. A modified hot-plate test sensitivie to mild analgesics. *Behav. Brain Res.* **1986**, *21*, 101-108, doi:10.1016/0166-4328(86)90088-4.

186. Bannon, A.W.; Malmberg, A.B. Models of nociception: hot-plate, tail-flick, and formalin tests in rodents. *Curr. Protoc. Neurosci.* **2007**, *41*, 8.9.1-8.9.16, doi:10.1002/0471142301.ns0809s41.

187. Can, A.; Dao, D.T.; Arad, M.; Terrillion, C.E.; Piantadosi, S.C.; Gould, T.D. The mouse forced swim test. *J. Vis. Exp.* **2012**, e3638, doi:10.3791/3638.

188. Azar, M.R.; Jones, B.C.; Schulteis, G. Conditioned place aversion is a highly sensitive index of acute opioid dependence and withdrawal. *Psychopharmacology* **2003**, *170*, 42-50, doi:10.1007/s00213-003-1514-y.

189. Shiotsuki, H.; Yoshimi, K.; Shimo, Y.; Funayama, M.; Takamatsu, Y.; Ikeda, K.; Takahashi, R.; Kitazawa, S.; Hattori, N. A rotarod test for evaluation of motor skill learning. *J. Neurosci. Methods* **2010**, *189*, 180-185, doi:10.1016/j.jneumeth.2010.03.026.

190. Flanagan, C.A. GPCR-radioligand binding assays. In *Methods Cell Biol.*; Elsevier: 2016; Volume 132, pp. 191-215.

191. Hulme, E.C.; Trevethick, M.A. Ligand binding assays at equilibrium: validation and interpretation. *Br. J. Pharmacol.* **2010**, *161*, 1219-1237, doi:10.1111/j.1476-5381.2009.00604.x.

192. Puls, K.; Olivé-Marti, A.-L.; Pach, S.; Pinter, B.; Erli, F.; Wolber, G.; Spetea, M. In vitro, in vivo and in silico characterization of a novel kappa-opioid receptor antagonist. *Pharmaceuticals* **2022**, *15*, 680, doi:10.3390/ph15060680.

193. Burlingham, B.T.; Widlanski, T.S. An intuitive look at the relationship of Ki and IC50: a more general use for the Dixon plot. *J. Chem. Educ.* **2003**, *80*, 214, doi:10.1021/ed080p214.

194. Guo, S.; Zhao, T.; Yun, Y.; Xie, X. Recent progress in assays for GPCR drug discovery. *Am. J. Physiol. Cell Physiol.* **2022**, *323*, C583-C594, doi:10.1152/ajpcell.00464.2021.

195. Schmidhammer, H.; Erli, F.; Guerrieri, E.; Spetea, M. Development of diphenethylamines as selective kappa opioid receptor ligands and their

pharmacological activities. *Molecules* **2020**, *25*, 5092, doi:10.3390/molecules25215092.

196. Otte, L.; Wilde, M.; Auwärter, V.; Grafinger, K.E. Investigation of the µ-and κ-opioid receptor activation by eight new synthetic opioids using the [35S]-GTPγS assay: U-47700, isopropyl U-47700, U-49900, U-47931E, N-methyl U-47931E, U-51754, U-48520, and U-48800. *Drug Test Anal.* **2022**, *14*, 1187-1199, doi:10.1002/dta.3238.

197. Lu, J.J.; Polgar, W.E.; Mann, A.; Dasgupta, P.; Schulz, S.; Zaveri, N.T. Differential in vitro pharmacological profiles of structurally diverse nociceptin receptor agonists in activating G protein and beta-arrestin signaling at the human nociceptin opioid receptor. *Mol. Pharmacol.* **2021**, *100*, 7-18, doi:10.1124/molpharm.120.000076.

198. Johnson, E.N.; Shi, X.; Cassaday, J.; Ferrer, M.; Strulovici, B.; Kunapuli, P. A 1,536-Well [35S]GTPγS scintillation proximity binding assay for ultra-high-throughput screening of an orphan Gαi-coupled GPCR. *Assay Drug Dev. Technol.* **2008**, *6*, 327-337, doi:10.1089/adt.2007.113.

199. Ferrer, M.; Kolodin, G.D.; Zuck, P.; Peltier, R.; Berry, K.; Mandala, S.M.; Rosen, H.; Ota, H.; Ozaki, S.; Inglese, J. A fully automated [35S] GTPγS scintillation proximity assay for the high-throughput screening of Gi-linked G protein-coupled receptors. *Assay Drug Dev. Technol.* **2003**, *1*, 261-273, doi:10.1089/15406580360545071.

200. Strange, P.G. Use of the GTPgS ([35S]GTPgS and Eu-GTPgS) binding assay for analysis of ligand potency and efficacy at G protein-coupled receptors. *Br. J. Pharmacol.* **2010**, *161*, doi:10.1111/bph.2010.161.issue-6.

201. Milligan, G. Principles: Extending the utility of [35S]GTPγS binding assays. *Trends Pharmacol. Sci.* **2003**, *24*, 87–90, doi:10.1016/s0165-6147(02)00027-5.

202. Kuhlman, B.; Bradley, P. Advances in protein structure prediction and design. *Nat. Rev. Mol. Cell Biol.* **2019**, *20*, 681-697, doi:10.1038/s41580-019-0163-x.

203. Schmidt, T.; Bergner, A.; Schwede, T. Modelling three-dimensional protein structures for applications in drug design. *Drug Discov. Today* **2014**, *19*, 890–897, doi:10.1016/j.drudis.2013.10.027.

204. Jumper, J.; Evans, R.; Pritzel, A.; Green, T.; Figurnov, M.; Ronneberger, O.; Tunyasuvunakool, K.; Bates, R.; Žídek, A.; Potapenko, A. Highly accurate protein structure prediction with AlphaFold. *Nature* **2021**, *596*, 583-589, doi:10.1038/s41586-021-03819-2.

205. Gulsevin, A.; Han, B.; Porta, J.C.; Mchaourab, H.S.; Meiler, J.; Kenworthy, A.K. Template-free prediction of a new monotopic membrane protein fold and assembly by AlphaFold2. *Biophys. J.* **2023**, *122*, 2041-2052, doi:10.1016/j.bpj.2022.11.011.

206. Martí-Renom, M.A.; Stuart, A.C.; Fiser, A.; Sánchez, R.; Melo, F.; Sali, A. Comparative protein structure modeling of genes and genomes. *Annu. Rev. Biophys. Biomol. Struct.* **2000**, *29*, 291–325, doi:10.1146/annurev.biophys.29.1.291.

207. Jisna, V.; Jayaraj, P. Protein structure prediction: conventional and deep learning perspectives. *Protein J.* **2021**, *40*, 522-544, doi:10.1007/s10930-021-10003-y.

208. Bhattacharya, S.; Roche, R.; Shuvo, M.H.; Bhattacharya, D. Recent advances in protein homology detection propelled by inter-residue interaction map threading. *Front. Mol. Biosci.* **2021**, *8*, 643752, doi:10.3389/fmolb.2021.643752.

209. Lesk, A.M.; Konagurthu, A.S. Protein structure prediction improves the quality of amino-acid sequence alignment. *Proteins* **2022**, *90*, 2144-2147, doi:10.1002/prot.26392.

210. Thompson, J.D.; Higgins, D.G.; Gibson, T.J. CLUSTAL W: improving the sensitivity of progressive multiple sequence alignment through sequence weighting, position-specific gap penalties and weight matrix choice. *Nucleic Acids Res.* **1994**, *22*, 4673-4680, doi:10.1093/nar/22.22.4673.

211. Sievers, F.; Higgins, D.G. Clustal omega. *Curr Protoc Bioinformatics* **2014**, *48*, 3.13. 11-13.13. 16, doi:10.1002/0471250953.bi0313s48.

212. Edgar, R.C. MUSCLE: multiple sequence alignment with high accuracy and high throughput. *Nucleic Acids Res.* **2004**, *32*, 1792-1797, doi:10.1093/nar/gkh340.

213. Molecular Operating Environment (MOE), C.C.G.U., Sherbooke St. West, Suite #910, Montreal, QC, Canada, H3A 2R7, 2021. Available online: https://www.chemcomp.com/Products.htm (accessed on 01.04.2021).

214. Yang, J.; Yan, R.; Roy, A.; Xu, D.; Poisson, J.; Zhang, Y. The I-TASSER Suite: protein structure and function prediction. *Nat. Methods* **2015**, *12*, 7-8, doi:10.1038/nmeth.3213.

215. Waterhouse, A.; Bertoni, M.; Bienert, S.; Studer, G.; Tauriello, G.; Gumienny, R.; Heer, F.T.; Beer, T.A.P.d.; Rempfer, C.; Bordoli, L.; Lepore, R.; Schwede, T. SWISS-MODEL: homology modelling of protein structures and complexes. *Nucleic Acids Res.* **2018**, *46*, W296-W303, doi:10.1093/nar/gky427.

216. Baker lab at University of Washington. Robetta: Structure prediction server. Available online: https://robetta.bakerlab.org/ (accessed on 01.10.2023).

217. Labute, P. The generalized Born/volume integral implicit solvent model: estimation of the free energy of hydration using London dispersion instead of atomic surface area. *J. Comput. Chem.* **2008**, *29*, 1693-1698, doi:10.1002/jcc.20933.

218. Ramachandran, G.N.; Ramakrishnan, C.; Sasisekharan, V. Stereochemistry of polypeptide chain configurations. *J. Mol. Biol.* **1963**, *7*, 95–99, doi:10.1016/s0022-2836(63)80023-6.

219. Abu-Hammad, A.; Zalloum, W.A.; Zalloum, H.; Abu-Sheikha, G.; Taha, M.O. Homology modeling of MCH1 receptor and validation by docking/scoring and protein-aligned CoMFA. *Eur. J. Med. Chem.* **2009**, *44*, 2583-2596, doi:10.1016/j.ejmech.2009.01.031.

220. Pedretti, A.; Vistoli, G. Modeling of human ghrelin receptor (hGHS-R1a) in its close state and validation by molecular docking. *Biorg. Med. Chem.* **2007**, *15*, 3054-3064, doi:10.1016/j.bmc.2007.01.057.

221. Warren, G.L.; Andrews, C.W.; Capelli, A.-M.; Clarke, B.; LaLonde, J.; Lambert, M.H.; Lindvall, M.; Nevins, N.; Semus, S.F.; Senger, S.; Tedesco, G.; Wall, I.D.; Woolven, J.M.; Peishoff, C.E.; Head, M.S. A critical assessment of docking programs and scoring functions. *J. Med. Chem.* **2006**, *49*, 5912–5931, doi:10.1021/jm050362n.

222. Ferreira, L.G.; Dos Santos, R.N.; Oliva, G.; Andricopulo, A.D. Molecular docking and structure-based drug design strategies. *Molecules* **2015**, *20*, 13384–13421, doi:10.3390/molecules200713384.

223. Jones, G.; Willett, P.; Glen, R.C.; Leach, A.R.; Taylor, R. Development and validation of a genetic algorithm for flexible docking. *J. Mol. Biol.* **1997**, *267*, 727–748, doi:10.1006/jmbi.1996.0897.

224. Corbeil, C.R.; Williams, C.I.; Labute, P. Variability in docking success rates due to dataset preparation. *J. Comput. Aided Mol. Des.* **2012**, *26*, 775-786, doi:10.1007/s10822-012-9570-1.

225. Friesner, R.A.; Banks, J.L.; Murphy, R.B.; Halgren, T.A.; Klicic, J.J.; Mainz, D.T.; Repasky, M.P.; Knoll, E.H.; Shelley, M.; Perry, J.K. Glide: a new approach for rapid, accurate docking and scoring. 1. Method and assessment of docking accuracy. *J. Med. Chem.* **2004**, *47*, 1739-1749, doi:10.1021/jm0306430.

226. Halgren, T.A.; Murphy, R.B.; Friesner, R.A.; Beard, H.S.; Frye, L.L.; Pollard, W.T.; Banks, J.L. Glide: a new approach for rapid, accurate docking and scoring. 2. Enrichment factors in database screening. *J. Med. Chem.* **2004**, *47*, 1750-1759, doi:10.1021/jm030644s.

227. Morris, G.M.; Huey, R.; Lindstrom, W.; Sanner, M.F.; Belew, R.K.; Goodsell, D.S.; Olson, A.J. AutoDock4 and AutoDockTools4: Automated docking with selective receptor flexibility. *J. Comput. Chem.* **2009**, *30*, 2785-2791, doi:10.1002/jcc.21256.

228. Trott, O.; Olson, A.J. AutoDock Vina: improving the speed and accuracy of docking with a new scoring function, efficient optimization, and multithreading. *J. Comput. Chem.* **2010**, *31*, 455-461, doi:10.1002/jcc.21334.

229. Wang, Z.; Sun, H.; Yao, X.; Li, D.; Xu, L.; Li, Y.; Tian, S.; Hou, T. Comprehensive evaluation of ten docking programs on a diverse set of protein–ligand complexes: the prediction accuracy of sampling power and scoring power. *Phys. Chem. Chem. Phys.* **2016**, *18*, 12964-12975, doi:10.1039/C6CP01555G.

230. Pagadala, N.S.; Syed, K.; Tuszynski, J. Software for molecular docking: a review. *Biophys. Rev.* **2017**, *9*, 91-102, doi:10.1007/s12551-016-0247-1.

231. Kuntz, I.D.; Blaney, J.M.; Oatley, S.J.; Langridge, R.; Ferrin, T.E. A geometric approach to macromolecule-ligand interactions. *J. Mol. Biol.* **1982**, *161*, 269-288, doi:10.1016/0022-2836(82)90153-X.

232. Rarey, M.; Kramer, B.; Lengauer, T.; Klebe, G. A fast flexible docking method using an incremental construction algorithm. *J. Mol. Biol.* **1996**, *261*, 470-489, doi:10.1006/jmbi.1996.0477.

233. Venkatachalam, C.M.; Jiang, X.; Oldfield, T.; Waldman, M. LigandFit: a novel method for the shape-directed rapid docking of ligands to protein active sites. *J. Mol. Graph. Model.* **2003**, *21*, 289-307, doi:10.1016/S1093-3263(02)00164-X.

234. Eldridge, M.D.; Murray, C.W.; Auton, T.R.; Paolini, G.V.; Mee, R.P. Empirical scoring functions: I. The development of a fast empirical scoring function to estimate the binding affinity of ligands in receptor complexes. *J. Comput. Aided Mol. Des.* **1997**, *11*, 425-445, doi:10.1023/A:1007996124545.

235. Gohlke, H.; Hendlich, M.; Klebe, G. Knowledge-based scoring function to predict protein-ligand interactions. *J. Mol. Biol.* **2000**, *295*, 337-356, doi:10.1006/jmbi.1999.3371.

236. Verdonk, M.L.; Cole, J.C.; Hartshorn, M.J.; Murray, C.W.; Taylor, R.D. Improved protein-ligand docking using GOLD. *Proteins* **2003**, *52*, 609–623, doi:10.1002/prot.10465.

237. Evers, A.; Hessler, G.; Matter, H.; Klabunde, T. Virtual screening of biogenic amine-binding G-protein coupled receptors: comparative evaluation of protein- and ligand-based virtual screening protocols. *J. Med. Chem.* **2005**, *48*, 5448–5465, doi:10.1021/jm050090o.

238. Jones, G.; Willett, P.; Glen, R.C. Molecular recognition of receptor sites using a genetic algorithm with a description of desolvation. *J. Mol. Biol.* **1995**, *245*, 43-53, doi:10.1016/S0022-2836(95)80037-9.

239. Wolber, G.; Dornhofer, A.A.; Langer, T. Efficient overlay of small organic molecules using 3D pharmacophores. *J. Comput. Aided Mol. Des.* **2006**, *20*, 773–788, doi:10.1007/s10822-006-9078-7.

240. Grant, J.A.; Pickup, B. A Gaussian description of molecular shape. *J. Phys. Chem.* **1995**, *99*, 3503-3510, doi:10.1021/j100011a016.

241. Kumar, A.; Zhang, K.Y.J. Advances in the development of shape similarity methods and their application in drug discovery. *Front. Chem.* **2018**, *6*, 315, doi:10.3389/fchem.2018.00315.

242. Fischer, A.; Smiesko, M.; Sellner, M.; Lill, M.A. Decision making in structure-based drug discovery: visual inspection of docking results. *J. Med. Chem.* **2021**, *64*, 2489-2500, doi:10.1021/acs.jmedchem.0c02227.

243. Spyrakis, F.; BidonChanal, A.; Barril, X.; Javier Luque, F. Protein flexibility and ligand recognition: challenges for molecular modeling. *Curr. Top. Med. Chem.* **2011**, *11*, 192-210, doi:10.2174/156802611794863571.

244. Hernández-Rodríguez, M.; C Rosales-Hernández, M.; E Mendieta-Wejebe, J.; Martínez-Archundia, M.; Correa Basurto, J. Current tools and methods in molecular dynamics (MD) simulations for drug design. *Curr. Med. Chem.* **2016**, *23*, 3909-3924, doi:10.2174/0929867323666160530144742.

245. Durrant, J.D.; McCammon, J.A. Molecular dynamics simulations and drug discovery. *BMC Biol.* **2011**, *9*, 71, doi:10.1186/1741-7007-9-71.

246. Hollingsworth, S.A.; Dror, R.O. Molecular dynamics simulation for all. *Neuron* **2018**, *99*, 1129-1143, doi:10.1016/j.neuron.2018.08.011.

247. Salo-Ahen, O.M.; Alanko, I.; Bhadane, R.; Bonvin, A.M.; Honorato, R.V.; Hossain, S.; Juffer, A.H.; Kabedev, A.; Lahtela-Kakkonen, M.; Larsen, A.S. Molecular dynamics simulations in drug discovery and pharmaceutical development. *Processes* **2021**, *9*, 71, doi:10.3390/pr9010071.

248. Liu, X.; Shi, D.; Zhou, S.; Liu, H.; Liu, H.; Yao, X. Molecular dynamics simulations and novel drug discovery. *Expert Opin. Drug Discov.* **2018**, *13*, 23-37, doi:10.1080/17460441.2018.1403419.

249. Bera, I.; Payghan, P.V. Use of molecular dynamics simulations in structure-based drug discovery. *Curr. Pharm. Des.* **2019**, *25*, 3339-3349, doi:10.2174/1381612825666190903153043.

250. Riniker, S. Fixed-charge atomistic force fields for molecular dynamics simulations in the condensed phase: an overview. *J. Chem. Inf. Model.* **2018**, *58*, 565-578, doi:10.1021/acs.jcim.8b00042.

251. Verlet, L. Computer" experiments" on classical fluids. I. Thermodynamical properties of Lennard-Jones molecules. *Phys. Rev.* **1967**, *159*, 98, doi:10.1103/PhysRev.159.98.

252. Vollmayr-Lee, K. Introduction to molecular dynamics simulations. *Am. J. Phys.* **2020**, *88*, 401-422, doi:10.1119/10.0000654.

253. Cheng, X.; Ivanov, I. Molecular dynamics. In *Computational Toxicology. Methods in Molecular Biology*, Reisfeld, B., Mayeno, A., Eds.; Humana Press: Totowa, NJ., 2012; Volume 929.

254. Shukla, R.; Tripathi, T. Molecular dynamics simulation in drug discovery: opportunities and challenges. In *Innovations and Implementations of Computer Aided Drug Discovery Strategies in Rational Drug Design*, Singh, S.K., Ed.; Springer: Singapore, 2021; pp. 295-316.

255. Maier, J.A.; Martinez, C.; Kasavajhala, K.; Wickstrom, L.; Hauser, K.E.; Simmerling, C. ff14SB: improving the accuracy of protein side chain and backbone parameters from ff99SB. *J. Chem. Theory Comput.* **2015**, *11*, 3696-3713, doi:10.1021/acs.jctc.5b00255.

256. Best, R.B.; Zhu, X.; Shim, J.; Lopes, P.E.; Mittal, J.; Feig, M.; MacKerell Jr, A.D. Optimization of the additive CHARMM all-atom protein force field targeting improved sampling of the backbone φ, ψ and side-chain χ1 and χ2 dihedral angles. *J. Chem. Theory Comput.* **2012**, *8*, 3257-3273, doi:10.1021/ct300400x.

257. Reif, M.M.; Hünenberger, P.H.; Oostenbrink, C. New interaction parameters for charged amino acid side chains in the GROMOS force field. *J. Chem. Theory Comput.* **2012**, *8*, 3705-3723, doi:10.1021/ct300156h.

258. Harder, E.; Damm, W.; Maple, J.; Wu, C.; Reboul, M.; Xiang, J.Y.; Wang, L.; Lupyan, D.; Dahlgren, M.K.; Knight, J.L. OPLS3: a force field providing broad coverage of drug-like small molecules and proteins. *J. Chem. Theory Comput.* **2016**, *12*, 281-296, doi:10.1021/acs.jctc.5b00864.

259. Nerenberg, P.S.; Head-Gordon, T. New developments in force fields for biomolecular simulations. *Curr. Opin. Struct. Biol.* **2018**, *49*, 129-138, doi:10.1016/j.sbi.2018.02.002.

260. Lin, F.-Y.; MacKerell, A.D. Force fields for small molecules. In *Biomolecular Simulations. Methods in Molecular Biology*, Bonomi, M., Camilloni, C., Eds.; Humana: New York, NY, 2019; Volume 2022, pp. 21-54.

261. Knapp, B.; Ospina, L.; Deane, C.M. Avoiding false positive conclusions in molecular simulation: the importance of replicas. *J. Chem. Theory Comput.* **2018**, *14*, 6127-6138, doi:10.1021/acs.jctc.8b00391.

262. Kräutler, V.; Van Gunsteren, W.F.; Hünenberger, P.H. A fast SHAKE algorithm to solve distance constraint equations for small molecules in molecular dynamics simulations. *J. Comput. Chem.* **2001**, *22*, 501-508, doi:10.1002/1096-987X(20010415)22:5%3C501::AID-JCC1021%3E3.0.CO;2-V.

263. Watanabe, M.; Karplus, M. Simulations of macromolecules by multiple time-step methods. *J. Phys. Chem.* **1995**, *99*, 5680-5697, doi:10.1021/j100015a061.

264. Ryckaert, J.-P.; Ciccotti, G.; Berendsen, H.J. Numerical integration of the cartesian equations of motion of a system with constraints: molecular dynamics of n-alkanes. *J. Comput. Phys.* **1977**, *23*, 327-341, doi:10.1016/0021-9991(77)90098-5.

265. Krieger, E.; Vriend, G. New ways to boost molecular dynamics simulations. *J. Comput. Chem.* **2015**, *36*, 996-1007, doi:10.1002/jcc.23899.

266. Olesen, K.; Awasthi, N.; Bruhn, D.S.; Pezeshkian, W.; Khandelia, H. Faster simulations with a 5 fs time step for lipids in the CHARMM force field. *J. Chem. Theory Comput.* **2018**, *14*, 3342-3350, doi:10.1021/acs.jctc.8b00267.

267. Gauthier, J.A.; Dickens, C.F.; Heenen, H.H.; Vijay, S.; Ringe, S.; Chan, K. Unified approach to implicit and explicit solvent simulations of electrochemical reaction energetics. *J. Chem. Theory Comput.* **2019**, *15*, 6895-6906, doi:10.1021/acs.jctc.9b00717.

268. Jorgensen, W.L.; Chandrasekhar, J.; Madura, J.D.; Impey, R.W.; Klein, M.L. Comparison of simple potential functions for simulating liquid water. *J. Chem. Phys.* **1983**, *79*, 926–935, doi:10.1063/1.445869.

269. Lomize, M.A.; Pogozheva, I.D.; Joo, H.; Mosberg, H.I.; Lomize, A.L. OPM database and PPM web server: resources for positioning of proteins in membranes. *Nucleic Acids Res.* **2012**, *40*, D370-D376, doi:10.1093/nar/gkr703.

270. Walton, E.B.; VanVliet, K.J. Equilibration of experimentally determined protein structures for molecular dynamics simulation. *Phys. Rev. E* **2006**, *74*, 061901, doi:10.1103/PhysRevE.74.061901.

271. Case, D.A.; Cheatham III, T.E.; Darden, T.; Gohlke, H.; Luo, R.; Merz Jr, K.M.; Onufriev, A.; Simmerling, C.; Wang, B.; Woods, R.J. The Amber biomolecular simulation programs. *J. Comput. Chem.* **2005**, *26*, 1668-1688, doi:10.1002/jcc.20290.

272. Brooks, B.R.; Brooks III, C.L.; Mackerell Jr, A.D.; Nilsson, L.; Petrella, R.J.; Roux, B.; Won, Y.; Archontis, G.; Bartels, C.; Boresch, S. CHARMM: the biomolecular simulation program. *J. Comput. Chem.* **2009**, *30*, 1545-1614, doi:10.1002/jcc.21287.

273. Berendsen, H.J.; van der Spoel, D.; van Drunen, R. GROMACS: A message-passing parallel molecular dynamics implementation. *Comput. Phys. Commun.* **1995**, *91*, 43-56, doi:10.1016/0010-4655(95)00042-E.

274. Phillips, J.C.; Braun, R.; Wang, W.; Gumbart, J.; Tajkhorshid, E.; Villa, E.; Chipot, C.; Skeel, R.D.; Kale, L.; Schulten, K. Scalable molecular dynamics with NAMD. *J. Comput. Chem.* **2005**, *26*, 1781-1802, doi:10.1002/jcc.20289.

275. Bock, A.; Bermudez, M.; Krebs, F.; Matera, C.; Chirinda, B.; Sydow, D.; Dallanoce, C.; Holzgrabe, U.; Amici, M.d.; Lohse, M.J.; Wolber, G.; Mohr, K. Ligand binding ensembles determine graded agonist efficacies at a G protein-coupled receptor. *J. Biol. Chem.* **2016**, *291*, 16375–16389, doi:10.1074/jbc.m116.735431.

276. Sydow, D. *Dynophores: Novel dynamic pharmacophores implementation of pharmacophore generation based on molecular dynamics trajectories and their graphical representation*; Freie Universität Berlin: Berlin, Germany, 2015.

277. Wermuth, C.; Ganellin, C.; Lindberg, P.; Mitscher, L. Glossary of terms used in medicinal chemistry (IUPAC Recommendations 1998). *Pure Appl. Chem.* **1998**, *70*, 1129-1143, doi:10.1351/pac199870051129.

278. Schaller, D.; Šribar, D.; Noonan, T.; Deng, L.; Nguyen, T.N.; Pach, S.; Machalz, D.; Bermudez, M.; Wolber, G. Next generation 3D pharmacophore modeling. *WIREs Comput Mol Sci.* **2020**, *10*, e1468, doi:10.1002/wcms.1468.

279. Seidel, T.; Wolber, G.; Murgueitio, M.S. Pharmacophore perception and applications. In *Applied Chemoinformatics: Achievements and Future Opportunities*, Engel, T., Gasteiger, J., Eds.; Wiley-VCH: Weinheim, Germany, 2018; pp. 259-282.

280. Wolber, G.; Langer, T. LigandScout: 3-D pharmacophores derived from protein-bound ligands and their use as virtual screening filters. *J. Chem. Inf. Model.* **2005**, *45*, 160–169, doi:10.1021/ci049885e.

281. Noonan, T.; Denzinger, K.; Talagayev, V.; Chen, Y.; Puls, K.; Wolf, C.A.; Liu, S.; Nguyen, T.N.; Wolber, G. Mind the gap - deciphering GPCR pharmacology using 3D pharmacophores and artificial intelligence. *Pharmaceuticals* **2022**, *15*, 1304, doi:10.3390/ph15111304.

282. Braga, R.C.; Andrade, C.H. Assessing the performance of 3D pharmacophore models in virtual screening: how good are they? *Curr. Top. Med. Chem.* **2013**, *13*, 1127-1138, doi:10.2174/1568026611313090010.

283. Kurogi, Y.; Guner, O.F. Pharmacophore modeling and three-dimensional database searching for drug design using catalyst. *Curr. Med. Chem.* **2001**, *8*, 1035-1055, doi:10.2174/0929867013372481.

284. Dixon, S.L.; Smondyrev, A.M.; Knoll, E.H.; Rao, S.N.; Shaw, D.E.; Friesner, R.A. PHASE: a new engine for pharmacophore perception, 3D QSAR model development, and 3D database screening: 1. Methodology and preliminary results. *J. Comput. Aided Mol. Des.* **2006**, *20*, 647-671, doi:10.1007/s10822-006-9087-6.

285. Taminau, J.; Thijs, G.; De Winter, H. Pharao: pharmacophore alignment and optimization. *J. Mol. Graph. Model.* **2008**, *27*, 161-169, doi:10.1016/j.jmgm.2008.04.003.

286. Sabe, V.T.; Ntombela, T.; Jhamba, L.A.; Maguire, G.E.; Govender, T.; Naicker, T.; Kruger, H.G. Current trends in computer aided drug design and a highlight of drugs discovered via computational techniques: A review. *Eur. J. Med. Chem.* **2021**, *224*, 113705, doi:10.1016/j.ejmech.2021.113705.

287. Sun, H. Pharmacophore-based virtual screening. *Curr. Med. Chem.* **2008**, *15*, 1018-1024, doi:10.2174/092986708784049630.

288. Giordano, D.; Biancaniello, C.; Argenio, M.A.; Facchiano, A. Drug design by pharmacophore and virtual screening approach. *Pharmaceuticals* **2022**, *15*, 646, doi:10.3390/ph15050646.

289. Mysinger, M.M.; Carchia, M.; Irwin, J.J.; Shoichet, B.K. Directory of useful decoys, enhanced (DUD-E): better ligands and decoys for better benchmarking. *J. Med. Chem.* **2012**, *55*, 6582-6594, doi:10.1021/jm300687e.

290. Jenkins, J.L.; Kao, R.Y.; Shapiro, R. Virtual screening to enrich hit lists from high-throughput screening: A case study on small-molecule inhibitors of angiogenin. *Proteins* **2003**, *50*, 81-93, doi:10.1002/prot.10270.

291. *ROCS 3.4.3.0: OpenEye Scientific Software*, Santa Fe, NM.

292. Hawkins, P.C.; Skillman, A.G.; Nicholls, A. Comparison of shape-matching and docking as virtual screening tools. *J. Med. Chem.* **2007**, *50*, 74-82, doi:10.1021/jm0603365.

293. Kearnes, S.; Pande, V. ROCS-derived features for virtual screening. *J. Comput. Aided Mol. Des.* **2016**, *30*, 609-617, doi:10.1007/s10822-016-9959-3.

294. Santino, F.; Gentilucci, L. Design of κ-opioid receptor agonists for the development of potential treatments of pain with reduced side effects. *Molecules* **2023**, *28*, 346, doi:10.3390/molecules28010346.

295. Spetea, M.; Windisch, P.; Guo, Y.; Bileviciute-Ljungar, I.; Schütz, J.; Asim, M.F.; Berzetei-Gurske, I.P.; Riba, P.; Kiraly, K.; Fürst, S. Synthesis and pharmacological activities of 6-glycine substituted 14-phenylpropoxymorphinans, a novel class of opioids with high opioid receptor affinities and antinociceptive potencies. *J. Med. Chem.* **2011**, *54*, 980-988, doi:10.1021/jm101211p.

296. Larson, D.L.; Jones, R.M.; Hjorth, S.A.; Schwartz, T.W.; Portoghese, P.S. Binding of norbinaltorphimine (norBNI) congeners to wild-type and mutant mu and kappa opioid receptors: molecular recognition loci for the pharmacophore and address components of kappa antagonists. *J. Med. Chem.* **2000**, *43*, 1573-1576, doi:10.1021/jm000059g.

297. Azevedo Neto, J.; Costanzini, A.; De Giorgio, R.; Lambert, D.G.; Ruzza, C.; Calò, G. Biased versus partial agonism in the search for safer opioid analgesics. *Molecules* **2020**, *25*, 3870, doi:10.3390/molecules25173870.

298. Gress, K.; Charipova, K.; Jung, J.W.; Kaye, A.D.; Paladini, A.; Varrassi, G.; Viswanath, O.; Urits, I. A comprehensive review of partial opioid agonists for the treatment of chronic pain. *Best Pract. Res. Clin. Anaesthesiol.* **2020**, *34*, 449-461, doi:10.1016/j.bpa.2020.06.003.

299. Wacker, D.; Wang, C.; Katritch, V.; Han, G.W.; Huang, X.-P.; Vardy, E.; McCorvy, J.D.; Jiang, Y.; Chu, M.; Siu, F.Y.; Liu, W.; Xu, H.E.; Cherezov, V.; Roth, B.L.; Stevens, R.C. Structural features for functional selectivity at serotonin receptors. *Science* **2013**, *340*, 615–619, doi:10.1126/science.1232808.

300. Ribeiro, J.M.L.; Filizola, M. Insights from molecular dynamics simulations of a number of G-protein coupled receptor targets for the treatment of pain and opioid use disorders. *Front. Mol. Neurosci.* **2019**, *12*, 207, doi:10.3389/fnmol.2019.00207.

301. Cheng, J.; Sun, X.; Li, W.; Liu, G.; Tu, Y.; Tang, Y. Molecular switches of the κ opioid receptor triggered by 6'-GNTI and 5'-GNTI. *Sci. Rep.* **2016**, *6*, 18913, doi:10.1038/srep18913.

302. Sharma, S.K.; Jones, R.M.; Metzger, T.G.; Ferguson, D.M.; Portoghese, P.S. Transformation of a κ-opioid receptor antagonist to a κ-agonist by transfer of a guanidinium group from the 5 '-to 6 '-position of naltrindole. *J. Med. Chem.* **2001**, *44*, 2073-2079, doi:10.1021/jm010095v.

303. Bileviciute-Ljungar, I.; Spetea, M.; Guo, Y.; Schütz, J.; Windisch, P.; Schmidhammer, H. Peripherally mediated antinociception of the mu-opioid receptor agonist 2-(4,5alpha-epoxy-3-hydroxy-14beta-methoxy-17-methylmorphinan-6beta-yl)aminoacetic acid (HS-731) after subcutaneous and oral administration in rats with carrageenan-induced hindpaw inflammation. *J. Pharmacol. Exp. Ther.* **2006**, *317*, 220–227, doi:10.1124/jpet.105.096032.

304. Kaserer, T.; Lantero, A.; Schmidhammer, H.; Spetea, M.; Schuster, D. μ Opioid receptor: novel antagonists and structural modeling. *Sci. Rep.* **2016**, *6*, 21548, doi:10.1038/srep21548.

305. Wang, Y.; Chen, Y.; Xu, W.; Lee, D.Y.; Ma, Z.; Rawls, S.M.; Cowan, A.; Liu-Chen, L.-Y. 2-Methoxymethyl-salvinorin B is a potent κ opioid receptor agonist with longer lasting action in vivo than salvinorin A. *J. Pharmacol. Exp. Ther.* **2008**, *324*, 1073-1083, doi:10.1124/jpet.107.132142.

306. Bock, A.; Chirinda, B.; Krebs, F.; Messerer, R.; Bätz, J.; Muth, M.; Dallanoce, C.; Klingenthal, D.; Tränkle, C.; Hoffmann, C. Dynamic ligand binding dictates partial agonism at a G protein–coupled receptor. *Nat. Chem. Biol.* **2014**, *10*, 18-20, doi:10.1038/nchembio.1384.

307. Bruning, J.B.; Parent, A.A.; Gil, G.; Zhao, M.; Nowak, J.; Pace, M.C.; Smith, C.L.; Afonine, P.V.; Adams, P.D.; Katzenellenbogen, J.A. Coupling of receptor conformation and ligand orientation determine graded activity. *Nat. Chem. Biol.* **2010**, *6*, 837-843, doi:10.1038/nchembio.451.

308. Ekroos, M.; Sjögren, T. Structural basis for ligand promiscuity in cytochrome P450 3A4. *PNAS* **2006**, *103*, 13682-13687, doi:10.1073/pnas.0603236103.

309. Bruning, J.B.; Chalmers, M.J.; Prasad, S.; Busby, S.A.; Kamenecka, T.M.; He, Y.; Nettles, K.W.; Griffin, P.R. Partial agonists activate PPARγ using a helix 12 independent mechanism. *Structure* **2007**, *15*, 1258-1271, doi:10.1016/j.str.2007.07.014.

310. Angell, R.M.; Angell, T.D.; Bamborough, P.; Bamford, M.J.; Chung, C.-w.; Cockerill, S.G.; Flack, S.S.; Jones, K.L.; Laine, D.I.; Longstaff, T. Biphenyl amide p38 kinase inhibitors 4: DFG-in and DFG-out binding modes. *Bioorg. Med. Chem. Lett.* **2008**, *18*, 4433-4437, doi:10.1016/j.bmcl.2008.06.028.

311. Gioia, D.; Bertazzo, M.; Recanatini, M.; Masetti, M.; Cavalli, A. Dynamic docking: A paradigm shift in computational drug discovery. *Molecules* **2017**, *22*, doi:10.3390/molecules22112029.

312. Kapetanovic, I. Computer-aided drug discovery and development (CADDD): in silico-chemico-biological approach. *Chem. Biol. Interact.* **2008**, *171*, 165-176, doi:10.1016/j.cbi.2006.12.006.

313. Sacan, A.; Ekins, S.; Kortagere, S. Applications and limitations of in silico models in drug discovery. In *Bioinformatics and drug discovery*, Larson, R., Ed.; Humana Press: Totowa, NJ, 2012; Volume 910, pp. 87-124.

314. Søndergaard, C.R.; Garrett, A.E.; Carstensen, T.; Pollastri, G.; Nielsen, J.E. Structural artifacts in protein− ligand X-ray structures: implications for the development of docking scoring functions. *J. Med. Chem.* **2009**, *52*, 5673-5684, doi:10.1021/jm8016464.

315. Liebeschuetz, J.; Hennemann, J.; Olsson, T.; Groom, C.R. The good, the bad and the twisted: a survey of ligand geometry in protein crystal structures. *J. Comput. Aided Mol. Des.* **2012**, *26*, 169-183, doi:10.1007/s10822-011-9538-6.

316. Leach, A.R.; Gillet, V.J.; Lewis, R.A.; Taylor, R. Three-dimensional pharmacophore methods in drug discovery. *J. Med. Chem.* **2010**, *53*, 539-558, doi:10.1021/jm900817u.

317. Shaker, B.; Ahmad, S.; Lee, J.; Jung, C.; Na, D. In silico methods and tools for drug discovery. *Computers in biology and medicine* **2021**, *137*, 104851, doi:10.1016/j.compbiomed.2021.104851.

318. Yusuf, M. Insights into the in-silico research: current scenario, advantages, limits, and future perspectives. *Life in Silico* **2023**, *1*, 13-25.

319. Azad, I.; Khan, T.; Maurya, A.K.; Irfan Azad, M.; Mishra, N.; Alanazi, A.M. Identification of Severe Acute Respiratory Syndrome Coronavirus-2 inhibitors through in silico structure-based virtual screening and molecular interaction studies. *J. Mol. Recognit.* **2021**, *34*, e2918, doi:10.1002/jmr.2918.

8. List of Publications

This list summarizes all publications that have been part of my doctoral studies between 2021–2024. Shared first authorship is denoted with the * symbol.

Article A

Puls, K.; Schmidhammer, H.; Wolber, G.; Spetea, M. Mechanistic characterization of the pharmacological profile of HS-731, a peripherally acting opioid analgesic, at the µ-, δ-, κ-opioid and nociceptin receptors. Molecules **2022**, 27, 919, doi:10.3390/molecules27030919.

Article B

Puls, K.*; Olivé-Marti, A.-L.*; Pach, S.; Pinter, B.; Erli, F.; Wolber, G.; Spetea, M. In vitro, in vivo and in silico characterization of a novel kappa-opioid receptor antagonist. Pharmaceuticals **2022**, 15, 680, doi:10.3390/ph15060680.

Article C

Puls, K.; Wolber, G. Solving an old puzzle: Elucidation and evaluation of the binding mode of Salvinorin A at the kappa opioid receptor. Molecules **2023**, 28, 718, doi:10.3390/molecules28020718.

Article D

Discovery of Novel, Selective, and Non-basic Agonists for the Kappa-Opioid Receptor Determined by Salvinorin A-Based Virtual Screening. (The manuscript has been submitted to the Journal of medicinal chemistry at 11.03.2024)

Article E

Noonan, T.; Denzinger, K.; Talagayev, V.; Chen, Y.; Puls, K.; Wolf, C.A.; Liu, S.; Nguyen, T.N.; Wolber, G. Mind the gap—deciphering GPCR pharmacology using 3D pharmacophores and artificial intelligence. Pharmaceuticals **2022**, 15, 1304, doi:10.3390/ph15111304.

Conference Abstract F

Puls, K.*; Pach, S.; Wolber, G.; Bermudez, M. Dynamic interaction patterns enable characterization of opioid-peptide binding to the atypical chemokine receptor 3. 12th International Conference on Chemical Structures (ICCS) **2022**, Noordwijkerhout, Netherlands.

Conference Abstract G

Puls, K.*; Wolber, G. Solving an Old Puzzle: How Salvinorin A Recognizes the Kappa Opioid Receptor. 8th ERNEST Meeting **2023**, Crete, Greece.